



Robert Tafner, Dipl.-Ing. Bakk. techn.

Observer-Based Parameter Identification Techniques: A Framework for Vehicle Dynamics Assessment

DOCTORAL THESIS

to achieve the university degree of
Doktor der technischen Wissenschaften

submitted to

Graz University of Technology

First Supervisor:

Univ.-Prof. Dipl.-Ing. Dr.techn. Martin Horn

Institute of Automation and Control
Graz University of Technology

Second Supervisor:

Prof. Dr. Antonella Ferrara

Dipartimento di Ingegneria Industriale e dell'Informazione
University of Pavia

Graz, October 2015

Affidavit

Eidesstattliche Erklärung

I declare that I have authored this thesis independently, that I have not used other than the declared sources/resources, and that I have explicitly indicated all material which has been quoted either literally or by content from the sources used. The text document uploaded to TUGRAZonline is identical to the present doctoral thesis.

Ich erkläre an Eides statt, dass ich die vorliegende Arbeit selbstständig verfasst, andere als die angegebenen Quellen/Hilfsmittel nicht benutzt, und die den benutzten Quellen wörtlich und inhaltlich entnommenen Stellen als solche kenntlich gemacht habe. Das in TUGRAZonline hochgeladene Textdokument ist mit der vorliegenden Dissertation identisch.

Graz, _____
Date Signature

Abstract

Assessment of the vehicle handling especially with respect to its lateral dynamics is an important aspect of the overall vehicle design and development process. However, a higher rate of vehicle update cycles, an increasing number of variants and a required high-quality comfort and/or driving reward render the evaluation process a challenging task. Consequently, virtual methods support the overall development process and increase time and cost efficiency significantly. The so-called model-based (objective) methodology aims to extract certain vehicle and/or driver model parameters from measurement data. These can then be used to simulate standard handling maneuvers, rather than performing them on a test track. State of the art parameter identification mechanisms are commonly performed offline and require extensive instrumentation of the test vehicle.

In this thesis, a novel approach is proposed based on observer-based parameter identification techniques. It introduces the advantages of online capability, time-efficient experiment execution and reduction of sensing devices due to estimation of specific system states. The sensing devices and estimated parameters are selected systematically, i.e. by exploiting observability measures and parameter sensitivity studies. State augmentation and unknown input recovery are the paradigms used for the joint estimation of states and parameters. Using the so-called sliding mode approach allows formulation of state observers that are invariant with respect to certain classes of perturbations. Its attractiveness is further increased by the finite time convergence property. Moreover, employing parameter identification algorithms based on higher-order sliding modes introduces robustness, finite convergence time and stability even for non-persistently excited systems.

Evaluation of the concepts is performed twofold. An industrial vehicle dynamics simulation tool provides data for the observation concepts. The resulting parameter estimates are integrated into the offline simulation of standard handling maneuvers, e.g. step input steering. Comparing these results with the reference data allows to draw conclusions on the expected accuracy of the method. Additionally, selected concepts are evaluated on experimental facilities, i.e. standard vehicles and an electric power steering test bench.

Acknowledgments

This thesis originated from my working time at the Alpen-Adria-Universität Klagenfurt and Graz University of Technology. I would like to thank both groups for their kindness.

First and foremost, I direct my thanks to Univ.-Prof. Dipl.-Ing. Dr.techn. Martin Horn for his technical guidance, the patience, encouragement and also the confidence for pursuing ideas that lightened the challenge.

Prof. Antonella Ferrara receives a special thank for her keen commitment and enthusiasm to support this project. I am grateful to Prof. Jaime A. Moreno and Prof. Leonid Fridman for their interest in my work and stimulating inputs.

Discussions with Dr. Markus Reichhartinger always opened my mind and inspired my future work. As a colleague and friend I am very thankful for his encouragement.

I would also like to thank Daniel Schwingshackl, Vamsi Makkapati and Dr. Jakob Rehrl. Moreover, Dr. Werner Kober for his support with experimental facilities and joining the research cooperation funded by the Austrian Research Promotion Agency (FFG).

A sincere 'Thank you' goes to my family. Especially to my parents for their support, kindness and warmth through all the years. Patrick and Katharina for teaching me the ability to focus back on the essential aspects of life.

Finally, the two persons making my life most delightful shall be mentioned: Susanne and Julia. Thank you for your love, believe and your willingness to make sacrifices!

Without you, I would not have become who I am.

Robert Tafner, Graz 06/10/2015

Contents

Abstract	vi
Notation	xix
Acronyms	xxii
1 Introduction	1
1.1 The Modern Vehicle Development Process	1
1.2 Vehicle Dynamics Assessment	2
1.2.1 Subjective Evaluation	4
1.2.2 Objective Evaluation	9
1.2.3 Model-based Objective Evaluation	18
1.2.4 State Observation for Vehicle Dynamics	24
1.3 Thesis Outline	24
2 Modelling of Selected Vehicle Dynamics	29
2.1 Vehicle Motion	30
2.1.1 Longitudinal Dynamics	31
2.1.2 Lateral Dynamics	33
2.2 Tire Dynamics	36
2.2.1 Stationary Tire Forces	38
2.2.2 Transient Tire Forces	44

2.3	Chassis Motion	45
2.3.1	Roll Dynamics	45
2.3.2	Pitch Dynamics	51
2.4	Steering Dynamics	55
2.4.1	Conventional Steering	55
2.4.2	Electric Power Steering System	56
2.5	Powertrain Dynamics	58
2.6	Human Perception	60
3	Analyses of Vehicle Dynamics Models	67
3.1	Theoretical Background	68
3.1.1	Parameter Sensitivity Analysis	68
3.1.2	Observability	71
3.1.3	Observability Measures	74
3.2	Application to Vehicle Dynamics Models	75
3.2.1	Longitudinal Dynamics	75
3.2.2	Lateral Dynamics	75
3.2.3	Roll Dynamics	93
3.2.4	Pitch Dynamics	96
3.2.5	Steering Dynamics	99
3.3	Concluding Remarks for the Parameter Identification	104
4	Observer-Based Parameter Identification Techniques	105
4.1	Theoretical Background	106
4.1.1	State Augmentation	107
4.1.2	Unknown Input Estimation	114
4.2	Applied Observer-Based Parameter Identification Techniques	121
4.2.1	Lateral Dynamics	121
4.2.2	Roll Dynamics	136
4.2.3	Pitch Dynamics	155
4.2.4	Steering Dynamics	155

4.2.5	Longitudinal and Powertrain Dynamics	161
4.2.6	Road Disturbance	163
4.3	Concluding Remarks on the Observer-based Parameter Identification Concepts	166
5	Validation of the Assessment Framework in Simulations	167
5.1	Implementation of the Parameter Identification Concepts: Peripherals	168
5.2	Observer-based Vehicle Parameter Identification	170
5.2.1	Source Model	170
5.2.2	Timeline of the Module Execution	171
5.2.3	Lateral Dynamics	173
5.2.4	Roll Dynamics	180
5.2.5	Pitch Dynamics	186
5.2.6	Steering Dynamics	188
5.2.7	Longitudinal and Powertrain Dynamics	188
5.2.8	Road Disturbances	190
5.2.9	Comments	193
5.3	Performance Assessment of the Model-based Handling Evaluation	194
5.3.1	Simulation of Open-loop Driving Maneuvers	195
5.3.2	Extraction and Comparison of Objective Metrics	201
5.3.3	Human Perception Simulation	203
5.3.4	Extraction of Objective Metrics	208
5.3.5	Comments	208
5.4	Concluding Remarks on the Simulation-based Evaluation	210
6	Experimental Evaluation of Selected Observer Concepts	211
6.1	The Implementation Setup	212
6.2	Lateral Dynamics (Experimental Vehicle A)	213
6.3	Roll Dynamics (Experimental Vehicle B)	221
6.4	Steering Dynamics (EPS Test Bench)	228
6.5	Concluding Remarks on the Experimental Evaluation	231

7 Conclusion	233
7.1 Thesis Objective and Main Contributions	233
7.2 Future Work	236
A Coordinate Frames	239
A.1 Coordinate Frames for Vehicle Motion Description	239
B Mathematical Supplements	243
B.1 Chapter 3 - Lateral Dynamics 3.2.2.II (Σ_{L2})	243
B.2 Chapter 3 - Lateral Dynamics 3.2.2.III (Σ_{L3})	245
B.3 Chapter 4 - Roll Dynamics 4.2.2.I (EKF)	249
C Objective Metrics of Standardized Test Maneuvers	251
C.1 Steady-state Circular Driving ISO4138	252
C.2 Step Input ISO7401	254
C.3 Sinusoidal Input (One Period) ISO7401	256
C.4 Sinusoidal Input (Continuous - Constant Frequency) ISO7401	258
C.5 Sinusoidal Input (Continuous - Varying Frequency) ISO7401	260
D Experimental Setup	263
D.1 Virtual Reference Vehicle (IPG CarMaker [®])	263
D.1.1 Virtual Vehicle Configuration	263
D.1.2 Measurement Setup	264
D.2 Experimental Vehicles	264
D.2.1 Some General Notes	264
D.2.2 Sensor Noise Characteristics	265
D.2.3 Sensor Configurations	266
D.3 Electric Power Steering Test Bench	267
D.3.1 Some General Notes	267
D.3.2 Data Acquisition and Measurement Devices	267
D.3.3 Test Bench Images	268

Bibliography

286

Notation

General

\mathbb{C}	Complex numbers
\mathbb{C}^-	Left-half open complex plane
x	Scalar
\mathbf{x}	Vector - reference system: intermediate axis system \mathcal{C}
\mathbf{A}	Matrix
${}^e\mathbf{x}$	Vector - reference system: earth-fixed axis system \mathcal{C}_e
${}^v\mathbf{x}$	Vector - reference system: vehicle-fixed axis system \mathcal{C}_v
${}^{wf}\mathbf{x}$	Vector - reference system: front wheel-fixed axis system \mathcal{C}_{wf}
${}^{wr}\mathbf{x}$	Vector - reference system: rear wheel-fixed axis system \mathcal{C}_{wr}
${}^vx_{x,f}$	Scalar - x-direction, front wheel, axis system \mathcal{C}_v
\hat{x}	Estimation value of x
\hat{x}^-	<i>A priori</i> estimation value of x
\hat{x}^+	<i>A posteriori</i> estimation value of x
\bar{x}	Nominal part of x (uncertain scalar)
Δx	Uncertain part of x (uncertain scalar)
x^*	Scaled value of x , i.e. $x^* = \frac{x}{X_{scal}}$
$\mathbf{x}_0, \mathbf{P}_0$	Initial values of \mathbf{x} and \mathbf{P} , e.g. $\mathbf{x}_0 := \mathbf{x}(t_0)$

\mathbb{N}_0	Natural numbers, including 0
\mathbb{R}	Real numbers
\mathbb{R}^n	n-dimensional space of real numbers

Mathematical Operators

\mathbf{A}^{-1}	Matrix inverse
\mathbf{A}^T	Matrix transpose
\mathbf{A}^H	Matrix conjugate-complex transpose
\dot{x}	Time derivative of x , i.e. $\dot{x} := \frac{dx}{dt}$
\ddot{x}	2 nd time derivative of x , i.e. $\ddot{x} := \frac{d^2x}{dt^2}$
$\bar{u}(s)$	Laplace transform of $u(t)$, i.e. $\bar{u}(s) := \mathcal{L}\{u(t)\}$
$[\cdot]^y$	Abbreviation used for sliding mode observers, i.e. $[\cdot]^y := \cdot ^y \text{sign}(\cdot)$
\equiv	"Identical equal to"
$:=$	"Defined by"
\approx	"Approximately equal to"

Latin Symbols

\mathbf{T}_{ev}	Transformation matrix from axis system "v" to "e"
\mathbf{a}	Translational acceleration vector, i.e. $\mathbf{a} = [a_x \ a_y \ a_z]^T$
\mathbf{v}	Translational velocity vector, i.e. $\mathbf{v} = [v_x \ v_y \ v_z]^T$
$a_{x,m}$	Measured longitudinal acceleration (distorted by pitch angle)
$a_{y,m}$	Measured lateral acceleration (distorted by roll angle)
m	Total vehicle mass
m_s	Mass of sprung vehicle parts
J_{xc}	Moment of inertia of chassis (+sprung parts) w.r.t. long. vehicle axis
J_{yc}	Moment of inertia of chassis (+sprung parts) w.r.t. lateral vehicle axis
J_z	Moment of inertia w.r.t. vertical vehicle axis

J_{ca}	Moment of inertia of aggregated parts below torque sensor (EPS)
J_{stw}	Moment of inertia of steering wheel angle
T_h	Steering wheel torque
T_w	Wheel torque
T_m	Assistant motor output torque
l_r	Distance between CoG and rear axle
l_f	Distance between CoG and front axle
l_{fe}	Distance l_f (with pneumatic trails)
l_{re}	Distance l_r (with pneumatic trails)
h_{rl}	Distance between roll center and CoG
h_{pl}	Distance between pitch center and CoG
n_p	Pneumatic trail
n_k	Kinematic trail
c_{α_f}	Lateral cornering stiffness front
$c_{\alpha_{fe}}$	Effective lateral cornering stiffness front (with steering elasticity)
c_{α_r}	Lateral cornering stiffness rear
c_y	Lateral tire stiffness
σ_α	Tire relaxation length
$c_\Sigma^r(\varphi)$	Effective roll stiffness
$d_\Sigma^r(\dot{\varphi})$	Effective roll damping
$c_\Sigma^p(\theta)$	Effective pitch stiffness
$d_\Sigma^p(\dot{\theta})$	Effective pitch damping
d_m	Damping coefficient (viscous friction) of electric motor
c_c	Steering column stiffness
d_c	Steering column damping
i_s	Static steering ratio

i_m	Transmission ratio from electric motor to the steering column
i_r	Transmission ratio from steering column to steering rack
g	Gravitational acceleration, i.e. $g \approx 9.8067\text{m}\cdot\text{s}^{-2}$

Greek Symbols

Σ	Abbreviation for a system definition, e.g. Σ_R for roll model
α	Rotational acceleration vector, i.e. $\alpha = [\alpha_x \ \alpha_y \ \alpha_z]^T$
ω	Rotational velocity vector, i.e. $\omega = [\omega_x \ \omega_y \ \omega_z]^T$
φ	Regression vector (Recursive Least Squares algorithm, Section 4.2.2.II)
Γ	Regression vector (Finite time parameter estimator, Section 4.2.2.II)
ρ	Parameter vector (Sensitivity analysis, Chapter 3)
θ	Parameter vector (Observer-based parameter estimation, Chapter 4)
Φ	Diffeomorphism
ζ, ξ, ϱ	Unknown inputs (not necessarily scalars)
τ	Time constant
α, κ	Observer gain parameters
λ, μ	————— ” —————
$\tilde{\lambda}$	Observer adaptive gain parameters
φ	Chassis roll angle
θ	Chassis pitch angle
ψ	Vehicle yaw angle
δ_h	Steering wheel angle
δ_s	Steering column angle
δ_w	Wheel angle
$\varphi\dots$	Position of the <u>a</u> ccelerator, <u>b</u> rake or <u>c</u> lutch pedal
ω_e	Engine speed
β	Vehicle sideslip angle

α_f	Tire slip angle (front)
α_{f_e}	Tire slip angle (front) with roll dynamics coupling
χ	Road inclination angle
Φ	Road bank angle
π	Constant, i.e. $\pi \approx 3.14159$

Acronyms

ABS	<u>A</u> nti- <u>l</u> ock <u>B</u> raking <u>S</u> ystem
ARAO	<u>A</u> daptive <u>R</u> oll <u>A</u> ngle <u>O</u> bserver
CAE	<u>C</u> omputer <u>A</u> ided <u>E</u> ngineering
CCF	<u>C</u> ross- <u>C</u> orrelation <u>F</u> unction
CoG	<u>C</u> enter of <u>G</u> ravity
DOE	<u>D</u> esign of <u>E</u> xperiments
EHPS	<u>E</u> lectro- <u>H</u> ydraulic <u>P</u> ower <u>S</u> teering
EKF	<u>E</u> xtended <u>K</u> alman <u>F</u> ilter
EPS	<u>E</u> lectric <u>P</u> ower <u>S</u> teering
ESP	<u>E</u> lectronic <u>S</u> tability <u>P</u> rogram
EU	<u>E</u> uropean <u>U</u> nion
FFT	<u>F</u> ast <u>F</u> ourier <u>T</u> ransform
FTPE	<u>F</u> inite <u>T</u> ime <u>P</u> arameter <u>E</u> stimation
GPS	<u>G</u> lobal <u>P</u> ositioning <u>S</u> ystem
GSTA	<u>G</u> eneralized <u>S</u> uper <u>T</u> wisting <u>A</u> lgorithm
HOSM	<u>H</u> igher- <u>O</u> rder <u>S</u> liding <u>M</u> ode
ICR	<u>I</u> ntantaneous <u>C</u> enter of <u>R</u> otation

IVM	<u>I</u> dentified <u>V</u> ehicle <u>M</u> odel
LTI	<u>L</u> inear <u>T</u> ime- <u>I</u> nvariant System
MLP	<u>M</u> ulti- <u>L</u> ayer <u>P</u> erceptron
OEM	<u>O</u> riginal <u>E</u> quipment <u>M</u> anufacturer
PE	<u>P</u> arameter <u>E</u> stimation
RED	<u>R</u> obust <u>E</u> xact <u>D</u> ifferentiator
RLS	<u>R</u> ecursive <u>L</u> east <u>S</u> quares
RLSPE	<u>R</u> ecursive <u>L</u> east <u>S</u> quares <u>P</u> arameter <u>E</u> stimator
RSE	<u>R</u> obust <u>S</u> tate <u>E</u> stimation
SMO	<u>S</u> liding <u>M</u> ode <u>O</u> bserver
STA	<u>S</u> uper <u>T</u> wisting <u>A</u> lgorithm
UIO	<u>U</u> nknown <u>I</u> nput <u>O</u> bserver
VBM	<u>V</u> ehicle <u>B</u> ehavior <u>M</u> odel
VDM	<u>V</u> ehicle <u>D</u> ynamics <u>M</u> odel
VSUIO	<u>V</u> ariable <u>S</u> tructure <u>U</u> nknown <u>I</u> nput <u>O</u> bserver

1

Introduction

1.1 The Modern Vehicle Development Process

Individual *mobility* has become a basic requirement of human beings. The means of transport are manifold and their applicability depend on the traveling distance. Thinking of road transport self-propelled vehicles provide high flexibility and individualism. Due to their propulsion, that is mostly based on internal combustion engines, the environmental burden is often subject of debates and results in more and more stringent emission standards for light duty vehicles, e.g. Euro 6 legislation [EUR06].

Additionally to the emission requirements, vehicle safety has also been facing some challenges within recent years. The introduction of active and passive safety systems (e.g. ABS, ESP) led to a significant reduction of road traffic fatalities in the EU countries whereas the number of accidents decreased only little over the last 20 years [EUR15].

The modern vehicle development process needs to adapt to the ever-changing customer requirements influenced by global trends such as *urbanization*, *eventual shortage of natural resources*, *environmental awareness* and *aging of the society* [SR08]. The latter is supported by the demography report of the EU [EUR10] showing an increase of the population aged 20-64 years. Especially the people of age 50+ are interested in buying *exclusive* and *individual* products without any compromises. The answer of the automobile market to that question is a tremendous increase in vehicle variants. However, long waiting times for innovations and exciting products are not accepted by the customers and consequently vehicle update cycles (so-called *time-to-market*) need to be reduced otherwise market shares might get lost to other OEMs. Figure 1.1 illustrates this conflict of objectives causing serious problems for the automobile market, i.e. keeping the high quality standards for an increasing number of variants and also developing new products in record times. A countermeasure to reduce development times and efforts is the introduction of the virtual development paradigm, i.e. numerous design and engineering

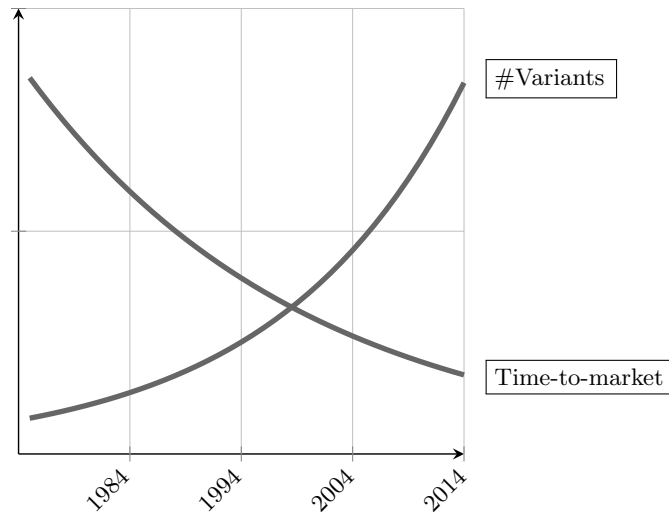


Figure 1.1: Conflicting requirements of decreasing product update cycle times and increasing number of vehicle variants [REN07, SR08, HE11].

problems are solved using CAE¹ tools. These support the aim to increase the quality level of developments in the concept phase already in order to reduce the requirements of testing hardware/prototypes and therefore development times [SR08].

In general, the design and evaluation of *vehicle handling* represents an integral part of the overall vehicle development task [SCH10]. The evaluation focuses not only on safety critical behavior, but also takes into account the fun factor a potential customer experiences when driving the vehicle. It is, besides design and image, a decisive factor for the buying decision of a specific vehicle [HE11]. As a consequence of the subjective experience by the customer, it is little surprising that the evaluation of vehicle dynamics is still mainly performed on a subjective basis [DEC09]. Although there exist already various alternative methods (e.g. objective evaluation) a replacement of subjective techniques in the near future is not foreseeable.

1.2 Vehicle Dynamics Assessment

The vehicle handling is referred to as the dynamic response (in terms of vehicle motion) to certain driver inputs, e.g. steering, throttle, brake and road disturbances [HE11, p.122]. The term *good* in this sense corresponds to an exact tracking of the driver dictated direction [ZOM91]. In general, the evaluation process might be performed in a *subjective* or *objective* manner.

¹Computer Aided Engineering.

Ideally, the following characteristics are inherent to the vehicle [MW04]

- intuitive and simple controllability,
- external disturbances must not distract the driver from its navigational task,
- clearly foreseeable handling limits,
- invariant (or close to) vehicle handling to any changes in the configuration (e.g. vehicle load, tires).

Interpretation of these requirements leads to the fact that the vehicle handling ideally shall be adapted to the driver skills. In view of the demography development [EUR10] the aging of the population complicates that adaption as the expectations on the vehicle handling of younger and older people are different (comfort vs. agility). Consequently, the importance of handling characteristics evaluation is strengthened in order to satisfy all potential customers.

Subjective evaluation generally refers to performing various driving tasks by expert and standard drivers followed by feeding back the characteristics of vehicle performance. Although the natural feedback would be verbal and ideally provide most information for the engineers, due to the heterogeneous vocabulary of the drivers this type of feedback would not be comparable. Furthermore, especially standard drivers are mostly unable to communicate their impressions in detail as they are lacking technical terms. Therefore, high efforts have been put on the translation of these verbal descriptions into numerical ratings of specific handling characteristics. Clearly, this might introduce some loss of information, as the expert drivers are not able to express their impressions in detail, but establishes a common basis for the feedback evaluation. Another difficulty subjective evaluation faces is the human being itself. It is known that the perception is different among humans, it changes with time (adaption) and it also depends on the current mood of a person [DEC09].

An alternative approach, that is not exposed to human variability is given by the *objective* evaluation. It refers to measurement of any vehicle responses due to driver inputs (steering, accelerating, braking) during specific, well-defined handling maneuvers. Clearly, the vehicle to be evaluated requires a high level of instrumentation such that the vehicle responses are recorded accurately. These measured signals can be further exploited for extraction of so-called objective metrics that describe the vehicle responses uniquely. For obtaining a synthesized rating, links between these objective metrics and subjective values fed back from test drivers need to be found. Once these links are identified ideally the evaluation of a specific vehicle can be conducted by measurement of vehicle responses, extraction of objective metrics and usage of subjective-objective links to generate a synthesized subjective evaluation without consulting any expert driver.

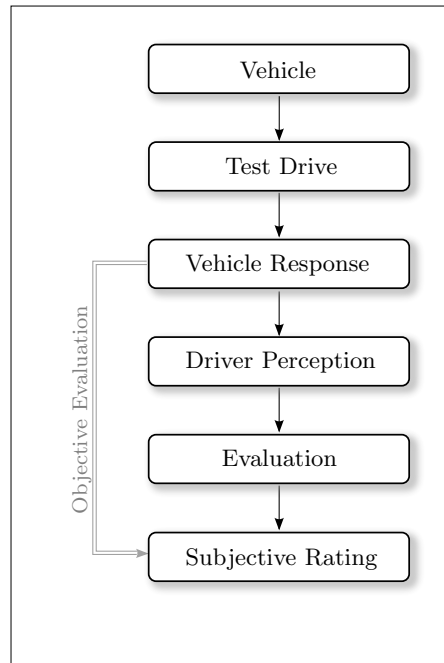


Figure 1.2: Flow diagram of the subjective evaluation process.

1.2.1 Subjective Evaluation

Introduction

Even though the vehicle development process is significantly supported by computer aided design methods and highly accurate measurement equipment the perception and evaluation of human beings with respect to vehicle dynamics is of great importance. That paradigm is commonly referred to as the subjective one. In general, the methodology mostly relies on highly experienced test drivers or specialized engineers that are required to have a good *memory of perception*, *power of discrimination* and a well-developed *filtering capability* [ZOM91]. From these requirements it is already obvious that the human influence on the overall process is the bottleneck of the methodology. Figure 1.2 shows the general process flow of the subjective evaluation. A test driver (not necessarily a single person) performs some handling maneuvers and feeds back the experience (perception) by filling out a designed questionnaire that is part of the evaluation. The rating(s) are analyzed statistically to calculate an overall grade per evaluation criterion. The gray line indicates the alternative process of objective evaluation. Its detailed process flow will be discussed later.

Driver Selection

In order to overcome inconsistent results due to individual preferences on the handling performance and variations in human perception the evaluation process is not only based

on a single person, but commonly relies on a group of several highly qualified engineers and drivers. The statistical evaluation of the results allows for identification of outliers and introduces additional robustness to the process.

Often discussed is the integration of untrained drivers into the evaluation group as these are closer to the future customer in terms of handling capabilities [MTTT80]. A well-evaluated vehicle (by expert drivers) is not guaranteed to be accepted by normal drivers as well [KRA11]. However, the expert driver is also capable of providing a detailed description of the handling differences and their cause whereas the standard driver might only point out the differences. And additionally, during the vehicle development phase it is only specialized personnel that is allowed to work with these prototype vehicles due to confidentiality reasons. Furthermore, in order to evaluate the vehicle handling its dynamics must be excited in a way that renders the handling differences visible [NKS01]. Clearly it is more likely that trained personnel is able to perform this task. Otherwise, the evaluation results might get distorted.

The aspect of defining a clear terminology for certain handling characteristics is indispensable for comparison of the subjective feedback. In fact, there is no standardization of the terminology and consequently the manufacturers do have their own specifications, which are highly related to the individual tuning philosophies [HEN04].

An excerpt of disciplines a vehicle is typically evaluated in, is depicted in Figure 1.3 and reads as *Straight line Directional Stability, Steering Precision, On/Off-Center Steering Response/Precision, Lane Change Performance, Load Change Reaction, Accelerating/Braking Performance, Driving Comfort*, see [HB02] and [ZOM91] for further details. Clearly, these disciplines can be subdivided further depending on the evaluation task. For example, if a suspension setting (or another modified vehicle part) should be evaluated, the questionnaire needs to be very specific (*low-level*, from a technical point of view). In contrast, if the evaluation task refers to a complete vehicle only *top-level* related questions are to be asked. In general, it is recommended to evaluate not more than 10 criteria per test run [HB02]. Additionally, if new variants of vehicle parts are to be evaluated it is a common practice to retain any information of the current vehicle setup from the engineers/test drivers. By doing so, any weaknesses in perception can not be compensated for by technical knowledge.

Mostly, the handling maneuvers are not chosen completely free by the drivers but there exist detailed lists that provide a comprehensive maneuver description, requirements on the test track as well as criteria the drivers need to look at [HB02].

Alternatively, in [CHE97] the selection is at the discretion of the drivers. But the results show a wide spread between different driver ratings, that most likely comes from the freely chosen vehicle excitations.

Questionnaire

The questionnaire aims to project the driver's perception into a comparable and homogenous data basis, i.e. the vocabulary of the driver to describe and assess certain

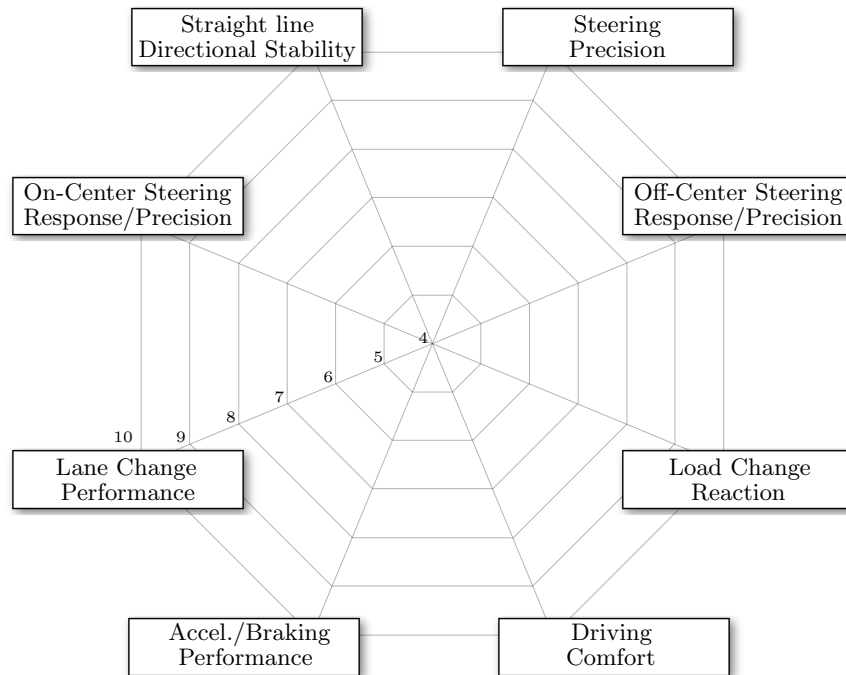


Figure 1.3: Typical disciplines of vehicle evaluation [HB02], [ZOM91].

handling characteristics needs to be transformed. Clearly, designing these is nontrivial and depends completely on the evaluation task. Not only the selection of questions has a great influence on the success of information extraction. But also the specific formulation of the question, i.e. extensive use of technical vocabulary might lead to confusion or misinterpretation and consequently a distortion of the information fed back from the drivers. Even the type of question, *open* or *restricted*, might limit the details in the answers [AND01, HL05]. Whereas an *open* question leaves the freedom of the answering detail to the human, a *restricted* question reduces the space of possible feedback significantly, i.e. harmonizes the information content from each driver. Aside the specific formulation of the questions, the selection of the latter is mainly driven by the evaluation objective and/or the specific driving maneuver. In other words, assuming the vehicle handling should be evaluated based on a double lane-change maneuver yields other questions as if the excitation was chosen to be a steady-state circular drive. Furthermore, evaluation of the vehicle suspension will result in other questions than assessing the engine performance. Examples of presented questionnaires in literature are manifold, e.g. [DEC09, DET05, HAR07, HB02, ZOM91]. An excerpt of questions related to the evaluation of the general vehicle handling is shown in Figure 1.4. This example demonstrates nicely the hierarchy of a questionnaire with regards to the considered vehicle assessment domains (sub-domains, etc.). Note that the formulation of these questions is kept simple such that normal drivers understand immediately which information is requested.

	Main Heading	Sub Heading	Sub Sub Heading	Question
01	Steady state turning	Over smooth roads	Cornering behaviour	Progressive behaviour with increasing lateral accel.
...				
12	Steady state turning	Over rough roads	Cornering behaviour	Ease with which a line is held
...				
22	Sudden braking in a turn			Roll stability
...				
29	Transient cornering	Turn in response		Body roll rate
...				
36	Straight line directional stability	Under acceleration		Tendency to pull to one side
...				
40	Obstacle avoidance	Single lane change	Balanced throttle	Controllability
...				
47	Response to steering impulse			Oscillation of vehicle

Figure 1.4: Excerpt of a questionnaire presented in [CHE97].

In comparison, the question "How is the steering on-center feel at $80\text{km}\cdot\text{h}^{-1}$?", as in [HAR07], is directed at experts. A more specific questionnaire is part of a collection presented in [KRA11] for the influence analysis of various vehicle suspension systems (configurable via electric linear actuators) onto the handling characteristics, see Figure 1.5. Aside the questions to the evaluator it also contains the rating itself that will be discussed in the next section.

Rating Scales

In order to somehow *measure* a driver's perception a rating scale needs to be defined. Generally, one distinguishes between an *open* and a *closed* scale. The open scale, standardized by the SAE Standard J1441 [J14], is made up of positive numbers where small values correspond to the rating *inadequate*. A quantitative increase enhances the grade of a specific handling feature. This type of scale, depicted in Figure 1.6(a), is also referred to as *unipolar* scale as there is no polarity change over the complete rating scale [ZOM91, ZSC09]. The discretization of grades is highly varying, e.g. 0-10 [ZOM91], 1-7 [CHE97], 0-60 [ISO99] and although the Standard J1441 recommends using 11 steps of grades, there is no clear definition on the advantages/disadvantages of more/less rating steps. To render the reading and interpretation of these scales easier the numbers are mostly supported by a verbal description. For some applications the grades are further divided into a coarse discretization scheme, e.g. *acceptable*, *not acceptable*. As argued in [ZOM91] the unipolar scale introduces the advantages of intuitive interpretation and it

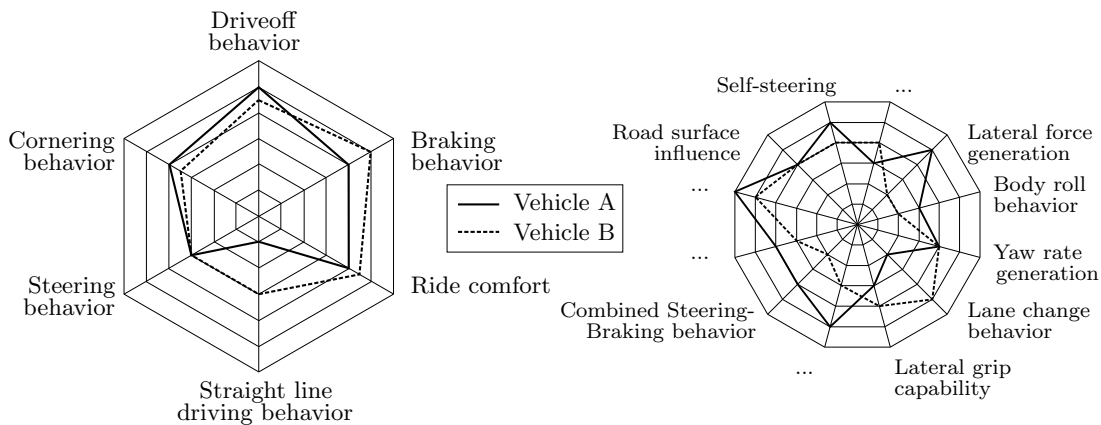
necessarily optimal with respect to its handling characteristics), that a better grade is achieved and one end of the scale refers to an improvement [BOT08]. The final grades of the various handling (sub)disciplines can be plotted in spider graphs, see Figures 1.7(a) and 1.7(b).

1.2.2 Objective Evaluation

The objective evaluation aims to identify vehicle handling characteristics in a *repeatable* and *measurable* manner. In contrast to the vaguely standardized subjective paradigm the situation is different for the objective approach. There, the specific driving tasks as well as the metrics to be extracted from measured vehicle responses are well defined. For so-called *open-loop* maneuvers the driver does not act as a controller and considers any vehicle reactions for generating a modified input, but applies pre-defined commands. Consequently, these maneuvers have the potential for evaluation of the pure vehicle responses rather than a driver-vehicle combination. In contrast, *closed-loop* maneuvers define a certain path/curvature that the driver, now acting as a controller (in the sense of control theory), has to follow within some certain limits. Generally, open-loop maneuvers have established to be more related to *driving behavior* whereas closed-loop tests are mainly used for *driving performance* assessment [HB02].

Figure 1.8 depicts the flow diagram of the objective evaluation process. In its initial phase the subjective evaluation is still required in order to identify the correlation between subjective ratings and objective metrics. Once these links have been determined a synthesized subjective rating can be generated based on the extracted objective metrics, ideally rendering the subjective evaluation redundant.

The driving maneuvers and the extracted characteristic values build the basis for the challenging correlation of objective values with subjective ratings. A standard approach



(a) Evaluation: Overall vehicle behavior. (b) Evaluation: Cornering behavior.

Figure 1.7: Graphical evaluation of handling disciplines.

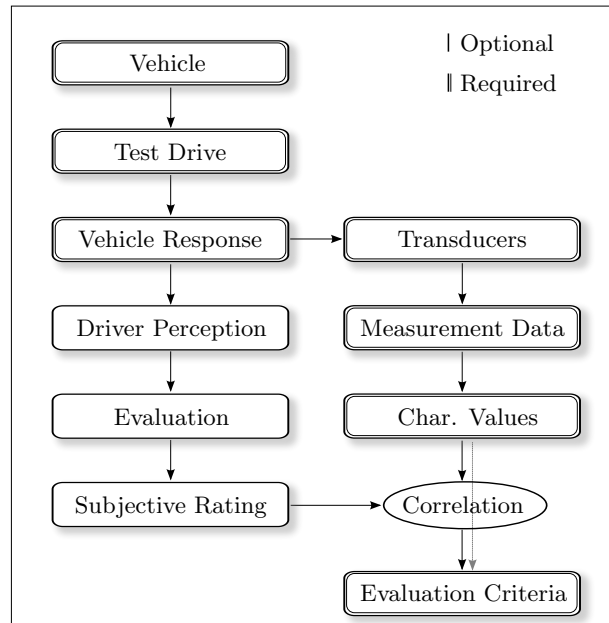


Figure 1.8: Objective evaluation based on metrics extracted from measurements [DEC09].

is exploiting multiple regression analysis for exploring any links between the two data sets [CHE97, ZOM91]. Based on the regression model a synthesized subjective evaluation can be generated. The boxes in Figure 1.8 marked with double-lines are process invariant, i.e. these sub-processes have to be executed whenever an objective evaluation is to be performed. This is opposed to the boxes with single-lines, as these are only executed for building a new data base for the correlation process (resulting in new evaluation criteria). Ideally, these boxes have to be performed once. The next paragraphs will shed some light on the standardized driving maneuvers, its characteristic values and the subjective-objective correlation. These maneuvers are related to the lateral driving behavior of the vehicle. Subjects as *Straight line driving*, *driving comfort* etc. are not objectives of this thesis, as is the so-called driveability². Only a side issue of the latter is evaluated, i.e. the longitudinal acceleration performance of the vehicle.

Standardized Driving Maneuvers

In the 1970s and 1980s an ISO committee, named TC 22/SC 9 "Vehicle dynamics and road-holding ability" was initiated with the objective to define standards and methods for vehicle dynamics evaluation such that all automotive manufacturing countries use the same methodologies [ZBR97]. The most important closed-loop, as well as open-loop

²The term *driveability* is more related to an evaluation of the longitudinal vehicle dynamics as well as vehicle-powertrain objectives [ZSM09]. Typical vehicle maneuvers for driveability evaluation are: idling, engine start, tip in, let off, acceleration, gear change, etc. [LS98].

maneuvers dealing with the cornering characteristics will be analyzed in the following. A comprehensive overview of driving situations (Figure 1.9), evaluation criteria and their development within the two last decades is discussed in [ZBR97] and [ZBR98].

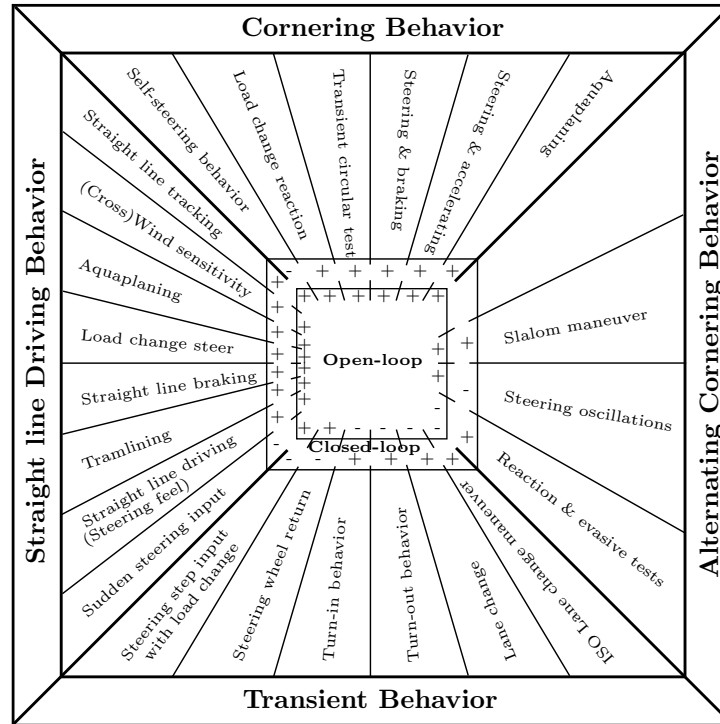


Figure 1.9: Overview of open- and closed-loop handling maneuvers [ZBR97].

Open-loop Driving Maneuvers

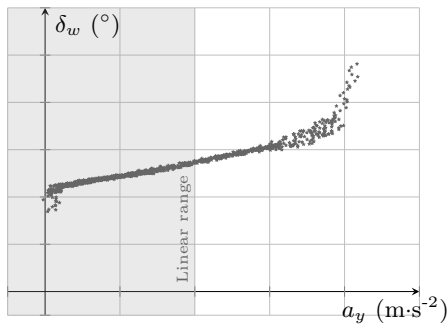
The standards ISO4138, ISO7401 and ISO13674 define these maneuvers with respect to the control inputs, i.e. steering wheel angle, accelerator/brake pedal position (i.e. longitudinal dynamics). For improvement of maneuver execution accuracy a steering robot might perform the control task [PHL08]. Recommended measurement variables as well as required transducer accuracies [ISO88a] are listed in Table 1.1. Appendix C provides the extracted objective metrics of all maneuvers.

Steady-state Circular Driving ISO4138

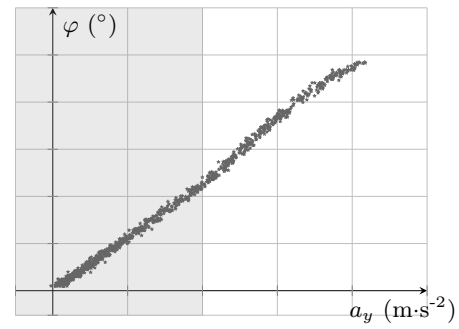
The standard ISO4138 [ISO12] defines the steady-state circular test that intends to reveal the vehicle characteristics for stationary driving. Although [DEC09] claims that the information extracted from steady-state values is very limited for subjective evaluation,

Sensor principle	Measurement quantity	Meas. range	Required accuracy	Reference
Meas. steering wheel	Steering wheel angle	$\pm 360^\circ$	$\pm 2^\circ$ for angles $\leq 180^\circ$ $\pm 4^\circ$ for angles $> 180^\circ$	[ISO88a]
	Steering wheel torque	$\pm 30\text{N}\cdot\text{m}$	$\pm 0.3\text{N}\cdot\text{m}$	[ISO88a]
Acceleration sensor	Longitudinal acceleration	$\pm 15\text{m}\cdot\text{s}^{-2}$	$\pm 0.15\text{m}\cdot\text{s}^{-2}$	[RH84]
	Lateral acceleration	$\pm 15\text{m}\cdot\text{s}^{-2}$	$\pm 0.15\text{m}\cdot\text{s}^{-2}$	[ISO88a]
Gyroscopic platform	Roll angle	$\pm 15^\circ$	$\pm 0.15^\circ$	[ISO88a]
	Pitch angle	$\pm 15^\circ$	$\pm 0.15^\circ$	[RH84]
	Yaw Velocity	$\pm 50^\circ/\text{s}$	$\pm 0.5^\circ/\text{s}$	[ISO88a]
Optical Speed Sensor	Longitudinal Velocity	0 to $50\text{m}\cdot\text{s}^{-1}$	$\pm 0.5\text{m}\cdot\text{s}^{-1}$	[ISO88a]
	Lateral Velocity	$\pm 10\text{m}\cdot\text{s}^{-1}$	$\pm 0.1\text{m}\cdot\text{s}^{-1}$	[ISO88a]
	Sideslip Angle	$\pm 15^\circ$	$\pm 0.15^\circ$	[ISO88a]

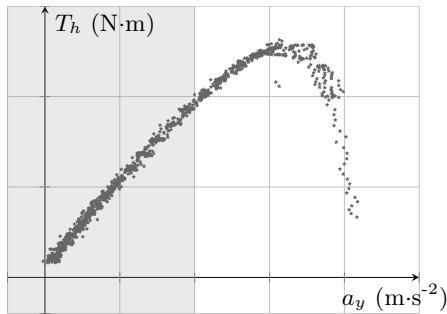
Table 1.1: Recommended measurement and transducer accuracies.



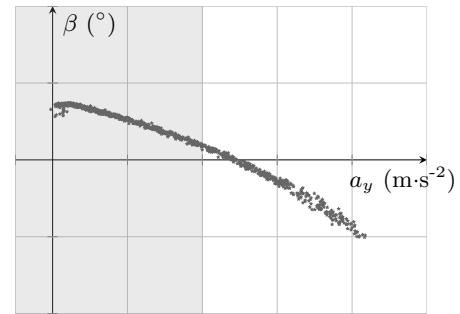
(a) Lat. accel. a_y vs. Wheel angle δ_w .



(b) Lat. accel. a_y vs. Roll angle φ .



(c) Lat. accel. a_y vs. Steer. torque T_h .



(d) Lat. accel. a_y vs. Sideslip angle β .

Figure 1.10: Simulation-based measurement results of steady-state circular driving (curvature radius $R=42\text{m}$). The *linear range* refers to these levels of lateral acceleration where the relation between steering angle and the latter can be modelled linearly.

this maneuver is useful for unveiling the so-called *self-steering characteristics*³ of the vehicle. According to [ZOM91], [RH84] there exist four different methods to perform

³The definition of the characteristic values is given in Appendix C.

the steady-state circular driving. However, herein only the methodology described in [ISO12] is discussed.

It is the driver's task to pilot the vehicle on a circular track (minimum radius $R=30\text{m}$ [ZOM91]) at constant (initially very low) velocity v_x . After reaching steady-state conditions⁴ the physical values of *steering wheel angle* δ_h (or wheel angle δ_w), *lateral acceleration* a_y and optionally *vehicle sideslip angle* β , *yaw rate* $\dot{\psi}$, *steering wheel torque* T_h and *vehicle roll angle* φ are measured for approximately $\tau_m = 3\text{s}$. After repeating the measurements at least three times the velocity is increased such that the lateral acceleration changes by $\Delta a_y = 0.5\text{m}\cdot\text{s}^{-2}$. The process is terminated if stationary conditions can not be reached any more.

Figure 1.10 illustrates the typical plots obtained from the steady-state circular driving.

Step Input ISO7401

The classic maneuver for evaluation of the transient vehicle response is given by the step input maneuver. As for the latter the vehicle shall be driven straight line at a longitudinal velocity $v_x = 80\text{km}\cdot\text{h}^{-1}$. The steering excitation needs to be applied rapidly, i.e. the steering velocity should be between $200^\circ/\text{s}$ and $500^\circ/\text{s}$ [ISO88a]. Again, the steering amplitude needs to be chosen such that a steady-state lateral acceleration level of $|a_y| = 4\text{m}\cdot\text{s}^{-2}$ (or $|a_y| = 2\text{m}\cdot\text{s}^{-2}$, $|a_y| = 6\text{m}\cdot\text{s}^{-2}$) is reached. Alternately, the steer steps should be applied in left and right directions. Figure 1.11(a) shows the excitation and vehicle response in terms of yaw rate $\dot{\psi}$.

Sinusoidal Input (One Period) ISO7401/ISO8725

The aim of the sinusoidal input maneuver is to investigate the transient response of the vehicle. Performing the maneuver requires a longitudinal velocity of $v_x = 80\text{km}\cdot\text{h}^{-1}$. If chosen higher or lower it should be in $20\text{km}\cdot\text{h}^{-1}$ steps. During the complete experiment the accelerator pedal position should be kept constant, even though the longitudinal velocity may decrease [ISO88a].

Starting with an initial yaw rate $\dot{\psi} = 0 \pm 0.5^\circ/\text{s}$ a full period of sinusoidal steering should be applied to the vehicle. The selection of the steering amplitude needs to cause a lateral acceleration level of $|a_y| = 4\text{m}\cdot\text{s}^{-2}$ during *steady-state cornering*⁵. Hence, before the ultimate experiment can be conducted some preliminary work, i.e. steering amplitude selection, needs to be performed. Figure 1.11(b) illustrates the steering excitation and the

⁴Conditions for reaching steady-state are [RH84]:

1. Standard deviation of the lateral acceleration is smaller than 5% of the average value (measurement window size $\tau_w = 3\text{s}$.)
2. Standard deviation of longitudinal velocity v_x is smaller than 5% of the average (τ_w as above).
3. Maximum deviation of the steering wheel angle δ_h from its average is smaller than 5% (τ_w as above).

⁵Optional acceleration levels are $|a_y| = 2\text{m}\cdot\text{s}^{-2}$ and $|a_y| = 6\text{m}\cdot\text{s}^{-2}$.

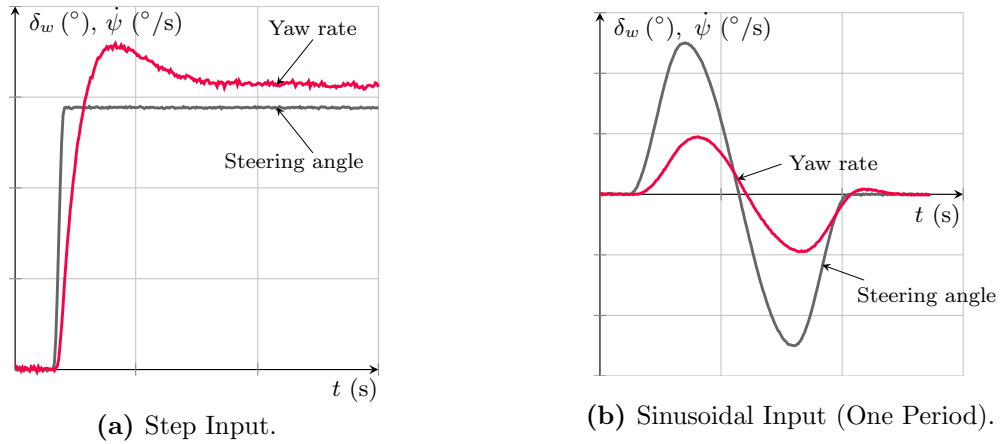


Figure 1.11: Maneuvers to evaluate the transient vehicle handling. Steering angle δ_w and vehicle response yaw rate $\dot{\psi}$.

vehicle response. The excitation frequency shall be $f_{ex}=0.5\text{Hz}$. For any further details see ISO7401 [ISO88a] and ISO8725 [ISO88b]. Table 1.1 lists the required measurements. The recommended objective metrics of both maneuvers, step and sinusoidal input (one period), are listed in Appendix C.

Sinusoidal Input (Continuous - Constant frequency) ISO7401/ISO13674

The continuous sinusoidal input is identical to the sinusoidal input (one period) in terms of maneuver execution. However, the steering wheel excitation needs to last for at least three periods, see Figure 1.12. Its frequency range should be up to 4Hz, increased step-wise. In the literature this maneuver is often referred to as *weave test*, e.g. [DEC09, PHL08]. Further details are provided in [ISO88a] and [ISO10].

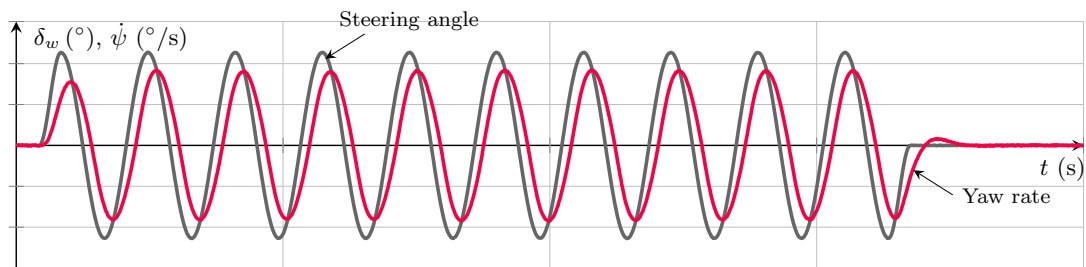


Figure 1.12: Sinusoidal Input (Continuous - Constant frequency). Steering angle δ_w and vehicle response yaw rate $\dot{\psi}$.

Sinusoidal Input (Continuous - Varying frequency) ISO8726

The objective of this maneuver is the extraction of certain vehicle responses in the frequency domain. The vehicle shall be driven in straight line (constant velocity $v_x = 80\text{km}\cdot\text{h}^{-1}$). In accordance with the latter maneuvers (sinusoidal cont. and single) the steering amplitude must be pre-determined such that a steady-state acceleration level of $|a_y| = 4\text{m}\cdot\text{s}^{-2}$ is achieved. Then, the sinusoidal excitation covers a frequency range of 0.1Hz to approx. 3Hz. A detailed description of the frequency response calculation from the measurements (Table 1.1) is provided in [ISO88c].

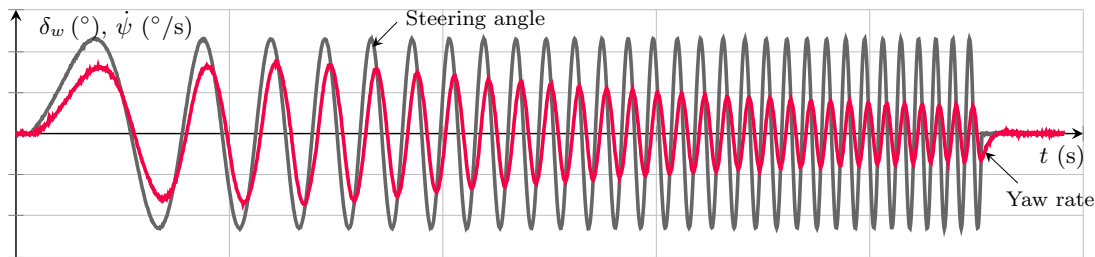


Figure 1.13: Sinusoidal Input (Continuous - Varying frequency). Steering angle δ_w and vehicle response yaw rate $\dot{\psi}$.

The maneuvers *Random Input* and *Pulse Input*, both defined in ISO7401, are not considered in this thesis and therefore omitted. See [ISO88a] for details.

Closed-loop Driving Maneuvers

In contrast to the open-loop maneuvers, that are almost independent from the driver due to the well-defined inputs, the closed-loop maneuvers are related to both driver and vehicle. Due to the varying driving styles the resulting vehicle responses depend highly on the human controller [NKS01].

Double Lane Change Maneuver ISO3888-1

The severe lane change maneuver ISO3888-1 is common for subjective evaluation and also vehicle performance assessment. However, for objective evaluation purposes this maneuver is difficult to use as the driver has great influence on its execution (e.g. selection of track limits) and consequently the objective metrics. The use of closed-loop maneuver data for objectifying driver ratings is discussed in [NKS01]. It illustrates the variance of the applied steering angles for different drivers (a group of experts and non-experts).

Standardization of the maneuver is given vaguely in [ISO99]. There, it is the track dimensions (Figure 1.14) and its marking with pylons that are defined clearly. The overall task of the driver should be self-explanatory, i.e. to navigate the vehicle through the pylon park. The recommended entry speed is $v_x = 80 \pm 3\text{km}\cdot\text{h}^{-1}$. The standard does not

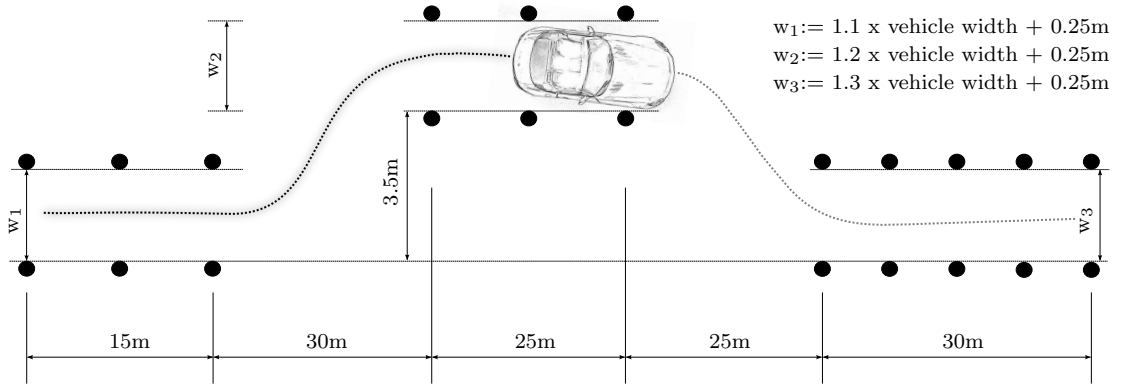


Figure 1.14: ISO Lane Change Maneuver ISO3888-1 [ISO99].

suggest⁶ any objective metrics to be extracted other than the passing time of the pylons park.

Subjective-Objective Correlation

The generation of a synthesized subjective evaluation requires some links between the extracted objective metrics (from either open- or closed-loop experiments) and subjective (reference) evaluations. In the following, after discussing the most common approach for finding these links, some literature review of work in the subjective-objective correlation domain is given. In general, finding these correlations is based on a statistical analysis. Commonly, the process is split into a two-step procedure [ZOM91]. First, correlations between extracted characteristic values need to be found. Metrics with low, new information content, i.e. high correlation with other metric(s), can be dropped. Only uncorrelated characteristic values should be used for the subsequent process. Second, a multiple regression analysis aims to identify a relation between subjective ratings and objective values. Once the regression parameters are identified a synthesized subject rating based on a linear regression might be formulated as [ZOM91]

$$y_i = a_{i,0} + \sum_{j=1}^n a_{i,j} \cdot c_{i,j}, \quad (1.1)$$

where y_i represents the i -th synthetic subjective rating, $a_{i,j}$ the n regressors to be determined and $c_{i,j}$ the n objective characteristic metrics.

A similar correlation process to identify the parameters of a linear model describing the driver ratings in terms of objective characteristic values is used in [CHE97] and [CC98]. Interestingly, in this approach the decision of the driving maneuvers "to be performed" is completely up to the drivers. Unfortunately, the end results of the correlation show a

⁶Due to inconsistent results of correlation between individual measured values and subjective evaluation criteria, e.g. [CHE97, p.26].

high variation that most likely are due to the natural driving concept. Exploiting only two objective metrics (related to the transient and the steady-state vehicle behavior) [WD78] provides a certain range of these values yielding a positive subjective evaluation. The work of [MOYS90] suggests extraction of four parameters⁷ (all related to the yaw response and the lateral acceleration of the vehicle) that are plotted on four axes. The effective area of the resulting rhombus can be used to assess the handling quality. Correlation with subjective evaluation is performed and re-analyzed in [CKA00]. However, the outcomes of these two publications are quite different. An extension to this four parameter method is presented in [ASH02] that investigates into nonlinear relations for the first time using neuro-fuzzy methods. Revealing several links that remain hidden when using classic simple/multiple regression techniques is reported.

A large number of extracted objective metrics (from open-loop maneuvers) is reduced to only five parameters showing high correlations with subjective ratings in [RA97, RA00]. These metrics are the time delays between steering angle and yaw rate, lateral acceleration, vehicle sideslip angle, its time derivative and the roll rate. The identification of a driver model is coupled with classic subjective-objective correlation in [HEN04]. Good correlation between objective metrics (*weave test*) and subjective ratings is found to be immanent in [DET05, HAR07] and used for evaluation of the straight line drive and characterization of steering feel. Interestingly, [HAR07] claims that the correlation of objective and subjective values is low for the maneuver *steady-state circular test*.

An extensive overview of state of the art subjective-objective correlation work is provided in [DEC09]. Furthermore, it proposes a modified questionnaire (subjective evaluation) such that the drivers have to provide feedback *how* they like the behavior and also the *intensity*. The answers are correlated with objective metrics using standard regression techniques.

Reconsidering the general idea of objective evaluation again, there is some contradiction how to handle the driver influence on the process. On the one hand side, the open-loop experiments do not suffer from any human variability, but on the other hand it is the human being that performs the evaluation, so excluding it completely (as for open-loop based evaluation) might not be a good decision.

The driver's sensitivity with respect to variations of the vehicle lateral dynamics is identified in [SHKH09]. Limited to the linear driving range and only considering standard drivers the resulting outcome of the work is a high sensitivity of the drivers to the response time of the yaw dynamics and the roll motion. Interestingly, the sensitivity to changes of the vehicle sideslip dynamics is low.

A promising approach is the addition of the driver's perception into the objectifying tool as in [SCH10]. This work extends the idea of [DEC09] and presents a detailed modelling approach of the human senses responsible for the driver's perception. Based on these (sensed vehicle responses) a correlation with subjective ratings is performed. Additionally, the parameters of a steering behavior model are identified from closed-loop

⁷Consequently the method is known as *four parameter method* in literature.

maneuver measurements and also used for a correlation with subjective ratings. Hence, there are two data sources for the correlation process, i.e. the objective metrics and the model parameters. However, that approach already refers to a so-called model-based objective evaluation, that is discussed within the next section.

Even though employing standard correlation techniques, the results of [KRA11] are interesting due to the great potential of the experimental setup, i.e. a vehicle with linear electric actuators for manipulating the suspension characteristics *at choice*. It offers a broad range of vehicle setups, e.g. active suspension systems, to be investigated with respect to subjective-objective correlation.

A combination of open- and closed-loop maneuver related objective metrics as well as subjective ratings from non-professional drivers is used in [ENG94]. It presents a procedure to analyze the straight line driving behavior. The work also discusses the calculation of a synthesized subjective rating based on a formula extracted from multiple regression analysis. The author mentions that the drivers applied highly varying control strategies and that in turn complicated the research. Some general comments and difficulties regarding the correlation method for evaluation of handling characteristics are formulated in [KN01]. Especially closed-loop maneuvers need to be analyzed with care as the vehicle responses change not only due to the vehicle-variant characteristics, but also the driver behavior (that adapts to the vehicle-variants), see also [NKS01]. Ideally, and this direction is followed by [JÜR97], the objective metrics should be independent of the vehicle and the maneuver, i.e. they can be derived directly from the *driving behavior* by identifying a driver model.

1.2.3 Model-based Objective Evaluation

Thus far, the presented approaches extract the objective metrics from measured vehicle responses. Alternatively, so-called *model-based* objective evaluation aims to identify parameters of vehicle and/or driver models and further exploits them as additional inputs for the correlation analysis. Additionally, the identified model parameters can be used for performing standard maneuvers in simulations and extract object metrics from there. Both approaches, modelling of the vehicle dynamics and the driver, will be reviewed with respect to the current state of the art. The general objective evaluation process (Figure 1.8) needs to be modified such, that it also includes the model parameter identification - this is shown in Figure 1.15. The correlation process now considers the subjective driver rating as well as model parameters and extracted objective metrics from simulation data. Once the synthesized subjective rating model has been parametrized, the correlation is obsolete, which is marked by the dashed, gray lines in Figure 1.15.

The process flow is not only related to the vehicle model-based objective evaluation, but can also be exploited for driver modelling based evaluation. By substituting the box *Vehicle Model* with *Driver Model* its validity still holds. Mathematical models, mostly physically motivated, aim to reproduce the real behavior of the system (vehicle or driver) as good as possible. The state of the art literature review revealed a current imbalance

between vehicle and driver modelling. Reasons might be, that modelling of the vehicle dynamics is mostly based on physical laws, whereas the driver as such, is far more complex and its modelling requires determining interdisciplinary relations (e.g. physiology, psychology, physics, control theory), see also [HEN04], [JÜR97].

A framework of vehicle models based on the phenomenological⁸ modelling paradigm is

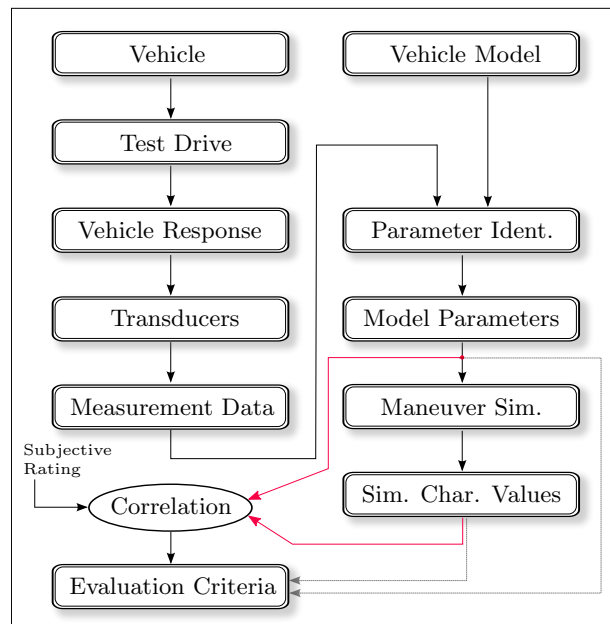


Figure 1.15: Objective evaluation based on characteristic values extracted from measurements [DEC09].

presented in [MEL03]. The aim of these models is to reproduce the driving behavior on a virtual basis. However, as the model parameters are not related to any physical vehicle parameters their identification is based on driving tests. An advantage of that modelling paradigm is the direct mapping between vehicle handling effects and the model parameters, i.e. a change in vehicle handling affects a single parameter only, whereas for classic (mechanical) models this is generally not the case. Furthermore, the identification of the models only requires in-vehicle measurements rather than test-bench experiments [ZOM02]. Although the work does not consider correlation between subjective ratings and model-based objective metrics it is clearly intended for support of the handling dynamics evaluation. In [ZOM02] an online⁹ parameter identification mechanism based on the covariance-intersection algorithm dealing with these phenomenological models is developed. In contrast, [KOB03] develops some offline parameter identification methods

⁸ *Phenomenological* models describe a certain phenomenon only, without considering underlying e.g. physical laws.

⁹ *Online* in this sense means that the data is supplied subsequently to the algorithm rather than in one block. Therefore it qualifies for in-vehicle operation as the parameters can be identified while performing handling maneuvers. The opposite of an online execution is then defined to be *offline*.

for mechanically motivated vehicle dynamics models. The identification process is based upon test-bench measurements and the model parameters validated by comparing simulation results and vehicle measurements for different types (limousine, mini-van). In [DSH⁺06] the work of [MEL03], [ZOM02] and [KOB03] is summarized and a fingerprint describing the vehicle dynamics with only a few characteristic parameters defined.

[PRE08] discusses an identification of model parameters related to an extended single-track model and also presents an innovative offline optimization algorithm for estimation of the nonlinear tire characteristics. Furthermore, the algorithm assessment is not only based on measurements of passenger cars, but also heavy-truck data. In accordance with the latter references, the vehicle handling evaluation exploiting these model-based approaches is not discussed.

A combination of online and offline model parameter identification is implemented by [MT08]. Model parameters related to the steady-state of the vehicle dynamics are identified and adapted online (lateral cornering stiffness of tires). A driver feedback mechanism ensures a time-optimal identification procedure. The remaining parameters of the double-track model are identified based on measurements of the transient vehicle responses and an optimization algorithm. A knowledge database (consisting of model parameters, characteristic values and subjective ratings) is further used for building a synthesized subjective rating (based on the identified model parameters).

An innovative identification method of the parameters related to a stationary tire model is discussed in [KOL09]. The requirements of measuring equipment are limited to a *standard*¹⁰ level, the excitation maneuver is selected as the steady-state circular test and the parameter identification is based on an offline optimization algorithm. However, the work is limited to the model parameter estimation and only points out that these can be further used for vehicle evaluation. In contrast, [HUN11] presents specific vehicle dynamics models (based on the single-track model) for the linear and nonlinear driving ranges. The parameters are identified using offline optimization techniques. These models are extended with the longitudinal vehicle dynamics and are further used for maneuver simulation and extraction of characteristics. A correlation analysis considering subjective ratings, objective metrics (from simulations) and model parameters completes the work.

In [GUT13] the influences of tire parameters on the vehicle handling characteristics are analyzed. Exploiting a considerable database consisting of subjective ratings and measured data from evaluation of various vehicle tire types a systematic correlation analysis is performed. A single-track model, with parameters fitted such that the error between model and measurement is minimized, supports the calculation of objective metrics for the correlation and consequently the overall vehicle development process.

Although not directly related to the model-based objective evaluation [ZAM94] and [BÖR04] estimate vehicle parameters (e.g. lateral tire cornering stiffness) adaptively

¹⁰*Standard* measurement equipment therein includes: an inertial measurement unit, a wheel vector transducer, an optical velocity sensor and an instrumented steering wheel.

(using online/offline optimization mechanisms). [LIM09] presents real-time algorithms (based on recursive least squares) for identifying different vehicle parameters¹¹. Exploiting additional GPS sensor measurements [RYU04] develops a state estimator and also identifies some vehicle parameters (roll dynamics, cornering stiffness, yaw moment of inertia) offline. The extension of the single-track model in terms of extrapolation to various vehicle configurations (tire configuration, roll stiffness etc.) is studied in [LAH12]. Identification of the parameters is based on an optimization scheme that operates on standard measurements related to the lateral and roll dynamics, i.e. yaw rate, lateral acceleration, vehicle sideslip and chassis roll angle. Table 1.2 summarizes the individual model parameter identification frameworks and lists the utilized measurement equipment as well as execution of parameter identification techniques, i.e. online vs. offline. Clearly, this list is not exhaustive as there exist numerous parameter identification concepts that are tailored to certain domains, e.g. roll dynamics identification. However, listing all these concepts is omitted intentionally as the thesis aims to provide a framework of parameter identification modules as do the presented references.

In contrast to vehicle parameter correlation an alternative approach is to replace the latter by a steering system model as discussed in [BAR04]. Various configurations of steering torque generation are evaluated by drivers and correlated with model parameters corresponding to the actual setup. [ZSC09] identifies the parameters of a steering model, but does not use them for correlation. In fact, these are used for a model supplying a reference steering torque to a dedicated actuator in an experimental vehicle to mimic the steering behavior of different vehicle variants. In [PFE06] the interactions between the steering system and an extended single-track model are analyzed regarding the on-center steering handling. However, although providing the basis for a model-based handling evaluation it is not the focus of that work.

The approach of [HAR02] aims to investigate the influence of the steering system on the overall vehicle evaluation. Simulations of a steering system model are used to validate objective metrics extracted from real handling maneuvers and altered steering system configurations. Furthermore, the models are exploited to gain better system understanding as well as effects of the individual parameters. However, model-based evaluation in the classic sense is not discussed either.

Changing the paradigm from vehicle to driver model identification results in another domain of model-based vehicle evaluation. Here, the analysis of the driver model reveals some information of the complete *vehicle-driver* system. Identifying the control element in closed-loop operation mode can be seen as conservation of the driver strategy [SCH10].

¹¹Axle cornering stiffness, vehicle mass, yaw moment of inertia and longitudinal position of the CoG.

Source	Objective	Identified Values	Exec.		Instrumentation					Data ^a	
			Offline	Online	Standard ^b	IMU ^c	VMS ^d	MSW ^e	Other	Sim.	Vehicle
[ZOM02]	VBM / VDM	(Related) lateral cornering stiffnesses, tire relaxation length, vehicle mass, road friction, roll stiffness, roll damping, roll inertia, const. road grade		○		○	○	○			●
[ZAM94]	VDM	(Related) cornering stiffnesses, steering ratio, sensor position, vehicle mass, yaw inertia, roll inertia, chassis roll damping, roll stabilizer (rear), rear axle stiffness, tire relaxation length, form factor tire curve, (normal load-depend.) friction factor	●			●	●	●	● ^f		●
[KOB03]	VDM	Nonlinear tire characteristic curves, roll lever, eigenfrequency & damping (roll dynamics), yaw inertia, tire relaxation length	●			●	●	●	● ^f		●
[PRE08]	VDM ^g	Nonlinear tire characteristics (lateral stiffnesses), yaw dynamics parameters (gain, damping, eigenfrequency of 2 nd -order transfer function)	●			●	●	●	● ^h		●
[MEL03]	VBM	Push/Pull damper characteristics (front/rear), pitch lever (front/rear), pitch inertia, yaw inertia, roll stiffness (front/rear), relaxation length (front/rear), normal load difference factors (front/rear), roll inertia, roll damping, roll lever (front/rear), roll moment distr., steering damping, lateral tire characteristics	●			○	○	○			●
[BÖR04]	VDM	Lateral cornering stiffness coefficient, road grade, vehicle mass		●		●	● ⁱ		● ^j		●
[MT08]	VDM	Lateral cornering stiffness (long. velocity - lat. accel. dependent map), long. vel. dependent yaw inertia and tire relaxation length (front/rear), roll damping	●	● ^k		●	●	●			●
[RRV00]	VDM	CoG height, roll center heights (front/rear), roll stiffness (front/rear), roll damping (front/rear), toe angles (front/rear), camber angles (front/rear), relaxation length		●		- ^l	-	-	-	-	●
[KOL09]	VDM	Nonlinear lateral tire characteristics (TM_Simple ^m model parameters)	●			●	●	●	● ^f		●
[RYU04]	VDM	Constant lateral cornering stiffness (front/rear), CoG position, yaw inertia, roll stiffness, roll damping	●			●	●		● ⁿ		●

Source	Objective	Identified Values	Exec.		Instrumentation					Data ^a	
			Offline	Online	Standard ^b	IMU ^c	VMS ^d	MSW ^e	Other	Sim.	Vehicle
[LAH12]	VDM	Roll lever, yaw inertia, roll inertia, roll center height (front/rear), steer compliance	•			◦	◦	◦	◦		•
[HUN11]	VDM	Constant lateral cornering stiffness (front/rear), tire relaxation length (front/rear), yaw inertia, gradients steering angle vs lat. acceleration, gradients sideslip angle vs. lat. acceleration (see [HUN11, p. 50] for details)	•		- ¹	-	-	-	-		•
[HH03]	VDM	Vehicle mass, road disturbances (inclination), internal combustion engine dynamics, suspension parameters (spring stiffnesses, damping coeffs.), roll dynamics	•	• ^o	- ¹	-	-	-	-		•

Table 1.2: Overview of relevant vehicle *parameter identification frameworks*. Clearly, this list is non-exhaustive - tailored solutions to individual problems are omitted and discussed within the scope of observer-based parameter identification techniques (Chapter 4).

^a If data is considered from simulations and real vehicle measurements only the latter is listed.

^b Acceleration, angular rate sensors and steering wheel angle. As available in ESP-equipped vehicles.

^c Inertial Measurement Unit.

^d Velocity Measurement System, e.g. optical velocity sensor.

^e Measurement Steering Wheel.

^f Wheel vector transducer.

^g Passenger cars & Heavy-duty.

^h Suspension travel measurement, wheel angle.

ⁱ Not used, implemented sideslip estimator.

^j Vertical accelerations, suspension travel, wheel angle.

^k In-vehicle lateral cornering stiffness map population. Map smoothing applied offline.

^l No information provided.

^m Tire Model TM_Simple [HIR09].

ⁿ Two-antenna GPS setup.

^o Using Neuro Fuzzy Mechanisms.

An extensive overview of driver models is provided in [PE07] and [JÜR97]. In summary, modelling can be based on the disciplines *control theory*, *physiology* or *psychology* [SCH10]. Driver models based on control theory structures, e.g. [DON77] are exploited for vehicle evaluation in e.g. [HOR85, REI90, WAG03, JÜR97, RIX05, SCH10]. The paradigm of *physiological* and *psychological* driver modelling is pursued in e.g. [HOU08, PIC04] and [KNS99].

1.2.4 State Observation for Vehicle Dynamics

The previous sections introduced the paradigm of objective evaluation and its model-based extension. Both require installation of extensive measurement equipment that is cost- and time-consuming. However, the parameter identification algorithms require accurate knowledge of the plant in- and outputs in order to estimate certain model parameters. State observers¹² are dynamical systems aiming to estimate system states (or more specifically their initial conditions) exploiting measurements of the plant inputs and available outputs [LUE71]. Hence, as some states might not be measurable physically or due to unavailability of sensor devices a state observer ideally solves the problem and renders all system states *known*. Vehicle dynamics related applications of (linear/nonlinear) state observers are manifold and only a few examples will be discussed. Estimation of the safety-related vehicle states yaw rate, sideslip angle and/or lateral velocity is presented in [AFK11, GIJ⁺08, GYNW10, KD97, IJF⁺06], lateral tire forces observation in [DVCL09, BCLT08, WMCL06, KIM09, NUT09] and observer-based calculation of the chassis roll angle in [SGMN08, MLC10, DM05]. Robust observers for active suspension systems are dealt with in [FRÖ08]. Furthermore, road bank angle and inclination are estimated in [KLC12, RG04, GIJ⁺09] and observer-based calculation of vehicle parameters in [MGV⁺09, RRV00, SOF08] respectively. Road-tire friction estimation is discussed in [PES06, TFG12]. In general, the design of these observer is related to certain requirements on the system structure, e.g. available measured outputs. Some observer structures are inherently robust¹³ to disturbances and/or able to estimate system state and unknown/uncertain parameters simultaneously. That invariance to perturbations increases the attractiveness of the nonlinear sliding mode paradigm for automotive application [MRF⁺08, SOF08, IFSD11, IFM15]. In summary, it is obvious that a large number of vehicle dynamics related applications are supported by observer-based structures. Especially those capable of simultaneously estimating states and parameters are of interest for the current application. Exploiting these dynamical systems should render some of the cost-intensive measurement equipment redundant and at the same time identify vehicle model parameters.

1.3 Thesis Outline

The fundamental objective of the thesis is the development of observer-based parameter identification methods for the vehicle dynamics evaluation process. Based on the outcome of the extensive literature research several questions and potentials for improvement have come up. In detail these are:

¹²Herein the terms *observer* and *estimator* will be used interchangeably. The term *filter* might lead to the assumption of solving a classic *filtering problem*, as defined in [STE94, p. 341]. However, in the sense of control theory the Kalman filter acts as optimal *observer* and these operate as *predictors*, compare [STE94, p. 341]. In this context, *observer*, *estimator* and *filter* act equally.

¹³For details see Chapter 4.

1. Objective evaluation involves instrumenting the vehicle with various, cost-intensive equipment. Not only is it inefficient in terms of costs, but also time, as it requires installation and configuration of the transducers. Replacing these measurement devices by low-cost equivalents, e.g. measuring angular rates rather than the angles, and furthermore estimating the signals of the replaced measuring devices would result in both, cost and time savings.
2. Model-based objective evaluation requires identification of model parameters. Under the assumption that some of the expensive measurement equipment is rendered redundant, would it be feasible to go one step further and use the observed signals for parameter estimation purposes? Or, alternatively use a combined technique, i.e. observer-based parameter identification, that estimates signals and model parameters simultaneously?
3. A well-known technique for estimating states and parameter jointly is the design of so-called *unknown input observers* [POZ04]. However, in order to estimate states robustly even in the presence of an unknown input certain requirements on the overall model structure exist. It needs to be ensured that the use of angular rates (rather than positions) still allows the employment of unknown input observers. In case of arising difficulties the design of the latter needs to be modified such, that the use of velocity measurement does not represent any restriction.
4. Given that the two previous questions can be answered positively, it is possible to perform the parameter identification in-vehicle and feed back the quality of the estimated parameters to the driver in real-time. Hence, time-optimal termination of the test drive can be achieved.
5. There is no common agreement of the proposed approaches which method, in terms of (model-based) objective evaluation, introduces the highest potential to replace/complement the subjective paradigm. A promising method is given in [SCH10] that exploits the idea of using perception signals (rather than measurements from transducers) for the objectifying work. These results will be integrated into the proposed evaluation framework such that objective metrics extracted from perception signals are also part of the extensive metrics database.

This thesis aims to provide a framework of different observer-based parameter identification techniques capable of estimating system states and parameters jointly. The effects of the low-cost measurement equipment w.r.t. increased measurement noise will be evaluated in both simulations¹⁴ and experiments. In summary, the design of observer-based parameter identification concepts that use only low-cost measurement equipment and allow in-vehicle parameter estimation make the approach unique. Simulations of

¹⁴For the simulations-based validation the in- and outputs to the observer mechanisms will be artificially augmented with noise.

standardized handling maneuvers allow the extraction of measured and sensed objective metrics that can be further used for correlation with subjective evaluation work. Note, that the latter will not be focus of this thesis.

The remaining chapters are organized as follows:

- **Chapter 2: Modelling of Selected Vehicle Dynamics**

This chapter reviews the modelling of the selected vehicle dynamics and builds the basis for the subsequent design of the observer-based parameter estimation techniques. These include longitudinal and lateral dynamics, pitch and roll dynamics. Modelling of an automotive steering system, powertrain and the driver's human senses (in order to transform the measurement signals into driver-related *or sensed* signals) concludes this chapter.

- **Chapter 3: Analyses of Vehicle Dynamics Models**

The models of Chapter 2 are put into state-space representation and a systematic approach identifies the model parameters influencing the system responses. Taking into considerations that some parameters can be easily determined by simple measurement techniques, the sets of model parameters to be identified during test drives will be proposed. Furthermore, two different driving maneuvers for the identification tasks as well as their effects on the parameter sensitivities will be discussed. Thereafter, the system property *observability*, in a quantitative way, allows some conclusions on the selection of sensors (w.r.t. the parameter identification task). Finally, an overview of *to be identified* vehicle parameters and selected sensor signals will be provided and further used within the next chapter.

- **Chapter 4: Observer-Based Parameter Identification Techniques**

The first part of the chapter is dedicated to a theoretical discussion of two different state and parameter identification techniques, namely *state augmentation* and *unknown input recovery*. Two academic examples illustrate the general ideas of the proposed approaches. The main part of the chapter deals with the design of observer-based parameter identification techniques for the individual problems. Again, in order to demonstrate the ideal performance of the concepts each proposed mechanism is evaluated in simulations¹⁵. A list of concepts integrated into the proposed framework is provided at the end of the chapter that contains the design paradigm, domain of application, estimated states and parameters and required measurements.

- **Chapter 5: Validation of the Assessment Framework in Simulations**

The complete framework consisting of the observer-based parameter identification schemes and the model-based objective handling evaluation are validated in simulations. For the generation of realistic vehicle dynamics measurements a professional

¹⁵This assumes non-existent parasitic dynamics.

state of the art simulation software package (IPG¹⁶ CarMaker[®]) is used. The first part of the chapter evaluates the observer concepts for certain driving maneuvers and provides a list of parameters characterizing its dynamics. Then, within the second part these parameters are used for simulation of standardized driving maneuvers and the results of the identified vehicle model and the source model (IPG CarMaker[®]) compared. Certain performance specifications are provided allowing to evaluate the accuracy of the mechanisms. Moreover, both measurement sources are considered for the extraction of objective metrics. At the end of the chapter the human sense models are integrated into the simulation process of the handling maneuvers. Finally, a comparison between measured and sensed vehicle responses is presented.

- **Chapter 6: Experimental Evaluation of Selected Observer Concepts**

Complementary to the evaluation of the observer concepts in simulations the latter are also validated by experimental work. Unfortunately, not all of the proposed concepts can be deployed to an experimental vehicle due to the lack of available (in-vehicle) transducer devices. In fact, the lateral and roll dynamics-related concepts are evaluated on the basis of real measurement data from experimental vehicles. Furthermore, the potential of a proposed robust state estimator (recovering also unknown inputs) will be demonstrated experimentally on a test bench of an electric power steering system available on-site.

- **Chapter 7: Conclusion**

At the end of the thesis a conclusion on the effective capability of the proposed framework to support the vehicle assessment process can be drawn. Furthermore, the main contributions of this thesis and an outlook to future research directions are discussed.

- **Appendices**

The introduction of axis systems used for vehicle dynamics applications is covered by Appendix A. Some mathematical supplements from the parameter sensitivity analysis (Chapter 3) and the observer design process (Chapter 4) are provided in Appendix B. Furthermore, an extensive overview of objective metrics to be extracted from standardized handling maneuvers is given in Appendix C and finally, the simulations and experimental setups used for concept evaluation are presented briefly in Appendix D.

¹⁶www.ipg.de

2

Modelling of Selected Vehicle Dynamics

The design of observer-based parameter identification mechanisms requires mathematical modelling of the underlying system dynamics. There exist different paradigms, e.g. motivated by physical laws, phenomenological effects and Black Box models, see also [IM11] for details. Commonly, the result is a set of partial and/or ordinary differential equations describing the system dynamics.

Referring to the terminology used in literature the majority of the proposed models can be interpreted as *Light Gray Box* models, i.e. the related physical laws are well known, but the model parameters are not. Hence, these parameters require estimation for gaining an accurate model of the real system. Solely the modelling of the powertrain dynamics exploits the idea of *Black Box* modelling, i.e. taking into considerations only the measurements of input and output signals as well as general assumptions on the model structure [LJU99]. However, preferably the models are based on principles of physics rather than Black Box models. That eases the interpretation of parameter variations, model understanding, analysis of system observability and estimation convergence. Only for exceptional cases where the modelling efforts are disproportionately large compared to Black Box models, the latter are to be favored.

The structure of the proposed vehicle model is depicted in Figure 2.1. The individual modules are selected such, that the vehicle motion (translational and rotational) including the chassis dynamics can be described accurately. Separating the domains into tailored subproblems allows design of versatile observer-based parameter identification mechanisms. The models itself are physically motivated as are its parameters. This is different to driving behavior models as used in [MEL03, ZOM02]. These rely on parameters directly related to vehicle evaluation. However, their versatility is limited w.r.t. application for other areas, e.g. vehicle controller design. The proposed models need to

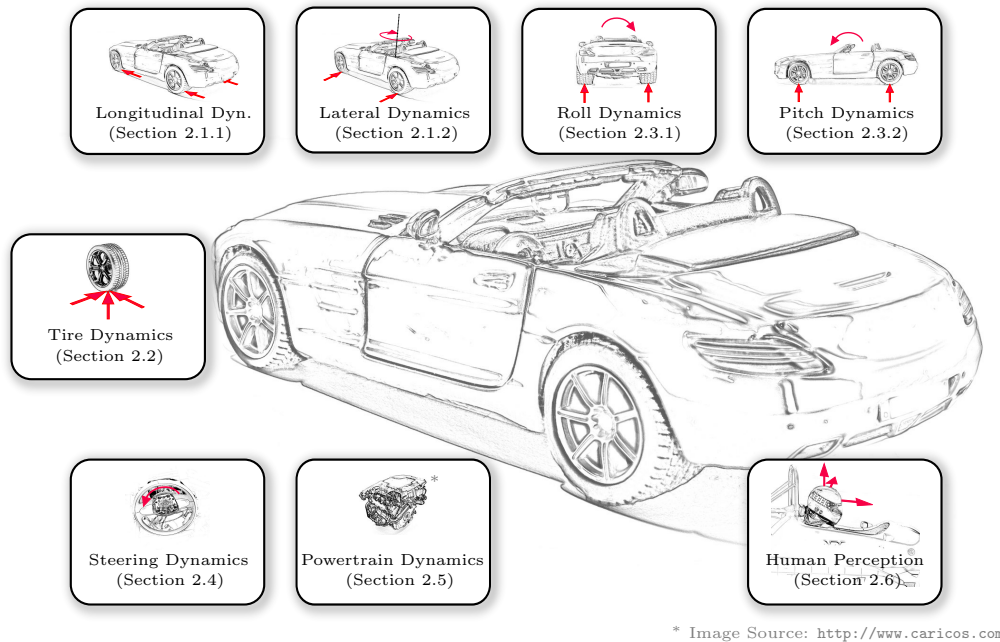


Figure 2.1: Modular structure of the vehicle model.

represent the real vehicle behavior as accurate as possible by taking into account the number of parameters to be identified. In [MEL03, p.47] the trade-off between model complexity/accuracy and number of parameters is discussed. Considering the real-time identification of model parameters and also the limited computational power in the vehicle, the conclusion of reducing the number of parameters to a minimum is trivial. In order to support vehicle handling evaluation significantly the mathematical models need to cover the description of vehicle (chassis) motion, steering, acceleration/braking and tire dynamics. Furthermore, environmental impacts (road disturbances) need to be added to the scope of the model. Consequently, the remaining chapter is organized as follows: first, the vehicle motion (longitudinal and lateral) will be discussed and proper modelling structures presented. Second, as the tires are influencing the vehicle motion greatly their modelling needs to be investigated in detail. Third, the vehicle chassis motion (roll and pitch) is to be dealt with and fourth, the steering dynamics will be considered. Fifth, the powertrain dynamics and driver perception models are proposed. Finally, at the end of this chapter a framework of mathematical models exists, building the basis for the subsequent state observer design mechanisms.

2.1 Vehicle Motion

For the modelling of a ground vehicle's motion in longitudinal and lateral direction it is assumed rigid, i.e. the chassis is firmly connected to the unsprung masses (wheels etc.).

Furthermore, the motion is restricted to be planar, consequently reducing the 3 rotational and 3 translational degrees of freedom to 3, i.e. 2 translational + 1 rotational (the DoF due to steering is not accounted for). Referring to the lateral motion of the vehicle (Section 2.1.2) these assumptions lead to the well-known single-track model proposed in 1940 [RS40]. It should be noted, that the coupling between the longitudinal and lateral dynamics is reduced to that extent, that the latter uses the longitudinal velocity as input. Most of the standardized driving maneuvers should be performed such, that the longitudinal velocity is kept almost constant anyway. Consequently, dynamics referring to the vehicle propulsion, i.e. engine and driveline dynamics are not considered for the lateral dynamics modelling. The longitudinal dynamics model (Section 2.1.1) is purely considering the acceleration and deceleration effects as well as drag forces. Mainly, this model will be exploited for designing a disturbance observer to recover the road inclination. Generally, this thesis focuses mainly on the lateral dynamics, which are highly important for the handling evaluation process. The longitudinal dynamics are considered less relevant and therefore the modelling efforts are kept low.

2.1.1 Longitudinal Dynamics

In order to reduce the influence of coupling effects between the longitudinal and lateral dynamics the vehicle is assumed to be driven on a straight line. The traction forces of the front/rear, left/right tires are lumped into a single force per axle, similar to the well-known single-track model (see 2.1.2). The dynamics of the vehicle under propulsion can be formulated by exploiting the conservation of linear momentum and read as

$$m \, {}_v a_x = \sum {}_v F_x, \quad (2.1a)$$

$$= {}_v F_{x,f} + {}_v F_{x,r} - {}_v F_{wind} - 2 {}_v F_r - {}_v F_g, \quad (2.1b)$$

where m represents the total vehicle mass, ${}_v F_{x,f}$ the longitudinal front axle force¹, ${}_v F_{x,r}$ the rear axles force, ${}_v F_{wind}$ the wind force, ${}_v F_r$ the tire rolling resistance and ${}_v F_g$ the resistance due to gravitational acceleration, i.e. road inclination. The longitudinal acceleration is given by ${}_v a_x$ and the vertical tire forces (depicted in Figure 2.2) read as ${}_v F_{z,f}$ and ${}_v F_{z,r}$. Modelling of the aerodynamic drag force ${}_v F_{aero}$ is kept simple and can be calculated as [HH03]

$${}_v F_{aero} = c_w A_v \frac{\rho_a}{2} {}_v v_x^2, \quad (2.2)$$

with c_w being the aerodynamic drag coefficient, A_v the front area of the vehicle, ρ_a the air density and ${}_v v_x$ the longitudinal vehicle velocity. The rolling resistance force ${}_v F_r$ of

¹The subscript "v" indicates the considered coordinate frame, see Appendix A and Section Notation for details.

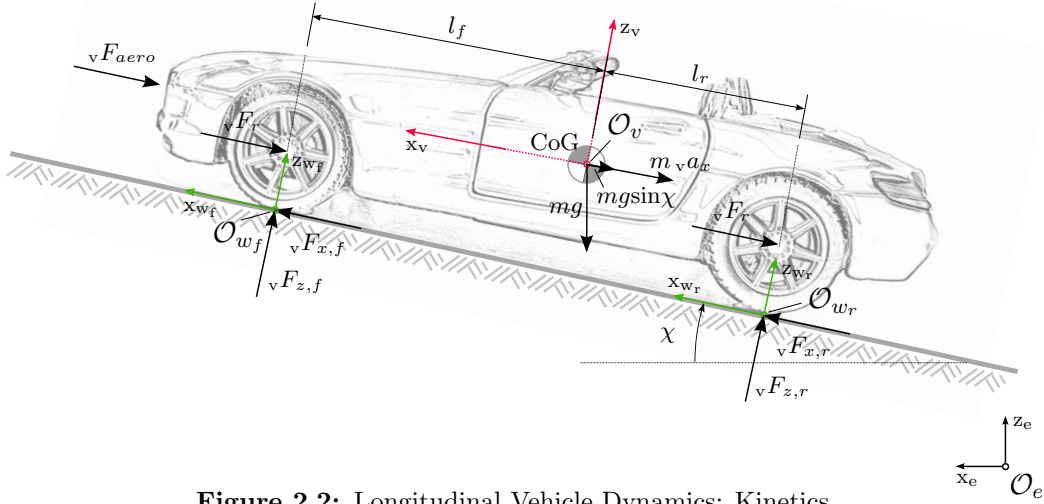


Figure 2.2: Longitudinal Vehicle Dynamics: Kinetics.

the tire is defined by [MW04]

$${}^vF_r = f_r {}^vF_z. \quad (2.3)$$

In general, the rolling resistance force is less than 1% of the vertical tire load vF_z [MW04]. The parameter f_r takes into account the road surface, tire model and tire pressure. Finally, the resistance due to road inclination vF_g is given by

$${}^vF_g = mg \sin \chi, \quad (2.4)$$

where χ refers to the road inclination angle².

Coupling with lateral dynamics In case the vehicle is not perfectly following a straight line coupling effects between longitudinal and lateral dynamics will arise. An additional term, known as curve resistance force ${}^vF_{cr}$, is introduced in (2.1) and for a steady-state circular drive reads as [MW04]

$${}^vF_{cr} = m {}^v a_y \left(\frac{l_r}{l_r + l_f} \sin \alpha_f + \frac{l_f}{l_r + l_f} \sin \alpha_r \right). \quad (2.5)$$

There ${}^v a_y$ is given by the lateral acceleration, α_f, α_r denote the tire slip angles and l_f, l_r represent the distances between CoG and front/rear axle (details will follow in the next section). Furthermore, due to the rotation of the vehicle-fixed axis system (w.r.t. the earth-fixed system, see Appendix A) the longitudinal acceleration becomes ${}^v a_x = {}^v \dot{v}_x - \dot{\psi} {}^v v_y$.

²A positive inclination angle refers to a climbing road.

Various extensions of the single-track model have been proposed through the years and the authors in [DSH⁺06] claim that an extended single-track model³ represents the vehicle dynamics up to frequencies of 3Hz in a satisfactorily manner.

Kinematics

Due to the assumptions of the single-track model (neglect of roll/pitch motion) the vehicle-fixed axis system \mathcal{C}_v coincides with the intermediate axis system \mathcal{C} . Consequently, only the transformation from the earth-fixed axis system \mathcal{C}_e to the vehicle-fixed axis system \mathcal{C}_v needs to be conducted. The origin of the latter is at the vehicle's center of gravity (CoG) and the distances to the wheel axis systems \mathcal{C}_{w_f} and \mathcal{C}_{w_r} are given by l_f and l_r respectively. Their origins coincide with the front and rear axles. Moreover, the axis system of the front wheel is rotated by the wheel angle δ_w with respect to the vehicle-fixed axis system. The instantaneous center of rotation is abbreviated by ICR (Figure 2.3) and R denotes its distance to the CoG.

The transformation between the earth-fixed and vehicle-fixed axis system due to a rotation by the angle ψ , referred to as yaw angle, is defined by the matrix \mathbf{T}_{ev}

$$\mathbf{T}_{ev} = \begin{bmatrix} \cos\psi & -\sin\psi & 0 \\ \sin\psi & \cos\psi & 0 \\ 0 & 0 & 1 \end{bmatrix}. \quad (2.6)$$

Consequently, defining the velocity vector ${}_v\mathbf{v} := [v_x \ v_y \ v_z]^T$ of the vehicle the transformation to and from the earth-fixed axis system reads as⁴

$${}_e\mathbf{v} = \mathbf{T}_{ev} {}_v\mathbf{v}, \quad (2.7)$$

$$\begin{aligned} {}_v\mathbf{v} &= \mathbf{T}_{ev}^{-1} {}_e\mathbf{v}, \\ &= \mathbf{T}_{ve} {}_e\mathbf{v}. \end{aligned} \quad (2.8)$$

The acceleration of the vehicle (in the vehicle-fixed axis system) is given by the time-derivative of the vehicle velocity ${}_e\mathbf{v}$ and transformation into the correct axis system [KOL09], i.e.

$$\begin{aligned} {}_v\mathbf{a} &= \mathbf{T}_{ev}^{-1} {}_e\mathbf{a}, \\ &= \mathbf{T}_{ev}^{-1} {}_e\dot{\mathbf{v}}, \\ &= \mathbf{T}_{ev}^{-1} \dot{\mathbf{T}}_{ev} {}_v\mathbf{v} + {}_v\dot{\mathbf{v}}. \end{aligned} \quad (2.9)$$

³The extensions comprise a roll model, nonlinear tire force curves, dynamic tire force models and steering elasticities, see [DSH⁺06] for details.

⁴Note that the rotation matrices are orthogonal matrices, hence $\mathbf{T}^{-1} = \mathbf{T}^T$.

Finally, the vehicle acceleration in component form yields

$${}_{\mathbf{v}} \begin{bmatrix} a_x \\ a_y \\ a_z \end{bmatrix} = {}_{\mathbf{v}} \begin{bmatrix} \dot{v}_x \\ \dot{v}_y \\ \dot{v}_z \end{bmatrix} + {}_{\mathbf{v}} \begin{bmatrix} -v_y \dot{\psi} \\ v_x \dot{\psi} \\ 0 \end{bmatrix}. \quad (2.10)$$

The vector of angular velocities is defined by

$${}_{\mathbf{v}} \boldsymbol{\omega} := [\omega_x \quad \omega_y \quad \omega_z]^T = [\dot{\varphi} \quad \dot{\theta} \quad \dot{\psi}]^T, \quad (2.11)$$

with $\dot{\varphi}$, $\dot{\theta}$ and $\dot{\psi}$ being the time derivatives of the roll φ , pitch θ and yaw ψ angles⁵. The angular acceleration ${}_{\mathbf{v}} \boldsymbol{\alpha}$ is the time derivative of ${}_{\mathbf{v}} \boldsymbol{\omega}$, i.e.

$${}_{\mathbf{v}} \boldsymbol{\alpha} = \frac{d}{dt} {}_{\mathbf{v}} \boldsymbol{\omega} = [\ddot{\varphi} \quad \ddot{\theta} \quad \ddot{\psi}]^T. \quad (2.12)$$

For the special case of the (planar) single-track model the z-component of (2.10) as well as the x- and y-components of (2.11) and (2.12) are identically zero.

Equations of Motion

The assumption of a rigid vehicle body allows the use of the Newton-Euler formalisms to describe the translational/rotational motion [JAZ14]. The principles of linear and angular momentum w.r.t. CoG read as

$$m {}_{\mathbf{v}} \mathbf{a} = \sum \mathbf{F} \quad \text{and} \quad J_z {}_{\mathbf{v}} \boldsymbol{\alpha} = \sum \mathbf{T}. \quad (2.13)$$

Taking into account the results of (2.10) and (2.12) the complete equations of motion of the standard single-track model in the vehicle-fixed axis system \mathcal{C}_v can be written as⁶

$$m \frac{d {}_{\mathbf{v}} v_x}{dt} = m {}_{\mathbf{v}} v_y \dot{\psi} + {}_{\mathbf{v}} F_{x,f} + {}_{\mathbf{v}} F_{x,r}, \quad (2.14a)$$

$$m \frac{d {}_{\mathbf{v}} v_y}{dt} = -m {}_{\mathbf{v}} v_x \dot{\psi} + {}_{\mathbf{v}} F_{y,f} + {}_{\mathbf{v}} F_{y,r}, \quad (2.14b)$$

$$J_z \frac{d \dot{\psi}}{dt} = l_f {}_{\mathbf{v}} F_{y,f} - l_r {}_{\mathbf{v}} F_{y,r}, \quad (2.14c)$$

with J_z denoting the moment of inertia w.r.t. the vertical vehicle axis. Commonly, the equations (2.14b) and (2.14c) are used to describe the lateral vehicle motion as the longitudinal velocity is assumed as system input. The second differential equation refers

⁵In general, the angular velocities (in vehicle-fixed coordinates) are assumed equal to the time derivatives of the angles (roll, pitch, yaw) in earth-fixed coordinates, see [KOB03, p.17] for details.

⁶Note that only the relevant equations are listed.

to the variable ${}_v v_y$ (vehicle lateral velocity). Often it is replaced by the vehicle's sideslip angle β , defined as the angle between the velocity vector and the longitudinal vehicle axis, see also Figure 2.3. Its calculation is given by

$$\beta = \text{atan} \left(\frac{{}_v v_y}{{}_v v_x} \right), \quad (2.15)$$

and assuming small angles its approximation reads as

$$\beta \approx \left(\frac{{}_v v_y}{{}_v v_x} \right). \quad (2.16)$$

It should be noted that the left subscript is intentionally written for the acting forces in (2.14a)-(2.14c) as these need to be converted from the wheel-fixed to the vehicle-fixed axis system, see Figure 2.4(a). In case of a front-steered vehicle (which is considered herein) this transformation reduces to the front wheel that is rotated by the wheel angle δ_w . Exploiting the transformation matrix \mathbf{T}_{vw_f}

$$\mathbf{T}_{vw_f} = \begin{bmatrix} \cos\delta_w & -\sin\delta_w & 0 \\ \sin\delta_w & \cos\delta_w & 0 \\ 0 & 0 & 1 \end{bmatrix}, \quad (2.17)$$

the transformation of the tire forces reads as

$${}_v \begin{bmatrix} F_{x,f} \\ F_{y,f} \\ F_{z,f} \end{bmatrix} = \mathbf{T}_{vw_f} {}_{w_f} \begin{bmatrix} F_{x,f} \\ F_{y,f} \\ F_{z,f} \end{bmatrix}. \quad (2.18)$$

The individual tire force components in vehicle-fixed coordinates are given by

$${}_v F_{x,f} = {}_{w_f} F_{x,f} \cos\delta_w - {}_{w_f} F_{y,f} \sin\delta_w, \quad (2.19a)$$

$${}_v F_{y,f} = {}_{w_f} F_{x,f} \sin\delta_w + {}_{w_f} F_{y,f} \cos\delta_w, \quad (2.19b)$$

$${}_v F_{z,f} = {}_{w_f} F_{z,f} \quad (2.19c)$$

Currently, equations (2.14a)-(2.14c) do not contain any information on the calculation of the road-tire forces. In general, their modelling leaves some design freedom to the user. Different tire force models (linear vs. nonlinear) will be discussed in the following.

2.2 Tire Dynamics

The vehicle tires represent the contact elements between the vehicle and the road surface. In terms of vehicle handling the tire characteristics have a tremendous influence on the

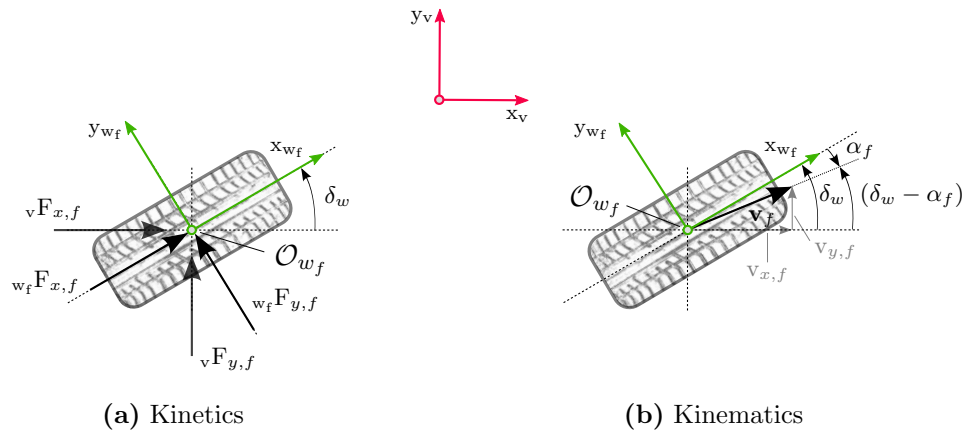


Figure 2.4: Front wheel schematics - Kinetics and Kinematics.

overall behavior. In general the basic functions of a tire can be summarized as [GIL92]:

- Generate longitudinal forces for acceleration (and deceleration) of the vehicle body.
- Generate lateral forces for cornering maneuvers.
- Prevent transmission of road shocks directly to the vehicle chassis.

These forces are generated between the tire element and the road surface via a small contact patch of postcard size [SHB14]. A shear mechanism acting on the tire elements passing through the contact patch is the main source of force generation (further details on the mechanics are discussed in [GIL92], [PAC12] and [MW04]). In terms of tire modelling there exist different approaches. [PAC12] denotes the main modelling paradigms as *experimental data-based*, *using similarity methods*, *simple* and *complex physical models*. This coincides with [ZAM94] as the modelling domains *physical*, *semi-empirical* and *empirical* do have a similar meaning as the ones before. Clearly, the choice of the tire model fully depends on the specific application. Whereas the latter are simpler (and consequently have less parameters) the former describe the tire dynamics in a highly accurate manner, but are more complex (i.e. great number of parameters). Typically, for model-based vehicle handling evaluation, the tire models are chosen simple (but as accurate as possible). Moreover, it reduces the workload if the number of parameters is small and their identification does not require extensive measurement equipment or a dedicated test bench. The tire force modelling is focused on the lateral acting direction as most of the maneuvers interesting for handling evaluation are driven at almost constant longitudinal speed and consequently, the coupling effects of the longitudinal and lateral forces can be neglected [KOB03, p.42].

Mostly, for vehicle dynamics relevant applications, e.g. stability control systems, assessment-related parameter identification, modelling of the lateral forces is based on empiri-

cal models, as the physical approaches are too complex and require good understanding of the material characteristics [VV08]. Examples of lateral tire force modelling based on simple models are manifold, e.g. [GYNW10, HUN11, PRE08, KOL09, NUT09, ZOM02, NÜS02].

Before introducing the most interesting tire modelling approaches the definition of *tire side slip angles* must be established as it is further required for calculation of lateral forces.

The velocities of the contact points (front and rear) constitute of two components. These are the vehicle velocity at the CoG and an additional component due to the rotation around the vehicle's z_v -axis, i.e. yaw motion. Hence, these read as

$${}_{\mathbf{v}}\mathbf{v}_f = \begin{bmatrix} v_x \\ v_y + l_f \dot{\psi} \\ 0 \end{bmatrix}, \quad {}_{\mathbf{v}}\mathbf{v}_r = \begin{bmatrix} v_x \\ v_y - l_r \dot{\psi} \\ 0 \end{bmatrix}. \quad (2.20)$$

For the rear wheel the axis system \mathcal{C}_{w_r} coincides with \mathcal{C}_v . Hence, no coordinate transformation is required. Considering Figure 2.4(b) the so-called slip angle⁷ α_f can be calculated as

$$\delta_w - \alpha_f = \text{atan} \left(\frac{{}_{\mathbf{v}}v_{f,y}}{{}_{\mathbf{v}}v_{f,x}} \right). \quad (2.21)$$

Here ${}_{\mathbf{v}}v_{f,y}$ is a scalar and refers to the y-component of the vector ${}_{\mathbf{v}}\mathbf{v}_f$. Assuming small angles for the steering and slip angles the trigonometric functions can be linearized, i.e. $\cos \alpha \approx 1, \sin \alpha \approx \alpha$. The front slip angle is then defined as

$$\alpha_f \approx \delta_w - \frac{{}_{\mathbf{v}}v_y}{{}_{\mathbf{v}}v_x} - \frac{l_f \dot{\psi}}{{}_{\mathbf{v}}v_x}. \quad (2.22)$$

Here, referring to (2.15) the term ${}_{\mathbf{v}}v_y {}_{\mathbf{v}}v_x^{-1}$ is equal to the sideslip angle β . Similarly the slip angle for the rear wheel can be computed as

$$\alpha_r = -\text{atan} \left(\frac{{}_{\mathbf{v}}v_{r,y}}{{}_{\mathbf{v}}v_{r,x}} \right) \approx -\frac{{}_{\mathbf{v}}v_y}{{}_{\mathbf{v}}v_x} + \frac{l_r \dot{\psi}}{{}_{\mathbf{v}}v_x}. \quad (2.23)$$

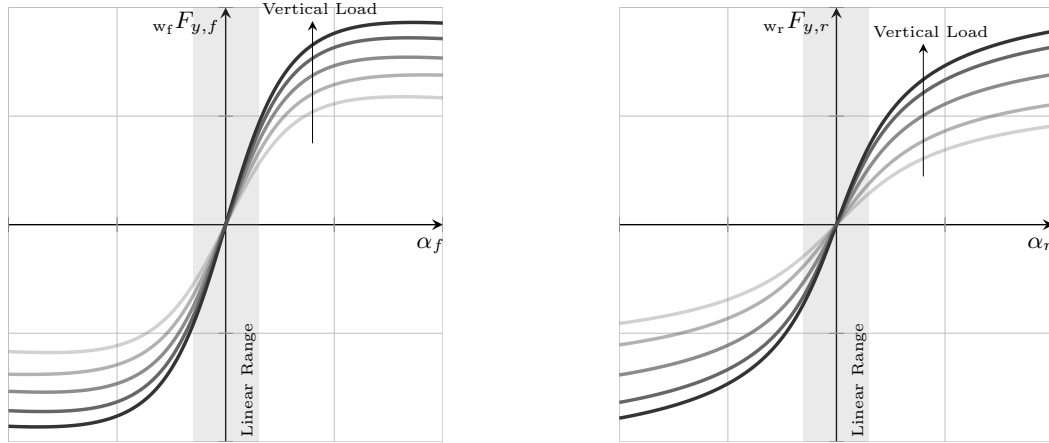
2.2.1 Stationary Tire Forces

The modelling of stationary tire forces refers to (as the name already suggests) steady-state conditions, i.e. the values influencing the lateral forces directly (e.g. slip angles, circumferential slip, camber angles) are constant or quasi-stationary (change very slowly w.r.t. the considered vehicle dynamics). For the subsequent tire force modelling, any

⁷The slip angle arises between the direction of wheel heading and the actual travel [GIL92]. It results from the deflection of the pneumatic tire under cornering conditions.

influences from camber and toe-in angles are not considered.

Typically the lateral tire forces are plotted against the slip angle of the tire, resulting in Figure 2.5. Due to the use of a single-track model the number of tires reduces from four to two (one per axle). From these curves it is obvious that the vertical load has a direct influence on the lateral force. The source of vertical load changes might either



(a) Front lateral tire force $w_f F_{y,f}$ vs. slip angle α_f .

(b) Rear lateral tire force $w_r F_{y,r}$ vs. slip angle α_r .

Figure 2.5: Lateral tire forces vs. slip angles.

be a static (additional vehicle mass) or a dynamic one (load transfer due to cornering). Regardless of the source, effectively it changes the curve shape.

Linear Tire Force Model

For small slip angles there exists a range (referred to as the *linear* or *proportional* range in literature) that allows linear modelling of the slip angle α and the lateral tire force F_y (Figure 2.5) characteristics, i.e.

$$F_{y,f}(\alpha_f) = c_{\alpha,f} \alpha_f, \quad (2.24a)$$

$$F_{y,r}(\alpha_r) = c_{\alpha,r} \alpha_r. \quad (2.24b)$$

Here the quantities $c_{\alpha,f}$, $c_{\alpha,r}$ represent the so-called lateral cornering stiffness factors that are defined as [GIL92, p.350]

$$c_{\alpha,f} = \left. \frac{\partial F_{y,f}}{\partial \alpha_f} \right|_{\alpha_f=0}, \quad c_{\alpha,r} = \left. \frac{\partial F_{y,r}}{\partial \alpha_r} \right|_{\alpha_r=0}. \quad (2.25)$$

The attentive reader might have noticed the disappearance of the subscripts denoting the axis system. As of now (for the remaining section) the tire forces defined refer to the

wheel-fixed axis system. Hence, depending on which wheel is considered a transformation to the vehicle-fixed coordinate system might be required.

Against the convention often seen in standard literature (e.g. SAE standards) it is assumed and based on Figures 2.3 and 2.4(b) that the slip angles are defined such that a rotation against the mathematical positive direction yields a positive slip angle. The resulting positive lateral tire force yields a *positive* cornering stiffness value. The validity of the linearization holds up to slip angles of approximately $\pm 3^\circ$ for dry road surfaces [MW04] which in terms of lateral acceleration refers to $|a_y| \approx 4\text{m}\cdot\text{s}^{-2}$.

A common extension to the linear modelling approach is the definition of a vertical load-dependent cornering stiffness, i.e. [MW04]

$$c_\alpha(F_z) = F_z \left(c_{\alpha_1} - c_{\alpha_2} \frac{F_z}{F_{z,nom}} \right). \quad (2.26)$$

Here c_{α_1} , c_{α_2} are parameters to be identified, F_z is the actual vertical tire force and $F_{z,nom}$ a nominal vertical tire force. The validity of this approach is again restricted to $|\alpha| = 0 - 3^\circ$. A load-dependent cornering stiffness is also exploited in [DVL⁺10], but the vertical tire forces need to be either measured or estimated. Obviously, measurement is cost-intensive and estimation requires observer structures as well as knowledge of certain vehicle parameters.

Magic Formula Model (MF)

A classic semi-empirical⁸ tire force model represents the *Magic formula* introduced by [PB97] in the 1990s. It models the longitudinal and lateral tire forces as well as the aligning torque by definition of a formula framework containing not less than 70+ formulas⁹. Lateral forces assuming pure slip (no longitudinal slip) can be modelled as

$$F_y(\alpha) = D \sin[C \operatorname{atan}(B\alpha - E(B\alpha - \operatorname{atan} B\alpha))]. \quad (2.27)$$

In literature the function argument is often sideslip $s_s := \tan\alpha$ [KD97]. However, assuming small slip angles a linearization of the trigonometric functions is reasonable and yields the function argument slip angle α . It should be noted, that each force model requires its own set of parameters. Figure 2.7 shows the slip-force curve and its characteristic points. Correspondence between the those points and the parameters is discussed in the following.

B denotes the *stiffness* factor, C the *shape* factor, D ($=F_{y,max}$) the *peak* factor and E the *curvature* factor. A graphical interpretation of variation w.r.t. the two shape factors C

⁸The term *semi-empirical* refers to a modelling paradigm that is based on measurement data (empirical). However, due to integration of physics-related knowledge it is called semi-empirical.

⁹These formulas consider pure and combined slip conditions as well as vertical load, road surface and wheel camber angle changes. Without any further discussion required it is obvious that the number of parameters is inappropriate for any online identification algorithm.

and E is investigated in [PAC12, p.175]. In general, these tire parameters are not constant, but vary with vehicle load, road surface etc. Moreover, a horizontal/vertical shift of the curve is allowed ([SHB14, PAC12]), e.g. for modelling of wheel camber effects, but not considered here.

Coherence between the model parameters and characteristic points of Figure 2.7 is given by the term $F_{y\infty}$, representing the horizontal asymptote, i.e. $F_{y\infty} := D \sin(\pi - \frac{C\pi}{2})$ [PB97] and the lateral cornering stiffness, i.e. $c_\alpha = BCD$.

Reconsidering again the problem of parameter identification it is in summary 8 parameters of the Magic Formula model that need to be estimated for front and rear axle of the single-track model.

Simplified Magic Formula Model (SMF)

In [AH05], [KNW07] and [GYNW10] simplifications of the MF model based on a reduced set of parameters have been presented and used for control, observation and parameter identification purposes. The approach of [AH05] reads as

$$F_y(\alpha) = D \sin(\text{atan } B\alpha), \quad (2.28)$$

and halves the number of unknown parameters compared to (2.27). Effectively, it operates on two per wheel and their interpretation is straightforward, as illustrates Figure 2.6. Comparing the SMF with the standard MF model reveals that the greater number of parameters provides an additional degree of freedom w.r.t. curve shaping. Due to the low number of parameters the shape of the SMF curve can only be influenced to some restricted extent.

As a result, the decrease of tire force after the maximum (for increasing slip angles) is not inherent to the simplified model. Although it is attractive due to the low number of parameters the systematic modelling error reduces its potential for accurate calculation of the lateral tire forces. For very small slip angles the model reduces to a linear one, i.e. $c_\alpha = BD$.

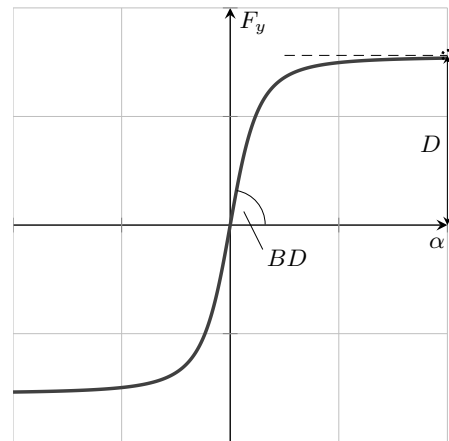


Figure 2.6: Graphical interpretation of the Simplified Magic Formula parameters.

TM_Simple

Combining the Magic Formula ideas with the so-called TMeasy¹⁰ [HRW07] model the resulting TM_Simple tire model [HIR09] exploits six parameters to describe the characteristics of the longitudinal and lateral tire forces. Focusing on the lateral tire forces the

¹⁰TMeasy is a semi-physical tire model for low frequency (vehicle dynamics) applications. The model parameters are reduced to a small number allowing for simple identification [HRW07].

model reads as [KOL09]

$$F_y(\alpha) = D \sin \left[B \left(1 - e^{-\frac{|\alpha|}{C}} \right) \text{sign}(\alpha) \right]. \quad (2.29)$$

For a graphical interpretation of its characteristic values the reader is referred to Figure 2.7. There, the maximum force and the limit value are denoted by $F_{y_{max}}$ and $F_{y_{\infty}}$ respectively. The slope of the curve at the origin is represented by c_{α} . The coherence between these values and the model parameters is defined by

$$D = F_{y_{max}}, \quad (2.30a)$$

$$B = \pi - \text{asin} \left(\frac{F_{y_{\infty}}}{F_{y_{max}}} \right), \quad (2.30b)$$

$$C = c_{\alpha}^{-1} B D. \quad (2.30c)$$

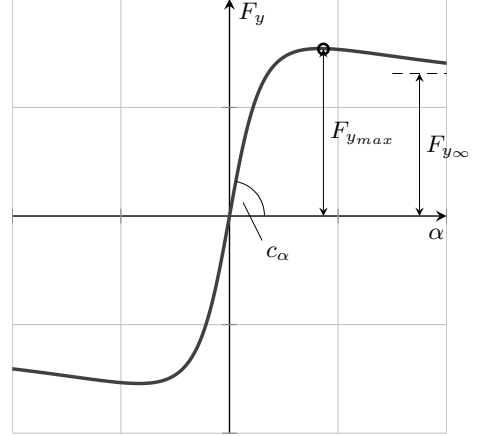


Figure 2.7: Characteristic points of the slip-force curves of MF and TM_Simple.

In order to include the effects of a varying vertical tire force F_z the parameters B, C, D can be modelled as functions of F_z , similar to (2.26), i.e.

$$\begin{bmatrix} F_{y_{max}}(F_z) \\ F_{y_{\infty}}(F_z) \\ c_{\alpha} \end{bmatrix} = \underbrace{\begin{bmatrix} a_1 \\ a_2 \\ a_3 \end{bmatrix}}_{=: \mathbf{a}} \left(\frac{F_z}{F_{z,nom}} \right) + \underbrace{\begin{bmatrix} b_1 \\ b_2 \\ b_3 \end{bmatrix}}_{=: \mathbf{b}} \left(\frac{F_z}{F_{z,nom}} \right)^2. \quad (2.31)$$

The vectors \mathbf{a} and \mathbf{b} have then to be identified which doubles the number of parameters, but also includes the effect of dynamic load transfer during cornering. Clearly, as the vertical forces can be interpreted as system inputs their values need to be known accurately.

Comparison of Tire Force Models

The qualitative shapes of the discussed models are summarized in Figure 2.8. Apparently, the shapes of the MF and SMF differ considerably. Especially the reproduction of the maximum force by the Simplified Magic Formula leaves potential for improvement. It seems that the model TM_Simple solves this issue by requiring an additional parameter only. From the perspective of parameter identification it is these two models (SMF and TM_Simple) that are attractive for further integration.

Although [OCGS06] illustrates a simple mechanism to identify the unknown parameters of the Magic Formula via genetic algorithms, extensive measurement equipment (incl. test bench) is required and the time horizon for the algorithm convergence is not appropriate for the real-time parameter identification objective.

The linear approach represents by far the simplest model whose parameters shall be identified. It is assumed to lack accuracy especially for slip angles exceeding the linear range. However, currently only the Magic Formula is not considered for any further work due to the number of parameters to be identified.

Some Comments on the Modelling The parameters of the discussed tire models are in general not constant, but change with vehicle load, road surface etc. However, for the current application it is reasonable to assume that the environmental conditions and also the actual vehicle load are known and do not vary to some extent. Then, the identified parameters might be assumed constant, but correspondent to the prevailing conditions. In fact, a change of e.g. vehicle load requires a new parameter identification run.

Pneumatic Trail

The ongoing introduction of tire force and also lateral dynamics models assumed that the lateral forces act directly at the wheel axis center, see Figure 2.4(a). As the lateral force build-up is not equally distributed over the tire contact patch (it is more shaped like a triangle [GIL92]) the resultant force contact point moves towards the rear of the surface. The distance from the center to the actual contact point is referred to as pneumatic trail. This effect further causes an aligning torque that is equal to the product of lateral force and pneumatic trail. Figure 2.9 shows the pneumatic trail n_p and the resulting aligning torque T_z . In general, n_p is not a constant, but depends on the vertical tire load F_z and slip angle α . For small slip angles ($\alpha = 0 - 2^\circ$) its variation can be approximated by a linear rela-

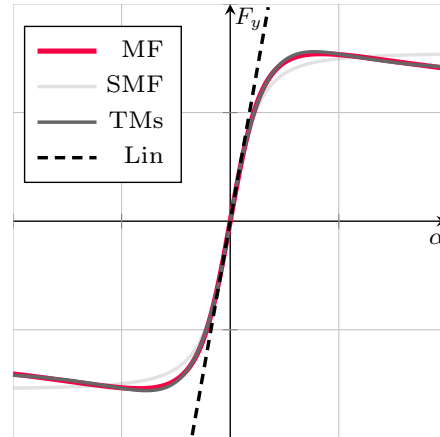


Figure 2.8: Comparison of the Magic Formula (MF), simplified Magic Formula (SMF), TM_Simple (TMs) and the linear modelling approach.

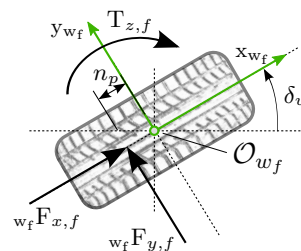


Figure 2.9: Kinetics at front wheel (including effects of pneumatic trail).

tionship [MW04], i.e.

$$n_p(F_z) = n_{p0} \frac{F_z}{F_{z,nom}}. \quad (2.32)$$

For larger slip angles it tends to zero, i.e. reducing the self-aligning moment although the lateral force increases [RAJ12]. The accuracy of the single-track model (2.14a)-(2.14c) can be increased if the distances between wheel axes and CoG are corrected by the pneumatic trails, i.e.

$$l_{f_e} := l_f - n_p, \quad l_{r_e} := l_r + n_p. \quad (2.33)$$

A modified version of the single-track model taking into account the pneumatic trail affects equation (2.14c) explicitly, i.e.

$$J_z \ddot{\psi} = l_{f_e} v F_{y,f} - l_{r_e} v F_{y,r}, \quad (2.34)$$

but also the calculation of the slip angles α_f (2.21) and α_r (2.23) needs to be adapted accordingly to

$$\alpha_f = \delta_w - \beta - \frac{l_{f_e} \dot{\psi}}{v v_x}, \quad \alpha_r = -\beta + \frac{l_{r_e} \dot{\psi}}{v v_x}. \quad (2.35)$$

2.2.2 Transient Tire Forces

Until now the slip angles or lateral forces have been considered to be stationary or at least quasi-stationary. If these tire models were applied for the simulation of transient handling maneuvers, such as step inputs or sinusoidal steering, the build-up of the tire forces is inherently assumed instantaneous. In reality, the deflection of the tire tread introduces a time lag such that the force build-up lags behind approximately one wheel rotation [MW04]. The standard modelling approach is to add a first-order system that is characterized by the so-called relaxation length σ_α , i.e.

$$\sigma_\alpha := \frac{c_\alpha}{c_y}, \quad (2.36)$$

where c_y represents the lateral tire stiffness¹¹. The relaxation length can be interpreted as the distance required to travel until the lateral tire forces are built-up. The dynamic system for calculation reads as

$$\frac{d\bar{F}_y}{dt} = \frac{1}{\tau_{lag}} (F_y - \bar{F}_y). \quad (2.37)$$

¹¹Not to be confused with the lateral tire *cornering* stiffness c_α .

The lagged tire force is denoted by \bar{F}_y and the time constant τ_{lag} is given by division of the relaxation length σ_α by the longitudinal vehicle speed ${}_v v_x$ [RAJ12]. More sophisticated modelling approaches as in [PB97] are not appropriate for the objective herein due to the high complexity.

2.3 Chassis Motion

2.3.1 Roll Dynamics

The rotation of the vehicle chassis around the x-axis (of the intermediate axis system¹²) is denoted as *roll motion*. Its excitation is caused by vehicle cornering, crosswinds, road roughness/bank angle and/or obstacles. During cornering the chassis rolls due to centrifugal forces to the outside of the turn. The intensity of the roll motion depends on the effective roll stiffness. Aside the standard damping elements of the vehicle suspension special roll stabilizers increase the stiffness of an axle to reduce the roll tendency.

The resulting roll angle and also the lateral acceleration of the driver's head (which is in turn affected by the roll motion of the chassis) are important measures for the vehicle evaluation process, e.g. [SCH10, MW04]. However, mostly the roll angle is measured or estimated for vehicle safety-related applications, i.e. roll-over detection systems, e.g. [DCREH10] or vehicle dynamics (roll) control, e.g. [RMC07].

In terms of roll dynamics modelling there exist different approaches in literature that vary w.r.t. model complexity and number of parameters. A complex 14-DoF full vehicle model including the roll center dynamics as well as nonlinear effects due to changes of the vehicle geometry is discussed in [SC08]. However, due to the model complexity the number of unknown, i.e. to be identified, parameters is too high to be used for real-time estimation methods. In [RAJ12] a 4-DoF model (roll motion, heave and vertical movement left/right) is developed. It includes the individual suspension elements and requires measurement of the relative displacements of tires and chassis. Commonly, the measurement of these quantities is not straightforward and requires installation of additional sensor equipment. As a consequence, the roll model to be developed will have a single degree of freedom. Especially due to its simplicity and low number of parameters that model is often used for roll dynamics modelling ([RAJ12, SHB14, DVL⁺10, SU11, RZSF⁺12, KOB03]). The work of [HMxCB06] investigates various low-order models for roll-over detection that should then serve as basis for a controller synthesis to prevent the occurrence of roll-over. Interestingly, the outcome of the study is a good matching between outcome of a simple model and real measurements. However, the requirement for linearity is paid by estimation quality losses for severe handling maneuvers as they happen in the case of roll-over. Clearly, that application is different to the current, as it is not the intention to forecast any roll-over incidents, but to provide a good estimate of the roll angle for standard handling maneuvers.

¹²See Appendix A for details.

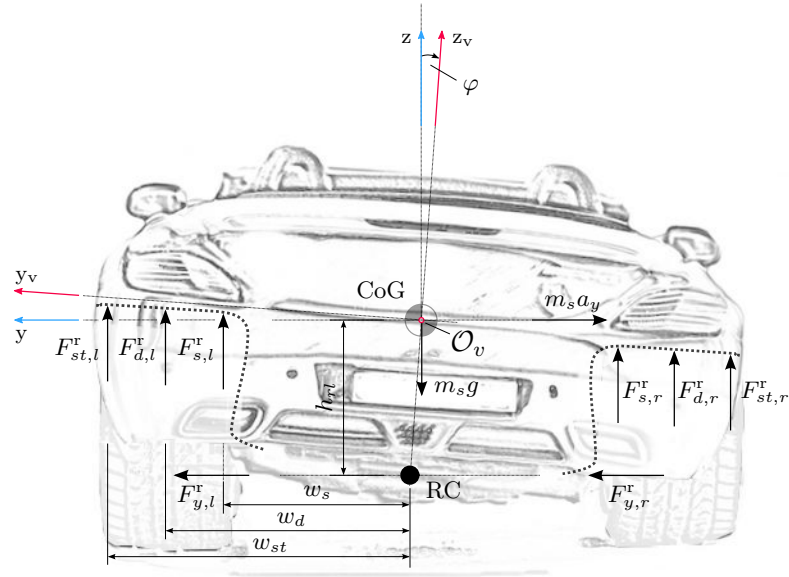


Figure 2.10: Schematics of the chassis roll motion.

In order to keep the number of parameters low the roll motion will be developed using a 1-DoF modelling assumption. In other words, the chassis can be interpreted as a rigid body that rotates around a fixed point, denoted by the so-called roll center RC. In fact, this is only a theoretical concept to simplify the modelling approach. In reality, there exists a roll center per axle whose position is defined by the suspension geometry. The connection of the front and rear roll center points is defined as roll axis.

Figure 2.10 illustrates the rotation of the vehicle chassis w.r.t. its longitudinal axis¹³. The front and rear chassis parts (including the suspension elements) are lumped into a rigid body (without any differentiation between front and rear axle) that is rotated around the roll center RC. Furthermore, the validity of the derived model requires several assumptions to hold:

1. The road bank angle is approximately zero and can be neglected. This implies the use of the model under test track conditions. Other than that, the calculated roll angle is affected by offsets and does not provide correct information of the chassis' roll angle.
2. The roll dynamics are only excited by the steering interactions of the driver. Disturbances (rough road, obstacles etc.) are not considered.
3. Coupling effects between yaw and roll dynamics can be disregarded. The same holds for the pitch dynamics.

¹³Note that the forces do not have a subscript as they refer to the intermediate axis system.

4. The roll motion does not affect the track width of the vehicle.
5. Front and rear suspension elements show the same characteristics and are lumped into a single element per vehicle side. Hence, differentiation between rear and front roll angle is not possible, as is an axis-individual suspension configuration.

The angle between the vertical axes of the intermediate axis system \mathcal{C} and the vehicle-fixed one \mathcal{C}_v is referred to as roll angle φ . The forces acting on the free vehicle chassis are due to the suspension elements and lateral tire forces. The former consist of the left/right spring forces $F_{s,l/r}^r$, left/right damping forces $F_{d,l/r}^r$ and the forces due to left/right roll stabilizers $F_{st,l/r}^r$. Here, the superscript "r" marks the forces to be related to roll dynamics¹⁴. The distances between the roll center and the virtual suspension elements (represented by the resulting forces only) read as w_s (spring elements), w_d (damping elements) and w_{st} (stabilizer elements). These distances are symmetric w.r.t. the roll center (and assumed constant despite the roll motion of the vehicle.). The distance between the center of gravity (CoG) and roll center RC is denoted as h_{rl} . The mass of the sprung parts reads as m_s and is equal to the total vehicle mass m reduced by the mass of the unsprung parts¹⁵ m_u .

Applying the conservation principle of angular momentum w.r.t. the roll center RC yields

$$J_{xc}\ddot{\varphi} = \sum T_x, \quad (2.38a)$$

$$= m_s a_y h_{rl} \cos\varphi + m_s g h_{rl} \sin\varphi + w_s \Delta F_s^r + w_d \Delta F_d^r + w_{st} \Delta F_{st}^r, \quad (2.38b)$$

where $\ddot{\varphi}$ represents the roll acceleration defined as the time derivative of the roll rate $\dot{\varphi}$, i.e.

$$\dot{\varphi} := \frac{d\varphi}{dt}, \quad \ddot{\varphi} := \frac{d^2\varphi}{dt^2}. \quad (2.39)$$

Due to the roll motion the position of the CoG changes and consequently the lever arm of the acting lateral force reduces to $h_{rl} \cos\varphi$. Additionally, the gravitational force affects the roll moment taking into account the distance $h_{rl} \sin\varphi$. In general, the rotation between the two axis systems by the angle φ can be described by the rotation matrix \mathbf{T}_{vi}^r , i.e.

$$\mathbf{T}_{vi}^r = \begin{bmatrix} 1 & 0 & 0 \\ 0 & \cos\varphi & \sin\varphi \\ 0 & -\sin\varphi & \cos\varphi \end{bmatrix}. \quad (2.40)$$

¹⁴This is required to differentiate the roll forces from pitch dynamics related ones (see Section 2.3.2).

¹⁵The unsprung parts of the vehicle are mainly the axles and tire elements [RAJ12].

Note that, although the intermediate axis system \mathcal{C} (see Appendix A) does not have a subscript, the rotation matrix \mathbf{T}_{vi}^r uses a subscript "i" to indicate the transformation direction. Considering the acceleration vector relevant for the roll motion defined in the intermediate axis system $\mathbf{a} := [a_x \ a_y \ a_z]^T$ with $a_x = 0$ and $a_z = g$, where g represents the gravitational acceleration, its transformation to the vehicle-fixed axis system reads as

$${}_{\vee}\mathbf{a} = \mathbf{T}_{vi}^r \mathbf{a}, \quad (2.41)$$

and yields the acceleration vector ${}_{\vee}\mathbf{a}$ in vehicle-fixed coordinates, i.e.

$${}_{\vee}\mathbf{a} = \begin{bmatrix} 0 \\ a_y \cos\varphi + g \sin\varphi \\ -a_y \sin\varphi + g \cos\varphi \end{bmatrix}. \quad (2.42)$$

Commonly, lateral acceleration sensors are installed chassis-fixed in the vehicle and hence sense the y-component of ${}_{\vee}\mathbf{a}$. Considering (2.38b) the left side of the formula can be interpreted as $m_s h_{rl} (a_y \cos\varphi + g \sin\varphi)$ which can be regarded as $m_s h_{rl} a_{y,m}$, where $a_{y,m}$ is an abbreviation of the y-component of ${}_{\vee}\mathbf{a}$, i.e.

$$a_{y,m} := a_y \cos\varphi + g \sin\varphi. \quad (2.43)$$

The terms ΔF_s^r , ΔF_d^r and $\Delta F_{st,\varphi}^r$ of (2.38b) denote the differences between the left and right suspension elements, i.e.

$$\Delta F_s^r := F_{s,l}^r - F_{s,r}^r, \quad (2.44a)$$

$$\Delta F_d^r := F_{d,l}^r - F_{d,r}^r, \quad (2.44b)$$

$$\Delta F_{st}^r := F_{st,l}^r - F_{st,r}^r. \quad (2.44c)$$

The moment of inertia J_{xc} is given by the moment of inertia w.r.t. the longitudinal axis of the sprung parts J_{xs} and corrected for the roll center, i.e. $J_{xc} = J_{xs} + m_s h_{rl}^2$. In the following the spring, damper and stabilizer forces need to be discussed in detail.

The spring force F_s is proportional to the displacement of the spring, i.e.

$$F_s^r = c_s^r (\Delta z_s^r) \Delta z_s^r, \quad (2.45)$$

where Δz_s^r denotes the vertical displacement of the spring element (positive for a length reduction of the spring) and $c_s^r (\Delta z_s^r)$ represents the spring stiffness that is in general a function of the displacement Δz_s^r . As previously mentioned the superscript "r" indicates the relevance for roll dynamics (as opposed to stiffness functions related to pitch dynamics presented in Section 2.3.2). Commonly, the front suspension springs are of linear

type, whereas the rear ones show progressive¹⁶ character [HH03]. Furthermore, [MW04] shows the nonlinear character¹⁷ of spring elements as used in air suspension systems. The deflection Δz_s^r can be formulated in terms of roll angle φ (assuming small angles) by $\Delta z_s^r \approx w_s \varphi$ such that the spring force F_s^r reads as

$$F_s^r \approx (-1)^i c_s^r(\varphi) w_s \varphi \quad i = 1, 2. \quad (2.46a)$$

The index i defines the force direction, i.e. $i = 1$ refers to the left (negative force for positive roll angles) and $i = 2$ to the right side.

In general the damping force is a nonlinear function of the deflection rate. A common approach is to model the characteristics as bilinear curve, i.e. different slopes for negative and positive deflection rates. As above, the force can be rewritten as a function of the roll rate $\dot{\varphi}$

$$F_d^r \approx (-1)^i d^r(\dot{\varphi}) w_d \dot{\varphi} \quad i = 1, 2, \quad (2.47)$$

where $d^r(\dot{\varphi})$ represents the roll rate-dependent damping coefficient. The passive roll stabilizer, integrated into the vehicle to reduce the roll angle during cornering [HE11], can be modelled as [SHB14]

$$F_{st}^r \approx (-1)^i \frac{c_{st}^r w_{st}}{2b_{st}^2} \varphi \quad i = 1, 2. \quad (2.48)$$

Here b_{st} reads as the stabilizer lever arm and c_{st}^r refers to the torsional stiffness factor of the passive stabilizer. Active elements are not discussed here, but details can be found in [SHB14].

Now, inserting the force models into (2.38b) leads to

$$J_{xc} \ddot{\varphi} = -c_{\Sigma}^r(\varphi) \varphi - d_{\Sigma}^r(\dot{\varphi}) \dot{\varphi} + m_s h_{rl} a_{y,m}, \quad (2.49)$$

with $a_{y,m} = a_y \cos \varphi + g \sin \varphi$ being the lateral acceleration measured in-vehicle (assuming a chassis-fixed acceleration sensor). Furthermore,

$$c_{\Sigma}^r(\varphi) := 2 w_s^2 c_s^r(\varphi) + w_{st}^2 \frac{c_{st}^r}{b_{st}^2}, \quad (2.50a)$$

$$d_{\Sigma}^r(\dot{\varphi}) := 2 w_d^2 d^r(\dot{\varphi}), \quad (2.50b)$$

describe the abbreviations of the effective stiffness and damping functions. The vertical tire deflection can be integrated by reducing the effective stiffness $c_{\Sigma}^r(\varphi)$ [AMM97] but that is not considered in this work¹⁸. Due to [MW04, p.29] the tire damping is not assumed relevant, as long as there is a damping suspension element. Furthermore, effects

¹⁶For higher values of vertical displacement the spring stiffness increases.

¹⁷The spring force is modelled by $F_s = c_1 \Delta z_s + c_2 \Delta z_s^3$.

¹⁸The tire vertical stiffness exceeds the spring stiffness by the order of a magnitude [MW04].

due to friction are not modelled explicitly in (2.49), but might be lumped into the effective stiffness $c_{\Sigma}^r(\varphi)$ and damping parameters $d_{\Sigma}^r(\dot{\varphi})$ respectively.

At the moment, the resulting model of the roll dynamics is nonlinear as the force models incorporate nonlinear effects. However, considering the simple nature of the roll model and its 1-DoF, the author of [AMM97] claims that due to the opposite suspension deflection during chassis roll the dominant nonlinearities do not have to be taken into account. For (2.49) that means replacing the roll angle and velocity-dependent parameters $c_{\Sigma}^r(\varphi)$ and $d_{\Sigma}^r(\dot{\varphi})$ by constants. Furthermore, as the distances between the CoG and the suspension elements, namely w_s , w_d and w_{st} , are almost identical an average distance $\tilde{w}_s := \frac{1}{3}(w_s + w_d + w_{st})$ can be assumed. Finally, the simplified model parameters can be formulated as

$$c_{\Sigma}^r := 2 \tilde{w}_s^2 c_s^r + \tilde{w}_s^2 \frac{c_{st}^r}{b_{st}^2}, \quad (2.51a)$$

$$d_{\Sigma}^r := 2 \tilde{w}_s^2 d^r, \quad (2.51b)$$

and the resulting linear model of the roll dynamics is given as

$$J_{xc}\ddot{\varphi} = -c_{\Sigma}^r\varphi - d_{\Sigma}^r\dot{\varphi} + m_s h_{rl} a_{y,m}. \quad (2.52)$$

That second-order model (or slightly different variations) are often seen for roll angle observation, e.g. [DVL⁺10], [SU11], [RZSF⁺12]. [RPTL11] also uses this simple roll modelling approach for a combined state and parameter estimation resulting in the roll angle as well as center of gravity (CoG) height.

Coupling with Lateral Dynamics The coupling between the roll and the lateral dynamics is modelled by a modification of the front and rear slip angles α_f , α_r respectively (2.35), i.e. α_{f_e} and α_{r_e}

$$\alpha_{f_e} = \delta_w - \frac{v v_y}{v v_x} - \frac{l_{f_e} \dot{\psi}}{v v_x} - \frac{h_{rl} \dot{\varphi}}{v v_x}, \quad (2.53a)$$

$$\alpha_{r_e} = -\frac{v v_y}{v v_x} + \frac{l_{r_e} \dot{\psi}}{v v_x} - \frac{h_{rl} \dot{\varphi}}{v v_x}. \quad (2.53b)$$

By merging the modified slip angle definitions with the single-track model equations (2.14b) and (2.34) a new set of equations accounting for the roll motion can be formulated.

Effects of Road Bank Angle on Roll Dynamics If the assumption does not hold that the road bank angle Φ is negligibly small, the total rotation angle between the intermediate axis system \mathcal{C} and the vehicle-fixed \mathcal{C}_v is given by the sum of vehicle roll angle φ and road bank angle Φ , i.e. $\varphi_m := \varphi + \Phi$, see Figure 2.11. Consequently, the transformation matrix as defined in (2.40) is now exploiting the angle φ_m and the

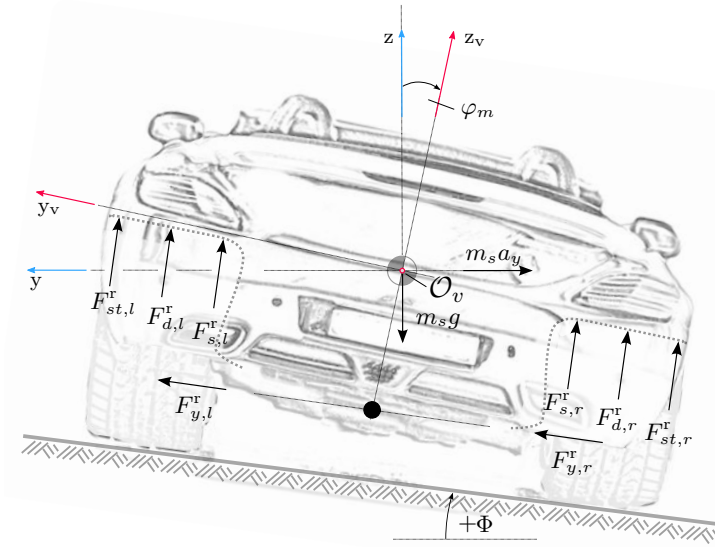


Figure 2.11: Road bank angle effects on roll dynamics.

resulting lateral acceleration is

$$a_{y,m} = a_y \cos\varphi_m + g \sin\varphi_m. \quad (2.54)$$

Combining that result with (2.52) the roll dynamics of the vehicle can be described. Note that the resulting model is not useful for state observer design as the measured roll angle or rate refer to φ_m or $\dot{\varphi}_m$, i.e. the sum of vehicle roll and road bank angle (or its time derivative).

2.3.2 Pitch Dynamics

The rotation of the vehicle chassis and hence the vehicle-fixed coordinate system \mathcal{C}_v around the y_v -axis is referred to as pitch motion (Figure 2.12). The resulting angle between the intermediate axis system \mathcal{C} and \mathcal{C}_v is denoted as pitch angle θ . Note that the angle θ is related to the chassis' pitch angle and does not include a road inclination angle. As presented in Section 2.1.1 the road inclination angle is denoted by χ .

The pitch dynamics modelling is similar to that of the roll dynamics presented previously. The employment of a 1-DoF model suggests the interpretation of the pitch dynamics as a torsional spring-mass-damper system, i.e. the pitch motion can be simplified to a rotation of the rigid body w.r.t. the pitch center (PC). Intentionally, the bounce (heave) movement of the chassis is not included into the model as the increase w.r.t. degrees of freedom yields more model parameters and also requires measurement of suspension displacement for a proper parameter identification mechanism. The suspension elements of the left and right hand-side are lumped into single front and rear elements. For the

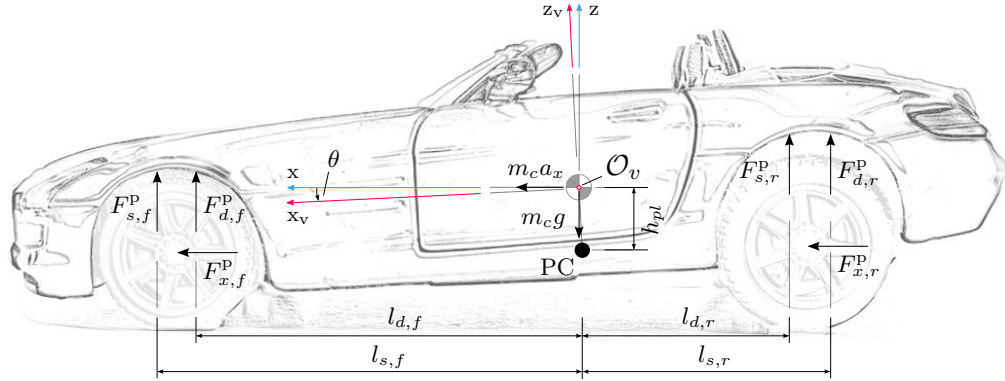


Figure 2.12: Schematics of the chassis pitch motion.

model validity to hold there are several assumptions necessary:

1. The road inclination angle is approximately zero and can therefore be neglected. This restricts the model use to test track conditions. Other than that, the longitudinal acceleration and pitch angle measurements are distorted and do not provide correct information.
2. The pitch dynamics are only excited by an intentional driver action, i.e. acceleration or deceleration. External excitations due to disturbances (rough road, obstacles etc.) are not considered.
3. The pitch motion is interpreted as a rotation of the sprung vehicle parts around a given point, named as pitch center (PC). Its position depends on the vehicle suspension type.
4. The longitudinal distances between CoG and front/rear axle are assumed constant. Suspension compliance is neglected.
5. Coupling effects with lateral/roll dynamics are negligible. Simultaneous excitation of lateral and pitch dynamics is not feasible.

Due to the vehicle acceleration or deceleration the change in vertical tire loads causes a pitch moment. The resulting suspension forces consist of the spring forces $F_{s,f}^P$, $F_{s,r}^P$ and the damping forces $F_{d,f}^P$, $F_{d,r}^P$. There are no (passive) stabilizing elements implemented in standard vehicles - active elements are not considered. The distances between the pitch center and the spring forces are $l_{s,f}$, $l_{s,r}$ (front/rear) and $l_{d,f}$, $l_{d,r}$ (front/rear) respectively. The parameter h_{pl} defines the height between the CoG and the pitch center. The moment of inertia J_{yc} comprises the moment of inertia w.r.t. the lateral axis of the sprung vehicle parts J_{ys} and a correction that accounts for the distance between CoG

and pitch center, i.e. $J_{yc} = J_{ys} + m_s h_{pl}^2$. For derivation of the equations of motion the conservation principle of angular momentum yields

$$J_{yc}\ddot{\theta} = \sum T_y, \quad (2.55a)$$

$$= F_{s,r}^P l_{s,r} + F_{d,r}^P l_{d,r} - F_{s,f}^P l_{s,f} - F_{d,f}^P l_{d,f} + m_s h_{pl} (a_x \cos\theta - g \sin\theta). \quad (2.55b)$$

The pitch rate $\dot{\theta}$ and the pitch acceleration $\ddot{\theta}$ are defined by

$$\dot{\theta} := \frac{d\theta}{dt}, \quad \ddot{\theta} := \frac{d^2\theta}{dt^2}. \quad (2.56)$$

Reconsidering the interpretation of the pitch motion as a rotation of the vehicle-fixed axis system \mathcal{C}_v by the angle θ w.r.t. the intermediate system \mathcal{C} its mathematical interpretation exploits the rotation matrix \mathbf{T}_{vi}^P , i.e.

$$\mathbf{T}_{vi}^P = \begin{bmatrix} \cos\theta & 0 & -\sin\theta \\ 0 & 1 & 0 \\ \sin\theta & 0 & \cos\theta \end{bmatrix}. \quad (2.57)$$

Defining the acceleration vector $\mathbf{a} := [a_x \quad 0 \quad g]^T$ it can be transformed considering \mathbf{T}_{vi}^P to ${}_v\mathbf{a}$ given by

$${}_v\mathbf{a} = \mathbf{T}_{vi}^P \mathbf{a} = \begin{bmatrix} a_x \cos\theta - g \sin\theta \\ 0 \\ a_x \sin\theta + g \cos\theta \end{bmatrix}. \quad (2.58)$$

Comparing the x-component of ${}_v\mathbf{a}$ with (2.55b) one sees that if the longitudinal acceleration is measured in vehicle-fixed coordinates the gravitational component is inherent to the measurement and the latter is defined by

$$a_{x,m} := a_x \cos\theta - g \sin\theta, \quad (2.59)$$

and consequently the equation of motion for the pitch dynamics reads as

$$J_{yc}\ddot{\theta} = F_{s,r}^P l_{s,r} + F_{d,r}^P l_{d,r} - F_{s,f}^P l_{s,f} - F_{d,f}^P l_{d,f} + m_s h_{pl} a_{x,m}. \quad (2.60)$$

The suspension spring forces $F_{s,r}^P$, $F_{s,f}^P$ are proportional to the suspension deflection Δz_f and Δz_r . Hereby, a positive deflection refers to a spring compression, i.e. reduction of its length. Approximating the deflections by $\Delta z_f \approx l_{s,f}\theta$ and $\Delta z_r \approx -l_{s,r}\theta$ the spring

forces are modelled by

$$F_{s,r}^p = -c_{s,r}^p(\theta) l_{s,r} \theta, \quad (2.61a)$$

$$F_{s,f}^p = c_{s,f}^p(\theta) l_{s,f} \theta. \quad (2.61b)$$

Moreover, the damping forces $F_{d,r}^p$, $F_{d,f}^p$ can be described by

$$F_{d,r}^p = -d_r^p(\dot{\theta}) l_{d,r} \dot{\theta}, \quad (2.62a)$$

$$F_{d,f}^p = d_f^p(\dot{\theta}) l_{d,f} \dot{\theta}. \quad (2.62b)$$

There, the spring stiffnesses $c_{s,r}^p(\theta)$, $c_{s,f}^p(\theta)$ and the damping coefficients $d_r^p(\dot{\theta})$, $d_f^p(\dot{\theta})$ are in general functions of the pitch angle θ and velocity $\dot{\theta}$ respectively. Combining (2.60), (2.61) and (2.62) yields

$$J_{yc} \ddot{\theta} = c_{\Sigma}^p(\theta) \theta + d_{\Sigma}^p(\dot{\theta}) \dot{\theta} + m_s h_{pl} a_{x,m}, \quad (2.63)$$

where

$$c_{\Sigma}^p(\theta) := -c_{s,r}^p(\theta) l_{s,r}^2 - c_{s,f}^p(\theta) l_{s,f}^2, \quad (2.64a)$$

$$d_{\Sigma}^p(\dot{\theta}) := -d_r^p(\dot{\theta}) l_{d,r}^2 - d_f^p(\dot{\theta}) l_{d,f}^2, \quad (2.64b)$$

represent the effective stiffness and damping factors depending on pitch angle θ and rate $\dot{\theta}$ respectively. The individual distances of spring and damping elements can be assumed equal such that there exists a front distance (between front suspension elements and PC) defined by $\tilde{l}_f := \frac{1}{2}(l_{s,f} + l_{d,f})$ and similarly a rear distance $\tilde{l}_r := \frac{1}{2}(l_{s,r} + l_{d,r})$. Exploiting the argumentation of the simplified roll dynamics with respect to the parameters c_{Σ}^p and d_{Σ}^p it is assumed that the opposite suspension deflection of rear and front elements renders the modelling of the dominant nonlinearities redundant. Consequently, $c_{\Sigma}^p(\theta)$ and $d_{\Sigma}^p(\dot{\theta})$ are assumed constant and independent of θ and $\dot{\theta}$. At the end, the linear model of the pitch dynamics reads as

$$J_{yc} \ddot{\theta} = c_{\Sigma}^p \theta + d_{\Sigma}^p \dot{\theta} + m_s h_{pl} a_{x,m}, \quad (2.65)$$

with

$$c_{\Sigma}^p := -c_{s,r}^p \tilde{l}_r^2 - c_{s,f}^p \tilde{l}_f^2, \quad (2.66)$$

$$d_{\Sigma}^p := -d_r^p \tilde{l}_r^2 - d_f^p \tilde{l}_f^2. \quad (2.67)$$

2.4 Steering Dynamics

2.4.1 Conventional Steering

In order to govern the heading direction of a vehicle the driver operates the steering wheel and rotates the tires around the kingpin axis. Herein, a front-steering system with fixed rear wheels is assumed. The static steering ratio, denoted by i_s , depends on the maximum angle of lock and is a function of the steering wheel angle δ_h , i.e.

$$i_s = f(\delta_h). \quad (2.68)$$

Commonly that function is approximated by linearization for certain ranges, i.e.

$$i_{s,lin}(\delta_{h,r}) = \left. \frac{df(\delta_h)}{d\delta_h} \right|_{\delta_h=\delta_{h,r}} \Rightarrow \delta_w = \frac{\delta_h}{i_{s,lin}}. \quad (2.69)$$

There $\delta_{h,r}$ represents a certain steering wheel angle (range). In fact, elasticities in the mechanical steering system (gear, linkage, shaft) affect the ratio between wheel angle and steering wheel angle additionally. Figure 2.13 depicts a standard steering system where the mechanical parts are assumed stiff and backlash-free. Moreover, the elasticities are lumped in a torsional stiffness C_S [BÖR04]. It shows the kinematic and pneumatic trails n_k and n_p respectively. In general, both are not constant, i.e. the pneumatic trail n_p depends on tire load and slip angle (Section 2.2.1) and the kinematic trail n_k is a function of the steering angle and the trail angle γ_t [MW04, p.752]. The offset steering is governed by the distance l_d whereas the latter depends on the angle of inclined kingpin axis and the camber angle. In order to keep the model simple, the wheel angle δ_w is assumed to represent a mean value of the left and right wheel angles $\delta_{w,l}$ and $\delta_{w,r}$.

The sum of the lateral tire forces ${}_{w_{f,l}}F_{y,f}$, ${}_{w_{f,r}}F_{y,f}$ (Figure 2.13) is denoted by the variable $F_{y,f}$ (subscripts omitted on purpose). Then, the resulting wheel angle (in due consideration of the steering elasticity) reads as

$$\delta_w = \frac{\delta_h}{i_s} - \frac{1}{C_s} F_{y,f} (n_p + n_k). \quad (2.70)$$

That steering elasticity also affects the interpretation of the front cornering stiffness. Combining (2.24a) and (2.53a) with (2.70) the tire force reads as

$$F_{y,f}(\alpha_{fe}) = \underbrace{\frac{c_{\alpha_f}}{1 + c_{\alpha_f} \frac{n_k + n_p}{C_S}}}_{=:c_{\alpha_{fe}}} \left(\delta_w - \beta - \frac{l_{fe}\dot{\psi}}{v_x} - \frac{h_{rl}\dot{\varphi}}{v_x} \right). \quad (2.71)$$

As a consequence, the cornering stiffness $c_{\alpha_{fe}}$ is no longer a constant, but accounts for steering elasticities and kinematic/pneumatic trails. Furthermore, the modifica-

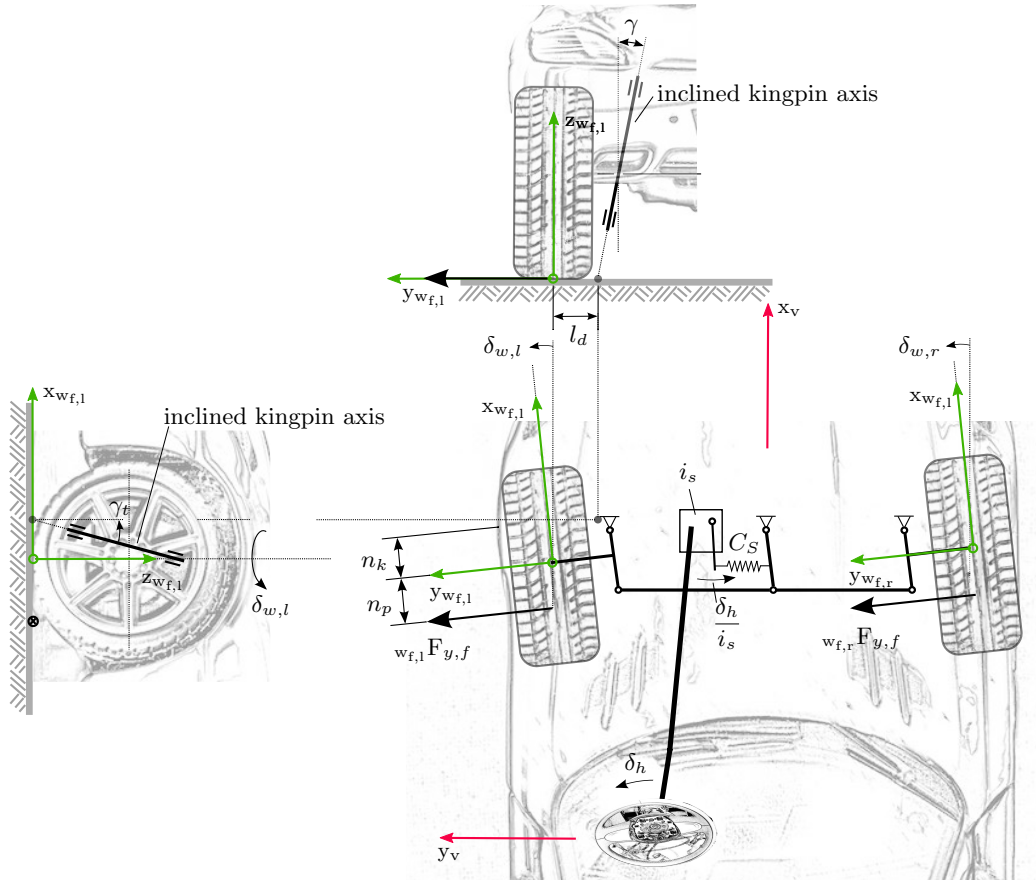


Figure 2.13: Front wheel schematics - Kinetics and Kinematics [MW04].

tions affect the coherence between parameters of the tire models Simplified Pacejka (SMF)/TM_Simple (TMs) and the lateral cornering stiffness. Note that the so-called *roll steering* effect [MW04] is not considered explicitly.

2.4.2 Electric Power Steering System

In modern passenger cars the conventional steering system is either implemented as electro-hydraulic power steering system (EHPS) or electric power steering (EPS) system. Comparing these two mechanisms, the latter provides advantages such as individual actuation, lower power consumption and additional functionality for enhanced vehicle safety and comfort, e.g. park assist [PH11]. Accordingly, a model of an electric power steering system will be integrated in the framework. Figure 2.14 shows the schematics of a typical EPS system. Therein, $T_{w,l}$, $T_{w,r}$ represent the left and right wheel torques interpreted as external inputs. These are given by the product of lateral tire forces and trail (pneumatic + kinematic). The electric motor EM is represented by its inertia J_m ,

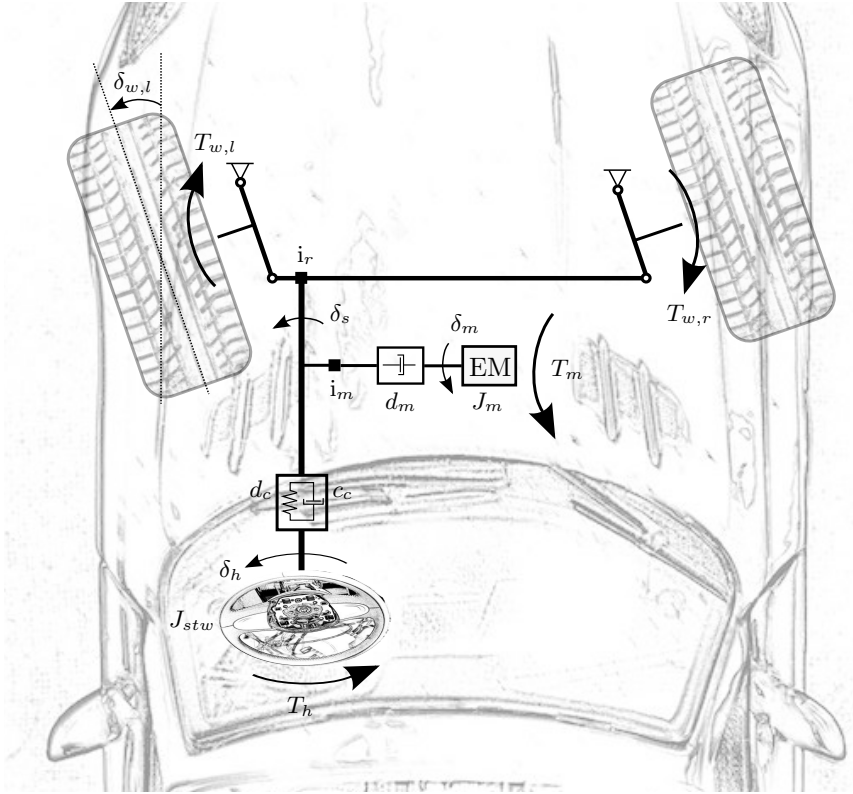


Figure 2.14: Electric Power Steering System Schematics.

the motor torque T_m and a damping coefficient d_m (viscous friction effects). The inertia of the steering wheel is given as J_{stw} , the stiffness of the column as c_c (torque sensor) and its damping coefficient as d_c . The transmission ratio from assistant motor to the column is defined by i_m and from steering column to the rack by i_r . Furthermore, T_h denotes the steering torque, δ_h the steering wheel angle, δ_m the motor angle, δ_s the column angle and $\delta_{w,l}$ the resulting (left) wheel angle.

The equations of the rotational motion can then be described by [ICDW11]

$$J_{stw} \ddot{\delta}_h = T_h - c_c (\delta_h - \delta_s) - d_c \dot{\delta}_h, \quad (2.72a)$$

$$J_{ca} \ddot{\delta}_s = c_c (\delta_h - \delta_s) - d_m i_m^2 \dot{\delta}_s + i_r^{-1} T_w + i_m T_m. \quad (2.72b)$$

The inertia J_{ca} constitutes of the column inertia J_c , motor inertia J_m and rack inertia J_r , i.e. $J_{ca} = J_c + i_m^2 J_m + i_r^{-2} J_r$. The external torque input T_w represents the sum of the left and right wheel torques $T_{w,l}$ and $T_{w,r}$.

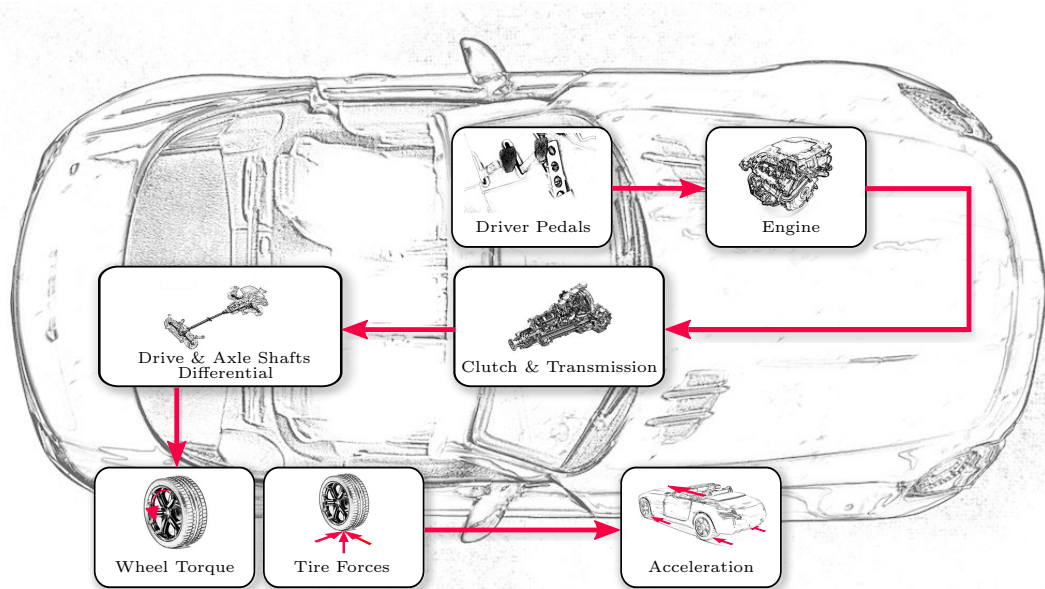


* Image Source: <http://www.caricos.com>

Figure 2.15: Modular structure of the vehicle powertrain.

2.5 Powertrain Dynamics

The acceleration performance of an automotive vehicle is governed by its maximum output torque at the wheels and the longitudinal tire forces [JAZ14]. The latter is not directly controllable as it mainly depends on the friction between road and tires. However, the torque available at the wheels is characterized by the powertrain, i.e. engine and driveline. Figure 2.15 depicts the most relevant components of a standard automotive powertrain¹⁹. The modelling of the powertrain dynamics serves the purpose to find a proper model of the dynamics from accelerator pedal position to vehicle acceleration. In general, a modular model structure of the components illustrated in Figure 2.15 would be preferable, but also requires adaption of the model to the actual vehicle configuration (w.r.t. its powertrain). For example, a vehicle with manual transmission necessitates different modelling than another with automatic transmission (e.g. dual clutch transmission), as do front-, rear-wheel or four-wheel driven vehicles.

The derived powertrain model is not intended to model oscillation or vibration effects subject of e.g. [TE09, FWE02].

Standard modelling procedures of the powertrain components are presented and discussed in the following for further use.

¹⁹Note that vehicles with hybrid propulsion require additional components and are not considered for the modelling.

Engine Dynamics

The internal combustion engine that is considered as *standard* propulsion source requires complex models to describe the physical effects of injection, combustion, gas exchange etc. required for torque generation, e.g. [HEY88, MT14]. However, these models are not useful for real-time application. Even when considering so-called mean-value²⁰ models the engine torque is a nonlinear function of many variables, such as fuel mass, air/fuel-ratio, recirculated exhaust gas ratio, engine speed, injection timing, number of injections and others [GO10].

A more interesting approach, especially with respect to the current application, is the use of a neural network to describe the resulting engine torque [HH03]. From a modelling perspective this refers to Black Box modelling as only the in- and outputs of the system *internal combustion engine* are relevant. Aside its high potential to describe nonlinear effects this method renders the knowledge of engine specific parameters unnecessary. Hence, the type of combustion engine only changes the input variables of the network whereas the size, operating principle etc. of the engine do not affect the system modelling at all. Furthermore, in contrast to linear models, aiming to approximate the engine's dynamics by several simplifications and consequently sacrificing accuracy the neural network retains these nonlinearities for a proper estimation of the effective torque. The latter can then be forwarded to the driveline model as system input.

Driveline Dynamics

For modelling of the driveline dynamics the elements of engine, clutch, transmission, drive shaft, differential and axle shafts need further considerations [KD97, GIL92]. Modelling of the engine is performed to that extent that its mechanical dynamics are modelled as [GO10]

$$J_e \frac{d\omega_e}{dt} = T_e - T_l, \quad (2.73)$$

where the engine torque (including losses) is denoted by T_e , the load torque is T_l , engine moment of inertia is J_e and engine speed ω_e . A simple model of the clutch and transmission is provided in [KD97]. Moreover, [RAJ12] discusses the modelling of a standard torque converter. Assuming an engaged clutch (which is reasonable during acceleration in a specific gear) and a transmission, where friction is neglected (as is its moment of inertia) the algebraic relation between the torques reads as

$$T_l = T_p \frac{1}{i_t}, \quad (2.74)$$

²⁰The term *mean-value* emphasizes that these models do not reflect the crankangle-based dynamics, but mean values of engine outputs [GO10, RAJ12].

with T_p being the torque output of the transmission and i_t the transmission ratio. The drive shaft is also assumed stiff, such that the torque of the transmission is equal to the torque of the differential. In terms of the axle shafts it is assumed that the vehicle is not excited in lateral direction and as a consequence these can be lumped into a single one. The differential drive is modelled similarly to the transmission, i.e. its inertia and friction are disregarded and the torque is affected by a coefficient i_f . Then, the most basic driveline model connecting engine and wheel is given by the algebraic relation

$$T_l = T_w \frac{1}{i_t i_f} \quad (2.75)$$

All these modelling assumptions are discussed in [KD97]. Finally, a correspondence between the engine torque and the vehicle acceleration (in longitudinal direction) can be formulated as

$$a_x = \frac{i_f i_t}{r \bar{m}} \left[T_e - J_e \frac{d}{dt} \omega_e - \frac{r {}_v F_{aero}}{i_f i_t} \right]. \quad (2.76)$$

This relation assumes a negligible road inclination and rolling resistance ${}_v F_R$. The aerodynamic drag force ${}_v F_{aero}$ is defined in (2.2). Furthermore, \bar{m} is defined by [MW04]

$$\bar{m} := m + \sum_{j=1}^n \frac{J_{Tj}}{r_j^2}, \quad (2.77)$$

where m denotes the total vehicle mass, J_{Tj} the sum of wheel inertia w.r.t. their rotation axis (per axle) and r_j the static tire radius related to axle j . Hence, for a standard vehicle (e.g. front-driven) the index n equals 1 - losses of the rear axle can be neglected.

2.6 Human Perception

The integration of the driver perception into the handling evaluation process is suggested in [DEC09] and implemented in [SCH10]. Before focusing on the modelling of the human senses the term *perception* will be introduced as "data acquisition of physical stimuli by the human senses" [SCH10, SL07]. This is contradictory to *cognition* including an individual interpretation of the perception.

A motion transformation of the measured signals to the driver axis system needs to be performed before these can be fed into the perception models. [SCH10] identified the most relevant senses related to handling evaluation, i.e. visual perception (velocities, sideslip angle, yaw rate), vestibular system (translational/angular accelerations), muscle spindles and Golgi tendon organs (steering wheel torque and angle).

Transformation of Acceleration Signals to Driver Head Axis System

The calculation of the driver perception signals requires transformation of the input signals (e.g. translational accelerations) into the coordinate system of the driver's head. Exploiting the assumption of a rigid body the angular accelerations are all invariant w.r.t. the actual position. In contrast, the translational accelerations need to be transformed from the vehicle's CoG to the considered axis system origin.

First, the position vector between the CoG and the origin \mathcal{O}_d ²¹ needs to be determined. Second, the human head dynamics need to be described in order to be able to calculate the position vector. And third, the accelerations w.r.t. the CoG will be transformed to \mathcal{O}_d .

Figure 2.16 illustrates the head movement w.r.t. to the vehicle chassis. There, the human body (apart from its head) is assumed static at a fixed position denoted by the vector ${}_{\mathbf{v}}\mathbf{x}_{d,stat} := [l_{h,x} \ l_{h,y} \ l_{h,z}]^T$. The roll and pitch movement of the head are denoted by φ_h and θ_h respectively. The dynamics of the head can be modelled by a spring-mass-damper system with linear characteristics. The resulting transfer function $G_{h,\varphi}(s)$ reads as [SCH10]

$$G_{h,\varphi}(s) = \frac{\bar{\varphi}_h(s)}{\bar{\varphi}(s)} = \frac{1}{\frac{J_h}{c_h} s^2 + 2\sqrt{\frac{J_h}{c_h}} s + 1}, \quad (2.78)$$

with $J_h = \frac{2}{5}m_h r_h^2 + m_h r_l^2$ being the moment inertia of the head w.r.t. to the rotation axis, m_h the mass of the head, r_h the head radius and r_l the distance between the head's CoG and the rotation axis. Furthermore, c_h denotes the rotation stiffness defined as $c_h = 10\pi \cdot J_h$. Parameter values are extracted from [SCH10]. For the sake of completeness, the missing parameters are standardized as $m_h = 5\text{kg}$, $r_h = 0.085\text{m}$ and $r_l = 0.2\text{m}$, see ÖNORM DIN 33402-2. The calculation of the pitch angle θ_h is straightforward as the head dynamics for the pitch rotation are identical.

Now, that the rotation angles are known, the position vector ${}_{\mathbf{v}}\mathbf{x}_{d,pos}$ relating the driver's head CoG to the vehicle's CoG can be calculated as

$$\begin{bmatrix} x_{d,od} \\ y_{d,od} \\ z_{d,od} \end{bmatrix} = \underbrace{\begin{bmatrix} l_{h,x} \\ l_{h,y} \\ l_{h,z} \end{bmatrix}}_{= {}_{\mathbf{v}}\mathbf{x}_{d,stat}} + \begin{bmatrix} r_l \cos\varphi_h \sin\theta_h \\ -r_l \sin\varphi_h \cos\theta_h \\ r_l \cos\varphi_h \cos\theta_h \end{bmatrix}. \quad (2.79)$$

²¹Note that the (driver) head-fixed axis system $\mathcal{C}_d = \{\mathcal{O}_d; x_d, y_d, z_d\}$ is not listed in Appendix A as it is not standardized. Its origin \mathcal{O}_d is located at the driver's head CoG and it is a right-hand side axis system. Its vertical axis points upwards, governed by the head roll and pitch angle. The x_d -axis points forwards (in driving direction). Rotary head motion is not modelled.

Finally, exploiting (2.79) and assuming the angular velocities in the vehicle-fixed axis system to be equal to the earth-fixed ones²² the transform of accelerations from CoG to any arbitrary point reads as [KOB03]

$$\underbrace{\begin{bmatrix} a_{x,od} \\ a_{y,od} \\ a_{z,od} \end{bmatrix}}_{=: {}_v\mathbf{a}_{od}} = \begin{bmatrix} a_x \\ a_y \\ a_z \end{bmatrix} + \begin{bmatrix} \ddot{\theta} z_{d,od} - \ddot{\psi} y_{d,od} - (\dot{\psi}^2 + \dot{\theta}^2) x_{d,od} + \dot{\theta} \dot{\varphi} y_{d,od} + \dot{\varphi} \dot{\psi} z_{d,od} \\ \ddot{\psi} x_{d,od} - \ddot{\varphi} z_{d,od} + \dot{\theta} \dot{\varphi} x_{d,od} - (\dot{\varphi}^2 + \dot{\psi}^2) y_{d,od} + \dot{\psi} \dot{\theta} z_{d,od} \\ \ddot{\varphi} y_{d,od} - \ddot{\theta} x_{d,od} - \dot{\varphi} \dot{\psi} x_{d,od} + \dot{\psi} \dot{\theta} y_{d,od} - (\dot{\varphi}^2 + \dot{\theta}^2) z_{d,od} \end{bmatrix}. \quad (2.80)$$

Now, the resulting acceleration vector at position \mathcal{O}_d can be transformed into driver head coordinates by ${}_d\mathbf{a}_{od} = \mathbf{T}_{dv} {}_v\mathbf{a}_{od}$ with

$$\mathbf{T}_{dv} = \begin{bmatrix} \cos\theta_h & 0 & \sin\theta_h \\ \sin\varphi_h \sin\theta_h & \cos\varphi_h & -\sin\varphi_h \cos\theta_h \\ -\cos\varphi_h \sin\theta_h & \sin\varphi_h & \cos\varphi_h \cos\theta_h \end{bmatrix}. \quad (2.81)$$

Transformation of Velocity Signals to Driver Head Axis System

The transformation of velocities from vehicle CoG to \mathcal{C}_d exploits (2.78), (2.79) and (2.81). Solely, the transformation (2.80) is different, i.e. [KOB03]

$$\underbrace{\begin{bmatrix} v_{x,od} \\ v_{y,od} \\ v_{z,od} \end{bmatrix}}_{=: {}_v\mathbf{v}_{od}} = \begin{bmatrix} v_x \\ v_y \\ v_z \end{bmatrix} + \begin{bmatrix} \dot{\theta} z_{d,od} - \dot{\psi} y_{d,od} \\ \dot{\psi} x_{d,od} - \dot{\varphi} z_{d,od} \\ \dot{\varphi} y_{d,od} - \dot{\theta} x_{d,od} \end{bmatrix}. \quad (2.82)$$

Finally, the velocity vector ${}_d\mathbf{v}_{od}$ can be calculated as ${}_d\mathbf{v}_{od} = \mathbf{T}_{dv} {}_v\mathbf{v}_{od}$.

Visual Perception

The eye acting as human visual sensor detects translational and angular velocities with some time delay. Hence, the transfer function of the visual sensor consists of a pure dead-time delay [WBGH06], i.e.

$$G_{eye,v}(s) = \frac{\bar{v}_{eye}(s)}{\bar{v}_m(s)} = e^{-\tau_e s}, \quad (2.83)$$

²²This is reasonable as only great values of road inclination or bank angle (e.g. steep bank curve) have a recognizable influence on the angular velocities. See [KOB03] for details.

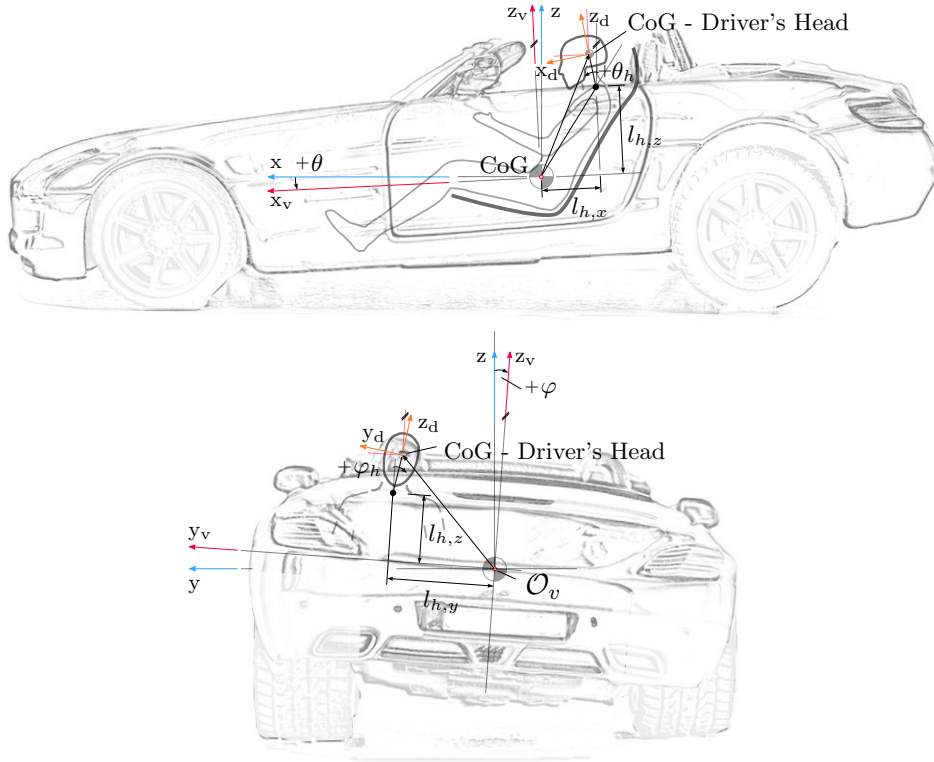


Figure 2.16: Lateral and rear view of driver's head position.

where the dead-time is given by $\tau_e = 0.15s$ for the central visual field [HS99]. The input signal of the transfer function is a velocity (in x-, y- or z-direction) transformed to the driver head-fixed coordinate system, i.e. equation (2.82). The transfer function of angular velocities $G_{eye,\omega}(s)$ is identical to (2.83). However, angular velocities do not have to be transformed and measured quantities can be fed to the transfer function directly.

Semi-circular Canals

The vestibular system consists of three semi-circular canals sensing angular accelerations and so-called otoliths sensing translational accelerations [SL07]. Due to similarities between the sensed signals and the yaw rate the model is based on a lead filter approximating a pure integrator at high input frequencies [WBGH06]. The transfer function of a semi-circular canal reads as

$$G_{scc}(s) = \frac{\bar{\omega}_{scc}(s)}{\bar{\alpha}_m(s)} = K \frac{1 + \tau_L s}{1 + \tau_i s} \underbrace{\frac{\tau_a s}{\tau_a s + 1}}_{=: A_{scc}(s)}. \quad (2.84)$$

For K , τ_L and τ_i different identification results can be found in literature, e.g. [HBS⁺05, HJ78]. Here, the values chosen are extracted from [WBGH06] and read as $K = 5.9$, $\tau_L = 0.11s$ and $\tau_i = 5.9s$. $A_{scc}(s)$ represents an adaption function as presented in [SCH10] to model the human sense adaption capabilities. The parameter τ_a is selected as $\tau_a = 80s$ [SCH10, WIL02]. Note that the system input of the transfer functions (one per rotation axis) are angular accelerations that need to be calculated, if not measured.

Otoliths The otoliths are sensitive to translational accelerations and for the mathematical modelling there exist numerous approaches differing in complexity [HJ78]. Here, a simple model combined with an adaption function valid for irregular otoliths²³, as discussed in [SCH10], is employed, i.e.

$$G_{oto}(s) = \frac{\bar{a}_{oto}(s)}{\bar{a}_m(s)} = \frac{1 + \tau_L s}{1 + \tau_i s} \underbrace{\frac{K_a \tau_a s + 1}{\tau_a s + 1}}_{=: A_{oto}(s)}. \quad (2.85)$$

Parameter values are given in [WBGH06] and [SCH10]. The adaption parameters are $K_a = 1.12$, $\tau_a = 87.5s$ and furthermore $\tau_L = 0.3s$, $\tau_i = 0.12s$. System inputs are the transformed, measured accelerations ${}_d\mathbf{a}_{od}$. There exists one transfer function per acceleration component.

Angular Rate Perception

Both, the semi-circular canals and the visual system provide angular rate as system output. Combining these two can be achieved by [WBGH06, VDS98]

$$\omega_p = \omega_{scc} + \Delta\omega - \tau_a \frac{d\Delta\omega_{filt}}{dt}, \quad (2.86)$$

where ω_p is the resulting angular rate of human perception, $\Delta\omega := \omega_{eye} - \omega_{scc}$ describes the difference in angular rate perception (between visual system and semi-circular canals), $\Delta\omega_{filt}$ is the low-pass filtered $\Delta\omega$. The low-pass filter time constant is given as $\tau_a = 3s$ [WBGH06].

Steering Wheel Perception

The muscle spindle is sensitive to muscle length and velocity [PIC04]. Its mathematical model assumes the displacement of the operating element (i.e. steering wheel in this case) as input [BB90]. Then the transfer function can be formulated as

$$G_{ms}(s) = \frac{\bar{\delta}_{h,ms}(s)}{\bar{\delta}_h(s)} = K \frac{\tau_l s + 1}{\tau_L s + 1} e^{-\tau_m s} \quad (2.87)$$

²³Due to [HJ78] the irregular otoliths show higher sensitivity as the regular ones w.r.t. rate of change.

with $K = 46.6$, $\tau_L = 0.02s$, $\tau_l = 0.103s$ and $\tau_m = 0.02s$ [SCH10, BB90].

Steering Torque Perception

The Golgi tendon organs (GTO), responsible for the regulation of the muscle tension [PIC04], are used for measuring the applied force [BB90]. In general, the input variable of the GTO is the muscle tension. However, based on the argumentation of [SCH10] the steering torque can be used directly as input to the model, i.e.

$$G_{gto}(s) = \frac{\bar{T}_{h,p}(s)}{\bar{T}_h(s)} = \frac{b_2s^2 + b_1s + b_0}{s^2 + a_1s + a_0} e^{-\tau_g s}. \quad (2.88)$$

The parameters are taken from [BB90, SCH10] and read as $b_2 = 0.5$, $b_1 = 0.8$, $b_0 = 0.24$, $a_1 = 1.6$, $a_0 = 0.64$, $\tau_g = 0.02s$.

3

Analyses of Vehicle Dynamics Models

The formulation of the proposed differential equations using an abstract formalism, i.e. the state-space representation, introduces increased readability and a certain degree of flexibility. For example, it is not necessary that the physical values of interest, e.g. the yaw rate, are identical to the state variables. However, before the state-space related observer design techniques can be applied some characteristics of the proposed models are to be analyzed, i.e. parameter sensitivity, observability and influence of sensor configurations on the state reconstruction objective.

The first part of this chapter deals with a theoretical introduction to the parameter sensitivity analysis, observability and also controllability/observability measures that are used for sensor configuration selection.

Thereafter, the presented theory will be applied to all models proposed in the previous chapter by exploiting a systematic approach of selecting the model parameters to be identified. In general, these parameters map the generic mathematical models to individual vehicle configurations. The herein proposed approach is twofold. First, a conducted parameter sensitivity study reveals the sensitivity of each system state to parameter changes. Second, results from existing literature will be exploited to quantify these parameters by static measurements. These two independent sources of information allow a systematic selection of the parameters to be identified later on.

Furthermore, a prerequisite allowing for employment of state estimators is the observability of the considered system. Consequently, it is necessary to show this property for all proposed models and sensor configurations respectively. Referring to the latter, the selection of sensors will be analyzed from the perspective of observation, i.e. measures of observability are exploited to provide some quantitative information how "well" the system can be observed given some system output. That extends the idea of basic

observability analysis commonly yielding only a binary result. Finally, these measures suggest a set of sensors for the task of state and parameter identification. This chapter aims to provide a set of parameters for the identification task and a suggestion of an effective sensor configuration for the models discussed in Chapter 2.

3.1 Theoretical Background

3.1.1 Parameter Sensitivity Analysis

In general, there are different approaches to examine the parametric sensitivity of a dynamical system, e.g. iterative simulations of a model with varying parameter sets. However, even if the computational power of standard personal computers increases steadily, the time consumption might become reasonable depending on the number of parameters and also their variation range.

In [KHA02] an interesting theoretical framework for sensitivity analysis of dynamical systems in *time* domain is proposed. A similar approach (extended by *frequency* domain analysis) is exploited in [NAL89] to investigate the sensitivity of vehicle dynamics systems to parameter variations. Herein, these frameworks (exactly speaking sensitivity functions in time domain) will be employed to evaluate the parametric sensitivity of the, in Chapter 2, proposed models.

First-order Sensitivity Functions

Given a general, nonlinear dynamical system represented in state-space form, i.e.

$$\frac{\partial \mathbf{x}}{\partial t} = \mathbf{f}(\mathbf{x}(t, \boldsymbol{\rho}), \boldsymbol{\rho}, \mathbf{u}(t)), \quad \mathbf{x}(t_0) = \mathbf{x}_0, \quad (3.1)$$

where $t \in \mathbb{R}^+$ denotes the time, $\mathbf{x}(t, \boldsymbol{\rho}) \in \mathbb{R}^n$ the state vector, $\mathbf{u}(t) \in \mathbb{R}^m$ the input vector, $\boldsymbol{\rho} \in \mathbb{R}^r$ the constant parameter vector and \mathbf{x}_0 the known initial condition¹. The function $\mathbf{f} : D_f \subseteq \mathbb{R}^n \times \mathbb{R}^r \times \mathbb{R}^m \rightarrow \mathbb{R}^n$ is assumed continuous in \mathbf{x} , $\boldsymbol{\rho}$ and \mathbf{u} (Remark: In a mathematically rigorous way it is $\mathbf{x}(t, \boldsymbol{\rho})$, $\mathbf{u}(t)$. However, the arguments are dropped sometimes for the reason of better readability.). Furthermore, $\mathbf{f}(\cdot)$ is continuously differentiable w.r.t. \mathbf{x} and $\boldsymbol{\rho}$ for all $(\mathbf{x}, \boldsymbol{\rho}, \mathbf{u}) \in D_f$ [KHA02]. Then, replacing $\boldsymbol{\rho}$ by the nominal parameter vector $\bar{\boldsymbol{\rho}}$, system (3.1) has a unique solution $\bar{\mathbf{x}}(t, \bar{\boldsymbol{\rho}})$. In [KHA02] it is shown explicitly that, if $\|\boldsymbol{\rho} - \bar{\boldsymbol{\rho}}\| < \varepsilon$, with $\varepsilon > 0$, system (3.1) has a unique solution $\mathbf{x}(t, \boldsymbol{\rho})$ that is close to $\bar{\mathbf{x}}(t, \bar{\boldsymbol{\rho}})$, i.e. the nominal one.

¹Note that the initial condition is independent of the parameter vector $\boldsymbol{\rho}$.

The partial derivative of (3.1) w.r.t. $\boldsymbol{\rho}$ yields²

$$\frac{\partial}{\partial t} \left(\frac{\partial \mathbf{x}}{\partial \boldsymbol{\rho}} \right) = \mathbf{A}_S(t, \boldsymbol{\rho}) \frac{\partial \mathbf{x}}{\partial \boldsymbol{\rho}} + \mathbf{B}_S(t, \boldsymbol{\rho}), \quad (3.2)$$

with

$$\mathbf{A}_S(t, \boldsymbol{\rho}) := \left. \frac{\partial \mathbf{f}(\mathbf{x}, \boldsymbol{\rho}, \mathbf{u})}{\partial \mathbf{x}} \right|_{\mathbf{x}=\mathbf{x}(t, \boldsymbol{\rho})}, \quad \mathbf{B}_S(t, \boldsymbol{\rho}) := \left. \frac{\partial \mathbf{f}(\mathbf{x}, \boldsymbol{\rho}, \mathbf{u})}{\partial \boldsymbol{\rho}} \right|_{\mathbf{x}=\mathbf{x}(t, \boldsymbol{\rho})}. \quad (3.3)$$

Due to the independence of the initial value \mathbf{x}_0 on the parameter vector $\boldsymbol{\rho}$ the initial value of (3.2) is given as $\left. \frac{\partial \mathbf{x}_0}{\partial \boldsymbol{\rho}} \right|_{\boldsymbol{\rho}=\bar{\boldsymbol{\rho}}} = \mathbf{0}$. The so-called sensitivity function $\mathbf{S}(t)$ is defined as

$$\mathbf{S}(t) := \left. \frac{\partial \mathbf{x}(t, \boldsymbol{\rho})}{\partial \boldsymbol{\rho}} \right|_{\boldsymbol{\rho}=\bar{\boldsymbol{\rho}}}, \quad (3.4)$$

solving the sensitivity equation

$$\frac{d}{dt} \mathbf{S}(t) = \mathbf{A}_S(t, \bar{\boldsymbol{\rho}}) \mathbf{S}(t) + \mathbf{B}(t, \bar{\boldsymbol{\rho}}), \quad \mathbf{S}(t_0) = \mathbf{0}, \quad (3.5)$$

uniquely. Note that the latter definitions refer to the nominal parameter vector $\bar{\boldsymbol{\rho}}$, i.e. the matrices $\mathbf{A}(t, \bar{\boldsymbol{\rho}})$ and $\mathbf{B}(t, \bar{\boldsymbol{\rho}})$ are defined as in (3.3), but evaluated for $\mathbf{x} = \bar{\mathbf{x}}(t, \bar{\boldsymbol{\rho}})$ and $\boldsymbol{\rho} = \bar{\boldsymbol{\rho}}$. In terms of structural composition the time-varying matrix $\mathbf{S}(t) \in \mathbb{R}^{n \times r}$ generally looks like

$$\mathbf{S}(t) = \left. \begin{bmatrix} \frac{\partial x_1}{\partial \rho_1} & \frac{\partial x_1}{\partial \rho_2} & \cdots & \frac{\partial x_1}{\partial \rho_r} \\ \frac{\partial x_2}{\partial \rho_1} & \frac{\partial x_2}{\partial \rho_2} & \cdots & \frac{\partial x_2}{\partial \rho_r} \\ \vdots & \vdots & \ddots & \vdots \\ \frac{\partial x_n}{\partial \rho_1} & \frac{\partial x_n}{\partial \rho_2} & \cdots & \frac{\partial x_n}{\partial \rho_r} \end{bmatrix} \right|_{\boldsymbol{\rho}=\bar{\boldsymbol{\rho}}}. \quad (3.6)$$

The elements $\frac{\partial x_i}{\partial \rho_j}$, with $i = 1 \dots n$ and $j = 1 \dots r$, are defined as *first-order sensitivity functions* and represent the sensitivity of the state x_i to parameter variations of ρ_j . In order to determine the sensitivity of a state variable x_i to the complete parameter vector $\boldsymbol{\rho}$ the i -th row of \mathbf{S} needs to be extracted. Moreover, the j -th column of \mathbf{S} reveals

²By assuming continuity and continuous differentiability of $\mathbf{f}(\cdot)$ the partial differentiation is commutative, see e.g. Theorem of Schwarz [LAN87, p.83].

information on the sensitivity of the complete state vector \mathbf{x} on a single parameter ρ_j . The structure of the time-varying dynamic matrix $\mathbf{A}_S \in \mathbb{R}^{n \times n}$ and the input matrix $\mathbf{B}_S \in \mathbb{R}^{n \times r}$ defined by (3.3) read as

$$\mathbf{A}_S(t, \boldsymbol{\rho}) = \begin{bmatrix} \frac{\partial}{\partial x_1} f_1(\mathbf{x}, \boldsymbol{\rho}, \mathbf{u}) & \dots & \dots & \frac{\partial}{\partial x_n} f_1(\mathbf{x}, \boldsymbol{\rho}, \mathbf{u}) \\ \frac{\partial}{\partial x_1} f_2(\mathbf{x}, \boldsymbol{\rho}, \mathbf{u}) & \frac{\partial}{\partial x_2} f_2(\mathbf{x}, \boldsymbol{\rho}, \mathbf{u}) & \dots & \frac{\partial}{\partial x_n} f_2(\mathbf{x}, \boldsymbol{\rho}, \mathbf{u}) \\ \vdots & \vdots & \ddots & \vdots \\ \frac{\partial}{\partial x_1} f_n(\mathbf{x}, \boldsymbol{\rho}, \mathbf{u}) & \frac{\partial}{\partial x_2} f_n(\mathbf{x}, \boldsymbol{\rho}, \mathbf{u}) & \dots & \frac{\partial}{\partial x_n} f_n(\mathbf{x}, \boldsymbol{\rho}, \mathbf{u}) \end{bmatrix}, \quad (3.7a)$$

$$\mathbf{B}_S(t, \boldsymbol{\rho}) = \begin{bmatrix} \frac{\partial}{\partial \rho_1} f_1(\mathbf{x}, \boldsymbol{\rho}, \mathbf{u}) & \frac{\partial}{\partial \rho_2} f_1(\mathbf{x}, \boldsymbol{\rho}, \mathbf{u}) & \dots & \frac{\partial}{\partial \rho_r} f_1(\mathbf{x}, \boldsymbol{\rho}, \mathbf{u}) \\ \frac{\partial}{\partial \rho_1} f_2(\mathbf{x}, \boldsymbol{\rho}, \mathbf{u}) & \frac{\partial}{\partial \rho_2} f_2(\mathbf{x}, \boldsymbol{\rho}, \mathbf{u}) & \dots & \frac{\partial}{\partial \rho_r} f_2(\mathbf{x}, \boldsymbol{\rho}, \mathbf{u}) \\ \vdots & \vdots & \ddots & \vdots \\ \frac{\partial}{\partial \rho_1} f_n(\mathbf{x}, \boldsymbol{\rho}, \mathbf{u}) & \dots & \dots & \frac{\partial}{\partial \rho_r} f_n(\mathbf{x}, \boldsymbol{\rho}, \mathbf{u}) \end{bmatrix}. \quad (3.7b)$$

Now, these sensitivity functions can be exploited to approximate the solution $\mathbf{x}(t, \boldsymbol{\rho})$, given the difference between $\bar{\boldsymbol{\rho}}$ and $\boldsymbol{\rho}$ is within the assumed ε -range. Then the solution reads as

$$\mathbf{x}(t, \boldsymbol{\rho}) \approx \mathbf{x}(t, \bar{\boldsymbol{\rho}}) + \underbrace{\mathbf{S}(t)(\boldsymbol{\rho} - \bar{\boldsymbol{\rho}})}_{=:\Delta \mathbf{x}(t, \Delta \boldsymbol{\rho})}. \quad (3.8)$$

Neglecting higher-order terms in the Taylor series expansion of $\mathbf{x}(t, \bar{\boldsymbol{\rho}} + \Delta \boldsymbol{\rho})$ leads to the approximative character of this method. Here, $\Delta \boldsymbol{\rho}$ denotes the difference between the parameter vectors $\boldsymbol{\rho}$ and $\bar{\boldsymbol{\rho}}$, i.e. $\Delta \boldsymbol{\rho} := \boldsymbol{\rho} - \bar{\boldsymbol{\rho}}$. The term $\Delta \mathbf{x}(t, \Delta \boldsymbol{\rho})$ represents the deviation of the solution $\mathbf{x}(t, \boldsymbol{\rho})$ (due to parameter variations) from the nominal $\bar{\mathbf{x}}(t, \bar{\boldsymbol{\rho}})$.

Second-order Sensitivity Functions

In general, calculation of the first-order sensitivity functions allows to evaluate the effect of parameter changes on the state variables. However, in some cases the first-order sensitivity functions might not provide the information required. Then, a second-order approach can be considered by building the partial derivative of (3.2) w.r.t. the parameter vector $\boldsymbol{\rho}$. Theoretically these second-order sensitivity functions do provide a higher

sensitivity to parameter changes. Further details can be found in [NAL89].

3.1.2 Observability

Given a linear, time-invariant system of the form

$$\frac{d\mathbf{x}}{dt} = \mathbf{A}\mathbf{x} + \mathbf{B}\mathbf{u}, \quad (3.9a)$$

$$y = \mathbf{C}\mathbf{x} \quad (3.9b)$$

where $\mathbf{x}(t) \in \mathbb{R}^n$ represents the state vector, $\mathbf{A} \in \mathbb{R}^{n \times n}$ the system matrix, $\mathbf{B} \in \mathbb{R}^{n \times m}$ the input matrix and $\mathbf{C} \in \mathbb{R}^{p \times n}$ the output matrix. The vectors $\mathbf{u}(t) \in \mathbb{R}^m$ and $\mathbf{y}(t) \in \mathbb{R}^p$ are referred to as system inputs and outputs respectively. Furthermore, the initial condition of (3.9) is defined as $\mathbf{x}_0 := \mathbf{x}(t_0)$.

Theorem 1. *System (3.9) or pair (\mathbf{C}, \mathbf{A}) is said to be observable if any unknown initial condition \mathbf{x}_0 can be recovered uniquely from knowledge of $\mathbf{u}(t)$ and $\mathbf{y}(t)$ over a finite time period $[0, T]$ with $T > 0$.*

In order to check for observability (of linear systems) there exist various necessary and sufficient criteria [POZ10, KAL11, MAR03]. Three of them are listed in the following:

1. The *observability Gramian* $\mathbf{Q}_G(t)$:

$$\mathbf{Q}_G(t) := \int_{t_0}^t e^{\mathbf{A}^T(t_0-\tau)} \mathbf{C}^T \mathbf{C} e^{\mathbf{A}(t_0-\tau)} d\tau, \quad (3.10)$$

needs to be positive definite for $t > 0$.

2. The *observability matrix* $\mathbf{O} \in \mathbb{R}^{np \times n}$ defined as

$$\mathbf{O} = \begin{bmatrix} \mathbf{C} \\ \mathbf{C}\mathbf{A} \\ \mathbf{C}\mathbf{A}^2 \\ \vdots \\ \mathbf{C}\mathbf{A}^{n-1} \end{bmatrix} \quad (3.11)$$

has full column rank.

3. Given an eigenvalue λ_i with $i = 1 \dots n$ and the corresponding eigenvector \mathbf{p}_i of the matrix \mathbf{A} , such that $\mathbf{A}\mathbf{p}_i = \lambda_i \mathbf{p}_i$ is fulfilled, then the system is called *observable* if for all eigenvectors $\mathbf{C}\mathbf{p}_i \neq \mathbf{0}$ holds.

Now, the considered class of systems is more generalized to nonlinear systems of the form

$$\frac{d\mathbf{x}}{dt} = \mathbf{f}(\mathbf{x}, \mathbf{u}), \quad (3.12a)$$

$$y = h(\mathbf{x}), \quad (3.12b)$$

with $\mathbf{x}(t) \in \mathbb{R}^n$, $\mathbf{u}(t) \in \mathbb{R}^m$, $\mathbf{y}(t) \in \mathbb{R}^p$, the initial state $\mathbf{x}_0 := \mathbf{x}(t_0)$ and the functions $\mathbf{f} : D_1 \subseteq \mathbb{R}^n \times \mathbb{R}^m \rightarrow \mathbb{R}^n$, $h : D_2 \subseteq \mathbb{R}^n \rightarrow \mathbb{R}$ are smooth. In terms of system classification (3.12) is referred to as multi-input single-output system. The more general case of a vector-valued output \mathbf{y} is considered in [NVDS90]. For the case of nonlinear systems the scope of observability is split into *locally*³ and *globally*⁴. The following definitions are from [BIR92].

Theorem 2. *System (3.12) is called locally observable in a point \mathbf{x}_p , if all unknown initial conditions \mathbf{x}_0 in a neighborhood $\mathcal{N} : \|\mathbf{x}_0 - \mathbf{x}_p\| < \varepsilon > 0$ of \mathbf{x}_p can be reconstructed uniquely from $\mathbf{u}(t)$ and $\mathbf{y}(t)$ with $t_0 \leq t \leq t_1 < \infty$. Furthermore, it is called locally observable if the previous condition holds for all $\mathbf{x}_p \in \mathbb{R}^n$ and $\mathbf{u} \in \mathbb{R}^m$.*

Remark: Interestingly, and this is different to the class of linear systems, the observability of a nonlinear system is also a function of the system input \mathbf{u} .

Theorem 3. *System (3.12) is called globally observable, if the unknown initial state vector \mathbf{x}_0 can be reconstructed uniquely from knowledge of $\mathbf{u}(t)$ and $\mathbf{y}(t)$ with $t_0 \leq t \leq t_1 < \infty$ for all $\mathbf{x}_0 \in \mathbb{R}^n$ and $\mathbf{u} \in \mathbb{R}^m$.*

The observation space \mathcal{O} (not to be confused with the origin of the axis systems of Appendix A) of system (3.12) is given by the output y and its time derivatives [HK77]

$$\mathcal{O} = \left\{ y \quad \frac{dy}{dt} \quad \frac{d^2y}{dt^2} \quad \dots \quad \frac{d^{n-1}y}{dt^{n-1}} \right\}. \quad (3.13)$$

Exactly speaking, the time derivatives of the output function y are functions of the state

³In literature, often a subtle differentiation between different types of observability is provided, see e.g. [NVDS90, HK77, GB81]. Herein, it is assumed sufficient to distinguish between *local* and *global* observability.

⁴This is in contrast to the class of linear, time-invariant systems, where the local observability implies the global and vice versa.

\mathbf{x} , but also the input vector \mathbf{u} and its time derivatives, i.e.

$$y = h(\mathbf{x}), \quad (3.14a)$$

$$\frac{dy}{dt} = \underbrace{\frac{\partial h(\mathbf{x})}{\partial \mathbf{x}} \mathbf{f}(\mathbf{x}, \mathbf{u})}_{=:\Psi_1(\mathbf{x}, \mathbf{u})} \quad (3.14b)$$

$$\frac{d^2 y}{dt^2} = \underbrace{\frac{\partial \Psi_1(\mathbf{x}, \mathbf{u})}{\partial \mathbf{x}} \mathbf{f}(\mathbf{x}, \mathbf{u}) + \frac{\partial \Psi_1(\mathbf{x}, \mathbf{u})}{\partial \mathbf{u}} \dot{\mathbf{u}}}_{=:\Psi_2(\mathbf{x}, \mathbf{u}, \dot{\mathbf{u}})} \quad (3.14c)$$

$$\vdots \quad (3.14d)$$

$$\frac{d^{n-1} y}{dt^{n-1}} = \underbrace{\frac{\partial \Psi_{n-2}}{\partial \mathbf{x}} \mathbf{f}(\mathbf{x}, \mathbf{u}) + \sum_{m=0}^{n-3} \frac{\partial \Psi_{n-2}}{\partial \mathbf{u}^m} \mathbf{u}^{m+1}}_{=:\Psi_{n-1}(\mathbf{x}, \mathbf{u}, \dots, \mathbf{u}^{(n-2)})}. \quad (3.14e)$$

The right-hand side of (3.14) can be combined into a function $\Phi(\mathbf{x}, \tilde{\mathbf{u}}) : \mathbb{R}^n \times \mathbb{R}^{m \times n-1} \rightarrow \mathbb{R}^n$, where $\tilde{\mathbf{u}} \in \mathbb{R}^{m \times n-1}$ holds the input \mathbf{u} and its time derivatives, i.e.

$$\Phi(\mathbf{x}, \tilde{\mathbf{u}}) := \begin{bmatrix} h(\mathbf{x}) & \Psi_1(\mathbf{x}, \mathbf{u}) & \dots & \Psi_{n-1}(\mathbf{x}, \tilde{\mathbf{u}}) \end{bmatrix}^T. \quad (3.15)$$

Theorem 4. *System (3.12) is called locally observable if there exists a neighborhood of the vector \mathbf{x} , such that (3.15) is a diffeomorphism between the neighborhood of \mathbf{x} and \mathbb{R}^n [POZ04].*

A necessary and sufficient condition for proof of (3.15) being a diffeomorphism is

$$\text{rank} \left(\frac{\partial \Phi(\mathbf{x}, \tilde{\mathbf{u}})}{\partial \mathbf{x}} \right) = n \quad (3.16)$$

Note that this is only a *sufficient* condition to show local observability.

Theorem 5. *System (3.12) is said to be globally observable in \mathbb{R}^n if it is locally observable in every point $\mathbf{x} \in \mathbb{R}^n$ [POZ04].*

3.1.3 Observability Measures

Thus far several criteria for analysis of the system's observability have been presented. However, the return value of these methods is a binary result - the system is *either* observable *or* not. Clearly, that information is an important prerequisite for the consecutive state observer design, but for some reasons (e.g. selection of sensing devices [FRÖ08], it might also be interesting to quantify a system's observability, e.g. *good* or *bad*. A criterion as the latter could ideally back up the choice of a sensor setup given the case there exist several options. In the following two different measures for linear, time-invariant systems are presented and will be applied in the remainder of this chapter to support the sensor selection process.

The so-called modal measures provide some interesting information on the intensity of an eigenvalue's influence on the system dynamics. An extensive overview of controllability measures for linear time-invariant systems is provided in [MOS11]. Due to the principle of duality [OGA01] these measures can also be applied to quantify the observability as well.

The first measure M_1 has been proposed in [LIT83] and requires transformation of a system (3.9) into its diagonal form to decouple the differential equations⁵. Then the observability measure is defined by

$$\kappa_{c,i} = \frac{\mathbf{p}_i^H \mathbf{C}^T \mathbf{C} \mathbf{p}_i}{\mathbf{p}_i^H \mathbf{p}_i} \quad i = 1 \dots n. \quad (3.17)$$

There, $\mathbf{p}_i \in \mathbb{R}^{n \times 1}$ denotes the right eigenvector corresponding to the i -th eigenvalue of \mathbf{A} .

A second measure M_2 introduced to quantify the controllability of a given system exploits the required signal energy to drive a system from a certain initial state \mathbf{x}_0 to the origin $\mathbf{0}$. The idea presented in [BR86] uses a defined control energy and investigates its effect on the state variables. The measure is defined as

$$\mu_{c,i} = \frac{1}{\sqrt{\mathbf{Q}_G^{-1}(t_{end})_{ii}}}, \quad (3.18)$$

with $\mathbf{Q}_G^{-1}(t_{end})$ being the inverse of the observability Gramian as presented in (3.10), evaluated for the time interval $[t_0, t_{end}]$. The subscript ii in (3.18) denotes the ii -th main diagonal element. A general detailed description of the interpretation of that measure is provided in [BR86]. Furthermore, referring to the definition of the observability Gramian (3.10) the upper integration limit can be chosen arbitrarily by the user. However, the selection criterion used here is based on an equal weighting of the system input and the eigendynamics as discussed in [MOS11].

⁵A common assumption to derive unique eigenvectors is that the system matrix \mathbf{A} has n different eigenvalues, if n denotes the size of the square matrix.

A Comment on the Use of Observability Measures Observability measures are exploited in [FRÖ08] for evaluation of various sensor configurations. Discrepancies between the quantified observability and resulting estimation accuracies led the author to the recommendation to select sensors based on simulations of observer concepts (operating on those different sensor configurations). However, influences on the estimation accuracy from e.g. observer gain tunings, measurement noise are not considered in there. As of that this recommendation is not followed and the use of observability measures favored.

3.2 Application to Vehicle Dynamics Models

3.2.1 Longitudinal Dynamics

The dynamics of the vehicle in longitudinal direction as well as the powertrain dynamics discussed in Sections 2.1.1 and 2.5 will be omitted in the subsequent analysis. This is due to the use of the *Black Box* modelling approach, that does not allow analysis of the system internals as these are assumed unknown per definition. Statistical learning algorithms, rather than observer-based parameter estimation techniques will be employed to identify the input-output characteristics.

3.2.2 Lateral Dynamics

The complexity of a model representing the lateral vehicle dynamics is mainly governed by the mathematical representation of the tire-road friction forces. Consequently, the analysis comprises three different tire force models with a varying number of model parameters. Additionally, an alternative structure defined by a different input compared to the classic single-track model will be presented and analyzed at the end of that section.

I Linear Tire Force Model

I.1 State-Space Model

The interpretation of the equations of motion w.r.t. to the lateral vehicle dynamics in state-space requires the definition of a state vector $\mathbf{x}(t) \in \mathbb{R}^n$. For the given physical model the state vector reads as

$$\mathbf{x} := \begin{bmatrix} x_1 & x_2 \end{bmatrix}^T = \begin{bmatrix} \dot{\psi} & \beta \end{bmatrix}^T. \quad (3.19)$$

Combining the equations (2.14b), (2.34) and taking into considerations the definition of the slip angles (2.53a) and (2.53b), the sideslip angle (2.15) and the linear tire force

model (2.24a), (2.71) a state-space formulation can be given as

$$\Sigma_{L1} : \begin{cases} \underbrace{\begin{bmatrix} \frac{dx_1}{dt} \\ \frac{dx_2}{dt} \end{bmatrix}}_{=: \dot{\mathbf{x}}} = \underbrace{\begin{bmatrix} a_{11} u_2^{-1} x_1 + a_{12} x_2 + b_{11} u_1 - b_{13} u_2^{-1} u_3 \\ (a_{21} u_2^{-2} - 1) x_1 + a_{22} u_2^{-1} x_2 + b_{21} u_2^{-1} u_1 - b_{23} u_2^{-2} u_3 \end{bmatrix}}_{=: \mathbf{f}(\mathbf{x}, \mathbf{u})}, & (3.20a) \\ y = h(\mathbf{x}), & (3.20b) \end{cases}$$

with $\mathbf{f} : D_f \subseteq \mathbb{R}^n \times \mathbb{R}^m \rightarrow \mathbb{R}^n$, $\mathbf{h} : D_h \subseteq \mathbb{R}^n \rightarrow \mathbb{R}$, the input vector $\mathbf{u}(t) \in \mathbb{R}^m$ defined by

$$\mathbf{u} := \begin{bmatrix} u_1 & u_2 & u_3 \end{bmatrix}^T = \begin{bmatrix} \delta_w & v v_x & \dot{\varphi} \end{bmatrix}^T, \quad (3.21)$$

and the output $y \in \mathbb{R}$. Furthermore, the abbreviations

$$a_{11} := \frac{-l_{f_e}^2 c_{\alpha_{f_e}} - l_{r_e}^2 c_{\alpha_r}}{J_z}, \quad a_{12} := \frac{-l_{f_e} c_{\alpha_{f_e}} + l_{r_e} c_{\alpha_r}}{J_z}, \quad (3.22a)$$

$$a_{21} := \frac{-l_{f_e} c_{\alpha_{f_e}} + l_{r_e} c_{\alpha_r}}{m}, \quad a_{22} := \frac{-c_{\alpha_{f_e}} - c_{\alpha_r}}{m}, \quad (3.22b)$$

$$b_{11} := \frac{l_{f_e} c_{\alpha_{f_e}}}{J_z}, \quad b_{13} := \frac{h_{rl}(-l_{f_e} c_{\alpha_{f_e}} + l_{r_e} c_{\alpha_r})}{J_z}, \quad (3.22c)$$

$$b_{21} := \frac{c_{\alpha_{f_e}}}{m}, \quad b_{23} := \frac{h_{rl}(-c_{\alpha_{f_e}} - c_{\alpha_r})}{m}. \quad (3.22d)$$

are introduced. Definition of the output mapping $h(\mathbf{x})$ will be analyzed later within the observability study. In general, the formulation of the lateral vehicle dynamics even with a linear lateral tire force model results in a nonlinear system description.

I.2 Parameter Sensitivity Analysis

Studying the effects of parameter variations on the system states x_1 and x_2 requires definition of a parameter vector $\boldsymbol{\rho}$. As a result system (3.20) can be written in the following form

$$\underbrace{\begin{bmatrix} \frac{dx_1}{dt} \\ \frac{dx_2}{dt} \end{bmatrix}}_{=: \dot{\mathbf{x}}} = \underbrace{\begin{bmatrix} \frac{-\rho_1^2 \rho_3 - \rho_2^2 \rho_4}{\rho_5 u_2} x_1 + \frac{-\rho_1 \rho_3 + \rho_2 \rho_4}{\rho_5} x_2 + \frac{\rho_1 \rho_3}{\rho_5} u_1 + \frac{-\rho_7 \rho_1 \rho_3 + \rho_7 \rho_2 \rho_4}{\rho_5 u_2} u_3 \\ \frac{-\rho_3 - \rho_4}{\rho_6 u_2} x_2 + \left(\frac{-\rho_1 \rho_3 + \rho_2 \rho_4}{\rho_6 u_2^2} - 1 \right) x_1 + \frac{\rho_3}{\rho_6 u_2} u_1 + \frac{\rho_7 (-\rho_3 - \rho_4)}{\rho_6 u_2^2} u_3 \end{bmatrix}}_{=: \begin{bmatrix} f_1(\mathbf{x}, \boldsymbol{\rho}, \mathbf{u}) & f_2(\mathbf{x}, \boldsymbol{\rho}, \mathbf{u}) \end{bmatrix}^T}, \quad (3.23)$$

with parameter vector $\boldsymbol{\rho} \in \mathbb{R}^r$ being defined as

$$\boldsymbol{\rho} := \begin{bmatrix} \rho_1 & \rho_2 & \rho_3 & \dots & \rho_7 \end{bmatrix}^T = \begin{bmatrix} l_{f_e} & l_{r_e} & c_{\alpha_{f_e}} & c_{\alpha_r} & J_z & m & h_{rl} \end{bmatrix}^T. \quad (3.24)$$

The system and input matrices $\mathbf{A}_{S_{L1}}(t, \boldsymbol{\rho}) \in \mathbb{R}^{n \times n}$ and $\mathbf{B}_{S_{L1}}(t, \boldsymbol{\rho}) \in \mathbb{R}^{n \times r}$ respectively, defined by (3.7a) and (3.7b), read as

$$\mathbf{A}_{S_{L1}}(t, \boldsymbol{\rho}) := \begin{bmatrix} \frac{-\rho_1^2 \rho_3 - \rho_2^2 \rho_4}{\rho_5 u_2} & \frac{-\rho_1 \rho_3 + \rho_2 \rho_4}{\rho_5} \\ \frac{-\rho_1 \rho_3 + \rho_2 \rho_4}{\rho_6 u_2^2} - 1 & \frac{-\rho_3 - \rho_4}{\rho_6 u_2} \end{bmatrix}, \quad (3.25a)$$

$$\mathbf{B}_{S_{L1}}(t, \boldsymbol{\rho}) := \begin{bmatrix} \frac{-2 \rho_1 \rho_3}{\rho_5 u_2} x_1 - \frac{\rho_3}{\rho_5} x_2 + \frac{\rho_3}{\rho_5} u_1 - \frac{\rho_3 \rho_7}{\rho_5 u_2} u_3 & -\frac{\rho_3}{\rho_6 u_2^2} x_1 \\ \frac{-2 \rho_2 \rho_4}{\rho_5 u_2} x_1 + \frac{\rho_4}{\rho_5} x_2 + \frac{\rho_4 \rho_7}{\rho_5 u_2} u_3 & \frac{\rho_4}{\rho_6 u_2^2} x_1 \\ \frac{-\rho_1^2}{\rho_5 u_2} x_1 - \frac{\rho_1}{\rho_5} x_2 + \frac{\rho_1}{\rho_5} u_1 - \frac{\rho_1 \rho_7}{\rho_5 u_2} u_3 & \frac{\partial f_2}{\partial \rho_3} \\ \frac{-\rho_2^2}{\rho_5 u_2} x_1 + \frac{\rho_2}{\rho_5} x_2 + \frac{\rho_2 \rho_7}{\rho_5 u_2} u_3 & \frac{\rho_2}{\rho_6 u_2^2} x_1 - \frac{1}{\rho_6 u_2} x_2 - \frac{\rho_7}{\rho_6 u_2^2} u_3 \\ \frac{\partial f_1}{\partial \rho_5} & 0 \\ 0 & \frac{\partial f_2}{\partial \rho_6} \\ \frac{-\rho_1 \rho_3 + \rho_2 \rho_4}{\rho_5 u_2} & \frac{-\rho_3 - \rho_4}{\rho_6 u_2^2} \end{bmatrix}^T. \quad (3.25b)$$

with

$$\begin{aligned} \frac{\partial f_2}{\partial \rho_3} &= -\frac{\rho_1}{\rho_6 u_2^2} x_1 - \frac{1}{\rho_6 u_2} x_2 + \frac{1}{\rho_6 u_2} u_1 - \frac{\rho_7}{\rho_6 u_2^2} u_3, \\ \frac{\partial f_1}{\partial \rho_5} &= -\frac{\rho_1^2 \rho_3 + \rho_2^2 \rho_4}{\rho_5^2 u_2} x_1 + \frac{-\rho_1 \rho_3 + \rho_2 \rho_4}{\rho_5^2} x_2 + \frac{\rho_1 \rho_3}{\rho_5^2} u_1 + \frac{\rho_1 \rho_3 \rho_7 - \rho_2 \rho_4 \rho_7}{\rho_5^2 u_2} u_3, \\ \frac{\partial f_2}{\partial \rho_6} &= \frac{-\rho_1 \rho_3 + \rho_2 \rho_4}{\rho_6^2 u_2^2} x_1 + \frac{-\rho_3 - \rho_4}{\rho_6^2 u_2} x_2 + \frac{\rho_3}{\rho_6^2 u_2} u_1 + \frac{\rho_3 \rho_7 + \rho_4 \rho_7}{\rho_6^2 u_2^2} u_3. \end{aligned}$$

for the system (3.23). Evaluating the matrices for the nominal parameters values $\bar{\boldsymbol{\rho}}$ and inserting $\mathbf{A}_{S_{L1}}(t, \bar{\boldsymbol{\rho}})$ and $\mathbf{B}_{S_{L1}}(t, \bar{\boldsymbol{\rho}})$ into (3.5) allows calculation of the numerical solution

Parameter	Symbol	Value	Unit
l_{f_e}	$\bar{\rho}_1$	1.087	m
l_{r_e}	$\bar{\rho}_2$	1.441	m
$c_{\alpha_{f_e}}$	$\bar{\rho}_3$	110000	N·rad ⁻¹
c_{α_r}	$\bar{\rho}_4$	130000	N·rad ⁻¹
J_z	$\bar{\rho}_5$	2152	kg·m ²
m	$\bar{\rho}_6$	1465	kg
$h_{r,l}$	$\bar{\rho}_7$	0.45	m

Table 3.1: Nominal parameter vector $\bar{\boldsymbol{\rho}}$ for parameter sensitivity evaluation of lateral dynamics ($\boldsymbol{\Sigma}_{L1}$).

related to the sensitivity functions $\mathbf{S}_{L1}(t) \in \mathbb{R}^{n \times r}$. Additionally to the $n \times r$ differential equations also the n nominal trajectories of $\bar{\mathbf{x}}(t, \bar{\boldsymbol{\rho}})$ need to be evaluated.

The choice of system excitation, i.e. driving maneuvers, is motivated such, that a.) the system is excited abruptly by a input step signal b.) is excited permanently by a harmonic function for analysis of the sensitivities. More precisely, the maneuvers refer to a pseudo-step⁶ and a sinusoidal steering excitation. The extracted information of the analysis can increase the transparency of the maneuver selection for the model parameter identification task of the next chapter. Execution-wise the steering angle amplitude is selected such that the linear range (see Figure 2.5) of the tire slip-force angle characteristics is not left. The longitudinal vehicle velocity is held constant at $v_x = 80\text{km}\cdot\text{h}^{-1}$ (as defined for the standard evaluation maneuvers - Section 1.2.2).

The values of the nominal parameter vector $\bar{\boldsymbol{\rho}}$ used for the simulation work are listed in Table 3.1. Clearly, the exact value of these parameters depends on the considered vehicle configuration. However, the physical range of these parameters is well known and in terms of parameter sensitivity analysis the nominal parameter value is of reduced importance. The quantitative effect of a parameter change $\Delta\rho$ on the state vector \mathbf{x} is abbreviated by

$$\Delta\mathbf{x}_{\rho_i} := \left. \frac{\partial\mathbf{x}}{\partial\rho_i} \right|_{\rho_i=\bar{\rho}_i} \Delta\rho_i \quad i = 1 \dots r \quad (3.27)$$

Here, ρ_i denotes the i -th element of the vector $\boldsymbol{\rho}$. The results of the simulations are illustrated in Figure 3.1. The subplots (a) and (b) show the effects of parameter changes on x_1 and x_2 during a pseudo-step steering excitation. Furthermore, (c) and (d) reveal information on the change of x_1 and x_2 due to parameter variations during a sinusoidal steering excitation. The plots (a) and (c) reveal that the model parameters ρ_2 , ρ_3 , ρ_1 and ρ_4 have the highest influence on x_1 when changed by some small value⁷. Note that

⁶A pseudo-step change can be interpreted as a sigmoid function. In practice, it is obtained by filtering an ideal step input and mainly differs by its continuous differentiability.

⁷More exactly, the simulated parameter variations are given by 1% of their nominal values.

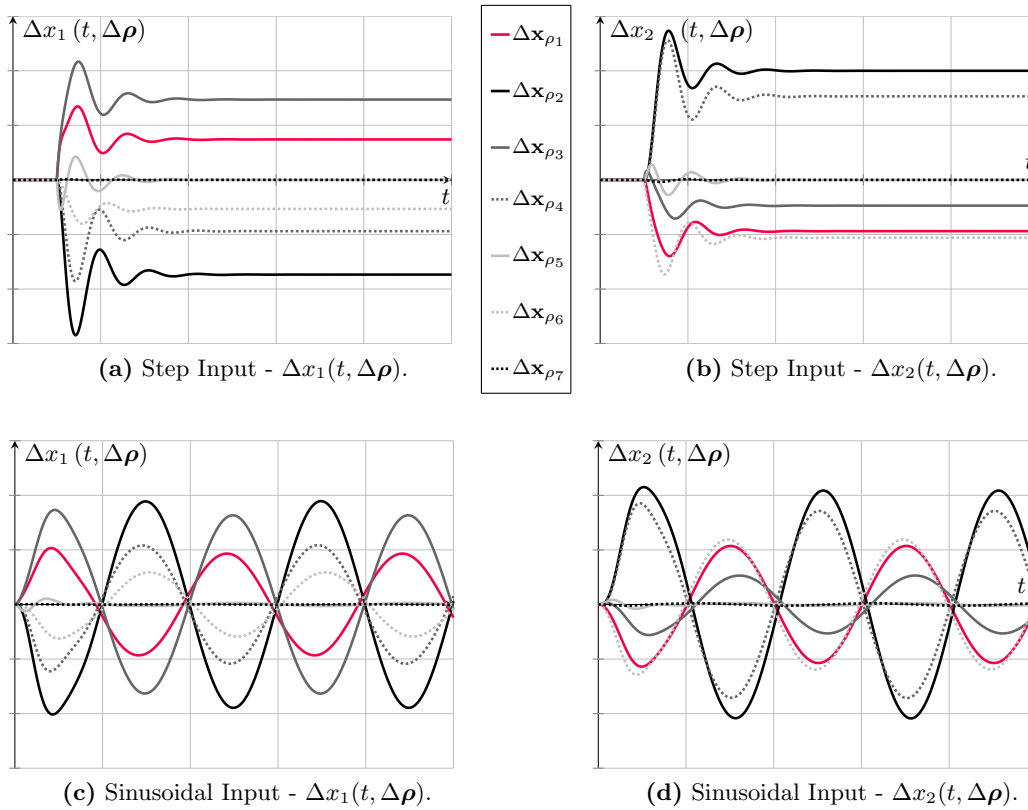


Figure 3.1: Sensitivities of state \mathbf{x} w.r.t. parameter variations $\Delta \rho$ for step and sinusoidal excitations (Σ_{L1}). The curves illustrate the relative change of the state values (w.r.t. the nominal case) when deviating the considered parameter by some small amount from its nominal quantity. In (a), (b) the steady-state values are of interest in order to analyze the influence of the individual parameters on the states. Plots (c), (d) show the state variations for some harmonic excitation. Note that $\Delta \mathbf{x}_{\rho_1}$ is an abbreviation for $\Delta \mathbf{x}(t, \Delta \rho_1)$.

the axes scaling of (a) and (c) is identical for a proper comparison of the sensitivities w.r.t. the excitation signal. The same holds for (b) and (d). Considering the magnitude of the influence of the individual parameters on x_1 there is no difference between the two simulated maneuvers. The situation looks similar for state x_2 , even though ρ_3 shows less influence on x_2 as for x_1 . In fact, the highest sensitivity of x_2 is on ρ_2 , ρ_4 , ρ_6 and ρ_1 . Similarly as for x_1 , the choice of maneuver does not introduce any changes to the previous results.

I.3 Model Parameter Identification by Static Measurements

An overview of measurement principles to determine vehicle parameters (e.g. inertia, planar CoG position, mass) is provided in [KOL09]. Following these results it is only

the tire parameters and the roll lever arm that are to be determined by identification⁸.

I.4 Model Parameter Selection

Bringing together the results of the previous two paragraphs it is the tire forces related parameters $c_{\alpha_{fe}}$, c_{α_r} and the planar position of CoG that are to be identified online. With regards to the objective of this thesis, providing model parameters for a subsequent vehicle handling evaluation, the vehicle related parameters can be assumed well known and constant during the identification work. Hence, and this coincides with the findings of [BÖR04] who classifies the urgency of parameter identification by a metric based on the standard deviation and maximum value of a parameter, the ones related to the tire forces are selected as those to be estimated.

I.5 Observability Analysis

In general, both state variables x_1 and x_2 can be measured by an angular rate and optical velocity sensor respectively. However, the latter is cost-intensive and its vehicle installation time consuming. Consequently, in this paragraph the effects of two different sensor configurations⁹ are investigated with respect to the observability of the system. Furthermore, quantitative metrics in form of observability measures reveal the potential how well the initial conditions can be recovered from measurements of a given sensor set.

The linear output mappings of the two sensor configurations $h_1(\mathbf{x})$ and $h_2(\mathbf{x})$ are defined as follows

$$y_1 = h_1(\mathbf{x}) = \begin{bmatrix} 1 & 0 \end{bmatrix} \mathbf{x}, \quad (3.28a)$$

$$y_2 = h_2(\mathbf{x}) = \begin{bmatrix} 0 & 1 \end{bmatrix} \mathbf{x}. \quad (3.28b)$$

The observability matrices \mathbf{O}_1 and \mathbf{O}_2 are defined as in (3.11) and read as

$$\mathbf{O}_1 = \begin{bmatrix} 1 & 0 \\ \frac{a_{11}}{u_2} & a_{12} \end{bmatrix}, \quad \mathbf{O}_2 = \begin{bmatrix} 0 & 1 \\ \frac{a_{21}}{u_2^2} - 1 & \frac{a_{22}}{u_2} \end{bmatrix} \quad (3.29)$$

From (3.29) and criterion 2 of Section 3.1.2 it is obvious that \mathbf{O}_1 has full rank as long as a_{12} is different from 0, i.e. $l_{fe} c_{\alpha_{fe}} \neq l_{re} c_{\alpha_r}$ must hold¹⁰. Similarly, \mathbf{O}_2 only suffers from

⁸The latter is also assumed known as discussed in Section 3.2.3.

⁹These configurations refer to *either* measurement of the yaw rate $\dot{\psi}$ *or* the vehicle sideslip angle β .

¹⁰From a vehicle handling point of view this is interesting as it can be interpreted as follows: assuming yaw rate measurement only, the system (3.20) is not observable if $l_{fe} c_{\alpha_{fe}} = l_{re} c_{\alpha_r}$. In other words, it is

Measure	$h_1(\mathbf{x})$	$h_2(\mathbf{x})$
M ₁ [LIT83]	$\kappa_{c,1} = 0.972$ $\kappa_{c,2} = 0.972$	$\kappa_{c,1} = 0.028$ $\kappa_{c,2} = 0.028$
M ₂ [BR86] ($t_{end} = 0.12$)	$\mu_{c,1} = 0.231$ $\mu_{c,2} = 0.620$	$\mu_{c,1} = 0.019$ $\mu_{c,2} = 0.231$

Table 3.2: Observability measures for sensor configurations $h_1(\mathbf{x})$ and $h_2(\mathbf{x})$ of Σ_{L1} .

a rank deficiency if

$${}_v v_x^2 = \frac{-l_{f_e} c_{\alpha_{f_e}} + l_{r_e} c_{\alpha_r}}{m}. \quad (3.30)$$

At this point some conditions for the observability have been worked out. However, the decision whether or not the system is observable is binary, i.e. *true* or *false*. It would be beneficial to gather some knowledge on the different effects of the two sensor configurations on the observability potential. Therefore, the observability measures, as defined by (3.17) and (3.18) shall reveal the differences in terms of quantitative observability for system (3.20) and the sensor configurations (3.28). The calculation of these measures is based on the parameters of Table 3.1 and the input u_2 , which refers to the longitudinal velocity ${}_v v_x$, is assumed constant (identically to the values of Section I.2). Then, the system can be treated as a linear one and the observability measures (3.17), (3.18) result in Table 3.2. From the obtained measures M₁ and M₂ it can be concluded that the installation of a yaw rate sensor is less susceptible to measurement noise [DP13] and the recovery of the initial states \mathbf{x}_0 of (3.20) is easier (compared to the same task but considering a vehicle sideslip measurement). The interpretation of the M₂ metric renders that conclusion more obvious, i.e. the higher values indicate a greater system excitation when stimulating the system by the same control energy¹¹.

II Simplified Magic Formula Tire Force Model

II.1 State-Space Model

The state-space formulation exploits the equations (2.14b), (2.34), (2.53a), (2.53b) and the sideslip angle (2.15). However, now the modelling of the lateral tire forces is based on equation (2.28), i.e. the Simplified Pacejka tire force model. Then a state-space notation

not observable, if the self-steering gradient equals zero, i.e. the turning response properties are neither *understeering* nor *oversteering*, but *neutral*. For further details consider [GIL92] or [ZOM91].

¹¹That interpretation is based on the controllability. However, due to the duality principle this also holds for the observability.

of the equations of motion can be formulated by

$$\Sigma_{L2} : \left\{ \begin{array}{l} \underbrace{\begin{bmatrix} \frac{dx_1}{dt} \\ \frac{dx_2}{dt} \end{bmatrix}}_{=: \mathbf{x}} = \underbrace{\begin{bmatrix} \frac{l_{f_e}}{J_z} D_f \varsigma_1 (B_f \alpha_{f_e}) - \frac{l_{r_e}}{J_z} D_r \varsigma_1 (B_r \alpha_{r_e}) \\ \frac{D_f}{m} u_2^{-1} \varsigma_1 (B_f \alpha_{f_e}) + \frac{D_r}{m} u_2^{-1} \varsigma_1 (B_r \alpha_{r_e}) - x_1 \end{bmatrix}}_{=: \mathbf{f}(\mathbf{x}, \mathbf{u})}, \\ y = h(\mathbf{x}), \end{array} \right. \quad (3.31a)$$

with

$$\alpha_{f_e} = \left(u_1 - x_2 - \frac{l_{f_e} x_1}{u_2} - \frac{h_{rl} u_3}{u_2} \right), \quad (3.32a)$$

$$\alpha_{r_e} = \left(-x_2 + \frac{l_{r_e} x_1}{u_2} - \frac{h_{rl} u_3}{u_2} \right), \quad (3.32b)$$

see also (2.53a), (2.53b). The state vector $\mathbf{x}(t) \in \mathbb{R}^n$ and the input vector $\mathbf{u}(t) \in \mathbb{R}^m$ are identical to (3.19), (3.21). Function $\varsigma_1(\cdot) : D_f \subseteq \mathbb{R} \rightarrow \mathbb{R}$ in (3.31a) is defined as $\varsigma_1(\cdot) := \sin(\text{atan}(\cdot))$ and can be further described by the identity

$$\sin(\text{atan}(x)) = \frac{x}{(1+x^2)^{\frac{1}{2}}}. \quad (3.33)$$

II.2 Parameter Sensitivity Analysis

Merging (3.31a), (3.32), (3.33) and introducing the parameter vector $\boldsymbol{\rho} \in \mathbb{R}^r$ as

$$\boldsymbol{\rho} := [\rho_1 \ \rho_2 \ \dots \ \rho_9]^T = [l_{f_e} \ l_{r_e} \ D_f \ B_f \ D_r \ B_r \ J_z \ m \ h_{rl}]^T, \quad (3.34)$$

results in the system formulation necessary for analysis of the parameter sensitivities, i.e.

$$\begin{bmatrix} \frac{dx_1}{dt} \\ \frac{dx_2}{dt} \end{bmatrix} = \underbrace{\begin{bmatrix} \frac{\rho_1 \rho_3 \rho_4}{\rho_7} \alpha_{f_e} \left(1 + \rho_4^2 \alpha_{f_e}^2\right)^{-\frac{1}{2}} - \frac{\rho_2 \rho_5 \rho_6}{\rho_7} \alpha_{r_e} \left(1 + \rho_6^2 \alpha_{r_e}^2\right)^{-\frac{1}{2}} \\ \frac{\rho_3 \rho_4}{\rho_8 u_2} \alpha_{f_e} \left(1 + \rho_4^2 \alpha_{f_e}^2\right)^{-\frac{1}{2}} + \frac{\rho_5 \rho_6}{\rho_8 u_2} \alpha_{r_e} \left(1 + \rho_6^2 \alpha_{r_e}^2\right)^{-\frac{1}{2}} - x_1 \end{bmatrix}}_{=: [f_1(\mathbf{x}, \boldsymbol{\rho}, \mathbf{u}) \quad f_2(\mathbf{x}, \boldsymbol{\rho}, \mathbf{u})]^T}. \quad (3.35)$$

Parameter	Symbol	Value	Unit
l_{f_e}	$\bar{\rho}_1$	1.087	m
l_{r_e}	$\bar{\rho}_2$	1.441	m
D_f	$\bar{\rho}_3$	5800	N
B_f	$\bar{\rho}_4$	18.97	-
D_r	$\bar{\rho}_5$	5200	N
B_r	$\bar{\rho}_6$	25	-
J_z	$\bar{\rho}_7$	2152	kg·m ⁻²
m	$\bar{\rho}_8$	1465	kg
h_{r_l}	$\bar{\rho}_9$	0.45	m

Table 3.3: Nominal parameter vector $\bar{\rho}$ for parameter sensitivity evaluation of lateral dynamics with Σ_{L2} .

Calculation of the matrix elements of $\mathbf{A}_{L2}(t, \rho)$ and $\mathbf{B}_{L2}(t, \rho)$ is omitted here, but can be found in Appendix B.

The simulation work is identical to the one discussed for system Σ_{L1} . For maneuver execution details consider I.2. The nominal parameters $\bar{\rho}$ of the system (3.35) are listed in Table 3.3. Figure 3.2 shows the simulation results of the two maneuvers pseudo-step (a)-(d) and sinusoidal steering (e)-(h)¹². The model parameters are grouped into vehicle- and tire-related parameters (left- and right-hand side of Figure 3.2).

Considering the plots (a), (b), (e) and (f) it is the parameters ρ_1 , ρ_2 , ρ_3 and ρ_8 that have the greatest influence on x_1 . As can be extracted from (c), (d), (g) and (h) the highest sensitivity of x_2 is on ρ_1 , ρ_2 , ρ_3 and ρ_5 .

II.3 Model Parameter Identification by Static Measurements

The determination of parameters by standard measurement techniques is identical to the results obtained for system Σ_{L1} as only the tire force model is adapted. Consequently, the results are to be extracted from there.

II.4 Model Parameter Selection

Summing up the results of the last two paragraphs the parameters of the identification process can be defined. Referring to the static measurements the vehicle related parameters are assumed known with sufficient accuracy. Hence, it is the tire model related parameters that need to be estimated. Even though the parameter sensitivity does not indicate the tire model related parameters as the ones with the greatest effects on the states x_1 and x_2 .

¹²The axes of the plots related to the same system states are identically scaled for allowing a comparison of the state deviation magnitude.

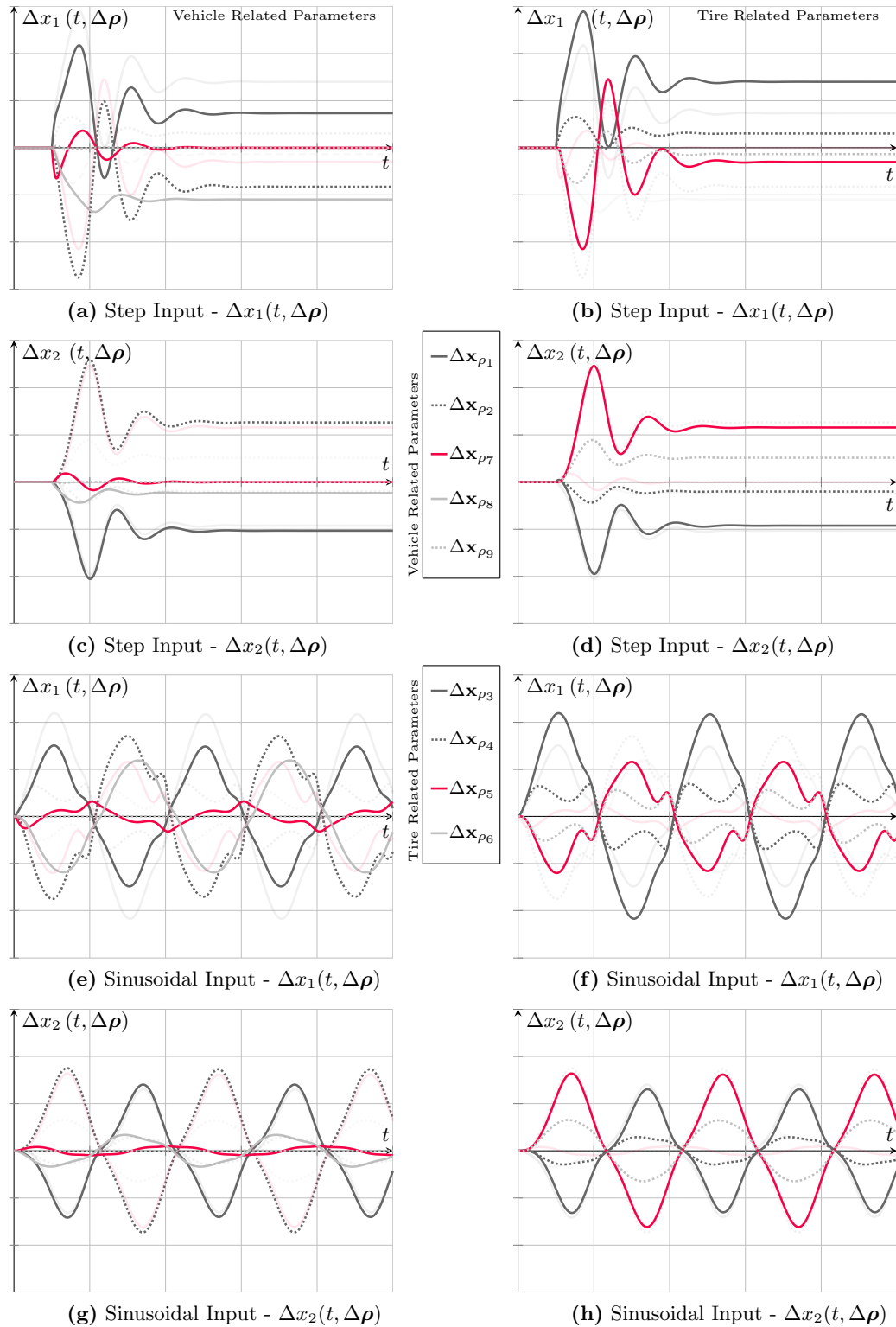


Figure 3.2: Sensitivities of state \mathbf{x} w.r.t. parameter variations $\Delta \rho$ for different handling maneuvers (Σ_{L2}).

However, from a metrological point of view the identification of these parameters makes complete sense, as their identification is mostly achieved by conducting test bench measurements. In summary, the parameters D_f , B_f , D_r and B_r are to be estimated by the proposed observer techniques.

II.5 Observability Analysis

The system (3.31a) will not serve directly as observer design model. Moreover, the state and parameter estimation will be formulated such, that the overall problem of model parameter identification is split into specific subproblems whose solution is provided by tailored observer designs. For these specific observers (and consequently system definitions) the observability will be analyzed in the related Chapter 4. Consequently, the analysis of the observability of (3.31) given some specific output is not of interest at that point.

III TM_Simple Tire Force Model

III.1 State-Space Model

Systems Σ_{L2} and Σ_{L3} differ in the employed tire force model. The derivation of the state equations is based on (3.19), (3.21), (2.14b) and (2.34). The tire force model reads as (2.29) and the resulting state-space formulation results in

$$\Sigma_{L3} : \begin{cases} \underbrace{\begin{bmatrix} \frac{dx_1}{dt} \\ \frac{dx_2}{dt} \end{bmatrix}}_{=: \dot{\mathbf{x}}} = \begin{bmatrix} \frac{l_{f_e}}{J_z} D_f \varsigma_2(B_f, C_f, \alpha_{f_e}) - \frac{l_{r_e}}{J_z} D_r \varsigma_2(B_r, C_r, \alpha_{r_e}) \\ \frac{1}{m u_2} \underbrace{\left[D_f \varsigma_2(B_f, C_f, \alpha_{f_e}) + D_r \varsigma_2(B_r, C_r, \alpha_{r_e}) \right]}_{=: \mathbf{f}(\mathbf{x}, \mathbf{u})} - x_1 \end{bmatrix}, & (3.36a) \\ y = h(\mathbf{x}), & (3.36b) \end{cases}$$

with the slip angles α_{f_e} and α_{r_e} as in (3.32). The function $\varsigma_2 : D_f \subseteq \mathbb{R} \times \mathbb{R} \times \mathbb{R} \rightarrow \mathbb{R}$ is defined by

$$\varsigma_2(B, C, \alpha) := \sin \left[B \left(1 - e^{-|\alpha| C^{-1}} \right) \text{sign}(\alpha) \right]. \quad (3.37)$$

III.2 Parameter Sensitivity Analysis

Before continuing with the analysis of the state vector's sensitivity to parameter variations some thoughts on the differentiability¹³ of (3.37) need to be discussed. Splitting

¹³For details consider [POZ10, KRE10].

the function definition for the cases of positive, negative and zero values of α results in

$$\varsigma_2(B, C, \alpha) = \begin{cases} \sin\left(B - B e^{-\alpha C^{-1}}\right) & \alpha > 0 \\ 0 & \alpha = 0 \\ -\sin\left(B - B e^{\alpha C^{-1}}\right) & \alpha < 0, \end{cases} \quad (3.38)$$

and for that function it is straightforward to show its differentiability for every value of $\alpha \in D \subseteq \mathbb{R}$. Furthermore, the derivative of ς_2 w.r.t. to α is given by

$$\frac{\partial}{\partial \alpha} \varsigma_2(B, C, \alpha) = \begin{cases} \cos\left(B - B e^{-\alpha C^{-1}}\right) \left[\frac{B}{C} e^{-\alpha C^{-1}}\right] & \alpha > 0 \\ \frac{B}{C} & \alpha = 0 \\ -\cos\left(B - B e^{\alpha C^{-1}}\right) \left[-\frac{B}{C} e^{\alpha C^{-1}}\right] & \alpha < 0, \end{cases} \quad (3.39)$$

or alternatively

$$\frac{\partial \varsigma_2(B, C, \alpha)}{\partial \alpha} = \cos\left(B \left(1 - e^{-|\alpha| C^{-1}}\right)\right) \left[\frac{B}{C} e^{-|\alpha| C^{-1}}\right] \quad \forall \alpha. \quad (3.40)$$

Now that the differentiability of the lateral tire force model is guaranteed¹⁴ the parameter vector $\boldsymbol{\rho} \in \mathbb{R}^r$ for the sensitivity analysis is given by

$$\boldsymbol{\rho} := \left[l_{f_e} \quad l_{r_e} \quad D_f \quad B_f \quad C_f \quad D_r \quad B_r \quad C_r \quad J_z \quad m \quad h_{rl} \right]^T. \quad (3.41)$$

Substituting the parameters in (3.36) by (3.41) the functions $f_1(\mathbf{x}, \boldsymbol{\rho}, \mathbf{u})$, $f_2(\mathbf{x}, \boldsymbol{\rho}, \mathbf{u})$ result in

$$\underbrace{\begin{bmatrix} \frac{dx_1}{dt} \\ \frac{dx_2}{dt} \end{bmatrix}}_{=:\dot{\mathbf{x}}} = \underbrace{\begin{bmatrix} \frac{\rho_1}{\rho_9} \rho_3 \tau_2(\rho_4, \rho_5, \alpha_{f_e}) - \frac{\rho_2}{\rho_9} \rho_6 \tau_2(\rho_7, \rho_8, \alpha_{r_e}) \\ \frac{\rho_3}{\rho_{10}} u_2^{-1} \tau_2(\rho_4, \rho_5, \alpha_{f_e}) + \frac{\rho_6}{\rho_{10}} u_2^{-1} \tau_2(\rho_7, \rho_8, \alpha_{r_e}) - x_1 \end{bmatrix}}_{=:\begin{bmatrix} f_1(\mathbf{x}, \boldsymbol{\rho}, \mathbf{u}) & f_2(\mathbf{x}, \boldsymbol{\rho}, \mathbf{u}) \end{bmatrix}^T}, \quad (3.42)$$

with α_{f_e} , α_{r_e} defined as in (3.32), but replacing the vehicle parameters by (3.41). Appendix B provides the partial derivatives defining the elements of the matrices $\mathbf{A}_{L3}(t, \boldsymbol{\rho})$ and $\mathbf{B}_{L3}(t, \boldsymbol{\rho})$.

¹⁴An assumption not mentioned explicitly is that the longitudinal velocity ${}_{\vee}v_x \neq 0$.

Parameter	Symbol	Value	Unit
D_f	$\bar{\rho}_3$	5800	N
B_f	$\bar{\rho}_4$	1.802	-
C_f	$\bar{\rho}_5$	0.095	rad
D_r	$\bar{\rho}_6$	5200	N
B_r	$\bar{\rho}_7$	1.875	-
C_r	$\bar{\rho}_8$	0.075	rad

Table 3.4: Tire model related nominal parameters of $\bar{\rho}$ related to the lateral dynamics (Σ_{L3}). Vehicle related model parameters are listed in Table 3.3.

The numerical simulation of the parameter sensitivity function based on the nominal parameters $\bar{\rho}$ listed in Table 3.4 results in plots as illustrated in Figure 3.3. The plots (a), (b), (e) and (f) as well as (c), (d), (g) and (h) related to certain excitation signals are scaled such, that the results are comparable. Furthermore, the analysis is based on the executed maneuvers pseudo-step and sinusoidal steering (details on the excitation parameters can be found in the sensitivity analysis of Σ_{L1}). Interpreting the results illustrated in Figure 3.3 the parameter sensitivities show a similar trend as for Σ_{L2} . Again, the state x_1 is most sensitive to the parameters ρ_1 , ρ_2 , ρ_3 and ρ_{10} . In terms of quantitative influence the situation is different for the two maneuvers as can be seen from plots (a), (b), (e) and (f). The state x_2 changes most if parameters ρ_2 , ρ_6 , ρ_1 and ρ_3 vary.

III.3 Model Parameter Identification by Static Measurements

Results can be obtained from system Σ_{L1} analysis as only the tire force model is adapted to the TM_Simple approach.

III.4 Model Parameter Selection

Not surprisingly the argumentation of the parameter selection for the identification process is similar as for the previous two lateral dynamics models. The vehicle related parameters are assumed to be identifiable from static measurements or *a priori* knowledge from vehicle design. However, the tire model related parameters are commonly unknown and need to be determined by in-vehicle observation techniques. Consequently, it is the parameters D_f , B_f , C_f , D_r , B_r and C_r that are selected for the *to be* proposed state observers.

III.5 Observability Analysis

As for the system Σ_{L2} an observability analysis can be omitted at that point as the overall problem of model parameter identification is split into several more specific observation problems. For these, observability will be discussed in Chapter 4.

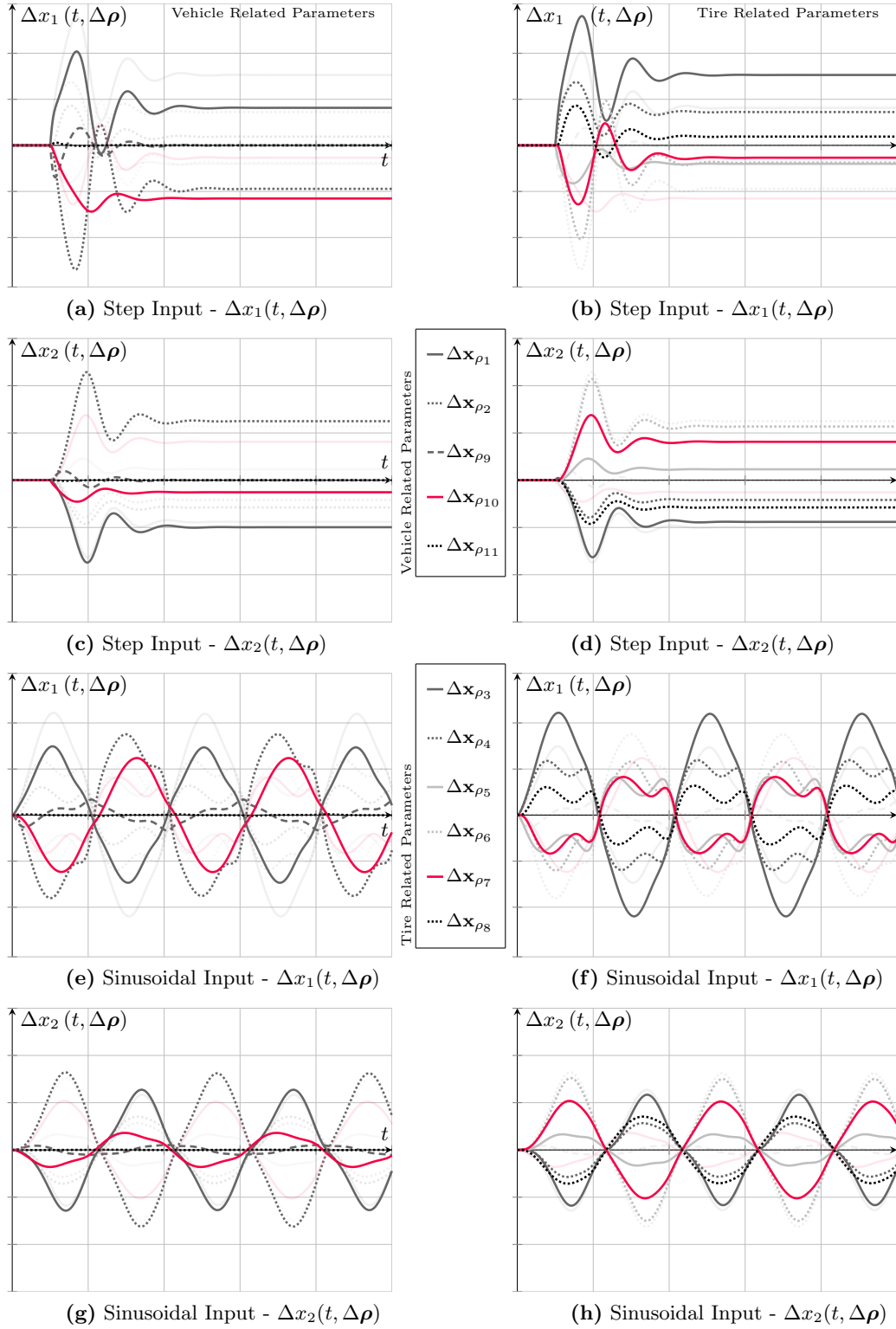


Figure 3.3: Sensitivities of state \mathbf{x} w.r.t. parameter variations $\Delta \rho$ for different handling maneuvers (Σ_{L3}).

IV Input-affine Linear Tire Force Model

Reconsidering again the systems Σ_{L2} and Σ_{L3} these are not input affine¹⁵. However, some of the discussed observer concepts require the underlying system model to be in input affine representation. Therefore, by regarding the lateral acceleration ${}_{\vee}a_y$ as system input (rather than the wheel angle δ_w) the equations of motion can be reformulated such, that the aforementioned prerequisite holds.

IV.1 State-Space Model

The equations of motion are based on (2.14b), (2.14c) (2.9) and (2.15) and generally read as

$$\frac{d\dot{\psi}}{dt} = \frac{l_{f_e} m}{J_z} {}_{\vee}a_y - \frac{l_{f_e} + l_{r_e}}{J_z} {}_{\vee}F_{y,r}, \quad (3.43a)$$

$$\frac{d\beta}{dt} = -\dot{\psi} + \frac{{}_{\vee}a_y}{{}_{\vee}v_x} \quad (3.43b)$$

Exploiting the state vector definition (3.19) and employing the linear tire force model (2.24) the state-space equations can be formulated as

$$\Sigma_{L4} : \left\{ \begin{array}{l} \underbrace{\begin{bmatrix} \frac{dx_1}{dt} \\ \frac{dx_2}{dt} \end{bmatrix}}_{=:\dot{\mathbf{x}}} = \underbrace{\begin{bmatrix} a_{11} u_2^{-1} x_1 + a_{12} x_2 + b_{11} u_1 - b_{13} u_2^{-1} u_3 \\ -x_1 + u_1 u_2^{-1} \end{bmatrix}}_{=:f(\mathbf{x},\mathbf{u})}, \\ y = h(\mathbf{x}), \end{array} \right. \quad (3.44a)$$

$$(3.44b)$$

with

$$a_{11} := -\frac{(l_{f_e} + l_{r_e}) l_{r_e} c_{\alpha_r}}{J_z}, \quad a_{12} := \frac{(l_{f_e} + l_{r_e}) c_{\alpha_r}}{J_z}, \quad (3.45a)$$

$$b_{11} := \frac{l_{f_e} m}{J_z}, \quad b_{13} := \frac{(l_{f_e} + l_{r_e}) h_w c_{\alpha_r}}{J_z}, \quad (3.45b)$$

and the input vector $\mathbf{u}(t) \in \mathbb{R}^m$ being defined as $\mathbf{u} := \begin{bmatrix} u_1 & u_2 & u_3 \end{bmatrix}^T = \begin{bmatrix} {}_{\vee}a_y & {}_{\vee}v_x & \dot{\psi} \end{bmatrix}^T$. The definition of the output mapping $h(\mathbf{x})$ will be discussed in the observability analysis. In general, any tire force model can be incorporated into (3.43) making the system representation attractive for observer design, as it operates on a reduced number of parameters. For example, the parameter $c_{\alpha_{f_e}}$, used in Σ_{L1} , does not appear in this formulation.

¹⁵The control input \mathbf{u} appears only linearly in the differential equation, see [NVDS90] for details.

IV.2 Parameter Sensitivity Analysis

The vector $\boldsymbol{\rho} \in \mathbb{R}^r$ holds the parameters of interest and reads as

$$\boldsymbol{\rho} := \begin{bmatrix} \rho_1 & \rho_2 & \dots & \rho_6 \end{bmatrix}^T = \begin{bmatrix} l_{f_e} & l_{r_e} & c_{\alpha_r} & J_z & m & h_{rl} \end{bmatrix}^T. \quad (3.46)$$

Then the state-space definition (3.44) using $\boldsymbol{\rho}$ can be written as

$$\begin{bmatrix} \frac{dx_1}{dt} \\ \frac{dx_2}{dt} \end{bmatrix} = \underbrace{\begin{bmatrix} -\frac{\rho_2 \rho_3 (\rho_1 + \rho_2)}{\rho_4 u_2} x_1 + \frac{\rho_3 (\rho_1 + \rho_2)}{\rho_4} x_2 + \frac{\rho_1 \rho_5}{\rho_4} u_1 + \frac{\rho_3 \rho_6 (\rho_1 + \rho_2)}{\rho_4 u_2} \\ -x_1 + \frac{u_1}{u_2} \end{bmatrix}}_{=: \begin{bmatrix} f_1(\mathbf{x}, \boldsymbol{\rho}, \mathbf{u}) & f_2(\mathbf{x}, \mathbf{u}) \end{bmatrix}^T}. \quad (3.47)$$

The matrices $\mathbf{A}_{L4}(t, \boldsymbol{\rho}) \in \mathbb{R}^{n \times n}$ and $\mathbf{B}_{L4}(t, \boldsymbol{\rho}) \in \mathbb{R}^{n \times r}$ defined by (3.3) are calculated as

$$\mathbf{A}_{L4}(t, \boldsymbol{\rho}) = \begin{bmatrix} -\frac{\rho_2 \rho_3 (\rho_1 + \rho_2)}{\rho_4 u_2} & \frac{\rho_3 (\rho_1 + \rho_2)}{\rho_4} \\ -1 & 0 \end{bmatrix}, \quad (3.48a)$$

$$\mathbf{B}_{L4}(t, \boldsymbol{\rho}) = \begin{bmatrix} -\frac{\rho_2 \rho_3}{\rho_4 u_2} x_1 + \frac{\rho_3}{\rho_4} x_2 - \frac{\rho_5}{\rho_4} u_1 + \frac{\rho_3 \rho_6}{\rho_4 u_2} u_3 & 0 \\ -\frac{\rho_3 (\rho_1 + 2\rho_2)}{\rho_4 u_2} x_1 + \frac{\rho_3}{\rho_4} x_2 + \frac{\rho_3 \rho_6}{\rho_4 u_2} u_3 & 0 \\ (\rho_1 + \rho_2) \left[-\frac{\rho_2}{\rho_4 u_2} x_1 + \frac{1}{\rho_4} x_2 + \frac{\rho_6}{\rho_4 u_2} u_3 \right] & 0 \\ (\rho_1 + \rho_2) \left[\frac{\rho_2 \rho_3}{\rho_4^2 u_2} x_1 - \frac{\rho_3}{\rho_4^2} x_2 - \frac{\rho_3 \rho_6}{\rho_4^2 u_2} u_3 \right] - \frac{\rho_1 \rho_5}{\rho_4^2} u_1 & 0 \\ \frac{\rho_1}{\rho_4} u_1 & 0 \\ \frac{\rho_3 (\rho_1 + \rho_2)}{\rho_4 u_2} & 0 \end{bmatrix}^T. \quad (3.48b)$$

From the definition of the parameter vector (3.46) it is obvious that the parameters are a subset of the $\boldsymbol{\Sigma}_1$ related $\boldsymbol{\rho}$ vector (3.24). Consequently, the nominal parameter values $\bar{\boldsymbol{\rho}}$ can be extracted from Table 3.1.

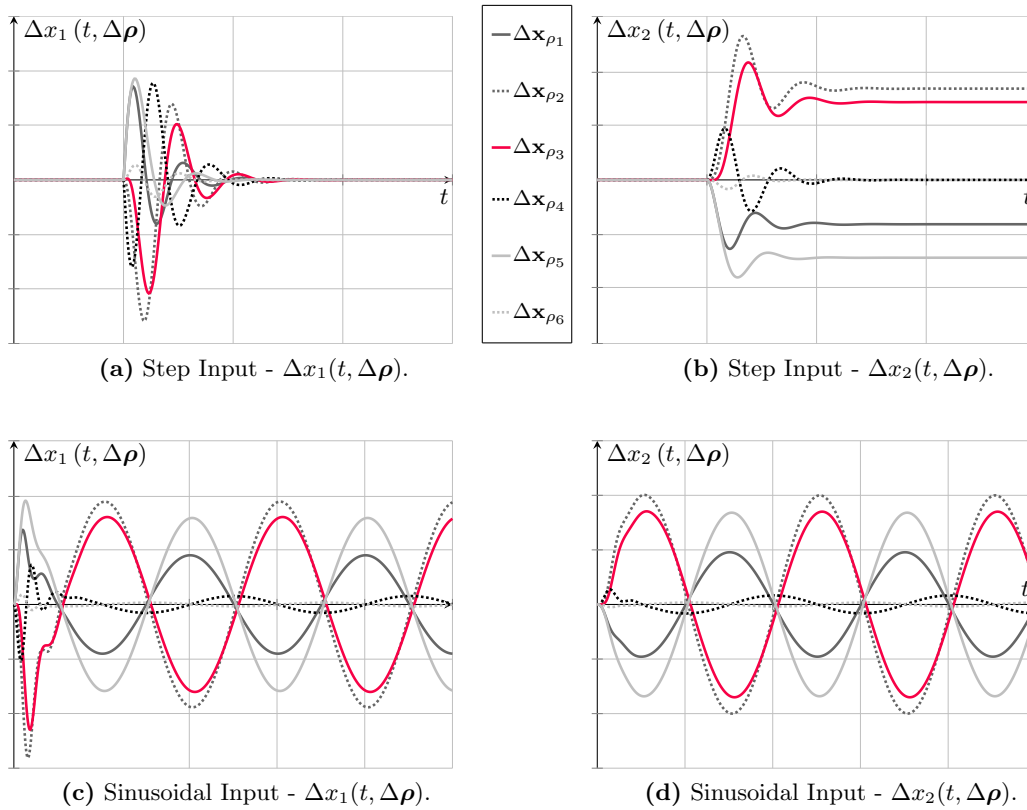


Figure 3.4: Sensitivities of state \mathbf{x} w.r.t. parameter variations $\Delta\boldsymbol{\rho}$ for step and sinusoidal excitations (Σ_{L4}). Note that $\Delta\mathbf{x}_{\rho_1}$ is an abbreviation for $\Delta\mathbf{x}(t, \Delta\rho_1)$.

The numerical simulation of the differential equations describing the parameter sensitivities of x_1 and x_2 is conducted by exciting the system with a pseudo-step and a sinusoidal lateral acceleration signal. Figure 3.4 illustrates the results of the simulation work. It is worth mentioning that the axes are not scaled equally for (a) and (c). Hence, a quantitative comparison of the results is not feasible¹⁶.

At a first glance it might be surprising that the sensitivity of x_1 to any variation of $\boldsymbol{\rho}$ diminishes for steady-state conditions, see (a) of Figure 3.4. However, reconsidering the approximation of the lateral acceleration by (2.10) that reads as

$${}_{\nu}a_y \approx {}_{\nu}v_x \left(\dot{\beta} + \dot{\psi} \right), \quad (3.49)$$

it is easy to see, as the time derivative of the sideslip angle β vanishes, the yaw rate $\dot{\psi}$ fully depends on the input quantity ${}_{\nu}a_y$ and is further independent of any model parameters. Evaluation of the parameter variation influence on x_1 and x_2 reveals that the

¹⁶The system response magnitude related to the pseudo-step is significantly higher than the one of the sinusoidal excitation.

Measure	$h_1(\mathbf{x})$	$h_2(\mathbf{x})$
M ₁ [LIT83]	$\kappa_{c,1} = 0.994$ $\kappa_{c,2} = 0.994$	$\kappa_{c,1} = 0.006$ $\kappa_{c,2} = 0.006$
M ₂ [BR86] ($t_{end} = 0.14$)	$\mu_{c,1} = 0.256$ $\mu_{c,2} = 3.198$	$\mu_{c,1} = 0.039$ $\mu_{c,2} = 0.256$

Table 3.5: Observability measures for sensor configurations $h_1(\mathbf{x})$ and $h_2(\mathbf{x})$ of Σ_{L4} .

results are consistent with respect to the two different driving maneuvers and both state variables. These show the highest sensitivity to the parameters ρ_2, ρ_3, ρ_5 . Interestingly, the parameter ρ_4 , referring to the rear lateral cornering stiffness c_{α_r} , is only at the last, but one position.

IV.3 Model Parameter Selection

The discussion of vehicle related parameters is omitted as it has been analyzed in I.4 and details can be extracted from there. With regards to the outcome of the parameter sensitivity analysis it makes sense to select the mentioned parameters ρ_2, ρ_3 and ρ_5 as the ones to be identified. However, the ease of determining vehicle related parameters is higher compared to the tire model parameters. As a consequence, the parameter ρ_3 is selected as the identification objective.

IV.4 Observability Analysis

Similar to the findings of Σ_{L1} the observability and its quantitative measures are to be evaluated for sensor configurations $h_1(\mathbf{x})$ and $h_2(\mathbf{x})$, given by the first and second state variable respectively, i.e.

$$y_1 = h_1(\mathbf{x}) = x_1 \quad \text{and} \quad y_2 = h_2(\mathbf{x}) = x_2. \quad (3.50a)$$

The observability matrices can be calculated as

$$\mathbf{O}_1 = \begin{bmatrix} 1 & 0 \\ a_{11} & a_{12} \end{bmatrix}, \quad \mathbf{O}_2 = \begin{bmatrix} 0 & 1 \\ -1 & 0 \end{bmatrix}. \quad (3.51)$$

The matrix \mathbf{O}_2 is regular independent of any parameters and \mathbf{O}_1 is regular if $a_{12} \neq 0$, which is reasonable considering its definition (3.45a) and the fact that the physical parameters are all > 0 .

Quantitative measures of the observability are listed in Table 3.5. From that the output y_1 suggests itself to be used for state reconstruction.

3.2.3 Roll Dynamics

V.1 State-Space Model

The model of the vehicle chassis' roll dynamics is based on the differential equation of (2.52). That linear differential equation with (assumed) constant coefficients can be formulated as a time-invariant state-space model by defining the state vector $\mathbf{x}(t) \in \mathbb{R}^n$ and input $u(t) \in \mathbb{R}$ as

$$\mathbf{x} := \begin{bmatrix} x_1 & x_2 \end{bmatrix}^T = \begin{bmatrix} \varphi & \dot{\varphi} \end{bmatrix}^T, \quad (3.52a)$$

$$u := a_{y,m}. \quad (3.52b)$$

Then the system reads as

$$\Sigma_R : \begin{cases} \underbrace{\begin{bmatrix} \frac{dx_1}{dt} \\ \frac{dx_2}{dt} \end{bmatrix}}_{=: \dot{\mathbf{x}}} = \underbrace{\begin{bmatrix} 0 & 1 \\ -a_{21} & -a_{22} \end{bmatrix}}_{=: \mathbf{A}} \begin{bmatrix} x_1 \\ x_2 \end{bmatrix} + \underbrace{\begin{bmatrix} 0 \\ b_2 \end{bmatrix}}_{=: \mathbf{b}} u, \\ y = h(\mathbf{x}), \end{cases} \quad (3.53a)$$

$$(3.53b)$$

with

$$a_{21} := \frac{c_{\Sigma}^r}{J_{xc}}, \quad a_{22} := \frac{d_{\Sigma}^r}{J_{xc}} \quad \text{and} \quad b_2 := \frac{m_s h_{rl}}{J_{xc}}. \quad (3.54)$$

V.2 Parameter Sensitivity Analysis

The model parameters that influence the characteristics of the roll dynamics are combined in the parameter vector $\boldsymbol{\rho} \in \mathbb{R}^r$, i.e.

$$\boldsymbol{\rho} := \begin{bmatrix} \rho_1 & \rho_2 & \rho_3 & \rho_4 & \rho_5 \end{bmatrix}^T = \begin{bmatrix} c_{\Sigma}^r & d_{\Sigma}^r & m_s & h_{rl} & J_{xs} \end{bmatrix}^T. \quad (3.55)$$

System (3.53) formulated in state-space and exploiting the definition of the parameter vector $\boldsymbol{\rho}$ reads as

$$\begin{bmatrix} \frac{dx_1}{dt} \\ \frac{dx_2}{dt} \end{bmatrix} = \underbrace{\begin{bmatrix} x_2 \\ -\frac{\rho_1}{\rho_5} x_1 - \frac{\rho_2}{\rho_5} x_2 + \frac{\rho_3 \rho_4}{\rho_5} u \end{bmatrix}}_{=: \begin{bmatrix} f_1(\mathbf{x}) & f_2(\mathbf{x}, \boldsymbol{\rho}, \mathbf{u}) \end{bmatrix}^T}. \quad (3.56)$$

Parameter	Symbol	Value	Unit
c_{Σ}^r	$\bar{\rho}_1$	140000	N·m·rad ⁻¹
d_{Σ}^r	$\bar{\rho}_2$	7000	N·m·s·rad ⁻¹
m_s	$\bar{\rho}_3$	1000	kg
h_{rl}	$\bar{\rho}_4$	0.45	m
J_{xc}	$\bar{\rho}_5$	400	kg·m ²

Table 3.6: Nominal parameter vector $\bar{\rho}$ for parameter sensitivity evaluation of roll dynamics with Σ_R .

Solving the differential equation (3.5) numerically requires definition of the matrices $\mathbf{A}_R(t, \boldsymbol{\rho}) \in \mathbb{R}^{n \times n}$ and $\mathbf{B}_R(t, \boldsymbol{\rho}) \in \mathbb{R}^{n \times r}$. Based on (3.3) these read as

$$\mathbf{A}_R(t, \boldsymbol{\rho}) := \begin{bmatrix} 0 & 1 \\ -\frac{\rho_1}{\rho_5} & -\frac{\rho_2}{\rho_5} \end{bmatrix}, \quad (3.57a)$$

$$\mathbf{B}_R(t, \boldsymbol{\rho}) := \begin{bmatrix} 0 & 0 & 0 & 0 & 0 \\ -\frac{x_1}{\rho_5} & -\frac{x_2}{\rho_5} & \frac{\rho_4}{\rho_5} u & \frac{\rho_3}{\rho_5} u & \frac{\rho_1}{\rho_5^2} x_1 + \frac{\rho_2}{\rho_5^2} x_2 - \frac{\rho_3 \rho_4}{\rho_5^2} u \end{bmatrix}. \quad (3.57b)$$

The nominal values of the parameter vector $\boldsymbol{\rho}$, namely $\bar{\rho}$, are listed in Table 3.6. The simulated driving maneuvers are selected such that transient and steady-state phases are well covered. More exactly, the performed maneuvers refer to a *pseudo-step* and a *sinusoidal* steering signal¹⁷. The obtained results from simulations are shown in Figure 3.5. A quantitative evaluation of the parameter variation effects on x_1 and x_2 reveals that ρ_1 has the highest influence. This is followed by a tie between ρ_3 and ρ_4 . For the pseudo-step signal the parameters ρ_2 and ρ_5 have no effect on both x_1 and x_2 once the system is in steady-state.

V.3 Model Parameter Identification by Static Measurements

To the best knowledge of the author there are no methods available to determine the fictitious values of c_{Σ}^r and d_{Σ}^r from static measurements. However, spring stiffnesses and damping coefficients of the vehicle suspensions as well as the suspension and vehicle geometry allows for calculation of these effective stiffness and damping values, c_{Σ}^r and d_{Σ}^r respectively. For the herein presented work, the assumption suggests itself (due to work of [KOL09]) to suppose the values of J_{xc} , m_s and h_{rl} as given. The latter might be

¹⁷For roll dynamics applications it is often seen that the excitation signal is a chirp signal. However, for the parameter sensitivity analysis it is assumed sufficient to excite the system with a sinusoidal of constant frequency.

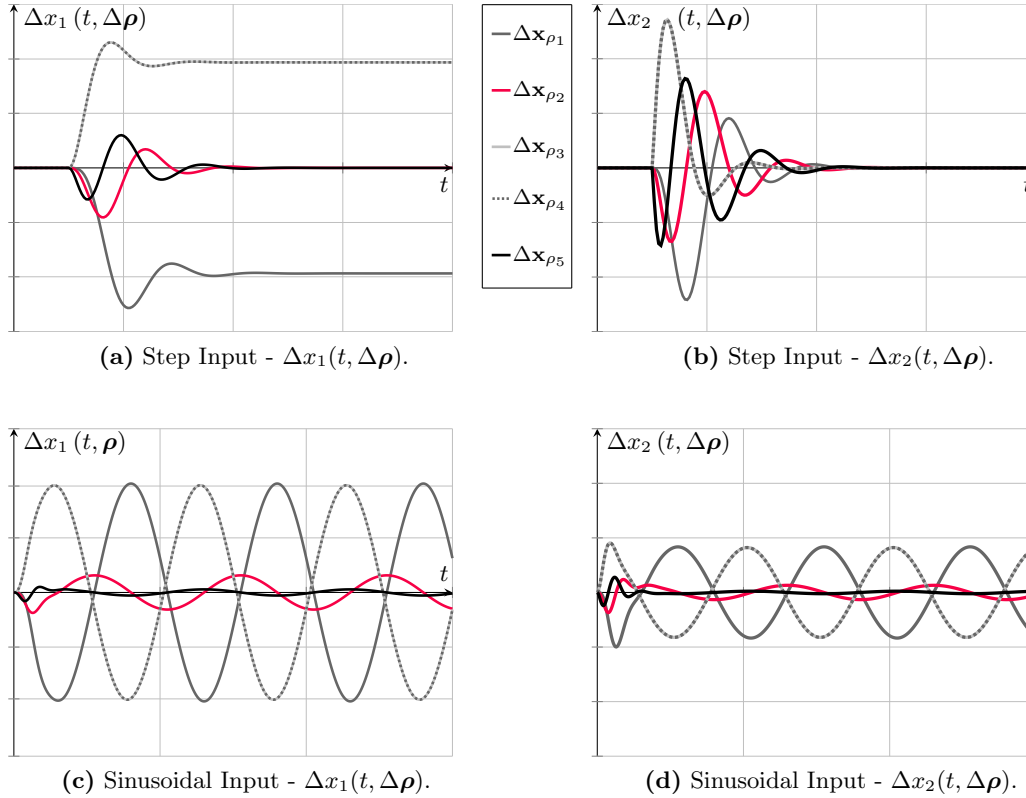


Figure 3.5: Sensitivities of state \mathbf{x} w.r.t. parameter variations $\Delta \rho$ (Σ_R). The axes of (a) and (c) as well as (b) and (d) are scaled identically.

difficult to be determined for real vehicles, but there exist static measurement techniques for the CoG height. Identification of roll center location is discussed in e.g. [MW04].

V.4 Model Parameter Selection

From the sensitivity analysis and the static measurement techniques the parameters of effective roll stiffness c_{Σ}^r and damping d_{Σ}^r are selected as objectives for the observer-based parameter identification. Regarding the roll stiffness this decision coincides with the sensitivity analysis outcome.

V.5 Observability Analysis

For vehicle handling evaluation it is a common practice to install angular position and velocity sensors (see Table 1.1). However, the design of a roll motion observer aims to operate on a single sensor only, i.e. either angular velocity or position. So, the sensor configuration considering regarding both systems states as measurable represents only the reference that most likely will not be available in practice. Consequently, the output

Measure	$h_1(\mathbf{x})$	$h_2(\mathbf{x})$
M ₁ [LIT83]	$\kappa_{c,1} = 0.004$ $\kappa_{c,2} = 0.004$	$\kappa_{c,1} = 0.996$ $\kappa_{c,2} = 0.996$
M ₂ [BR86] ($t_{end} = 0.14$)	$\mu_{c,1} = 0.296$ $\mu_{c,2} = 0.027$	$\mu_{c,1} = 7.106$ $\mu_{c,2} = 0.296$

Table 3.7: Observability measures for sensor configurations $h_1(\mathbf{x})$ and $h_2(\mathbf{x})$ of Σ_R .

mappings $h_1(\mathbf{x})$ and $h_2(\mathbf{x})$ of interest are defined as

$$y_1 = h_1(\mathbf{x}) = \begin{bmatrix} 1 & 0 \end{bmatrix} \mathbf{x} \quad \text{and} \quad y_2 = h_2(\mathbf{x}) = \begin{bmatrix} 0 & 1 \end{bmatrix} \mathbf{x}. \quad (3.58)$$

For the state-space representation (3.53) and the output mappings observability can be checked by e.g. the observability matrices \mathbf{O}_1 , \mathbf{O}_2 . These are full rank resulting in observability of all configurations by assuming the parameter a_{21} to be different from 0 which is completely reasonable, as it presents the scaled¹⁸ effective roll stiffness, see (3.54).

$$\mathbf{O}_1 = \begin{bmatrix} 1 & 0 \\ 0 & 1 \end{bmatrix}, \quad \mathbf{O}_2 = \begin{bmatrix} 0 & 1 \\ -a_{21} & -a_{22} \end{bmatrix}. \quad (3.59)$$

The observability measures $\kappa_{c,i}$ and $\mu_{c,i}$ are used to quantify the observability and furthermore backup the selection of the sensor set. Table 3.7 summarizes the observability measures for the two different sensor configurations (3.58). It reveals that the initial states of the system Σ_R are well observable if the second state variable (angular velocity) is measured. Even though, the system is also observable by considering only the first state variable (angular position) the estimation error is more susceptible to measurement noise [DP13].

This result is also supported by the requirement of low-cost sensor equipment, see Chapter 1. The in-vehicle measurement of angular rates (in this case roll rate) is simpler and more cost-efficient compared to the position measurement. Consequently, for the estimation of system states and unknown parameters the variable to be measured is given by the roll rate, i.e. the time derivative of the roll angle.

3.2.4 Pitch Dynamics

VI.1 State-Space Model

The differential equations modelling the motion of the chassis' pitch dynamics are provided in (2.65). The state vector $\mathbf{x}(t) \in \mathbb{R}^n$ consists of the pitch angle and its time

¹⁸By the moment of inertia w.r.t. the longitudinal axis J_{xc} .

derivative, i.e.

$$\mathbf{x} := \begin{bmatrix} x_1 & x_2 \end{bmatrix}^T = \begin{bmatrix} \theta & \dot{\theta} \end{bmatrix}^T. \quad (3.60)$$

The linear, time-invariant system representing a simplified model of the pitch dynamics reads as

$$\Sigma_P : \begin{cases} \underbrace{\begin{bmatrix} \frac{dx_1}{dt} \\ \frac{dx_2}{dt} \end{bmatrix}}_{=: \dot{\mathbf{x}}} = \underbrace{\begin{bmatrix} 0 & 1 \\ -a_{21} & -a_{22} \end{bmatrix}}_{=: \mathbf{A}} \begin{bmatrix} x_1 \\ x_2 \end{bmatrix} + \underbrace{\begin{bmatrix} 0 \\ b_2 \end{bmatrix}}_{=: \mathbf{b}} u, \\ y = h(\mathbf{x}), \end{cases} \quad (3.61a)$$

with

$$a_{21} := \frac{c_{\Sigma}^p}{J_{yc}}, \quad a_{22} := \frac{d_{\Sigma}^p}{J_{yc}} \quad \text{and} \quad b_2 := \frac{m_s h_{pl}}{J_{yc}}. \quad (3.62)$$

The output mapping $h(\mathbf{x})$ will be discussed and defined later in this section.

VI.2 Parameter Sensitivity Analysis

As for the roll dynamics, see (3.55), the parameter vector $\boldsymbol{\rho} \in \mathbb{R}^r$ is composed of

$$\boldsymbol{\rho} := \begin{bmatrix} \rho_1 & \rho_2 & \dots & \rho_5 \end{bmatrix}^T = \begin{bmatrix} c_{\Sigma}^p & d_{\Sigma}^p & m_s & h_{pl} & J_{yc} \end{bmatrix}^T. \quad (3.63)$$

Merging the definition of the parameter vector (3.63), the state-space formulation (3.61) the system might be represented as shown in (3.56) for the roll dynamics. Furthermore, the identical system and matrix structure of Σ_R and Σ_P yields matrices $\mathbf{A}_P(t, \boldsymbol{\rho}) \in \mathbb{R}^{n \times n}$ and $\mathbf{B}_P(t, \boldsymbol{\rho}) \in \mathbb{R}^{n \times r}$ only differing w.r.t. their parameter interpretation.

The nominal values of the parameter vector $\boldsymbol{\rho}$ required for the numerical solution of the parameter sensitivity functions are presented in Table 3.8. Excitation signals are selected as a pseudo-step and sinusoidal function. Especially for the pitch dynamics, where the actuators are the accelerator and the brake pedals exciting the system sinusoidally is practically almost impossible. Hence these results are more of theoretical interest.

Figure 3.6 depicts the simulation results and obviously x_1 and x_2 are most sensitive to changes of the parameters ρ_1 , ρ_3 and ρ_4 .

VI.3 Model Parameter Identification by Static Measurements

Here, the same assumptions are valid as presented in Section V.3. Hence, the model parameters J_{yc} , m_s and h_{pl} are assumed to be identifiable via static measurements.

Parameter	Symbol	Value	Unit
c_{Σ}^p	$\bar{\rho}_1$	131700	$\text{N}\cdot\text{m}\cdot\text{rad}^{-1}$
d_{Σ}^p	$\bar{\rho}_2$	13750	$\text{N}\cdot\text{m}\cdot\text{s}\cdot\text{rad}^{-1}$
m_s	$\bar{\rho}_3$	1000	kg
h_{pl}	$\bar{\rho}_4$	0.45	m
J_{yc}	$\bar{\rho}_5$	1800	$\text{kg}\cdot\text{m}^2$

Table 3.8: Nominal parameter vector $\bar{\rho}$ for parameter sensitivity evaluation of pitch dynamics with Σ_P .

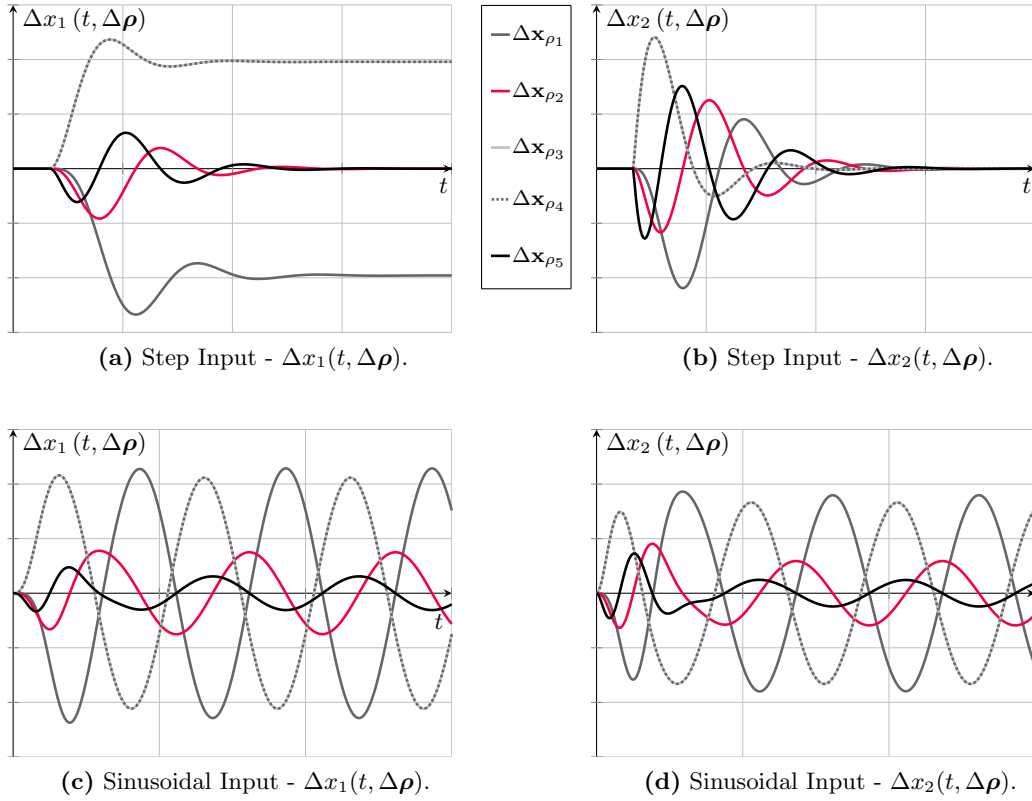


Figure 3.6: Sensitivities of state \mathbf{x} w.r.t. parameter variations $\Delta \rho$ (Σ_P). The axes of (a) and (c) as well as (b) and (d) are scaled identically.

VI.4 Model Parameter Selection

By arguing similarly as in Section V.4 the effective pitch stiffness c_{Σ}^p and damping d_{Σ}^p are selected for parameter identification.

Measure	$h_1(\mathbf{x})$	$h_2(\mathbf{x})$
M_1 [LIT83]	$\kappa_{c,1} = 0.014$ $\kappa_{c,2} = 0.014$	$\kappa_{c,1} = 0.987$ $\kappa_{c,2} = 0.987$
M_2 [BR86] ($t_{end} = 0.08$)	$\mu_{c,1} = 0.155$ $\mu_{c,2} = 0.010$	$\mu_{c,1} = 0.496$ $\mu_{c,2} = 0.155$

Table 3.9: Observability measures for sensor configurations $h_1(\mathbf{x})$ and $h_2(\mathbf{x})$ of Σ_P .

VI.5 Observability Analysis

Identically to the roll dynamics, the aim is to install only a single sensor in the vehicle, either sensing the pitch angular position or its time derivative, the angular rate. Consequently, the sensor setup is identical to (3.58). Furthermore, due to the identical system matrix structures of Σ_R and Σ_P the resulting observability matrices yield exactly (3.59), but a_{21} being defined as in (3.62). Hence, observability of sensor configuration y_1 (measuring pitch angular position) is independent of any model parameters. Moreover, given the moment of inertia J_{yc} is finite and the total pitch stiffness c_{Σ}^p different from zero, observability of sensor configuration y_2 (measuring pitch angular rate) can be concluded. Table 3.9 lists the observability measures for both sensor configurations. From the knowledge of the roll dynamics analysis it is little surprising that sensor setup $h_2(\mathbf{x})$ is the preferable one as argued there.

3.2.5 Steering Dynamics

VII.1 State-Space Model

The two second-order differential equations (2.72) define the dynamics of the electric power steering system. However, as the absolute angular positions are not relevant for the objective to recover the steering torque T_h and wheel torque T_w , the state vector $\mathbf{x}(t) \in \mathbb{R}^n$ is defined as

$$\mathbf{x} := \begin{bmatrix} x_1 & x_2 & x_3 \end{bmatrix}^T = \begin{bmatrix} \omega_h & \omega_s & \delta_d \end{bmatrix}^T. \quad (3.64)$$

The scalar input $u \in \mathbb{R}$ is regarded as $u := T_m$ and the disturbance vector $\boldsymbol{\zeta}(t) \in \mathbb{R}^q$ as

$$\boldsymbol{\zeta} := \begin{bmatrix} \zeta_1 & \zeta_2 \end{bmatrix}^T = \begin{bmatrix} T_h & T_w \end{bmatrix}^T. \quad (3.65)$$

The variables ω_h and ω_s denote the time derivatives of the corresponding angles¹⁹ and $\delta_d := \delta_h - \delta_s$. Based on these definitions the electric-power assisted steering dynamics

¹⁹ $\omega_h := \frac{d\delta_h}{dt}$ and $\omega_s := \frac{d\delta_s}{dt}$.

can be formulated as state-space model [ICDW11]

$$\Sigma_S : \left\{ \begin{array}{l} \begin{array}{l} \frac{dx_1}{dt} \\ \frac{dx_2}{dt} \\ \frac{dx_3}{dt} \end{array} = \underbrace{\begin{bmatrix} -\frac{d_c}{J_{stw}} & 0 & -\frac{c_c}{J_{stw}} \\ 0 & -\frac{d_m i_m^2}{J_{ca}} & \frac{c_c}{J_{ca}} \\ 1 & -1 & 0 \end{bmatrix}}_{=: \mathbf{A}} \begin{bmatrix} x_1 \\ x_2 \\ x_3 \end{bmatrix} + \underbrace{\begin{bmatrix} 0 & \frac{1}{J_{stw}} & 0 \\ \vdots & \vdots & \vdots \\ \frac{i_m}{J_{ca}} & 0 & \frac{i_r^{-1}}{J_{ca}} \\ 0 & 0 & 0 \end{bmatrix}}_{=: [\mathbf{b} \quad \mathbf{D}]} \begin{bmatrix} u \\ \zeta_1 \\ \zeta_2 \end{bmatrix} \\ \mathbf{y} = \mathbf{C} \mathbf{x}. \end{array} \right. \quad (3.66a)$$

The definition of the output mapping will be further discussed in the analysis of the observability. A linear state controller, operating on $u = -\mathbf{k}^T \mathbf{x}$, is employed for dampening oscillations between the steering moment T_h and the angular acceleration of the steering wheel angle δ_h , see [ICDW11]. The controlled system with modified system matrix $\tilde{\mathbf{A}} := \mathbf{A} - \mathbf{b}\mathbf{k}$ with $\mathbf{k} := [k_1 \quad k_2 \quad k_3]^T$ reads as

$$\Sigma_{\tilde{S}} : \left\{ \begin{array}{l} \begin{array}{l} \frac{dx_1}{dt} \\ \frac{dx_2}{dt} \\ \frac{dx_3}{dt} \end{array} = \underbrace{\begin{bmatrix} -\frac{d_c}{J_{stw}} & 0 & -\frac{c_c}{J_{stw}} \\ -\frac{i_m k_1}{J_{ca}} & \tilde{a}_{22} & \frac{c_c - i_m k_3}{J_{ca}} \\ 1 & -1 & 0 \end{bmatrix}}_{=: \tilde{\mathbf{A}}} \begin{bmatrix} x_1 \\ x_2 \\ x_3 \end{bmatrix} + \underbrace{\begin{bmatrix} \frac{1}{J_{stw}} & 0 \\ 0 & \frac{i_r^{-1}}{J_{ca}} \\ 0 & 0 \end{bmatrix}}_{=: \tilde{\mathbf{D}}} \begin{bmatrix} \zeta_1 \\ \zeta_2 \end{bmatrix} \\ \mathbf{y} = \mathbf{C} \mathbf{x}. \end{array} \right. \quad (3.67a)$$

with $\tilde{a}_{22} := -i_m (d_m i_m + k_2) J_{ca}^{-1}$. For the time being the control objective of the LQR-based state controller is purely suppression of inherent oscillations, i.e. there is no scheme for active driver-specific steering characteristics adaption implemented.

VII.2 Parameter Sensitivity Analysis

Other than before the parameter sensitivity knowledge will not be used to select parameters for an identification process. Moreover, it reveals information useful for the *a priori* parameter identification process²⁰ and quantifies a percentage deviation of the

²⁰That deals with the determination of all listed parameters relevant to the steering system. It shall also provide information on the required parameter accuracy and the expected state deviations assuming non-ideal parameters.

states assuming inaccurate parameters. The parameter vector $\boldsymbol{\rho} \in \mathbb{R}^r$ reads as

$$\boldsymbol{\rho} := \begin{bmatrix} \rho_1 & \rho_2 & \dots & \rho_7 \end{bmatrix}^T = \begin{bmatrix} J_{stw} & J_{ca} & c_c & d_c & d_m & i_m & i_r \end{bmatrix}^T. \quad (3.68)$$

As system (3.67) is linear the matrix $\mathbf{A}_S(t, \boldsymbol{\rho}) \in \mathbb{R}^{n \times n}$ does have the same structure as the system matrix \mathbf{A} (but the parameters being replaced by (3.68)) and furthermore using the abbreviations

$$\frac{\partial f_2}{\partial \rho_2} = \frac{\rho_6 k_1}{\rho_2^2} x_1 + \frac{\rho_5 \rho_6^2 + \rho_6 k_1}{\rho_2^2} x_2 - \frac{\rho_3 - \rho_6 k_3}{\rho_2^2} x_3 - \frac{1}{\rho_7 \rho_2^2} d_2, \quad (3.69a)$$

$$\frac{\partial f_2}{\partial \rho_6} = -\frac{k_1}{\rho_2} x_1 - \frac{2 \rho_5 \rho_6 + k_2}{\rho_2} x_2 - \frac{k_3}{\rho_2} x_3, \quad (3.69b)$$

$\mathbf{B}_S(t, \boldsymbol{\rho}) \in \mathbb{R}^{n \times r}$ results in

$$\mathbf{B}_S(t, \boldsymbol{\rho}) = \begin{bmatrix} \frac{\rho_4}{\rho_1^2} x_1 + \frac{\rho_3}{\rho_1^2} x_3 - \frac{1}{\rho_1^2} d_1 & 0 & 0 \\ 0 & \frac{\partial f_2}{\partial \rho_2} & 0 \\ -\frac{1}{\rho_1} x_3 & \frac{1}{\rho_2} x_3 & 0 \\ -\frac{1}{\rho_1} x_1 & 0 & 0 \\ 0 & -\frac{\rho_6^2}{\rho_2} x_2 & 0 \\ 0 & \frac{\partial f_2}{\partial \rho_6} & 0 \\ 0 & -\frac{1}{\rho_7^2 \rho_2} d_2 & 0 \end{bmatrix}^T. \quad (3.70)$$

Simulation of the parameter sensitivity functions requires the definition of the nominal values of the parameter vector $\boldsymbol{\rho}$ as listed in Table 3.10. The disturbance input d_1 is regarded as system input for the sensitivity analysis and the excitation signal is selected as pseudo-step and sinusoidal function. Motivation of their selection has been discussed within the preceding analyses. Obviously, these represent the vehicle maneuvers input step and sinusoidal steering excitation. Figure 3.7 illustrates the simulation results for the two excitation signals.

Parameter	Value	Unit
J_{stw}	0.025	kg·m ²
J_{ca}	0.14	kg·m ²
c_c	110	N·m·rad ⁻¹
d_c	0.5	N·m·s·rad ⁻¹
i_m	18.3	-
i_r	108	-

Table 3.10: Nominal parameter vector $\bar{\rho}$ for parameter sensitivity evaluation of the steering system $\Sigma_{\bar{g}}$.

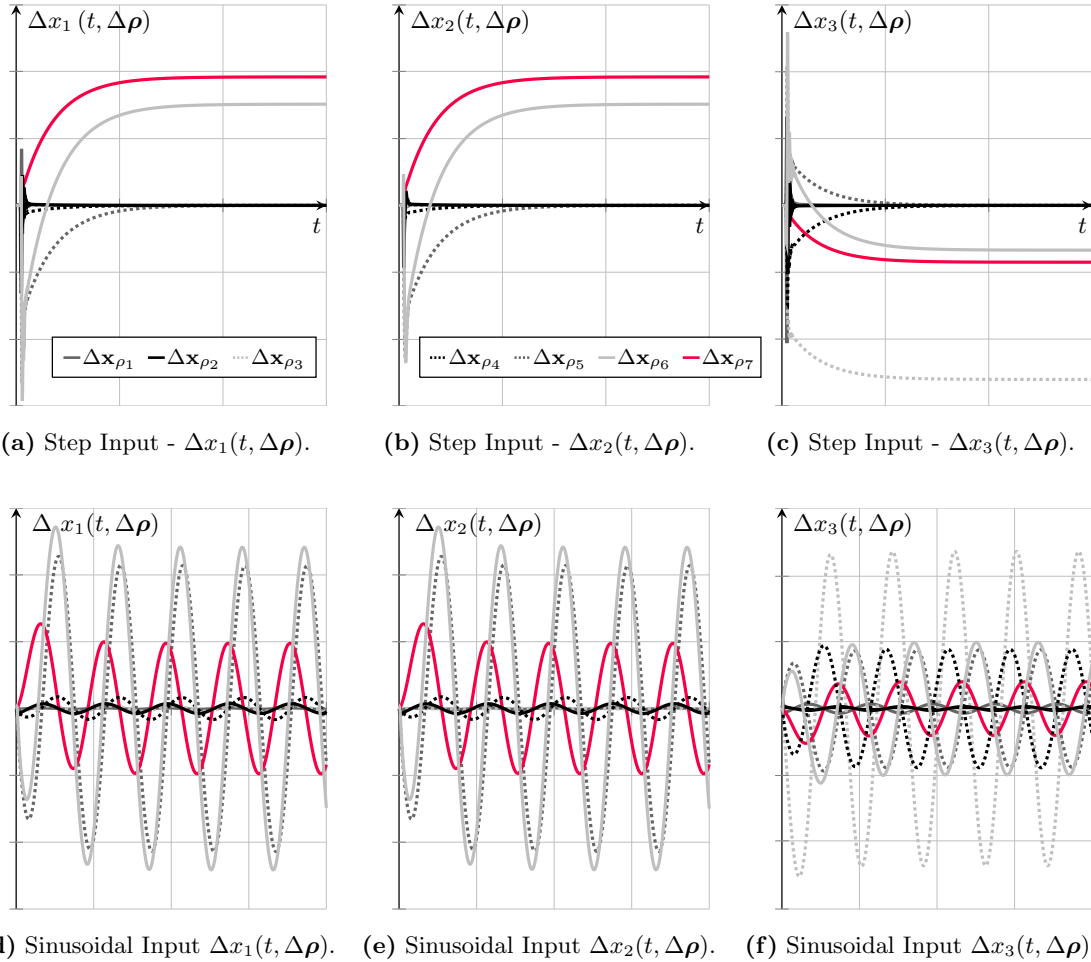


Figure 3.7: Sensitivities of state \mathbf{x} w.r.t. parameter variations $\Delta \rho$ ($\Sigma_{\bar{g}}$).

VII.3 Observability Analysis

The availability of measured system states depends on the number of sensors installed in the considered vehicle. In general, at least two of the three system states should be (indirectly) measurable²¹.

The first system state, i.e. steering wheel angular rate can be computed by considering the steering wheel angle (measured in every modern automotive vehicle) and building the time derivative. However, due to measurement noise appropriate filtering might be required as discussed in Chapters 4, 5, 6.

The torsion angle between steering wheel and motor shaft, represented by x_3 , can be recovered from a torque sensor, supposed c_c is known accurately. In summary, three different sensor configurations, namely $\mathbf{y}_1 \in \mathbb{R}^n$, $\mathbf{y}_2 \in \mathbb{R}^{n-1}$ and $\mathbf{y}_3 \in \mathbb{R}$ are considered, i.e.

$$\mathbf{y}_1 = \mathbf{C}_1 \mathbf{x} = \begin{bmatrix} x_1 & x_2 & x_3 \end{bmatrix}^T, \quad (3.71a)$$

$$\mathbf{y}_2 = \mathbf{C}_2 \mathbf{x} = \begin{bmatrix} x_1 & x_3 \end{bmatrix}^T, \quad (3.71b)$$

$$y_3 = \mathbf{c}_3^T \mathbf{x} = x_3, \quad (3.71c)$$

with the matrices \mathbf{C}_1 , \mathbf{C}_2 , \mathbf{c}_3 of appropriate dimensions. In the following the observability analysis is performed for \mathbf{C}_2 and \mathbf{c}_3 as the first sensor configuration provides already full state information. The observability matrices \mathbf{O}_2 and \mathbf{O}_3

$$\mathbf{O}_2 = \begin{bmatrix} 1 & 0 & -\frac{d_c}{J_{stw}} & 1 & \frac{d_c^2}{J_{stw}^2} - \frac{c_c}{J_{stw}} & -\frac{d_c}{J_{stw}} \\ 0 & 0 & 0 & -1 & \frac{c_c}{J_{stw}} & \frac{d_m i_m^2}{J_{ca}} \\ 0 & 1 & -\frac{c_c}{J_{stw}} & 0 & \frac{d_c c_c}{J_{stw}^2} & -\frac{c_c}{J_{stw}} - \frac{c_c}{J_{ca}} \end{bmatrix}^T, \quad (3.72a)$$

$$\mathbf{O}_3 = \begin{bmatrix} 0 & 0 & 1 \\ 1 & -1 & 0 \\ -\frac{d_c}{J_{stw}} & \frac{d_m i_m^2}{J_{ca}} & -\frac{c_c}{J_{stw}} - \frac{c_c}{J_{ca}} \end{bmatrix}, \quad (3.72b)$$

are both full (column) rank, i.e. system $\Sigma_{\tilde{g}}$ is observable for both configurations. The observability measures M_1 and M_2 , listed in Table 3.11, show the high observability

²¹Referring to the actual sensor setups of a state of the art passenger car.

potential of the sensor configurations \mathbf{C}_1 and \mathbf{C}_2 . However, it is little surprising that the full knowledge of the system state also shows the highest rating in terms of quantitative observability measure. Considering the sensor configuration \mathbf{c}_3 even though the system is observable in theory the recovery of the initial conditions is more susceptible to measurement noise²².

Measure	\mathbf{C}_1	\mathbf{C}_2	\mathbf{c}_3
M ₁ [LIT83]	$\kappa_{c,1} = 1.0$	$\kappa_{c,1} = 0.976$	$\kappa_{c,1} = 0.253 \cdot 10^{-3}$
	$\kappa_{c,2} = 1.0$	$\kappa_{c,2} = 0.976$	$\kappa_{c,2} = 0.253 \cdot 10^{-3}$
	$\kappa_{c,3} = 1.0$	$\kappa_{c,3} = 0.396$	$\kappa_{c,3} = 0.012 \cdot 10^{-3}$
M ₂ [BR86] ($t_{end} = 0.016$)	$\mu_{c,1} = 0.070$	$\mu_{c,1} = 0.046$	$\mu_{c,1} = 3.938 \cdot 10^{-5}$
	$\mu_{c,2} = 0.181$	$\mu_{c,2} = 0.008$	$\mu_{c,2} = 4.938 \cdot 10^{-5}$
	$\mu_{c,3} = 2.975$	$\mu_{c,3} = 0.774$	$\mu_{c,3} = 0.045$

Table 3.11: Observability measures for sensor configurations \mathbf{C}_1 , \mathbf{C}_2 and \mathbf{c}_3 ($\Sigma_{\tilde{g}}$).

3.3 Concluding Remarks for the Parameter Identification

The presented analysis of the vehicle dynamics related models provides a basis to continue with the observer design process. Aside the necessary prerequisite of observability also individual sensor configurations with respect to observability measures have been discussed. Table 3.12 summarizes the individual models, the *to be* identified parameters and also the considered system measurements/sensor configurations.

Σ	Domain	Known Parameters	(To be) Ident. Parameters	Measurement
Σ_{L1}	Lateral	$l_{f_e}, l_{r_e}, J_z, m, h_{rl}$	$c_{\alpha_{f_e}}, c_{\alpha_r}$	$\dot{\psi}$
Σ_{L2}	— " —	— " —	$D_{f/r}, B_{f/r}$	$\dot{\psi}$
Σ_{L3}	— " —	— " —	$D_{f/r}, B_{f/r}, C_{f/r}$	$\dot{\psi}$
Σ_{L4}	— " —	— " —	c_{α_r}	$\dot{\psi}$
Σ_R	Roll	m_s, J_{x_c}, h_{rl}	$c_{\Sigma}^r, d_{\Sigma}^r$	$\dot{\varphi}$
Σ_P	Pitch	m_s, J_{y_c}, h_{pl}	$c_{\Sigma}^p, d_{\Sigma}^p$	$\dot{\theta}$

Table 3.12: Overview of vehicle dynamics models, parameters and measurements.

From the last column of Table 3.12 it can be seen that only angular rates are to be measured. Hence, the requirement for low-cost sensor equipment is fully met.

²²Note that the sensor configuration \mathbf{c}_3^T or alternatively the single measurement of x_1 are generally observable, but for the sake of unknown input recovery the number of measurements needs to match or exceed the number of unknowns. Hence, single channel measurements are only interesting for pure state estimation (without unknown inputs).

4

Observer-Based Parameter Identification Techniques

The preceding analysis of the vehicle dynamics models revealed those parameters that need to be estimated by e.g. observer-based parameter identification techniques. Furthermore, it also identified those quantities that have to be known *a priori* of the estimation process. Additionally, the observability of the given systems has been analyzed that is vital for any following observer design. And finally, it also shed some light on the measurements required and also available in-vehicle, i.e. the use of angular rate sensors for the identification task appears preferable to the position measurements. However, the vehicle handling evaluation requires also information of certain angular positions, e.g. chassis roll angle. Therefore, these signals need to be estimated from the available system descriptions and measurements. Commonly, the mechanisms denoted as state observers aim to reconstruct the system states or more specifically their initial conditions. In case there exist unknown model parameters the task of state estimation becomes more challenging as not only the states, but also the uncertainties, i.e. the model parameters, are to be identified. In literature *robust* state estimation refers to the state reconstruction of a system affected by disturbances such that there is (almost) no difference to the results as if there is no disturbance acting. The simultaneous recovery of states and parameters is referred to as *joint* parameter and state estimation.

Herein, two different paradigms of state *and* parameter estimation are discussed. *State augmentation* requires definition of the nominal model dynamics and then augments it with artificial parameter dynamics. Consequently, the state vector does not only hold the states, but also the parameters. Obviously, due to the system modifications also its properties such as observability need to be evaluated again. Mostly, even if the given system is linear, the state augmentation renders the system nonlinear and the observability evaluation more difficult.

An alternative approach is known as *unknown input reconstruction* paradigm. The idea is as follows: the uncertainties or unmodelled dynamics are lumped into a virtual system input that will be recovered by robust unknown input observer structures.

The remaining chapter is organized as follows: First, the theoretical background of the applied mechanisms is introduced; second, the concepts of observer-based parameter identification are discussed and third, a concept evaluation is performed in simulations. These assume *ideal*¹ conditions and should be interpreted as a proof of concept, whereas the more realistic simulations are conducted in Chapter 5 where the simulated measurements are provided by a detailed multi-body simulations software package.

4.1 Theoretical Background

The identification of parameters related to a certain system model can be conducted in different ways. A main classification criterion is the execution point in time of the algorithm and/or the availability of measurement data. Algorithms executed right after the completion of measurement are known as *offline* approaches. That is opposed to algorithms operating at the same time as the measurements are taken and extracting the new information from these in real-time. These are referred to as *online* approaches. The requirement for in-vehicle applicability necessitates the proposed parameter identification algorithms to be online capable. In the following two different well-known approaches will be discussed theoretically and are later applied to the vehicle dynamics models in order to estimate unknown model parameters in real-time. Exactly speaking, both methods use state observation concepts to recover unknown system states and also model parameters. It is the interpretation, how these uncertain parameters are regarded within the model description, that yields the different paradigms of state and parameter estimation.

In general, the state observation task aims to recover the (unknown) initial conditions of system states from measured system inputs and outputs. More precisely, the estimated state vector $\hat{\mathbf{x}}(t)$ should asymptotically converge to the real state $\mathbf{x}(t)$, i.e.

$$\lim_{t \rightarrow \infty} \mathbf{x}(t) = \lim_{t \rightarrow \infty} \hat{\mathbf{x}}(t). \quad (4.1)$$

The emphasis shall be put here on *asymptotically* as the discussed concept of variable structure observation allows robust² and finite time convergence of the estimation error, i.e.

$$\mathbf{x}(t) = \hat{\mathbf{x}}(t) \quad \forall t \geq \tau_c, \quad (4.2)$$

where $\tau_c < \infty$ denotes the convergence time.

¹*Ideal* in this sense refers to the non-existence of unmodelled dynamics and measurement noise.

²*Robust* with respect to model uncertainties, unmodelled dynamics and disturbance inputs. This is commonly not related to measurement noise.

4.1.1 State Augmentation

Given a nonlinear system of the form

$$\frac{d\mathbf{x}}{dt} = \mathbf{f}(\mathbf{x}, \mathbf{x}_\rho, \mathbf{u}), \quad (4.3)$$

with $\mathbf{x}(t) \in \mathbb{R}^n$ being the state vector, $\mathbf{u}(t) \in \mathbb{R}^m$ the input vector, $\mathbf{x}_\rho \in \mathbb{R}^k$ the vector of constant parameters to be identified³ and the function $\mathbf{f} : D_f \subseteq \mathbb{R}^n \times \mathbb{R}^k \times \mathbb{R}^m \rightarrow \mathbb{R}^n$. The initial conditions of \mathbf{x} and \mathbf{x}_ρ are defined as $\mathbf{x}_0 := \mathbf{x}(t_0)$ and $\mathbf{x}_{\rho_0} := \mathbf{x}_\rho(t_0)$. Then, by definition of a new *augmented* state vector $\mathbf{x}_a(t) \in \mathbb{R}^{n+k}$, i.e.

$$\mathbf{x}_a := \begin{bmatrix} x_{a_1} & \dots & x_{a_{n+k}} \end{bmatrix}^T = \begin{bmatrix} \underbrace{x_1 \dots x_n}_{n \times 1} \vdots \underbrace{x_{\rho_1} \dots x_{\rho_k}}_{k \times 1} \end{bmatrix}^T, \quad (4.4)$$

system (4.3) can be rewritten as

$$\frac{d\mathbf{x}_a}{dt} = \underbrace{\begin{bmatrix} f_1(\mathbf{x}_a, \mathbf{u}) \\ f_2(\mathbf{x}_a, \mathbf{u}) \\ \vdots \\ f_n(\mathbf{x}_a, \mathbf{u}) \\ f_{n+1}(\mathbf{x}_a, \mathbf{u}) \\ \vdots \\ f_{n+k}(\mathbf{x}_a, \mathbf{u}) \end{bmatrix}}_{=: \mathbf{f}_a(\mathbf{x}_a, \mathbf{u})} \quad \left. \begin{array}{l} \left. \begin{array}{l} \left. \begin{array}{l} f_1(\mathbf{x}_a, \mathbf{u}) \\ f_2(\mathbf{x}_a, \mathbf{u}) \\ \vdots \\ f_n(\mathbf{x}_a, \mathbf{u}) \end{array} \right\} n \times 1 \\ \left. \begin{array}{l} f_{n+1}(\mathbf{x}_a, \mathbf{u}) \\ \vdots \\ f_{n+k}(\mathbf{x}_a, \mathbf{u}) \end{array} \right\} k \times 1 \end{array} \right\} \end{array} \right. \quad (4.5)$$

where the last k elements of the function $\mathbf{f}_a(\mathbf{x}_a, \mathbf{u}) : D_f \subseteq \mathbb{R}^{n+k} \times \mathbb{R}^m \rightarrow \mathbb{R}^{n+k}$ are identically zero as the model parameters are assumed constant. Obviously, the increase of the system order from n to $n+k$ necessitates a repetition of the system observability analysis.

For that type of system description common state observation concepts can be applied straightforwardly. Those intrinsically estimate the system states and model parameters due to the modified system description.

Extended Kalman Filter

The classic Kalman Filter (KF) provides the best linear approach to minimize a weighted 2-norm of the estimation error's expectation value [SIM06]. A common assumption for

³The vector \mathbf{x}_ρ is generally a subset of the parameter vector $\boldsymbol{\rho}$ presented for the each vehicle model in Section 3.2. Additionally, emphasis is put on the term *constant*. That is important for the subsequent parameter dynamics modelling process.

the filter derivation is the Gaussianity of the measurement and process noise. If fulfilled, the first- and second-order statistics describe the probability density function of the Gaussian noise completely. However, the standard Kalman Filter operates on a linear system model, but often due to the nonlinear characteristics of real systems that is not helpful. Aside a linearized Kalman Filter version [SIM06] the so-called Extended Kalman Filter (EKF) is the most common employed KF variant. Its derivation will be discussed briefly within the next paragraph, but can be found in more detail in [GA01, GIB11, SIM06].

Given a nonlinear system description by

$$\frac{d\mathbf{x}}{dt} = \mathbf{f}(t, \mathbf{x}, \mathbf{u}, \mathbf{w}), \quad \mathbf{x}_0 := \mathbf{x}(t_0), \quad (4.6a)$$

$$\mathbf{y} = \mathbf{h}(t, \mathbf{x}, \mathbf{u}, \mathbf{v}). \quad (4.6b)$$

where $t \in \mathbb{R}^+$, $\mathbf{x}(t) \in \mathbb{R}^n$ represents the state vector⁴, $\mathbf{u}(t) \in \mathbb{R}^m$ the system input, $\mathbf{w}(t) \in \mathbb{R}^r$ a stochastic process noise, $\mathbf{y}(t) \in \mathbb{R}^p$ the system output, $\mathbf{v}(t) \in \mathbb{R}^q$ the stochastic measurement noise⁵ and the mappings $\mathbf{f} : D_f \subseteq \mathbb{R}^+ \times \mathbb{R}^n \times \mathbb{R}^m \times \mathbb{R}^r \rightarrow \mathbb{R}^n$ and $\mathbf{h} : D_h \subseteq \mathbb{R}^+ \times \mathbb{R}^n \times \mathbb{R}^m \times \mathbb{R}^q \rightarrow \mathbb{R}^p$. The noise terms \mathbf{w} and \mathbf{v} are assumed white Gaussian random variables with zero-mean, i.e. $E[\mathbf{w}(t)] = 0$, $E[\mathbf{v}(t)] = 0$ and covariance matrices [GIB11]

$$E[\mathbf{w}(t)\mathbf{w}^T(\tau)] = \mathbf{Q}(t)\delta(t - \tau), \quad (4.7a)$$

$$E[\mathbf{v}(t)\mathbf{v}^T(\tau)] = \mathbf{R}(t)\delta(t - \tau), \quad (4.7b)$$

$$E[\mathbf{w}(t)\mathbf{v}^T(\tau)] = \mathbf{0} \quad \forall t, \tau \in \mathbb{R}^+, \quad (4.7c)$$

with $\delta(\cdot)$ denoting the Dirac delta function and $E[\cdot]$ the expectation value. Furthermore, the positive definite matrices $\mathbf{Q}(t) \in \mathbb{R}^{r \times r}$ and $\mathbf{R}(t) \in \mathbb{R}^{q \times q}$ refer to as covariance matrices of the process and measurement noise respectively. For brevity, the following notation [SIM06] can be used

$$X \sim \mathcal{N}(\bar{x}, \sigma^2), \quad (4.8)$$

where X is the random variable, \bar{x} its mean value and σ^2 its standard deviation. The operator \mathcal{N} indicates that random variable X is modelled by an e.g. normal distribution

⁴Note that the state vector is not necessarily an augmented vector, hence there is no subscript "a".

⁵Any effects of the process noise on the system output \mathbf{y} are lumped into the term \mathbf{v} and hence no explicit dependence on \mathbf{w} is assumed here.

$\mathcal{N}(0, 1)$. Then, the process and measurement noise terms can be written as

$$\mathbf{w}(t) \sim \mathcal{N}(0, \mathbf{Q}(t) \delta(t - \tau)), \quad (4.9)$$

$$\mathbf{v}(t) \sim \mathcal{N}(0, \mathbf{R}(t) \delta(t - \tau)). \quad (4.10)$$

For a mathematically more rigorous background of the stochastics see e.g. [SIM06, GIB11, PP02]. Commonly, the derivation of the Extended Kalman Filter (EKF) is presented in discrete-time domain due to the eventual implementation of the filter on a digital hardware platform. Consequently, (4.6) needs to be discretized w.r.t. time using e.g. the *Runge-Kutta* method [KRE10], i.e.

$$\mathbf{x}_{k+1} = \mathbf{x}_k + \frac{\boldsymbol{\delta}_1 + 2\boldsymbol{\delta}_2 + 2\boldsymbol{\delta}_3 + \boldsymbol{\delta}_4}{6}, \quad (4.11)$$

with the coefficients $\boldsymbol{\delta}_1, \boldsymbol{\delta}_2, \boldsymbol{\delta}_3, \boldsymbol{\delta}_4$ defined by

$$\boldsymbol{\delta}_1 = \tau_s \mathbf{f}(k\tau_s, \mathbf{x}_k, \mathbf{u}_k, \mathbf{w}_k), \quad (4.12a)$$

$$\boldsymbol{\delta}_2 = \tau_s \mathbf{f}\left(k\tau_s, \mathbf{x}_k + \frac{\boldsymbol{\delta}_1}{2}, \mathbf{u}_k, \mathbf{w}_k\right), \quad (4.12b)$$

$$\boldsymbol{\delta}_3 = \tau_s \mathbf{f}\left(k\tau_s, \mathbf{x}_k + \frac{\boldsymbol{\delta}_2}{2}, \mathbf{u}_k, \mathbf{w}_k\right), \quad (4.12c)$$

$$\boldsymbol{\delta}_4 = \tau_s \mathbf{f}((k+1)\tau_s, \mathbf{x}_k + \boldsymbol{\delta}_3, \mathbf{u}_k, \mathbf{w}_k). \quad (4.12d)$$

For brevity the abbreviation $\mathbf{x}_k := \mathbf{x}(k\tau_s)$, $k \in \mathbb{N}_0$ is introduced with τ_s being the sampling time. Then, the resulting discrete-time system reads as

$$\mathbf{x}_{k+1} = \mathbf{f}_k(\mathbf{x}_k, \mathbf{u}_k, \mathbf{w}_k), \quad \mathbf{x}_0 := \mathbf{x}(0), \quad (4.13a)$$

$$\mathbf{y}_k = \mathbf{h}_k(\mathbf{x}_k, \mathbf{u}_k, \mathbf{v}_k). \quad (4.13b)$$

Before introducing the EKF equations it is necessary to define two different types of estimates, namely the *a priori* and *a posteriori* estimates. The *a posteriori* state and error covariance estimates⁶ are defined by [SIM06]

$$\hat{\mathbf{x}}_k^+ = E \left[\mathbf{x}_k \mid \mathbf{y}_1, \mathbf{y}_2, \dots, \mathbf{y}_k \right], \quad (4.14a)$$

$$\mathbf{P}_k^+ = E \left[\left(\mathbf{x}_k - \hat{\mathbf{x}}_k^+ \right) \left(\mathbf{x}_k - \hat{\mathbf{x}}_k^+ \right)^T \right]. \quad (4.14b)$$

⁶Exactly speaking $\mathbf{P}_k^{+/-}$ represent only approximations of the error covariance matrices due to linearization errors inherent to the Extended Kalman Filter.

From the definition of $\hat{\mathbf{x}}_k$ it is obvious that all last k measurement samples are used for the updated estimation of the state \mathbf{x}_k . In contrast, the *a priori* state and error covariance estimates read as

$$\hat{\mathbf{x}}_k^- = E \left[\mathbf{x}_k \mid \mathbf{y}_1, \mathbf{y}_2, \dots, \mathbf{y}_{k-1} \right], \quad (4.15a)$$

$$\mathbf{P}_k^- = E \left[\left(\mathbf{x}_k - \hat{\mathbf{x}}_k^- \right) \left(\mathbf{x}_k - \hat{\mathbf{x}}_k^- \right)^T \right], \quad (4.15b)$$

and use only the $(k-1)$ last measurements for the state update. Now, the idea for deriving the Extended Kalman Filter is to approximate the right-hand side of (4.13a) by a Taylor series expansion (neglecting any higher-order terms) at the point $(\hat{\mathbf{x}}_k^+, \mathbf{u}_k, \mathbf{0})$ and of (4.13b) at the point $(\hat{\mathbf{x}}_k^-, \mathbf{u}_k, \mathbf{0})$ respectively. The resulting system equations provide the basis for the design of a standard Kalman Filter that finally yields the iterative equations of the discrete-time Extended Kalman Filter, i.e.

$$\left. \begin{array}{l} \text{Correction} \\ \mathbf{C}_k = \frac{\partial}{\partial \mathbf{x}_k} \mathbf{h}_k \left(\hat{\mathbf{x}}_k^-, \mathbf{u}_k, \mathbf{0} \right), \end{array} \right\} \quad (4.16a)$$

$$\mathbf{K}_k = \mathbf{P}_k^- \mathbf{C}_k^T \left(\mathbf{C}_k \mathbf{P}_k^- \mathbf{C}_k^T + \mathbf{R}_k \right)^{-1}, \quad (4.16b)$$

$$\left. \begin{array}{l} \hat{\mathbf{x}}_k^+ = \hat{\mathbf{x}}_k^- + \mathbf{K}_k \left(\mathbf{y}_k - \mathbf{h}_k \left(\hat{\mathbf{x}}_k^-, \mathbf{u}_k, \mathbf{0} \right) \right), \end{array} \right\} \quad (4.16c)$$

$$\mathbf{P}_k^+ = \left(\mathbf{I} - \mathbf{K}_k \mathbf{C}_k \right) \mathbf{P}_k^-, \quad (4.16d)$$

$$\left. \begin{array}{l} \text{Prediction} \\ \mathbf{A}_k = \frac{\partial}{\partial \mathbf{x}_k} \mathbf{f}_k \left(\hat{\mathbf{x}}_k^+, \mathbf{u}_k, \mathbf{0} \right), \end{array} \right\} \quad (4.16e)$$

$$\mathbf{N}_k = \frac{\partial}{\partial \mathbf{w}_k} \mathbf{f}_k \left(\hat{\mathbf{x}}_k^+, \mathbf{u}_k, \mathbf{0} \right), \quad (4.16f)$$

$$\hat{\mathbf{x}}_{k+1}^- = \mathbf{f}_k \left(\hat{\mathbf{x}}_k^+, \mathbf{u}_k, \mathbf{0} \right), \quad (4.16g)$$

$$\mathbf{P}_{k+1}^- = \mathbf{A}_k \mathbf{P}_k^+ \mathbf{A}_k^T + \underbrace{\mathbf{N}_k \mathbf{Q}_k \mathbf{N}_k^T}_{=:\bar{\mathbf{Q}}_k}. \quad (4.16h)$$

Hereby, $\mathbf{C}_k \in \mathbb{R}^{p \times n}$ denotes the linearized output mapping, $\mathbf{K}_k \in \mathbb{R}^{n \times p}$ refers to the Kalman filter gain, $\mathbf{A}_k \in \mathbb{R}^{n \times n}$ the dynamic matrix of the linearized system, $\bar{\mathbf{Q}}_k \in \mathbb{R}^{n \times n}$ the (weighted⁷) covariance matrix of the process noise \mathbf{w}_k and $\mathbf{R}_k \in \mathbb{R}^{p \times p}$ the covariance

⁷By the partial derivative of the function \mathbf{f}_k w.r.t. the process noise \mathbf{w}_k .

matrix of the measurement noise \mathbf{v}_k . Both, $\bar{\mathbf{Q}}_k$ and \mathbf{R}_k are positive definite matrices. Furthermore, the initial conditions of the state $\hat{\mathbf{x}}^+(0) =: \hat{\mathbf{x}}_0^+$ and error covariance estimate read as

$$\hat{\mathbf{x}}_0^+ = E[\mathbf{x}_0], \quad (4.17)$$

$$\mathbf{P}_0^+ = E\left[\left(\mathbf{x}_0 - \hat{\mathbf{x}}_0^+\right)\left(\mathbf{x}_0 - \hat{\mathbf{x}}_0^+\right)^T\right]. \quad (4.18)$$

With respect to the stability of the EKF a good overview is provided in [TØN07] and the important results are given by [LSBJ95, RGYU99, RAP04]. Moreover, stability of a parameter estimating EKF and convergence of these parameters is dealt with in [LJU79]. An increasingly popular alternative to the EKF avoiding the necessary assumption of Gaussianity⁸ is given by the Unscented Kalman Filter (UKF) [JU97, WVDM00] that operates directly on the state distribution, approximated by a set of points. As claimed in [VDMW01] the UKF outperforms the EKF for many applications. However, it suffers from the difficulty of finding an appropriate set of points describing the state distribution. And from a practical point of view the information distortion given a non-Gaussian random variable might be negligible.

Example: EKF-based Model Parameter Identification

Given a second-order LTI system with state vector $\mathbf{x} \in \mathbb{R}^n$ defined as

$$\frac{dx_1}{dt} = x_2, \quad (4.19a)$$

$$\frac{dx_2}{dt} = -\alpha_1 x_1 - \alpha_2 x_2 + u, \quad (4.19b)$$

$$y = x_1, \quad (4.19c)$$

and $\alpha_1 > 0$ being the known, α_2 the *unknown* (but *constant*) model parameter. Consequently, $x_{\rho_1} \in \mathbb{R}$ is scalar and defined as $x_{\rho_1} := \alpha_2$. The initial conditions of the state vector $\mathbf{x} := [x_1 \ x_2]^T$ are denoted by $\mathbf{x}_0 := \mathbf{x}(t_0 = 0)$. In order to allow application of the EKF for estimation of the system states and also unknown parameter α_1 a new, augmented state vector $\mathbf{x}_a \in \mathbb{R}^{n+1}$ is introduced as

$$\mathbf{x}_a := \begin{bmatrix} x_{a_1} & x_{a_2} & x_{a_3} \end{bmatrix}^T = \begin{bmatrix} x_1 & x_2 & x_{\rho_1} \end{bmatrix}^T, \quad (4.20)$$

⁸The EKF inherently assumes the states as Gaussian random variables, represented uniquely by their means and variances. Note that generally random variables are not represented uniquely by their 1st and 2nd statistical moments. These are then propagated through the system using a linearization of the nonlinear system dynamics [HAY01].

where the new state variable x_{a_3} refers to α_2 . As the parameter is assumed constant the resulting nonlinear system is given by

$$\frac{d\mathbf{x}_a}{dt} = \mathbf{f}_a(\mathbf{x}_a, u), \quad (4.21a)$$

$$y = x_{a_1}, \quad (4.21b)$$

with the function $\mathbf{f}_a(\mathbf{x}_a, u)$ defined as

$$\mathbf{f}_a(\mathbf{x}_a, u) := \begin{bmatrix} f_1(\mathbf{x}_a, u) \\ f_2(\mathbf{x}_a, u) \\ f_3(\mathbf{x}_a, u) \end{bmatrix} = \begin{bmatrix} x_{a_2} \\ -\alpha_1 x_{a_1} - x_{a_2} x_{a_3} + u \\ 0 \end{bmatrix} \quad (4.22)$$

The modification of the system structure requires analysis of the observability even if it has been evaluated for the original system already. Based on Theorem 4 (Section 3.1.2) and (3.16) a conclusion on the local observability can be drawn. The Jacobian matrix of the diffeomorphism $\Phi(\mathbf{x}_a, u)$, regarded as local observability matrix $\mathbf{Q}_L(\mathbf{x}_a, u)$, as in (3.15), reads as

$$\mathbf{Q}_L(\mathbf{x}_a, u) := \frac{\partial}{\partial \mathbf{x}_a} \Phi(\mathbf{x}_a, u) = \begin{bmatrix} 1 & 0 & 0 \\ 0 & 1 & 0 \\ -1 & x_{a_2} & x_{a_3} \end{bmatrix}, \quad (4.23)$$

and consequently $\Phi(\mathbf{x}_a, u)$ is a diffeomorphism iff $x_{a_3}(t) \neq 0, \forall t > 0$ and system (4.21) is locally observable. For the implementation of the EKF the system is discretized w.r.t. time using the Runge-Kutta method in (4.11) and (4.12).

The (white) process noise \mathbf{w}_k and measurement noise v_k are assumed Gaussian random variables defined by

$$\mathbf{w}_k \sim \mathcal{N}(0, \bar{\mathbf{Q}}), \quad (4.24a)$$

$$v_k \sim \mathcal{N}(0, r), \quad (4.24b)$$

where the covariance matrix $\bar{\mathbf{Q}}$ and the scalar r are constant and independent of time. Table 4.1 lists the parameters used for the simulation and Figure 4.1 illustrates the state and parameter estimates.

Some Comments on the Simulation Results The graphical illustration of the state variables and the parameter estimate as shown in Figure 4.1(c) reveals the convergence property of the system state \hat{x}_{a_3} to the value of the unknown parameter α_2 . Clearly,

Parameter	Description	Value
\mathbf{x}_0	Initial condition of the state vector \mathbf{x}	$[0 \ 0]^T$
α_1	Known model parameter of (4.19)	20
α_2	Unknown model parameter of (4.19)	9
$\bar{\mathbf{Q}}$	Process noise covariance matrix	$\text{diag}([1\text{e-}7 \ 1\text{e-}7 \ 1\text{e-}2])$
$\hat{\mathbf{x}}_{a,0}^+$	Initial condition of the estimated state vector	$[-0.25 \ 0.65 \ 0.5]^T$
\mathbf{P}_0^+	Initial condition of the error covariance estimate	$\text{diag}([1\text{e-}1 \ 1\text{e-}1 \ 1\text{e}0])$
r	Measurement noise covariance	$1\text{e-}5$

Table 4.1: Simulation parameters of the plant and the EKF.

the estimation error of the first state variable, also measured, is almost zero from the very beginning of the simulations due to the tuning of the filter. The small values of the measurement variance r and the initial error covariance estimate \mathbf{P}_0^+ , see Table 4.1, result in a Kalman gain, that forces the state estimates $\hat{x}_{a_{1,k}}^+$ to y_k immediately. Another fact important to mention is the tuning of the $\bar{\mathbf{Q}}$ matrix. It is obvious that the process noise variance of \hat{x}_{a_3} exceeds that of \hat{x}_{a_1} and \hat{x}_{a_2} by the order of five magnitudes. A sloppy interpretation would be the following: the mathematical model of the $\hat{x}_{a_1}, \hat{x}_{a_2}$ dynamics is more reliable than the random-walk model of the third state variable, i.e. the unknown parameter estimate. This is a very typical setup of the process noise covariance matrix when augmenting the state vector with model parameters. In general, the tuning of the covariance matrices related to the process noise $\bar{\mathbf{Q}}$ and measurement noise \mathbf{R} (or in this example scalar r) is not straightforward and requires some expertise. Consequently, numerous publications propose automatic tuning of these matrices, e.g. [ORR06, BDP11, SGG14].

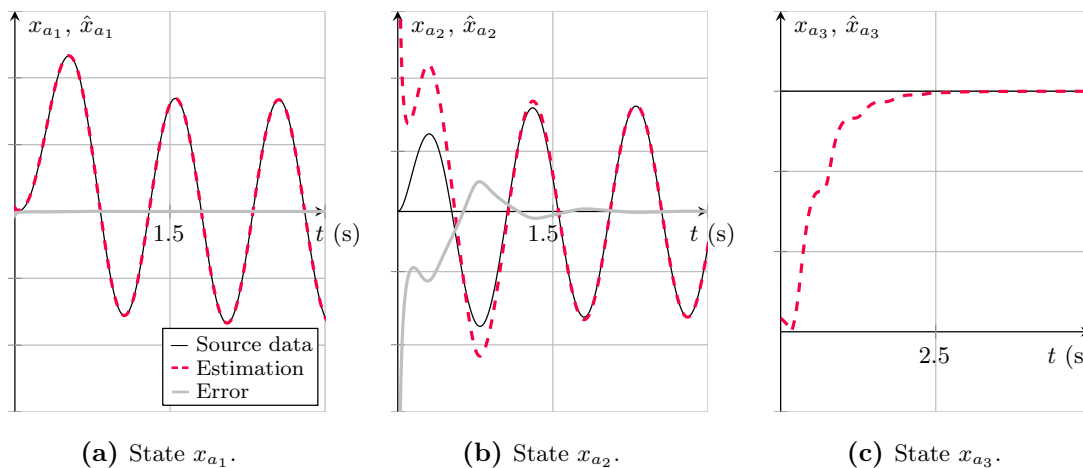


Figure 4.1: Joint state and parameter estimation simulation results of system (4.19).

4.1.2 Unknown Input Estimation

In contrast to state vector augmentation the approach of unknown input estimation lumps the uncertain or completely unknown parameters into a virtual input. Again vector $\mathbf{x}_\rho \in \mathbb{R}^k$ shall be considered that holds all unknown parameters. Then, exploiting the physical meaning of its elements at least their nominal ranges can be assumed known. That allows separation into known (nominal) part and an unknown one, i.e.

$$\mathbf{x}_\rho = \bar{\mathbf{x}}_\rho + \Delta\mathbf{x}_\rho. \quad (4.25)$$

Here, $\bar{\mathbf{x}}_\rho$ represents the nominal and $\Delta\mathbf{x}_\rho$ the unknown part of the vector \mathbf{x}_ρ . Now, considering system (4.3) and the separation of the state vector it can be written as

$$\frac{d\mathbf{x}}{dt} = \mathbf{f}(\mathbf{x}, \bar{\mathbf{x}}_\rho, \mathbf{u}) + \underbrace{\Delta\mathbf{f}(\mathbf{x}, \Delta\mathbf{x}_\rho, \mathbf{u})}_{=:\zeta}. \quad (4.26)$$

The objective of the observer design is now to estimate the system states $\mathbf{x} \in \mathbb{R}^n$ robustly even if an unknown input $\zeta \in \mathbb{R}^n$ acts on the system⁹. For the considered class of systems so-called *unknown input* observers can be constructed. Ideally, recovery of the unknown input allows further identification of the parameter uncertainties $\Delta\mathbf{x}_\rho$. However, due to stochastic (measurement noise) and also deterministic (unmodelled system dynamics) noise effects the recovered unknown input gets distorted and that might lead to inaccurately recovered parameter uncertainties.

Conventional Sliding Modes

In the 1970s the sliding mode approach began to rise and still it is one of the most popular control strategies for handling systems affected by bounded uncertainties [STP12]. Interpreted as a special kind of variable structure systems the characteristic attribute is the real-time hard switching between different system structures. An inherent property of those variable structure systems is the occurrence of a so-called *sliding mode*, in case the system switching occurs at an infinite frequency [PIS00]. The naming is derived from the fact, that the system can be thought of as sliding on a discontinuity surface (or manifold) into the origin. That hyperplane \mathcal{S} is defined as follows

$$\mathcal{S} = \{\mathbf{x} \in \mathbb{R}^n : \boldsymbol{\sigma}(\mathbf{x}) = \mathbf{0}\}. \quad (4.27)$$

Moreover, that manifold represents an invariant set, i.e. if the trajectories are on the manifold once, they remain there. Interestingly, and that is one of the main characteristics related to sliding modes, the design of the manifold prescribes the reduced-order motion of the system once in sliding mode. Furthermore, during sliding the system is

⁹For now it is only assumed that $\zeta(t)$ is bounded by some constant $\Omega < \infty$. The mathematically more rigorous restrictions on the unknown input are defined in the related parts of this chapter.

invariant to external disturbances and even internal parameter uncertainties, if some assumptions on the system structure, see [DRA69] for details, are fulfilled.

In general, the design of a sliding mode control¹⁰ concept is twofold. First, an appropriate manifold defining the controlled systems dynamics in sliding mode needs to be designed [SEFL14, BDK09]. Second, a discontinuous control law is to be formulated such that the system trajectories reach the manifold within finite time. This phase is referred to as *reaching* phase, whereas the motion on the sliding surface is called *sliding* phase.

The basic ideas of the sliding mode technique will be demonstrated by a simple introductory example.

Example: Stabilization of a Double Integrator with Unknown Input (UI)

Given a second-order LTI system defined as

$$\frac{dx_1}{dt} = x_2, \quad (4.28a)$$

$$\frac{dx_2}{dt} = u + \Delta_u, \quad (4.28b)$$

representing a double-integrator. The initial conditions $\mathbf{x}_0 := \mathbf{x}(t_0)$ are chosen arbitrarily, but different from $\mathbf{0}$.

Obviously, as the system is not asymptotically stable inherently, the origin $\mathbf{x}_e = \mathbf{0}$ shall be stabilized using the sliding mode control concept. For now, the uncertain input $\Delta_u \in \mathbb{R}$ is assumed as $\Delta_u = 0$.

First, a sliding manifold \mathcal{S} , governing the sliding motion, needs to be designed. Here, the sliding variable $\sigma \in \mathbb{R}$ is defined by

$$\sigma := \mathbf{S} \mathbf{x}, \quad (4.29)$$

with $\mathbf{S} \in \mathbb{R}^n$ given as $\mathbf{S} := [\lambda \ 1]$, where λ is constant and strictly positive. Now, assuming a sliding mode can be enforced, i.e. $\sigma \equiv 0$, there happens an *order-reduction* of the initial system, as $x_2 = -\lambda x_1$. Consequently, a single differential equations, namely

$$\frac{dx_1}{dt} = -\lambda x_1, \quad (4.30)$$

is sufficient to describe the system dynamics. This order-reduction (in sliding mode) is an intrinsic feature meaning that, whatever the system dynamics are before the sliding phase, they are completely determined by the design of the sliding manifold \mathcal{S} during

¹⁰Note that the presented findings are related to the control objective, i.e. stabilization of a given system. However, they are transferable to the problem of state observer design assuming the system being represented in estimation error coordinates. Then the observation task can be interpreted as stabilization problem.

sliding! For the present problem the definition of a linear sliding surface yields asymptotically decaying system states. Once the sliding manifold is designed it is the task to construct a controller that enforces the sliding mode. Calculation of the sliding variable derivative w.r.t. time and defining it as discontinuous¹¹, i.e.

$$\frac{d\sigma}{dt} = u + \lambda x_2 \stackrel{!}{=} -\eta[\sigma]^0. \quad (4.31)$$

Here, η is a strictly positive constant. For brevity, the operator $[\cdot]$ is introduced as $[x]^y := |x|^y \operatorname{sign}(x)$ and $[x]^0 := \operatorname{sign}(x)$. Moreover, the definition of the sign function is given by

$$\operatorname{sign}(x) = \begin{cases} 1 & x > 0, \\ \in [-1, 1] & x = 0, \\ -1 & x < 0. \end{cases} \quad (4.32)$$

The control law is then defined as $u = -\lambda x_2 - \eta[\sigma]^0$ and using the Lyapunov function candidate $V(\sigma) = \frac{1}{2} \sigma^2$ it can be shown that the *reachability condition* (see e.g. [SEFL14, UGS09])

$$\sigma \dot{\sigma} < -\eta|\sigma|, \quad (4.33)$$

ensuring finite time convergence of σ and attainment of a sliding mode, holds. The closed-loop system using the discontinuous control law reads as

$$\frac{dx_1}{dt} = x_2, \quad (4.34a)$$

$$\frac{dx_2}{dt} = -\lambda x_2 - \eta[\sigma]^0. \quad (4.34b)$$

Since the right-hand side of (4.34) is no longer continuous the Lipschitz condition¹² does not hold and conventional methods can not be applied for solving the differential equations. Therefore, solutions to problem (4.34) are commonly understood in the sense of Filippov, see [FIL88, UGS09] for further details.

Now, the uncertainty Δ_u is assumed different from zero, but bounded with a (Lipschitz)

¹¹Note that due to nullifying σ and accepting a discontinuous $\dot{\sigma}$ this concept is denoted as 1-sliding.

¹²The function $\mathbf{f}(t, \mathbf{x})$ needs to fulfill the inequality

$$\|\mathbf{f}(t, \mathbf{x}) - \mathbf{f}(t, \mathbf{y})\| \geq L \|\mathbf{x} - \mathbf{y}\| \quad \forall t, \mathbf{x}, \mathbf{y}, \quad (4.35)$$

in some connected set, then the function is said to be (locally) Lipschitz [KHA02] and L denotes the Lipschitz constant.

bounded derivative, i.e.

$$|\Delta_u(t)| < \Delta_u^+ < \infty \quad \text{and} \quad \left| \frac{d}{dt} \Delta_u(t) \right| < \bar{\Delta}_u^+ < \infty \quad \forall t. \quad (4.36a)$$

Then (4.31) changes, as the *matched*¹³ uncertainty appears in the time-derivative of σ , resulting in

$$\frac{d\sigma}{dt} = u + \lambda x_2 + \Delta_u \stackrel{!}{=} -\tilde{\eta}[\sigma]^0. \quad (4.37)$$

The control signal can then be calculated as $u = -\lambda x_2 - \tilde{\eta}[\sigma]^0$ with $\tilde{\eta} := (\eta + \Delta_u^+)$. By checking the reachability condition $\sigma \dot{\sigma}$, i.e.

$$\sigma \dot{\sigma} = \sigma \Delta_u - (\eta + \Delta_u^+) |\sigma|, \quad (4.38)$$

and applying the worst case approximation

$$\sigma \Delta_u \leq |\sigma \Delta_u| = |\sigma| |\Delta_u| < |\sigma| \Delta_u^+, \quad (4.39)$$

it can be seen that σ converges to zero within finite time and rejects the disturbance completely¹⁴. In other words, the system motion during the sliding phase is not affected by the perturbation at all! Denoting the time to terminate the reaching phase, i.e. driving σ to zero, by τ_{c1} , it is obvious that $\forall t \geq \tau_{c1} < \infty$,

$$0 \equiv \lambda x_2 + u_{eq} + \Delta_u, \quad (4.40)$$

holds. The concept of the so-called *equivalent control* u_{eq} [UTK92] can be seen as the average effect of the discontinuous control¹⁵ such that the system trajectories remain on the sliding surface. An approximation of the equivalent term can be obtained by low-pass filtering of the discontinuous control, denoted by

$$\hat{u}_{eq} = -\lambda x_2 - \left(\tilde{\eta}[\sigma]^0 \right)_{lpf}. \quad (4.41)$$

Now, combining (4.40) and (4.41) it can be seen that an estimate of the uncertainty/un-

¹³An uncertainty is called *matched*, if the attained sliding mode is invariant to the acting perturbation. Therefore, the well-known *matching* condition [DRA69] needs to hold. For further details see also [UGS09, SEFL14].

¹⁴It should be noted that the discussed invariance to matched disturbances only holds during the sliding motion. This is in contrast to the *reaching phase*, i.e. the time period before the sliding motion is induced, where the system is sensitive to disturbances.

¹⁵Theoretically switching at infinite frequency. Due to imperfections in the practical implementation high-frequent, but finite.

known input Δ_u can be obtained¹⁶ from the equivalent control term, i.e.

$$\left(\tilde{\eta}|\sigma|^0\right)_{l_{pf}} =: \hat{\Delta}_u. \quad (4.42)$$

In summary, once the controlled system (4.28) is in a sliding mode, its dynamics are completely defined by the sliding surface, i.e. it tends to the origin asymptotically. Alternatively to the linear sliding surface definition (4.29) a nonlinear surface can be designed as

$$\sigma := x_2 + \kappa|x_1|^{\frac{1}{2}}, \quad (4.43)$$

with κ strictly positive. This ensures finite time convergence of the trajectories to the origin $\mathbf{0}$. The controller structure is identical to the previous one, but considers the alternative definition of the sliding variable. Consequently, u reads as

$$u = -\tilde{\eta}|\sigma|^0, \quad (4.44)$$

where $\tilde{\eta}$ is a positive constant, see (4.37) for its choice. In the literature that concept is known as control *with prescribed convergence law* [SEFL14]. Interestingly, this control concepts leads to a second-order sliding motion and considering the uncompensated system dynamics (4.28) to a complete *dynamical collapse* (during sliding) ending up in algebraic equations for the system states, i.e. $x_1 = x_2 = 0$. However, as the second-order sliding motion only takes place at the origin there are discussions in the sliding mode community whether it is reasonable to use the term *second-order sliding mode* here. However, due to the finite time convergence of the system prescribed by the nonlinear sliding surface that concept belongs to the class of *terminal sliding mode* (TSM), see e.g. [VG93, ZPW94, FRI12, RH14] for details.

Higher-order Sliding Modes

The inherent deficiencies of the 1-sliding approach are its restriction of relative degree¹⁷ 1, i.e. the control has to appear in the first time derivative of the sliding variable explicitly, and the occurrence of the *chattering* effect due to discontinuous control signal character.

¹⁶A discussion of the filter design influence on the equivalent control approximation accuracy is found in [UTK92].

¹⁷Given a nonlinear, input-affine SISO system $\dot{\mathbf{x}} = \mathbf{a}(\mathbf{x}) + \mathbf{b}(\mathbf{x})u$, $y = c(\mathbf{x})$ then the system's relative degree ρ , with $1 \leq \rho \leq n$, of the output y w.r.t. the input u is defined by

$$L_{\mathbf{b}} L_{\mathbf{a}}^{i-1} c(\mathbf{x}) = 0 \quad i = 1, 2, \dots, \rho - 1 \quad \text{and} \quad L_{\mathbf{b}} L_{\mathbf{a}}^{\rho-1} c(\mathbf{x}) \neq 0,$$

with the *Lie-Derivative*

$$L_{\mathbf{b}} L_{\mathbf{a}}^k c(\mathbf{x}) := \frac{\partial \left(L_{\mathbf{a}}^k c(\mathbf{x}) \right)}{\partial \mathbf{x}} \mathbf{b}(\mathbf{x}).$$

Further details can be found in [KHA02].

Higher-order sliding modes aim to bring r -time derivatives of the sliding variable to zero, i.e. $\sigma = \dot{\sigma} = \dots = \sigma^{r-1} = 0$ [PB02], where r denotes the order of the sliding motion [LEV93]. The herein considered higher-order sliding mode concepts belong to the class of second-order sliding modes (SOSM). Well-known and widely used examples of controllers yielding 2-sliding are the *twisting* [LEV93], *sub-optimal* [BFU98] and *quasi-continuous* [LEV05] algorithms. Further 2-sliding controllers have been presented in [LEV07]. However, measurement/knowledge of the sliding variable derivative w.r.t. time is required. An interesting controller for relative degree 1 systems, but providing a second-order sliding mode, is the *super-twisting* algorithm (STA) [LEV93, LEV03]. The control signal of a super-twisting algorithm generally reads as

$$u = \alpha_1 |\sigma|^{\frac{1}{2}} + \nu, \quad (4.45a)$$

$$\frac{d\nu}{dt} = \alpha_2 |\sigma|^0, \quad (4.45b)$$

with α_1, α_2 being strictly positive and known as the controller gains¹⁸, σ the sliding variable and ν a correction term compensating disturbances (as shown in the example below).

Example (cont'd): Stabilization of a Double Integrator with UI

Due to its applicability to relative degree 1 systems its design is very similar to the one presented for the conventional 1-sliding modes. Moreover, it provides invariance to a certain class of disturbances and finite time convergence. However, the main advantage is the *continuous* control signal. The sliding surface shall be given as in (4.29) and a super-twisting controller can be designed as follows. Differentiating the sliding variable w.r.t. time leads to

$$\frac{d\sigma}{dt} = \underbrace{\lambda x_2 + \Delta_u}_{=: \tilde{\Delta}_u} - \alpha_1 |\sigma|^{\frac{1}{2}} - \nu, \quad (4.46a)$$

$$\frac{d\nu}{dt} = \alpha_2 |\sigma|^0. \quad (4.46b)$$

Then, by choosing the controller gains as in [LEV98], i.e.

$$\alpha_1 = 1.5 \left(\tilde{\Delta}_u^+ \right)^{\frac{1}{2}} \quad \text{and} \quad \alpha_2 = 1.1 \tilde{\Delta}_u^+, \quad (4.47)$$

¹⁸The tuning of the STA coefficients is based on the upper bound of the uncertainty, see e.g. [LEV93, LEV98, DFL05].

Parameter	Description	Value
Δ_u	Disturbance acting on the plant input	$1 + \sin(0.2\pi t) + \sin(8\pi t)$
λ	Sliding surface design parameter, see (4.29)	3
$\tilde{\eta}$	Controller gain of C_1 (4.37) and C_2 (4.44)	9
κ	Sliding surface design parameter, see (4.43)	3
α_1, α_2	Controller gains of C_3 (4.45)	20, 50

Table 4.2: Simulation parameters of the plant and the sliding mode controllers.

with $\tilde{\Delta}_u^+$ given by¹⁹

$$\left| \frac{d}{dt} \tilde{\Delta}_u(t) \right| < \tilde{\Delta}_u^+ < \infty \quad (4.48)$$

the condition $\sigma \equiv 0, \dot{\sigma} \equiv 0$ holds $\forall t \geq \tau_{c_2} < \infty$ [LEV98, MO12]. From (4.46a) it is obvious that once σ and $\dot{\sigma}$ are zero ν provides information of the uncertainty Δ_u *without* filtration (as required in the case of 1-sliding). Moreover, due to the continuity of the term $\alpha_1[\sigma]^{\frac{1}{2}}$ and hiding the discontinuity $\alpha_2[\sigma]^0$ under the integral, the super-twisting control is continuous. In terms of convergence the use of (4.29) results in an asymptotic behavior, rather than finite time²⁰.

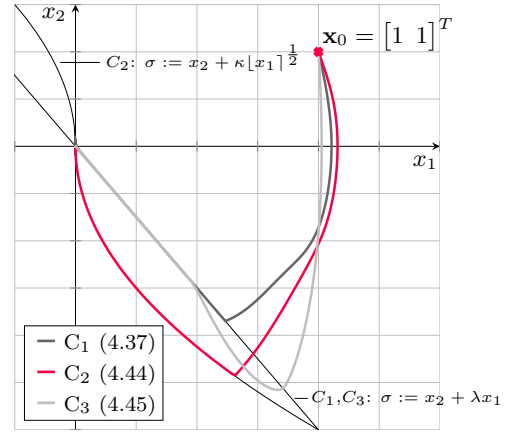


Figure 4.2: Phase portrait of the stabilized system trajectories (4.28).

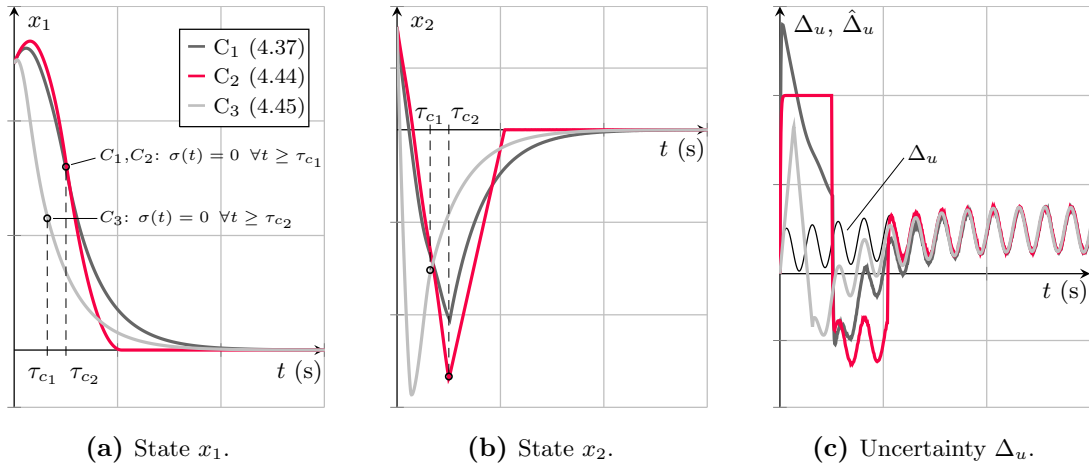


Figure 4.3: Simulation results of stabilized double integrator (4.28).

¹⁹Inherently a bounded state x_2 is assumed.

²⁰This can be overcome by employing the nonlinear sliding surface (4.43).

4.2 Applied Observer-Based Parameter Identification Techniques

4.2.1 Lateral Dynamics

The analysis of Section 3.2.2 revealed a significant influence of the tire model related parameters on the overall system behavior. Moreover, their determination is mostly based on offline identification techniques exploiting test bench measurement data, e.g. [AHH03, OCGS06]. The challenging in-vehicle estimation of the parameters commonly employs expensive measurement equipment and the observer design might become difficult due to the increasing model complexity, e.g. [BCLT08, DVL⁺10]. Often, these methods do not aim for providing parameters of the tire force models directly, but robust vehicle state estimates and therefore adapt the tire model parameters. Reconsidering the use of the SMF tire model (Section 3.2.2.II) four parameters need to be identified. So, augmenting the state vector by four unknown parameters results in a sixth-order system and even in simulations that concept is already very sensitive to its tuning w.r.t. the filter convergence properties.

Herein, a tailored identification procedure will be presented that is capable of estimating model parameters related to 3.2.2.I (Lin), 3.2.2.II (SMF) and 3.2.2.III (TMs) obtained from a small number of driving experiments. For some of the observation techniques the input-affine linear tire force model (see 3.2.2.IV) will be employed rather than the standard single-track model, as in 3.2.2.I.

The proposed design should allow robust, online estimation of model parameters without requiring installation of expensive sensor equipment, i.e. use of signals such as lateral velocity, tire forces (longitudinal, lateral, vertical) is not intended. The overall task is divided into a two-stage identification procedure that can be summarized as follows:

- Stage I aims to identify the lateral cornering stiffness, see (2.25). Coherence between cornering stiffness and tire model parameters is given in Section 2.2.1. A slow sinusoidal steering with low amplitude is selected as system excitation.
- Stage II identifies the maximum lateral tire forces during extensive vehicle excitation. Either a slow sinusoidal maneuver or a steady-state circular drive (up to the limits of adhesion) are to be performed.

Due to the separation of the overall objective, the observer designs provide tailored solutions to the specific problems. Furthermore, the resulting identification techniques for the lateral cornering stiffnesses can also be used for the linear lateral model, see Section 3.2.2.I.

So, exploiting the proposed observer concepts will allow straightforward identification of model parameters related to the SMF and TM_Simple models and requires only a few distinct driving maneuvers. The detailed procedure of model parameters extraction from the specified characteristic points will be covered in the Chapter 5.

I Lateral Cornering Stiffness Observer

In general, the so-called lateral cornering stiffness represents the slope of the slip-force characteristics at the origin, see (2.25). Even though the linear characteristics between the slip angle and the tire force are only valid for a restricted range, due to its simplicity the linear tire force model is often seen in practical implementations. Moreover, identification of the lateral stiffness quantity is subject of many publications, e.g. [STJP06, BCLT08, WI09, LNO15]. Herein, two different concepts based on observation techniques will be discussed aiming to determine the lateral cornering stiffness parameters from yaw measurements as discussed in 3.2.2.I and 3.2.2.IV.

I.1 Extended Kalman Filter (EKF)

State Augmentation

The state-space formulation Σ_{L1} (3.20) builds the basis for the estimation problem. In addition to state estimation of x_1 and x_2 , namely the yaw rate and vehicle sideslip angle, the (constant) model parameters $c_{\alpha_{fe}}$ and c_{α_r} shall be identified. Therefore, the state vector (3.19) needs to be augmented by a parameter vector $\mathbf{x}_\rho \in \mathbb{R}^k$ defined as $\mathbf{x}_\rho := [x_{\rho_1} \ x_{\rho_2}]^T = [c_{\alpha_{fe}} \ c_{\alpha_r}]^T$. That leads to the augmented state vector $\mathbf{x}_a \in \mathbb{R}^{n+k}$ given as

$$\mathbf{x}_a := \left[\underbrace{x_{a_1} \ x_{a_2}}_{=: \mathbf{x}} \quad \underbrace{x_{a_3} \ x_{a_4}}_{=: \mathbf{x}_\rho} \right]^T = \left[\dot{\psi} \ \beta \ c_{\alpha_{fe}} \ c_{\alpha_r} \right]^T. \quad (4.49)$$

The extended state-space formulation for state and parameter observer design reads as

$$\frac{d\mathbf{x}_a}{dt} = \mathbf{f}_a(\mathbf{x}_a, \mathbf{u}), \quad (4.50a)$$

$$y = h_a(\mathbf{x}_a, \mathbf{u}), \quad (4.50b)$$

with $\mathbf{f}_a : D_{f_a} \subseteq \mathbb{R}^{n+k} \times \mathbb{R}^m \rightarrow \mathbb{R}^{n+k}$, $h_a : D_{h_a} \subseteq \mathbb{R}^{n+k} \rightarrow \mathbb{R}$. For any further details see 3.2.2.I.1. The vector-valued function $\mathbf{f}_a(\cdot) := [f_1(\cdot) \ f_2(\cdot) \ f_3(\cdot) \ f_4(\cdot)]^T$ is defined by

$$\begin{bmatrix} f_1(\mathbf{x}_a, \mathbf{u}) \\ f_2(\mathbf{x}_a, \mathbf{u}) \\ f_3(\mathbf{x}_a, \mathbf{u}) \\ f_4(\mathbf{x}_a, \mathbf{u}) \end{bmatrix} := \begin{bmatrix} a_{11}(\mathbf{x}_a)u_2^{-1}x_{a_1} + a_{12}(\mathbf{x}_a)x_{a_2} + b_{11}(\mathbf{x}_a)u_1 - b_{13}(\mathbf{x}_a)u_3u_2^{-1} \\ a_{21}(\mathbf{x}_a)u_2^{-2}x_{a_1} + a_{22}(\mathbf{x}_a)u_2^{-1}x_{a_2} + b_{21}(\mathbf{x}_a)u_1u_2^{-1} - b_{23}(\mathbf{x}_a)u_3u_2^{-2} \\ 0 \\ 0 \end{bmatrix}. \quad (4.51)$$

The low excitation of the lateral dynamics allows to neglect the coupling effects with the roll dynamics, i.e. input u_3 can be omitted for both observer design paradigms.

Observability Analysis

Augmentation of the system states with parameters affects the system structure significantly and its observability analysis as presented in Section 3.2.2.I.5 is not valid anymore. The nonlinear system character requires a local observability analysis using the criterion (3.16). A diffeomorphism $\Phi(\mathbf{x}_a, \mathbf{u}, \dot{\mathbf{u}}, \ddot{\mathbf{u}})$ can be formulated as in (3.15), i.e.

$$\Phi(\mathbf{x}_a, \mathbf{u}, \dot{\mathbf{u}}, \ddot{\mathbf{u}}) := \begin{bmatrix} y(\mathbf{x}_a) & \dot{y}(\mathbf{x}_a, \mathbf{u}) & \ddot{y}(\mathbf{x}_a, \mathbf{u}, \dot{\mathbf{u}}) & \dddot{y}(\mathbf{x}_a, \mathbf{u}, \dot{\mathbf{u}}, \ddot{\mathbf{u}}) \end{bmatrix}^T. \quad (4.52)$$

Its partial derivative w.r.t. \mathbf{x}_a is denoted by the matrix $\mathbf{Q}_L(t) \in \mathbb{R}^{(n+k) \times (n+k)}$ and defined as

$$\mathbf{Q}_L(t) := \frac{\partial}{\partial \mathbf{x}_a} \Phi(\mathbf{x}_a, \mathbf{u}, \dot{\mathbf{u}}, \ddot{\mathbf{u}}). \quad (4.53)$$

The (local) observability matrix $\mathbf{Q}_L(t)$ is interpreted as a function of time, as the trajectories of the state variable $\mathbf{x}(t)$ and the system input $\mathbf{u}(t)$ are known *a priori* of the matrix evaluation. Unfortunately, an analytical calculation of the determinant's zero is not feasible (even with sophisticated mathematics software) and thus the regularity of $\mathbf{Q}_L(t)$ needs to be evaluated numerically. Therefore, two subsets of the physically possible values of $c_{\alpha_{fe}}$ and c_{α_r} are defined as $C_f := [55000 : 5000 : 120000]$ and $C_r := [75000 : 5000 : 150000]$. Then, for every simulation run two values of C_f and C_r are extracted and used for $c_{\alpha_{fe}}$ and c_{α_r} . Furthermore, the results are calculated for two different (constant) longitudinal velocities. The results are illustrated in Figures 4.4(a) and 4.4(b). Therein, c_{α}^* denotes all possible²¹ combinations of $c_{\alpha_{fe}} \in C_f$ and $c_{\alpha_r} \in C_r$. In Figure 4.4 the area shaded in light gray represents the range space of the determinant

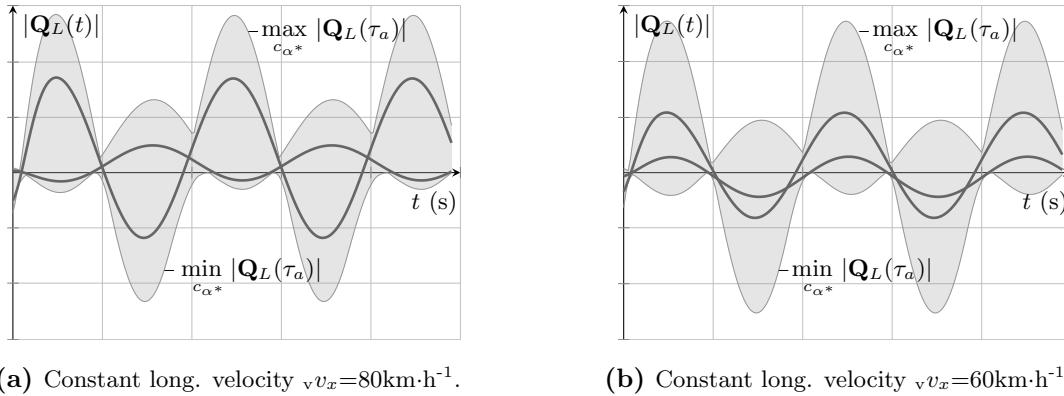


Figure 4.4: Determination of the observability for varying parameters $c_{\alpha_{fe}}$, c_{α_r} and a constant long. vehicle velocity v_{vx} .

²¹And also feasible from a vehicle dynamics point of view, e.g. the difference between front and rear stiffness should be within a certain range.

$|\mathbf{Q}_L(t)|$ for all tested combinations of lateral stiffness values. That range is enclosed by the minimal and maximal values of $\mathbf{Q}_L(t)$ at a certain time instant denoted by τ_a . The dark gray curves represent two arbitrarily chosen parameter setups, in order to demonstrate the variation in time of the local observability. Clearly, there exist points in time where a rank deficiency of $\mathbf{Q}_L(t)$ occurs and observability might be lost²². However, as these points are finite and the observability is regained once the zero line is crossed, a possibility to robustify the observation concept is to evaluate the observability matrix $\mathbf{Q}_L(t)$ online and turn off any state estimation if the determinant is sufficiently close to zero.

EKF Design

Now, that the augmented system has been introduced and its (local) observability discussed the design of an EKF is identical as presented in Section 4.1.1. Some comments on the tuning of the filter parameters will be provided in the example at the end of this section.

I.2 Variable Structure Unknown Input Observer (VSUIO)

An alternative estimation concept of the lateral cornering stiffness uses the unknown input observer technique, rather than state augmentation. The starting point of the design represents Σ_{L4} , i.e. the state-space representation of the single-track model using lateral acceleration as system input, see 3.2.2.IV. The state vector definition is given in (3.19) and the system equations are based on (3.44) and read as

$$\frac{dx_1}{dt} = \tilde{a}_{11} c_{\alpha_r} u_2^{-1} x_1 + \tilde{a}_{12} c_{\alpha_r} x_2 + b_{11} u_1, \quad (4.54a)$$

$$\frac{dx_2}{dt} = -x_1 + u_1 u_2^{-1}, \quad (4.54b)$$

$$y = x_1, \quad (4.54c)$$

with the scaled input $\tilde{u}_1 := u_1 u_2^{-1}$ and modified model parameters, compare with (3.45a)

$$\tilde{a}_{11} := -\frac{(l_{f_e} + l_{r_e}) l_{r_e}}{J_z}, \quad \tilde{a}_{12} := \frac{(l_{f_e} + l_{r_e})}{J_z}. \quad (4.55)$$

For the definition of b_{11} see (3.45b). Furthermore, the influence of the roll dynamics on the slip angles α_{f_e} and α_{r_e} is neglected. Then, the assumed unknown model parameter c_{α_r} can be separated into a nominal \bar{c}_{α_r} and an uncertain part Δc_{α_r} , i.e.

$$c_{\alpha_r} = \bar{c}_{\alpha_r} + \Delta c_{\alpha_r}. \quad (4.56)$$

²²Theorem 4, p. 73, is only a sufficient condition for local observability.

Merging (4.56) with (4.54) results in a system

$$\frac{dx_1}{dt} = \tilde{a}_{11} \bar{c}_{\alpha_r} u_2^{-1} x_1 + \tilde{a}_{12} \bar{c}_{\alpha_r} x_2 + b_{11} u_1 + \xi(x_1, x_2), \quad (4.57a)$$

$$\frac{dx_2}{dt} = -x_1 + u_1 u_2^{-1}, \quad (4.57b)$$

$$y = x_1, \quad (4.57c)$$

with an unknown input $\xi(x_1, x_2)$ given by an expression containing the uncertain parameters and states, i.e.

$$\xi(x_1, x_2) := \underbrace{\left[\tilde{a}_{11} u_2^{-1} x_1 + \tilde{a}_{12} x_2 \right]}_{=: \Gamma(x_1, x_2)} \Delta c_{\alpha_r}. \quad (4.58)$$

Due to the boundedness of the inputs u_1, u_2 the state variables x_1 and x_2 are bounded too²³. Hence, the unknown input $\xi(x_1, x_2)$ is upper bounded by

$$\left| \xi(x_1, x_2) \right| < \xi^+ < \infty, \quad (4.59)$$

for any x_1, x_2 and u_2 . This also assumes a longitudinal velocity that is significantly different from zero. Moreover, if the input u_2 , i.e. longitudinal velocity ${}_v v_x$, is assumed constant during the identification experiment, it can be regarded as a model parameter and the system characteristics become linear. Hence, its general matrix/vector form can be defined as

$$\frac{d\mathbf{x}}{dt} = \mathbf{A}\mathbf{x} + \mathbf{B}\mathbf{u} + \mathbf{D}\boldsymbol{\xi}, \quad (4.60a)$$

$$\mathbf{y} = \mathbf{C}\mathbf{x}, \quad (4.60b)$$

with $\mathbf{A} \in \mathbb{R}^{n \times n}$, $\mathbf{B} \in \mathbb{R}^{n \times m}$, $\mathbf{D} \in \mathbb{R}^{n \times q}$, $\mathbf{C} \in \mathbb{R}^{p \times n}$, $\boldsymbol{\xi} \in \mathbb{R}^q$, $\mathbf{x} \in \mathbb{R}^n$, $\mathbf{u} \in \mathbb{R}^m$ and $\mathbf{y} \in \mathbb{R}^p$.

Robust State Estimation

A priori to the design of an unknown input observer its general existence needs to be ensured. The additional (unknown) input to the system complicates the standard observability criteria and special care needs to be taken. For the ongoing analysis the notion of *indistinguishable* states needs to be introduced [HK77, MD08]. Suppose that for system (4.60) \mathbf{x}_0 represents an initial state vector and $\mathbf{u}, \boldsymbol{\xi}$ the known and unknown inputs.

²³System (4.54) is Bounded-Input-Bounded-Output (BIBS) stable. See [KHA02] for further details.

Then, the following theorem can be formulated [MD08]

Theorem 6. *Suppose $\bar{\mathbf{x}}_0 \neq \mathbf{x}_0$ and $\mathbf{y}(t, \mathbf{x}_0, \mathbf{u}, \xi) = \mathbf{y}(t, \bar{\mathbf{x}}_0, \mathbf{u}, \bar{\xi}) \forall t > 0$ for some, distinct unknown inputs $\xi, \bar{\xi}$, then $\bar{\mathbf{x}}_0$ is said to be a strongly indistinguishable state of \mathbf{x}_0 .*

Applying this theory to the lateral dynamics system with an unknown input yields indistinguishable dynamics based on the following argumentation. Consider system (4.57) and a second instance of it that actually does have a different unknown input $\bar{\xi}(z_1, z_2)$ with z_1, z_2 being the state variables of the system

$$\frac{dz_1}{dt} = \tilde{a}_{11} \bar{c}_{\alpha_r} u_2^{-1} z_1 + \tilde{a}_{12} \bar{c}_{\alpha_r} z_2 + b_{11} u_1 + \bar{\xi}(z_1, z_2), \quad (4.61a)$$

$$\frac{dz_2}{dt} = -z_1 + u_1 u_2^{-1}, \quad (4.61b)$$

$$y = z_1. \quad (4.61c)$$

Then, by defining the state errors $e_1 := x_1 - z_1$ and $e_2 := x_2 - z_2$ their dynamics can be formulated by

$$\frac{de_1}{dt} = \tilde{a}_{11} \bar{c}_{\alpha_r} u_2^{-1} e_1 + \tilde{a}_{12} \bar{c}_{\alpha_r} e_2 + \Delta\xi(e_1, e_2), \quad (4.62a)$$

$$\frac{de_2}{dt} = -e_1, \quad (4.62b)$$

with $\Delta\xi(e_1, e_2) := \xi(x_1, x_2) - \bar{\xi}(z_1, z_2)$. Now, given that the output signals of the two systems are identical (as argued in Theorem 6) yields $e_1 \equiv 0$. From (4.62b) it follows that $e_2(t) = K$, where K denotes some constant that is generally different from zero²⁴. Consequently, migrating these details into (4.62a) the correspondence

$$-\tilde{a}_{12} \bar{c}_{\alpha_r} K = \Delta\xi(0, e_2), \quad (4.63)$$

follows directly. In other words, even though the system outputs y are identical the differences in terms of unknown inputs are compensated by the second system state. The consequence of that observation are indistinguishable dynamics of (4.57) and the inability to design an observer that allows reconstruction of the system's initial states. This theory is further backed up by the introduced of strong observability [HAU83, SEFL14] that requires the transfer matrix $(\mathbf{A}, \mathbf{D}, \mathbf{C})$ to have no invariant zeros. For system (4.57) even the weaker criterion of strong detectability²⁵, fails as the transfer function from unknown input ξ to system output y shows a zero at the origin $s = 0$. Now, the challenging question is how to overcome that problem. In fact, the initial condition of state x_2 can be selected almost at choice by taking into account the design

²⁴Considering an initial state $z_2(t_0) \neq 0$.

²⁵Strong detectability requires the invariant zeros of $(\mathbf{A}, \mathbf{D}, \mathbf{C})$ to be in \mathbb{C}^- , see [HAU83, ES98].

of experiments. It is clear that the estimate's initial condition is determined by the user. But, assuming the lateral dynamics are not excited at all before conducting the identification experiment it is reasonable to consider the initial condition of the plant identical to zero²⁶. Therefore, with regards to (4.57b) the input $\tilde{u}_1 := u_1 u_2^{-1}$, state x_1 and also its initial condition are known. Hence, by numerical integration an estimate of x_2 can be obtained, i.e.

$$\hat{x}_2(t) = \int_0^t -x_1(\tau) + \tilde{u}_1(\tau) d\tau, \quad (4.64)$$

with the initial condition $x_2(0) = 0$. Clearly, in general obtaining estimates from numerical integration is not recommended²⁷. However, for this special setup it appears to be a feasible solution and due to the short duration of the integration process, as will be demonstrated by simulation-based work (Chapter 5) and also experimental validation (Chapter 6), the obtained results are promising.

Now, focusing back on the identification of the uncertain lateral cornering stiffness Δc_{α_r} the system to be considered is reformulated to

$$\frac{dx_1}{dt} = \tilde{a}_{11} \bar{c}_{\alpha_r} u_2^{-1} x_1 + \tilde{u}_a + \xi(x_1, x_2), \quad (4.65a)$$

$$y = x_1, \quad (4.65b)$$

with $\tilde{u}_a := \tilde{a}_{12} \bar{c}_{\alpha_r} \hat{x}_2 + b_{11} u_1$ being an augmented input vector that also holds the estimates of x_2 . That system is definitely strong observable and allows the introduction of a so-called finite time parameter estimator [MG11] based on higher-order sliding modes. Consequently, it yields finite time convergence of the parameters as opposed to the asymptotic behavior of standard least-squares-based algorithms, e.g. [IM11]. The concept employs a so-called *generalized* super-twisting algorithm (GSTA) [MOR09], that includes linear correction terms (in contrast to the classic super-twisting algorithm), that are stronger than the nonlinear ones, given that the trajectories are far away from the origin. Note that, for a certain set of parameters the GSTA degenerates to the standard STA.

²⁶It shall be emphasized that the discussed initial condition of the vehicle, does not refer to the very initial state of the vehicle, i.e. at its resting position. It moreover refers to the condition before any lateral excitation of the vehicle is conducted. Hence, it might be driven in a straight line beforehand.

²⁷Given the fact that x_2 is based on measured values of x_1 and also \tilde{u}_1 their noise might not be perfectly zero-mean. Therefore, the longer the integration interval is, the more influence the mean value of the measurement noise will have.

The finite time parameter estimation algorithm can be formulated as

$$\frac{d\hat{x}_1}{dt} = \tilde{a}_{11} \bar{c}_{\alpha_r} u_2^{-1} \hat{x}_1 + \tilde{u}_a + \Gamma(\hat{x}_1, \hat{x}_2) \hat{\theta} - \alpha_1 \phi_1(e_1), \quad (4.66a)$$

$$\frac{d\hat{\theta}}{dt} = -\alpha_2 \phi_2(e_1) \Gamma(\hat{x}_1, \hat{x}_2), \quad (4.66b)$$

with the correction terms $\phi_1(e_1)$ and $\phi_2(e_1)$

$$\phi_1(e_1) := \mu_1 |e_1|^{\frac{1}{2}} + \mu_2 e_1, \quad (4.67a)$$

$$\phi_2(e_1) := \frac{1}{2} \mu_1^2 |e_1|^0 + \frac{3}{2} \mu_1 \mu_2 |e_1|^{\frac{1}{2}} + \mu_2^2 e_1. \quad (4.67b)$$

Furthermore, e_1 denotes the estimation error $e_1 := \hat{x}_1 - x_1$ between the measurement x_1 and \hat{x}_1 provided by the FTPE algorithm. Moreover, $\alpha_1, \alpha_2, \mu_1$ are strictly positive constants and $\mu_2 \geq 0$. Interestingly, the nonlinear algorithm provides bounded parameter estimates $\hat{\theta} := \Delta \hat{c}_{\alpha_r}$ even if persistence of excitation is not guaranteed. For the proof of stability and convergence time estimate consider [MG11].

Comment on the Extension to Front Cornering Stiffness Estimation The presented sliding mode-based concept aims to recover the uncertain parameter Δc_{α_r} . However, once that is known only half of the objective is accomplished. In other words, knowledge of the rear lateral cornering stiffness does not reveal any information on the front values. Hence, system (3.43) needs to be reformulated such, that the front force enters (3.43a), rather than the rear one. From a structural perspective the model looks like (4.57), but the new unknown input ξ is now a function of the states x_1, x_2 and also the input δ_w . Regardless of the structural changes w.r.t. the unknown input the parameter estimation algorithm can be designed identically to that presented.

An Idea for Estimation of the Uncertain Parameter and Initial Condition

In the following an alternative idea for joint estimation of the uncertain parameter and also the initial condition will be presented. Note that this approach is only discussed theoretically, but not evaluated in simulations or experiments.

Again system (4.54) and also (4.56) are considered. Then, from the knowledge that the initial condition of $x_2(t)$ can not be recovered by means of observers at least

$$x_2(t) = \underbrace{x_2(0)}_{=:x_{2,0}} + \underbrace{\int_0^t -x_1(\tau) + \tilde{u}_1(\tau) d\tau}_{=:x_{2,int}(t)}, \quad (4.68)$$

holds. Now, merging (4.54), (4.56) and (4.68) yields

$$\frac{dx_1}{dt} = \tilde{a}_{11} (\bar{c}_{\alpha_r} + \Delta c_{\alpha_r}) u_2^{-1} x_1 + \tilde{a}_{12} (\bar{c}_{\alpha_r} + \Delta c_{\alpha_r}) (x_{2,0} + x_{2,int}) + b_{11} u_1, \quad (4.69a)$$

$$y = x_1. \quad (4.69b)$$

And this can be formulated as a parameter identification problem as in (4.66) with $\hat{\theta}$ and $\mathbf{\Gamma}(\hat{x}_1, \hat{x}_{2,int})$ being defined as

$$\hat{\theta} := \left[\Delta \hat{c}_{\alpha_r} \quad \hat{x}_{2,0} \quad \Delta \hat{c}_{\alpha_r} \hat{x}_{2,0} \right]^T, \quad (4.70a)$$

$$\mathbf{\Gamma}(\hat{x}_1, \hat{x}_{2,int}) := \left[\tilde{a}_{11} u_2^{-1} \hat{x}_1 + \tilde{a}_{12} \hat{x}_{2,int} \quad \tilde{a}_{12} \bar{c}_{\alpha_r} \quad \tilde{a}_{12} \right]. \quad (4.70b)$$

Example: Estimation of Lateral Cornering Stiffness Parameters

A simulation-based proof of concept should demonstrate the applicability of the proposed observer concepts for the estimation of the lateral cornering stiffness values. Therefore, ideal reference plants Σ_{L1} and Σ_{L4} , as in (3.9) and (3.44), with the model parameters as listed in Table 4.3 are implemented. The signal parameters of the system excitation are selected such that the lateral acceleration is low ($< 4\text{m}\cdot\text{s}^{-2}$) and the transients in the tire force generation are negligible, i.e. sinusoidal steering with an amplitude $\delta_w = 1^\circ$ and frequency $f = 0.25\text{Hz}$. Both observer concepts, the EKF and the sliding mode parameter estimator, are evaluated in simulations based on the tuning as in Table 4.3. The source model states and their estimates as well as the identified lateral cornering stiffness values can be taken from Figures 4.5 and 4.6. In accordance with the presented sliding mode-based parameter identification algorithm only the rear cornering stiffness is identified. The model parameter of the front tire needs design and implementation of an additional mechanism such that $\Delta c_{\alpha_{fe}}$ is recovered from the unknown input.

Some Comments on the EKF The tuning of the EKF follows the suggestions provided in the introductory example of Section 4.1.1. In order to demonstrate the quick convergence of the estimated state variables the filter is activated at $t_{act} = 1\text{s}$. The light gray shading in Figure 4.5 stresses this delayed filter activation. In general, the uncertainties of the front and rear lateral cornering stiffness are estimated accurately. Even though the EKF is more expensive in terms of computational efforts it also estimates both uncertainties simultaneously. However, the drawback is certainly the lack of a straightforward filter tuning as the setup of the $\bar{\mathbf{Q}}$ matrix can be difficult.

Some Comments on the VSUIO From Figures 4.6(a), (b), (e) and (f) it can be concluded that the state x_1 and the unknown input ξ are estimated robustly. From the error plots (b) and (f) the finite time convergence is obvious. A main advantage is the

Parameter	Description	Value	Unit
l_{fe}	Distance front axle to CoG	1.1	m
l_{re}	Distance rear axle to CoG	1.4	m
J_z	Moment of inertia w.r.t. z-axis	2100	kg·m ²
m	Vehicle mass	1400	kg
${}_v v_x$	Longitudinal velocity	80	km·h ⁻¹
$c_{\alpha_{fe}}$	Lateral cornering stiffness (front)	83000	N·rad ⁻¹
c_{α_r}	Lateral cornering stiffness (rear)	95000	N·rad ⁻¹
$\hat{\mathbf{x}}_{a,0}^+$	Initial (augmented) state vector (EKF)	$[-0.07 \ -0.0026 \ 4e4 \ 6e4]^T$	-
\mathbf{P}_0^+	Initial error covariance matrix (EKF)	diag([1 1 1 1])	-
r	Covariance of the meas. noise (EKF)	3e-6	-
$\bar{\mathbf{Q}}$	Covariance of the process noise (EKF)	diag([1e-11 1e-11 1e3 1e3])	-
μ_1	Gain nonlinear error correction term (VSUIO), see (4.67)	5e3	-
μ_2	Gain linear error correction term (VSUIO), see (4.67)	1	-
α_1	Parameter estimator gain (VSUIO), see (4.66)	0.75e-2	-
α_2	Parameter estimator gain (VSUIO), see (4.66)	5e3	-

Table 4.3: Simulation parameters of the plant, EKF and VSUIO.

recovery of the unknown input without requirement of standard filtration techniques that would annihilate the claim for finite time recovery. Consequently, it a.) avoids the tuning of a filter constant for calculation of the equivalent error injection term and b.) provides better (in terms of accuracy) estimates of the unknown parameter. Generally, the employment of a low-pass filter in order to estimate the equivalent output injection term introduces a phase lag between the estimate and the real values. That incorrect causal relation between estimated uncertainty and state variables can lead to distortions of the identified parameters.

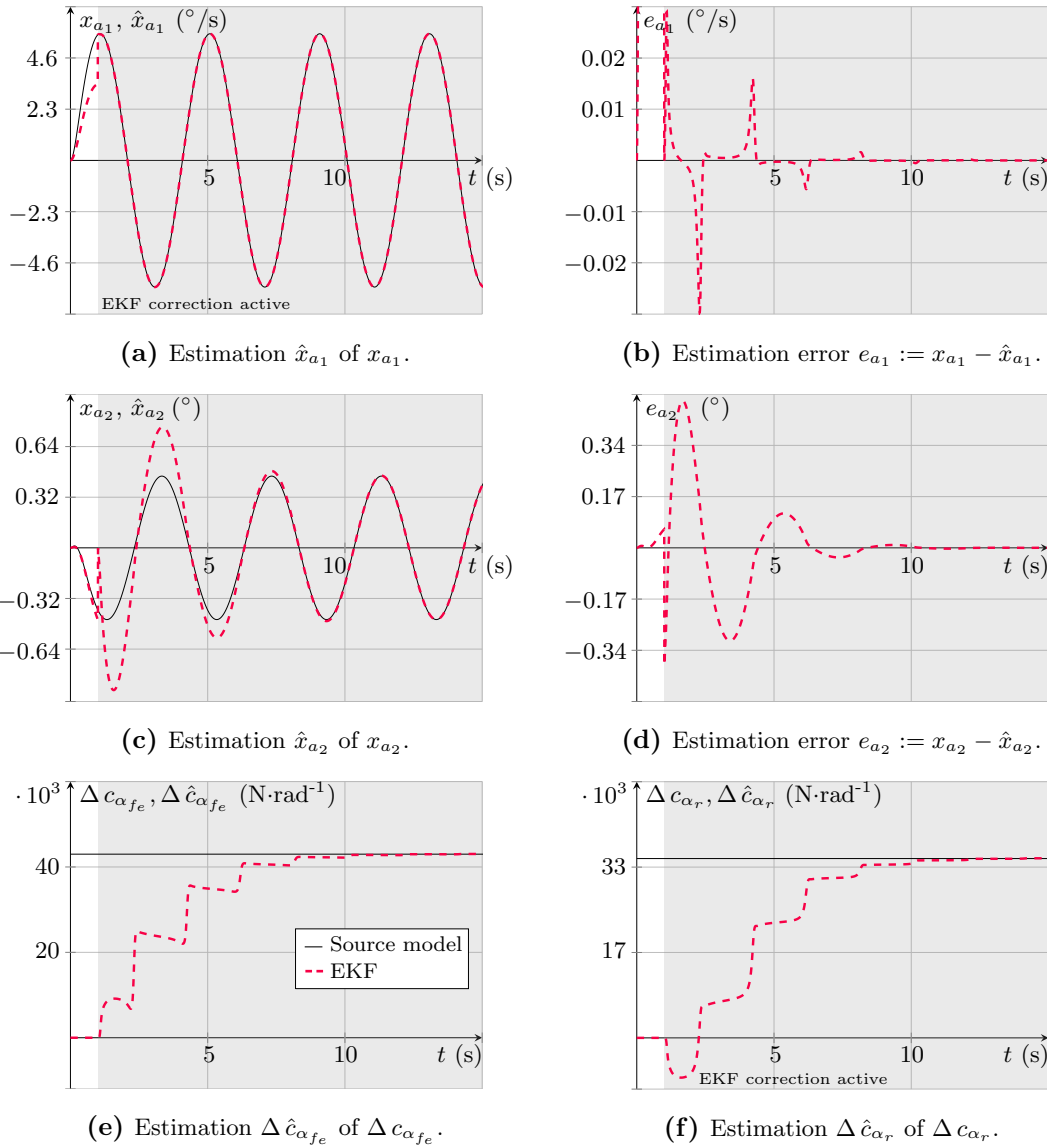


Figure 4.5: Ideal reference simulation results: Robust state estimation of Σ_{L1} (EKF).

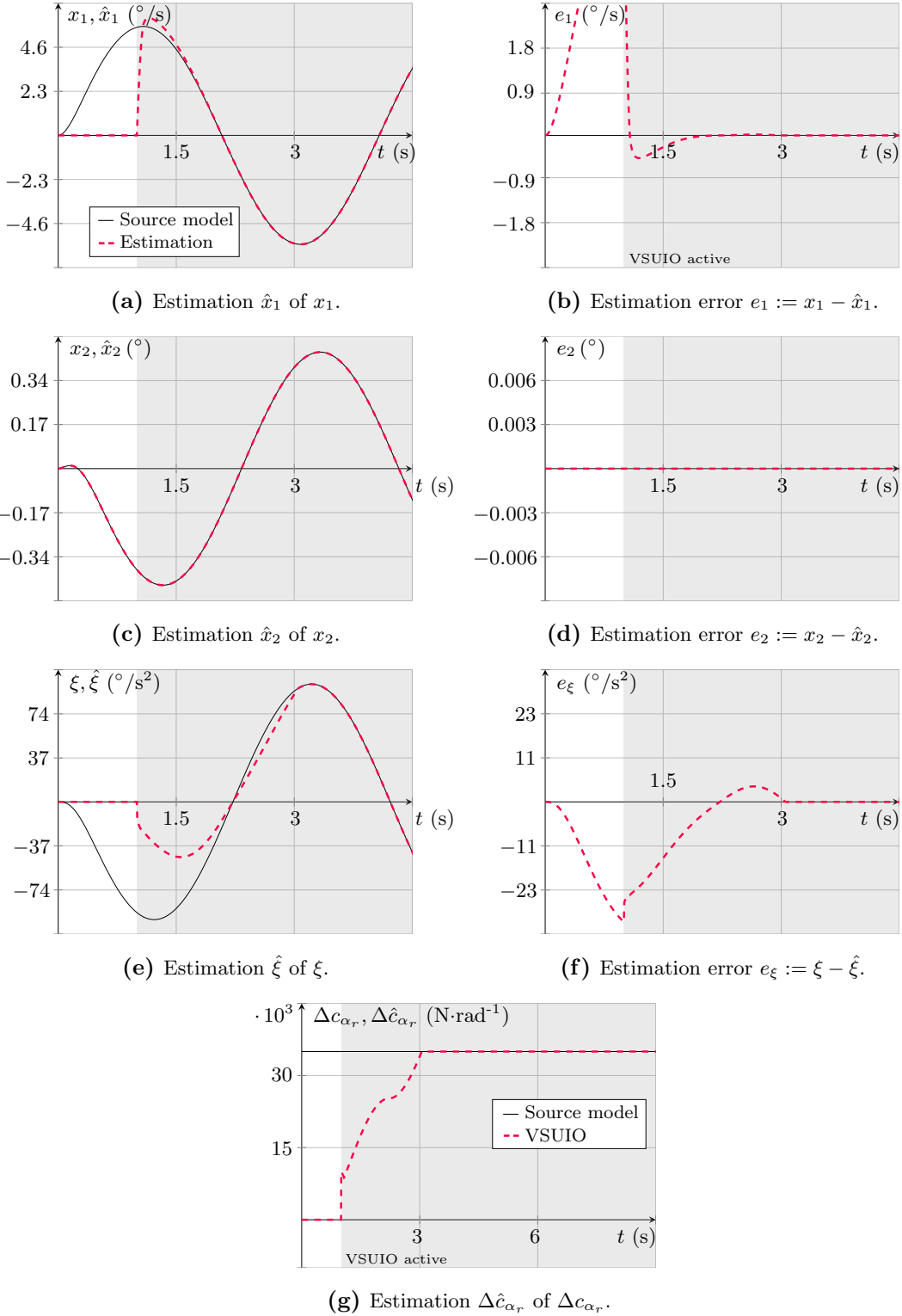


Figure 4.6: Ideal reference simulation results: Robust state estimation of Σ_{L4} (VSUIO).

II Lateral Tire Force Observer

II.1 Variable Structure Unknown Input Observer (VSUIO)

The objective of the lateral tire force observer is already suggested by its name. More specifically, knowledge of the maximum arising lateral tire force would be beneficial for the estimation of the tire force model parameter D , see the definition of SMF (2.28) and TMSimple (2.29) and (2.30a).

In contrast to the sliding mode observer in [BCL09] requiring sophisticated tuning rules of the observer gains the herein presented concept exploits a first-order state-space model (2.14a), (2.14c), (2.10) for the subsequent observer design process. Defining the state variable $x_1 := \dot{\psi}$, the input signal $u := {}_v a_y$ and the uncertainty²⁸ $\zeta_u := {}_v F_{y,r}$ the differential equation reads as

$$\frac{dx_1}{dt} = k_1 u + k_2 \zeta_u, \quad (4.71a)$$

$$y = x_1, \quad (4.71b)$$

with the constants k_1 and k_2 defined by

$$k_1 := \frac{l_{fe} m}{J_z} \quad \text{and} \quad k_2 := -\frac{l_{fe} + l_{re}}{J_z}. \quad (4.72)$$

The *strongly* observable²⁹ system allows an observer design of the form [FB07]

$$\frac{d\hat{x}_1}{dt} = k_1 u + \lambda_1 [e_1]^{\frac{1}{2}} + \gamma, \quad (4.73a)$$

$$\frac{d\gamma}{dt} = \lambda_2 [e_1]^0. \quad (4.73b)$$

Variable e_1 denotes the estimation error $e_1 := x_1 - \hat{x}_1$, and $\lambda_1, \lambda_2 > 0$. From the error dynamics

$$\frac{de_1}{dt} = \omega - \lambda_1 [e_1]^{\frac{1}{2}}, \quad (4.74)$$

$$\frac{d\omega}{dt} = k_2 \frac{d\zeta_u}{dt} - \lambda_2 [e_1]^0, \quad (4.75)$$

²⁸The considered class of uncertainties is a.) bounded and b.) does have a (Lipschitz) bounded derivative for any $t > 0$.

²⁹See [SEFL14] for details.

Parameter	Description	Value	Unit
l_{fe}	Distance front axle to CoG	1.1	m
l_{re}	Distance rear axle to CoG	1.4	m
J_z	Moment of inertia w.r.t. z-axis	2100	kg·m ²
m	Vehicle mass	1400	kg
S_f	Front tire model parameters (TM_Simple), i.e. $[D_f B_f C_f]$	[5300 2.127 0.1358]	-
S_r	Rear tire model parameters (TM_Simple), i.e. $[D_r B_r C_r]$	[4100 2.1638 0.0934]	-
\hat{x}_0	Initial state vector (VSUIO)	-0.25	rad·s ⁻¹
ν_0	Initial condition of ν (VSUIO)	2	rad·s ⁻²
λ_1	Observer gain factor (VSUIO), see (4.73)	4.743	-
λ_2	Observer gain factor (VSUIO), see (4.73)	11	-

Table 4.4: Simulation parameters of the plant and VSUIO.

where $\omega := k_2 \zeta_u - \gamma$, it becomes obvious that the unknown input ζ_u and its derivative with respect to time need to be bounded, i.e.

$$\left| \zeta_u(t) \right| < \zeta_u^+ < \infty, \quad (4.76a)$$

$$\left| \frac{d}{dt} \zeta_u(t) \right| < \dot{\zeta}_u^+ < \infty, \quad \forall t > 0. \quad (4.76b)$$

Then, choosing the observer gains λ_1 and λ_2 as suggested in e.g. [LEV98] e_1 and ω are driven to zero in finite time τ_c , i.e.

$$\frac{de_1(t)}{dt} = 0 \quad \Rightarrow \quad \omega(t) = 0 \quad \Rightarrow \quad k_2 \zeta_u(t) = \gamma(t) \quad \forall t \geq \tau_c. \quad (4.77)$$

And therefrom the unknown input ζ_u can be reconstructed (without explicit filtration of a discontinuous term).

Certainly, this concept can also be applied for recovery of the front lateral force. Therefore, the state-space formulation needs to be adapted such, that the uncertainty ζ_u comprises the front lateral force ${}_v F_{y,f}$. Alternatively, from knowledge of ${}_v a_y$ and the estimated ${}_v \hat{F}_{y,r}$ the front lateral force can be obtained, see (2.13).

Example: Estimation of the Rear Lateral Tire Force

The proposed observation concept will be first evaluated using an ideal source plant based on a single-track model with nonlinear (TM_Simple) tire force models. Parameters of the reference system are provided in Table 4.4. Excitation of the vehicle is

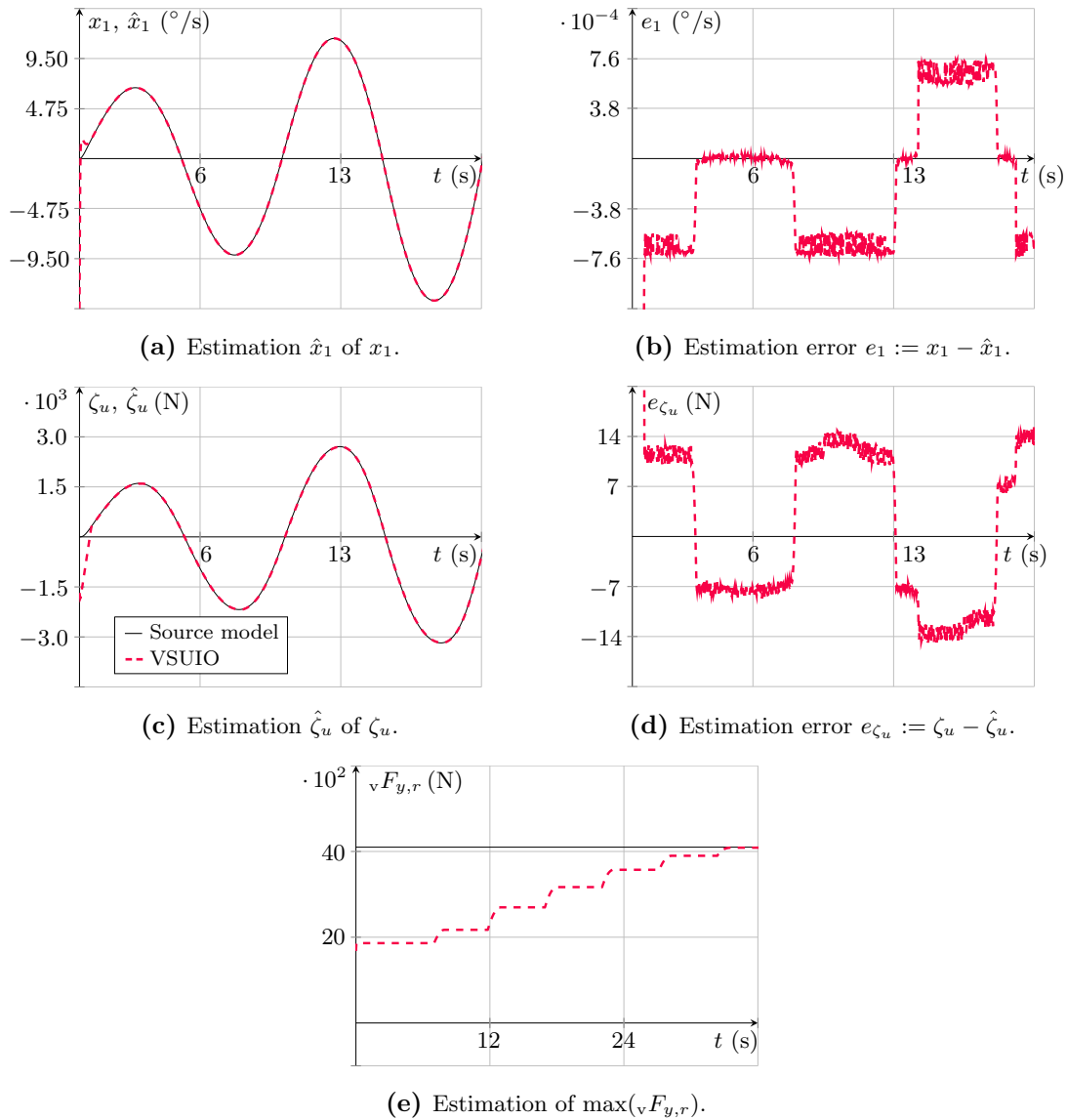


Figure 4.7: Ideal reference simulation results: Recovery of the tire force ${}_v F_{y,r}$.

performed sinusoidally with constant frequency $f \approx 0.1\text{Hz}$ and an increasing steering amplitude until the driver feels the loss of adhesion. The longitudinal velocity should be almost constant, i.e. ${}_v v_x \approx 80\text{km}\cdot\text{h}^{-1}$. Alternatively, a steady-state circular drive with increasing vehicle velocity at a track of constant curvature radius can also be performed. Results of the simulations under ideal conditions are presented in Figure 4.7.

The estimation of the maximum force, see Figure 4.7(e), is based on a comparison of the actual value and the current maximum, i.e. the actual value is the new maximum if greater than the old, and dropped otherwise.

III Vehicle Sideslip Observer

The estimation of the sideslip angle of a motor-driven vehicle is discussed in many publications, e.g. [IJF⁺06, BCL09, GYNW10, AFK11, GCRP14]. For the application of vehicle handling evaluation the sideslip angle is only of reduced importance as there is a redundancy (for lateral accelerations up to $|a_y| < 4\text{m}\cdot\text{s}^{-2}$) between the sideslip angle and the yaw rate/lateral acceleration [DEC09]. Therefore, the necessity of a designated vehicle sideslip observer development is not given. However, this section provides an idea how an estimator design could benefit from the obtained results.

Assume that the parameters of the tire model SMF or TM_Simple have been identified with the previously proposed observer techniques and the parameter extraction discussed in Section 5.2.3. Then, either system Σ_{L2} or Σ_{L3} can be used directly for an observer design. Their nonlinear characters suggest the use of an Extended [BCL09] or an Unscented Kalman Filter [AFK11] to estimate the sideslip angle. Alternatively, one can plug in the nonlinear tire models, see (2.28), (2.29), into Σ_{L4} and design a state observer as proposed in [GYNW10].

4.2.2 Roll Dynamics

The importance of the actual roll angle for vehicle safety related applications motivated numerous publications to estimate the former using state observation schemes. Commonly, the *a priori* knowledge of roll dynamics related parameters is necessarily assumed, e.g. in [ADM04, RG04, DM05, SGMN08, MLC10, TXH07]. But then, these approaches are not only able to estimate the chassis' roll, but also the road bank angle. Furthermore, most of these observation mechanisms do not require expensive sensor equipment. Commonly, angular rate sensors (for yaw and roll rates) are sufficient. In contrast, given the case the model parameters are not accurately known *a priori* their identification requires measurement of the roll angle, as proposed in e.g. [AHH03, ZOM02, KOB03]. However, it necessitates the installation of costly measurement equipment to obtain the roll angle in-vehicle. Joint estimation of the latter and its related (unknown) model parameters is presented to some extent in [RPTL11] and also the authors publications [TRH12a, TRH12b, TRH14b]. The latter concepts are designed such, that only cost-efficient sensing of the roll rate and lateral acceleration is sufficient. Moreover, the model parameters of effective stiffness and damping, as presented in Section 2.3.1, can be obtained in real-time.

For the identification of the uncertainties of the roll dynamics model, as presented in Section 3.2.3, two different concepts are proposed. The first is based on state augmentation and the second exploits a reconstructed unknown input to identify the parameters. Namely these are the effective roll stiffness c_{Σ}^r and damping d_{Σ}^r , based on the findings of Section 3.2.3.V.3.

I Extended Kalman Filter (EKF)

The use of an EKF as parameter estimator requires state augmentation and consequently yields an extended system formulation. Even if the observer design is more straightforward than for the variable structure-based mechanism this is paid by a more difficult filter tuning requiring some expertise.

State Augmentation

The definitions of the state and input vectors (3.52) and the state-space representation of Σ_R (3.53) build the basis of the design process. For the estimation of the model parameters c_Σ^r and d_Σ^r the augmented state vector $\mathbf{x}_a \in \mathbb{R}^{n+k}$ is introduced

$$\mathbf{x}_a := \begin{bmatrix} x_{a_1} & x_{a_2} & x_{a_3} & x_{a_4} \end{bmatrix}^T = \begin{bmatrix} \varphi & \dot{\varphi} & c_\Sigma^r & d_\Sigma^r \end{bmatrix}^T. \quad (4.78)$$

Then, the resulting state-space formulation for the design of a joint state and parameter estimation reads as

$$\frac{d\mathbf{x}_a}{dt} = \mathbf{f}_a(\mathbf{x}_a, u), \quad (4.79a)$$

$$y = h_a(\mathbf{x}_a), \quad (4.79b)$$

with $\mathbf{f}_a : D_{f_a} \subseteq \mathbb{R}^{n+k} \times \mathbb{R} \rightarrow \mathbb{R}^{n+k}$, $h_a : D_{h_a} \subseteq \mathbb{R}^{n+k} \rightarrow \mathbb{R}$. The input signal $u(t)$ is given by the measured lateral acceleration $u := a_{y,m}$, see (2.43) and (3.52b). The vector-valued function $\mathbf{f}_a(\cdot) := \begin{bmatrix} f_1(\cdot) & f_2(\cdot) & f_3(\cdot) & f_4(\cdot) \end{bmatrix}^T$ is defined by

$$\begin{bmatrix} f_1(\mathbf{x}_a, u) \\ f_2(\mathbf{x}_a, u) \\ f_3(\mathbf{x}_a, u) \\ f_4(\mathbf{x}_a, u) \end{bmatrix} := \begin{bmatrix} x_{a_2} \\ -x_{a_1} x_{a_3} - x_{a_2} x_{a_4} + k u \\ 0 \\ 0 \end{bmatrix}. \quad (4.80)$$

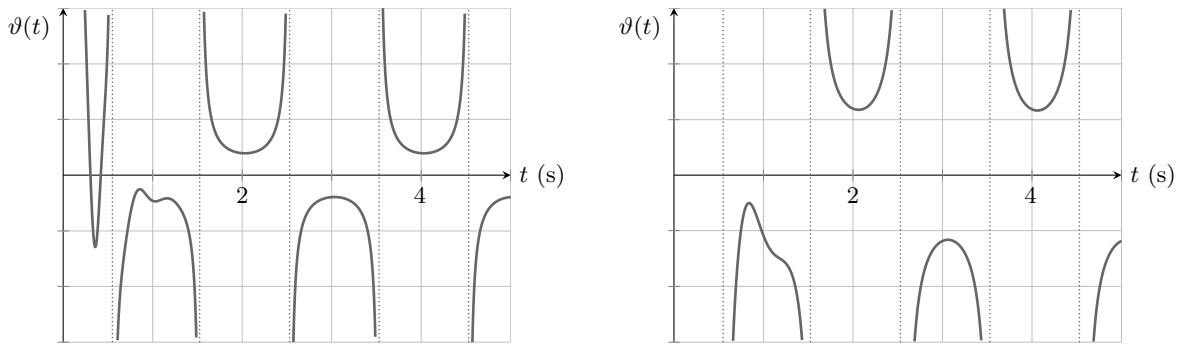
Observability Analysis

The state augmentation renders the analysis of Section 3.2.3.V.5 obsolete due to the modified system formulation. A diffeomorphism $\Phi(\mathbf{x}_a, u, \dot{u}, \ddot{u})$ as in (3.15) and (4.52) is used and the matrix $\mathbf{Q}_L(t)$ denotes its partial derivative, see (4.53). In contrast to Section 4.2.1.I.1 the regularity of $\mathbf{Q}_L(t)$ can be evaluated analytically. Further details are given in Appendix B.

A rank deficiency of the local observability matrix occurs if the expression

$$\vartheta := \frac{du}{dt} - \frac{k^2 u^2 - 2k u x_{a_1} x_{a_3} - k u x_{a_2} x_{a_4} + x_{a_1}^2 x_{a_3}^2 + x_{a_1} x_{a_2} x_{a_3} x_{a_4} + x_{a_2}^2 x_{a_3}}{k x_{a_2}}, \quad (4.81)$$

equals zero. Its evaluation is performed numerically for a given experiment. Figures 4.8(a) and 4.8(b) show the values of $\vartheta(t)$ for a sinusoidal system excitation and two different sets of model parameters. Apart from the initial phase where $\vartheta(t)$ crosses the zero line local observability can be concluded for the remaining time. However, these results are only valid for the actual set of model parameters and system input. Depending on the *a priori knowledge* of the system states and inputs the evaluation of the observability might be performed in advance or online.



(a) Numerical evaluation of (4.81) - parameter set S_1 (Table 4.5).

(b) Numerical evaluation of (4.81) - parameter set S_2 (Table 4.5).

Figure 4.8: Local observability evaluation by numerical simulation of (4.79), (4.80).

Parameter	Description	Value	Unit
m_s	Vehicle chassis mass	1000	kg
J_{xc}	Vehicle chassis moment of inertia w.r.t. x-axis	500	kg·m ²
h_{rl}	Roll lever arm	0.4	m
S_1	Effective roll stiffness and damping - Set 1 $[c_{\Sigma}^r \ d_{\Sigma}^r]$	[170000 5000]	N·m·rad ⁻¹ , N·m·s·rad ⁻¹
S_2	Effective roll stiffness and damping - Set 2 $[c_{\Sigma}^r \ d_{\Sigma}^r]$	[60000 3400]	N·m·rad ⁻¹ , N·m·s·rad ⁻¹

Table 4.5: Simulation parameters for local observability analysis of (4.79), (4.80).

EKF Design

Using the system formulation (4.79), (4.80) the EKF design as explained in Section 4.1.1 can be performed.

II Variable Structure Unknown Input Observer (VSUIO)

The state-space system Σ_R relevant for the observer design is defined by (3.52), (3.53) and reads as

$$\frac{dx_1}{dt} = x_2, \quad (4.82a)$$

$$\frac{dx_2}{dt} = -\bar{a}_{21}x_1 - \bar{a}_{22}x_2 + b_2u + \varrho(x_1, x_2), \quad (4.82b)$$

$$y = x_2, \quad (4.82c)$$

with an unknown input $\varrho(x_1, x_2)$ being defined as

$$\varrho(x_1, x_2) := -\Delta a_{21}x_1 - \Delta a_{22}x_2. \quad (4.83)$$

The introduction of an unknown input results from the objective to identify the effective stiffness and damping model parameters that are assumed to be known inaccurately. Hence, they can be split into a nominal³⁰ and an uncertain part, i.e.

$$a_{21} := \bar{a}_{21} + \Delta a_{21}, \quad a_{22} := \bar{a}_{22} + \Delta a_{22}. \quad (4.84)$$

Here, $\bar{a}_{21/22}$ denote the *nominal* and $\Delta a_{21/22}$ the *uncertain* parts of the model parameters. In general, system (4.82) equals the vector-matrix notation of (4.60). Design of robust observation concepts that provide vanishing estimation errors even in the presence of an unknown input are discussed in e.g. [ES98]. An observer consisting of combined linear and nonlinear correction terms is given by

$$\frac{d\hat{\mathbf{x}}}{dt} = \mathbf{A}\hat{\mathbf{x}} + \mathbf{B}\mathbf{u} - \mathbf{G}_l\mathbf{C}\mathbf{e} + \mathbf{G}_n\boldsymbol{\nu}, \quad (4.85)$$

with the standard replica of the system, $\hat{\mathbf{x}} \in \mathbb{R}^n$ being the state estimate, $\mathbf{e} \in \mathbb{R}^n$ the estimation error, $\boldsymbol{\nu} \in \mathbb{R}^p$ the discontinuous injection term and $\mathbf{G}_l\mathbf{C}\mathbf{e}$, $\mathbf{G}_n\boldsymbol{\nu}$ the linear and nonlinear correction terms respectively. Its existence requires two structural conditions on the system to be fulfilled. These are discussed in [SPU08] and refer to

1. The *observer matching conditions*, i.e.

$$\text{rank}(\mathbf{C}\mathbf{D}) = \text{rank}(\mathbf{D}) = q \quad (4.86)$$

with \mathbf{C} being the output matrix, \mathbf{D} the unknown input matrix and q being the number of unknown inputs. This condition is also referred to as *relative degree condition*.

³⁰The specification of nominal parameters is simple as their feasible physical ranges are generally known.

2. The transfer matrix between the unknown inputs $\boldsymbol{\xi}$, see (4.60), and the output \mathbf{y} needs to be minimum-phase, i.e. the invariant zeros of the triple $(\mathbf{A}, \mathbf{D}, \mathbf{C})$ have to be in \mathbb{C}^- .

The second condition refers to the notion of *strong observability* and *strong detectability* that are introduced and further discussed in [HAU83, MD08, SEFL14]. Focusing back on the problem of the robust state estimation related to the roll dynamics model in (4.82) it is not hard to see that the relative degree condition is fulfilled. However, neither strong observability nor strong detectability are given as the transfer function from unknown input to the output is not minimum-phase, i.e. there exists a zero that is not in \mathbb{C}^- . Consequently, as discussed in [HAU83, MD08] an unknown input observer for (4.82) does not exist.

Interpretation of the differential equations (4.82) as mechanical system allow the following description of the challenge: normally the position x_1 is the measurable and uncertainties w.r.t. forces (acting on the time derivative of x_2) are interpreted as perturbations. Then, observation concepts as presented in [DFL05, DFP06] are able to robustly estimate the states and also provide for recovery of the unknown input. However, for the actual setup it is the velocity that is measured. And as the unknown input ϱ can not be expressed by the output y (and its time derivatives), as it would be the case for a strongly observable system, the observer can not be designed.

Introduction of a diffeomorphism Φ allows transformation of the state \mathbf{x} to $\mathbf{z} \in \mathbb{R}^n$ exploiting the definition of the *Lie-Derivative* it reads as

$$\Phi(\mathbf{x}, u) := \begin{bmatrix} z_1 \\ z_2 \end{bmatrix} = \begin{bmatrix} c(\mathbf{x}) \\ L_{\mathbf{a}}c(\mathbf{x}) + L_{\mathbf{b}}c(\mathbf{x})u \end{bmatrix} = \begin{bmatrix} y \\ \dot{y} \end{bmatrix}. \quad (4.87)$$

Note that the formulation of the diffeomorphism refers to a general, nonlinear and input-affine system. Then, system (4.82) can be re-written in z -coordinates as

$$\frac{dz_1}{dt} = z_2, \quad (4.88a)$$

$$\frac{dz_2}{dt} = \bar{f}(z_1, z_2, v) + \zeta(z_1, z_2), \quad (4.88b)$$

$$y = z_1, \quad (4.88c)$$

with v as the new input, i.e. $v := \frac{du}{dt}$, ζ the unknown input and \bar{f} the nominal system dynamics, i.e.

$$\zeta(z_1, z_2) := -\Delta a_{21} z_1 - \Delta a_{22} z_2, \quad (4.89a)$$

$$\bar{f}(z_1, z_2, v) := -\bar{a}_{21} z_1 - \bar{a}_{22} z_2 + b_2 v. \quad (4.89b)$$

Moreover, ζ and \bar{f} are assumed bounded [POZ10] in any compact set of the state-space. Given the fact that the underlying system is a mechanical one this assumption clearly holds. The upper bound of the uncertainty ζ is denoted by

$$\left| \zeta(z_1, z_2) \right| < \zeta^+ < \infty \quad \forall z_1, z_2. \quad (4.90)$$

Interestingly, the change of coordinates does not affect the model parameters \bar{a}_{21} , \bar{a}_{22} , b_2 at all. However, the relative degree of the system output y w.r.t. the unknown input ζ is now 2. Note also, that the increase of the relative degree yields a violation of the observer matching condition, as in (4.86). But, for the considered 2-sliding observer based on the super-twisting algorithm that is not a problem. Basically, the state transformation can be interpreted as the integration of an integrator at the input of the original system³¹. Now, defining the *new* system as the series connection of the old system and an integrator, it is easy to understand that the latter "cancels" the zero (of the transfer function from ϱ to x_2) at the origin. But, this necessitates the calculation of the input signal's time derivative, i.e. $v = \frac{du}{dt}$.

Even though the state variables have been transformed by (4.87) the structure of the resulting system (4.88) is completely identical to (4.82)³². Therefore, by building the time derivative of the input signal u it is possible to employ a second-order (STA-based) observer for the estimation of the states z_1 and z_2 that is invariant to the unknown input ζ . Furthermore, it is possible to recover an estimate for the latter.

Technically, the diffeomorphism in (4.87) does contain uncertain parameters, i.e. a_{21} and a_{22} . However, the transformation is for the definition of a new system that fulfills the requirement of no internal dynamics, i.e. $\rho = n$, see [SEFL14, DFL05]. So, the inverse diffeomorphism is never used for any transformation back into the x -coordinates³³. As will be presented in the following section, the estimation of the roll angle itself will be conducted by an additional state observer concept.

For the objective of identifying uncertain parameters Δa_{21} and Δa_{22} , as in (4.83), and system state estimation of x_1 , referring to the roll angle φ of the vehicle chassis, it is necessary to define individual tasks for tailored submodules, as shown in Figure 4.9. First, a robust exact differentiator (RED) calculates the time derivative of the system input u for further use in system (4.88). Second, a robust state observer recovers the system states z_1 and z_2 and also provides an estimate of the unknown input ζ . Third, two different parameter identification algorithms estimate the uncertainties Δa_{21} , Δa_{22} . And forth, an adaptive Luenberger observer estimates the actual roll angle by exploiting knowledge of the identified effective roll stiffness and damping. Note that the latter is required as the robust state observation is performed in z - rather than x -coordinates. More precisely, the z -coordinates refer to roll rate and acceleration, whereas the x -coordinates are representing roll angle and rate respectively.

³¹In [KPM12] this idea is used to apply 2-sliding control algorithms to systems of relative degree 1.

³²Clearly, the state variables and consequently their physical interpretation are different now.

³³The main objective of the robust state estimation is the recovery of the unknown input.

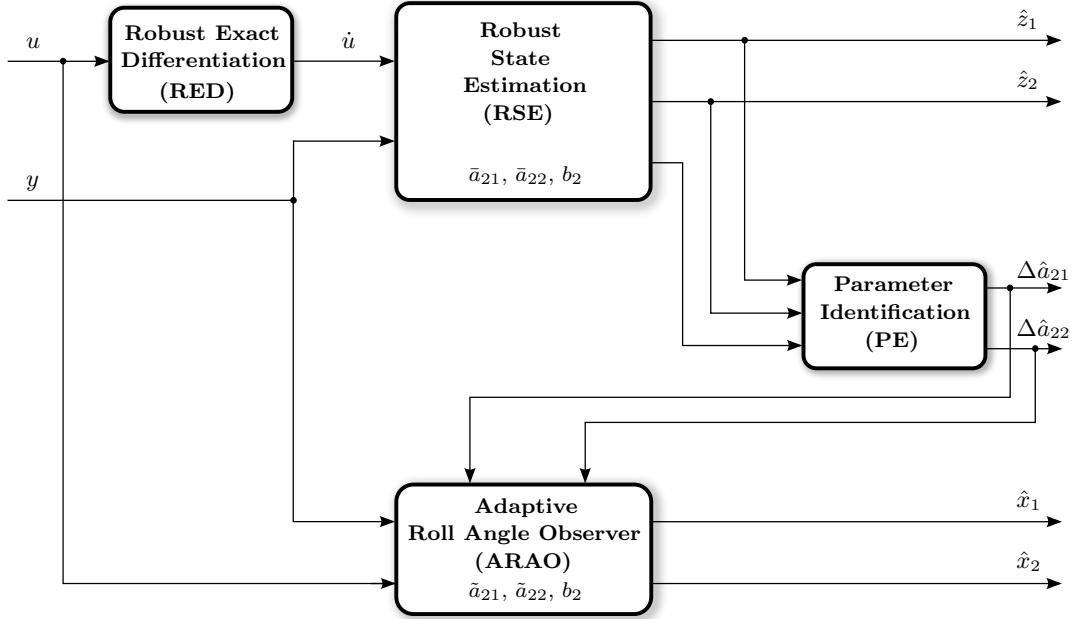


Figure 4.9: Schematics of the proposed concept for roll model parameters identification.

Robust Exact Differentiation (RED)

The transformation of the original system into (4.88) requires real-time differentiation of the system input u w.r.t. time providing highly accurate and phase shift-free³⁴ estimates. A robust exact³⁵ differentiator as presented in [LEV98] is employed to fulfill these requirements.

Differentiating a given signal with respect to time can be formulated as a control problem, given that the control loop is identical to that depicted in Figure 4.10. The concept is based on an introduction of an artificial plant (an integrator) that should track some given reference value. A variable structure control concept, e.g. [LEV98], provides inherent robustness and finite time convergence.

In a mathematically more rigorous way the plant is given by

$$\frac{d\hat{u}}{dt} = v, \quad (4.91)$$

where \hat{u} defines the estimate of the input signal u and v the control output or the time derivative of \hat{u} . Note that the class of input functions u is restricted to bounded functions with Lipschitz-bounded derivatives and some small amount of noise [LEV98]. Now, by

³⁴Intrinsically, standard differentiating concepts introduce a certain amount of phase shift between the real signals and the estimated derivatives.

³⁵For an accurate definition of the terminology *robust* and *exact* the reader is referred to [LEV98].

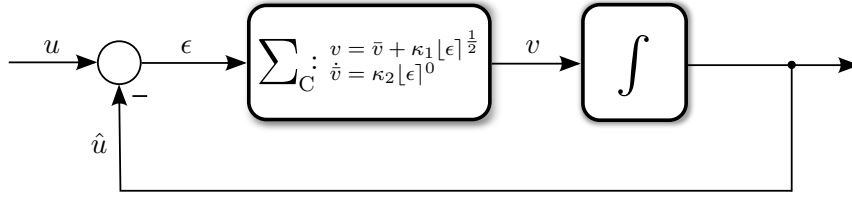


Figure 4.10: Time differentiation realized as control loop. The control signal v approximates the derivative of u w.r.t. time. Due to the advantages of robustness and finite time convergence Σ_C is based on the super-twisting algorithm.

introducing the error coordinate ϵ , being defined as

$$\epsilon := u - \hat{u}, \quad (4.92)$$

it is the objective to drive that error ϵ to zero within finite time, i.e. $\epsilon \equiv 0 \forall t \geq \tau_{c_1}$. One possible solution is the use of a super-twisting controller

$$v = \bar{v} + \kappa_1 |\epsilon|^{\frac{1}{2}}, \quad (4.93a)$$

$$\frac{d\bar{v}}{dt} = \kappa_2 |\epsilon|^0, \quad (4.93b)$$

with $\kappa_1, \kappa_2 > 0$. Systematic tuning of these parameters is discussed in e.g. [RH11, LEV98]. Transforming the system into error coordinates it reads as

$$\frac{d\epsilon}{dt} = \underbrace{\frac{du}{dt} - \bar{v} - \kappa_1 |\epsilon|^{\frac{1}{2}}}_{=: \bar{\epsilon}}, \quad (4.94a)$$

$$\frac{d\bar{\epsilon}}{dt} = \frac{d^2 u}{dt^2} - \kappa_2 |\epsilon|^0. \quad (4.94b)$$

For that type of system stability proofs of finite time convergence exist, e.g. [LEV98, MO12]. From (4.94b) it becomes obvious that the second time derivative of the signal u needs to be bounded, i.e.

$$\left| \frac{d^2}{dt^2} u(t) \right| < u^+ < \infty \quad \forall t. \quad (4.95)$$

After convergence of ϵ and $\bar{\epsilon}$ to the origin within finite time τ_{c_1} , i.e. $\epsilon \equiv 0$, $\bar{\epsilon} \equiv 0$, the definition of $\bar{\epsilon}$ reveals that v provides an estimate for the derivative of u w.r.t. time.

Furthermore, if the input signal $u(t)$ is corrupted by some bounded noise term $|\nu(t)| \leq \varepsilon_n$,

then it can be shown that the accuracy of the time derivative estimate is given by

$$\left| v - \frac{du}{dt} \right| < \tilde{\kappa}_1 \sqrt{\varepsilon_n} \quad \forall t \geq \tau_{c_1}, \quad (4.96)$$

where the constant $\tilde{\kappa}_1$ is a function of κ_1, κ_2 , see [LEV98] for details.

Robust State Estimation (RSE)

Due to its invariance to a certain class of disturbances the sliding mode paradigm is well suited to solve the problem of state reconstruction in the presence of uncertainties. In the following an STA³⁶-based higher-order sliding mode observer [LEV93], is implemented to reconstruct the states z_1 and z_2 .

The formulation of a robust state observer [DFL05] is based on a replica of the state equations (4.88) and injection terms, i.e.

$$\frac{d\hat{z}_1}{dt} = \hat{z}_2 + \lambda_1 |e_1|^{\frac{1}{2}}, \quad (4.97a)$$

$$\frac{d\hat{z}_2}{dt} = -\bar{a}_{21}\hat{z}_1 - \bar{a}_{22}\hat{z}_2 + b_2v + \lambda_2 |e_1|^0, \quad (4.97b)$$

with the estimation errors e_1 and e_2 defined as $e_1 := z_1 - \hat{z}_1$ and $e_2 := z_2 - \hat{z}_2$. Then, the error dynamics read as

$$\frac{de_1}{dt} = e_2 - \lambda_1 |e_1|^{\frac{1}{2}}, \quad (4.98a)$$

$$\frac{de_2}{dt} = -\bar{a}_{21}e_1 - \underbrace{-\bar{a}_{22}e_2 + \zeta(z_1, z_2)}_{=: \xi(z_1, z_2, \hat{z}_2)} - \lambda_2 |e_1|^0. \quad (4.98b)$$

Convergence of the estimation errors employing a super-twisting algorithm is guaranteed if the condition

$$\left| \xi(z_1, z_2, \hat{z}_2) \right| < \xi^+ < \infty, \quad (4.99)$$

holds³⁷ for any z_1, z_2 and $|\hat{z}_2| \leq 2 \sup |z_2|$, see [DFL05] for details. Due to the boundedness of the system input v , the system states of (4.88) (BIBS stable) and the uncertainty ζ , see (4.90), the existence of ξ^+ is guaranteed. Suggestions for the tuning of the observer

³⁶This second-order algorithm has been selected over conventional 1-sliding concepts due to the advantages of a.) finite time convergence, b.) required knowledge of the sliding variable only (rather than its time derivatives) and c.) chattering reduction. Furthermore, it allows the rejection of Lipschitz perturbations exactly [MOR09].

³⁷Note that the term $-\bar{a}_{21}e_1$ can be neglected due to the accurate knowledge of x_1 .

gains λ_1 and λ_2 are given in [LEV93, LEV98]. Herein, the gains are chosen as

$$\lambda_1 = 1.5 \left(\xi^+ \right)^{\frac{1}{2}} \quad \text{and} \quad \lambda_2 = 1.1 \xi^+. \quad (4.100)$$

Then, the solutions of system (4.98) converge to the origin $(e_1, e_2) = (0, 0)$ within finite time τ_{e_2} , i.e.

$$e_1(t) = e_2(t) = 0 \quad \forall t \geq \tau_{e_2}. \quad (4.101)$$

A proof of stability is omitted here, but can be found in e.g. [LEV98, DFL05, MO12]. Furthermore, for the estimation of the convergence time τ_{e_2} different methods have been proposed by [LEV98, DFL05, PP09, MO12, UTK13]. These can be useful for the activation of the parameter identification mechanism to be started once the estimation errors have vanished.

Adaptive Robust State Estimation (ARSE)

So far, the quantitative knowledge of the uncertainty bound ξ is assumed *a priori* (and constant) in order to be able to tune the observer gains appropriately. However, commonly it is difficult to obtain reasonable values for the bound. Often it is chosen too conservatively resulting in a high gains³⁸. In case of a time-varying perturbation it might be helpful to adjust the bound as well. Consequently, adaptive gain schemes are increasingly considered, e.g. [GMF12, STP12, UP13, ES15]. Exactly speaking, the observer gains are generally no longer static, but might read as

$$\tilde{\lambda}_1 := \tilde{\lambda}_1(e_1, e_2, \dots, e_n, t) \quad \text{and} \quad \tilde{\lambda}_2 := \tilde{\lambda}_2(e_1, e_2, \dots, e_n, t). \quad (4.102)$$

The algorithm presented in the following is known as adaptive gain super-twisting algorithm [STP12] and changes the observer gains adaptively until a sliding motion is established. A so-called *detector* determines the entering and leaving of a domain $\Lambda := |e_1| - \mu$, where μ is some positive constant. Needless to say, but the definition of the detector is not unique and leaves some design freedom to the user. For the current application it is chosen as a band around the sliding variable e_1 [TRH14b]. Whenever the trajectories enter the domain Λ the observer gains are decreased. In contrast, if the trajectories are outside that domain the gains are increased in order to push them (back). Mathemati-

³⁸These increase the tendency to *chattering*. Even though this problem is more related to the control task it should be noted here.

cally speaking, this reads as

$$\frac{d\tilde{\lambda}_1}{dt} = \begin{cases} \kappa [\Lambda]^0 & \text{if } \tilde{\lambda}_1 > \tilde{\lambda}^-, \\ \eta & \text{else,} \end{cases} \quad (4.103a)$$

$$\tilde{\lambda}_2 = \varepsilon \tilde{\lambda}_1. \quad (4.103b)$$

The quantity $\tilde{\lambda}^-$ represents a lower bound for the gain $\tilde{\lambda}_1$. Its initial value is defined as $\tilde{\lambda}_{1,0} := \tilde{\lambda}_1(t_0)$ and $\tilde{\lambda}_{1,0} > \tilde{\lambda}^-$ needs to hold. Furthermore, κ , η and ε are positive constants. More specifically, κ governs the rate of observer gain change, η is some small constant that is only used whenever the lower bound of $\tilde{\lambda}_1$, namely $\tilde{\lambda}^-$, is fallen below. The value of ε scales the ratio between the values of $\tilde{\lambda}_1$ and $\tilde{\lambda}_2$. Furthermore, $\eta \geq \mu$ needs to hold. A stability proof of the adaptive gain super-twisting algorithm and an estimation of the convergence time are both provided in [STP12].

Now, that two different observer concepts, based on static and adaptive gains, are introduced the objective of unknown input recovery shall be focused on again. Due to the convergence of the estimation errors e_1 , e_2 within finite time τ_{c_3} equation (4.98b) becomes

$$\frac{de_2}{dt} \equiv 0 \quad \Rightarrow \quad 0 \equiv \zeta(z_1, z_2) - \nu_{eq} \quad \forall t \geq \tau_{c_3}. \quad (4.104)$$

Here, the term $\nu_{eq} := \left(\tilde{\lambda}_2 [e_1]^0 \right)_{eq}$ represents the equivalent output injection term that is required to maintain the system's sliding motion. Even if ν_{eq} refers to the adaptive gain scheme in that case, it should be emphasized that it can also be extracted from the static gain mechanism. Reconsidering (4.104) it is obvious that the identification of ν_{eq} allows for recovery of the uncertainty $\zeta(z_1, z_2)$, i.e.

$$\hat{\nu}_{eq} := \left(\tilde{\lambda}_2 [e_1]^0 \right)_{lpf}. \quad (4.105)$$

For the switching frequency tending to infinity and the filter time constant τ_f to zero $\hat{\nu}_{eq} \rightarrow \nu_{eq}$ holds [UGS09]. The approximative character of the estimate can be emphasized by defining

$$\nu_{eq} = \hat{\nu}_{eq} + \Delta\nu_{eq}, \quad (4.106)$$

where $\Delta\nu_{eq}$ accounts for the errors due to the filtration process and noise. Finally, an estimate of the uncertainty $\zeta(z_1, z_2)$ is given by $\hat{\nu}_{eq} = \hat{\zeta}(z_1, z_2)$.

Alternatively to avoid the explicit filtration in order to obtain equivalent output injection term another route might be chosen by implementing a higher-order robust exact differentiator [LEV05] as presented in Section 4.2.4 or step-by-step sliding mode observer [FES06].

Parameter Identification (PE)

The extraction of the uncertain parameters Δa_{21} and Δa_{22} from the recovered uncertainty $\hat{\zeta}$ is performed by two different approaches. The first is based on a classic Recursive Least Squares (RLS) algorithm and the second uses a more recent algorithm, i.e. a generalized super-twisting algorithm providing finite time convergence [MG11]. These two mechanisms are abbreviated with RLSPE (Recursive Least Squares Parameter Estimator) and FTPE (Finite Time Parameter Estimator) respectively.

Referring to (4.89) the uncertainty constitutes of a linear combination of system states z_1, z_2 and the unknown parameters Δa_{21} and Δa_{22} . The finite time convergence of the robust state observation ensures estimation errors of $e_1 \equiv 0, e_2 \equiv 0$ after a time τ_{c_2} . The estimate of the uncertainty $\hat{\zeta}(z_1, z_2)$ reads as

$$\hat{\zeta}(z_1, z_2) = -\Delta\hat{a}_{21} z_1 - \Delta\hat{a}_{22} z_2, \quad \forall t \geq \tau_{c_2} \quad (4.107)$$

where $\Delta\hat{a}_{21}, \Delta\hat{a}_{22}$ represent estimates of $\Delta a_{21}, \Delta a_{22}$. It is important to note again, that the latter are unknown, but constant. Defining a parameter vector $\hat{\theta}$ and a regression vector φ as

$$\hat{\theta} := \begin{bmatrix} \Delta\hat{a}_{21} & \Delta\hat{a}_{22} \end{bmatrix}^T \quad \text{and} \quad \varphi := -\begin{bmatrix} z_1 & z_2 \end{bmatrix}, \quad (4.108a)$$

the identification of the unknown parameters can be formulated as a linear regression problem

$$\hat{\zeta}(z_1, z_2) = \varphi \hat{\theta}. \quad (4.109)$$

The implementation of the RLS algorithm will be discrete w.r.t. time, hence the parameter and regression vectors need to be discretized at equidistant time intervals, represented by the sampling period τ_s , i.e.

$$\mathbf{v}_k := \mathbf{v}(k \tau_s) \quad k \in \mathbb{N}_0, \quad (4.110)$$

where \mathbf{v} stands for the quantity to be discretized in time, e.g. $\hat{\theta}, \varphi$. Then the discrete-time implementation of an RLS algorithm can be written as [LJU99]

$$\mathbf{L}_k = \frac{\mathbf{P}_{k-1} \varphi_k^T}{\Lambda + \varphi_k \mathbf{P}_{k-1} \varphi_k^T}, \quad (4.111a)$$

$$\hat{\theta}_k = \hat{\theta}_{k-1} + \mathbf{L}_k \left[\hat{\zeta}_k - \varphi_k \hat{\theta}_{k-1} \right], \quad (4.111b)$$

$$\mathbf{P}_k = \Lambda^{-1} \left[\mathbf{I} - \mathbf{L}_k \varphi_k \right] \mathbf{P}_{k-1}. \quad (4.111c)$$

There, the matrix \mathbf{P}_k is an approximation of the estimation error covariance matrix [IM11], \mathbf{L}_k can be interpreted as a weighting factor how much the new parameter estimate is affected by the estimation error $\Delta\zeta := \left[\hat{\zeta}_k - \boldsymbol{\varphi}_k^T \hat{\boldsymbol{\theta}}_{k-1} \right]$. Furthermore, the quantity Λ (in that case a scalar value) is referred to as a *forgetting factor* that attenuates the influence of older measurement values on the actual parameter estimation. In the literature there exist numerous algorithms to adapt Λ during operation, e.g. [WAN09]. However, for the current application a constant value $\Lambda < 1$ is used.

Assuming uncorrelated and zero-mean $\boldsymbol{\varphi}$ and $\Delta\nu$ and persistent excitation³⁹ the estimations of the RLS algorithm are consistent, e.g. [SS89, DFP06].

In summary, the presented parameter estimation concept exploits the equivalent injection error term, approximated by low-pass filtering of the high-frequency switching term and uses the extracted information for solving the formulated regression problem. The parameters convergence asymptotically [IM11]. This is different for the alternative approach extracted from [MG11] that converges in finite time. Moreover, it can be shown that the states remain bounded, even if the system is not excited persistently. Basically, the parameter estimation problem of system (4.88) can be formulated as

$$\frac{d\tilde{z}_2}{dt} = -\bar{a}_{21}z_1 - \bar{a}_{22}\tilde{z}_2 + b_2v - \alpha_1 \left(\mu_1 [e_{z_2}]^{\frac{1}{2}} + \mu_2 e_{z_2} \right) + \boldsymbol{\Gamma}(\hat{z}_1, \tilde{z}_2) \hat{\boldsymbol{\theta}}, \quad (4.112a)$$

$$\frac{d\hat{\boldsymbol{\theta}}}{dt} = -\alpha_2 \left(\frac{\mu_1^2}{2} [e_{z_2}]^0 + \frac{3}{2} \mu_1 \mu_2 [e_{z_2}]^{\frac{1}{2}} + \mu_2^2 e_{z_2} \right) \boldsymbol{\Gamma}(\hat{z}_1, \tilde{z}_2)^T, \quad (4.112b)$$

with the error e_{z_2} being defined as $e_{z_2} := \hat{z}_2 - \tilde{z}_2$, where \hat{z}_2 and \tilde{z}_2 are the estimates of the real state z_2 provided by the state observer and the parameter identification algorithm respectively. The gains α_1 , α_2 , μ_1 are strictly positive constants, $\mu_2 \geq 0$, the vector $\boldsymbol{\Gamma}(z_1, \tilde{z}_2)$ holds the state estimates, i.e. $\boldsymbol{\Gamma}(\hat{z}_1, \tilde{z}_2) := - \begin{bmatrix} \hat{z}_1 & \tilde{z}_2 \end{bmatrix}$ and the parameter vector $\hat{\boldsymbol{\theta}}$ is identical to (4.108a).

Note that, even though the same observer as discussed in (4.97) is employed, its objective is purely the robust estimation of the states z_1, z_2 and not the recovery of the unknown input ζ . This renders the tuning of the low-pass filter redundant and eases the setup of the parameter identification mechanism. The stability proof and an estimate of the convergence time are provided in [MG11].

Adaptive Roll Angle Observation (ARAO)

From the presented observer-based parameter identification methods the uncertain model parameters of system (4.88) can now be assumed identified. However, due to the required system transformation (4.87) it is the roll rate and acceleration, rather than the roll angle and rate, that are estimated during the state observation process. Therefore, an additional observer concept based on system (4.82) using the identified model parameters

³⁹For the definition of persistent excitation see e.g. [LJU99, IM11].

as additional input needs to be designed to get an estimate of the roll angle.

Then, a standard Luenberger observer [LUE71] can be designed as

$$\frac{d\hat{x}_1}{dt} = \hat{x}_2 + l_1 (y - \hat{x}_2), \quad (4.113a)$$

$$\frac{d\hat{x}_2}{dt} = -\tilde{a}_{21}\hat{x}_1 - \tilde{a}_{22}\hat{x}_2 + b_2u + l_2 (y - \hat{x}_2), \quad (4.113b)$$

where the expressions \tilde{a}_{21} and \tilde{a}_{22} vary with time, i.e. $\tilde{a}_{21} = a_{21} + \Delta a_{21}(t)$ and $\tilde{a}_{22} = a_{22} + \Delta a_{22}(t)$. The terms $\Delta a_{21}(t)$ and $\Delta a_{22}(t)$ are interpreted as a time-varying difference between the real parameters a_{21}, a_{22} and the estimated ones $\tilde{a}_{21}, \tilde{a}_{22}$. Formulation of the error dynamics⁴⁰, with $e_1 := x_1 - \hat{x}_1$ and $e_2 := x_2 - \hat{x}_2$, results in

$$\frac{de_1}{dt} = (1 - l_1) e_2, \quad (4.114a)$$

$$\frac{de_2}{dt} = -a_{21}e_1 - (a_{22} + l_2) e_2 + \varsigma(\hat{x}_1, \hat{x}_2), \quad (4.114b)$$

where the input ς is defined by

$$\varsigma(\hat{x}_1, \hat{x}_2) := -\Delta a_{21}(t)\hat{x}_1 - \Delta a_{22}(t)\hat{x}_2. \quad (4.115)$$

Ideally, for vanishing Δa_{21} Δa_{22} the input $\varsigma(\hat{x}_1, \hat{x}_2)$ disappears too. Unfortunately, due to imperfections in the parameter estimation algorithms and also parasitic system dynamics there remains some deviation between the real and the estimated parameters. Hence, information on the effects of $\varsigma(\hat{x}_1, \hat{x}_2)$ would be useful to determine the quality of the roll angle estimation.

$$G_1(s) = \frac{\bar{e}_1(s)}{\bar{\varsigma}(s)} = \frac{1 - l_1}{s^2 + (a_{22} + l_2)s + a_{21}(1 - l_1)}, \quad (4.116a)$$

$$G_2(s) = \frac{\bar{e}_2(s)}{\bar{\varsigma}(s)} = \frac{s}{s^2 + (a_{22} + l_2)s + a_{21}(1 - l_1)}. \quad (4.116b)$$

$G_1(s)$ and $G_2(s)$ define the transfer functions of the input ς to the errors e_1 and e_2 respectively. Under the assumption that all components, i.e. observer (4.97), robust exact differentiator (4.94), parameter identification algorithm (4.112), are tuned correctly and the corresponding errors converge, then the uncertainties $\Delta a_{21}(t)$ and $\Delta a_{22}(t)$ are bounded for times $t \geq \tau_c$, where τ_c denotes an overall convergence time accounting for all convergence times of the involved structures. These upper bounds are then defined

⁴⁰Note that the unknown input f of (4.82) can now be disregarded due to the estimates of the parameter uncertainties $\Delta a_{21}(t)$ and $\Delta a_{22}(t)$.

by

$$|\Delta a_{21}(t)| \leq \Delta a_{21}^+ \quad \text{and} \quad |\Delta a_{22}(t)| \leq \Delta a_{22}^+ \quad \forall t \geq \tau_c. \quad (4.117)$$

Furthermore, the system matrix of (4.114) can be formulated as

$$\mathbf{A}_e := \begin{bmatrix} 0 & (1 - l_1) \\ -a_{21} & -(a_{22} + l_2) \end{bmatrix}, \quad (4.118)$$

and by appropriate choice of the vector $\mathbf{l} := [l_1 \quad l_2]^T$ that matrix is a Hurwitz matrix. Consequently, assuming a bounded input, the output as well as the states [KHA02] are also bounded. Hence, by correct design of \mathbf{l} in (4.114) it is clear that both $e_1(t)$ and $e_2(t)$ are bounded. This in turn reveals the boundedness of the estimates \hat{x}_1 and \hat{x}_2 where the bounds are defined as \hat{x}_1^+ and \hat{x}_2^+ and a (conservative) bound of the input signal $\varsigma(\hat{x}_1, \hat{x}_2)$ might be calculated as

$$|\varsigma(\hat{x}_1, \hat{x}_2)| = |-\Delta a_{21}(t) \hat{x}_1 - \Delta a_{22}(t) \hat{x}_2| \quad (4.119a)$$

$$\leq |-\Delta a_{21}(t) \hat{x}_1| + |-\Delta a_{22}(t) \hat{x}_2| \quad (4.119b)$$

$$< \Delta a_{21}^+ \hat{x}_1^+ + \Delta a_{22}^+ \hat{x}_2^+ \quad (4.119c)$$

And finally, assuming an harmonic input ς the upper bounds of the errors $e_1(t)$ and $e_2(t)$ can be approximated by

$$e_1(t) \approx |G_1(j\omega)| \left(\Delta a_{21}^+ \hat{x}_1^+ + \Delta a_{22}^+ \hat{x}_2^+ \right) \sin(\omega t + \angle G_1(j\omega)), \quad (4.120a)$$

$$e_2(t) \approx |G_2(j\omega)| \left(\Delta a_{21}^+ \hat{x}_1^+ + \Delta a_{22}^+ \hat{x}_2^+ \right) \sin(\omega t + \angle G_2(j\omega)) \quad (4.120b)$$

Example: Model Parameter Identification of the Roll Dynamics

The proposed observer-based parameter identification techniques are to be evaluated in simulations using an ideal reference system. This is further motivated as within the next chapter these concepts will be applied to measurement data obtained from a vehicle dynamics simulation software and then it is difficult to distinguish inherent deficiencies of the mechanisms and effects due to unmodelled dynamics.

Table 4.6 summarizes the model parameters of the plant and all relevant tuning factors of the observer concepts. The excitation of the system is performed by a sinusoidal signal with amplitude $a_{y,m} = 7\text{m}\cdot\text{s}^{-2}$ and constant frequency $f = 0.5\text{Hz}$. Rather than using a frequency sweep the process of parameter identification is designed such, that different excitation frequencies will be applied sequentially. As a result, for each of these frequencies a certain set of parameters is identified.

Parameter	Description	Value	Unit
a_{21}	Reference (scaled) roll stiffness, see (3.53)	150	$\text{rad}^{-1} \cdot \text{s}^{-2}$
a_{22}	Reference (scaled) roll damping, see (3.53)	6	$\text{rad}^{-1} \cdot \text{s}^{-1}$
b_2	System input weight, see (3.53)	2	m^{-1}
\bar{a}_{21}	Nominal model parameter (scaled stiffness)	30	$\text{rad}^{-1} \cdot \text{s}^{-2}$
\bar{a}_{22}	Nominal model parameter (scaled damping)	2	$\text{rad}^{-1} \cdot \text{s}^{-1}$
$\hat{\mathbf{x}}_0^+$	Initial state vector (EKF)	$[-0.04 \ 0.08 \ -\bar{a}_{21} \ -\bar{a}_{22}]^T$	-
\mathbf{P}_0^+	Initial error covariance matrix (EKF)	$\text{diag}([1\text{e-}5 \ 1\text{e-}5 \ 1\text{e-}3 \ 1\text{e-}3])$	-
r	Covariance of the meas. noise (EKF)	$3\text{e-}7$	-
$\bar{\mathbf{Q}}$	Covariance of the process noise (EKF)	$\text{diag}([1\text{e-}9 \ 1\text{e-}9 \ 1\text{e-}4 \ 1\text{e-}6])$	-
λ_1	Static observer gain (VSUIO-RSE), see (4.97)	16	-
λ_2	Static observer gain (VSUIO-RSE), see (4.97)	45	-
κ	Adaptive observer gain change coeff. (VSUIO-ARSE), see (4.103a)	50	-
μ	Detector width (VSUIO-ARSE), see (4.103a)	$5\text{e-}4$	-
$\tilde{\lambda}^-$	Lower bound of adaptive gain $\tilde{\lambda}_1$, see (4.103a)	17	-
$\tilde{\lambda}_{1,0}$	Initial value of the adaptive gain $\tilde{\lambda}_1$	25	-
η	Small gain to push $\tilde{\lambda}_1$ above $\tilde{\lambda}^-$	$1\text{e-}2$	-
ε	Gain factor $\tilde{\lambda}_2$	1.2	-
$\hat{\mathbf{x}}_0$	Initial state vector (VSUIO-RSE)	$[-0.04 \ 0.08]^T$	-
f_c	Cut-off frequency low-pass filter (RLSPE)	30	Hz
Λ	Forget. factor (RLSPE), see (4.111)	0.9999	-
μ_1	Nonlinear term (FTPE), see (4.112)	3	-
μ_2	Linear term (FTPE), see (4.112)	11	-
α_1	Parameter estimator gain (FTPE), see (4.112)	3	-
α_2	Parameter estimator gain (FTPE), see (4.112)	30	-

Table 4.6: Simulation parameters of the plant, EKF, VSUIO-(A)RSE, RLSPE and FTPE.

Simulation results of the EKF-based state augmentation scheme are shown in Figure 4.11. From (b) it is obvious that the estimation error of state x_1 vanishes after $t \approx 11\text{s}$. Furthermore, the unknown parameter deviations Δa_{21} and Δa_{22} are identified after 10 seconds of operation.

Evaluation of the second concept in simulations is performed on a reduced set of mechanisms involved, i.e. the robust exact differentiator and also the adaptive Luenberger observer are omitted. These will be added when testing the performance on measurement data from the professional vehicle dynamics simulation software. In other words the system is assumed to be in form (4.88), i.e. operates in z -coordinates. Moreover, the input signal is not the output of the differentiator. The system excitation is identical to the previous experiment. For the VSUIO concept the distinction between the static and adaptive gain algorithms is performed by the abbreviations RSE (static) and ARSE (adaptive) respectively. From the results obtained one concept will be selected and further used within the next chapter. The same holds true for the parameter iden-

tification mechanism, i.e. at the end of this section only one shall be brought forward to the remaining part of this thesis. Figure 4.12 depicts the simulation results from a sinusoidal system excitation. Overall that concept shows a good convergence rate of either the states and the parameters. The estimation errors have vanished to reasonably low values after $t \approx 4s$.

Some Comments on the VSUIO For the variable structure unknown input observer there are two aspects that need to be focused on: a.) what is the benefit of the adaptive gain scheme and b.) which of the two proposed parameter estimators is the better choice. Starting with the static gain scheme it necessitates some knowledge of the uncertainty bounds in order to guarantee stability of the system. In contrast, the adaptive scheme claims to avoid this requirement.

For the considered system only e_1 is known and can be incorporated into the detector formulation. However, in general there is some lower bound on the gains λ_1 and λ_2 that guarantees convergence of the algorithm. So, assuming $\tilde{\lambda}_1$ is smaller than this lower bound, the error $|e_1|$ will leave the band μ and consequently $\tilde{\lambda}_1$ (and also $\tilde{\lambda}_2$) will be increased to push back the error. However, during the time e_1 is not within the μ -band the parameter identification needs to be stopped as the assumption that e_1 and e_2 are both zero is violated. Consequently, in order to get a satisfactorily behavior of the adaptive scheme for the unknown input recovery the lower bounds of the adaptive gains $\tilde{\lambda}_1, \tilde{\lambda}_2$ are ideally above the lower bound of those gains that guarantee convergence. In summary, for the current application even the adaptive gain scheme inherently requires some estimate of the perturbation's upper boundary.

Considering the obtained simulation results it appears from Figures 4.12(b) and 4.12(d) that the adaptive algorithm shows less noise after convergence. However, this is due to a slightly different tuning of the two algorithms. In general, both provide good estimates of the states and unknown input. Due to the higher flexibility (at the price of more parameters to be tuned) the adaptive scheme is selected as the one to be brought forward. Focusing on the parameter estimators it is a lot clearer which algorithm to favor. There, the RLS algorithm exploits the estimates of the unknown input from filtering the discontinuous term, i.e. obtaining an estimate for the equivalent output error injection. Intrinsicly, the filtering process introduces some phase shift between the state estimates and the recovered input. From (4.107) it is obvious that this phase shift causes an incorrect mapping of the state estimates onto the unknown input and that further results in a distortion of the parameter estimates. In fact, the damping coefficient is underestimated. The only possibility to overcome this deficiency is to assume perfect knowledge of the system input frequency and compensate for the phase shift. Even though in practice this will be difficult to perform, results obtained from a phase-shift correction, denoted by RLSPE*, can be extracted from Figures 4.12(g) and 4.12(h). Compared with the uncorrected estimates of the RLSPE algorithm the offset in the damping parameter is obvious. Alternatively, the FTPE algorithm not only provides finite time convergence

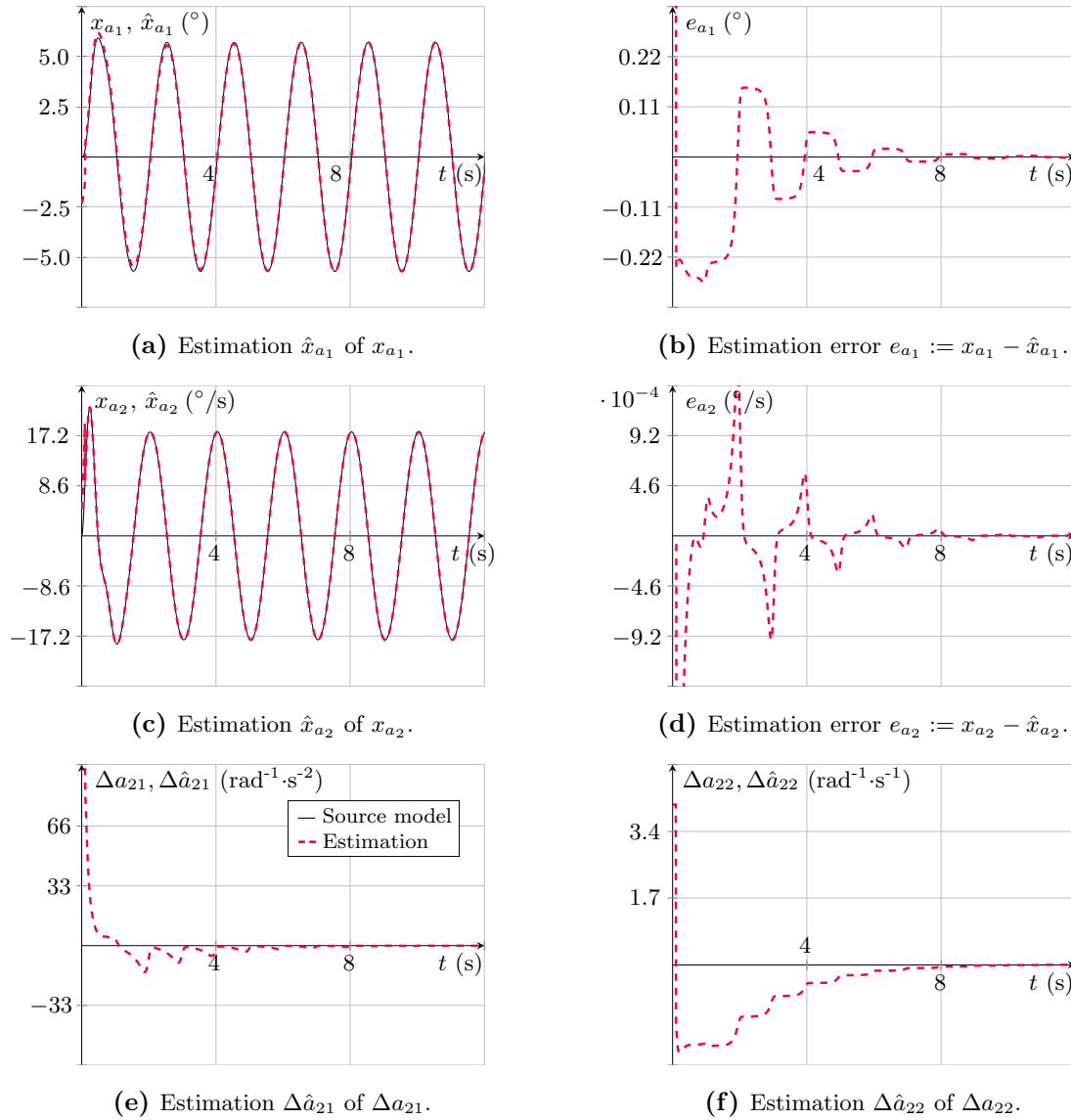


Figure 4.11: Ideal reference simulation results: Robust state estimation of Σ_R (EKF).

(as opposed to the asymptotic of the RLSPE), but also avoids the filtration process to extract an estimate of the uncertainty. Even though the number of differential equations to be solved for the combination VSUIO+FTPE is higher than for VSUIO+RLSPE the advantageous parameter estimation accuracy (see Figure 4.12(h)) leads to the decision to drop the concept of the RLS algorithm and only use FTPE to estimate the unknown model parameters.

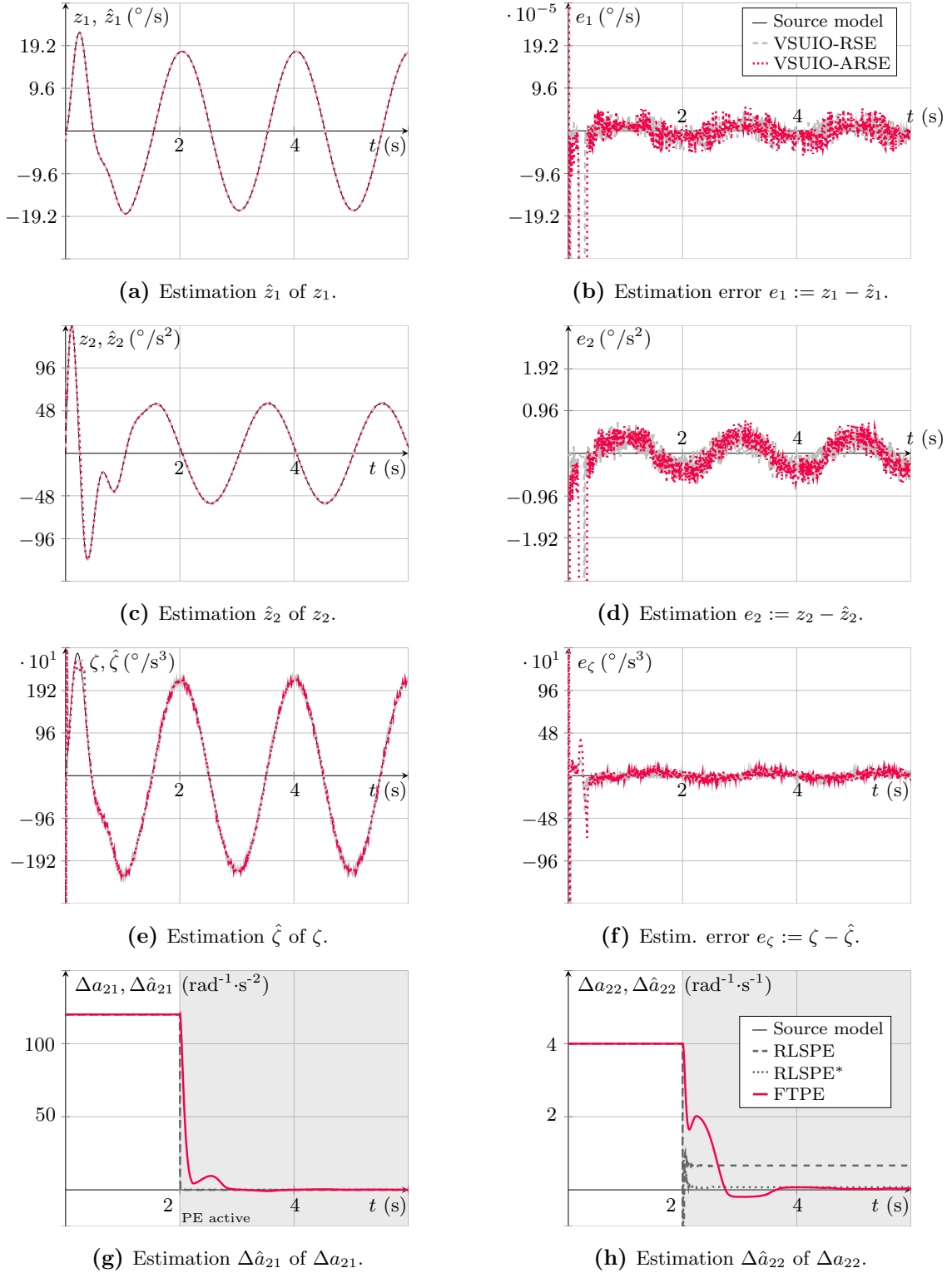


Figure 4.12: Ideal reference simulation results: Robust state estimation of Σ_R (VSUIO).

4.2.3 Pitch Dynamics

I Extended Kalman Filter

The mathematical structures of the roll and pitch state-space models (Σ_R and Σ_P respectively) are identical as (3.53) and (3.61) reveal. Consequently, the state observation and parameter identification task can be solved by the same concepts as presented in the previous section, e.g., a standard Extended Kalman Filter, see Section 4.2.2.I. The alternative concept of the unknown input observer is not considered here.

4.2.4 Steering Dynamics

I Variable Structure Unknown Input Observer (VSUIO)

The electric power steering (EPS) modelling and state-space formulations are provided in Sections 2.4.2 and 3.2.5. In contrast to the previous observer concepts the objective of the EPS state observer is also the recovery of unknown inputs, i.e. steering and wheel torques T_h and T_w respectively. But then, these inputs are not further used for a model parameter identification. System (3.67) does not fulfill the observer matching condition (4.86) and consequently the observer (4.85) does not exist. Fortunately, the invariant zeros of $(\tilde{\mathbf{A}}, \tilde{\mathbf{D}}, \mathbf{C})$ are in \mathbb{C}^- . Hence, the transfer matrix of (3.67) between the unknown inputs and the measured outputs is minimum-phase, but not relative degree 1. In [FES06] the relative degree condition is weakened and classic sliding mode observers are combined with robust exact differentiators in order to generate additional output signals. Furthermore, in [FB06] an algorithm for systems violating the observer matching condition is presented that transforms the given systems into a canonical form allowing design of finite time observer concepts even if the relative degree condition is not fulfilled. That algorithm will be applied to the given system $\Sigma_{\tilde{\zeta}}$ and a so-called step-by-step sliding mode observer [BBD96, FES06] can be designed.

The new state vector $\mathbf{z} \in \mathbb{R}^n$ is defined as

$$\mathbf{z} := \begin{bmatrix} z_1 & z_2 & z_3 \end{bmatrix}^T = \begin{bmatrix} x_1 & x_3 & x_1 - x_2 \end{bmatrix}^T, \quad (4.121)$$

and obtained by a state transformation $\mathbf{z} = \mathbf{T}\mathbf{x}$, with $\mathbf{T} \in \mathbb{R}^{n \times n}$ given by

$$\mathbf{T} := \begin{bmatrix} \mathbf{c}_1^T & \mathbf{c}_2^T & (\mathbf{c}_2 \mathbf{A})^T \end{bmatrix}^T. \quad (4.122)$$

Therein, \mathbf{c}_i denotes the i -th row, with $i = 1, 2$, of the output matrix \mathbf{C}_2 as in (3.71b).

The transformed system with $\bar{\mathbf{A}} := \mathbf{T}\tilde{\mathbf{A}}\mathbf{T}^{-1}$, $\bar{\mathbf{D}} := \mathbf{T}\tilde{\mathbf{D}}$, $\bar{\mathbf{B}} := \mathbf{T}\tilde{\mathbf{B}}$ and $\bar{\mathbf{C}} := \mathbf{C}\mathbf{T}^{-1}$, reads as

$$\begin{bmatrix} \frac{dz_1}{dt} \\ \frac{dz_2}{dt} \\ \frac{dz_3}{dt} \end{bmatrix} = \underbrace{\begin{bmatrix} -\frac{d_c}{J_{stw}} & -\frac{c_c}{J_{stw}} & 0 \\ 0 & 0 & 1 \\ \bar{a}_{31} & \bar{a}_{32} & \bar{a}_{33} \end{bmatrix}}_{=: \bar{\mathbf{A}}} \begin{bmatrix} z_1 \\ z_2 \\ z_3 \end{bmatrix} + \underbrace{\begin{bmatrix} J_{stw}^{-1} & 0 \\ 0 & 0 \\ J_{stw}^{-1} & \frac{-i_r^{-1}}{J_{ca}} \end{bmatrix}}_{=: \bar{\mathbf{D}}} \begin{bmatrix} \zeta_1 \\ \zeta_2 \end{bmatrix}, \quad (4.123a)$$

$$\bar{\mathbf{y}} = \underbrace{\begin{bmatrix} 1 & 0 & 0 \\ 0 & 1 & 0 \end{bmatrix}}_{=: \bar{\mathbf{C}}} \mathbf{z}, \quad (4.123b)$$

with $\zeta_1 := d_1, \zeta_2 := d_2$ (introduced to distinguish the elements of $\bar{\mathbf{D}}$ from the unknown inputs) and

$$\bar{a}_{31} := \frac{-J_{ca} d_c + J_{stw} (i_m k_1 + i_m^2 d_m + i_m k_2)}{J_{ca} J_{stw}}, \quad (4.124a)$$

$$\bar{a}_{32} := \frac{-J_{ca} c_c - J_{stw} (c_c - i_m k_3)}{J_{ca}}, \quad (4.124b)$$

$$\bar{a}_{33} := \frac{-i_m^2 d_m - i_m k_2}{J_{ca}}. \quad (4.124c)$$

For system (4.123) a step-by-step super-twisting observer can be formulated as

$$\frac{d\hat{z}_1}{dt} = \bar{a}_{11} \hat{z}_1 + \bar{a}_{12} \hat{z}_2 + \gamma_1(z_1, \hat{z}_1, z_2, \hat{z}_2), \quad (4.125a)$$

$$\frac{d\hat{z}_2}{dt} = \hat{z}_3 + E \gamma_2(z_2, \hat{z}_2), \quad (4.125b)$$

$$\frac{d\hat{z}_3}{dt} = \bar{a}_{31} \hat{z}_1 + \bar{a}_{32} \hat{z}_2 + \bar{a}_{33} \hat{z}_3 + E \gamma_3(z_2, \hat{z}_2), \quad (4.125c)$$

where \bar{a}_{ij} denotes the element of matrix $\bar{\mathbf{A}}$ located at the i -th row and j -th column. The correction terms $\gamma_1(\cdot)$, $\gamma_2(\cdot)$ and $\gamma_3(\cdot)$ are designed on the basis of the super-twisting algorithm (4.45) and higher-order exact differentiators [LEV99]. More specifically these

are defined by

$$\gamma_1(z_1, \hat{z}_1, z_2, \hat{z}_2) := \bar{a}_{11} e_1 + \bar{a}_{12} e_2 + \kappa_1 [e_1]^{\frac{1}{2}} + \nu_1, \quad (4.126a)$$

$$\frac{d\nu_1}{dt} = \kappa_2 [e_1]^0, \quad (4.126b)$$

$$\gamma_2(z_2, \hat{z}_2) := \kappa_3 [e_2]^{\frac{2}{3}}, \quad (4.126c)$$

$$\gamma_3(z_2, \hat{z}_2) := \bar{a}_{32} e_2 + \kappa_4 [e_2]^{\frac{1}{3}} + \nu_2, \quad (4.126d)$$

$$\frac{d\nu_2}{dt} := \kappa_5 [e_2]^0, \quad (4.126e)$$

with the estimation errors defined as $e_1 := z_1 - \hat{z}_1$, $e_2 := z_2 - \hat{z}_2$ and $e_3 := z_3 - \hat{z}_3$. Variable E in (4.125b) and (4.125c) is typical for the step-by-step observer, as it governs the (de)activation of individual observer terms. Herein, its definition is given by

$$E = \begin{cases} 1 & \text{if } |e_1| = |z_1 - \hat{z}_1| < \varepsilon_1 \quad \text{with } \varepsilon_1 > 0, \\ 0 & \text{else.} \end{cases} \quad (4.127)$$

Writing the system in estimation error coordinates allows intuitive interpretation of the observer characteristics and reads as

$$\frac{de_1}{dt} = \bar{d}_{11} \zeta_1 - \kappa_1 [e_1]^{\frac{1}{2}} - \nu_1, \quad (4.128a)$$

$$\frac{d\nu_1}{dt} = \kappa_2 [e_1]^0, \quad (4.128b)$$

$$\frac{de_2}{dt} = e_3 - E \kappa_3 [e_2]^{\frac{2}{3}}, \quad (4.128c)$$

$$\frac{de_3}{dt} = \bar{a}_{31} e_1 + \bar{a}_{33} e_3 + \bar{d}_{31} \zeta_1 + \bar{d}_{32} \zeta_2 - E \kappa_4 [e_2]^{\frac{1}{3}} - \nu_2, \quad (4.128d)$$

$$\frac{d\nu_2}{dt} = \kappa_5 [e_2]^0. \quad (4.128e)$$

The coefficients \bar{d}_{ij} are the elements of the matrix $\bar{\mathbf{D}}$ at i -th row and j -th column. Convergence of the estimation errors e_1 , e_2 and e_3 of the *two* observer concepts (4.128a), (4.128b) and (4.128c), (4.128d), (4.128e) can be analyzed individually. The equations

(4.128a) and (4.128b) can be rewritten (introducing $\tilde{\nu} := \bar{\zeta}_1 - \nu_1$) as

$$\frac{de_1}{dt} = \tilde{\nu} - \kappa_1 [e_1]^{\frac{1}{2}}, \quad (4.129a)$$

$$\frac{d\tilde{\nu}}{dt} = \frac{d\bar{\zeta}_1}{dt} - \kappa_2 [e_1]^0. \quad (4.129b)$$

The uncertainty $\bar{\zeta}_1(t) := \bar{d}_{11} \zeta_1(t)$ needs to be bounded, with a (Lipschitz) bounded derivative, i.e.

$$\left| \bar{\zeta}_1(t) \right| < \bar{\zeta}_1^+ < \infty, \quad (4.130a)$$

$$\left| \frac{d}{dt} \bar{\zeta}_1(t) \right| < \check{\zeta}_1^+ < \infty \quad \forall t > 0. \quad (4.130b)$$

Then, assuming that the observer gains are chosen appropriately, see e.g. (4.47), convergence of the super-twisting algorithm for $\forall t \geq \tau_{c_1} < \infty$ can be shown [DFP06, MO12], i.e. $e_1 \equiv 0$, $\tilde{\nu} \equiv 0$. Hence, after the convergence time τ_{c_1} the quantity of ν_1 can be exploited to gather an estimate $\hat{\zeta}_1$ for ζ_1 , i.e.

$$\hat{\zeta}_1 = \bar{d}_{11}^{-1} \nu_1. \quad (4.131)$$

Moreover, it is guaranteed that the absolute value of the estimation error e_1 is quantitatively below ε_1 and activation of the *second* higher-order sliding mode observer established.

The equations (4.128c) and (4.128d) define the error dynamics of the recently activated observer aiming to drive e_2 and e_3 to zero. Considering (4.128d) the term $\bar{a}_{31} e_1$ can be neglected as it is for sure below the threshold ε_1 and therefore small compared to the remaining terms. And alternatively, one could always argue to add another linear term to $\gamma_3(\cdot)$ canceling the appearance of e_1 in the dynamics of e_3 as the former is well known (z_1 is measured). Therefore, introducing an uncertainty

$$\xi(z_3, \hat{z}_3, \zeta_1, \zeta_2) := \bar{a}_{33} (z_3 - \hat{z}_3) + \bar{d}_{31} \zeta_1 + \bar{d}_{32} \zeta_2, \quad (4.132)$$

with an upper bound ξ^+ given as

$$\left| \xi(z_3, \hat{z}_3, \zeta_1, \zeta_2) \right| < \xi^+ < \infty, \quad (4.133)$$

for any z_3 , \hat{z}_3 , ζ_1 and ζ_2 . According to [LEV05] and [LL14] the gains κ_3 , κ_4 , κ_5 can be tuned as

$$\kappa_3 = 2 \left(\xi^+ \right)^{\frac{1}{3}}, \quad \kappa_4 = 1.5\sqrt{2} \left(\xi^+ \right)^{\frac{2}{3}}, \quad \kappa_5 = 1.1 \xi^+. \quad (4.134)$$

Parameter	Description	Value	Unit
J_{stw}	Steering wheel inertia (source model)	0.035	kg·m ²
J_{ca}	Sum of inertia (column, motor, rack)	0.25	kg·m ²
c_c	Column stiffness (source model)	95	N·m·rad ⁻¹
d_c	Column damping (source model)	0.8	N·m·s·rad ⁻¹
i_m	Transmission ratio electric motor to column	21	-
i_r	Transmission ratio column to rack	75	-
$\hat{\mathbf{x}}_0$	Initial state vector (VSUIO)	$[-4.5 \ -6.75 \ 0.25]^T$	-
κ_1	Observer gain (VSUIO), see (4.128a)	100	-
κ_2	Observer gain (VSUIO), see (4.128b)	500	-
κ_3	Observer gain (VSUIO), see (4.128c)	15.9	-
κ_4	Observer gain (VSUIO), see (4.128d)	133.6	-
κ_5	Observer gain (VSUIO), see (4.128e)	550	-
ε_1	Error band threshold, see (4.127)	1e-4	rad·s ⁻¹

Table 4.7: Simulation parameters of the source model and VSUIO.

A modification allowing for smaller observer gains would be the integration of the estimated $\hat{\zeta}_1$ into (4.126d). Then it drops out of the error dynamics, if perfectly estimated. After the finite time period τ_{c_2} the estimation errors converge to the origin, i.e. $(e_2, e_3) = (0, 0)$ and (4.128d) becomes

$$\frac{de_3}{dt} \equiv 0 \quad \Rightarrow \quad 0 \equiv \bar{d}_{31} \zeta_1 + \bar{d}_{32} \zeta_2 - \nu_2, \quad \forall t \geq \tau_{c_2}. \quad (4.135)$$

Then, an estimate of the unknown input ζ_2 , namely $\hat{\zeta}_2$, can be recovered from (4.135) and yields

$$\hat{\zeta}_2 = \bar{d}_{32}^{-1} \left(\nu_2 - \bar{d}_{31} \hat{\zeta}_1 \right), \quad (4.136)$$

with ζ_1 being approximated by the estimate $\hat{\zeta}_1$ as in (4.131).

Example: Reconstruction of Steering Torque and Wheel Moment

Table 4.7 lists the model and also the observer-relevant parameters. Actually, the electric motor is only used for dampening of oscillations, but is not set up to support the driver significantly. The steering torque T_h that is to be recovered by the state estimator is chosen as a sinusoidal signal with amplitude $T_h = 4\text{N}\cdot\text{m}$ and frequency $f = 0.5\text{Hz}$. Calculation of the wheel moment is currently obtained from a simple differential equation taking into account the rack displacement. The robust state estimates as well as the recovered inputs, i.e. steering torque T_h and wheel moment T_w obtained from the simulations are plotted in Figure 4.13. In summary, the results look promising and the observer will be evaluated further within the next chapters.

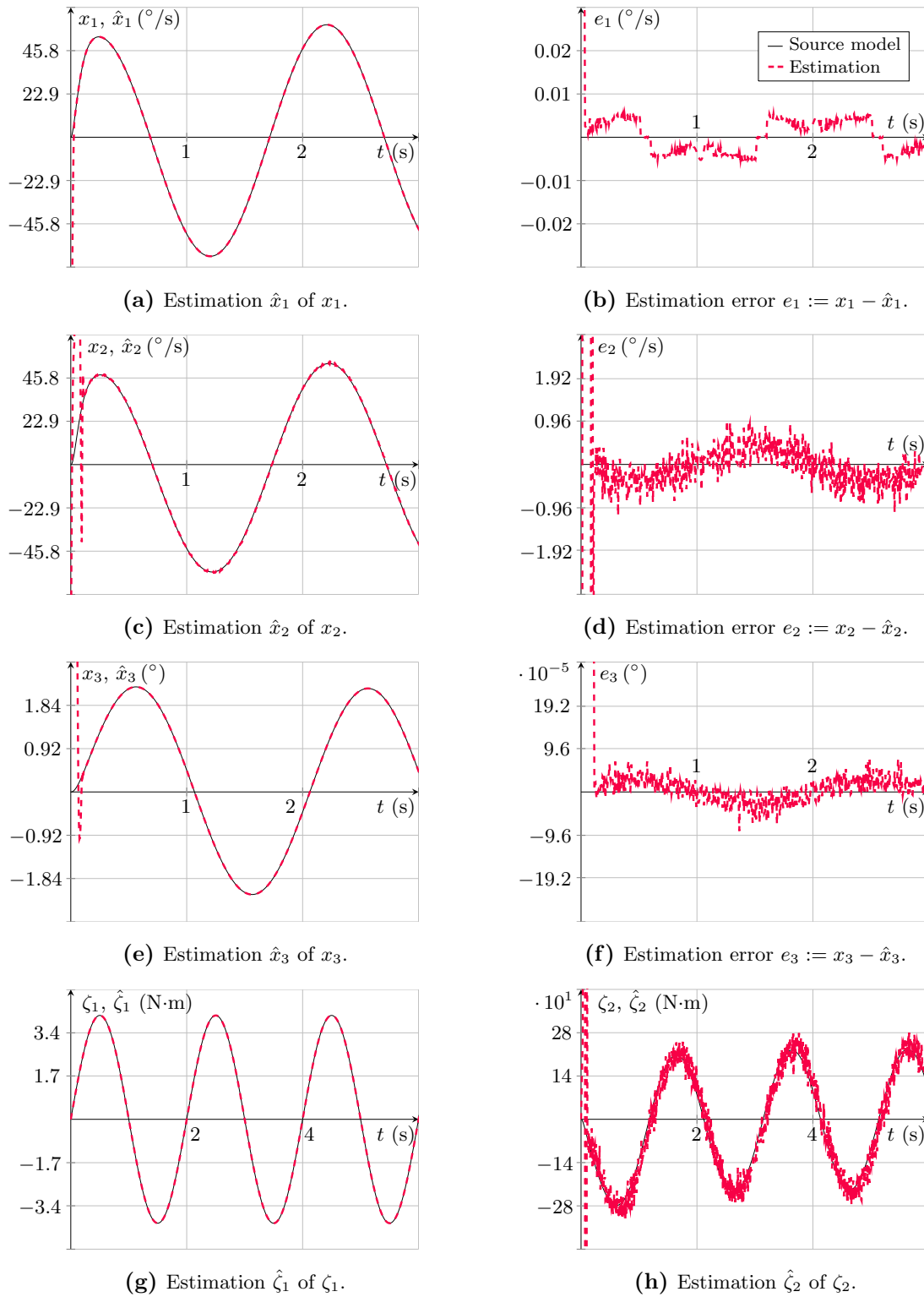


Figure 4.13: Ideal reference simulation results: Robust state estimation of $\Sigma_{\bar{s}}$.

4.2.5 Longitudinal and Powertrain Dynamics

The modelling of the powertrain dynamics in Section 2.5 also considered the dynamics of the (combustion) engine. Within this section the engine is modelled by a Black Box approach due to the nonlinearities, the number of unknown parameters and the lack of measurement signals available. Generally, two different approaches are investigated further in the following. The first approximates the complete chain of mechanical systems from the accelerator pedal position to the longitudinal acceleration signal by an artificial neural network. The second only approximates the behavior of the internal combustion engine (ICE) and provides an estimate of the engine torque given the actual accelerator pedal position and engine speed. Then, the calculation of the longitudinal acceleration is based on the simplified driveline models as presented in Section 2.5. The idea of approximating the ICE with an artificial neural network is presented in [HH03] to estimate the net torque of a gasoline-fed reciprocating engine. However, that method suffers from two drawbacks: First, the engine torque that is treated as system output is not measured directly, but estimated by some ECU-internal software function, that varies between the different suppliers. Hence, the internal torque estimation limits the Black Box estimation quality of the real torque. Second, the model of the driveline again contains parameters that should be known *a priori* and some additional parameter identification mechanism would be required. As a consequence, the Black Box model is designed such, that it takes as input the accelerator pedal position as well as engine speed and provides an estimate of the longitudinal acceleration. Figure 4.14 sketches the modular powertrain and its approximation by a feedforward neural network⁴¹. In general, these networks are often used for nonlinear regression and classification tasks due to their powerful modelling capabilities [KEC01].

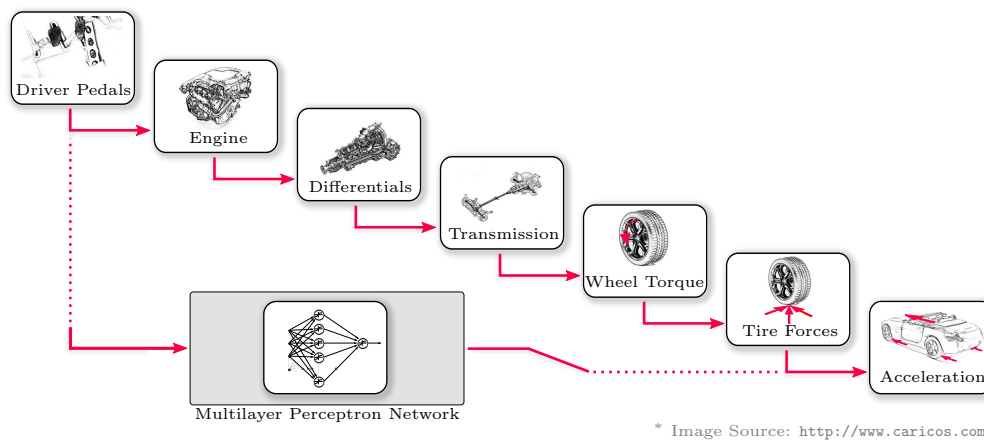


Figure 4.14: Approximation of the powertrain (and longitudinal) dynamics by a neural network structure.

⁴¹For a general introduction to neural networks see [KEC01]. Practical application to automotive topics is reviewed in [HH03].

A powerful, but also critically viewed theorem is the so-called Kolmogorov theorem [GP89]. It claims that any continuous function can be implemented exactly by a network consisting of certain number of neurons in the input and hidden layer as well as the output layer. Certainly, that claim makes the paradigm of neural networks interesting for Black Box modelling. Briefly, the general structure and the terminology used shall be introduced, before focusing on the modelling task itself. Figure 4.15 shows a feedforward neural network, also denoted as multilayer perceptron (MLP), that models a general, continuous and nonlinear function $f : D_f \subseteq \mathbb{R}^n \rightarrow \mathbb{R}$.

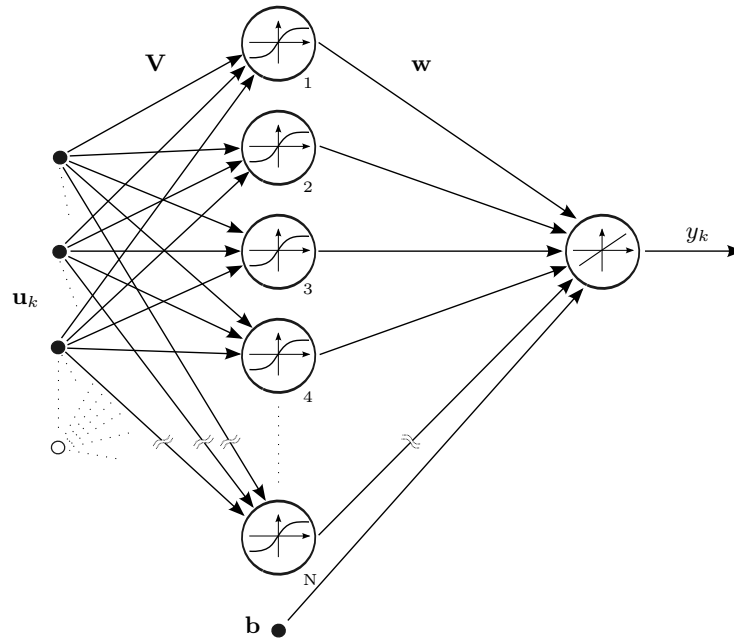


Figure 4.15: Schematics of an MLP network [KEC01].

Therein, $\mathbf{u}_k \in \mathbb{R}^n$ denotes the input vector at time instant $k\tau_s$, i.e. $\mathbf{u}_k := \mathbf{u}(k\tau_s)$ with $k \in \mathbb{N}_0$, $\mathbf{V} \in \mathbb{R}^{N \times n}$ the matrix of hidden layer weights, $\mathbf{w} \in \mathbb{R}^N$ the vector of output layer weights, $\mathbf{b} \in \mathbb{R}^N$ an offset value vector, N the number of neurons in the hidden layer and $y_k \in \mathbb{R}$ the scalar output at time instant $k\tau_s$, i.e. $y_k := y(k\tau_s)$ with τ_s being the sampling time. Then, the output function can be described as

$$y_k(\mathbf{u}_k, \mathbf{V}, \mathbf{w}, \mathbf{b}) = \sum_{i=1}^N w_i f_i(\mathbf{v}_i^T \mathbf{u}_k) + b_i, \quad (4.137)$$

where $f_i(\cdot) : D \subseteq \mathbb{R} \rightarrow \mathbb{R}$ is known as the *activation function* of the i -th hidden neuron,

. Furthermore, it is assumed as a sigmoid function, i.e.

$$f(x) = \frac{1}{1 + e^{-x}}. \quad (4.138)$$

Furthermore, the vector \mathbf{v}_i^T refers to the i -th row of matrix \mathbf{V} and w_i, b_i are the i -th elements of the appropriate vectors.

In [HH03] different architectural types of neural networks have been tested for the modelling of the internal combustion engine and it was found that the MLP structure shows good accuracy paid by the price of a time-intensive learning phase in order to find optimal values of \mathbf{V} and \mathbf{w} . The simulation-based evaluation of the neural structure will be given in Chapter 5.

4.2.6 Road Disturbance

An inherent assumption of the designed robust state observation concepts considers the road inclination and/or bank angle to be negligible. Figure 2.2 shows the inclination angle χ between the earth-fixed system \mathcal{C}_e and the vehicle-fixed system \mathcal{C}_v that might arise due to an inclined road. In general, it is the sum of the pitch angle and the inclination angle that defines the rotation angle between these two coordinate systems. With respect to the roll motion, Figure 2.11 illustrates the effect of a banked road on the roll angle, that is defined by the sum of the chassis roll, i.e. φ and the road bank angle Φ . As these additional external angles act as disturbances on the acceleration and angular rate sensors it needs to be validated before conducting any experiments that the assumptions of a flat road hold. Consequently, it is the task of the two proposed concepts to identify the road inclination and bank to support the driver in the decision whether the current road segment is feasible for any parameter identification work.

Due to the execution point of time the concepts are operated⁴², the design requires either to use kinematic relations that do not rely on any unknown or uncertain parameters and/or defines specific maneuvers that allow direct calculation of the inclination or bank angles.

I Road Inclination Estimation

The motivation to determine the actual road inclination is manifold, e.g. for look-ahead driver assistance systems [SJ08], transmission control [KN05] or correct longitudinal motion estimation [HH03, GIJ⁺09]. Herein, the objective of identifying the road inclination supports the decision whether the current track is feasible for performing any vehicle handling experiments. Figure 2.2 illustrates a vehicle climbing an inclined road, i.e. a rotation of the vehicle-fixed axis system \mathcal{C}_v and the earth-fixed \mathcal{C}_e by an angle $\theta - \chi$. There, θ represents the pitch angle of the vehicle (as in Section 2.3.2) and χ

⁴²At that stage of the overall process no vehicle model parameters have yet been identified.

the road inclination angle⁴³. The measured (in vehicle-fixed coordinates) longitudinal acceleration can be expressed using the transformation matrix as in (2.57), but taking into account the rotation angle as $\theta - \chi$. That yields an $a_{x,m}$ of

$$a_{x,m} = a_x \cos(\theta - \chi) - g \sin(\theta - \chi). \quad (4.139)$$

Given the observer objective, i.e. evaluating the inclination angle of a considered track section, the pitch dynamics of the vehicle can be neglected without any loss of information. In other words, the road inclination estimation requires the vehicle to be driven at constant (low) speed such that the pitch dynamics are not excited significantly. Additionally, the coupling between lateral and longitudinal dynamics, described in (2.5) and (2.10), is neglected. Consequently, another requirement for the observer activation can be formulated and refers to a straight line driving when estimating the road inclination. Applying these assumptions on (4.139) and assuming small inclination angles⁴⁴ the measured longitudinal acceleration reduces to

$$a_{x,m} = a_x + g\chi. \quad (4.140)$$

Referring to (2.10) and the assumption of the non-existent lateral dynamics, i.e. $\dot{\psi} \approx 0$, the derivative of the velocity w.r.t. time equals the acceleration, i.e. taking into account (4.140)

$$\frac{d_{\vee} v_x}{dt} = a_{x,m} - g\chi. \quad (4.141)$$

And transferring this simple differential equation into state-space representation by introducing the state vector $x_1 \in \mathbb{R}$ as $x_1 := v_x$, the input $u \in \mathbb{R}$ as $u := a_{x,m}$ and the output $y \in \mathbb{R}$ as $y := v_x$ results in

$$\frac{dx_1}{dt} = u - \Delta_u, \quad (4.142a)$$

$$y = x_1, \quad (4.142b)$$

with $\Delta_u := g\chi$ being a bounded⁴⁵ unknown input. Comparing (4.142) with the system (4.71) the similarities are obvious. Hence, an unknown input observer, as presented in Section 4.2.1.II, can be designed in order to gather an estimate of the road inclination, namely $\hat{\chi}$. For any further details on the observer design reconsider Section 4.2.1.II.

⁴³Note that these two rotations do have opposite positive directions.

⁴⁴This assumption should be clear from that point of view, that evaluation of the handling characteristics requires an almost flat road track. Given the case that the road inclination is obvious the driver is able to stop any experiments independently of the estimation results.

⁴⁵Certainly, the road inclination can not exceed some finite value.

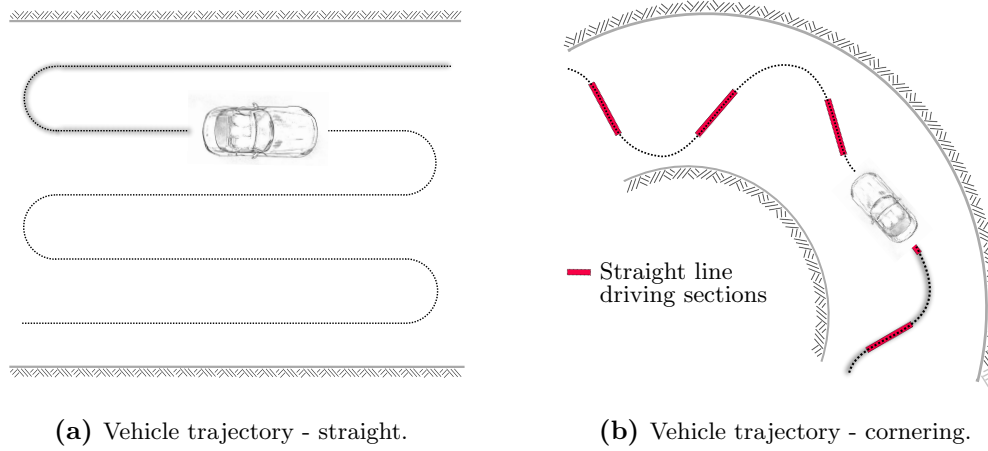


Figure 4.16: Suggested vehicle trajectories for the road bank determination.

II Road Grade Estimation

Figure 2.11 shows the effect of a banked road on the vehicle-fixed axis system and the roll dynamics related state variables. The lateral acceleration and also the vehicle sideslip angle are affected by a banked road, see e.g. (2.54). Therefore, various state observer-based methods for estimating the actual road inclination in order to improve safety-related assistance systems have been proposed, e.g. [TSE01, RG04, SGMN08, KLC12, MKDN12]. However, these approaches have in common that the model parameters of the roll dynamics need to be known *a priori*. An observer framework consisting of kinematic relations only is presented in [GIJ⁺09]. Herein, an estimate of the road bank angle is obtained, during periods the vehicle is driven almost in a straight line. Then the effects of the lateral vehicle motion on the lateral acceleration are negligible. Simplifying (2.54), i.e.

$$a_{y,m} = a_y \cos(\varphi + \Phi) + g \sin(\varphi + \Phi), \quad (4.143)$$

by assuming a roll angle $\varphi \approx 0$ and a lateral acceleration $a_y \approx 0$, then due to the small angles the trigonometric functions can be linearized and the resulting road bank angle estimation reads as

$$a_{y,m} \approx g\Phi. \quad (4.144)$$

In order to evaluate the suitability of a given road section or test track for the parameter identification process, i.e. the road bank angle should be approximately zero, specific vehicle driving trajectories (for a straight and curved track) are suggested and illustrated in Figures 4.16(a) and 4.16(b).

4.3 Concluding Remarks on the Observer-based Parameter Identification Concepts

The simulation results of the observer-based parameter identification techniques based on ideal source models revealed the advantages and disadvantages of different concepts. Even though some are promising from a theoretical point of view their application under realistic conditions might be difficult. To conclude the current chapter all mechanisms that will be part of the simulation⁴⁶-based evaluation (Chapter 5) are listed in Table 4.8.

Domain	Concept	Estim. Parameters	Estimated States	Measurements	Equations
Lateral (Cornering Stiffness)	EKF	$c_{\alpha_{f_e}}, c_{\alpha_r}$	$\dot{\psi}, \beta$	$\dot{\psi}, \delta_w, v v_x$	(4.50), (4.51), (4.16)
	VSUIO	— " —	— " —	$\dot{\psi}, v a_y, v v_x$	(4.64), (4.66), (4.67)
Lateral (Tire Force)	VSUIO	$v F_{y,f}, v F_{y,r}$	$\dot{\psi}$	$\dot{\psi}, v a_y, (\delta_w)$	(4.73)
Roll	EKF	$c_{\Sigma}^r, d_{\Sigma}^r$	$\varphi, \dot{\varphi}$	$\dot{\varphi}, a_{y,m}$	(4.79), (4.80), (4.16)
	VSUIO + FTPE	— " —	$\varphi, \dot{\varphi}, \ddot{\varphi}$	— " —	(4.93), (4.97), (4.103), (4.112), (4.113)
Pitch	EKF	$c_{\Sigma}^p, d_{\Sigma}^p$	$\theta, \dot{\theta}$	$\dot{\theta}, a_{x,m}$	(3.61), (4.50), (4.51), (4.16)
Steering	VSUIO	T_w, T_h	$\omega_h, \omega_s, \delta_h - \delta_s$	$\omega_h, \delta_h - \delta_s$	(4.125), (4.126)
Longitudinal, Powertrain	MLP	-	a_x	ω_e, φ_{acc}	(4.137)
Road Disturbance	VSUIO	-	χ, Φ	$a_{x,m}, v v_x, a_{y,m}$	(4.141), (4.144)

Table 4.8: Overview of proposed observer-based parameter identification techniques, estimated parameters and states, required measurements and relevant equations.

⁴⁶The source models are represented by a professional vehicle dynamics simulation software.

5

Validation of the Assessment Framework in Simulations

The validation of the proposed observer-based parameter identification mechanisms to meet certain performance specifications needs to be conducted in a more realistic simulation environment than presented in Chapter 4. Embedding the concepts into such a framework should sensitize the reader to the emerging difficulties and required modifications of the observer peripherals when being applied under real-world conditions. The results presented in the sequel of this chapter serve a twofold strategy. Firstly, the application to realistic simulation data (rather than the idealized source models as in Chapter 4) represents the next step towards the in-vehicle application (and also validation) of the concepts. Secondly, those concepts not applicable in-vehicle due to the lack of sensing devices are at least tested and evaluated within a realistic simulation framework and uprising problems or concept deficiencies will be revealed quickly.

Moreover, the evaluation of the overall assessment framework does not only cover the observer concepts, but also the model-based handling evaluation that deals with the integration of the identified parameters into vehicle models and subsequent simulation of open-loop handling maneuvers. Consequently, that allows a comparison of vehicle responses from effectively performed maneuvers and simulated ones.

Focusing back onto the observer concepts, it is the extension of the latter by peripheral modules that handle their activation and also provide feedback of the actual parameter estimation quality to the driver. This allows for time-optimal termination of the maneuvers performed during parameter identification. The ideal¹ source models recently assumed will now be replaced by the output of a professional vehicle dynamics simulation

¹In the sense that parasitic dynamics are not existent, i.e. the system dynamics of the plant and observer replica are identical. Moreover, under ideal conditions the signals are not affected by measurement noise.

software package, i.e. IPG² CarMaker[®]. Feeding the proposed observer concepts with that data does not only result in parameter estimates, but also reveals the capability of the simple models to represent the real-world behavior of the vehicle. Furthermore, robustness to measurement noise, system excitation as well as effects due to parasitic dynamics will be discussed. The aforementioned, identified vehicle parameters are supplied to a generic vehicle model that serves as basis for the offline simulation of the standardized open-loop maneuvers, as presented in Section 1.2.2. The obtained results will then be compared with the identical maneuvers, but performed by the more complex multi-body vehicle model of IPG CarMaker[®]. By doing so, the potential of the overall mechanism to replace the real handling maneuver execution by the simulations-based method is analyzed.

Furthermore, the integration of human perception models (Section 2.6) allows extraction of "sensed" objective metrics and comparison of the measured vehicle responses and those that the human being senses. The resulting broad database of objective metrics can be further used for the generation of a generic (subjective) rating. However, the scope of the thesis ends after the extraction of the objective metrics and any correlations between these and subjective ratings remain an open issue.

5.1 Implementation of the Parameter Identification Concepts: Peripherals

For the convergence of the parameter estimation errors generally a required assumption is persistent excitation of the system, e.g. [LJU99]. Clearly, for the simulations in Chapter 4 the system excitations (and simulation start and end points in time) are selected such that this holds. However, under real driving conditions it needs to be ensured, that the parameter identification algorithms are only activated if the vehicle is excited sufficiently³. The employed activation algorithms are based on certain thresholds of representative measurements and also calculations, e.g. signal amplitude and frequency. Figure 5.1 illustrates the observer-based parameter identification module, in this case an Extended Kalman Filter, and its peripherals. For the given example of the roll dynamics, the aforementioned activation is based on the steering angle δ_h , its time derivative $\omega_h := \frac{d\delta_h}{dt}$ and the longitudinal velocity ${}_v v_x$. Furthermore, the excitation frequency is determined internally as the roll model parameter identification is expected to be performed during a sinusoidal steering maneuver. The situation changes slightly for the variable structure-based concepts as there the robust state estimation does not need any explicit (de-)activation. Theoretically, it is not even required for the finite time parameter estimation algorithm as its trajectories do not diverge in the case of

²For details consider www.ipg.de.

³Even though the term *sufficiently* is quite vague, it is difficult to provide exact information on the activation of the parameter identification. In practice, thresholds related to certain vehicle in- and outputs will be adjusted based on some expertise and trial and error runs.

stopped system excitation [MG11]. However, in practice the parameter estimation lags the system excitation by a conservative amount of time in order to ensure convergence of the state estimation errors.

The second peripheral structure added to each observation concept is the so-called quality evaluation module. It feeds back the actual difference between an open-loop model estimate⁴ and the measurement. It allows the driver to decide on termination of the current parameter identification run. This results in a high efficiency with respect to maneuver duration and consequently time on the test track.

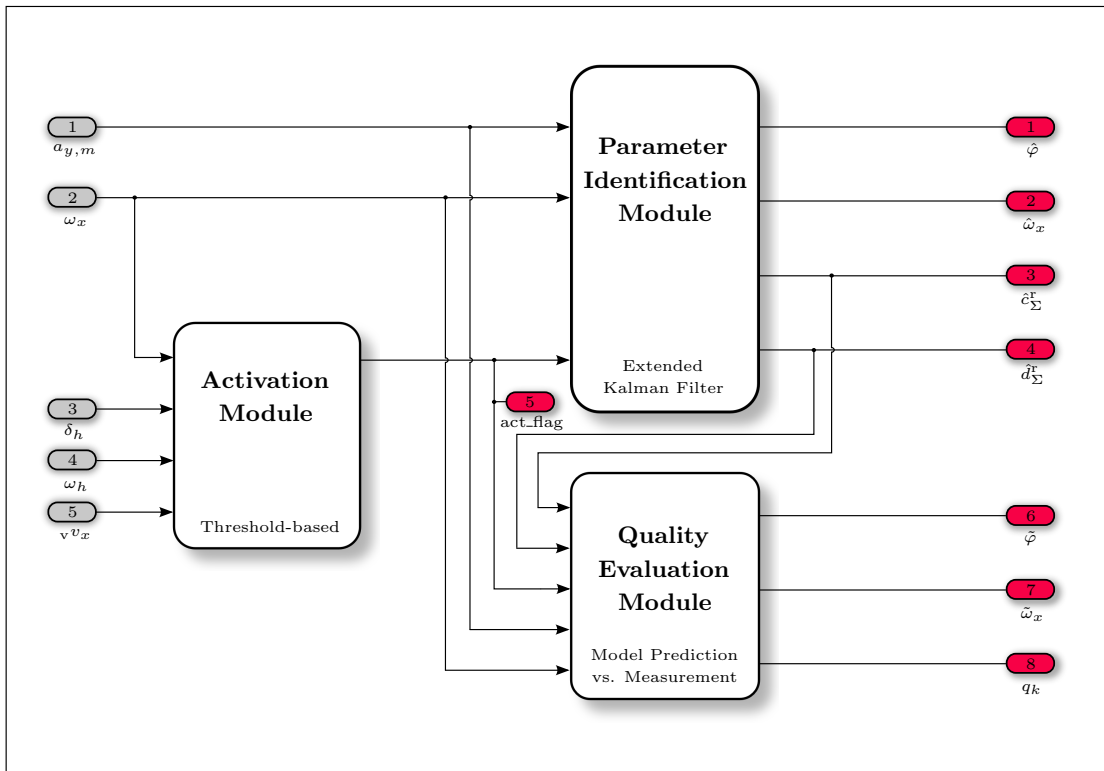


Figure 5.1: Observer peripherals - (de-)activation and estimation quality modules.

For the example of the roll dynamics the estimates $\tilde{\varphi}$, $\tilde{\omega}_x$ are obtained from the adaptive roll angle observer in (4.113), but setting the correction gains l_1 and l_2 to zero. Defining a discrete-time estimation error \tilde{e}_k , i.e. $\tilde{e}_k := \omega_{x,k} - \tilde{\omega}_{x,k}$, with $e_k = e(k\tau_s)$, τ_s being the sampling time and $k \in \mathbb{N}_0$, calculation of an absolute sum over a user-defined time

⁴This refers to a time-varying system that takes into account the parameter estimates of the observer concepts, but uses no measurement information for (observer-like) corrections.

window of length N_w can be conducted, i.e.

$$\tilde{e}_{tot,k} = \sum_{i=k-N_w+1}^k |\tilde{e}_i|. \quad (5.1)$$

The resulting value of $\tilde{e}_{tot,k}$ is then mapped into a representative quantity that allows the driver to continue or stop the maneuver. Denoted by the variable q_k the mapping is defined as

$$q_k = \begin{cases} 1 & \tilde{e}_{tot,k} < g_1, \\ i & g_{i-1} \leq \tilde{e}_{tot,k} < g_i \\ 5 & \text{else.} \end{cases} \quad \text{with } i = 2, 3, 4, \quad (5.2)$$

Therein g_1 to g_4 are user-defined thresholds for the determination of the actual estimation quality. Results of the concept will be demonstrated within the evaluation part of the roll model parameter identification techniques, see Section 5.2.4.

5.2 Observer-based Vehicle Parameter Identification

5.2.1 Source Model

The multi-body vehicle dynamics simulation software package IPG CarMaker[®] is used to generate the reference data. In general, the embedded 17-DoF vehicle model allows accurate simulation of realistic vehicle behavior and is highly flexible with respect to vehicle configurations, i.e. suspension setup, chassis type and geometry, engine type and performance, vehicle tires, vehicle load etc. Due to a sophisticated driver model that is part of the software package the simulation of highly dynamical driving maneuvers is also feasible. Details of the virtual vehicle used for the evaluation work are provided within Appendix D.

In order to render the scenarios (parameter identification and handling evaluation) more realistic the simulation outputs of the source model, i.e. IPG CarMaker[®], are artificially augmented with measurement noise. The statistical characteristics of the (assumed) Gaussian noise is also given in Appendix D and based on real vehicle measurements.

A Comment on the Availability of Steering System Measurements An essential number of evaluated concepts uses measurements of the steering system as input. A common modelling approach transforms the steering wheel angle δ_h to the wheel angle δ_w by a static transmission ratio, see (2.69). In fact, elasticities of the steering system and acting lateral tire forces perturb the wheel angle dynamically. For the purpose of simulation-based evaluation the wheel angle is available as a measurement and is used as such. In contrast, the in-vehicle evaluation requires the use of (2.69) as the wheel

angle can neither be measured, nor the influence of the lateral forces estimated as the steering stiffness is commonly not known. Further details will be provided in Chapter 6 and Appendix D.

The reference data obtained from IPG CarMaker[®] is not only used for the validation of the observation concepts, but also to compare effectively performed standardized handling maneuvers and simulated ones. The latter also takes into account the identified vehicle parameters.

5.2.2 Timeline of the Module Execution

Even though the observer concepts are designed and implemented as stand-alone modules the order of execution is significant. Figure 5.2 sketches the flow chart of the module execution process. Starting with the identification of static vehicle parameters, see Chapter 3 for details, the proving ground needs to be evaluated for suitability first. That is required due to the modelling assumptions of the chassis roll and pitch motions, i.e. the ground must not be affected by an inclination and/or bank angle different from zero. Consequently, the proposed mechanisms of Section 4.2.6 are the first to be employed.

Assuming an adequate test track the model parameters of the chassis roll and pitch motions are identified by the corresponding observation concepts, see Sections 4.2.2 and 4.2.3. Knowledge of the effective stiffness and damping parameters allows the estimation of the roll and pitch angles and consequently compensation of their effects on the longitudinal and lateral accelerations⁵. In the following, the nonlinear characteristics of the lateral tire force vs. slip angle are to be identified employing the concepts proposed in Section 4.2.1. These identified model parameters characterize the actual vehicle configuration such that the handling evaluation can be conducted by simulations, rather than real execution⁶ of the maneuvers.

From the flow chart in Figure 5.2 it can also be extracted that some observation concepts presented in Chapter 4, i.e. steering dynamics (Section 4.2.4) and longitudinal dynamics (Section 4.2.5) are not directly necessary for the handling evaluation work. Their objectives and scopes will be discussed within the validation analysis.

Some Comments on the Notation In Chapter 2 the time derivatives of the roll, pitch and yaw angles have been introduced as $\dot{\varphi}$, $\dot{\theta}$ and $\dot{\psi}$ respectively, see (2.11). In the course of the simulation-based evaluation these values are also estimated by observation mechanisms. As the readability of estimated values, e.g. $\hat{\varphi}$, is sub-optimal the notation of angular velocities and accelerations is changed from e.g. $\dot{\psi}$ to ω_z , see (2.11), and $\ddot{\psi}$ to $\dot{\omega}_z$ respectively. This affects only Chapter 5.

⁵Measured in the vehicle-fixed axis system \mathcal{C}_v .

⁶Herein, the term "real execution" refers to the simulation of the corresponding maneuver with IPG CarMaker[®] software.

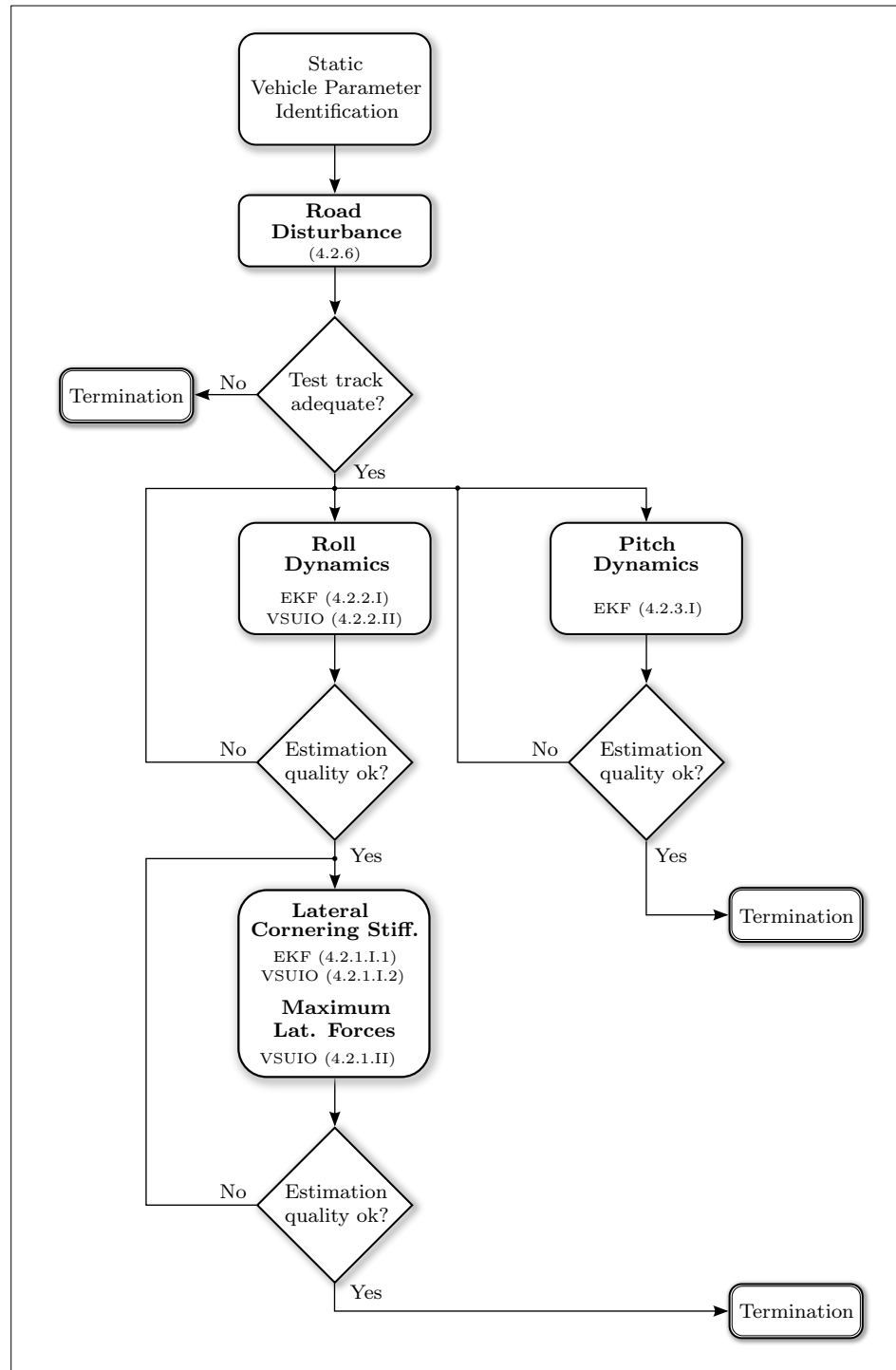


Figure 5.2: Flow chart of the vehicle model parameter identification process.

5.2.3 Lateral Dynamics

The proposed parameter identification techniques, see Section 4.2.1, aim to identify the model parameters of a nonlinear tire force model, i.e. (2.28) or (2.29). In the following the focus is put on the model TM_Simple, but the outcomes can easily be transferred to SMF tire model, e.g. [TRH14a]. The overall parameter identification process is separated into two individual problems, i.e. identification of the maximum lateral tire forces (Section 4.2.1.II) and tire cornering stiffness (Section 4.2.1.I). As a consequence, the design of experiments needs to ensure vehicle operation in the gray shaded areas of Figure 5.3. In fact, to identify the lateral cornering stiffness of the front and rear tires (or equivalently axles due to the use of the single-track model) the steering input needs to be low, such that the *proportional range* is not left. Herein, the maneuver is selected to be sinusoidal, rather than constant⁷ (*Maneuver I*).

From the estimation of the lateral tire forces it is possible to extract information on its maximum value. Hence, the vehicle needs to be operated within the slip-force range denoted by *Maneuver II* in Figure 5.3. Once the driver "feels" the loss of adhesion the maneuver can be terminated. In order to increase the robustness of the estimates to human variability ideally the maneuver is repeated several times allowing to average the individual results. However, there is no information available, whether the identified maximum represents the real one. In other words, there is some clear dependency on the maneuver execution and the quality of the estimates.

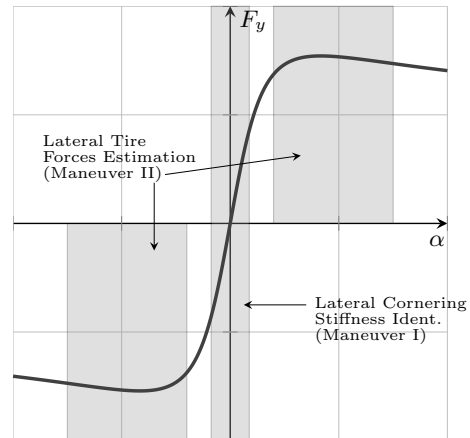


Figure 5.3: Suggested vehicle operational areas for the parameter identification of lateral tire slip-force characteristics.

Lateral Cornering Stiffness

In Section 4.2.1.I two different concepts have been proposed to estimate the lateral cornering stiffness values of the front and the rear tires. This redundancy increases the robustness of the parameter estimation process due to the diverse observer design paradigms. Under the assumption that both algorithms provide feasible estimates a scalar value for the front and lateral cornering stiffnesses can be obtained by averaging the results of both sources.

In general, the EKF estimates the front and rear cornering stiffness values $c_{\alpha_{fe}}$ and c_{α_r} simultaneously. However, due to its modelling basis, i.e. system Σ_{L1} (3.20), it takes into account any unmodelled dynamics of the steering system. In contrast, the VSUIO

⁷This is a necessary assumption of the VSUIO design process, see Section 4.2.1.I.2 for details.

Parameter	Description	Value	Unit
$\bar{c}_{\alpha_{fe}}$	Nominal (effective) front cornering stiffness	50000	N·rad ⁻¹
\bar{c}_{α_r}	Nominal rear cornering stiffness	70000	N·rad ⁻¹
$\hat{\mathbf{x}}_{a,0}^+$	Initial (augmented) state vector (EKF)	$[-0.087 \ 0 \ 7e4 \ 7e4]^T$	-
\mathbf{P}_0^+	Initial error covariance matrix (EKF)	diag([1 1 1e4 1e4])	-
r	Covariance of the meas. noise (EKF)	2.6e-7	-
$\bar{\mathbf{Q}}$	Covariance of the process noise (EKF)	diag([1e-9 1e-9 5e1 5e1])	-
$\tilde{\mathbf{x}}_0$	Initial state vector (VSUIO)	$[0 \ 1e4]^T$	-
μ_1	Gain nonlinear error corr. term (VSUIO), see (4.67)	1e2	-
μ_2	Gain linear error corr. term (VSUIO), see (4.67)	1e4	-
α_1	Parameter estimator gain (VSUIO), see (4.66)	0.015	-
α_2	Parameter estimator gain (VSUIO), see (4.66)	5e3	-

Table 5.1: Parameters of the EKF and VSUIO for the simulation-based concept evaluation.

concept, based on Σ_{L4} , does not require the information of the steering angle (at least for the estimation of the rear cornering stiffness), but uses lateral acceleration as system input. For the estimation of the front stiffness the situation becomes identical to the EKF. From the previous findings it is obvious that the employment of the VSUIO concept requires two individual instances as the uncertainty structure varies between front and rear axle.

The observer parameters used for their evaluation are summarized in Table 4.3. In terms of parameter tuning the front and rear instances are identical. The tuning efforts of the EKF concept, i.e. adjusting the elements of the matrix \mathbf{Q} are significantly higher than those of the sliding mode observers⁸. There exist well-known tuning rules that allow a systematic adjustment of the observer gains. In contrast, for the EKF it is an iterative process that includes the adjustment of the parameters and evaluation in simulations. Figure 5.4 shows the evaluation results of the EKF concept. The *a priori* estimate corrections (by yaw rate measurements) are performed throughout the complete experiment. Availability of the yaw rate ω_z as a measurement becomes obvious in Figure 5.4(a) and (b) as the estimation error is almost zero right from the beginning of the experiment. The vehicle sideslip angle β is estimated and from (c) and (d) the influence of the parameter estimates on its prediction can be concluded. Figure (e) shows the estimates of front and rear cornering stiffness values $\hat{c}_{\alpha_{fe}}$, \hat{c}_{α_r} .

⁸The EKF inherently takes into account the (measurement) noise characteristics. Hence, any changes of those noise statistics result in a necessary re-tuning of the filter parameters. This is not the case for the sliding mode concepts as the tuning is independent of the noise.

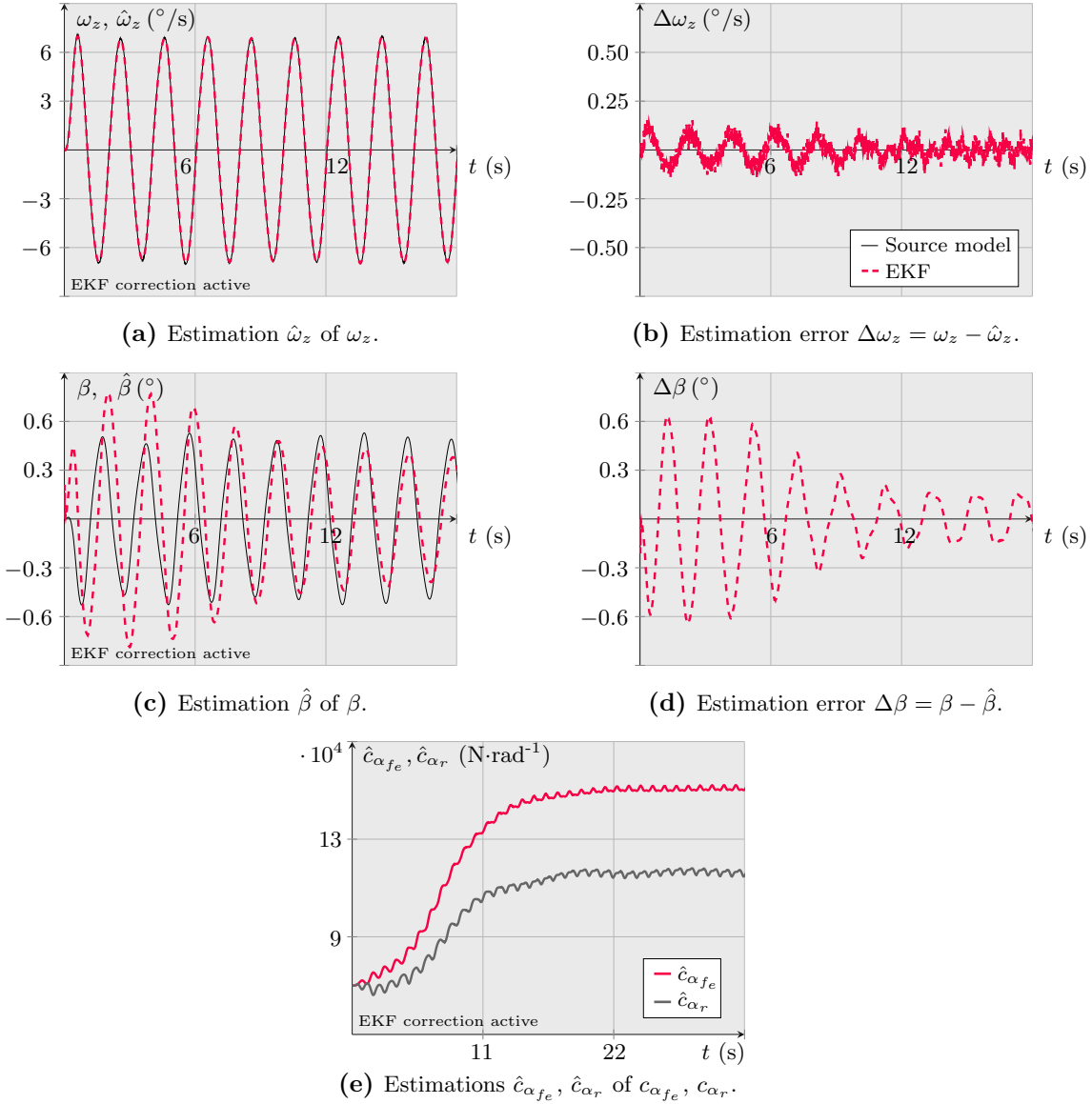


Figure 5.4: Simulation-based estimation results of the (effective) front and rear lateral cornering stiffnesses, $c_{\alpha_{fe}}$, c_{α_r} and vehicle states ω_z , β using the EKF concept. Maneuver: sinusoidal steering with $\delta_h = \pm 20^{\circ}$, $f_{ex} = 0.5\text{Hz}$, $v_x = 80 \pm 2\text{km}\cdot\text{h}^{-1}$. Correcting the *a priori* estimates of the EKF by the measured yaw rate ω_z is activated right from the beginning of the experiment. The decrease of the estimation error w.r.t. vehicle sideslip angle β due to the variation of the stiffness parameters can be seen in (d).

Conversion of the time series into scalar parameters is conducted by taking average values of the estimates between $t \approx 22\text{s}$ and $t \approx 33\text{s}$.

Simulation-based evaluation results obtained from the alternative observer concept VSUIO are depicted in Figure 5.5.

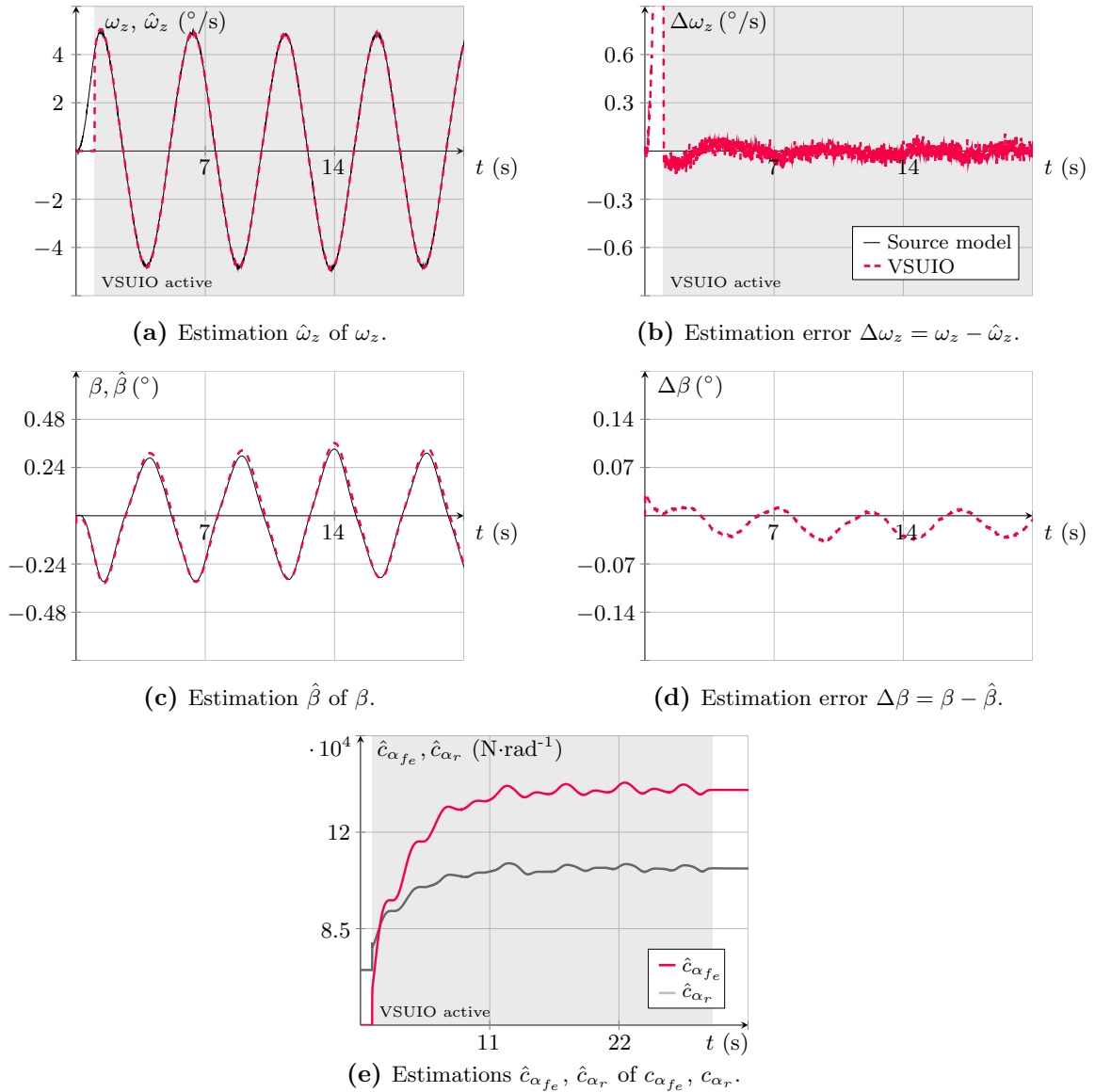


Figure 5.5: Simulation-based estimation results of the VSUIO concept related to the (effective) lateral cornering stiffness identification. Maneuver: sinusoidal steering with $\delta_h \pm 15^\circ$, $f_{ex} = 0.2\text{Hz}$, $v_x = 80 \pm 2\text{km}\cdot\text{h}^{-1}$.

The subplots (a) and (b) show the measured yaw rate ω_z and also its estimate $\hat{\omega}_z$ of VSUIO. Any results of the front VSUIO are omitted as no additional information can be extracted therefrom apart from the estimated cornering stiffness values. Moreover, these plots illustrate the times when the activation of the parameter identification module (Figure 5.1) is active (gray areas). For that experiment, the start of the parameter estimation is delayed intentionally, in order to demonstrate the fast parameter convergence. During the simulation runs it was found that the activation time of VSUIO is not

critical for the obtained results. So is its deactivation, as the system trajectories do not diverge even in the case of a non-excited system [MG11]. Scalar parameter extraction is again performed by averaging the estimation signals between $t \approx 15$ s and $t \approx 30$ s. Table 5.2 lists the obtained values of identified cornering stiffnesses.

Parameter	Concept	Value	Unit
$[\hat{c}_{\alpha_{fe}} \ \hat{c}_{\alpha_r}]$	EKF	[151180 116670]	N·rad ⁻¹
$[\hat{c}_{\alpha_{fe}} \ \hat{c}_{\alpha_r}]$	VSUIO	[135320 106910]	N·rad ⁻¹

Table 5.2: Identified cornering stiffness values of the concepts EKF and VSUIO.

Lateral Tire Forces

The maximum arising front and rear lateral tire forces need to be estimated to allow identification of the tire model parameters D_f and D_r . Theoretically, the observer can be implemented as specified in (4.73). However, the in-vehicle measurement of the lateral acceleration is affected by the arising chassis roll motion, i.e. roll angle $\varphi \neq 0$ (2.43). Assuming a flat test track ensures that the lateral acceleration measurement is only affected by the chassis' roll angle and that can be easily compensated for. According to Figure 5.2 the roll model parameters are already identified at the stage of lateral tire forces estimation. Hence, the results of the ARAO concept (4.113) can be exploited to obtain corrected measurement values of lateral acceleration.

Parameter	Description	Value	Unit
$\hat{\mathbf{x}}_0$	Initial state vector (VSUIO)	0.35	rad·s ⁻¹
ν_0	Initial condition of ν (VSUIO)	2	rad·s ⁻²
λ_1	Observer gain factor (VSUIO), see (4.73a)	5.81	-
λ_2	Observer gain factor (VSUIO), see (4.73b)	16.5	-
c_{Σ}^R	Effective roll stiffness (ARAO)	65640	N·m·rad ⁻¹
d_{Σ}^R	Effective roll damping (ARAO)	5194	N·m·s·rad ⁻¹
$[l_1 \ l_2]^T$	Observer gain vector (ARAO), see (4.113)	$[-10.25 \ 47.22]^T$	-

Table 5.3: Parameters of the VSUIO concept for the simulation-based observer validation of lateral tire force estimation.

Table 5.3 lists the observer parameters of both the VSUIO and ARAO concepts. The vehicle excitation needs to be designed such that the range of operation (in terms of slip-force characteristics) is within the specified area of Figure 5.3 (Maneuver II). Herein, the steering signal is chosen to be of type slow step input that drives the vehicle to its limits of adhesion (in the lateral dynamics sense). Alternatively, the vehicle could also be excited sinusoidally. However, due to the high input transients the dynamic build-up of the lateral tire forces gains more influence on the results compared to the slowly-growing

Parameter	Value	Unit
$\max(\hat{F}_{y,f})$	6355	N
$\max(\hat{F}_{y,r})$	4736	N

Table 5.4: Identified maximum lateral tire forces using the VSUIO technique.

forces of the moderate step input. The vehicle responses to the driver's input are depicted in Figure 5.6. It also shows the estimated values, i.e. yaw rate ω_z and rear lateral tire force ${}_{\vee}F_{y,r}$ of the VSUIO concept. Note, that from the recovery of the unknown input, see (4.77), an estimate ${}_{\vee}\hat{F}_{y,r}$ can be obtained, see Figure 5.6(d). Moreover, from (2.14b), the front lateral tire force ${}_{\vee}\hat{F}_{y,f}$ can be recovered, see (c). Calculation of the actual maximum value is kept simple, i.e. if the actual value exceeds the actual maximum set it as new maximum, otherwise drop it. Results are plotted in (c) and (d). The reference values of the lateral tire force maxima are extracted from the source model force measurements.

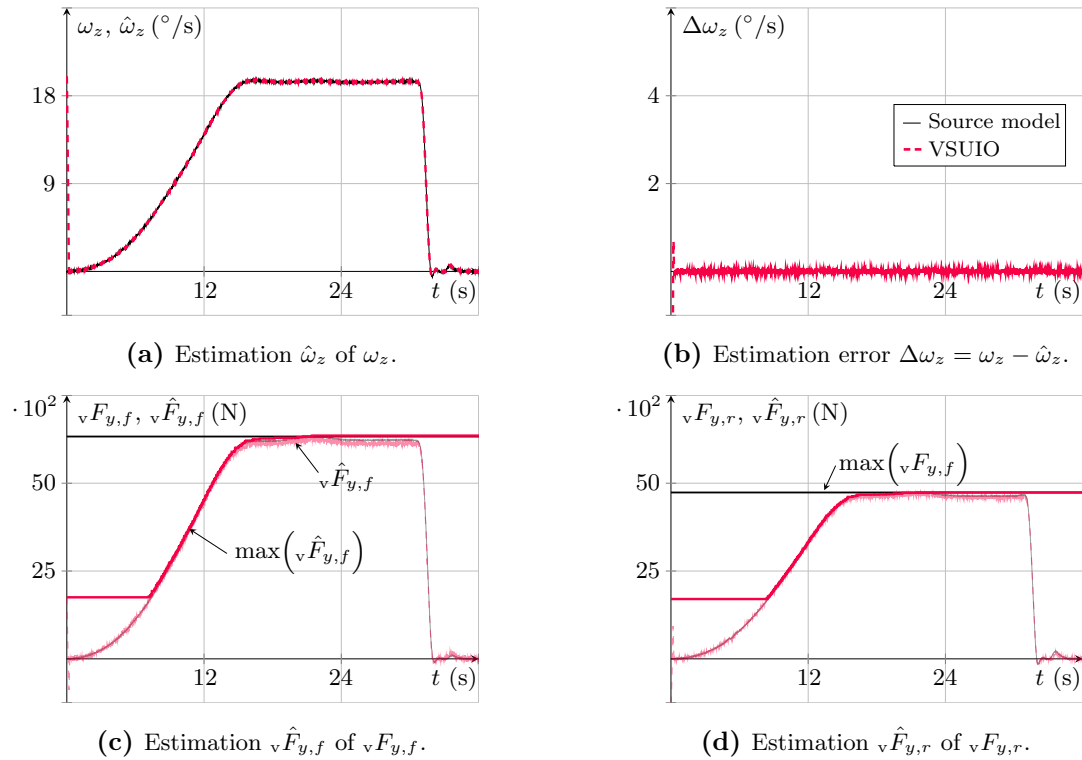


Figure 5.6: Simulation-based estimation results of the lateral tire forces estimation (VSUIO). Maneuver: slow steer step with $\delta_{h,\max} = 120^\circ$, $\omega_h \approx 4^\circ/\text{s}$, ${}_{\vee}v_x = 80 \pm 3\text{km}\cdot\text{h}^{-1}$. The recovered tire forces of the front and rear axles are depicted in (c) and (d). The red curves show the actual estimates of the maxima.

Tire Force Model Parameter Recovery

The objective is to identify the model parameters B , C and D of the TM_Simple model, see (2.29), from the estimated characteristic points of the slip-force curves. For the coherence between model parameters and those points the reader is referred to (2.30). Clearly, the equation system is under-determined and the parameters can not be recovered uniquely. Therefore, an assumption on the value of B has to be made. The latter is responsible for characterizing the degressive part of the curve, i.e. for high slip angles. In view of the given application, vehicle operation at such high slip angles is only of minor interest. Therefore, the idea is to set parameter B to some value, such that the tire forces decrease slightly once the maximum point has been reached. From (2.30b) it is obvious that the ratio between $F_{y_{max}}$ and $F_{y_{\infty}}$ governs parameter B . Simulations have shown that adjusting the end value $F_{y_{\infty}}$ to approx. 90% of the maximum results in a slightly degressive slip-force curve and allows identification of the two remaining parameters⁹. Consequently, from (2.30a) and the estimated $\max(\sqrt{v}\hat{F}_y)$ parameter D follows. Subsequently, merging (2.30c) and the cornering stiffness estimate \hat{c}_{α} results in parameter C . By executing this method for the front and rear parameters an analytic description of the slip-force characteristics is obtained. Figure 5.7 compares the real and estimated curves of the front and rear tires. Moreover, the identified tire model parameters are listed in Table 5.5.

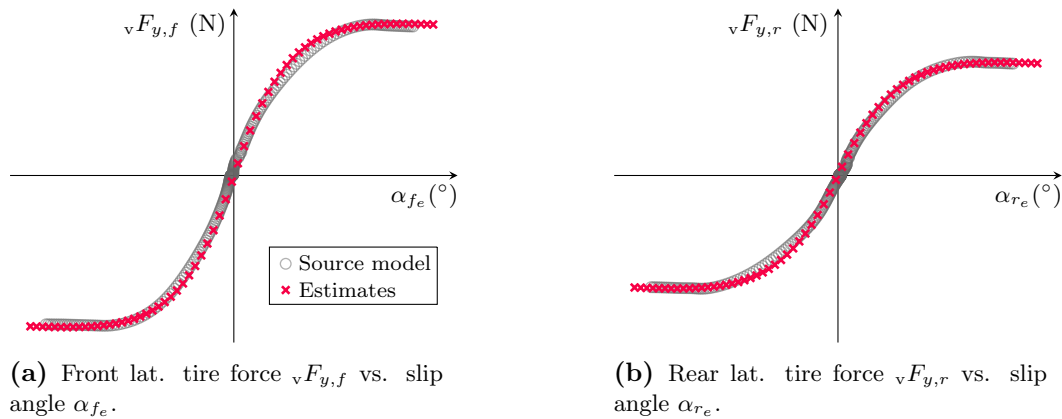


Figure 5.7: Comparison of the real and estimated lateral slip-force characteristic curves.

\hat{D}_f (N)	\hat{B}_f (-)	\hat{C}_f (rad)	\hat{D}_r (N)	\hat{B}_r (-)	\hat{C}_r (rad)
6355	1.888	$8.38 \cdot 10^{-2}$	4736	1.974	$8.36 \cdot 10^{-2}$

Table 5.5: Identified model parameters of front and rear lateral tire force models.

⁹Furthermore, it has shown that this setup places the maximum tire force w.r.t. slip angle within the first third of the expected lateral slip range.

5.2.4 Roll Dynamics

Similarly as presented for the estimation of the lateral cornering stiffness also the parameters of the roll model are determined by two completely independent structures. The first is implemented as an Extended Kalman Filter (Section 4.2.2.I) and based on state augmentation (Section 4.1.1), whereas the second uses the unknown input reconstruction technique (Section 4.1.2) and higher-order sliding mode observers (Section 4.2.2.II). Both concepts are used for the identification of the roll model-related effective stiffness c_{Σ}^r and damping d_{Σ}^r .

The vehicle excitation signal is selected in accordance with the roll dynamics-related frequency range of interest, i.e. $f_{ex} \approx 0.2 - 3.0\text{Hz}$ [KOB03]. Theoretically, the vehicle should be excited at constant, approximately equidistant, operating points (in terms of frequency) and once steady-state conditions have been reached the measurements/identification need to be performed. Then, this procedure can be repeated for the next operating point. The steering angle amplitude is to be held constant during the complete process. However, in practice this time-consuming maneuver is often replaced by a sinusoidal chirp function with steadily increasing frequency. Herein, the time-specific constraints are not relevant (especially under consideration of the simulation-based evaluation). Therefore, the first approach, i.e. exciting the vehicle with constant input frequencies and changing the latter step-wise within the interesting frequency range, is chosen. More specifically, the roll dynamics are excited with frequencies of 0.1, 0.2, 0.5, 1.0, 1.5 and 2.0Hz. To this extent it is assumed that higher input frequencies are realistic only during test bench-based evaluation of the roll dynamics rather than real road-driving.

Table 4.6 lists the implemented parameters of the observation concepts. With regards to the Extended Kalman filter setup the diagonal elements of the process noise matrix $\bar{\mathbf{Q}}$ require the highest tuning efforts, as these are adjusted during iterative simulation runs until the estimation error convergence shows satisfactory behavior. In contrast to the unknown process noise characteristics, the measurement noise can be determined from stationary measurements (Appendix D). Even though theoretically the parameter tuning of the VSUIO is straightforward due to the involvement of four different submodules a certain process order needs to be followed. Starting with the adjustment of the RED gains it is inevitable to get good estimates of the derivative of the input signal w.r.t. time. Inherently, the differentiating concept amplifies high-frequency terms such as measurement noise on the input signal. Consequently, the time-derivative estimates are low-pass filtered¹⁰. Once these are found the adaptive gain algorithm of ARSE needs to be supplied with a number of parameters, see (4.103), avoiding the often

¹⁰In [LEV98] the *a posteriori* low-pass filtering is suggested and therein it is shown that there is still a benefit in terms of derivative estimation accuracy compared to standard differentiating low-pass filter structures.

Parameter	Description	Value	Unit
\bar{a}_{21}	Nom. roll model param. (scaled stiffness)	55.6	$\text{rad}^{-1} \cdot \text{s}^{-2}$
\bar{a}_{22}	Nom. roll model param. (scaled damping)	2.78	$\text{rad}^{-1} \cdot \text{s}^{-1}$
$\hat{\mathbf{x}}_{a,0}^+$	Initial (augmented) state vector (EKF)	$[0.04 \ -0.1 \ -\bar{a}_{21} \ -\bar{a}_{22}]^T$	-
\mathbf{P}_0^+	Initial error covariance matrix (EKF)	$\text{diag}([1\text{e-}5 \ 1\text{e-}5 \ 1\text{e-}3 \ 1\text{e-}3])$	-
r	Covariance of the meas. noise (EKF)	$2.93\text{e-}7$	-
$\bar{\mathbf{Q}}$	Covariance of the process noise (EKF)	$\text{diag}([1\text{e-}10 \ 1\text{e-}10 \ 1\text{e-}4 \ 1\text{e-}5])$	-
κ_1	RED gain 1, see (4.93a)	23.1	-
κ_2	RED gain 2, see (4.93b)	260.6	-
f_c	Low-pass filter (RED) cut-off frequency	20	Hz
n_{lpf}	Filter order low-pass filter (RED)	3	-
κ	Observer adaptive gain (ARSE), see (4.103a)	200	-
μ	Detector width (ARSE), see (4.103a)	$1.5\text{e-}4$	-
$\tilde{\lambda}^-$	Lower bound of adaptive gain $\tilde{\lambda}_1$, see (4.103a)	6.71	-
$\tilde{\lambda}_{1,0}$	Initial value of the adaptive gain $\tilde{\lambda}_1$	8.05	-
η	Small gain to push $\tilde{\lambda}_1$ above $\tilde{\lambda}^-$	$1\text{e-}2$	-
ε	Gain factor $\tilde{\lambda}_2$	1.64	-
$\hat{\mathbf{x}}_0$	Initial state vector (RSE)	$[0.04 \ -0.1]^T$	-
μ_1	Gain nonlinear error correction term (FTPE), see (4.112)	5	-
μ_2	Gain linear error correction term (FTPE), see (4.112)	3	-
α_1	Parameter estimator gain (FTPE)	3	-
α_2	Parameter estimator gain (FTPE)	10	-
$[l_1 \ l_2]^T$	Observer gain vector (ARAO), see (4.113)	$[-10.25 \ 47.22]^T$	-

Table 5.6: Parameters of the EKF and VSUIO (RED, ARSE, FTPE, ARAO) concepts for the simulation-based observer validation of roll dynamics-related state and parameter estimation.

assumed knowledge of the uncertain input term bounds¹¹. For the finite time parameter estimation (FTPE) algorithm a weighting of the linear and nonlinear terms needs to be determined allowing a fast convergence with low estimation fluctuations once the system is in steady-state. Finally, the adaptive roll dynamics observer (ARAO) requires the specification of error dynamics eigenvalues. As the system parameters vary during the identification, these are set up for the nominal case. Obviously, this affects the error convergence dynamics, but updating the Luenberger gains within every time step is assumed unnecessary.

Evaluation of the observer concepts is performed graphically for the case of an excitation frequency of $f_{ex} = 1.0\text{Hz}$. Figure 5.8 compares the reference signals and estimates.

¹¹Inspecting the definition of the unknown input, see (4.89), and the change of input excitation frequency, it appears even more feasible to use an adaptive gain scheme.

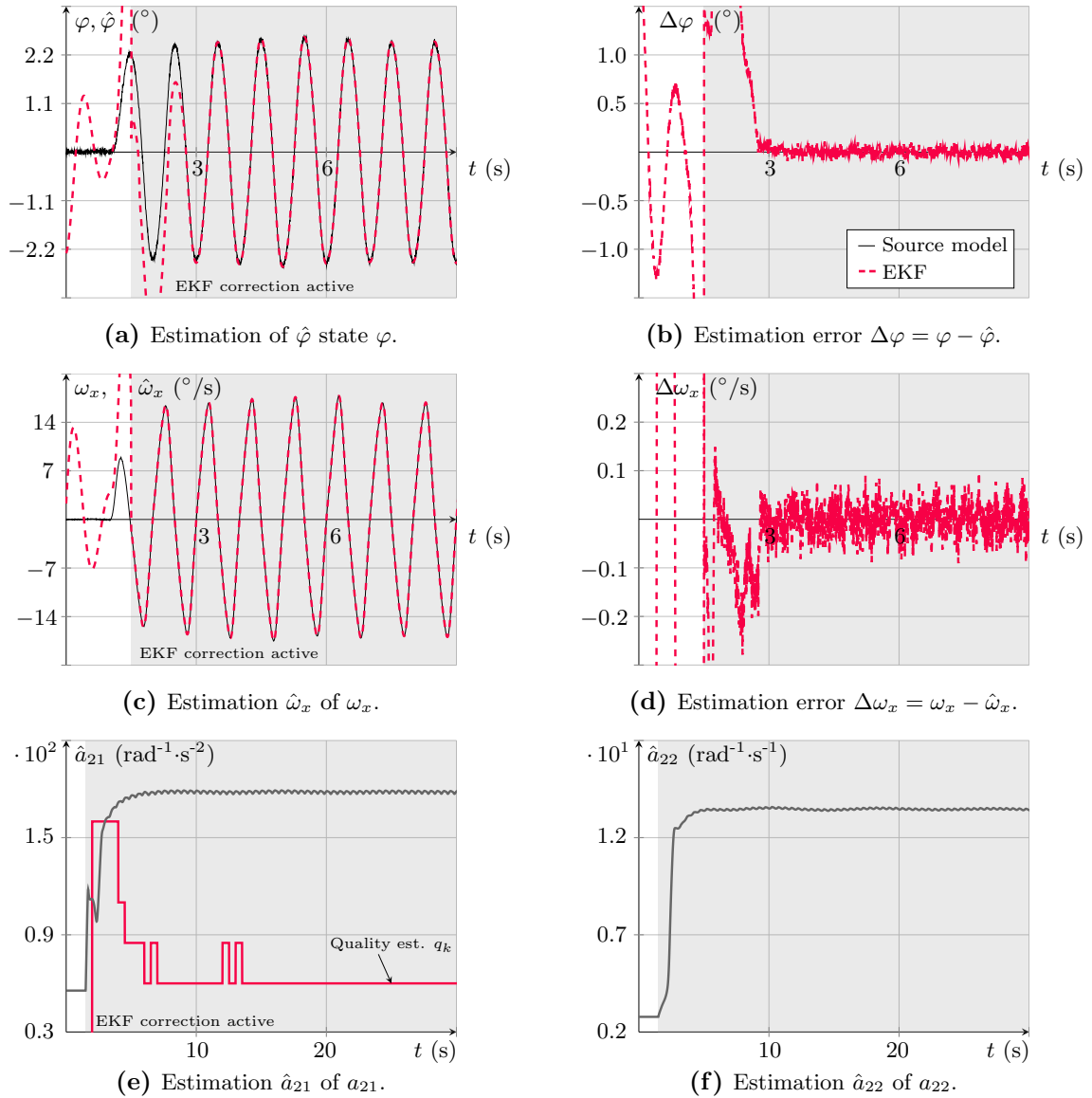


Figure 5.8: Simulation-based estimation results of the parameters a_{21} and a_{22} as well as states (roll angle φ and velocity ω_x) using the EKF concept. Maneuver: sinusoidal steering with $\delta_h = \pm 45^\circ$, $f_{ex} = 1.0\text{Hz}$, $v_{vx} = 80 \pm 2\text{km}\cdot\text{h}^{-1}$. Correction of the *a priori* estimates by the measured roll velocity ω_x is indicated by the gray boxes in (a)-(f).

The gray boxes indicate the (threshold-based) activation of the EKF correction mechanism by measurements. Furthermore, from Figure 5.8(e) and (f) it can be concluded that the estimation values converge after a time $t \approx 10\text{s}$ such that the experiment could be terminated after that time. This is further backed up by consideration of the estimation quality signal illustrated in (e). It provides the driver with the information of the actual estimation performance and allows to decide on the time of maneuver termination.

The evaluation results of the VSUIO concept, see Figure 5.9, require comprehensive analysis as more individual concepts are involved in the observation process. In the subplots (a) and (b) the measured lateral acceleration and lateral jerk are depicted. Furthermore, it shows the estimates of the RED mechanism. Due to the artificial increase of the systems relative degree it is not the roll angle φ and rate ω_x that are estimated, but the roll rate and the acceleration α_x . State estimation results and errors are plotted in (c)-(f). Furthermore, (d) shows the time-varying character of the observer gain $\tilde{\lambda}_1$. The gray dotted lines in (e) and (f) show the results of FTPE and also reveal the influence of the parameter estimates, see (g) and (h), on the estimation error of α_x . In terms of maneuver termination convergence of the parameter estimates is given after time $t \approx 20$ s. Even if that appears to be slower than the EKF concept a comparison is rather difficult due to completely different observer tunings.

For the estimation of the chassis roll angle φ the identified parameters of the roll model are supplied to the adaptive roll angle observer (ARAO). Its recovery of the roll angle is illustrated in Figure 5.10. Again, the gray boxes indicate the activation of FTPE, i.e. estimation of roll model parameters.

Both concepts show good estimation performances for the operating point of $f_{ex} = 1.0$ Hz. Now, the consistency of the obtained results over the complete range of excitation frequency, i.e. $f_{ex} = 0.1 - 2.0$ Hz shall be determined. Therefore, both concepts are supplied with the specific lateral acceleration signals and results in terms of identified parameters obtained. Figures 5.11(a) and (b) show the estimated roll model parameters c_{Σ}^r , d_{Σ}^r vs. excitation frequency f_{ex} . Actually, the positive aspect of the experiments is consistent results of EKF and VSUIO over the complete range of frequencies. More interestingly, the parameters are not constant, but affected by the excitation frequency. An interpretation of the decreasing stiffness and increasing damping is based on the characteristics of the underlying vehicle suspension. As discussed in Appendix D the damping elements show nonlinear characteristics between damping forces and velocity. Without any doubts also the effects of unmodelled dynamics (that arise due to the numerous simplifications of the roll model in Section 2.3.1) are lumped into the model parameters. For the generic vehicle handling evaluation a weighted average¹² is calculated.

¹²The weighting of the results is performed such, that those results of the excitation frequencies do have a higher impact on the overall result, that are neither the highest nor the lowest.

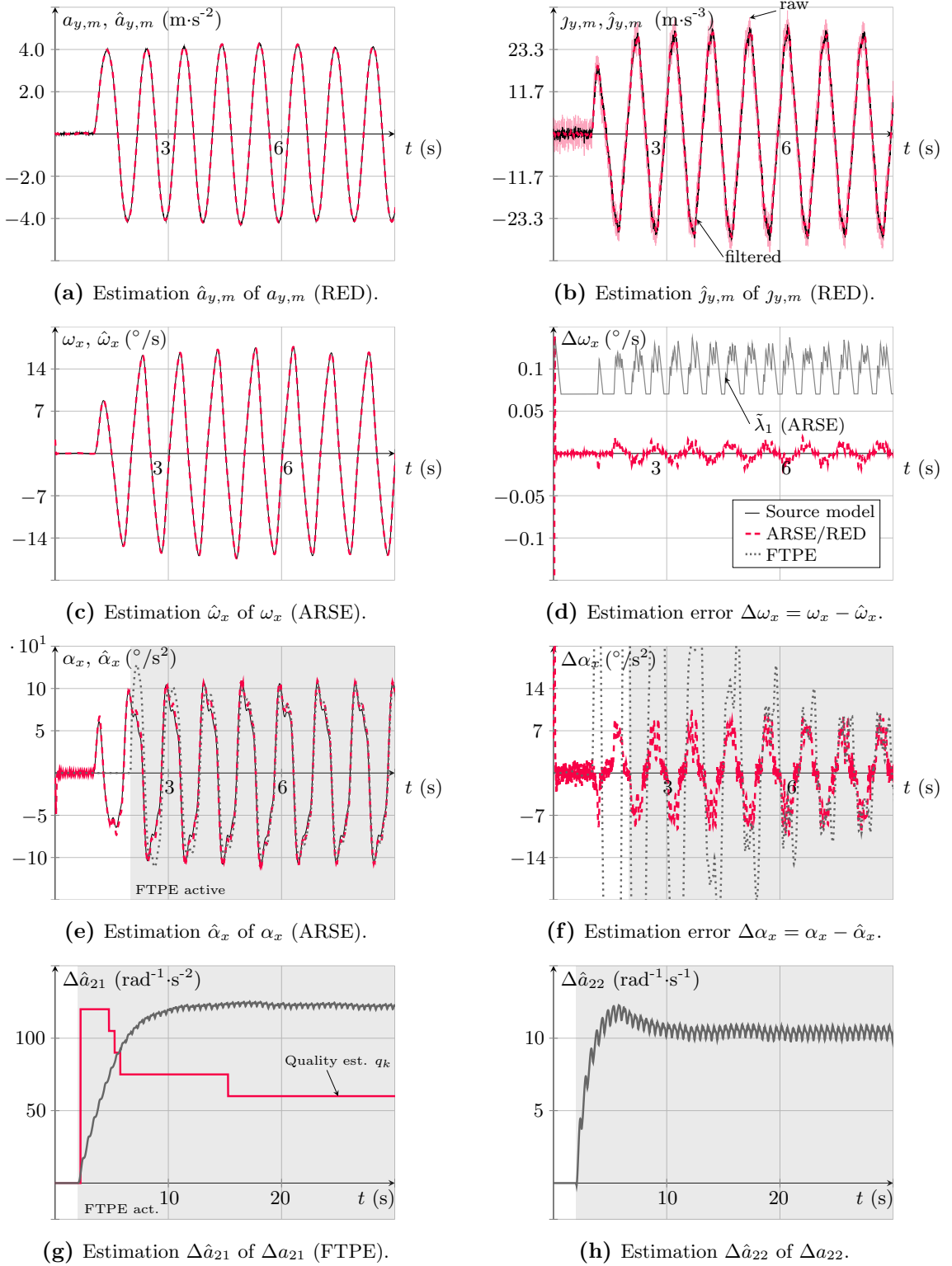


Figure 5.9: Simulation-based estimation results of the uncertain parameters Δa_{21} and Δa_{22} as well as states (roll velocity ω_x and acceleration α_x) using the VSUIO concept. Maneuver: sinusoidal steering with $\delta_h = \pm 45^\circ$, $f_{ex} = 1.0\text{Hz}$, $v_x = 80 \pm 2\text{km}\cdot\text{h}^{-1}$. The gray boxes in (e)-(h) indicate the activation of the parameter estimation algorithm FTPE.

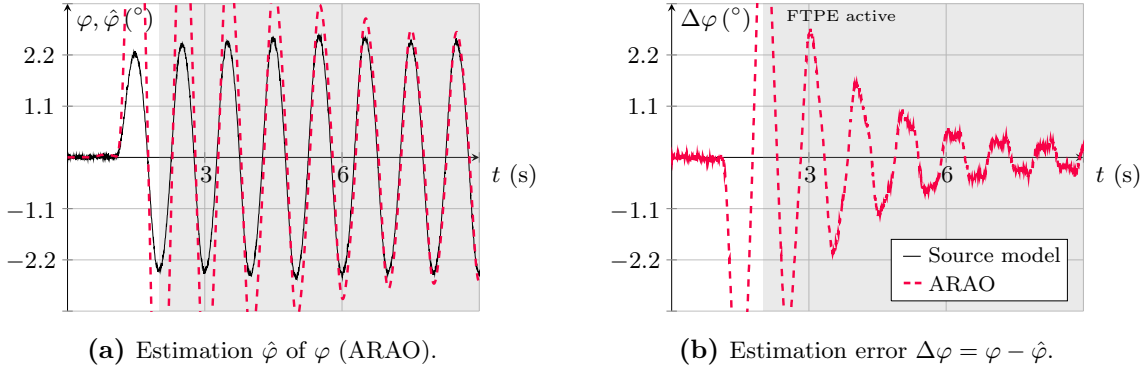


Figure 5.10: Simulation-based estimation results of the roll angle φ and rate ω_x using the VSUIO concept (ARAO). Maneuver as in Figure 5.9. The gray areas indicate the activation of the parameter estimation algorithm.

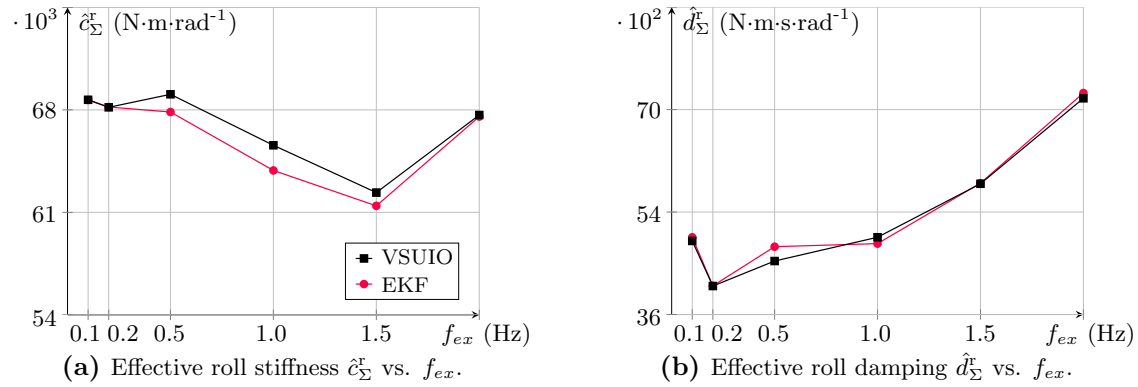


Figure 5.11: Simulation-based estimation results of the roll model parameters c_Σ^r and d_Σ^r for an excitation frequency range of $f_{ex} = 0.1 - 2.0$ Hz. The results show consistent results of the VSUIO and EKF concepts and also reveal the effects of unmodelled dynamics on the estimations of the parameters.

Even though the design paradigms of the two proposed concepts are rather different, the obtained results are similar. Clearly, for the simulation of handling maneuvers the employed roll model requires only one set of parameters. Thus, the weighted averages of EKF and VSUIO are merged such that at the end of the procedure a single pair of roll stiffness and damping values is obtained.

Parameter	Concept	Value	Unit
$[\hat{c}_\Sigma^r \quad \hat{d}_\Sigma^r]$	EKF	[66614 5220]	$[\text{N}\cdot\text{m}\cdot\text{rad}^{-1} \quad \text{N}\cdot\text{m}\cdot\text{s}\cdot\text{rad}^{-1}]$
$[\hat{c}_\Sigma^r \quad \hat{d}_\Sigma^r]$	VSUIO	[65970 5166]	$[\text{N}\cdot\text{m}\cdot\text{rad}^{-1} \quad \text{N}\cdot\text{m}\cdot\text{s}\cdot\text{rad}^{-1}]$

Table 5.7: Identified effective roll stiffness and damping parameters using the concepts EKF and VSUIO.

5.2.5 Pitch Dynamics

The observer-based parameter identification of the pitch dynamics is identical to the EKF-based concept designed for the roll dynamics. Consequently, in terms of parameter tuning, see Table 5.8 for the actual configuration, all EKF-related comments valid for the roll and lateral dynamics, do hold for the pitch dynamics as well. The covariance of the measurement noise is chosen by two orders of a magnitude higher compared to the results of the roll rate sensor noise analysis, see Appendix D, as the estimation quality of the states and parameters showed better matching with reference values using the modified noise covariance. The process noise characteristics are obtained from extensive simulation-based evaluation of different tuning setups.

Parameter	Description	Value	Unit
\bar{a}_{21}	Nominal pitch model parameter (scaled stiffness)	38.89	$\text{rad}^{-1}\cdot\text{s}^{-2}$
\bar{a}_{22}	Nominal pitch model parameter (scaled damping)	2.78	$\text{rad}^{-1}\cdot\text{s}^{-1}$
$\hat{\mathbf{x}}_{a,0}^+$	Initial (augmented) state vector (EKF)	$[1\text{e-}4 \ -1\text{e-}3 \ -\bar{a}_{21} \ -\bar{a}_{22}]^T$	-
\mathbf{P}_0^+	Initial error covariance matrix (EKF)	$\text{diag}([1 \ 1 \ 1\text{e}2 \ 1\text{e}2])$	-
r	Covariance of the meas. noise (EKF)	$3\text{e-}5$	-
\mathbf{Q}	Covariance of the process noise (EKF)	$\text{diag}([1\text{e-}12 \ 1\text{e-}4 \ 5\text{e}1 \ 5\text{e}0])$	-

Table 5.8: Parameters of the EKF concept for the simulation-based observer validation of pitch dynamics-related state and parameter estimation.

In terms of vehicle excitation the situation complicates for the pitch dynamics when compared to the roll dynamics. For the latter, the vehicle can be easily excited by actuating the steering wheel. However, in order to get persistent excitation of the pitch dynamics the driver needs to alternately actuate the accelerator and brake pedals. Figure 5.12 shows the evaluation of the pitch dynamics observer concept in simulations. In (a) the vehicle actuation signal, i.e. gas and brake pedal positions (φ_{acc} , φ_{brk}), are plotted. The resulting longitudinal acceleration signal shows an asymmetric reaction on the excitation which is reasonable considering the forces acting on the wheels that come from either the engine or the brakes. The reference and estimated pitch rate and angle signals are depicted in (c) and (d). Especially the accurate estimates in (d) of the pitch angles shall be noted. However, from the parameter identification results in (e) and (f) highly varying values of effective pitch stiffness and also damping can be noticed. Even in the presence of a low-pass filtering algorithm the parameters are not constant. In other words the proposed observation concept is capable of providing robust estimates of the pitch angle and also time-varying model parameters. However, it is not possible to extract a single set of parameter, i.e. effective pitch stiffness and damping, that describes the system characteristics for a certain range of operation.

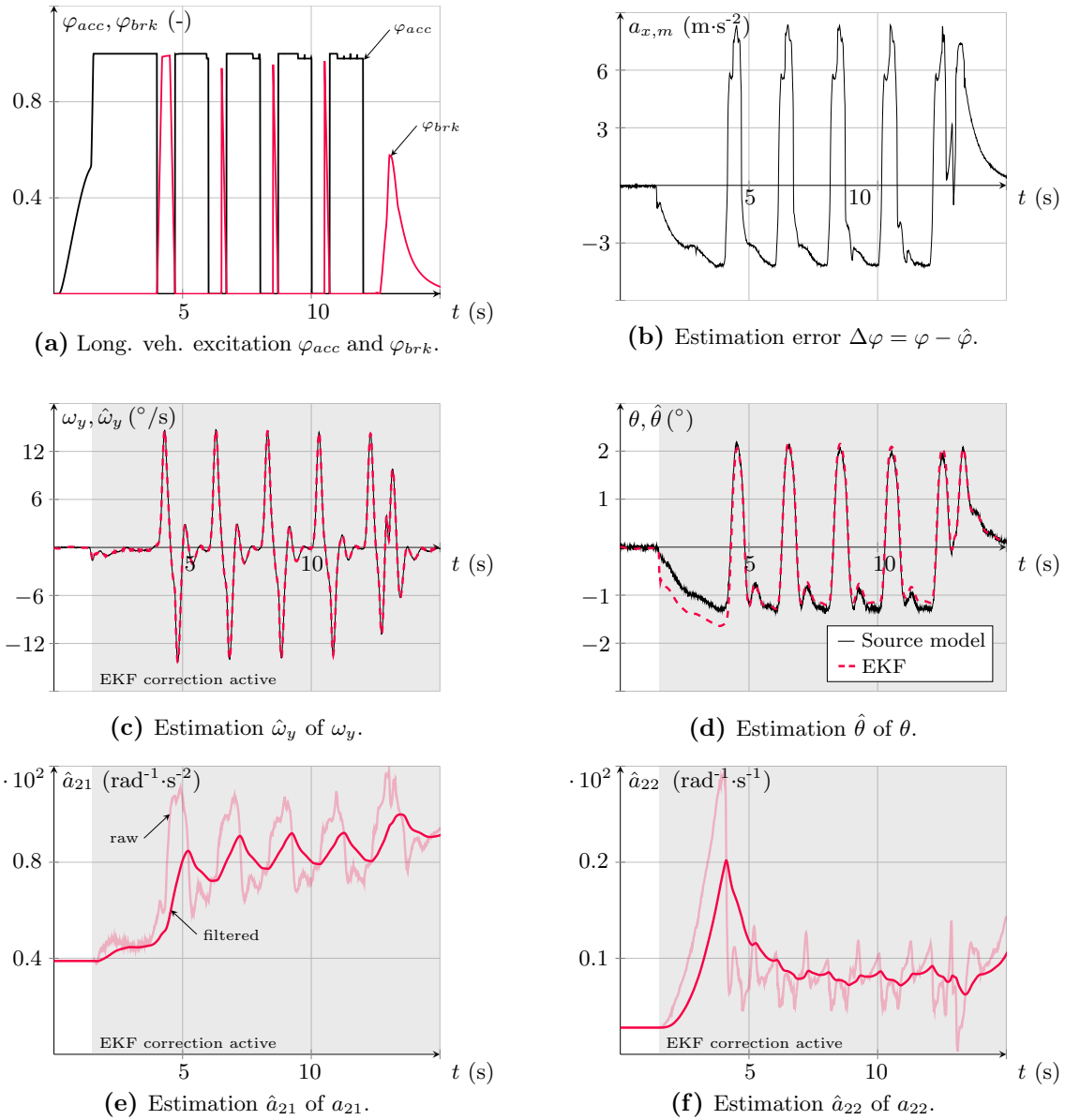


Figure 5.12: Simulation-based estimation results of the parameters a_{21} and a_{22} as well as states (pitch angle θ and velocity ω_y) using the EKF concept. Alternating full acceleration and braking excitation in 1st gear. Correction of *a priori* estimates by the measured pitch rate ω_y is indicated by the gray boxes, see (c)-(f).

Recapitulating the modelling of the pitch dynamics, it is based on the assumption that the motion can be described by an angular spring-mass-damper system. However, in reality that does not account for the asymmetric mass distribution of the vehicle, i.e. the weight of the engine is concentrated near the front axle, whereas for the rear vehicle part there does not exist any counterbalance.

Altogether, that result is not critical for the handling evaluation of the vehicle as to the best knowledge of the author there do not exist any standardized handling maneuvers that take into account the pitch dynamics of the vehicle. Ergo, the adaptive pitch dynamics observer is ready for in-vehicle implementation, but for evaluating the handling its supplied model parameters are of minor usefulness.

5.2.6 Steering Dynamics

Due to the lack of a detailed steering model in IPG CarMaker[®] the evaluation of the observer concept for recovery of steering torque T_h and wheel torque T_w is based solely on measurement data from an EPS test bench. Results will be provided in Chapter 6 and the test bench is presented in Appendix D.

5.2.7 Longitudinal and Powertrain Dynamics

The dynamics of the longitudinal vehicle motion, taking into account the powertrain and longitudinal slip-force characteristics, is the only domain that is modelled based on a neural network concept. Approximating the system, that takes as input the driver's accelerator pedal position and delivers the longitudinal acceleration of the vehicle as output, by standard system theory-based mechanisms is not feasible for this application. Therefore, the idea presented in Section 4.2.5 and based on [HH03] aims to identify the gains of a multilayer perceptron network. The practical realization of the network is performed by the help of the Neural Network Toolbox of Matlab[®]. It allows definition of the network structure, provides the graphical interfaces for data supply and configuration work and also validates the trained network on data provided by the user. Herein, extensive simulation tests have shown that a single hidden layer with 30 perceptrons shows high potential to provide accurate results of the actual longitudinal acceleration when being supplied with gas pedal position and engine speed. Due to the dependency of the longitudinal dynamics on the actual gear there exists one MLP per gear.

The underlying idea for vehicle assessment w.r.t. the longitudinal dynamics is the following: given the scenario that vehicle A shall be compared to vehicle B in terms of longitudinal acceleration capability. Then, vehicle A performs a few test runs, i.e. full load accelerations, and the input and output signals are captured for the neural network training. Feeding the MLP with the gathered data a neural network setup (one per gear) will be obtained. Then, if vehicle B shall be assessed the identified acceleration performance model of A can be embedded into some rapid-prototyping hardware and the acceleration performances compared online. Clearly, for a feasible comparison the environmental parameters, e.g. road surface, asphalt temperature, wind and the test track itself shall be close to those of vehicle A evaluation.

Herein, the idea is to compare a real vehicle to the virtual one provided by IPG CarMaker[®] exploiting the procedure described above. On the one hand side it should demonstrate the applicability of the method to real vehicle measurement data and also reveal the ro-

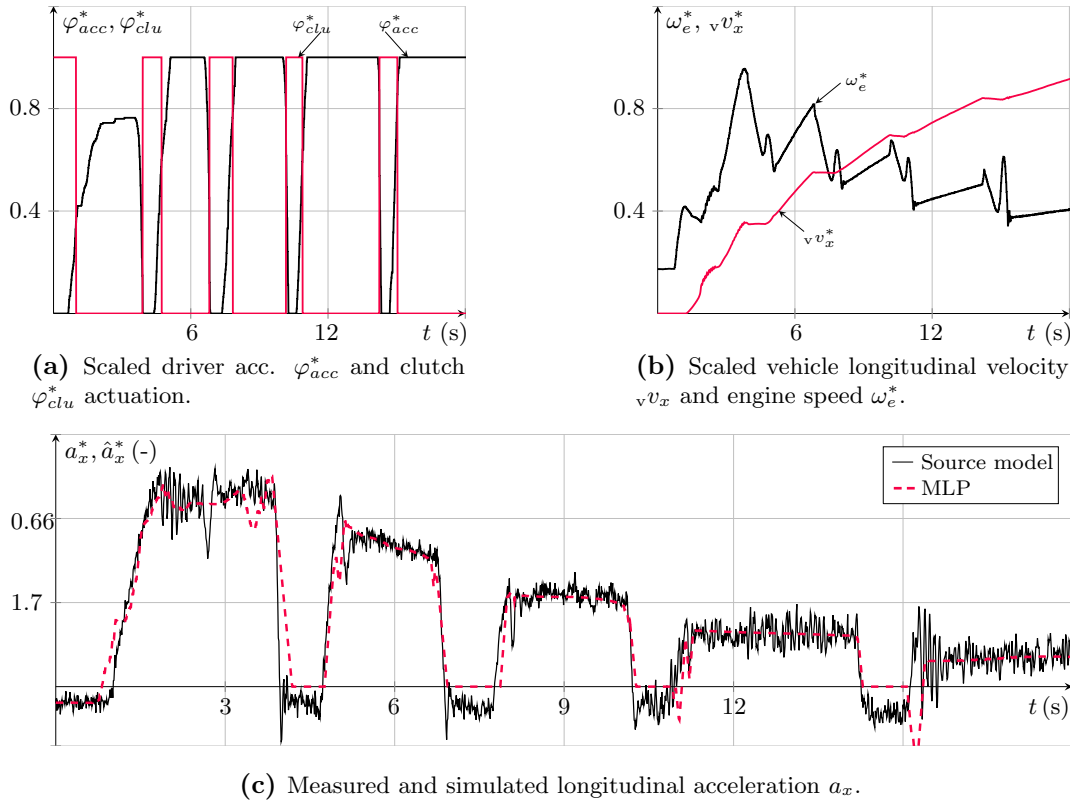


Figure 5.13: Simulation-based validation of the longitudinal dynamics modelling approach using an MLP network. During a full-load acceleration run of the vehicle the measured results can be compared with estimates of the MLP approach. In general, the method shows a good fitting between simulations and real-world, but lacks robustness when being applied to other source model variants.

bustness of the method as the environmental conditions will definitely not be identical. Figure 5.13 shows the vehicle actuation (accelerator φ_{acc}^* and clutch φ_{clu}^* pedal positions), see (a), as well as longitudinal velocity $v v_x^*$ and engine speed ω_e^* , see (b). Note that these measurements are scaled as a matter of confidentiality, indicated by the superscript '*'. In Figure 5.13(c) the measured and also estimated values of longitudinal acceleration, a_x^* and \hat{a}_x^* respectively, of a single full-load acceleration run are plotted. In general, the obtained estimates look promising and capture the acceleration characteristics of the vehicle quite well. There are some outliers due to shifting effects that are not covered by the model, but apart from that the overall quality is good. However, when being applied to a different vehicle, i.e. not the one the network has been trained on, the estimate quality decreases tremendously and the obtained results are not useful at all. This lack of robustness might come from the small data amount (only covering the full-load acceleration experiment) that is supplied to the network. Small changes in accelerator

pedal actuation dynamics can already lead to divergence of the estimates. Integration of additional measurement signals, e.g. clutch pedal position, gas pedal velocity etc. significantly increase the amount of network training time required, but do not result in a better stability of the network, when being applied to an alternative vehicle. In summary, the required excessive data amount and thereof resulting extensive amount of network training time render the approach unattractive for the application of longitudinal dynamics assessment. As a consequence, the latter will not be subject of the remaining thesis.

5.2.8 Road Disturbances

In order to ensure the assumptions of flat road conditions (for the lateral, roll and pitch dynamics parameter identifications) two mechanisms are employed to estimate the road inclination and road bank angle. The difficulty arises from the restriction to not use any vehicle information that is subject to the subsequent identification tasks. As an example, in literature there exist approaches to estimate the road bank angle exploiting observer techniques, e.g. [TSE01], [SGMN08], [MLC10], [KLC12]. But as a prerequisite these models require some vehicle parameter knowledge, e.g. the slip-force characteristics. Based on any differences between the real measurements and the internal model forecasts the actual bank angle is estimated. Herein, referring to the flow chart in Figure 5.2 that information is not available at that time and hence these concepts are not relevant for the current application.

Estimation of the road inclination relies on a simple model coupled with a robust state estimator based on sliding modes, see Section 4.2.6.I. For the road bank angle its recovery is not specifically based on observation mechanisms, but exploits a deliberate order of maneuver execution that allows drawing conclusions on the actual bank angle, see Section 4.2.6.II.

Some Comments on the Road Disturbance Observation In the sequel two concepts for the estimation of the road inclination and also bank angle are evaluated in simulations. In terms of performance specifications the permissible inclination and bank angles of a test track for the objective of handling evaluation are specified in [ISO88a, RH84] and read as $\pm 1.15^\circ$. As a sensitivity analysis of the parameter identification algorithms with respect to perturbations due to road inclination or bank angle has not been performed, the limits as suggested by the standard ISO7401 are used as angles the algorithms need to be capable to detect.

A prerequisite of the methods is clearly the correction of any offsets on the acceleration signals, when the vehicle is at rest. Otherwise, the estimates will also be affected by these offsets.

Parameter	Description	Value
λ_1	Observer gain factor (VSUIO), see (4.73a)	2.59
λ_2	Observer gain factor (VSUIO), see (4.73b)	3.3

Table 5.9: Parameters of the VSUIO concept for the simulation-based observer validation of the road inclination estimation.

Inclination

The basis for the observer design in terms of modelling is given by (4.141). Assuming the measurement of the longitudinal vehicle velocity ${}_{\nu}v_x$ and also acceleration¹³ $a_{x,m}$ the structure of the system is identical to (4.71), i.e. the model of the lateral force estimation mechanism. Consequently, the same observer structure can be used to recover the unknown input, i.e. $g\chi$, the weighted road inclination angle. The tuning of the observer parameters is straightforward and the values used within the simulation-based evaluation listed in Table 5.9.

For the concept evaluation the vehicle follows a straight trajectory that avoids any steering actuation as coupling affects with the lateral dynamics will distort the inclination estimation. Figure 5.14 shows a maneuver, where the vehicle is driven across the (to be tested) proving ground. From (b) the high potential of identifying any positive or negative road inclination can be deduced. Consequently, employing this concept at the very beginning of the vehicle parameter identification process allows the driver to evaluate the proving ground for its suitability.

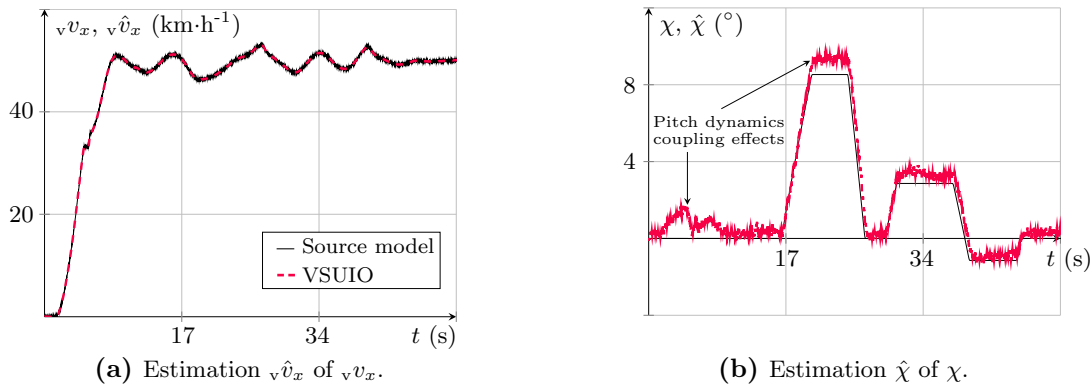


Figure 5.14: Simulation-based evaluation of the road inclination estimation. The vehicle is driven on a track with artificially introduced positive and negative road inclines. As the pitch angle is not available at this stage of the overall process, any effects from the chassis' pitch dynamics have to be accepted.

¹³Note that the measured longitudinal acceleration refers to $a_{x,m}$ which is affected by the chassis' pitch angle, as in (2.59). However, due to the low, constant longitudinal velocity the coupling effects from the pitch dynamics are assumed acceptable.

Bank Angle

Theoretically, the road bank angle could be estimated by the same mathematical principle as the inclination, if the lateral velocity v_y is measured. As this is not the case, an alternative mechanism exploiting the effect of the bank angle on the lateral acceleration measurement, see (2.54), is utilized. The theoretical background is described in Section 4.2.6.II and will now be evaluated in simulations. It should be emphasized again, that at the time of module execution no useful information on either the lateral dynamics (slip-force characteristics) nor the roll dynamics (roll angle) is available. Figures 4.16(a) and (b) illustrate the maneuvers that shall be performed on the proving ground. Importantly, the road bank angle detection algorithm shall be deactivated if the longitudinal velocity exceeds some threshold, e.g. $v_{x,thresh} \approx 15\text{km}\cdot\text{h}^{-1}$. This measure ensures that the influence of any chassis roll motion is kept low. Furthermore, the algorithm shall only be active if the steering wheel angle δ_h is within some specified range, e.g. $\delta_h = \pm 5^\circ$. Basically, there are two different scenarios that are investigated further. The first refers to follow an S-shaped trajectory including longer straight sections (perpendicular to the road inclination to be determined) as illustrated in Figure 5.15(a). The lateral

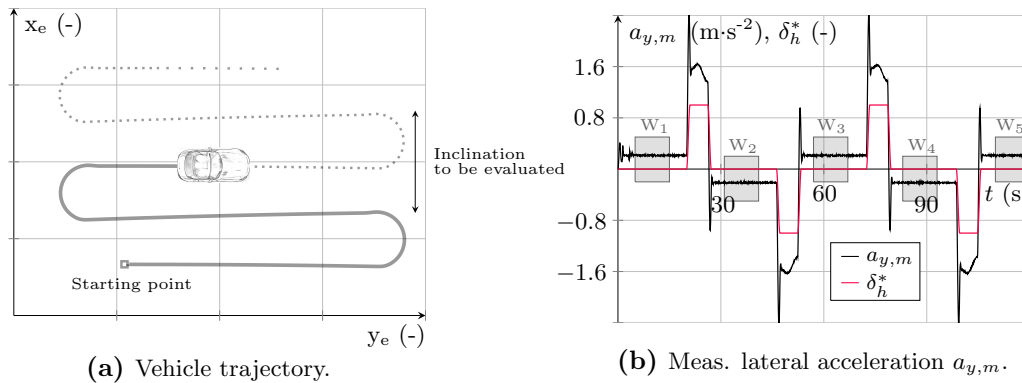


Figure 5.15: Road bank angle determination of a proving ground (dynamic platform) to be assessed for parameter identification work. The actual bank angle can be extracted from the measurements of lateral acceleration during the straight line driving.

acceleration measurement is observed whenever the steering wheel angle is within the specified range, illustrated by $W_1 \dots W_5$ in (b), and an estimation of the road bank angle extracted from (2.54). Calculating averaged values for those time windows provides the driver/engineer with information to further evaluate the suitability of the test track for assessment work.

A second scenario is the evaluation of the road bank angle during cornering, see Figure 5.16(a). Again, the trajectory to follow shall be designed such, that it contains straight line driving and also cornering. As the algorithm is deactivated anyway once the steering wheel angle exceeds the activation threshold the (higher) steering amplitude (due to the previous straight line driving) is not problematic. As discussed previously, whenever the

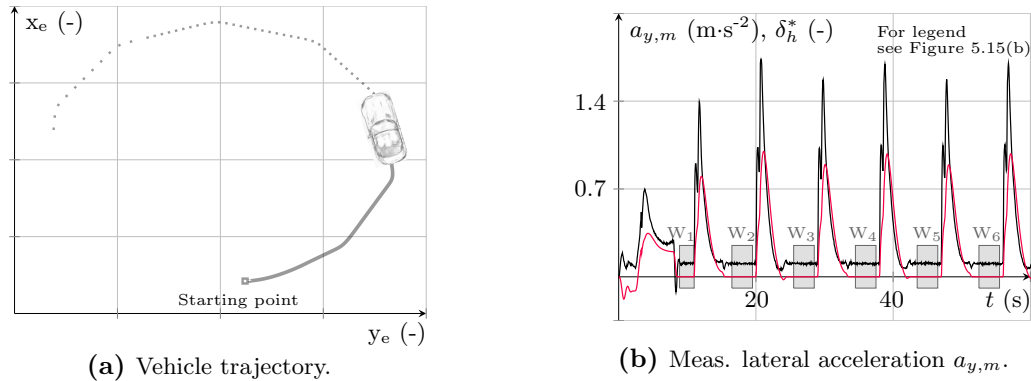


Figure 5.16: Road bank angle determination of a proving ground (curvature) to be assessed. The straight line driving section can be exploited to determine the road bank angle from the lateral acceleration measurements.

steering wheel position is within the activation limits the algorithm extracts the road bank angle from the lateral measurement. Figure 5.16(b) shows the algorithm activation phases $W_1 \dots W_6$ that hold the information on the existing road bank angle.

5.2.9 Comments

The observer-based parameter estimation concepts have now all been evaluated in simulations, but operating on noise-affected measurement signals that are generated by a rather complex vehicle model implemented in IPG CarMaker[®]. Results of the lateral and roll dynamics-related concepts look promising and will be further analyzed within the simulation-based handling evaluation. There, the accuracy of the models (in combination with the identified parameters) will be validated against the measurements of the source model. Also, the (partly observer-based) mechanisms to determine the suitability of a test track for handling evaluation work showed promising results. With respect to the pitch dynamics the robust state estimation, yielding an estimate of the pitch angle, performed satisfactorily. However, the estimated model parameters showed clear non-constant characteristics. Obviously, due to the simple modelling approach any arising parasitic dynamics are lumped into the parameter estimates. Therefore, this model is not assumed feasible for integration into the handling evaluation process. For the modelling of the longitudinal dynamics (from driver accelerator pedal to vehicle longitudinal acceleration) the situation is even worse. Estimation performance is acceptable, if the MLP is applied to vehicle data the network has been trained for, but in terms of extrapolation capabilities the approach showed some real deficiencies and is therefore not pursued any further.

5.3 Performance Assessment of the Model-based Handling Evaluation

Following the idea of model-based vehicle handling evaluation, i.e. the simulation of standardized handling maneuvers exploiting an identified vehicle model, this approach will be further evaluated taking into account the model parameters identified within the last section. Table 5.10 lists the static (s) and identified (i) parameters that can be further used for the simulation of the handling maneuvers as described in Section 1.2.2. The employed single-track vehicle model is based on the equations (2.14b), (2.14c)/(2.34), (2.29), (2.53a), (2.52). Moreover, it takes into account the transient build-up of the tire forces, see (2.37). The outcome of the subsequent section aims to answer the question whether the identified vehicle model is accurate enough to simulate the handling maneuvers, rather than performing it on a test track¹⁴. Comparing the results of CarMaker[®], which is referred to as the source model, taking into account the acceptable sensor accuracies of the handling evaluation process, see Table 1.1, and exploiting the identified vehicle model (IVM) allows to draw a conclusion on that question.

Parameter	Description	Source	Value	Unit
l_f	Distance front axle to CoG	(s)	1.108	m
l_r	Distance rear axle to CoG	(s)	1.42	m
J_{xc}	Moment of inertia (chassis) w.r.t. x-axis	(s)	360	kg·m ²
J_z	Moment of inertia w.r.t. z-axis	(s)	2152.3	kg·m ²
m	(Total) Vehicle mass	(s)	1463	kg
m_s	Vehicle chassis mass (only sprung parts)	(s)	1301	kg
h_{rl}	Distance between CoG and roll center	(s)	0.49	m
n_p	Static pneumatic trail (front and rear)	(s)	0.05	m
c_y	Lateral tire stiffness (front and rear)	(s)	200000	N·m ⁻¹
c_{Σ}^r	Effective roll stiffness	(i)	66292	N·m·rad ⁻¹
d_{Σ}^r	Effective roll damping	(i)	5193	N·m·s·rad ⁻¹
D_f	TM.Simple parameter (front)	(i)	6355	N
B_f	TM.Simple parameter (front)	(i)	1.888	-
C_f	TM.Simple parameter (front)	(i)	8.38 10 ⁻²	rad
D_r	TM.Simple parameter (rear)	(i)	4736	N
B_r	TM.Simple parameter (rear)	(i)	1.974	-
D_r	TM.Simple parameter (rear)	(i)	8.36 10 ⁻²	rad

Table 5.10: Summary of the model parameters used for the handling evaluation.

The last part of this chapter is dedicated to the integration of the human perception modelling, see Section 2.6, into the evaluation process. It reviews the human sensor models from a system theory perspective. Evaluation of the open-loop maneuvers is repeated and the results analyzed in time domain.

¹⁴In fact, executing the maneuvers on a test track refers to simulation of these using the IPG CarMaker[®] software.

5.3.1 Simulation of Open-loop Driving Maneuvers

In the following, the results obtained by the source model and those of IVM are compared. From Appendix C it is clear that the steering angle can be selected such, that the vehicle response in terms of lateral acceleration is at $a_y = 2, 4$ or $6\text{m}\cdot\text{s}^{-2}$. However, for keeping the number of simulated maneuvers (and consequently objective metrics) reasonably low, only the level of $a_y = 4\text{m}\cdot\text{s}^{-2}$ is analyzed further. The same holds true for possible excitation frequencies, e.g. maneuver sinusoidal input (const. frequency). There, only $f_{ex} = 0.5\text{Hz}$ is considered.

Steady-state Circular Driving ISO4138

The subsequently simulated driving maneuver reveals the stationary driving characteristics of a vehicle. Actually, it is the task of the driver to follow a circular trajectory, with $R=42\text{m}$, for increasing longitudinal velocities. The latter is increased step-wise and kept constant for some time in order to gather measurements. For a more detailed maneuver description the reader is referred to Section 1.2.2 or [RH84]. Figure 5.17 shows the results of the source model (IPG CarMaker[®]) and also the estimates using the identified vehicle model (IVM) with parameters presented in the previous section. Figure 5.17(d) does not, as suggested in e.g. [ISO88a], plot the steering torque T_h vs. lateral acceleration a_y as there is no mechanism implemented yet, that provides simulation values of the steering torque. Consequently, to complete the series of plots the yaw rate takes the place of the steering torque.

The overall fitting is good, even though for higher lateral accelerations (beyond the "linear range") there is some deviation between the source and the identified vehicle model. Especially the wheel angle δ_w and also the sideslip angle β show an obvious deviation for those high lateral acceleration levels. However, with regards to the simplicity of the vehicle model this appears reasonable.

A Comment on the Driver Modelling Theoretically, the steady-state circular driving maneuver is of open-loop type. However, its implementation and simulation requires the identified vehicle model to follow a precomputed yaw rate. Hence, rather than performing the maneuver with some type of feed-forward control the more robust way is to design a simple (but robust) controller that is capable of piloting the single-track model along the given (constant w.r.t. yaw rate) trajectory. Therefore, an adaptive super-twisting algorithm [STP12] is designed and implemented that takes the actual yaw rate error as input and supplies a steering angle to the model for tracking the reference.

Step Input ISO7401

The first maneuver to assess the transient behavior of the vehicle is the step input excitation. In contrast to the remaining experiments three different levels of lateral

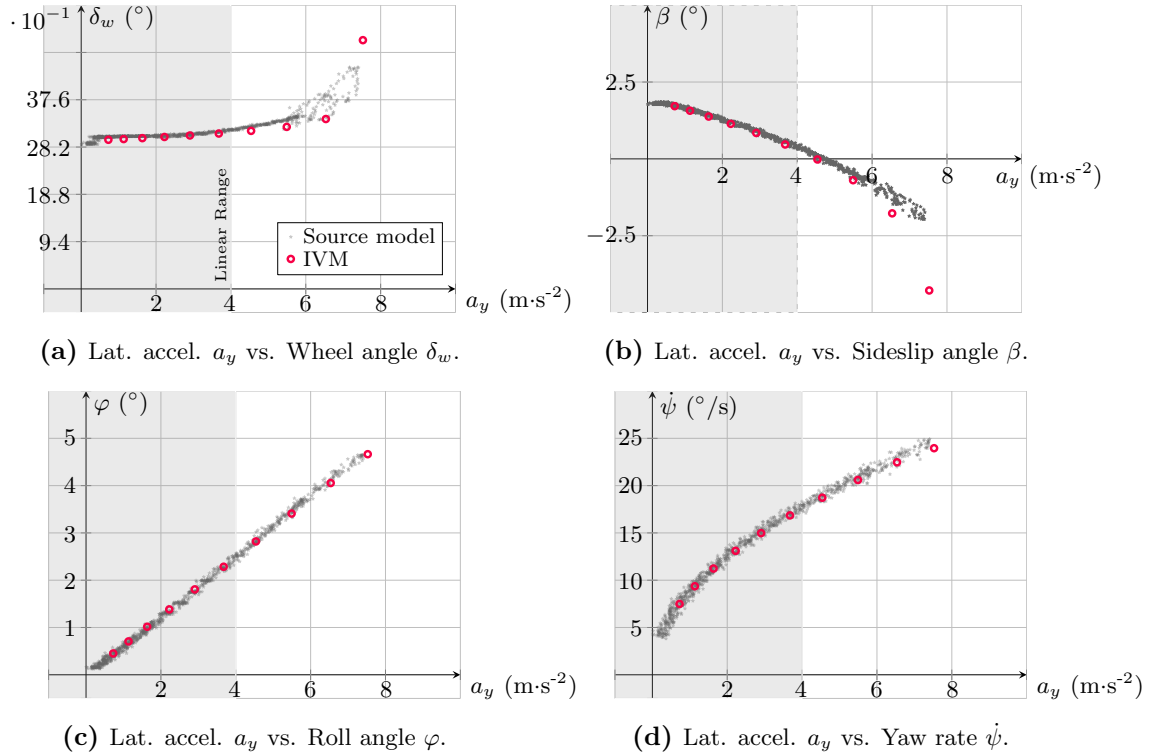


Figure 5.17: Result comparison between source model (IPG CarMaker[®]) and identified vehicle model. Maneuver: Steady-state circular driving with curvature radius $R=42\text{m}$, $v_x = 0 - 70\text{km}\cdot\text{h}^{-1}$. The identified vehicle model does not provide any estimates of the steering torque T_h , therefore it is replaced by the yaw rate $\dot{\psi}$ in (d).

acceleration, i.e. $a_y = 2, 4, 6\text{m}\cdot\text{s}^{-2}$, are simulated by both, the source model and the IVM. Details on the handling maneuver execution are provided in Section 1.2.2. An interesting aspect of the simulation results in Figure 5.18 is the extrapolation capability of the identified vehicle model (IVM) to higher lateral acceleration levels, such as $a_y = 6\text{m}\cdot\text{s}^{-2}$. Obviously, the estimates are not perfectly matching the references of the source model, but are close. For a quantitative evaluation of the IVM outputs the permissible sensor accuracy limits, as in Table 1.1, envelope the black simulation results as gray shades. Ideally, the results of the IVM stay within those limits. Then, the accuracy of the model forecasts has the potential to support the handling evaluation process significantly. For the lower levels of acceleration levels, i.e. $a_y = 2, 4\text{m}\cdot\text{s}^{-2}$ the fitting between source and identified vehicle model is satisfactorily.

Sinusoidal Input (One Period) ISO7401/ISO8725

The sinusoidal excitation (one period) is the alternative or additional maneuver for assessing the transient vehicle behavior. A detailed description of the maneuver parameters

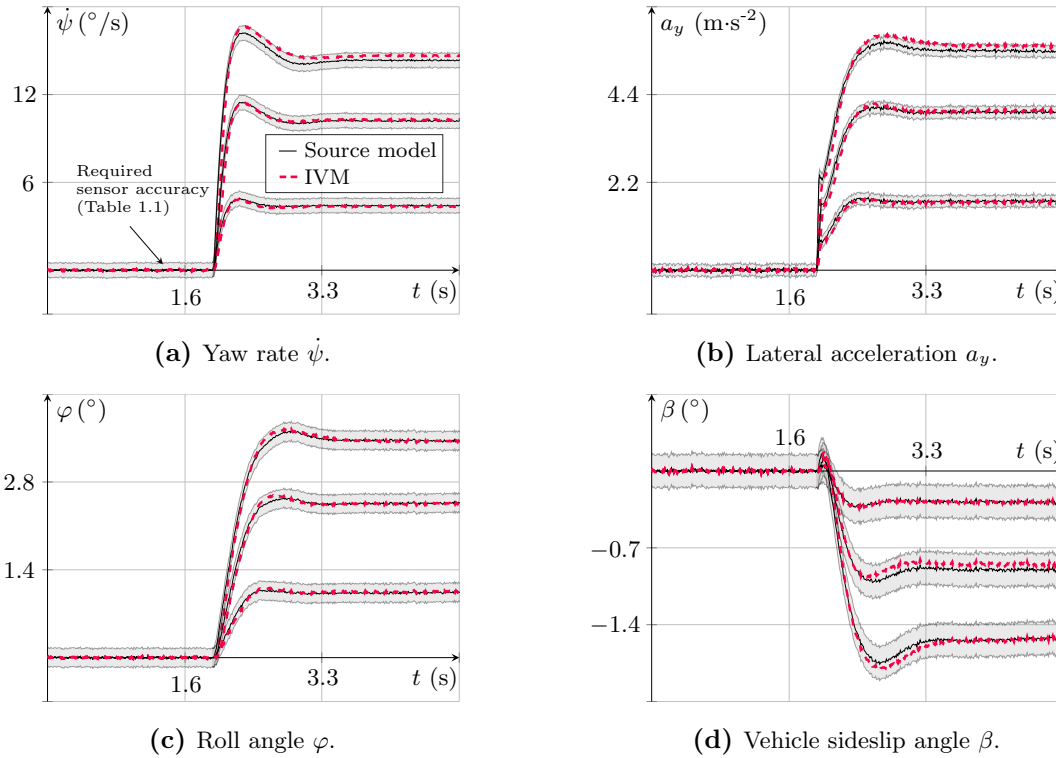


Figure 5.18: Result comparison between source and identified vehicle model. Maneuver: Step steering with $\delta_h = 14/30/42^\circ$, $\omega_h \approx 500^\circ/\text{s}$, $v_x = 80 \pm 2 \text{ km}\cdot\text{h}^{-1}$. The required sensor accuracy envelopes the references in (a)-(d).

is given in Section 1.2.2. Before conducting this maneuver the required steering angle needs to be determined by a step input yielding a steady-state lateral acceleration of $a_y \approx 4 \text{ m}\cdot\text{s}^{-2}$. Then the excitation frequency is specified to be $f_{ex} = 0.5 \text{ Hz}$. Figure 5.19 shows the results of both, source model and IVM. The overall fitting between the two models is good for all considered signals. The results of the IVM exhibit some small time lag compared to the source model. However, for such a transient maneuver clearly the (unmodelled) dynamic load transfer of the vertical tire forces, and consequently variation of pneumatic trail (2.32) does have an influence on the responses of the vehicle.

Sinusoidal Input (Continuous - Constant frequency) ISO7401/ISO13674

Similarly, as for the previous maneuver the vehicle is again excited sinusoidally. However, now the number of periods is increased from one to at least three [ISO88a]. As the remaining maneuver parameters are identical further details are omitted. Figure 5.20 shows the vehicle responses in terms yaw rate $\dot{\psi}$, vehicle sideslip angle β , roll angle φ and lateral acceleration a_y . Additionally to the time-based plots a common approach to visualize the characteristics of steering angle vs. lateral acceleration is depicted in Figure

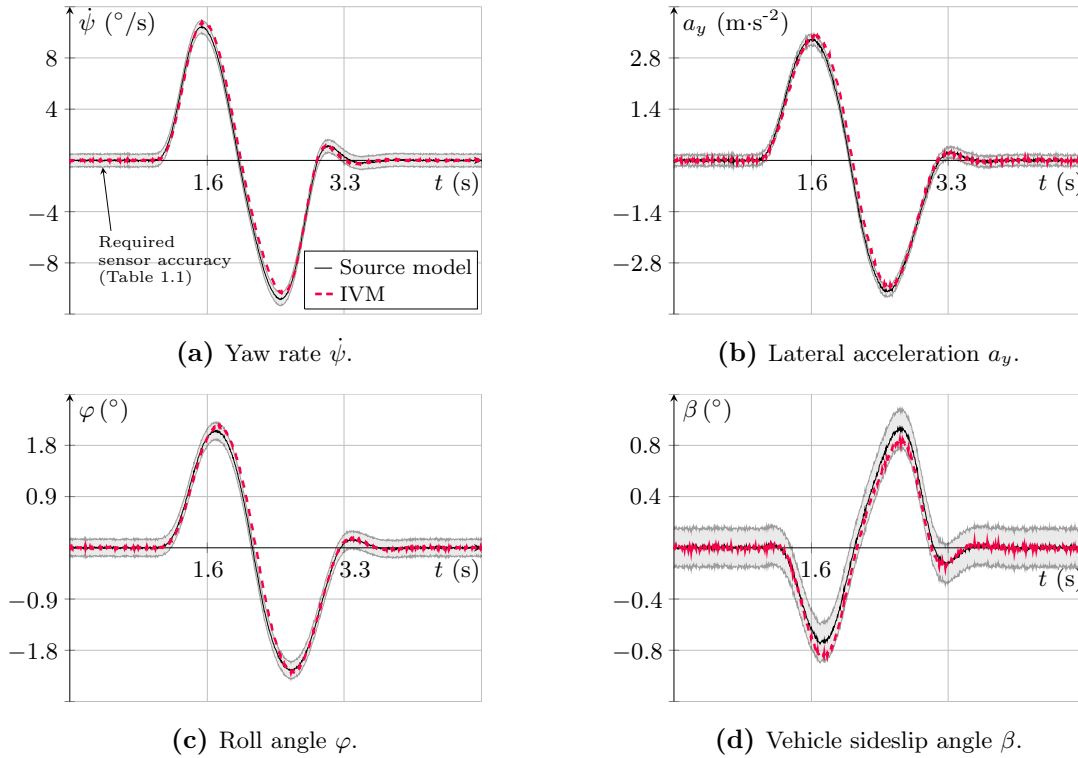


Figure 5.19: Result comparison between source and identified vehicle model. Maneuver: Sinusoidal steering (one period) with $\delta_h = \pm 30^\circ$, $f_{ex} = 0.5\text{Hz}$, $v_x = 80 \pm 2\text{km}\cdot\text{h}^{-1}$.

5.21 showing the resulting ellipsoidal curve. For both figures the discrepancy between source model and IVM is low and the estimates are within the permissible range.

Sinusoidal Input (Continuous - Varying frequency) ISO8726

Extending the sinusoidal vehicle excitation in the sense that the frequency varies now over some predefined range, rather than being constant, allows the identification of the frequency responses of $\delta_w \rightarrow \dot{\psi}$ and $\delta_w \rightarrow a_y$. In fact, the vehicle is excited by frequencies within the range $f_{ex} = 0.1 - 3.0\text{Hz}$. From the obtained measurements (under steady-state conditions), Fast-Fourier-Transforms (FFT) [OSB99] and bilinear transforms [CHE95], an approximation of the frequency responses can be calculated. The IVM is excited identically and therefrom gains and phase shifts at the discrete frequency points can be approximated by FFT and cross-correlation function (CCF) techniques respectively. Figure 5.22 shows the results of the source model and the estimates obtained from the IVM.

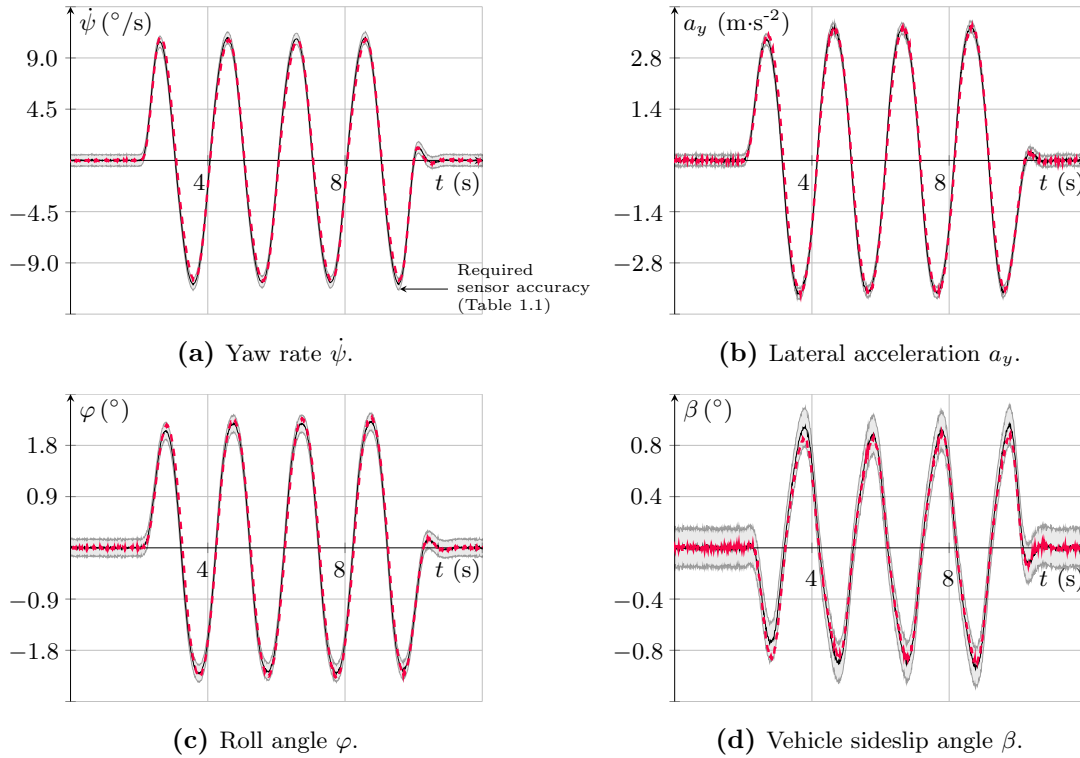


Figure 5.20: Result comparison between source and identified vehicle model. Maneuver: Sinusoidal steering (continuous - const. frequency) with $\delta_h = \pm 30^\circ$, $f_{ex} = 0.5\text{Hz}$, $v_x = 80 \pm 2\text{km}\cdot\text{h}^{-1}$.

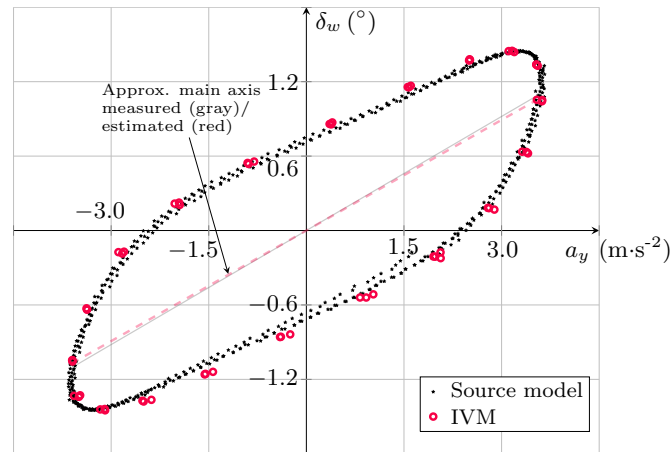


Figure 5.21: Source vs. identified vehicle model for sinusoidal steering (const. frequency). Lateral acceleration a_y vs. Wheel angle δ_w .

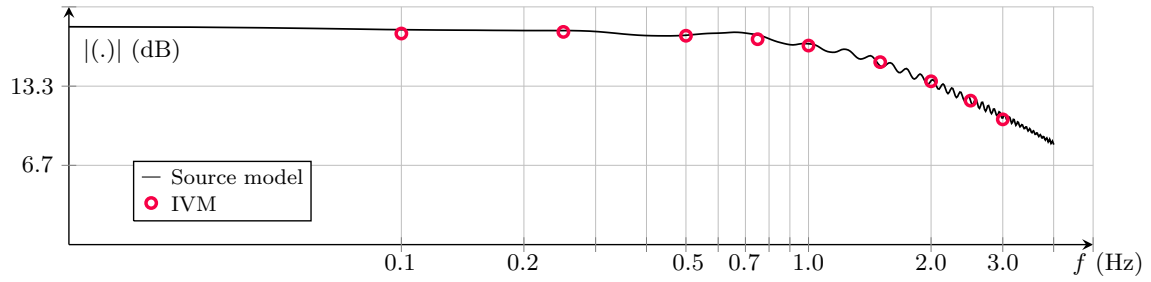
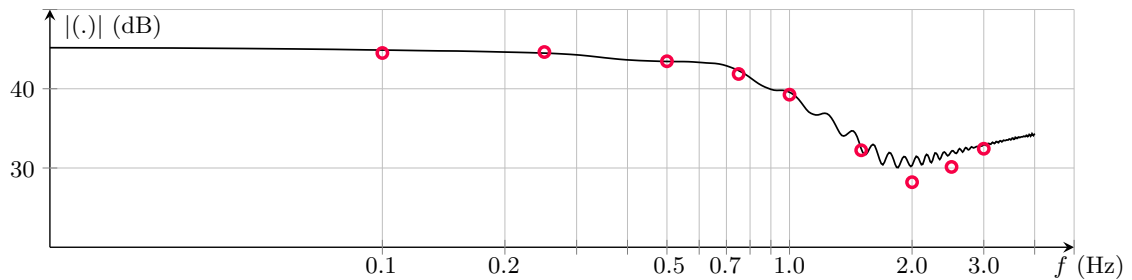
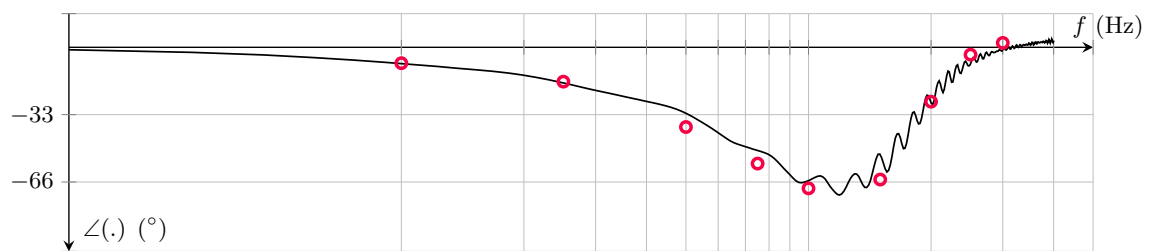
(a) Magnitude plot of the frequency response $\delta_w \rightarrow \psi$.(b) Phase plot of the frequency response $\delta_w \rightarrow \psi$.(c) Magnitude plot of the frequency response $\delta_w \rightarrow a_y$.(d) Phase plot of the frequency response $\delta_w \rightarrow a_y$.

Figure 5.22: Result comparison between source and identified vehicle model. Maneuver: Sinusoidal steering (continuous - varying freq.) with $\delta_h = \pm 30^\circ$, $f_{ex} = 0.1 - 3.0\text{Hz}$, $v_x = 80 \pm 2\text{km}\cdot\text{h}^{-1}$. The frequency response estimation of the source model is based on FFT calculations. Magnitude and phase at the discrete frequency points of the identified vehicle model are calculated by using FFT and CCF techniques.

Interestingly, there is a mismatch between the two when considering the phase plot of the yaw rate response. For higher frequencies, i.e. $f_{ex} > 1\text{Hz}$, the phase shift between steering angle and yaw rate is significantly overestimated. From a vehicle dynamics perspective it is the tire force build-up dynamics that are too slow within the IVM, if the excitation frequency exceeds 1Hz. However, that deviation is not critical due the following reasons:

- None of the herein considered objective metrics is related to constant frequency excitation above 1Hz. Therefore, the accuracy of the model-based predicted vehicle responses for higher frequencies is of minor importance.
- Modelling of the transient tire force build-up is kept as simple as possible. Even the lateral tire stiffness c_y is set to some reasonable value, rather than the precise one (no information available of the IPG CarMaker[®] internals). Moreover, elasticities in the vehicle suspension setup, (dynamic) toe-in and camber angles, dynamic load transfer between tires are completely neglected¹⁵. It is not astonishing that the neglect of these influences affects the results negatively at some stage of the evaluation process. To overcome that problem the underlying model needs to be modified to such an extent that it includes the discussed influences.

5.3.2 Extraction and Comparison of Objective Metrics

The time-based evaluation of the results in terms of fitting between the source and identified vehicle model revealed a good matching between the two sources. Now, extraction of objective metrics shall demonstrate a percentage error that will be introduced when employing the identified vehicle model instead of real-world execution of the standard handling maneuvers. The extraction of these metrics (Appendix C) is performed manually and the definition of the errors is shown on the example of the step input related metric $\text{SI}(\dot{\psi}/\delta_w)_{T_1}$, i.e.

$$\Delta\text{SI}(\dot{\psi}/\delta_w)_{T_1} = \frac{\left(\text{SI}(\dot{\psi}/\delta_w)_{T_1} - \hat{\text{SI}}(\dot{\psi}/\delta_w)_{T_1}\right)}{\text{SI}(\dot{\psi}/\delta_w)_{T_1}}. \quad (5.3)$$

There, $\hat{\text{SI}}(\cdot)$ refers to the objective metric that is extracted from the simulation results of IVM. Figure 5.23 shows the percentage errors of the maneuver-specific objective metrics. With regards to the metrics obtained from the steady-state circular drive the slopes of the characteristics δ_w vs. a_y and β vs. a_y at an acceleration level of $a_y=6\text{m}\cdot\text{s}^{-2}$ are significantly different from the source model. Considering the plots in Figure 5.17(a) and (d) the overall fitting is quite well, but the metrics refer to the slopes of the characteristics and these are obviously different (for some points). In order to calculate these slopes the data set is approximated by a spline and the derivative w.r.t. a_y evaluated. So, it

¹⁵The transient tire force build-up is a rather complex process, see e.g. [PAC12] for details.

percentage of difference appears high, the same holds true as described previously, i.e. the estimates of IVM are still within the required sensor accuracy range. For the sinusoidal input with varying frequency the fitting is well and that is also reflected by the results in Figure 5.23(e). The discussed deviation of the phase shift between frequency responses of source model and IVM for excitation frequencies above 1Hz is not transformed into the objective metrics. Here, it is only worth mentioning that the metrics of resonance peaks and eigenfrequency were not applicable.

5.3.3 Human Perception Simulation

The idea of modelling the human perception is to gain further insights into the assessment process. Transforming the basis of the objective metrics extraction to the driver (rather than the vehicle) shall reveal additional information to model the linkage between the metrics and the subjective evaluation, see [SCH10] for further details. Herein, it is not the aim to develop that correlation and build the linkage. In fact, the signals shall be transferred to what the human being "feels" during the drive and then extract the metrics. That broad database (together with the standard metrics) can then be used for further scientific work in order to identify any relations between objective metrics and subjective assessment.

Before integrating the modelled human sensors (Section 2.6) into the simulation environment and discussing the obtained results from virtually performing the standard handling maneuvers, the *to be expected* behavior of the models shall be analyzed.

The semi-circular canals are responsible for the perception of angular rates. As the input signal is the angular acceleration it approximates (at least for a certain frequency band) an integrator, Figure 5.24(a) and (b). In literature there exist (at least) two different modelling approaches of the semi-circular canals, i.e. with and without adaption. In [WBGH06] it is claimed that for dynamic environments (e.g. aircraft/car simulators) the adaption term is not required as the adaption time constants are a lot higher than those of the system dynamics. However, based on [SCH10] the adaption terms are included herein. Consequently, as can be seen in (b), low-frequent excitation signals are attenuated significantly. Focusing on the perception of translational accelerations the otoliths have to be investigated further. Independent from the use of an adaption term, the human perception of trans. accelerations is only sensitive up to $f_{ex}=2\text{Hz}$ [SCH10]. In Figure 5.24(c) and (d) this is marked by the gray boxes. Implementation-wise the high-frequency gain of the transfer function $G_{oto}(s)$ is compensated by a low-pass filtering element with appropriate selection of the cut-off frequency. Finally, the perception of the steering angle can be modelled with the transfer function $G_{ms}(s)$ and obviously represents a lead-element in the control sense as does $G_{oto}(s)$. In the following the maneuvers discussed in Section 5.3.1 are simulated again with consideration of the modelled human senses. Solely the steady-state circular maneuver is not repeated as its integra-

tion here is not useful¹⁶. The vehicle responses will be visualized in terms of yaw rate, lateral acceleration, roll angle and vehicle sideslip angle. The latter is captured by the visual perception that is modelled as pure time delay, as in (2.83).

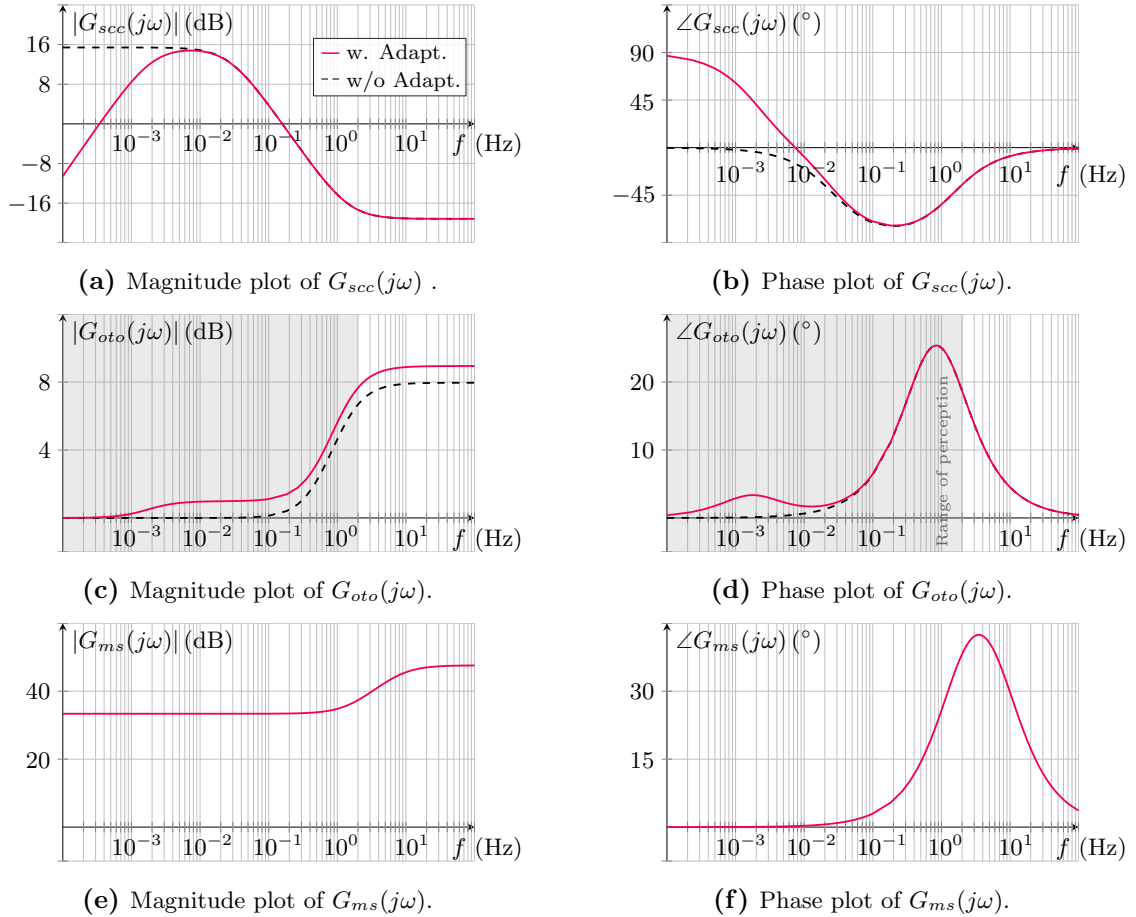


Figure 5.24: Frequency responses of the human perception (semi-circular canals, otoliths and steering wheel). The modelling is presented in Section 2.6.

Some Notes on the Implementation The semi-circular canals take as input signals the angular accelerations that are normally not measured in-vehicle. To overcome that problem robust exact differentiators (as in Section 4.2.2.II) are implemented to estimate yaw, roll and pitch accelerations. Furthermore, the output of the semi-circular canals is an angular velocity. For the lateral dynamics this is not a problem, but for roll dynamics an additional integrator needs to be added¹⁷.

¹⁶A simple argument refers to the adaption of the otoliths to actual constant yaw rates. This would mean that tracking a given static yaw rate with a constant steering angle is not possible.

¹⁷It is that integration that smooths the signal and cancels the noise almost completely in Figures 5.25-5.29.

For a better comparison between measured and sensed quantities a scaling of the latter might be performed such that the values match under steady-state conditions. Herein, no specific scaling is applied.

A Comment on the Notation For the subsequent analysis it is important to differentiate between *measured* and *sensed* signals. Therefore, only the sensed signals will be denoted by an additional subscript that refers to either the otoliths ("oto"), the semi-circular canals ("scc"), the muscle spindles ("ms") or the visual sense ("vis").

Step Input ISO7401

The sudden excitation of the vehicle by actuating the steering wheel step-wise causes the driver to sense the vehicle responses as presented in Figure 5.25. As already anticipated once the motion is constant the yaw rate that the driver senses, vanishes due to the inherent adaption capability of the semi-circular canals. The same holds true for the roll angle. In terms of lateral acceleration perception there is a distinct peak in the step response that is not seen in the measured signals. The vehicle sideslip angle remains unchanged apart from the introduced dead-time.

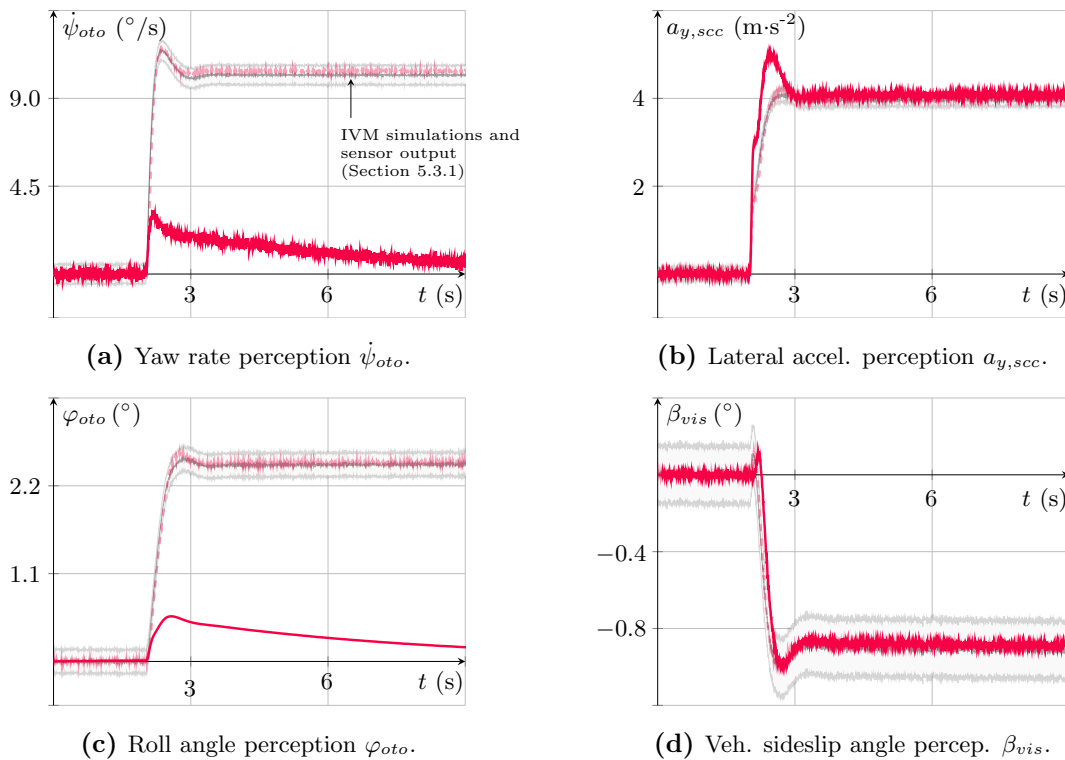


Figure 5.25: Human perception signals of the step input maneuver, see also Figure 5.18. The raw sensor signals are shown in the background of (a)-(d).

Sinusoidal Input (One Period) ISO7401/ISO8725

The second maneuver for evaluation of the transient vehicle characteristics contains a one-period enduring sinusoidal steering maneuver. In contrast to the step input there is no constant excitation during this maneuver that would cause the perception signals to vanish. Figure 5.26 shows the human perception signals. As expected from Figure 5.24(a) the sensed yaw rate and roll angle are attenuated with respect to their magnitudes. That is opposed to the lateral acceleration that shows an increased amplitude and due to the lead-character of the otolith's transfer function a positive phase shift, see Figure 5.26, acts on the lateral acceleration.

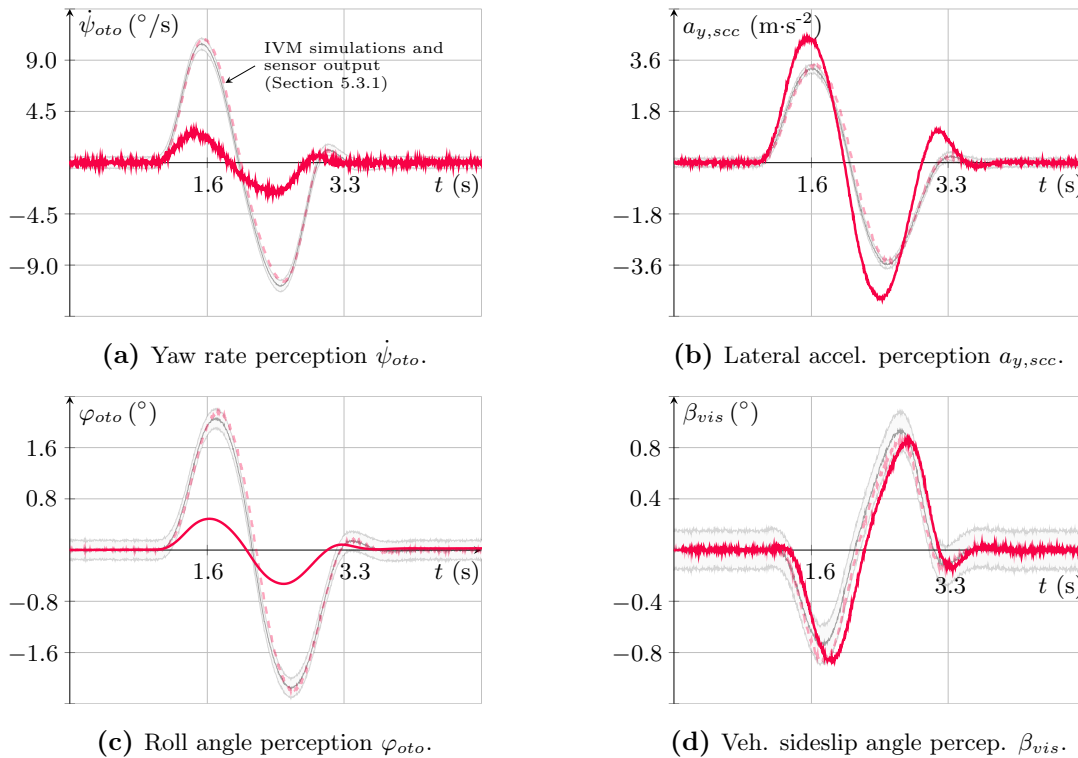


Figure 5.26: Human perception signals of the sinusoidal input (one period) maneuver, see also Figure 5.19. The background of (a)-(d) shows the raw sensor signals.

Sinusoidal Input (Continuous - Constant frequency) ISO7401/ISO13674

A steering signal with constant frequency applied to the vehicle yields the perception signal results as depicted in Figure 5.27. In terms of interpretation there is no difference compared to the previously presented maneuver, i.e. sinusoidal steering (one period). Furthermore, the excitation frequencies are identical, so the only difference is the existence of steady-state conditions.

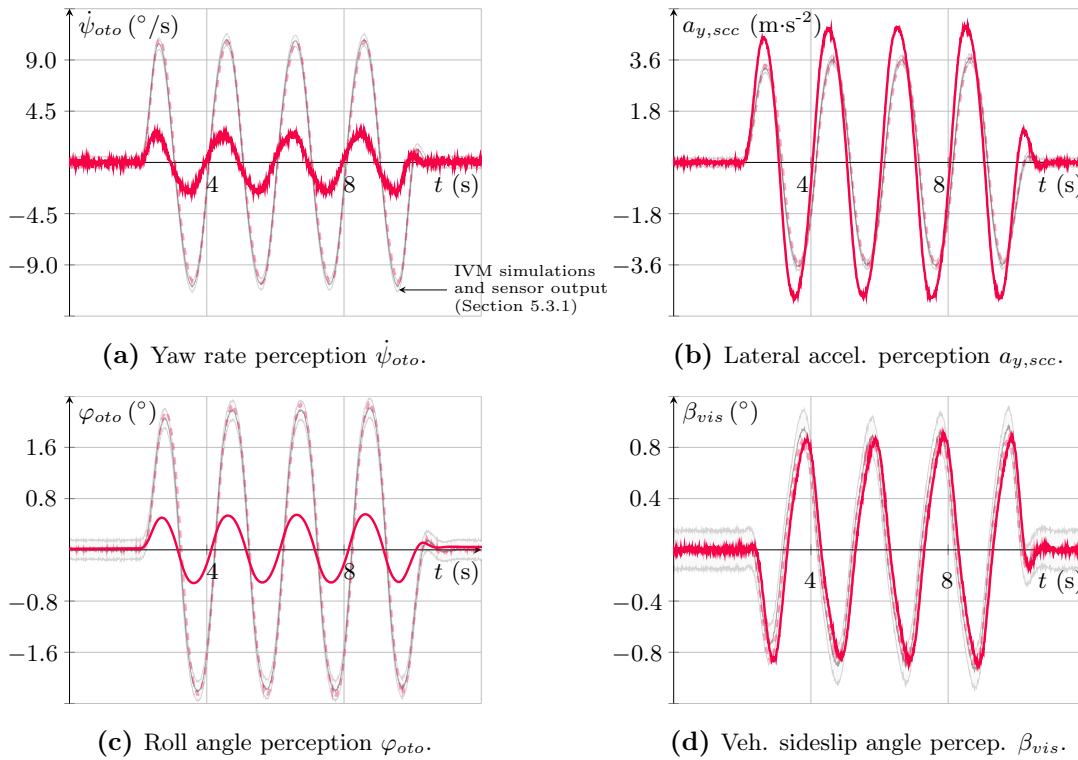


Figure 5.27: Human perception signals for the sinusoidal steering (const. frequency) maneuver, see also Figure 5.20.

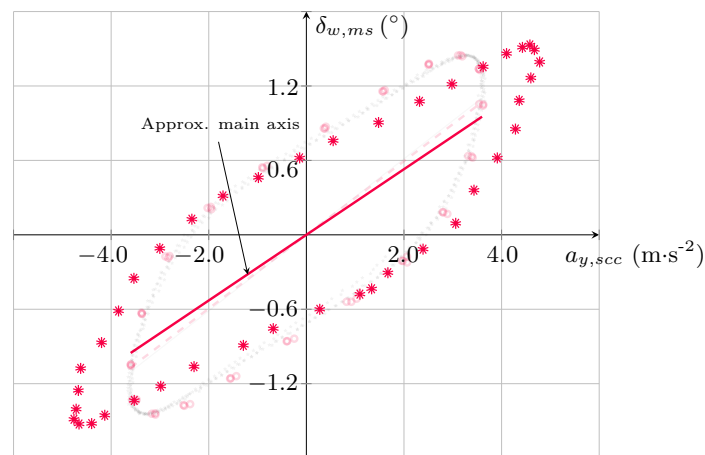


Figure 5.28: Lateral accel. percep. $a_{y,sc}$ vs. Wheel angle percep. $\delta_{w,ms}$.

Moreover, the ellipsoidal that illustrates the characteristics of lateral acceleration against steering angle is shown in Figure 5.28 for the case of perception signals.

Sinusoidal Input (Continuous - Varying frequency) ISO8726

Before concluding the analysis of the human perception signal evaluation the last maneuver, i.e. sinusoidal steering excitation with varying frequency is simulated. It allows approximation of the system's frequency responses, i.e. $\delta_{w,ms} \rightarrow \dot{\psi}_{oto}$ and $\delta_{w,ms} \rightarrow a_{y,scc}$. The methods for extraction of the magnitudes and phase shifts with respect to certain frequencies are identical to the ones described in Section 5.3.1. The obtained estimates of magnitude and phase plots can be extracted from Figure 5.29. Quantitatively, the interpretation of (a) can be directly extracted from Figure 5.24(a), i.e. the magnitude for low and high excitation frequencies is attenuated significantly due to the characteristics of $G_{scc}(s)$.

5.3.4 Extraction of Objective Metrics

In general, the same objective metrics as specified in Appendix C can be extracted. However, due to the different character of the sensed vehicle responses care needs to be taken, whether the metrics are still meaningful, e.g. for $SI(\dot{\psi}/\delta_w)_{R_{ss}}$ this is no longer the case!

5.3.5 Comments

This second part of Chapter 5 reviewed the performance of state estimates related to the identified vehicle model (considering the obtained parameter from Section 5.2). Comparing the source model (IPG CarMaker[®]) and IVM results for certain standardized vehicle handling maneuvers that are part of the objective vehicle dynamics assessment work, revealed the potential of the method to support the overall assessment process. The performance specifications of the maximum permissible deviations between source model and IVM are based on given sensor accuracies, see e.g. [PHL08]. The required accuracy is achieved for almost all performed maneuvers and looks overall very promising.

Furthermore, the integration of the human sense models allows the extraction of objective metrics that are based on a human being, rather than sensing devices. These values do have the potential to be further used for correlations with subjective assessment as in [SCH10].

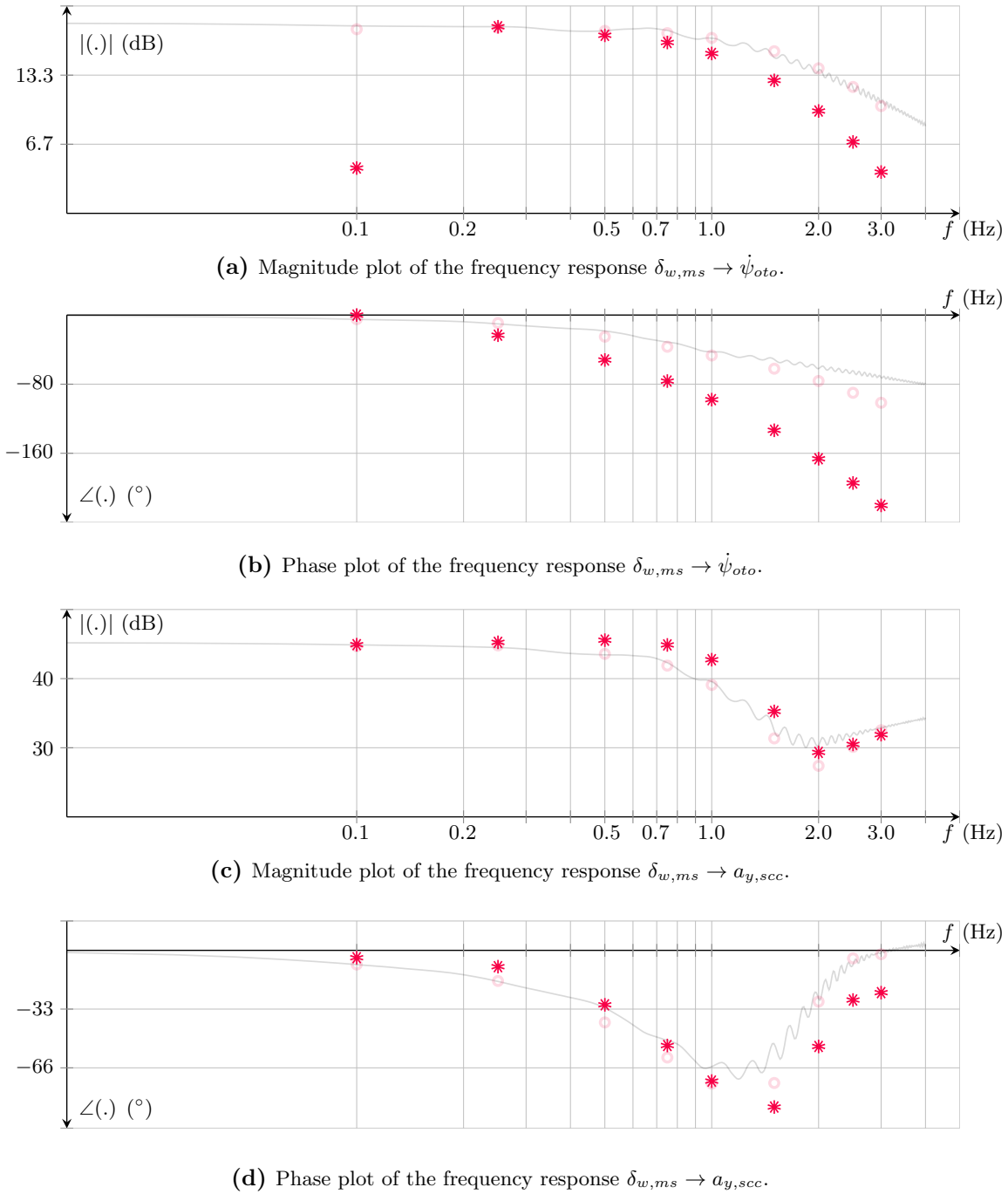


Figure 5.29: Estimated frequency responses of the vehicle dynamics affected by the human sense models of muscle spindles $G_{ms}(j\omega)$ and semi-circular canals $G_{sccl}(j\omega)$ as well as otoliths $G_{oto}(j\omega)$. Note that e.g. $G_{ms}(j\omega)$ represents the frequency response of the system modelled by (2.87).

5.4 Concluding Remarks on the Simulation-based Evaluation

In summary, the observer-based parameter identification techniques as well as the handling evaluation in simulations showed good performance in terms of accuracy when compared to the source model IPG CarMaker[®]. Clearly, the simulations of standardized driving maneuvers also revealed the limits of accurate vehicle response estimates. This is paid by the simple models as assumed in Chapter 2. However, when sticking to the specified objective values, e.g. ISO7401, ISO4138 etc. the differences are within an acceptable range that has the potential to provide some considerable time and cost reduction to the overall vehicle dynamics assessment process.

6

Experimental Evaluation of Selected Observer Concepts

It has been the aim of the previous chapters to systematically present the modelling of vehicle dynamics, analyze their sensitivities with respect to model parameters, select appropriate system outputs as an outcome of the sensor selection process and propose observer-based parameter identification mechanisms. As the name suggests the latter estimate non-measurable system states and uncertain model parameters simultaneously. Validation of these concepts in a custom-built simulation environment has been subject of the last chapter. Now, the deployment of those concepts to real-world systems concludes the development process, intends to back up the findings of Chapter 5 and extends them to scenarios of experimental application. Ideally, not only the observer-based identification techniques would be evaluated under real conditions. A comparison between offline simulated and effectively performed handling maneuvers under real-world conditions could reveal the integration potential of the proposed concepts into the overall handling evaluation process. However, this would require the availability of an experimental vehicle that is (at least) instrumented with those sensors listed in Table 1.1. Unfortunately, that comparison can not be conducted due to the lack of experimental facilities.

Nevertheless, some selected concepts of Chapter 4 are tested on real vehicle measurement data. Moreover, the robust state estimator related to the electric steering system (EPS), see Section 4.2.4, is deployed to a dedicated test bench of an EPS system, that is available for experimental work.

Generally, in comparison to the complex simulations environment consisting of e.g. IPG CarMaker[®], it is expected for real-world application that effects due to measurement noise, time discretization, parasitic dynamics play an even more prominent role in evaluating the observer performance. Speaking of the latter, for most of the selected concepts

ground truth data of the mechanical systems, e.g. lateral tire slip-force characteristics, effective roll stiffness, is not available. Consequently, evaluation is restricted to a comparison between measurement data and model predictions (under considerations of the identified parameters). Solely for the electric steering system reference data of the recovered inputs, i.e. driver steering torque T_h and wheel torque T_w , exists.

Focusing on the presented concepts of Chapter 4 it is the parameter and state estimation of the lateral dynamics (Section 4.2.1), roll dynamics (Section 4.2.2) and robust state estimation of the electric steering system (Section 4.2.4) that are evaluated on experimental facilities.

6.1 The Implementation Setup

Ideally, the implementation of the proposed concepts is performed on a rapid-prototyping platform (as described in Appendix D). The challenging problem that arises by doing so, is the inherent *low* sampling time of vehicle-related measurements of $\tau_s = 0.01\text{s}$. Due to reasons of CAN performance it is not expected at the moment that the sampling times will reduce dramatically within the foreseeable future. However, from the simulation results¹ it is already clear that such high sampling times cause a massive degradation of the estimation performances and therefore render the implementation of the proposed concepts unfeasible.

However, for the given application the need to access the vehicle's CAN data bus is only given temporarily. In other words, if the necessary sensor devices are integrated into a stand-alone platform that performs its own data measurements, there are no restrictions on the chosen sampling rate apart from the specifications of the processing unit that is installed. In fact, any difficulties of up-sampling strategies that will arise with the actual experimental vehicles will then be obsolete. Therefore, "real" in-vehicle implementation of the proposed algorithms is not realized. Nevertheless, the sampling rate of the measured vehicle data is artificially increased such that the observer concepts that are implemented in the Matlab[®]/Simulink[®] environment get new data every $\tau_s = 0.001\text{s}$.

Alternatively, rather than using prediction-based algorithms for online increase of the sampling rates the introduction of an artificial time delay will be discussed. A data buffer that holds samples of e.g. time instants k and $(k - 1)$ allows calculation of minor time steps (in between $(k - 1)$ and k) by simple interpolation techniques. That data is then fed to the observers, but with a certain amount of time lag. From the perspective of the observer the data rate is constant, but delayed with respect to the measurement. However, as the observation results are not further used by any real-time application the introduction of the time delay is acceptable. It only needs to be ensured when inspecting the estimation results that the time synchronization between measurements

¹The results of Chapter 5 are achieved by executing the proposed concepts with a sampling time $\tau_s = 0.001\text{s}$.

and estimates is correct.

Scaling of the Variables In the sequel of this chapter the main results of the experimental evaluation will be presented. To some extent the measured vehicle data is part of industrial cooperations and due to data confidentiality a scaling of the results is required. In general, the notation

$$x^*(t) := \frac{x(t)}{x_{scal}}, \quad (6.1)$$

defines a scaled variable $x^*(t)$, with x_{scal} being a (not further specified) constant. Moreover, publication of any vehicle related parameters as well as observer tunings is omitted on purpose. Note that the notation of scaled variables is only used within figures.

6.2 Lateral Dynamics (Experimental Vehicle A)

Model parameter identification and performance evaluation of those results is based on the measurement data gathered from experimental vehicle A, see Appendix D.2 for further details.

Identification of the lateral tire slip-force characteristics refers to the parameter estimation of the tire model `TM_Simple` as specified in (2.29). Those six parameters are recovered by separating the overall identification task into the estimation of lateral cornering stiffness and maximum tire force (per wheel). From the latter and the assumption of a slightly degressive curve for quantities of slip exceeding the maximum-related value, see Section 5.2.3, the parameters B , C and D can be extracted².

Lateral Cornering Stiffness

Knowledge extraction of the actual front and rear lateral cornering stiffness values requires the vehicle to be operated within the so-called proportional range, i.e. the characteristics between lateral force and slip are assumed linear. The two proposed concepts, namely the Extended Kalman filter (EKF) and the variable structure unknown input observer (VSUIO) are applied sequentially. Figure 6.1 shows the estimates of the yaw rate ω_z , vehicle sideslip angle β and the front and rear lateral cornering stiffness values $c_{\alpha_{fe}}$ and $c_{\alpha_{re}}$. Again, the presented quantities are scaled due to data confidentiality. From the plots (a)-(f) it is obvious that the *a priori* estimates are corrected by measurements of the yaw rate permanently throughout the complete experiment. Due to the aggressive tuning of the filter parameters, allowing for fast convergence of the states and parameters, the latter show significant variations with time and are therefore low-pass filtered, see (e) and (f). Furthermore, it is worth mentioning that the ordinates of (a) and (b) as well as (c) and (d) show the same ranges, i.e. the remaining error is directly

²For a detailed description of the maneuvers refer to Section 5.2.3 and Figure 5.3.

related to the estimated signal. Calculation of scalar parameter values from the time series of $\hat{c}_{\alpha_{fe}}$ and \hat{c}_{α_r} relies on averaging of values for the last fourth w.r.t. time t in (e) and (f). In contrast to the simulations-based validation of the concepts the estimates are not obviously converging to a constant value, but remain within some boundary. This effect is likely to be caused by measurement noise and parasitic dynamics whose influence is projected onto the parameter estimates.

Evaluation of the VSUIO concept is shown in Figure 6.2. Therein, the start of the finite time parameter estimation algorithm is delayed by some time lag. That is purely for representations to show the convergence of the VSUIO. For practical applications, the parameter estimation might start right with the vehicle sideslip estimation process. In contrast to the EKF concept two instances of the VSUIO module need to be designed, i.e. one for the front and one for the rear cornering stiffness estimation. Similarly as for the results of the EKF, the ordinates of (a), (b) and (c), (d) do have the same ranges such that the resulting errors are comparable with the estimated quantities. The plots of (e) and (f) already show the low-pass filtered estimates of the front and rear lateral cornering stiffness values. For the qualitative analysis of the parameter estimates the same holds true as discussed for the EKF.

Interestingly, when comparing the two concepts applied to real-vehicle data the use of different excitation maneuvers is obvious³. With respect to the excitation durations the two maneuvers are approximately the same, but the steering amplitudes are different. For the actual tuning of the EKF the steering amplitude needed to be above a certain threshold in order to gain convergence of the parameters.

Final values of the lateral cornering stiffness value for the front and rear tire can then be obtained by merging the results of EKF and VSUIO.

A General Comment on the Calculation of the Wheel Angle Both concepts⁴ need the steering angle of the wheel as system input. In practice, it is often calculated from the measured steering wheel angle δ_h , as defined in (2.4.1), with neglecting any elasticity of the steering system. The (nonlinear) static steering transmission is identified by the use of wheel alignment turn plates. Even though there exist measuring techniques for obtaining accurate quantities of steering angles, due to cost and installation time drawbacks, these are rarely used.

Maximum Lateral Tire Forces

In Chapter 5.2 the experiments to be preferred for the estimation of maximum forces have been introduced as either slow step input (similar to a steady-state circular maneuver) or sinusoidal steering. Even though theoretically these are the preferences, for experimental

³The attentive reader might have noticed that within Section 5.2.3 as well.

⁴For the VSUIO-based mechanisms this only refers to the instance estimating the front cornering stiffness uncertainty.

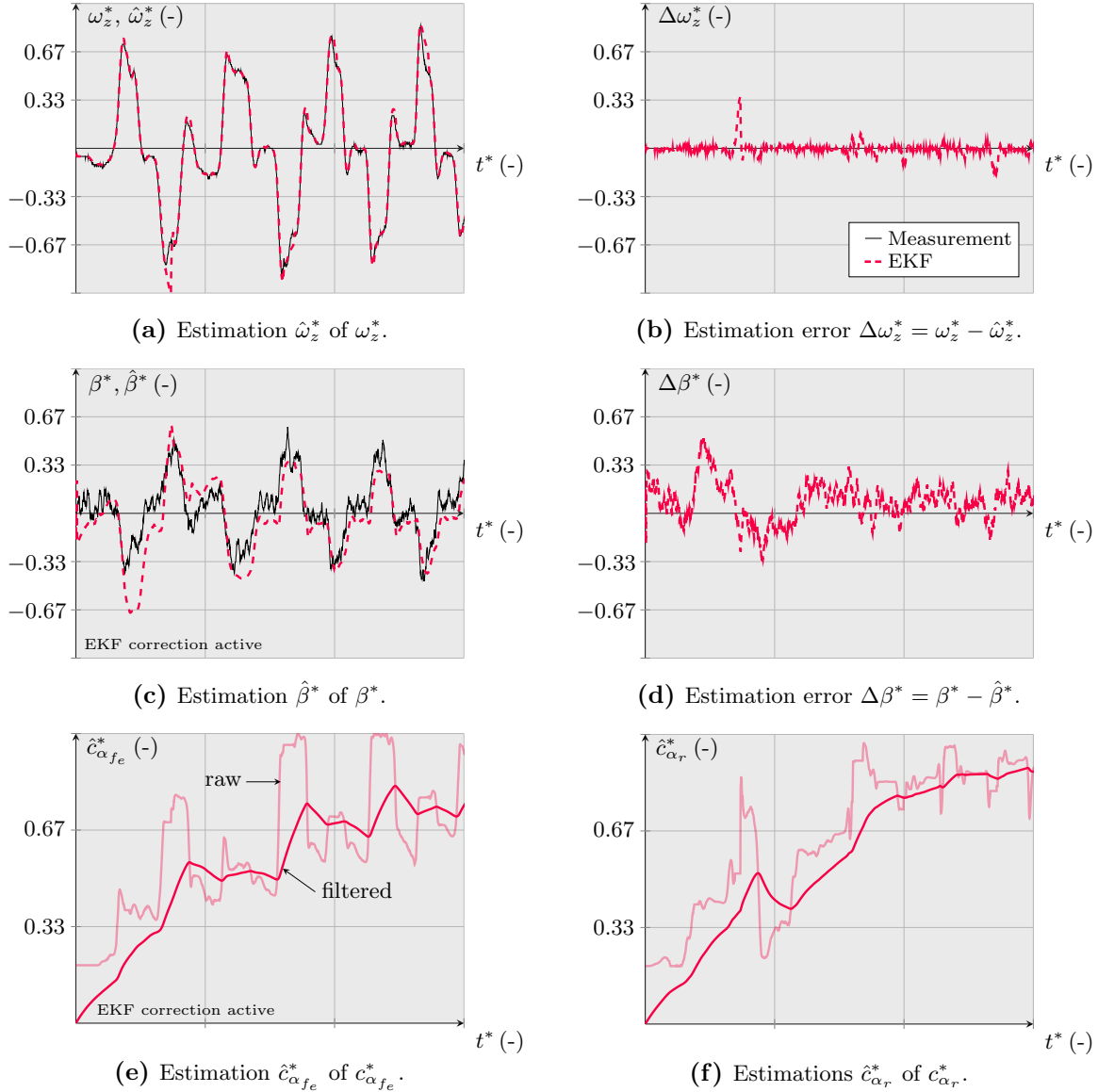


Figure 6.1: Experimental evaluation of the lateral cornering stiffness estimating EKF. Maneuver: sinusoidal-like steering with low amplitude in order to stay within the *proportional range*.

validation a highly dynamical driven lane change maneuver shall reveal the maxima of front and rear forces.

This decision obeys the availability of historic measurement data as an experimental vehicle with necessary sensor devices (e.g. optical velocity measurements) for the validation of the results is not available.

The estimation of the tire forces requires the lateral acceleration (compensated for any

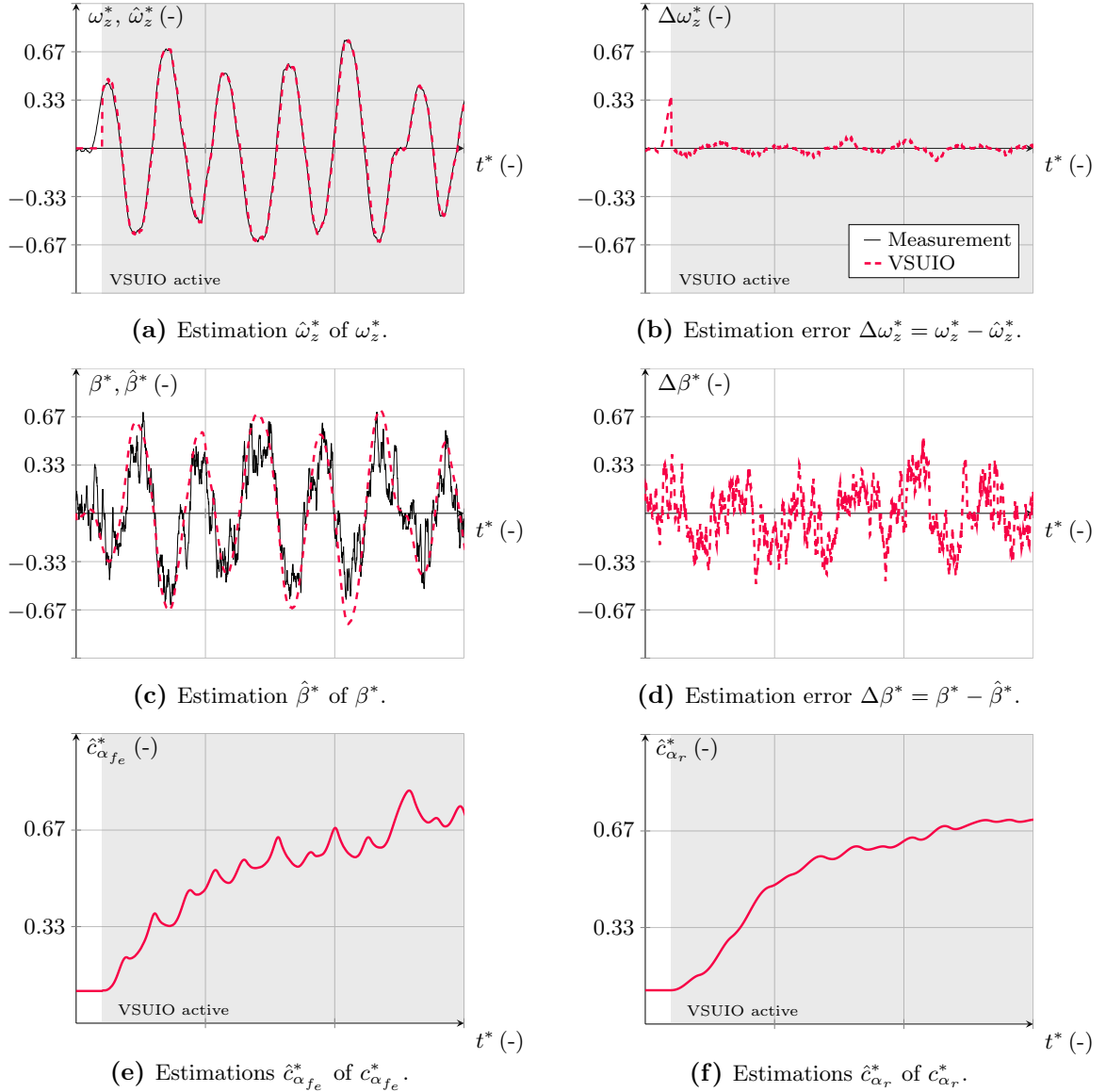


Figure 6.2: Experimental evaluation of the lateral cornering stiffness estimating VSUIO. Maneuver: sinusoidal steering with low amplitude in order to stay within the *proportional range*. From (c) it is obvious that the signal of the measured sideslip angle is significantly affected by measurement noise for those low levels of excitation.

effects of the chassis' roll motion) as system input. As the roll angle φ is not measurable an estimation scheme, e.g. ARAO in Section 5.2, needs to be employed. But, unfortunately the experimental vehicle that is equipped with the optical velocity sensor does not provide any measurement data of either roll angle or rate. In fact, an approx-

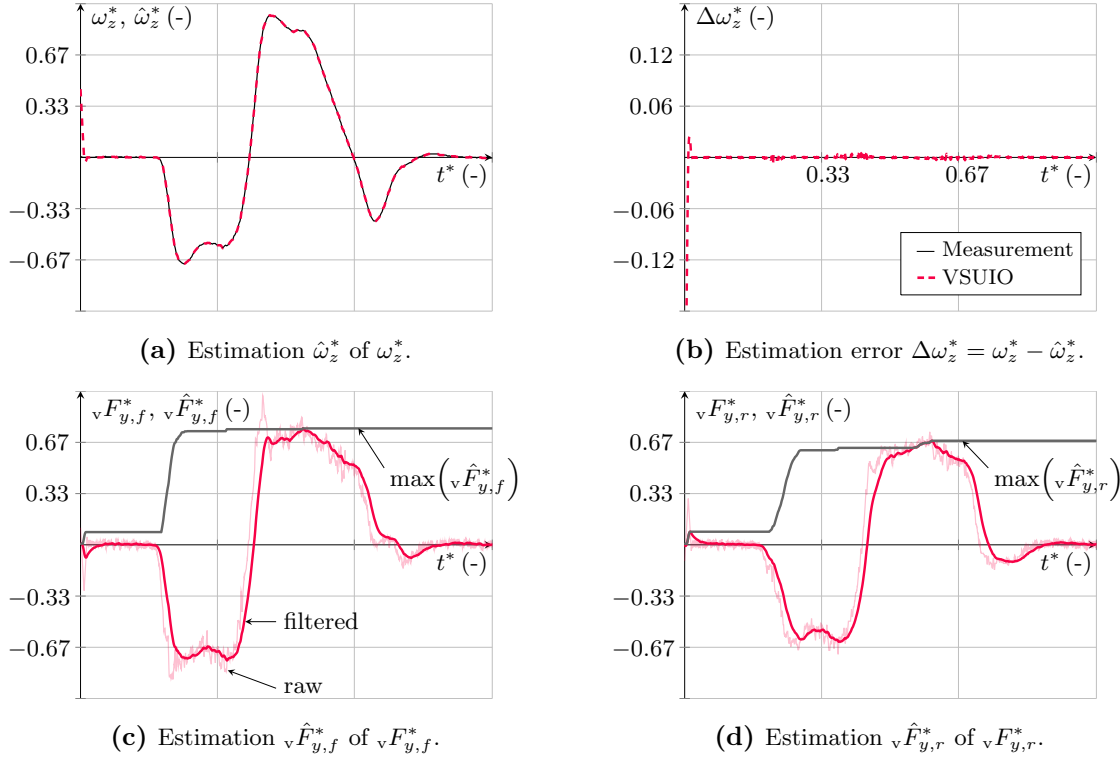


Figure 6.3: Experimental evaluation of the VSUIO concept to estimate maximum lateral tire forces of the front and rear wheels. Maneuver: highly dynamical lane change maneuver driven at approximately constant longitudinal velocity.

imation of the roll angle can only be obtained from an open-loop estimation⁵ that uses the measured lateral acceleration as input. Additionally, the high rates of roll angular velocity emphasize the nonlinear effects of the damping elements on the roll motion and complicate the calculation of a compensated lateral acceleration. Despite the arising problems, these estimates of the front and rear forces will be further used for obtaining the required tire model parameters.

Figure 6.3 shows the estimates and errors of the yaw rate and also the maxima of the absolute tire forces. In order to robustify the estimates to measurement and time-discretization noise a low-pass filtering scheme is accommodated. Any introduced time lags due to the filtration process are acceptable as only the maximum values are of interest. The gray lines in Figure 6.3(c) and (d) show the estimates of the maxima.

Reconstruction of the Model Parameters The mechanism of converting the identified characteristic points of the front and rear lateral tire slip-force curves into model parameters is identical to Section 5.2.3. It assumes a constant parameter B that gov-

⁵The model parameters are taken from the estimation results of vehicle B. This is assumed feasible as it affects the identification and performance evaluation identically.

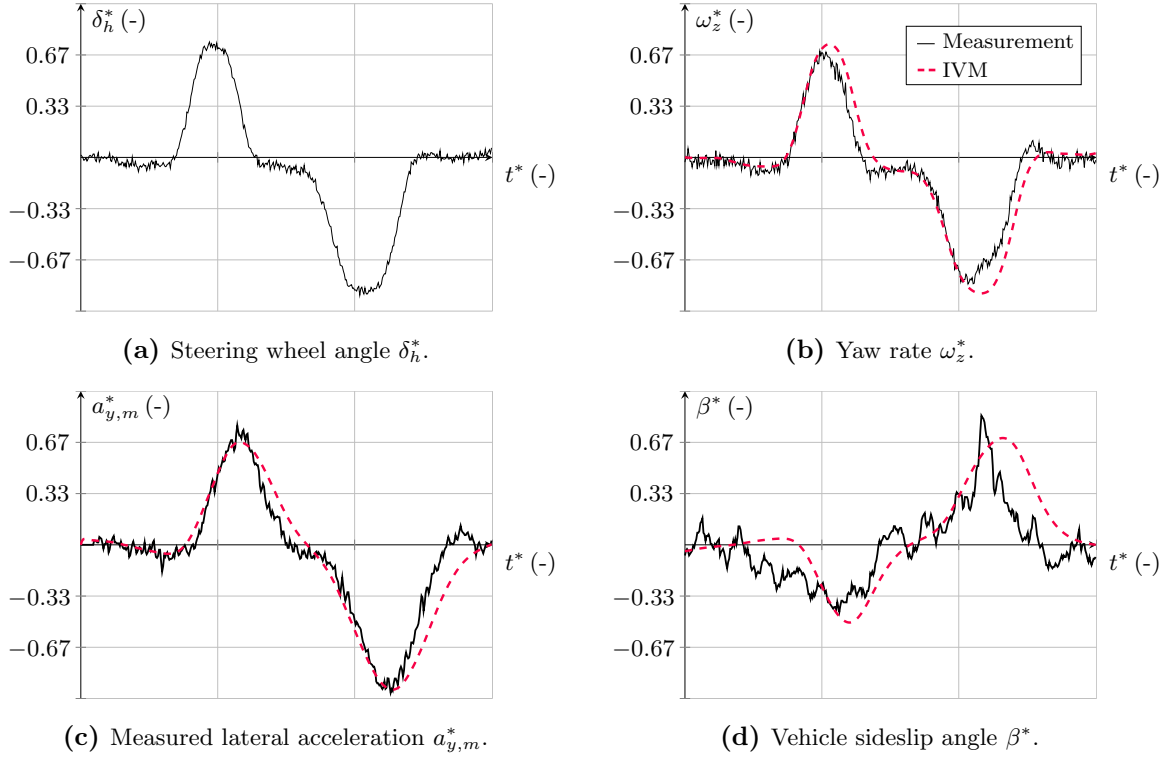


Figure 6.4: Experimental validation of the identified lateral slip-force curves. Maneuver: moderate steering excitation such that the proportional range, i.e. $|a_{y,m}| < 4\text{m}\cdot\text{s}^{-2}$ is not left. Constant longitudinal velocity to reduce any coupling effects between longitudinal and lateral vehicle dynamics.

erns the degressive part of the curve and from that the remaining parameters can be recovered. The resulting parameters are not listed explicitly, but used within the next section to validate the tire model on vehicle measurement data.

Results Performance Assessment

The validation of the estimated lateral slip-force characteristics is performed for three different excitation levels. Proper selection of the validation maneuvers ensures that the steering actuation is intensified from the first to the last experiment. At the end the model with its identified parameters will be applied to the data from a handling maneuver that brings the vehicle to the edge of stability. Even though the model prediction accuracy for that region of operation is of minor importance for the given application, it shows the extrapolation capability of the approach.

In general, the validation model is identical to that of Section 5.3 and denoted by the abbreviation IVM. The first maneuver and the resulting vehicle responses are shown in Figure 6.4. It shows the measurements of steering wheel angle δ_h and the responses

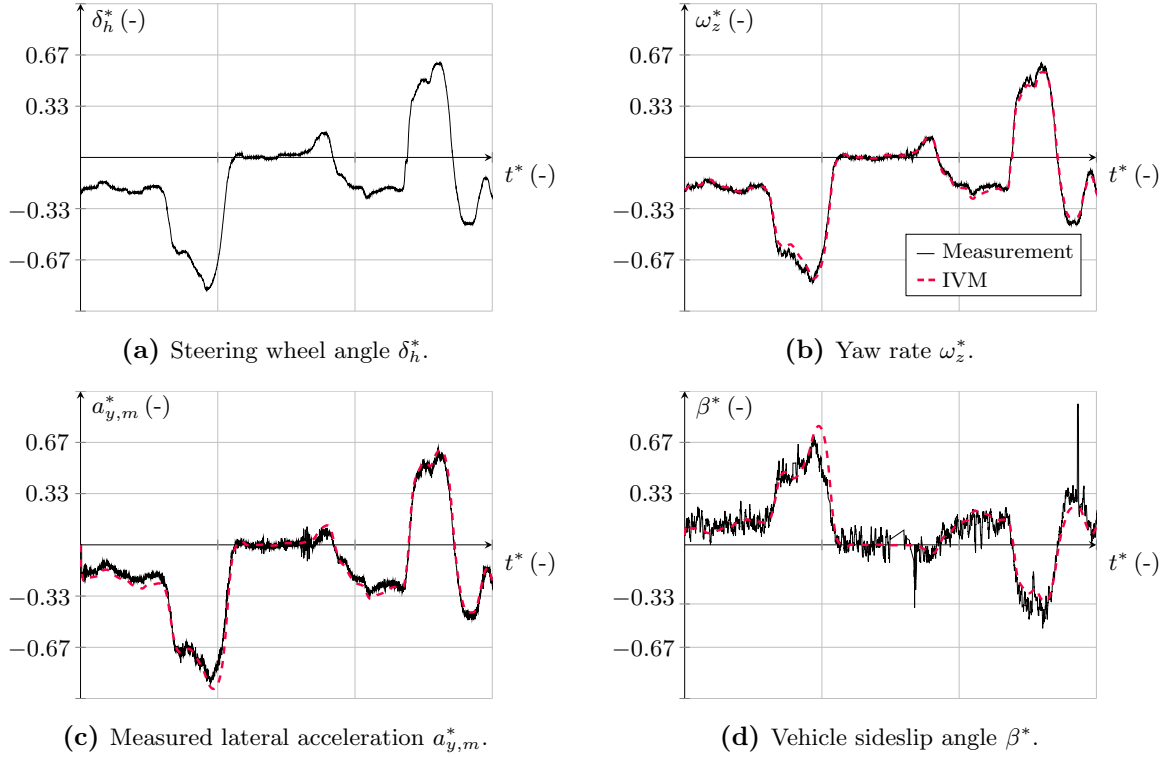


Figure 6.5: Experimental validation of the lateral dynamics. Maneuver: dynamic steering excitation resulting in lateral accelerations $|a_{y,m}| > 4\text{m}\cdot\text{s}^{-2}$. Here, the nonlinear characteristics between force and slip gain importance.

in terms of yaw rate ω_z , measured lateral acceleration $a_{y,m}$ and vehicle sideslip angle β . During this maneuver the vehicle is operated within the proportional area, i.e. the lateral acceleration is $|a_{y,m}| < 4\text{m}\cdot\text{s}^{-2}$.

The estimates of yaw rate and lateral acceleration fit the measurements quite well. Solely the vehicle sideslip angle appears to have some phase lag compared to the measurement. However, due to the small magnitudes of the steering angle and resulting low sideslip angles effects of the sensor noise on the measurements are significant.

The second maneuver is designed such, that the proportional range is left occasionally. Then, the nonlinear characteristics of the slip-force curve gain importance for the estimations of responses, such as yaw rate, sideslip angle etc. Figure 6.5 shows the fitting between measurements and identified vehicle model estimates. Overall, the accuracy of the model shows great potential for further handling maneuvers to be simulated. Now, also the matching between measured and estimated vehicle sideslip angle is within completely acceptable ranges.

Finally, and this is the most surprising result, a vehicle maneuver that is performed highly dynamical with arising lateral accelerations $|a_{y,m}| > 9\text{m}\cdot\text{s}^{-2}$ is considered. Even though for the process of handling evaluation such high lateral acceleration levels are

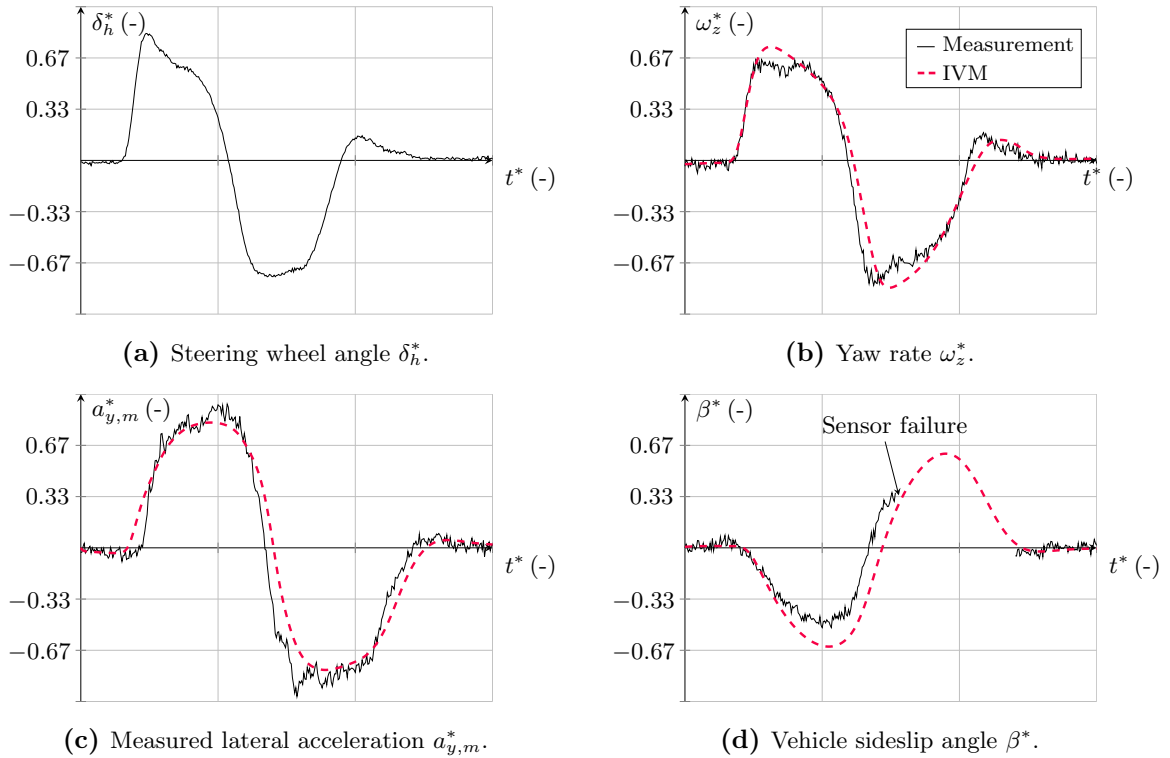


Figure 6.6: Experimental evaluation of the lateral dynamics. Maneuver: highly dynamical single lane change. The maximum of lateral acceleration is $|a_{y,m}| > 9\text{m}\cdot\text{s}^{-2}$.

not of interest, it shows the extrapolation capability that is obtained by the model. The maneuver itself represents a lane change driven at roughly constant velocity. Unfortunately, during the experiment execution the optical velocity sensor failed to gather all measurements.

Figure 6.6 shows the driver's input in terms of steering angle and the resulting vehicle responses. Furthermore, in (d) it illustrates the data gap that arose due to the sensor fault. But, more importantly, the measurements and model predictions are both quantitatively and qualitatively on a good level. From these data points of the sideslip angle measurements illustrated in (d) it can also be concluded that the sideslip predictions seem to be good.

Comments

In summary, the slip-force curve identifying mechanisms have been validated for real-world experiments. The concepts EKF and VSUIO provide good estimates of the cornering stiffness values and in combination with the maximum lateral force identification the parameters of the TM_Simple model can be recovered.

It should be clear from the simple modelling approach of the tire forces (and also vehicle

dynamics) that the actual set of parameters, i.e. B , C and D of front and rear tires is only valid for the road conditions and vehicle configuration at present! In fact, any changes with respect to these require a repetition of the identification process.

6.3 Roll Dynamics (Experimental Vehicle B)

The change of testing platform from experimental vehicle A to B is necessary, as the former is not equipped with a measurement device sensing any roll motion-related physical values, rather than lateral acceleration (in the vehicle-fixed axis system). For vehicle B the angular velocity of the chassis motion around the x-axis is captured and therefore allows application of the observer-based concepts presented in Section 4.2.2. On the one hand side this refers to an EKF and, on the other hand side there is a more sophisticated framework (Figure 4.9 for estimation of roll-related model parameters and also roll angle) that is based on sliding modes. Both concepts regard the measured lateral acceleration as system input and the roll rate as output.

With regards to the design of the maneuver to be performed for the identification, some aspects have already been covered in Section 5.2.4. So, from the perspective of correct process execution the excitation refers to application of constant excitation frequencies that are spread equidistantly over the frequency range of interest. However, this contradicts the aim for time effectiveness and often for practical applications the excitation is designed as a sinusoidal chirp signal with constant amplitude and increasing frequency. Note that, with respect to the employed roll dynamics model the input is lateral acceleration. However, the actuation signal the driver handles refers to steering wheel angle. Consequently, and this can also be seen in Figures 6.7 and 6.8, it is the steering wheel amplitude that is kept constant, rather than lateral acceleration. The latter clearly is a reaction of the vehicle and due to its frequency response characteristics modified by some magnitude, depending on the excitation.

Figure 6.7 shows the experimental results obtained from the EKF mechanism. In (a) the roll exciting lateral acceleration $a_{y,m}$ is depicted and (b), (c) show the vehicle responses as well as their estimates. Focusing on (b) there is a reference roll angle illustrated that needs some further explanation. In-vehicle measurement of the roll angle is not possible for any of the experimental vehicles. But, exploiting the measurements of roll rate ω_x and correcting it by the help of some sophisticated signal processing mechanisms, an *estimate* can be obtained that allows interpretation as *pseudo-reference*. However, there is one obvious difficulty with this estimate, i.e. at the time of the maneuver execution no information on the test track inclinations were available. So, even if the measured roll rate used as basis for the pseudo-reference generation is compensated for slow perturbations due to road disturbances, it does not guarantee the vanishing of all inherent effects due to the road conditions. Hence, rather than using the pseudo-reference roll angle as estimation performance indicator it should only show that the estimated roll angle is not completely off the reference.

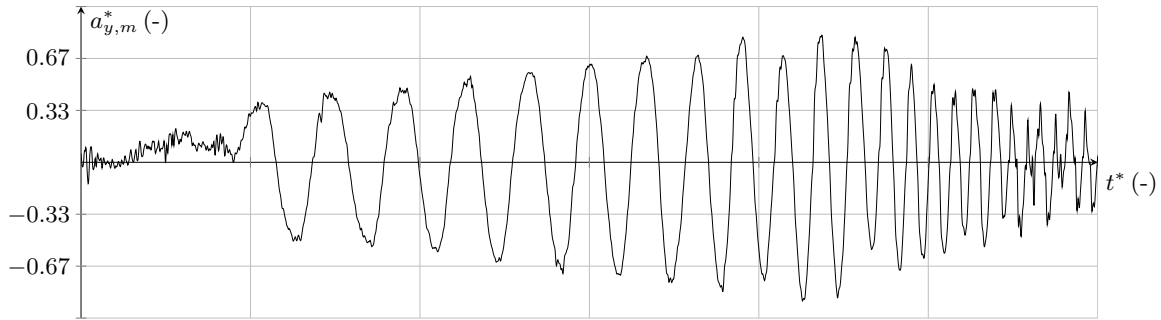
Another interesting aspect depicted in (b), (c), (d) and (e) is the module activation based on certain signals, see Section 5.1 for details. The gray boxes indicate that the EKF takes into account the measurements of roll rate in order to correct the *a priori* estimates of the internal system model. These corrections ensure proper estimates of the parameters, rather than considering only the internal random-walk model.

Figures 6.7(d) and (e) show the estimation of the model parameters. The request for fast convergence of the parameters results in nervous traces of parameter estimates and suggests the use of low-pass filtering. There is, and this backs up the results of Section 5.2.4, some influence of the excitation frequency on the parameter estimates. But, in order to keep the model complexity low, the time series in (d) and (e) might be averaged for the last thirds of the signals to obtain single value estimates.

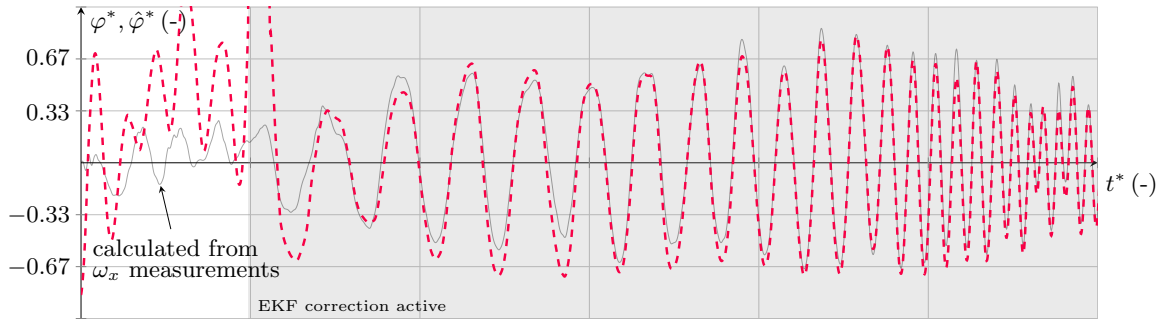
For the variable structure based unknown input observer (VSUIO) the situation is a bit more complex as it involves several submodules that need further analysis. This will be conducted on the basis of the identical measurement data used for the EKF concept. The tuning of the involved mechanisms should follow a certain procedure in order to ensure correctness of the estimates. First, correct time differentiation of the input signal can only be guaranteed, if the RED algorithm is set up correctly. Thereafter, the (adaptive) robust state estimation, finite time parameter estimation and adaptive roll angle observer can be adjusted accordingly, preferably in the order mentioned. Then, the overall state and parameter estimation concept will yield results as presented in Figure 6.8.

For the VSUIO mechanism the time derivative of the input signal, namely the lateral acceleration $a_{y,m}$, needs to be calculated, see $j_{y,m}$ in (b). By using low-pass filtering techniques the inherent high-frequency gain of the differentiator can be counteracted, such that the calculated jerk is not affected heavily by noise. In [LEV98] it is also claimed that the application of the low-pass filter after the differentiator is still the better choice compared to differentiating linear low-pass filter structures. In general, the amount of measurement noise that can be expected from a standard sensor is not considered as a serious problem as showed the simulation-based robustness analysis in [TRH14b]. Therein, the expectable amount of low-cost sensor measurement noise has been intensified by a factor of 3 and still the resulting parameter estimates are close to the results obtained for a standard amount of noise.

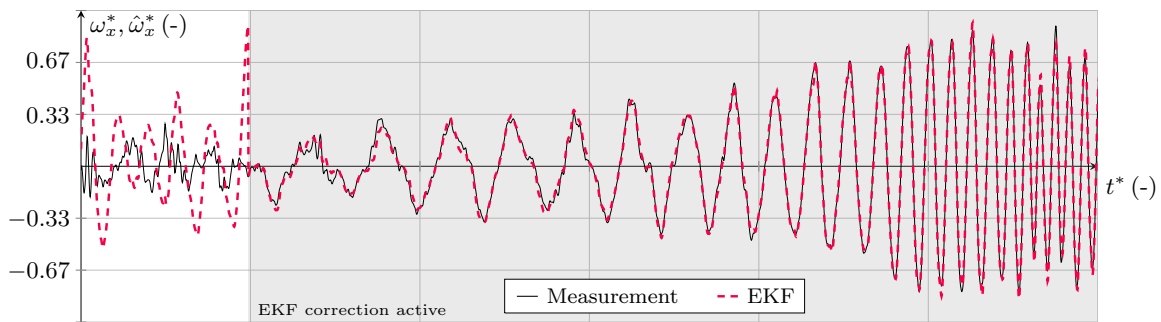
Figure 6.8(c) shows the observation results with respect to the roll rate ω_x . In the background the adaptive character of the observer gain $\tilde{\lambda}_1$ is illustrated. The last subplot of Figure 6.8 deals with the roll acceleration and its estimates by ARSE and FTPE. The recovered uncertain parts of the parameters a_{21} and a_{22} , see (4.84), are depicted in Figure 6.9(a) and (b). The applied low-pass filters actually serve the purpose to smooth the nervous estimates that stem from an aggressively tuned FTPE algorithm, ensuring low convergence times. Extraction of single values can again be obtained by building averages of the time series for approximately the last thirds of the signals.



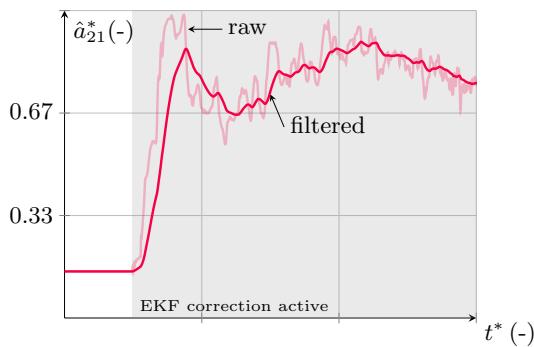
(a) Measured lateral acceleration $a_{y,m}^*$.



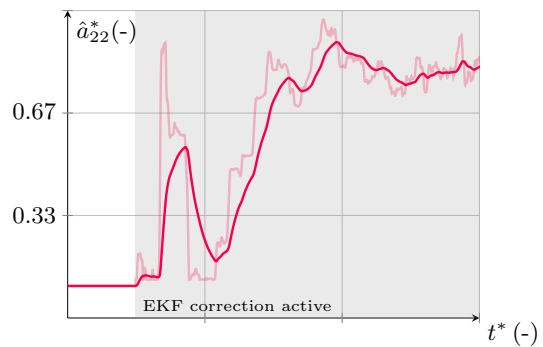
(b) Estimation $\hat{\varphi}^*$ of φ^* .



(c) Estimation $\hat{\omega}_x^*$ of ω_x^* .



(d) Estimation \hat{a}_{21}^* of a_{21}^* .



(e) Estimation \hat{a}_{22}^* of a_{22}^* .

Figure 6.7: Roll dynamics parameter identification - experimental evaluation of the EKF concept. Maneuver: sinusoidal steering with constant steering angle, but varying frequency ($f_{ex} = 0.3 - 2.2\text{Hz}$). The longitudinal velocity is kept constant $v_{vx} \approx 80\text{km}\cdot\text{h}^{-1}$.

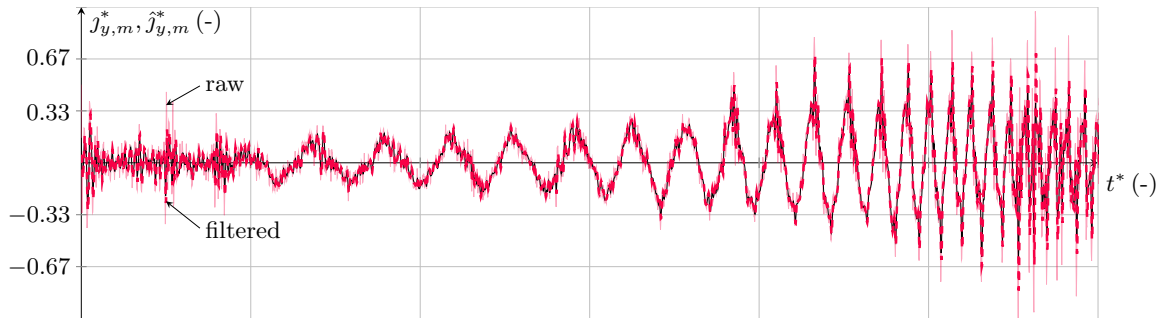
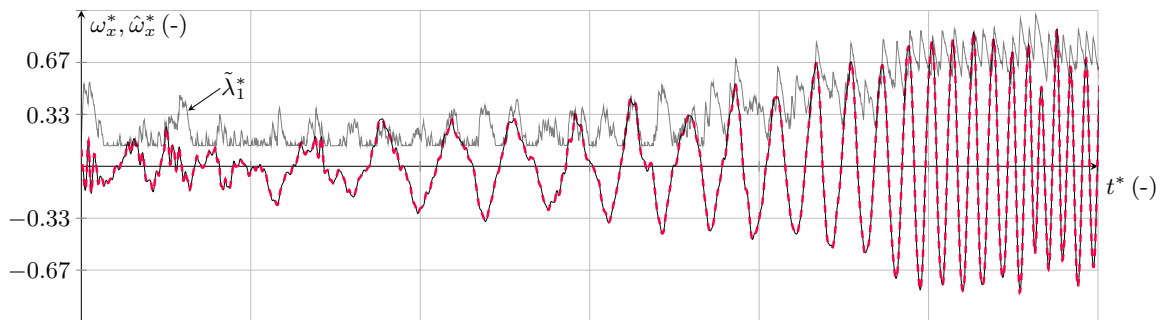
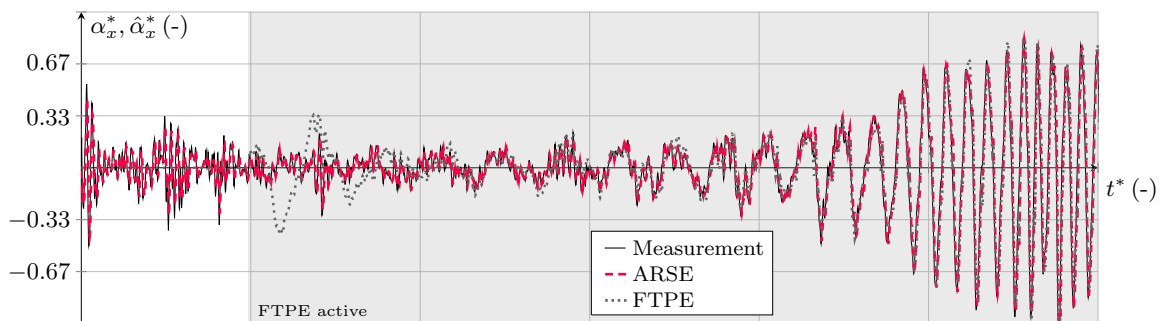
(a) Estimation $\hat{a}_{y,m}^*$ of $a_{y,m}^*$ (RED).(b) Estimation $\hat{J}_{y,m}^*$ of $J_{y,m}^*$ (RED).(c) Estimation $\hat{\omega}_x^*$ of ω_x^* (ARSE).(d) Estimation $\hat{\alpha}_x^*$ of α_x^* (ARSE, FTPE).

Figure 6.8: Roll dynamics parameter identification - experimental evaluation of the VSUIO concept (RED, ARSE and FTPE). Maneuver: as in Figure 6.7.

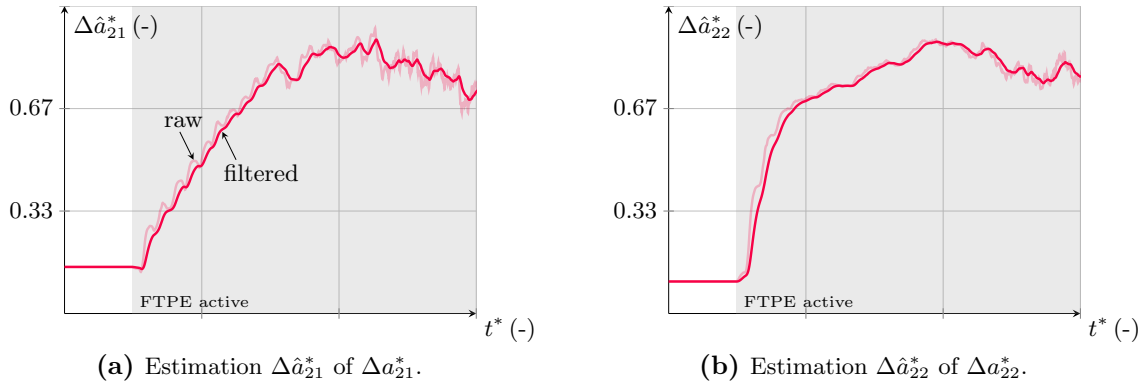


Figure 6.9: Roll dynamics parameter identification - experimental evaluation of the VSUIO concept (FTPE). Maneuver: as in Figure 6.7. The estimated parameters are smoothed by employing a first-order low-pass filtering structure.

Now, exploiting the obtained roll model parameters and forwarding them to the adaptive roll angle observer (ARAO) allows achievement of the results plotted in Figure 6.10. Again, even if the roll angle is shown in (a) that refers to an offline calculated estimate from the measurements of ω_x . Further details on the approximation of the reference roll angle are provided at the beginning of this section.

A Comment on the Sensor Noise of the Lateral Acceleration An often discussed drawback of the VSUIO concept is its requirement for differentiating the system input once in order to increase the relative degree from plant output to unknown input artificially. Argumentation against that procedure often uses the problem of measurement noise on the lateral acceleration signal. From the previous section it should be clear, and this is further underlined by [TRH14b], that the noise is not a severe problem. Moreover, the integration of the algorithms into a stand-alone hardware that embeds user-specific (high-quality) acceleration sensors rebuts the argumentation against the differentiation completely.

Results Performance Assessment

Assessment of the identified roll model parameters comprises two different maneuvers. The first is similar to the parameter identification run and contains sinusoidal steering with constant amplitude, but varying frequency. The range actually varies from $f_{ex} \approx 0.3 - 2.0$ Hz. This validation maneuver is selected in order to demonstrate the estimation performance of the roll angle and rate for various excitation frequencies. Figure 6.11 shows the system input, i.e. measured lateral acceleration $a_{y,m}$ and also the roll rate ω_x (measured and predicted)⁶. Both parameter sets, i.e. of the EKF and VSUIO concepts,

⁶Note that, due to the lack of the angular position measurement it is the velocity that serves as ground truth data.

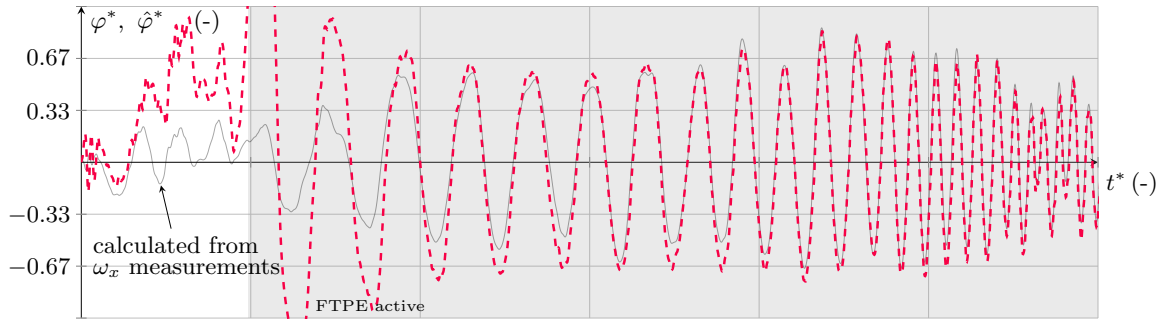
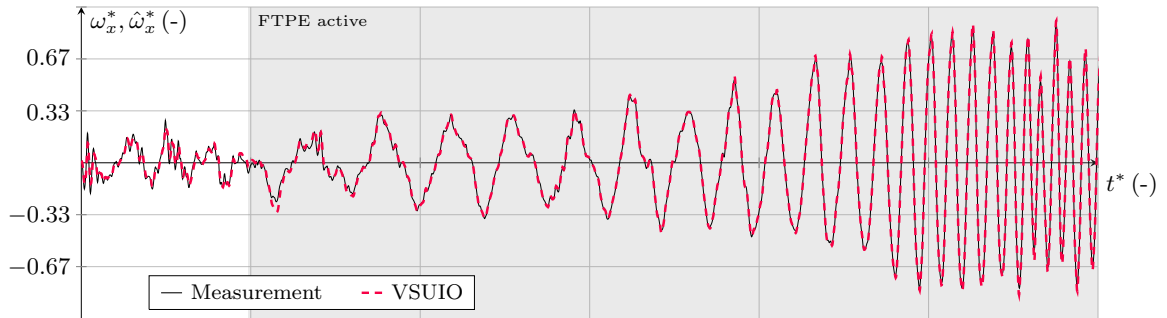
(a) Estimation $\hat{\varphi}^*$ of φ^* (ARAO).(b) Estimation $\hat{\omega}_x^*$ of ω_x^* (ARAO).

Figure 6.10: Roll dynamics parameter identification - experimental evaluation of the VSUIO concept (ARAO). Maneuver: as in Figure 6.7. The illustrated roll angle measurement in (a) is obtained by sophisticated offline signal processing algorithms based on the measured roll rate ω_x .

are employed and the results compared against each other. Obviously, the parameters are quite similar and the results of EKF- and VSUIO-based predictions with respect to the chassis' roll rate can hardly be distinguished. In summary, the fitting between measurements and model predictions looks promising.

The second experiment is more related to a highly dynamical driving maneuver, i.e. an aggressively performed double lane change. Consequently, this second maneuver aims to reveal the potential of the extrapolation capability. In general, for the objective of parameter identification the excitation levels w.r.t. the lateral acceleration are within a range of $|a_{y,m}| \approx 4\text{m}\cdot\text{s}^{-2}$. However, for this maneuver that level is exceeded by far. Considering Figure 6.12, the lateral acceleration $a_{y,m}$ is depicted in (a) and the chassis' response, i.e. roll rate ω_x , in (b). Similarly to the previous experiment, there are no obvious differences between the two parameter sets from EKF and VSUIO. Both show good matching with the measurement data.

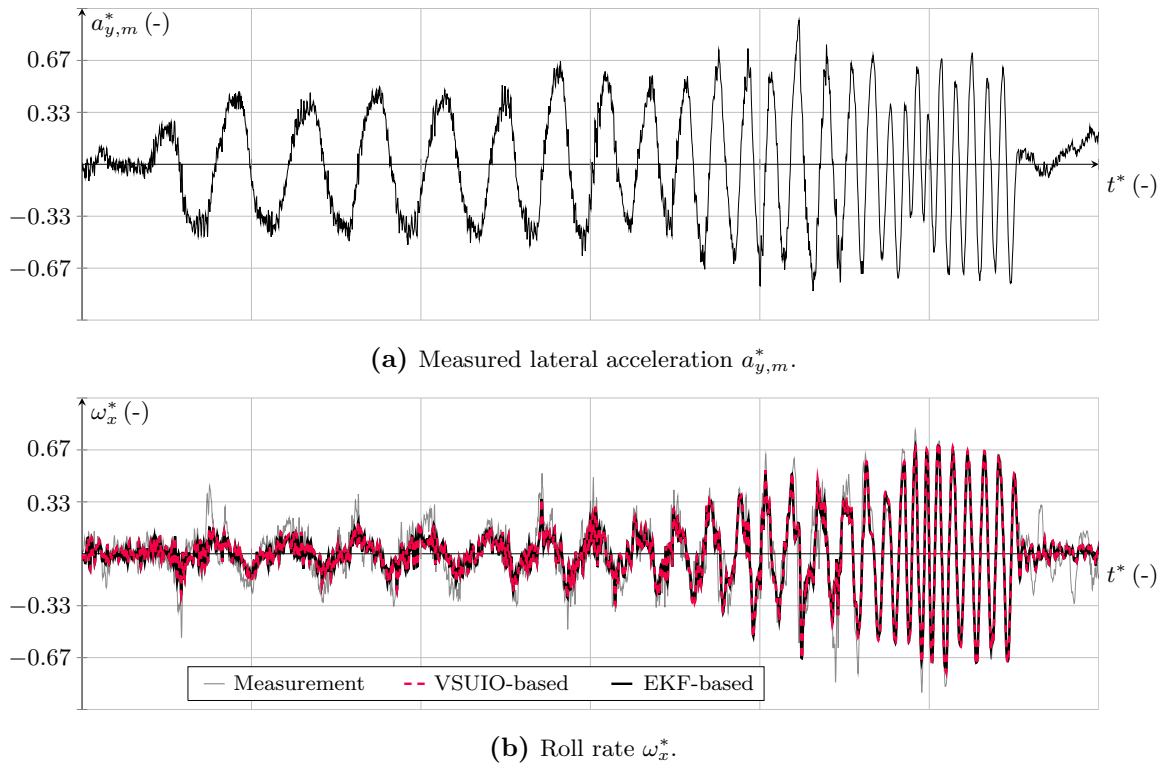


Figure 6.11: Validation of roll model parameter estimation. Maneuver: sinusoidal sweep steering ($f_{ex} = 0.3 - 2.0\text{Hz}$) at const. longitudinal velocity $v_x \approx 80\text{km}\cdot\text{h}^{-1}$. Both parameter sets (VSUIO- and EKF-based) are used and compared against the real measurements.

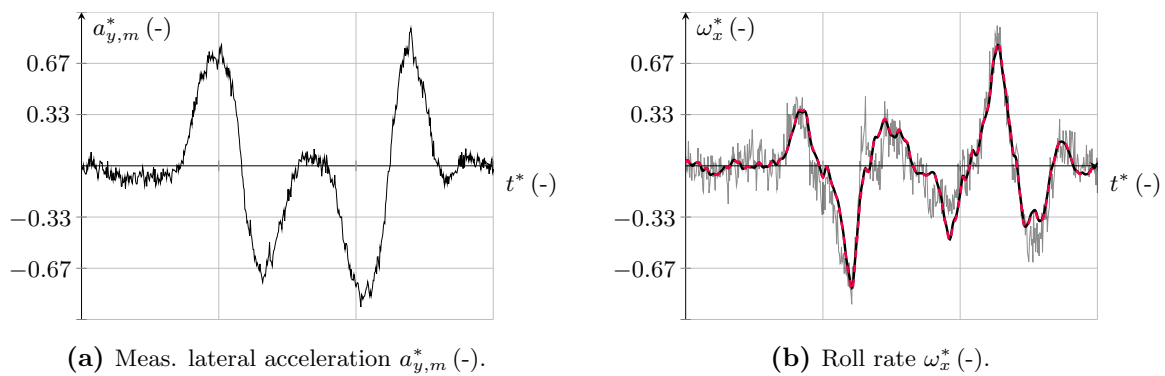


Figure 6.12: Validation of roll model parameter estimation. Maneuver: double lane change (longitudinal velocity $v_x \approx 70\text{km}\cdot\text{h}^{-1}$). Again, model predictions based on both sets of parameters (VSUIO- and EKF-based) are evaluated and compared against the real measurements, i.e. roll rate ω_x .

6.4 Steering Dynamics (EPS Test Bench)

The proposed robust state estimator (Section 4.2.4) will be evaluated on an Electric Power Steering (EPS) test bench available on-site for experimental work. Further details of the test bench setup are provided in Appendix D, Section D.3.

In terms of measured system variables the steering wheel sensor provides an angular position data of δ_h and also a time-derivative. But, the sampling rate of the derivative is ten times lower than that of the position. Consequently, it is also approximated by a robust exact differentiation concept as discussed in Section 4.2.4.II. Measurement of the steering column twist δ_d is obtained from a torque sensor that is available for any standard electric power steering systems, as suggested in e.g. [PFE06]. However, from the torque sensor position in Figures D.2(a) and (b) it is clear that the measured torque value does not coincide with the driver input torque. Therefore, in order to obtain an accurate quantity of the driver torque, an estimation scheme needs to be employed. In contrast, the installation of a measurement steering wheel would also solve that problem, but is cost- and time-intensive. Moreover, the motor torque that serves as plant input can be assumed to be known accurately.

For the evaluation of the observation concept the excitation maneuver consists of two phases, i.e. the steering wheel actuation within the first section is kept moderate (with respect to angular velocity and also steering torque). Within the second phase the steering actions are more dynamical resulting in both, higher angular rates and steering torque. Furthermore, the high transients of the second experiment phase shall reveal the capability of the sliding mode observer to respond rapidly to any changes of the wheel torque. The experimental results are shown in Figure 6.13. In (a) the measured and estimated steering wheel angular velocities are illustrated. Plot (b) shows the estimates of column angular velocity ω_s and its reference (see Appendix D for details). And, (c) visualizes the twisting angles (estimate and reference⁷). The non-measured angular velocity ω_s is estimated accurately, even if the unknown input ζ_2 , see (3.66), acts on the system.

The recovered unknown inputs of steering torque T_h and also wheel torque T_w are shown in Figure 6.14. By using higher-order low-pass filtering techniques the undesired effects of an aggressive observer tuning (allowing for estimation of high transients in a satisfactorily way) and also measurement noise can be reduced. Alternatively, an adaptive gain scheme, e.g. [STP12], can also solve the problem of the aggressive (static) observer gains.

Clearly, recovery of the steering torque in Figure 6.14(a) shows good matching with the reference. Unfortunately, for the EPS test bench the steering torque is not directly measurable. That would require installation of a measurement steering wheel. But, the accurate knowledge of the model parameters and assumption of no model imperfections

⁷The reference can be obtained from the output of the torque sensor.

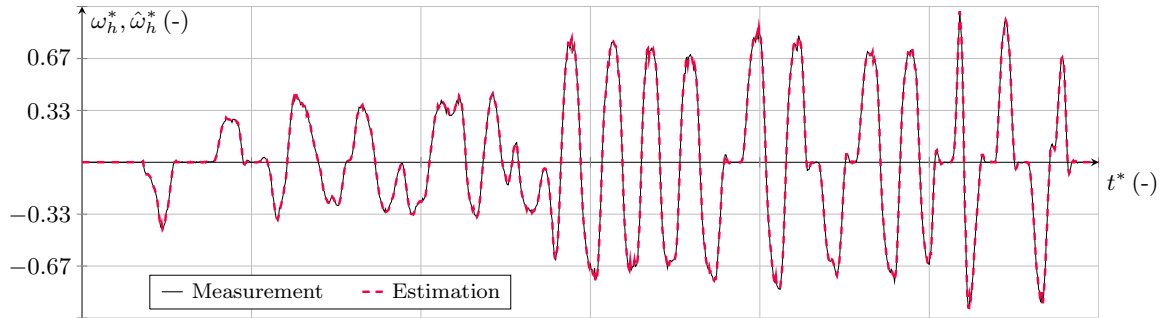
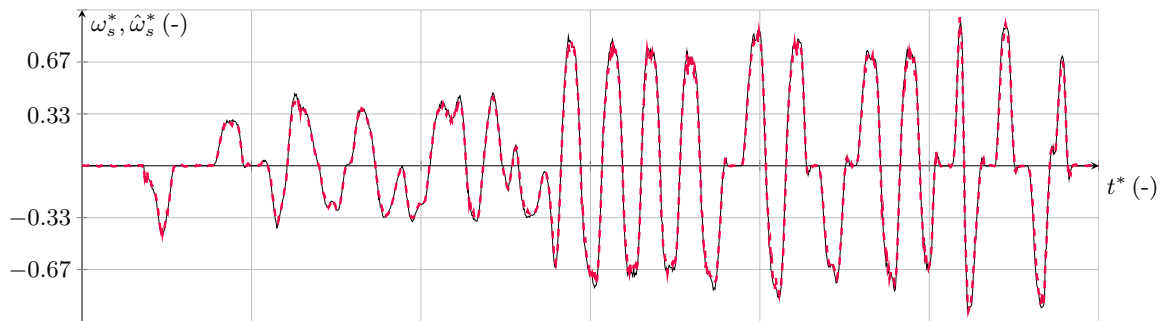
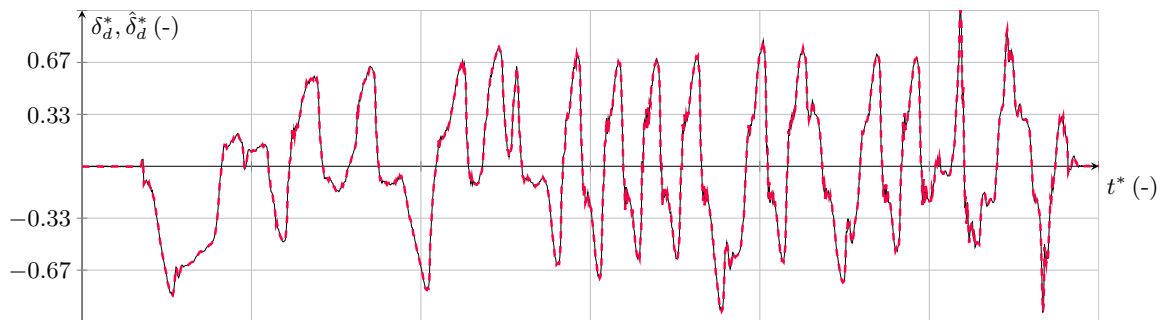
(a) Estimation $\hat{\omega}_h^*$ of ω_h^* .(b) Estimation $\hat{\omega}_s^*$ of ω_s^* .(c) Estimation $\hat{\delta}_d^*$ of δ_d^* .

Figure 6.13: Experimental evaluation of the robust state estimation related to the EPS system. The experiment is performed such, that moderate actuation as well as highly dynamical steering are covered.

w.r.t. to the first channel of (4.123), allow calculation of a reference value for T_h ⁸. Moreover, the arising lateral forces that cause the wheel torque T_w , are implemented for the EPS test bench by spring-damper elements, see also Figure D.2(d). Theoretically, the measurement of those forces could be conducted by installed load cells. In practice

⁸In comparison to the observer-based calculation of the steering torque this method requires the explicit differentiation of ω_h w.r.t. time.

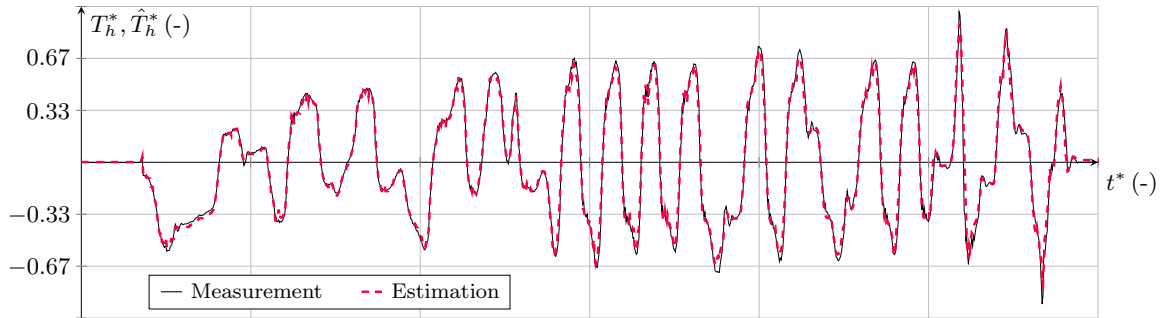
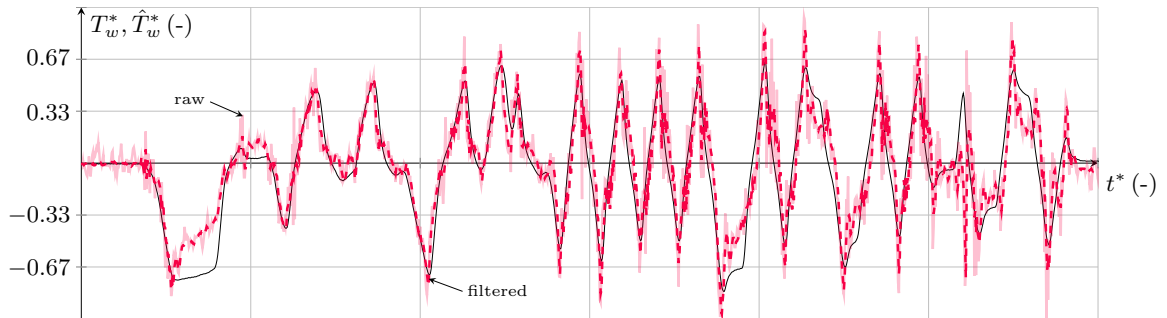
(a) Estimation \hat{T}_h^* of T_h^* .(b) Estimation \hat{T}_w^* of T_w^* .

Figure 6.14: Recovered unknown inputs of steering torque T_h and wheel torque T_w during the experimental evaluation of the EPS-related VSUIO concept.

however, the force quantities are obtained from feeding the displacement measurements of the steering rack into a second-order system that calculates, based on the spring stiffness and damping coefficients, the forces at the steering rack corresponding to the arising wheel torques. In summary, the variable structure unknown input observer has been tested successfully for the robust state estimation of the EPS-related system states, i.e. steering velocity ω_h , column angular rate ω_s and twisting angle of the steering column δ_d . Moreover, the recovered unknown inputs that refer to the steering torque T_h and wheel torque T_w are matching their references well. Even for high slew rates of the wheel torque the estimates are close to the reference values. In terms of further use, the recovered steering wheel torque can be used for the assessment work whereas the wheel torque (or corresponding lateral tire forces) can be exploited for feedback generation of the actual road conditions to the driver.

6.5 Concluding Remarks on the Experimental Evaluation

Three different concepts related to the lateral and roll dynamics as well as steering dynamics have been successfully migrated to an experimental environment. The estimation of the lateral slip-force characteristics based on two individual concepts, namely sliding modes and Extended Kalman filter showed good estimation performance despite the presence of measurement noise and parasitic dynamics. At this point one important advantage of the sliding mode technique shall be mentioned. In contrast to the EKF that is tuned for the noise characteristics, the gain setup of the sliding mode-based observation techniques is completely independent of any noise properties! The obtained parameters were tested using a model to predict vehicle responses in terms of yaw rate etc. and the fitting between estimates and measurements are promising. However, for the sake of integration to the handling evaluation process further extensive testing needs to be conducted. The experimental validation presented in here can only be considered as a first step. In order to draw any conclusions on the prediction accuracy a fully instrumented experimental vehicle would be required that allows identification of the vehicle parameters. Based on these, the comparison between offline simulated and effectively performed handling maneuvers, as in Section 5.3, would reveal the capability of the overall method to be integrated into the model-based assessment process.

Identically, the evaluation of the roll dynamics needs to be pursued further, i.e. validation of the estimation results on the basis of an instrumented experimental vehicle. Only the estimates of the EPS system are evaluated to an extent that reliable reference values are available.

In general, it can be concluded that the first evaluation phase is successfully completed and further experimental validation required.

7

Conclusion

7.1 Thesis Objective and Main Contributions

This thesis aims to extend state of the art work related to the model-based vehicle dynamics assessment process by means of observer-based parameter identification techniques and use of cost-efficient measurement equipment. This is derived from the fact that existing approaches commonly apply the parameter identification algorithms offline and/or do rely on cost-intensive measurement equipment. Offline in that sense refers to the decoupling and sequential execution of the test drive and parameter estimation.

Basically, the presented framework allows online estimation of unknown vehicle model parameters from a set of measurement signals using state observation techniques. Adherence to cost-efficiency is ensured by installation of low-cost sensing devices, e.g. mainly angular rate and translational acceleration sensors. Moreover, due to the estimation of states, related to certain vehicle dynamics, the necessity of measuring all vehicle responses is obsolete.

Herein, a systematic approach for the design of the observation principles has been investigated. Starting with the modelling of the vehicle motion, the obtained results (i.e. the sets of differential equations) are represented by means of the state-space formulation. Sensitivities of state variables are analyzed further with respect to parameter variations. The findings from that analysis provide a theoretical overview of those parameters that influence the system states significantly (when being varied). Consequently, that information can be exploited for the selection of parameters to be estimated. The sensor configuration is not only based on the availability of experimental facilities, but also supported by observability measures providing quantitative information on the observability of the system (w.r.t. different system outputs). The designed observation mechanisms differ from existing approaches e.g. in the fact that angular velocities, rather than positions are used for the estimation corrections. A simulated vehicle dynamics assessment

process shows the potential of the observers to estimate the vehicle parameters and also demonstrates the accuracy of the model predictions exploiting these parameter estimates. Complementary, selected observation structures are evaluated experimentally, taking into account real vehicle measurement data. Moreover, the robust estimation of steering system related states is evaluated on a test bench representing an Electric Power Steering system. Both, the simulations-based and also experimental evaluation runs show satisfactorily accuracy of the state and parameter estimates. However, the experimental evaluation of the concepts needs to be conducted more extensively for different vehicle types and configurations.

The sequel of this section discusses the main contributions of this thesis and also reviews the extent to which the formulated questions of Section 1.3 could be answered.

Tailored vehicle dynamics models for observer design process

The evaluation of the vehicle handling requires accurate information regarding the vehicle motion that is commonly obtained from measurement devices. Theoretically, the motion could also be described by mathematical models, but these rely on numerous parameters. In order to maintain the possibility for online estimation of selected parameters, one is obliged to find trade-off between their number and the resulting model accuracy. Herein, for the longitudinal and lateral vehicle motions as well as the roll and pitch motions of the chassis these models were defined such, that the number of unknown parameters is kept low, allowing for observer-based parameter identification. Nevertheless, as demonstrated in Section 5.3.1 the models describe the vehicle motion accurately enough to provide data for the extraction of objective metrics. These can be further used for the assessment process.

Systematic selection of sensor types based on observability measures

Normally, the measurement setup is well-known *a priori* to the observer design process. For the vehicle dynamics assessment recommendations suggest the types and accuracies of sensors to be installed, e.g. [PHL08]. Herein, the approach is chosen differently, as the selection of sensor types is based on a system analysis exploiting observability measures. The latter do not provide the standard binary results of observability, but return a quantitative feedback how "well" the system is observable (w.r.t. a certain output). In fact, these results coincide with the assumption to install only low-cost measurement devices, e.g. gathering angular velocities.

Systematic selection of vehicle model parameters to be identified

Design of the observer-based parameter identification mechanisms requires the definition of those parameters that need to be estimated. Therefore, two sources of information are considered. First, the efforts are taken into account to obtain certain vehicle parameters from static measurements, e.g. vehicle mass, planar CoG position. Second, a parameter

sensitivity analysis reveals information on the influence of certain parametric changes on the state variables. Merging these sources allows a systematic selection of the parameters to be estimated by observer-based schemes.

Adapted observer design for mechanical systems using velocity measurements

Existing robust observation mechanisms based on (higher-order) sliding modes, e.g. [DFL05] consider a mechanical system, where the forces are perturbed and the position is regarded as system output. Herein, it is not the position, but the velocity that is measured. This minor change of the system output renders the usability of standard observation concepts obsolete due to certain system architectural restrictions, i.e. the relative degree of the output w.r.t. the unknown perturbation does not equal the system order. Therefore, an environment consisting of several peripheral mechanisms, e.g. a robust exact differentiator, is proposed (see Section 4.2.2.II). Generally, it can be deployed to any mechanical system consisting of the same structure as described. Herein, it is used for the estimation of roll dynamics related states and parameters.

Utilization of finite time parameter estimation concepts for an automotive application

Interpretation of parametric uncertainties as an unknown input to a system allows its recovery by sliding mode observers in finite time. Knowledge of the unknown input structure and the availability of the robustly estimated system states allows the identification of the parameters using standard least-squares approaches, e.g. [DFP06, TRH14b]. However, due to an asymptotic convergence the property of a finite parameter estimation error convergence time is lost. Herein, considering the roll dynamics, the employment of the robust exact differentiator (HOSM), adaptive robust estimator (HOSM) and finite time parameter estimation (GSTA) ensures overall finite time convergence.

Moreover, to the best knowledge of the author the finite time parameter estimation algorithm, that is also applied for the estimation of the lateral cornering stiffness, has not yet been used for automotive applications. Its employment allows time-efficient tuning of the observer gains, robust estimates of the parameters and it does not diverge, even if the system is not excited persistently.

Driver feedback of model prediction accuracy

A mechanism is designed and implemented, that compares the predictions of the model using estimated parameters and real measurements. Transformed into a rating the driver receives some information of the actual parameter quality and is able to terminate the test drive, if those rates are within specified limits. This guarantees time- and cost-efficiency.

Evaluation of the concepts in simulations and experiments

The proposed parameter identification concepts have been evaluated in a specific environment including the software package IPG CarMaker[®] and implementations of the mechanisms within MATLAB[®]/Simulink[®]. Comparing the results of standard handling maneuvers, e.g. step input, sinusoidal input simulated in CarMaker[®] and predicted by models using the identified parameters, showed that the latter are within the permissible sensor accuracies for the assessment process. This demonstrates on the one hand side the validity of the proposed observer-based parameter identification concepts and on the other hand the framework's potential to support the model-based vehicle dynamics assessment.

Referring to the specific observer concepts, the lateral slip-force characteristics are recovered from a combination of sliding mode concepts and an Extended Kalman filter. The parameters of the roll dynamics are successfully identified by higher-order sliding mode concepts and an EKF. The redundant implementation of the concepts increases the reliability of the parameter estimates. For the pitch dynamics an EKF is proposed, that provides accurate estimates of the pitch angle. However, the parameter estimates show a high variance (due to the inherent system nonlinearities) and hence are not feasible for offline simulation work. Moreover, the longitudinal dynamics modelling based on multi-layer perceptrons showed good results for the training data, but suffered from robustness issues when being applied to alternative vehicle data. This might come from the lack of extensive measurement data to train the network. Finally, two concepts for estimation of the road disturbances are proposed, that are ideally employed at the very beginning of the process to evaluate the suitability of the test track for evaluation work. Experimental evaluation could only be performed to such an extent that the predictions of an identified vehicle model are compared to certain vehicle measurements. However, the lack of extensive measurement equipment does not allow to draw final conclusions on the accuracy of the methods applied in-vehicle. This step needs to be conducted eventually. Furthermore, a wider spectrum of vehicles (different types and configurations) shall provide additional information on the robustness and accuracy of the concepts.

7.2 Future Work

The sequel of this chapter discusses some suggestions for enhancement of the proposed mechanisms and future perspectives.

Improvement of the model accuracies and extraction of parameters

In order to estimate state variables and model parameters simultaneously (online) the number of parameters to be identified needs to be kept low. This allows slim and robust observer designs. However, from the evaluation work in Chapter 5 some potential improvements were identified. These include integration of a load-dependent pneumatic

trail, as in (2.32) and transient tire force build-up (2.37) also within the underlying observer design models. Furthermore, explicit consideration of the steering elasticity can increase the accuracy of the transformation from steering wheel angle δ_h to wheel angle δ_w .

Another idea not covered explicitly is the extraction of wheel-specific slip-force characteristics, rather than axle-related ones. Exploiting a calculated dynamic load transfer of vertical tire forces allows separation of the axle forces into wheel-specific quantities.

Integration of a steering system model into the offline evaluation procedure

Currently, the steering system is only integrated to that extent in the offline handling evaluation that its influence on the (front) lateral cornering stiffness is considered. In combination with the robust state estimation mechanism allowing recovery of relevant system input torques it should be possible to extract further information from the steering system. That can be used for evaluation work. Currently, a steering system model allowing to predict the arising steering torque offline is completely missing.

Estimation of human perception-related dynamics

The integration of the human perception models allows extraction of objective metrics related to the driver senses, rather than measurement devices. However, the identified model parameters correspond to the vehicle dynamics and do not take into account the human at all. Therefore, a question of research could be to merge these two approaches, i.e. human sense and vehicle dynamics modelling. Employment of observation concepts allows identification of parameters, that can be further used for correlation analysis with subjective ratings, see Chapter 1. Interestingly, these parameters would inherently conserve somehow information of the vehicle as well as driver perception.

Modification of the observer-based parameter identification methods

Essentially, the modifications of the vehicle dynamics models as well as the integration of the human perception into the observer structures require a complete re-design of the observer-based parameter identification techniques. Sticking to the proposed concepts this task deals also with the implementation and evaluation of (4.69), i.e. the finite-time identification of the (uncertain) cornering stiffness and the initial condition of the vehicle sideslip angle. Moreover, it includes the analysis of a sampling time decrease and its effects on the parameter estimates as well as introduction of possible counteractions, e.g. to be found in the field of discrete-time sliding modes [MON02, BJ06].

Vehicle dynamics assessment validation

The focus of this thesis is purely put on the extraction of objective metrics from model-based simulations. The resulting database consists of objective metrics extracted from

standard vehicle responses as well as human perception signals. At the moment strong correlation between subjective ratings and the database (especially the human perception signals) can only be assumed as presented in e.g. [DEC09, SCH10]. Consequently, performing an extensive statistics analysis that reveals further insights between the correlations of subjective and objective ratings remains an open issue.

A

Coordinate Frames

A.1 Coordinate Frames for Vehicle Motion Description

The standard ISO8855 [ISO91] (for german-speaking countries DIN70000) defines the following coordinate systems for description of the vehicle motion. Figures A.1(a)-(e), A.2(a), A.2(b) illustrate these coordinate systems.

Earth-fixed axis system $\mathcal{C}_e = \{\mathcal{O}_e; \mathbf{x}_e, \mathbf{y}_e, \mathbf{z}_e\}$ - A right-hand orthogonal axis system fixed to the earth. The spanned plane of the x_e - and y_e -axes coincides with a horizontal plane, e.g. the road surface. The orthogonal z_e -axis points upwards.

Vehicle-fixed axis system $\mathcal{C}_v = \{\mathcal{O}_v; \mathbf{x}_v, \mathbf{y}_v, \mathbf{z}_v\}$ - A right-hand side orthogonal axis system with origin \mathcal{O}_v at choice (typically chosen as the vehicle's center of gravity). However, alternatively it might be selected as half of the vehicle's wheel in order to be independent of the load. The x_v -axis points forwards (vehicle's longitudinal plane of symmetry), the y_v -axis points to the driver's left-hand side and the z_v -axis points upwards. The orientation of the vehicle-fixed coordinate system with respect to the earth-fixed system is defined by three consecutive rotations about the CARDAN angles 1.) yaw ψ , 2.) pitch θ , 3.) roll φ . Further details are given in [ISO91].

Intermediate axis system $\mathcal{C} = \{\mathcal{O}; \mathbf{x}, \mathbf{y}, \mathbf{z}\}$ - A right-hand side orthogonal axis system in which the xy -plane is parallel to the $x_e y_e$ -plane of the earth-fixed axis system. The x -axis is the projection of the x_v -axis onto the $x_e y_e$ -plane. The z -axis points upwards. The origin \mathcal{O} coincides with \mathcal{O}_v .

Wheel axis system $\mathcal{C}_w = \{\mathcal{O}_w; \mathbf{x}_w, \mathbf{y}_w, \mathbf{z}_w\}$ - A right-hand side orthogonal axis system where the x_w -axis is the intersection of the wheel plane and the $x_e y_e$ -plane with a positive direction forwards. The $x_w y_w$ -plane is parallel to the $x_e y_e$ -plane. And the z_w -axis points upwards. The origin \mathcal{O}_w is in the center of the tire-road contact patch.

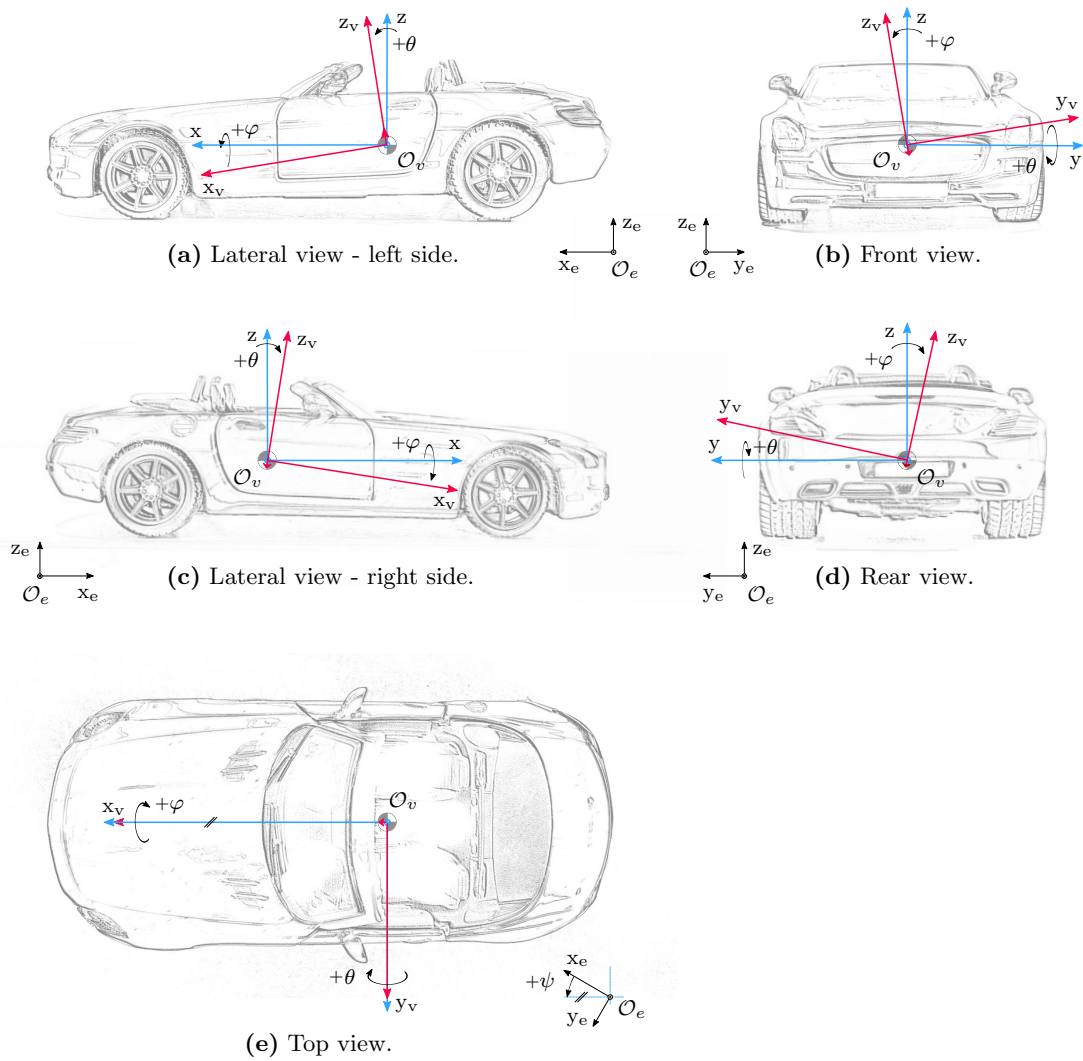
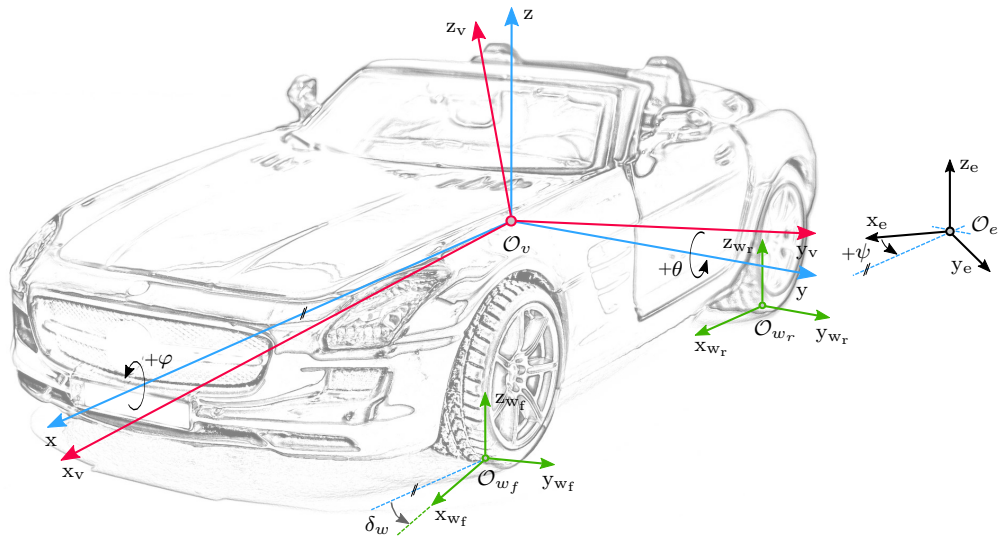
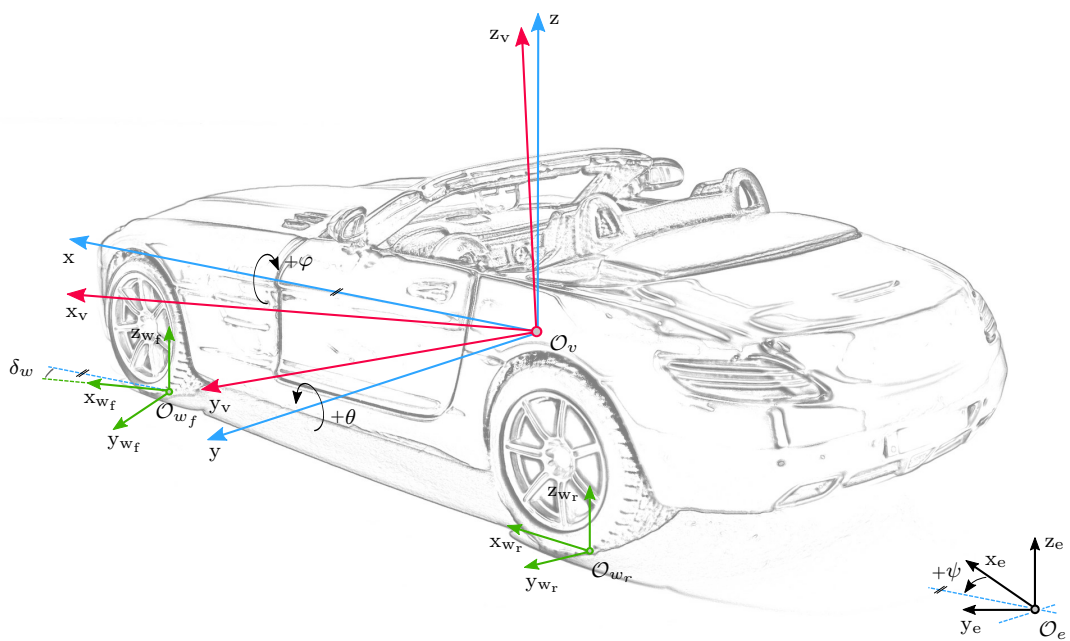


Figure A.1: Axis systems as defined in ISO8855 [ISO91] - lateral, front, rear and top views.



(a) Front View.



(b) Rear View.

Figure A.2: Axis systems as defined in ISO8855 [ISO91] - three-dimensional front and rear views.

B

Mathematical Supplements

B.1 Chapter 3 - Lateral Dynamics 3.2.2.II (Σ_{L2})

II.2 Parameter Sensitivity Analysis The calculation of the matrices $\mathbf{A}_{L2}(t, \boldsymbol{\rho})$ and $\mathbf{B}_{L2}(t, \boldsymbol{\rho})$ is defined in (3.3) and requires partial differentiation of the functions $f_1(\mathbf{x}, \boldsymbol{\rho}, \mathbf{u})$ and $f_2(\mathbf{x}, \boldsymbol{\rho}, \mathbf{u})$, see (3.35), w.r.t. the state vector \mathbf{x} and the parameter vector \mathbf{u} . For brevity the abbreviations

$$\gamma_f := \left[1 + \rho_4^2 \alpha_{f_e}^2 \right] \quad \text{and} \quad \gamma_r := \left[1 + \rho_6^2 \alpha_{r_e}^2 \right],$$

are introduced. The partial derivatives read as

$$\frac{\partial f_1}{\partial x_1} = -\frac{\rho_1^2 \rho_3 \rho_4}{\rho_7 u_2} \gamma_f^{-\frac{1}{2}} \left[1 - \rho_4^2 \alpha_{f_e}^2 \gamma_f^{-1} \right] - \frac{\rho_2^2 \rho_5 \rho_6}{\rho_7 u_2} \gamma_r^{-\frac{1}{2}} \left[1 - \rho_6^2 \alpha_{r_e}^2 \gamma_r^{-1} \right],$$

$$\frac{\partial f_1}{\partial x_2} = -\frac{\rho_1 \rho_3 \rho_4}{\rho_7} \gamma_f^{-\frac{1}{2}} \left[1 - \rho_4^2 \alpha_{f_e}^2 \gamma_f^{-1} \right] + \frac{\rho_2 \rho_5 \rho_6}{\rho_7} \gamma_r^{-\frac{1}{2}} \left[1 - \rho_6^2 \alpha_{r_e}^2 \gamma_r^{-1} \right],$$

$$\frac{\partial f_2}{\partial x_1} = -\frac{\rho_1 \rho_3 \rho_4}{\rho_8 u_2^2} \gamma_f^{-\frac{1}{2}} \left[1 - \rho_4^2 \alpha_{f_e}^2 \gamma_f^{-1} \right] + \frac{\rho_2 \rho_5 \rho_6}{\rho_8 u_2^2} \gamma_r^{-\frac{1}{2}} \left[1 - \rho_6^2 \alpha_{r_e}^2 \gamma_r^{-1} \right] - 1,$$

$$\frac{\partial f_2}{\partial x_2} = -\frac{\rho_3 \rho_4}{\rho_8 u_2} \gamma_f^{-\frac{1}{2}} \left[1 - \rho_4^2 \alpha_{f_e}^2 \gamma_f^{-1} \right] - \frac{\rho_5 \rho_6}{\rho_8 u_2} \gamma_r^{-\frac{1}{2}} \left[1 - \rho_6^2 \alpha_{r_e}^2 \gamma_r^{-1} \right].$$

Furthermore, the derivatives of $f_1(\mathbf{x}, \boldsymbol{\rho}, \mathbf{u})$ w.r.t. to $\boldsymbol{\rho}$ yield

$$\frac{\partial f_1}{\partial \rho_1} = \frac{\rho_3 \rho_4 \alpha_{f_e}}{\rho_7} \gamma_f^{-\frac{1}{2}} + \left[-\frac{\rho_1 \rho_3 \rho_4}{\rho_7 u_2} \gamma_f^{-\frac{1}{2}} + \frac{\rho_1 \rho_3 \rho_4^3 \alpha_{f_e}^2}{\rho_7 u_2} \gamma_f^{-\frac{3}{2}} \right] x_1,$$

$$\frac{\partial f_1}{\partial \rho_2} = -\frac{\rho_5 \rho_6 \alpha_{r_e}}{\rho_7} \gamma_r^{-\frac{1}{2}} + \left[-\frac{\rho_2 \rho_5 \rho_6}{\rho_7 u_2} \gamma_r^{-\frac{1}{2}} + \frac{\rho_2 \rho_5 \rho_6^3 \alpha_{r_e}^2}{\rho_7 u_2} \gamma_r^{-\frac{3}{2}} \right] x_1,$$

$$\frac{\partial f_1}{\partial \rho_3} = \frac{\rho_1 \rho_4 \alpha_{f_e}}{\rho_7} \gamma_f^{-\frac{1}{2}},$$

$$\frac{\partial f_1}{\partial \rho_4} = \frac{\rho_1 \rho_3 \alpha_{f_e}}{\rho_7} \gamma_f^{-\frac{1}{2}} - \frac{\rho_1 \rho_3 \rho_4^2 \alpha_{f_e}^3}{\rho_7} \gamma_f^{-\frac{3}{2}},$$

$$\frac{\partial f_1}{\partial \rho_5} = -\frac{\rho_2 \rho_6 \alpha_{r_e}}{\rho_7} \gamma_r^{-\frac{1}{2}},$$

$$\frac{\partial f_1}{\partial \rho_6} = -\frac{\rho_2 \rho_5 \alpha_{r_e}}{\rho_7} \gamma_r^{-\frac{1}{2}} + \frac{\rho_2 \rho_5 \rho_6^2 \alpha_{r_e}^3}{\rho_7} \gamma_r^{-\frac{3}{2}},$$

$$\frac{\partial f_1}{\partial \rho_7} = -\frac{\rho_1 \rho_3 \rho_4 \alpha_{f_e}}{\rho_7^2} \gamma_f^{-\frac{1}{2}} + \frac{\rho_2 \rho_5 \rho_6 \alpha_{r_e}}{\rho_7^2} \gamma_r^{-\frac{1}{2}},$$

$$\frac{\partial f_1}{\partial \rho_8} = 0,$$

$$\frac{\partial f_1}{\partial \rho_9} = \left[-\frac{\rho_1 \rho_3 \rho_4}{\rho_7 u_2} \gamma_f^{-\frac{1}{2}} + \frac{\rho_1 \rho_3 \rho_4^3 \alpha_{f_e}^2}{\rho_7 u_2} \gamma_f^{-\frac{3}{2}} + \frac{\rho_2 \rho_5 \rho_6}{\rho_7 u_2} \gamma_r^{-\frac{1}{2}} - \frac{\rho_2 \rho_5 \rho_6^3 \alpha_{r_e}^2}{\rho_7 u_2} \gamma_r^{-\frac{3}{2}} \right] u_3,$$

and finally the derivatives of $f_2(\mathbf{x}, \boldsymbol{\rho}, \mathbf{u})$ w.r.t. $\boldsymbol{\rho}$ are given by

$$\frac{\partial f_2}{\partial \rho_1} = \left[-\frac{\rho_3 \rho_4}{\rho_8 u_2^2} \gamma_f^{-\frac{1}{2}} + \frac{\rho_3 \rho_4^3 \alpha_{f_e}^2}{\rho_8 u_2^2} \gamma_f^{-\frac{3}{2}} \right] x_1,$$

$$\frac{\partial f_2}{\partial \rho_2} = \left[\frac{\rho_5 \rho_6}{\rho_8 u_2^2} \gamma_r^{-\frac{1}{2}} - \frac{\rho_5 \rho_6^3 \alpha_{r_e}^2}{\rho_8 u_2^2} \gamma_r^{-\frac{3}{2}} \right] x_1,$$

$$\frac{\partial f_2}{\partial \rho_3} = \frac{\rho_4 \alpha_{f_e}}{\rho_8 u_2} \gamma_f^{-\frac{1}{2}},$$

$$\frac{\partial f_2}{\partial \rho_4} = \frac{\rho_3 \alpha_{f_e}}{\rho_8 u_2} \gamma_f^{-\frac{1}{2}} - \frac{\rho_3 \rho_4^2 \alpha_{f_e}^3}{\rho_8 u_2} \gamma_f^{-\frac{3}{2}},$$

$$\frac{\partial f_2}{\partial \rho_5} = \frac{\rho_6 \alpha_{r_e}}{\rho_8 u_2} \gamma_r^{-\frac{1}{2}},$$

$$\frac{\partial f_2}{\partial \rho_6} = \frac{\rho_5 \alpha_{r_e}}{\rho_8 u_2} \gamma_r^{-\frac{1}{2}} - \frac{\rho_5 \rho_6^2 \alpha_{r_e}^3}{\rho_8 u_2} \gamma_r^{-\frac{3}{2}},$$

$$\frac{\partial f_2}{\partial \rho_7} = 0,$$

$$\frac{\partial f_2}{\partial \rho_8} = -\frac{\rho_3 \rho_4 \alpha_{f_e}}{\rho_8^2 u_2} \gamma_f^{-\frac{1}{2}} - \frac{\rho_5 \rho_6 \alpha_{r_e}}{\rho_8^2 u_2} \gamma_r^{-\frac{1}{2}},$$

$$\frac{\partial f_2}{\partial \rho_9} = \left[-\frac{\rho_3 \rho_4}{\rho_8 u_2^2} \gamma_f^{-\frac{1}{2}} + \frac{\rho_3 \rho_4^3 \alpha_{f_e}^2}{\rho_8 u_2^2} \gamma_f^{-\frac{3}{2}} - \frac{\rho_5 \rho_6}{\rho_8 u_2^2} \gamma_r^{-\frac{1}{2}} + \frac{\rho_5 \rho_6^3 \alpha_{r_e}^2}{\rho_8 u_2} \gamma_r^{-\frac{3}{2}} \right] u_3.$$

B.2 Chapter 3 - Lateral Dynamics 3.2.2.III (Σ_{L3})

III.2 Parameter Sensitivity Analysis The elements of the matrices $\mathbf{A}_{L3}(t, \boldsymbol{\rho})$ and $\mathbf{B}_{L3}(t, \boldsymbol{\rho})$ result from the partial derivatives of the functions $\mathbf{f}_1(\mathbf{x}, \boldsymbol{\rho}, \mathbf{u})$ and $\mathbf{f}_2(\mathbf{x}, \boldsymbol{\rho}, \mathbf{u})$, see (3.42), w.r.t. \mathbf{x} and $\boldsymbol{\rho}$. The following abbreviations are used to increase readability

$$\tau_{2_f} := \sin \left(\rho_4 - \rho_4 e^{-\frac{|\alpha_{f_e}|}{\rho_5}} \right) [\alpha_{f_e}]^0, \quad \tau_{2_r} := \sin \left(\rho_7 - \rho_7 e^{-\frac{|\alpha_{r_e}|}{\rho_8}} \right) [\alpha_{r_e}]^0,$$

with

$$\alpha_{f_e} = u_1 - x_2 - \frac{\rho_1 x_1}{u_2} - \frac{\rho_{11} u_3}{u_2}, \quad \alpha_{r_e} = -x_2 + \frac{\rho_2 x_1}{u_2} - \frac{\rho_{11} u_3}{u_2}.$$

Then, the partial derivatives of $\mathbf{f}_1(\mathbf{x}, \boldsymbol{\rho}, \mathbf{u})$ and $\mathbf{f}_2(\mathbf{x}, \boldsymbol{\rho}, \mathbf{u})$ w.r.t. $\boldsymbol{\rho}$ read as

$$\frac{\partial f_1}{\partial \rho_1} = \frac{\rho_3}{\rho_9} \tau_{2f} + \frac{\rho_1 \rho_3}{\rho_9} \left[-\frac{\rho_4}{\rho_5 u_2} x_1 \xi_f \right],$$

$$\frac{\partial f_1}{\partial \rho_2} = -\frac{\rho_6}{\rho_9} \tau_{2r} + \frac{\rho_1 \rho_3}{\rho_9} \left[\frac{\rho_7}{\rho_8 u_2} x_1 \xi_r \right],$$

$$\frac{\partial f_1}{\partial \rho_3} = \frac{\rho_1}{\rho_9} \tau_{2f},$$

$$\frac{\partial f_1}{\partial \rho_4} = \frac{\rho_1 \rho_3}{\rho_9} \left[1 - e^{-\frac{|\alpha_{fe}|}{\rho_5}} \right] \cos \left(\rho_4 - \rho_4 e^{-\frac{|\alpha_{fe}|}{\rho_5}} \right) [\alpha_{fe}]^0,$$

$$\frac{\partial f_1}{\partial \rho_5} = \frac{\rho_1 \rho_3}{\rho_9} \left[-\frac{\rho_4}{\rho_5^2} \alpha_{fe} \xi_f \right],$$

$$\frac{\partial f_1}{\partial \rho_6} = \frac{\rho_2}{\rho_9} \tau_{2r},$$

$$\frac{\partial f_1}{\partial \rho_7} = -\frac{\rho_2 \rho_6}{\rho_9} \left[1 - e^{-\frac{|\alpha_{re}|}{\rho_8}} \right] \cos \left(\rho_7 - \rho_7 e^{-\frac{|\alpha_{re}|}{\rho_8}} \right) [\alpha_{re}]^0,$$

$$\frac{\partial f_1}{\partial \rho_8} = \frac{\rho_2 \rho_6}{\rho_9} \left[\frac{\rho_7}{\rho_8^2} \alpha_{re} \xi_r \right],$$

$$\frac{\partial f_1}{\partial \rho_9} = -\frac{\rho_1 \rho_3}{\rho_9^2} \tau_{2f} + \frac{\rho_2 \rho_6}{\rho_9^2} \tau_{2r},$$

$$\frac{\partial f_1}{\partial \rho_{10}} = 0,$$

$$\frac{\partial f_1}{\partial \rho_{11}} = -\frac{\rho_1 \rho_3 \rho_4 u_3}{\rho_5 \rho_9 u_2} \xi_f + \frac{\rho_2 \rho_6 \rho_7 u_3}{\rho_8 \rho_9 u_2} \xi_r,$$

$$\frac{\partial f_2}{\partial \rho_1} = \frac{\rho_3}{\rho_{10} u_2} \left[-\frac{\rho_4}{\rho_5 u_2} x_1 \xi_f \right],$$

$$\frac{\partial f_2}{\partial \rho_2} = \frac{\rho_6}{\rho_{10} u_2} \left[\frac{\rho_7}{\rho_8 u_2} x_1 \xi_r \right],$$

$$\frac{\partial f_2}{\partial \rho_3} = \frac{1}{\rho_{10} u_2} \tau_{2f},$$

$$\frac{\partial f_2}{\partial \rho_4} = \frac{\rho_3}{\rho_{10} u_2} \left[1 - e^{-\frac{|\alpha_{fe}|}{\rho_5}} \right] \cos \left(\rho_4 - \rho_4 e^{-\frac{|\alpha_{fe}|}{\rho_5}} \right) [\alpha_{fe}]^0,$$

$$\frac{\partial f_2}{\partial \rho_5} = \frac{\rho_3}{\rho_{10} u_2} \left[-\frac{\rho_4}{\rho_5^2} \alpha_{fe} \xi_f \right],$$

$$\frac{\partial f_2}{\partial \rho_6} = \frac{1}{\rho_{10} u_2} \tau_{2r},$$

$$\frac{\partial f_2}{\partial \rho_7} = \frac{\rho_6}{\rho_{10} u_2} \left[1 - e^{-\frac{|\alpha_{re}|}{\rho_8}} \right] \cos \left(\rho_7 - \rho_7 e^{-\frac{|\alpha_{re}|}{\rho_8}} \right) [\alpha_{re}]^0,$$

$$\frac{\partial f_2}{\partial \rho_8} = \frac{\rho_6}{\rho_{10} u_2} \left[-\frac{\rho_7}{\rho_8^2} \alpha_{re} \xi_r \right],$$

$$\frac{\partial f_2}{\partial \rho_9} = 0,$$

$$\frac{\partial f_2}{\partial \rho_{10}} = -\frac{\rho_3}{\rho_{10}^2 u_2} \tau_{2f} - \frac{\rho_6}{\rho_{10}^2 u_2} \tau_{2r},$$

$$\frac{\partial f_2}{\partial \rho_{11}} = -\frac{\rho_3 \rho_4 u_3}{\rho_5 \rho_{10} u_2^2} \xi_f + -\frac{\rho_6 \rho_7 u_3}{\rho_8 \rho_{10} u_2^2} \xi_r.$$

Furthermore, the partial derivatives of $\mathbf{f}_1(\mathbf{x}, \boldsymbol{\rho}, \mathbf{u})$ and $\mathbf{f}_2(\mathbf{x}, \boldsymbol{\rho}, \mathbf{u})$ w.r.t. \mathbf{x} result as

$$\frac{\partial f_1}{\partial x_1} = -\frac{\rho_1 \rho_3}{\rho_9} \left[\frac{\rho_1 \rho_4}{\rho_5 u_2} \xi_f \right] - \frac{\rho_2 \rho_6}{\rho_9} \left[\frac{\rho_2 \rho_7}{\rho_8 u_2} \xi_r \right],$$

$$\frac{\partial f_1}{\partial x_2} = -\frac{\rho_1 \rho_3}{\rho_9} \left[\frac{\rho_4}{\rho_5} \xi_f \right] + \frac{\rho_2 \rho_6}{\rho_9} \left[\frac{\rho_7}{\rho_8} \xi_r \right],$$

$$\frac{\partial f_2}{\partial x_1} = -\frac{\rho_3}{\rho_{10} u_2} \left[\frac{\rho_1 \rho_4}{\rho_5 u_2} \xi_f \right] + \frac{\rho_6}{\rho_{10} u_2} \left[\frac{\rho_2 \rho_7}{\rho_8 u_2} \xi_r \right] - 1,$$

$$\frac{\partial f_2}{\partial x_2} = -\frac{\rho_3}{\rho_{10} u_2} \left[\frac{\rho_4}{\rho_5} \xi_f \right] - \frac{\rho_6}{\rho_{10} u_2} \left[\frac{\rho_7}{\rho_8} \xi_r \right],$$

with

$$\xi_f := e^{-\frac{|\alpha_{fe}|}{\rho_5}} \cos \left(\rho_4 - \rho_4 e^{-\frac{|\alpha_{fe}|}{\rho_5}} \right) \quad \text{and} \quad \xi_r := e^{-\frac{|\alpha_{re}|}{\rho_8}} \cos \left(\rho_7 - \rho_7 e^{-\frac{|\alpha_{re}|}{\rho_8}} \right).$$

B.3 Chapter 4 - Roll Dynamics 4.2.2.I (EKF)

Observability Analysis System (4.79), (4.80) is formulated as input-affine system, i.e.

$$\frac{d\mathbf{x}}{dt} = \mathbf{a}(\mathbf{x}) + \mathbf{b}(\mathbf{x})u, \quad (\text{B.3})$$

$$y = h(\mathbf{x}) \quad (\text{B.4})$$

with $\mathbf{a}(\mathbf{x}) : D_a \subseteq \mathbb{R}^{n+k} \rightarrow \mathbb{R}^{n+k}$ and $\mathbf{b}(\mathbf{x}) : D_b \subseteq \mathbb{R}^{n+k} \rightarrow \mathbb{R}^{n+k}$. Note that for brevity the subscript "a" is omitted, so that vector \mathbf{x} refers to the augmented state vector \mathbf{x}_a as in Section 4.2.2.I. Then for (4.79) a diffeomorphism can be defined as

$$\Phi(\mathbf{x}, \tilde{\mathbf{u}}) := [\Phi_1(\mathbf{x}, \tilde{\mathbf{u}}) \quad \Phi_2(\mathbf{x}, \tilde{\mathbf{u}}) \quad \Phi_3(\mathbf{x}, \tilde{\mathbf{u}}) \quad \Phi_4(\mathbf{x}, \tilde{\mathbf{u}})]^T, \quad (\text{B.5})$$

with the elements Φ_i , $i=1..4$, i.e.

$$\Phi_1(\mathbf{x}, \tilde{\mathbf{u}}) = h(\mathbf{x}), \quad (\text{B.6a})$$

$$\Phi_2(\mathbf{x}, \tilde{\mathbf{u}}) = L_a h + L_b c u, \quad (\text{B.6b})$$

$$\Phi_3(\mathbf{x}, \tilde{\mathbf{u}}) = L_a^2 c + L_b L_a c u + L_a L_b c u + L_b^2 c u + L_b c \dot{u}, \quad (\text{B.6c})$$

$$\begin{aligned} \Phi_4(\mathbf{x}, \tilde{\mathbf{u}}) = & L_a^3 c + 2 L_b L_a^2 c u + L_a^2 L_b c u + L_a L_b^2 c u + L_a L_b^2 c u^2 + \\ & + L_b^2 L_a c u^2 + L_b^3 c u^2 + L_a L_b c \dot{u} + L_b L_a c \dot{u} + L_a L_b c \dot{u} + \\ & + L_b^2 c \dot{u} + L_b^2 c u \dot{u} + L_b c \ddot{u}, \end{aligned} \quad (\text{B.6d})$$

and the vector $\tilde{\mathbf{u}} := [u \quad \dot{u} \quad \ddot{u}]$. The observability matrix \mathbf{Q}_L is defined as the Jacobian matrix of Φ , i.e.

$$\mathbf{Q}_L(\mathbf{x}, \tilde{\mathbf{u}}) := \frac{\partial \Phi(\mathbf{x}, \tilde{\mathbf{u}})}{\partial \mathbf{x}} = \begin{bmatrix} \frac{\partial \Phi_1(\mathbf{x}, \tilde{\mathbf{u}})}{\partial \mathbf{x}} \\ \frac{\partial \Phi_2(\mathbf{x}, \tilde{\mathbf{u}})}{\partial \mathbf{x}} \\ \frac{\partial \Phi_3(\mathbf{x}, \tilde{\mathbf{u}})}{\partial \mathbf{x}} \\ \frac{\partial \Phi_4(\mathbf{x}, \tilde{\mathbf{u}})}{\partial \mathbf{x}} \end{bmatrix}. \quad (\text{B.7})$$

In contrast to Section 4.2.2.I matrix \mathbf{Q}_L operates on the arguments \mathbf{x} and $\tilde{\mathbf{u}}$ rather than time t . The reason is as follows: if the state trajectories and input values are known *a priori* of the observability analysis they can be inserted into the Jacobian matrix and then it reduces to a time-dependent matrix. However, if they are not known *a priori*,

and observability is evaluated in real-time, then the arguments are state vector \mathbf{x} and vector of input (derivatives) $\tilde{\mathbf{u}}$.

Reconsidering again system description (4.80) the observability matrix can be calculated as

$$\mathbf{Q}_L(\mathbf{x}, \tilde{\mathbf{u}}) = \begin{bmatrix} 0 & 1 & 0 & 0 \\ -x_3 & -x_4 & -x_1 & -x_2 \\ x_3 x_4 & x_4^2 - x_3 & \frac{\partial \Phi_3}{\partial x_3} & \frac{\partial \Phi_3}{\partial x_4} \\ \frac{\partial \Phi_4}{\partial x_1} & \frac{\partial \Phi_4}{\partial x_2} & \frac{\partial \Phi_4}{\partial x_3} & \frac{\partial \Phi_4}{\partial x_4} \end{bmatrix}, \quad (\text{B.8})$$

with the partial derivatives

$$\frac{\partial \Phi_3}{\partial x_3} = x_1 x_4 - x_2, \quad (\text{B.9a})$$

$$\frac{\partial \Phi_3}{\partial x_4} = x_1 x_3 + 2 x_2 x_4 - k u, \quad (\text{B.9b})$$

$$\frac{\partial \Phi_4}{\partial x_1} = -x_3 x_4^2 + x_3^2, \quad (\text{B.9c})$$

$$\frac{\partial \Phi_4}{\partial x_2} = -x_4^3 + 2 x_3 x_4, \quad (\text{B.9d})$$

$$\frac{\partial \Phi_4}{\partial x_3} = -x_1 x_4^2 + 2 x_1 x_3 - k u + 2 x_2 x_4, \quad (\text{B.9e})$$

$$\frac{\partial \Phi_4}{\partial x_4} = 2 k u x_4 - 2 x_1 x_3 x_4 - 3 x_2 x_4^2 + 2 x_2 x_3 - k \dot{u}. \quad (\text{B.9f})$$

Matrix \mathbf{Q}_L is not full rank if the following condition holds

$$\frac{du}{dt} = \frac{k^2 u^2 - 2 k u x_1 x_3 - k u x_2 x_4 + x_1^2 x_3^2 + x_1 x_2 x_3 x_4 + x_2^2 x_3}{k x_2}, \quad (\text{B.10})$$

which means that system (4.79) is locally observable, if (B.10) does not hold.

C

Objective Metrics of Standardized Test Maneuvers

In the following the objective metrics extracted from vehicle responses gathered from standardized excitation maneuvers are listed. The standards ISO7401 [ISO88a], ISO 8725 [ISO88b], ISO 4138 [ISO12], ISO13674 [ISO10] and ISO8726 [ISO88c] provide information/recommendations on the exact maneuver execution and metrics to be extracted. Furthermore, [DEC09, SCH10, ZOM91, RH84] supply additional information on objective metrics.

The standard maneuvers performed during the simulation part of the process are:

1. Step Input ISO7401 (SI)
2. Steady-state Circular Driving ISO4138 (SC)
3. Sinusoidal Input (One Period) ISO7401/ISO8725 (SS¹)
4. Sinusoidal Input (Continuous - Constant frequency) ISO7401/ISO13674 (SO)
5. Sinusoidal Input (Continuous - Varying frequency) ISO8726 (FR²)

In order to identify the various objective metrics uniquely there are different sub- and superscripts introduced. Figure C.1 depicts an indicator for the global metric number, in- and output signals, metric abbreviation, information source and lateral acceleration level. The majority of the maneuvers are executed for different acceleration levels, such that there exist 3 variants of a single metric (corresponding to 3 different lateral acceleration levels³). Furthermore, the information source for metrics extraction is either the standard

¹Often that maneuver is referred to as Single Sine maneuver.

²The vehicle responses of that maneuver can be exploited for estimation of the vehicle's frequency response.

³The standard ISO7401 [ISO88a] suggests levels of $a_y = 2,4,6\text{m}\cdot\text{s}^{-2}$.

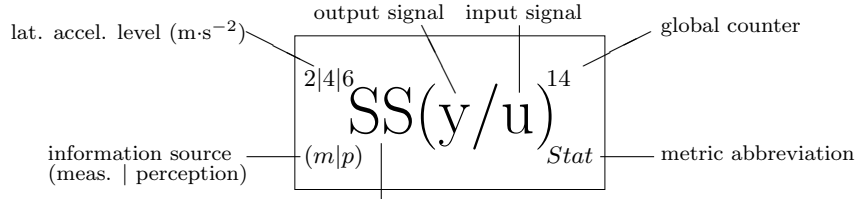


Figure C.1: Objective metrics representation design.

measurement or the calculated driver perception signal. So theoretically, for every metric there exist 6 variants⁴. Definitely, the following list is not exhaustive and only illustrates a number of (important) existing objective metrics ([ISO88a, ISO12, ISO10, DEC09, SCH10]).

C.1 Steady-state Circular Driving ISO4138

Lateral acceleration levels a_y : -

Information source: Standard measurements

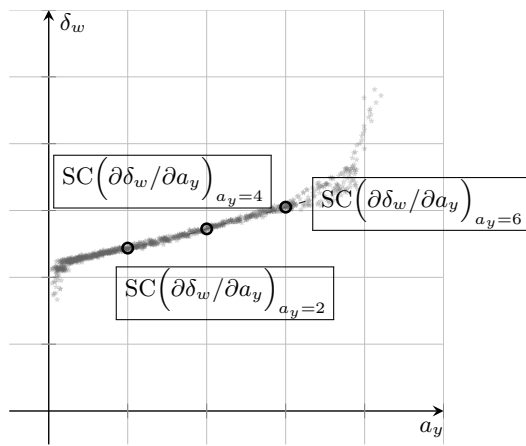
Objective Metric	Signal In (S1)	Signal Out (S2)	Description	Source
$SC(\partial\delta_w/\partial a_y)_{a_y=2}$	STW angle δ_w	Lat. accel. a_y	Gradient steering angle, i.e. $\frac{\partial\delta_w}{\partial a_y}$ evaluated at $a_y = 2\text{m}\cdot\text{s}^{-2}$.	[ISO12]
$SC(\partial\delta_w/\partial a_y)_{a_y=4}$	— " —	— " —	Gradient steering angle at $a_y = 4\text{m}\cdot\text{s}^{-2}$.	[ISO12]
$SC(\partial\delta_w/\partial a_y)_{a_y=6}$	— " —	— " —	Gradient steering angle at $a_y = 6\text{m}\cdot\text{s}^{-2}$.	[ISO12]
$SC(\partial\beta/\partial a_y)_{a_y=2}$	Sideslip angle β	Lat. accel. a_y	Gradient sideslip angle, i.e. $\frac{\partial\beta}{\partial a_y}$ evaluated at $a_y = 2\text{m}\cdot\text{s}^{-2}$.	[ISO12]
$SC(\partial\beta/\partial a_y)_{a_y=4}$	— " —	— " —	Gradient sideslip angle at $a_y = 4\text{m}\cdot\text{s}^{-2}$.	[ISO12]
$SC(\partial\beta/\partial a_y)_{a_y=6}$	— " —	— " —	Gradient sideslip angle at $a_y = 6\text{m}\cdot\text{s}^{-2}$.	[ISO12]
$SC(\partial\varphi/\partial a_y)_{a_y=2}$	Roll angle φ	Lat. accel. a_y	Gradient roll angle, i.e. $\frac{\partial\varphi}{\partial a_y}$ evaluated at $a_y = 2\text{m}\cdot\text{s}^{-2}$.	[ISO12]
$SC(\partial\varphi/\partial a_y)_{a_y=4}$	— " —	— " —	Gradient roll angle at $a_y = 4\text{m}\cdot\text{s}^{-2}$.	[ISO12]
$SC(\partial\varphi/\partial a_y)_{a_y=6}$	— " —	— " —	Gradient roll angle at $a_y = 6\text{m}\cdot\text{s}^{-2}$.	[ISO12]

The *self-steering* characteristics can be extracted from $SC(\partial\delta_w/\partial a_y)$ evaluated at $a_y = 2, 4, 6\text{m}\cdot\text{s}^{-2}$. Due to the constant radius R of the track, a positive self-steering gradient refers to positive values of the aforementioned metrics [ZOM91].

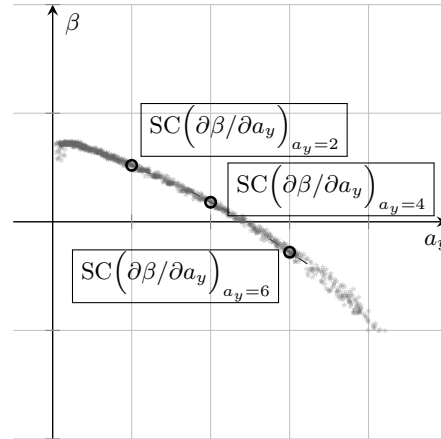
⁴For the subsequently presented metrics these subscripts are omitted.

Objective Metric	Signal In (S1)	Signal Out (S2)	Description	Source
$SC(\partial T_h/\partial a_y)_{a_y=2}$	STW torque T_h	Lat. accel. a_y	Gradient steering torque, i.e. $\frac{\partial T_h}{\partial a_y}$ evaluated at $a_y = 2\text{m}\cdot\text{s}^{-2}$	[ISO12]
$SC(\partial T_h/\partial a_y)_{a_y=4}$	— " —	— " —	Gradient steering torque at $a_y = 4\text{m}\cdot\text{s}^{-2}$	[ISO12]
$SC(\partial T_h/\partial a_y)_{a_y=6}$	— " —	— " —	Gradient steering torque at $a_y = 6\text{m}\cdot\text{s}^{-2}$	[ISO12]

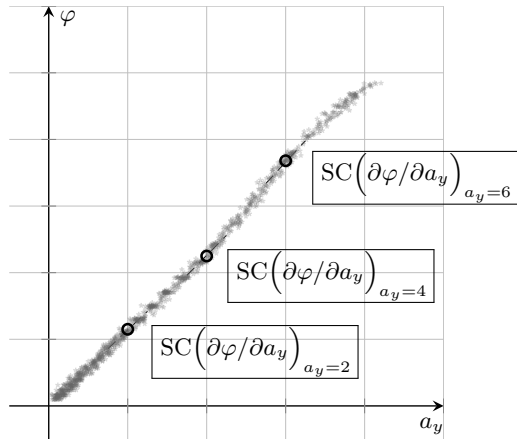
Table C.1: Objective metrics of the maneuver *Steady-state Circular Driving* (ISO4138).



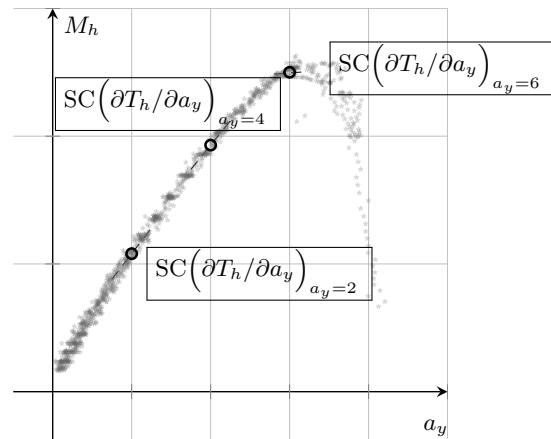
(a) Lat. accel. a_y vs. Steering angle δ_w .



(b) Lat. accel. a_y vs. Sideslip angle β .



(c) Lat. accel. a_y vs. Roll angle φ .



(d) Lat. accel. a_y vs. Steer. torque T_h .

Figure C.2: Graphical representation of the objective metrics (maneuver *SC*).

C.2 Step Input ISO7401

Lateral acceleration levels a_y : $2,4,6\text{m}\cdot\text{s}^{-2}$

Information source: Standard measurements + driver perception signals

Objective Metric	Signal In (S1)	Signal Out (S2)	Description	Ref.
$SI(\dot{\psi}/\delta_w)_{\tau_1}$	STW angle δ_w	Yaw rate $\dot{\psi}$	Response time - Time interval from reaching 50% (w.r.t. steady-state value) of S1 to 90% of the steady-state value of S2.	[ISO88a]
$SI(\dot{\psi}/\delta_w)_{R_{ss}}$	———— " ————	———— " ————	Steady-state ratio - Between the steady-state values of S1 and S2 $\left(= \frac{\dot{\psi}_{ss}}{\delta_{w,ss}} \right)$.	[ISO88a]
$SI(\dot{\psi}/\delta_w)_{\tau_2}$	———— " ————	———— " ————	Peak response time - Time interval from reaching 50% (w.r.t. steady-state value) of S1 and the peak value of S2.	[ISO88a]
$SI(\dot{\psi}/\delta_w)_{os}$	———— " ————	———— " ————	Overshoot value - Percentage value of relation steady-state vs maximum value of S2 $\left(= \frac{\dot{\psi}_{max} - \dot{\psi}_{ss}}{\dot{\psi}_{ss}} \right)$.	[ISO88a]
$SI(\dot{\psi}/\delta_w)_{tb}$	———— " ————	———— " ————	TB value - Product of the yaw rate peak response time and steady-state sideslip angle $\left(= ST(\dot{\psi}/\delta_w)_{\tau_2} \cdot \beta_{ss} \right)$.	[ISO88a]
$SI(a_y/\delta_w)_{\tau_1}$	STW angle δ_w	Lat. accel. a_y	Response time - Time interval from reaching 50% (w.r.t. steady-state value) of S1 to 90% of the steady-state value of S2.	[ISO88a]
$SI(a_y/\delta_w)_{R_{ss}}$	———— " ————	———— " ————	Steady-state ratio - Between the steady-state values of S1 and S2 $\left(= \frac{a_{y,ss}}{\delta_{w,ss}} \right)$.	[ISO88a]
$SI(a_y/\delta_w)_{\tau_2}$	———— " ————	———— " ————	Peak response time - Time interval from reaching 50% (w.r.t. steady-state value) of S1 and the peak value of S2.	[ISO88a]
$SI(a_y/\delta_w)_{os}$	———— " ————	———— " ————	Overshoot value - Percentage value of relation steady-state vs maximum value of S2 $\left(= \frac{a_{y,max} - a_{y,ss}}{a_{y,ss}} \right)$.	[ISO88a]

Table C.2: Objective metrics of the maneuver *Step Input* (ISO7401).

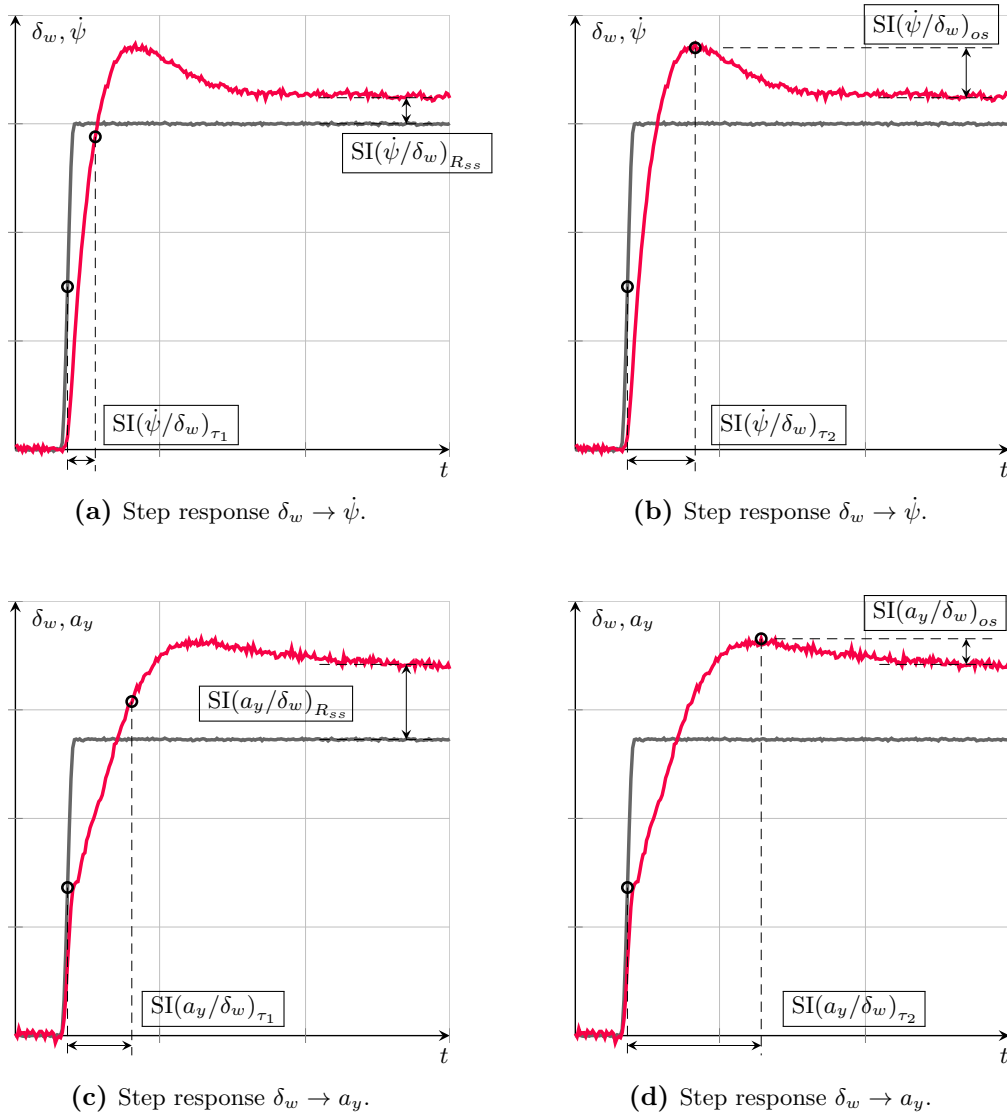


Figure C.3: Graphical representation of the objective metrics (maneuver SI).

C.3 Sinusoidal Input (One Period) ISO7401

Lateral acceleration levels a_y : 2,4,6m·s⁻²

Information source: Standard measurements + driver perception signals

Objective Metric	Signal In (S1)	Signal Out (S2)	Description	Ref.
$SS(\dot{\psi}/\delta_w)_{A+}$	STW angle δ_w	Yaw rate $\dot{\psi}$	Positive signal amplitude - Relating to S2.	[DEC09]
$SS(\dot{\psi}/\delta_w)_{A-}$	———— " ———	———— " ———	Negative signal amplitude - Relating to S2.	[DEC09]
$SS(\dot{\psi}/\delta_w)_{\tau_{A+}}$	———— " ———	———— " ———	Time lag pos. signal amplitude - Time interval from excitation start (S1) to the positive peak value of S2.	[DEC09]
$SS(\dot{\psi}/\delta_w)_{\tau_{A-}}$	———— " ———	———— " ———	Time lag neg. signal amplitude - Time interval from excitation start (S1) to the negative peak value of S2.	[DEC09]
$SS(\dot{\psi}/\delta_w)_{A_G^+}$	———— " ———	———— " ———	Pos. yaw rate gain - Ratio of positive amplitudes between S2 and S1.	[ISO88a]
$SS(\dot{\psi}/\delta_w)_{A_G^-}$	———— " ———	———— " ———	Neg. yaw rate gain - Ratio of negative amplitudes between S2 and S1.	
$SS(\dot{\psi}/\delta_w)_{A_{ratio}}$	———— " ———	———— " ———	Yaw rate ratio - Between $SS(\dot{\psi}/\delta_w)_{A-}$ to $SS(\dot{\psi}/\delta_w)_{A+}$.	[ISO88b]
$SS(\dot{\psi}/\delta_w)_{\tau_{lag}^+}$	———— " ———	———— " ———	Time lag pos. signal amplitudes - Time lag between S2 and S1 (for positive half-wave).	[ISO88a], [ISO88b]
$SS(\dot{\psi}/\delta_w)_{\tau_{lag}^-}$	———— " ———	———— " ———	Time lag neg. signal amplitudes - Time lag between S2 and S1 (for negative half-wave).	[ISO88a], [ISO88b]
$SS(\dot{\psi}/\delta_w)_{\tau_{ratio}}$	———— " ———	———— " ———	Time lag ratio - $SS(\dot{\psi}/\delta_w)_{\tau_{lag}^-}$ to $SS(\dot{\psi}/\delta_w)_{\tau_{lag}^+}$.	[ISO88b]
$SS(a_y/\delta_w)_{A+}$	STW angle δ_w	Lat. accel. a_y	Positive signal amplitude - Relating to S2.	[DEC09]
$SS(a_y/\delta_w)_{A-}$	———— " ———	———— " ———	Negative signal amplitude - Relating to S2.	[DEC09]
$SS(a_y/\delta_w)_{\tau_{A+}}$	———— " ———	———— " ———	Time lag pos. signal amplitude - Time interval from excitation start (S1) to the positive peak value of S2.	[DEC09]
$SS(a_y/\delta_w)_{\tau_{A-}}$	———— " ———	———— " ———	Time lag neg. signal amplitude - Time interval from excitation start (S1) to the negative peak value of S2.	[DEC09]
$SS(a_y/\delta_w)_{A_G^+}$	———— " ———	———— " ———	Pos. lat. accel. gain - Ratio of positive amplitudes between S2 and S1.	[ISO88a]
$SS(a_y/\delta_w)_{A_G^-}$	———— " ———	———— " ———	Neg. lat. accel. gain - Ratio of negative amplitudes between S2 and S1.	
$SS(a_y/\delta_w)_{A_{ratio}}$	———— " ———	———— " ———	Lat. accel. ratio - Between $SS(a_y/\delta_w)_{A-}$ and $SS(a_y/\delta_w)_{A+}$.	[ISO88b]
$SS(a_y/\delta_w)_{\tau_{lag}^+}$	———— " ———	———— " ———	Time lag pos. signal amplitudes - Time lag between S2 and S1 (for positive half-wave).	[ISO88a], [ISO88b]

Objective Metric	Signal In (S1)	Signal Out (S2)	Description	Ref.
$SS(a_y/\delta_w)_{\tau_{lag}^-}$	— " —	— " —	Time lag neg. signal amplitudes - Time lag between S2 and S1 (for negative half-wave).	[ISO88a], [ISO88b]
$SS(a_y/\delta_w)_{\tau_{ratio}}$	— " —	— " —	Time lag ratio - $SS(a_y/\delta_w)_{\tau_{lag}^-}$ to $SS(a_y/\delta_w)_{\tau_{lag}^+}$.	[ISO88b]

Table C.3: Objective metrics of the maneuver *Step Input* (ISO7401).

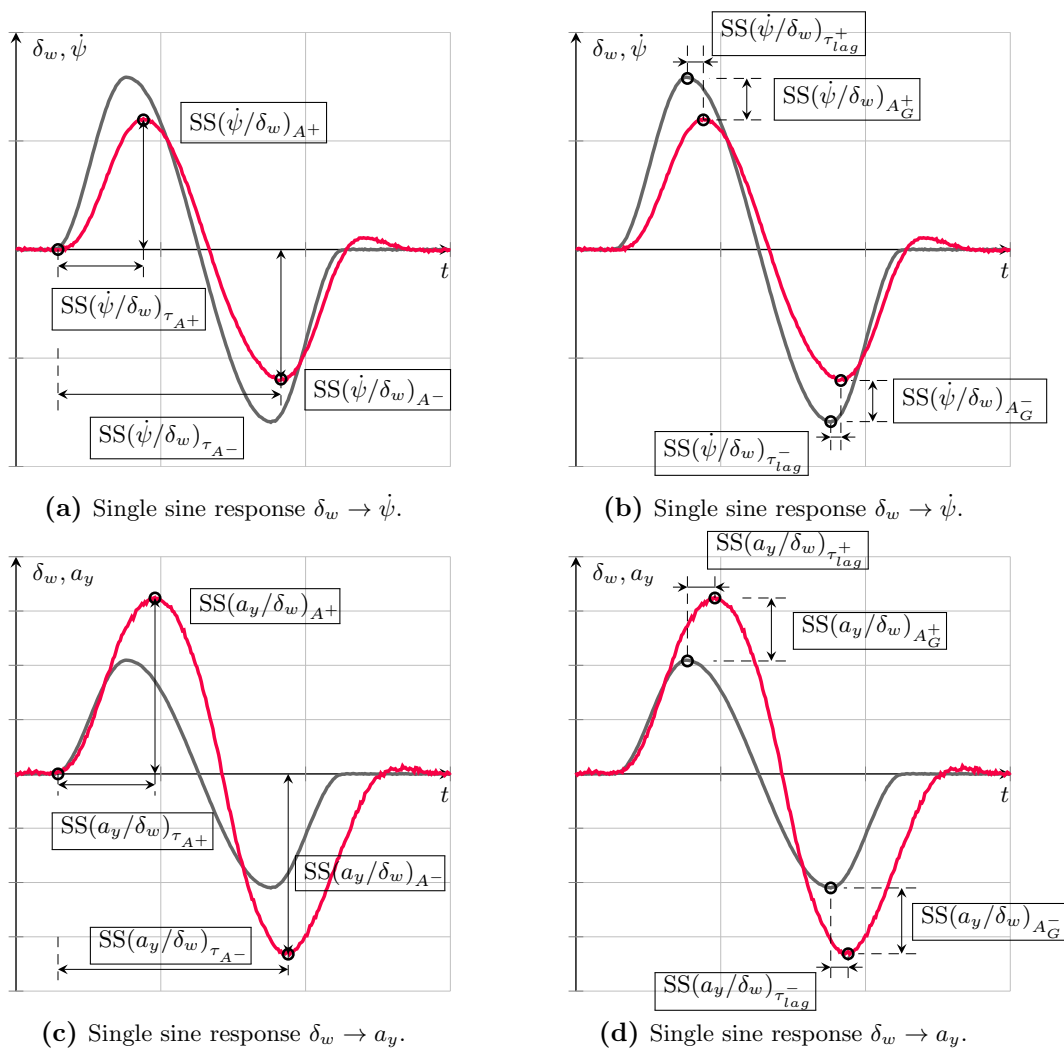


Figure C.4: Graphical representation of the objective metrics (maneuver SS).

C.4 Sinusoidal Input (Continuous - Constant Frequency) ISO7401

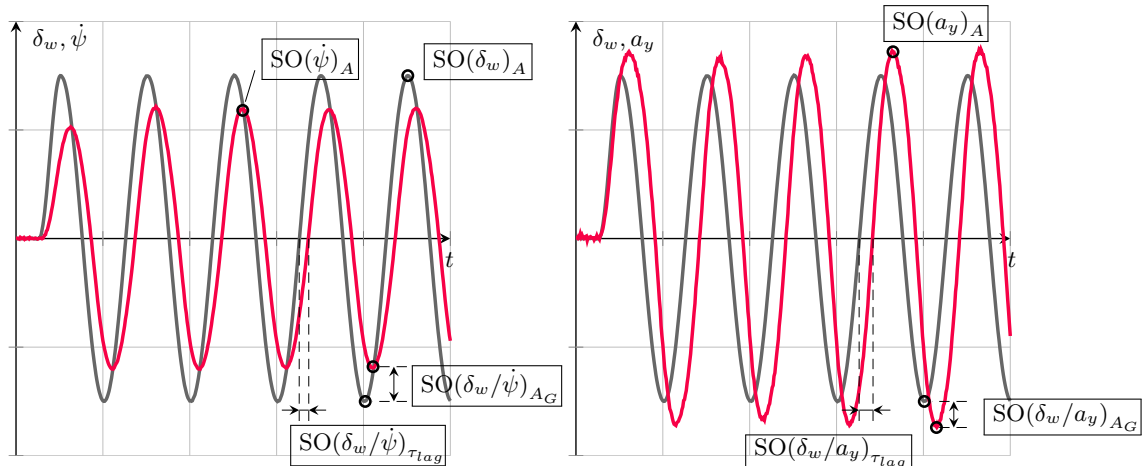
Lateral acceleration levels a_y : 2,4,6ms⁻²

Signal excitation frequency f_{ex} : 0.5,1.0Hz

Information source: Standard measurements + driver perception signals

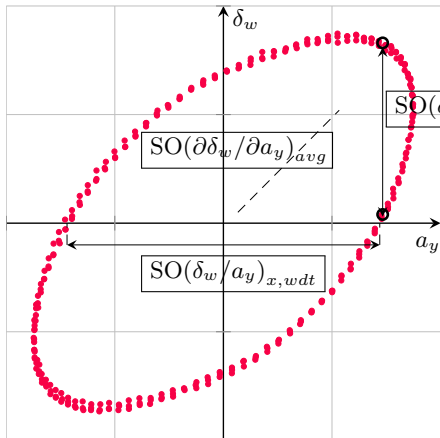
Objective Metric	Signal In (S1)	Signal Out (S2)	Description	Source
$SO(\delta_w)_A$	STW angle δ_w	-	Mean signal amplitude steering angle (excluding first signal period).	[ISO88a]
$SO(\dot{\psi})_A$	-	Yaw rate $\dot{\psi}$	Mean signal amplitude yaw rate (excluding first signal period).	[ISO88a]
$SO(a_y)_A$	-	Lat. accel. a_y	Mean signal amplitude lateral acceleration (excluding first signal period).	[ISO88a]
$SO(\dot{\psi}/\delta_w)_{AG}$	STW angle δ_w	Yaw rate $\dot{\psi}$	Yaw rate gain - Ratio between $SO(\dot{\psi})_A$ and $SO(\delta_w)_A$.	[ISO88a]
$SO(a_y/\delta_w)_{AG}$	———— " ————	Lat. accel. a_y	Lateral acceleration gain - Ratio between $SO(a_y)_A$ and $SO(\delta_w)_A$.	[ISO88a]
$SO(\dot{\psi}/\delta_w)_{\tau_{lag}}$	———— " ————	Yaw rate $\dot{\psi}$	Time delay - Between steering wheel angle and yaw rate (to be determined after first signal period).	[ISO88a]
$SO(a_y/\delta_w)_{\tau_{lag}}$	———— " ————	Lat. accel. a_y	Time delay - Between steering wheel angle and lateral acceleration (to be determined after first signal period).	[ISO88a]
$SO(a_y/\delta_w)_{x,wdt}$	———— " ————	———— " ————	Horizontal width of the ellipse.	[DEC09]
$SO(a_y/\delta_w)_{y,wdt}$	———— " ————	———— " ————	Vertical width of the ellipse.	[DEC09]
$SO(a_y/\delta_w)_{area}$	———— " ————	———— " ————	Area of ellipse	[DEC09]
$SO(\partial a_y/\partial \delta_w)_{avg}$	———— " ————	———— " ————	Average slope of the main axis (ellipse).	[DEC09]
$SO(a_y/\delta_w)_{y,wdt,80\%}$	———— " ————	———— " ————	Vertical width of the ellipse at 80% of the max. amplitude.	[DEC09]

Table C.4: Objective metrics of the maneuver *Sinusoidal Input (Continuous - Constant Frequency)* (ISO7401).

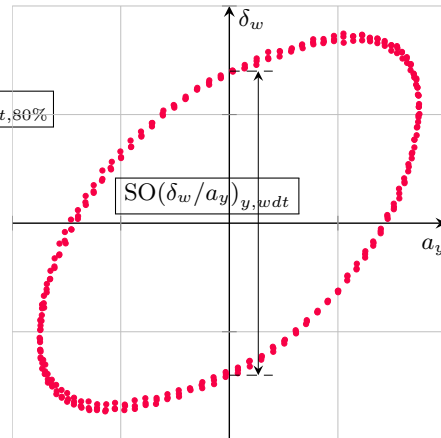


(a) Sinusoidal input cont. $\delta_w \rightarrow \dot{\psi}$.

(b) Sinusoidal input cont. $\delta_w \rightarrow a_y$.



(c) Ellipsoidal δ_w vs. a_y .



(d) Ellipsoidal δ_w vs. a_y .

Figure C.5: Graphical representation of the objective metrics (maneuver SO).

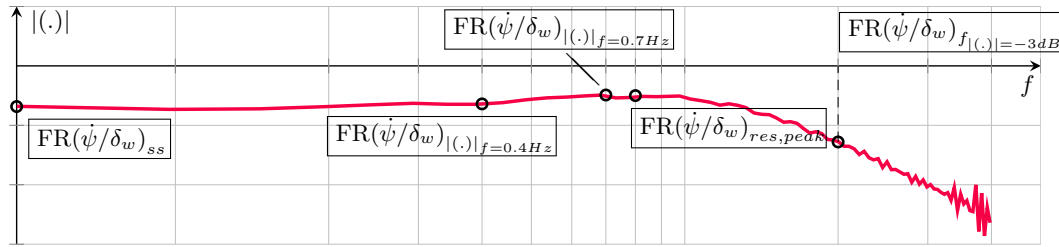
C.5 Sinusoidal Input (Continuous - Varying Frequency) ISO7401

Lateral acceleration levels a_y : 2,4,6m·s⁻²

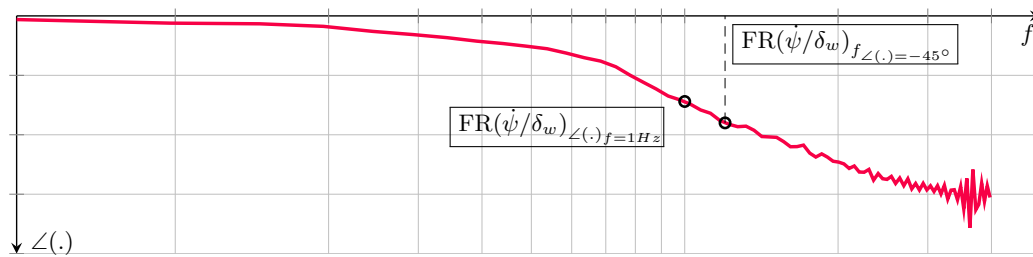
Information source: Standard measurements + driver perception signals

Objective Metric	Signal In (S1)	Signal Out (S2)	Description	Ref.
$FR(\dot{\psi}/\delta_w)_{ss}$	STW angle δ_w	Yaw rate $\dot{\psi}$	Steady-state gain - δ_w to $\dot{\psi}$.	[DEC09]
$FR(\dot{\psi}/\delta_w)_{res,peak}$	———— " ———	———— " ———	Resonance peak.	[DEC09]
$FR(\dot{\psi}/\delta_w)_{\angle(\cdot),f=1\text{Hz}}$	———— " ———	———— " ———	Phase for excitation signal frequency of 1Hz.	[DEC09]
$FR(\dot{\psi}/\delta_w)_{f_{\angle(\cdot)}=-45^\circ}$	———— " ———	———— " ———	Signal excitation frequency for a phase shift of -45° .	[DEC09]
$FR(\dot{\psi}/\delta_w)_{f_{ \cdot }=-3\text{dB}}$	———— " ———	———— " ———	Signal excitation frequency for a magnitude decay of -3dB .	[DEC09]
$FR(\dot{\psi}/\delta_w)_{\tau_{eq}}$	———— " ———	———— " ———	Equivalent time lag $\left(= \frac{1}{2\pi \cdot f_{\angle(\cdot)}=-45^\circ} \right)$.	[DEC09]
$FR(\dot{\psi}/\delta_w)_{ \cdot f=0.4\text{Hz}}$	———— " ———	———— " ———	Gain (dB) for a signal excitation of $f=0.4\text{Hz}$.	[SCH10]
$FR(\dot{\psi}/\delta_w)_{ \cdot f=0.7\text{Hz}}$	———— " ———	———— " ———	Gain (dB) for a signal excitation of $f=0.7\text{Hz}$.	[SCH10]
$FR(\dot{\psi}/\delta_w)_{eig}$	———— " ———	———— " ———	Eigenfrequency of yaw rate dynamics.	[SCH10]
$FR(a_y/\delta_w)_{ss}$	STW angle δ_w	Lat. accel. a_y	Steady-state gain - δ_w to a_y .	[DEC09]
$FR(a_y/\delta_w)_{res,peak}$	———— " ———	———— " ———	Resonance peak.	[DEC09]
$FR(a_y/\delta_w)_{\angle(\cdot),f=1\text{Hz}}$	———— " ———	———— " ———	Phase for excitation signal frequency of 1Hz.	[DEC09]
$FR(a_y/\delta_w)_{f_{\angle(\cdot)}=-45^\circ}$	———— " ———	———— " ———	Signal excitation frequency for a phase shift of -45° .	[DEC09]
$FR(a_y/\delta_w)_{f_{ \cdot }=-3\text{dB}}$	———— " ———	———— " ———	Signal excitation frequency for a magnitude decay of -3dB .	[DEC09]
$FR(a_y/\delta_w)_{\tau_{eq}}$	———— " ———	———— " ———	Equivalent time lag $\left(= \frac{1}{2\pi \cdot f_{\angle(\cdot)}=-45^\circ} \right)$.	[DEC09]
$FR(a_y/\delta_w)_{ \cdot f=0.4\text{Hz}}$	———— " ———	———— " ———	Gain (dB) for a signal excitation of $f=0.4\text{Hz}$.	[SCH10]
$FR(a_y/\delta_w)_{ \cdot f=0.7\text{Hz}}$	———— " ———	———— " ———	Gain (dB) for a signal excitation of $f=0.7\text{Hz}$.	[SCH10]
$FR(a_y/\delta_w)_{ \cdot f=1.0\text{Hz}}$	———— " ———	———— " ———	Gain (dB) for a signal excitation of $f=1.0\text{Hz}$.	[SCH10]

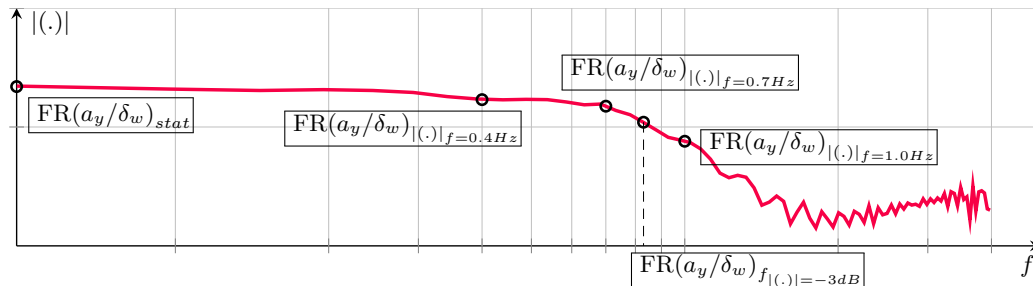
Table C.5: Objective Metrics of the maneuver *Sinusoidal Input (Continuous - Varying Frequency)* (ISO7401).



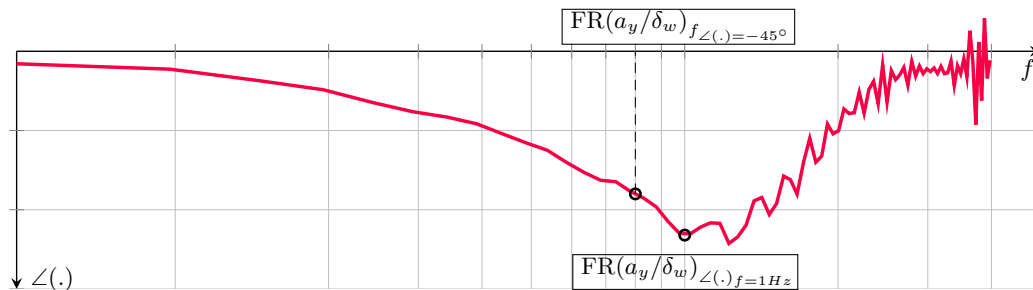
(a) Magnitude plot of the frequency response $\delta_w \rightarrow \dot{\psi}$.



(b) Phase plot of the frequency response $\delta_w \rightarrow \dot{\psi}$.



(c) Magnitude plot of the frequency response $\delta_w \rightarrow a_y$.



(d) Phase plot of the frequency response $\delta_w \rightarrow a_y$.

Figure C.6: Graphical representation of the objective metrics (maneuver FR).

D

Experimental Setup

D.1 Virtual Reference Vehicle (IPG CarMaker[®])

The software package IPG¹ CarMaker[®] is a well-known state of the art tool for simulation of vehicle dynamics and its control. A multi-body, 17-DoF vehicle model allows versatile configurations with respect to engine, suspension, steering, tires, braking system, vehicle geometry, aerodynamics, sensor configuration etc. Furthermore, it can be fully embedded into the Simulink[®] environment allowing for simple integration of modified vehicle assistance systems, driver models and so on. For the actual application only its basic functionality is in use.

D.1.1 Virtual Vehicle Configuration

For the objective of reference data generation further used within the evaluation process of the observer-based parameter identification algorithms a standard vehicle configuration is treated as the *virtual vehicle*. It uses a rigid vehicle body, a steering system with static² transmission ratio, an IPG-Tire model [SH92], a standard powertrain with manual gearbox and a suspension setup that is further discussed in the following.

The suspension springs are modelled by linear deflection-force characteristics with different stiffness values for the front and rear components. At least locally the deflection velocity-force characteristics of the damping elements can be represented linearly. But for both operational ranges, i.e. push and pull, the characteristic lines consist of two individual slopes that are either used dependent on the actual deflection velocity. So, in summary four slopes characterize the full operational range of the damper. Moreover,

¹www.ipg.de

²*Static* in a sense, that the transmission ratio between steering wheel angle and steering angle of the tire varies over the actuation range, but elasticities are not considered.

Parameter	Description	Value	Unit
l_f	Distance front axle to CoG	1.108	m
l_r	Distance rear axle to CoG	1.42	m
J_{xc}	Moment of inertia (chassis) w.r.t. x-axis	360	kg·m ²
J_{yc}	Moment of inertia (chassis) w.r.t. y-axis	1800	kg·m ²
J_z	Moment of inertia w.r.t. z-axis	2152	kg·m ²
m	(Total) Vehicle mass	1463	kg
m_s	Vehicle chassis mass (only sprung parts)	1301	kg
h_{rl}	Distance between CoG and roll center	0.49	m
h_{pl}	Distance between CoG and pitch center	0.49	m
\tilde{w}_s	Avg. distance between CoG and suspension parts	0.55	m
\tilde{l}_f^p	Avg. distance between front suspension parts and COG	1.08	m
\tilde{l}_r^p	Avg. distance between rear suspension parts and COG	1.4	m
n_p	(Constant) Pneumatic trail	0.05	m

Table D.1: Model parameters of the virtual vehicle (IPG CarMaker[®]).

front and rear elements can be parametrized differently, rendering the overall damping characteristics nonlinear. The models of the roll stabilizers are exploiting a single stiffness value that can be adjusted independently for front and rear suspension.

The most relevant model parameters of the virtual vehicle required for the observer setups are listed in Table D.1.

D.1.2 Measurement Setup

The definition of certain virtual sensing devices, e.g. accelerations at specific vehicle positions, as well as standard output signals provides a wide range of extractable vehicle state information during the simulation runs. A list of the considered measurement channels used for the validation is provided in Table D.2.

Generally, data acquisition is performed with a sampling time $\tau_s = 0.001$ s. In order to render the validation scenarios more realistic the virtual measurements are augmented by noise disturbances. Statistical characteristics extracted from a noise analysis performed on real vehicle measurement data are provided in Section D.2. For those signals no information is available generic values within the expectable range are considered.

D.2 Experimental Vehicles

D.2.1 Some General Notes

Both experimental vehicles are mid-sized and can be categorized into the compact class. Configurations are standard without any modifications of the suspension, steering etc.

Domain	Signal
Longitudinal Dynamics	Longitudinal velocity v_x
	(Measured) Longitudinal acceleration $a_{x,m}$
Lateral Dynamics	Longitudinal acceleration a_x
	(Measured) Lateral acceleration $a_{y,m}$
	Lateral acceleration a_y
Tire Dynamics	Vehicle sideslip angle β
	Lateral (front) tire forces $F_{y,f}$
	Lateral (rear) tire forces $F_{y,r}$
	Front slip angle α_{fe}
Roll Dynamics	Rear slip angle α_r
	Roll angle φ
	Roll rate $\dot{\varphi}$
Pitch Dynamics	Roll acceleration $\ddot{\varphi}$
	Pitch angle θ
Powertrain Dynamics	Pitch rate $\dot{\theta}$
	Engine speed ω_e
	Actual gear n
	Pedal positions $\varphi_{acc}, \varphi_{brk}, \varphi_{clu}$

Table D.2: Vehicle measurement channels that are used within the IPG CarMaker[®] - Matlab[®]/Simulink[®] evaluation environment.

D.2.2 Sensor Noise Characteristics

Analysis of the noise characteristics affecting the measured signals is performed for two reasons. First, the characteristics of the noise process, i.e. its mean and standard deviation will be further used for the tuning of the EKF structures. And second, as the assumed Gaussian distribution is fully characterized by its mean and standard deviation, overlaying noise histograms with an approximated normal distribution validates the assumption of Gaussian noise. Even though the Gaussianity is not necessarily required for the Kalman Filter, see [SIM06], identifying its variance is helpful.

Practically measurements are taken for a duration >90 s while the vehicle is at rest and the resulting signals analyzed. Figure D.1 shows the extracted noise characteristics of the longitudinal acceleration a_x , lateral acceleration a_y , yaw rate $\dot{\psi}$ and roll rate $\dot{\varphi}$. These signals serve as measurements for the Kalman filter correction mechanisms. For the remaining in-vehicle measurements mean and standard deviation are not inspected in detail as their exact knowledge is not relevant for the tuning. It should be noted again that the sliding mode-based techniques do not take into considerations the noise characteristics at all. Especially not for the tuning of the observer gains!

Mean and standard deviations of the analyzed signals are listed in Table D.3.

Measurement	Variance σ^2	Mean Value μ	Unit
Longitudinal acceleration a_x	$5.93 \cdot 10^{-4}$	$-1.97 \cdot 10^{-6}$	$\text{m}\cdot\text{s}^{-2}$
Lateral acceleration a_y	$3.15 \cdot 10^{-4}$	$-4.48 \cdot 10^{-6}$	$\text{m}\cdot\text{s}^{-2}$
Roll rate ω_x	$1.4 \cdot 10^{-7}$	$-1.44 \cdot 10^{-7}$	$\text{rad}\cdot\text{s}^{-1}$
Yaw rate ω_z	$1.54 \cdot 10^{-7}$	$5.33 \cdot 10^{-8}$	$\text{rad}\cdot\text{s}^{-1}$

Table D.3: Measurement noise characterization of the vehicle transducer devices (for EKF tuning).

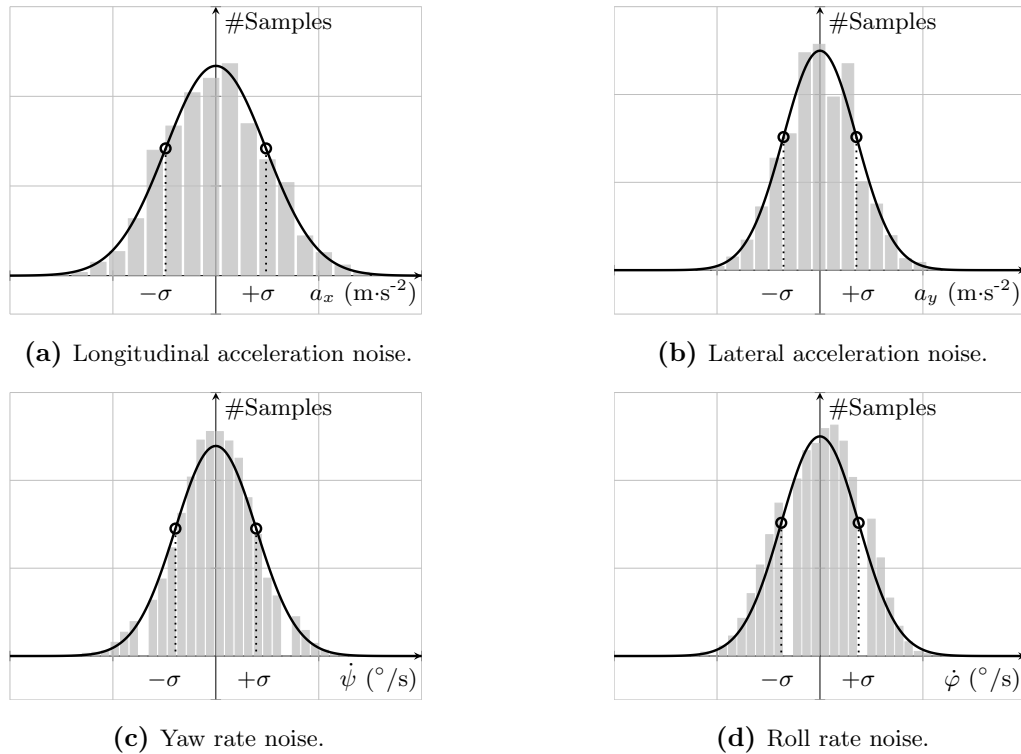


Figure D.1: Noise characteristics analysis of the in-vehicle sensors.

D.2.3 Sensor Configurations

The rapid-prototyping hardware dSpace MicroAutoBox 1401/1504³ is often used for in-vehicle function development. Herein, the implemented observation concepts (Matlab[®]/Simulink[®]) can be easily transferred to that platform using the Simulink Coder[™]. In terms of device specifications the MicroAutoBox operates on a floating-point 800MHz processor and the most important connections to the vehicle are the 24 12-bit analog-digital I/O channels and 4 CAN channels. Table D.4 lists the obtained measurements and related sensor devices (or at least similar types) of the installed and used types.

³See www.dspace.com for further details.

Domain	Sensor Type	Signal	Exp. Vehicle
Longitudinal Dynamics	Vehicle CAN	Long. velocity v_{v_x}	A, B
”	e.g. Bosch DRS-MM 3.7K [GMB15b]	Long. acceleration $a_{x,m}$	A, B
Lateral Dynamics	”	Yaw rate $\dot{\psi}$	A, B
”	”	Lateral acceleration $a_{y,m}$	A, B
”	e.g. Kistler Correxit [®] S-350 [AG15]	Vehicle sideslip angle β (Lateral velocity v_{v_y})	A
Roll Dynamics	e.g. Bosch SMG10x [GMB15a]	Roll rate $\dot{\phi}$	B
Powertrain Dynamics	Vehicle CAN	Accelerator pedal φ_{acc} , Brake pedal φ_{brk} , Clutch pedal φ_{clu}	B
Powertrain Dynamics	Vehicle CAN	Actual gear n	A, B
Powertrain Dynamics	Vehicle CAN	Engine speed ω_e	A, B
Steering System	Vehicle CAN	Steering wheel angle δ_w	A, B

Table D.4: Overview of in-vehicle measurements of the two experimental vehicles and possible sensor types (effectively used sensors must not be published).

D.3 Electric Power Steering Test Bench

D.3.1 Some General Notes

The test bench of an Electric Power Steering system consists of a rigid metal frame that accommodates an original steering system as installed in a compact-sized middle-class vehicle. Artificial reaction force generation due the steering actuation is performed by spring-damper elements that react on a deflection of the steering rack. With regards to the architectural type the EPS system refers to a servo unit (i.e. an electric motor) that sits right at the pinion connecting steering rack and column. In contrast to other types the assistant forces do not have to be transmitted via the steering column allowing for higher assistance power [PH11].

D.3.2 Data Acquisition and Measurement Devices

The rapid-prototyping system, i.e. a dSpace MicroAutoBox as described above executes the function prototypes and performs the data acquisition. In order to allow communication between the rapid-prototyping hardware, the electric motor control and the sensors a CAN bus is implemented.

In terms of measurement devices a torque sensor, that reads the requested driver input, is located right above the servo unit. The steering angle sensor that also provides an estimate of the velocity is at the upper end of the steering column right before the steering wheel⁴. In order to obtain estimates of the acting forces a potentiometer-based sensor principle provides measurements of the steering rack displacement. Then, exploiting

⁴When referring to a view point from the pinion to the steering wheel.

knowledge of the spring packs stiffnesses and damping coefficients a second-order model calculates the force from measurements of the deflection. The displacement can be further used to calculate the actual angular velocity of the steering column. Theoretically, this task can also be accomplished by considering the angular velocity of the electric motor (without calculation of a time derivative). More technical details on the EPS test bench can be found in [WEY15].

D.3.3 Test Bench Images

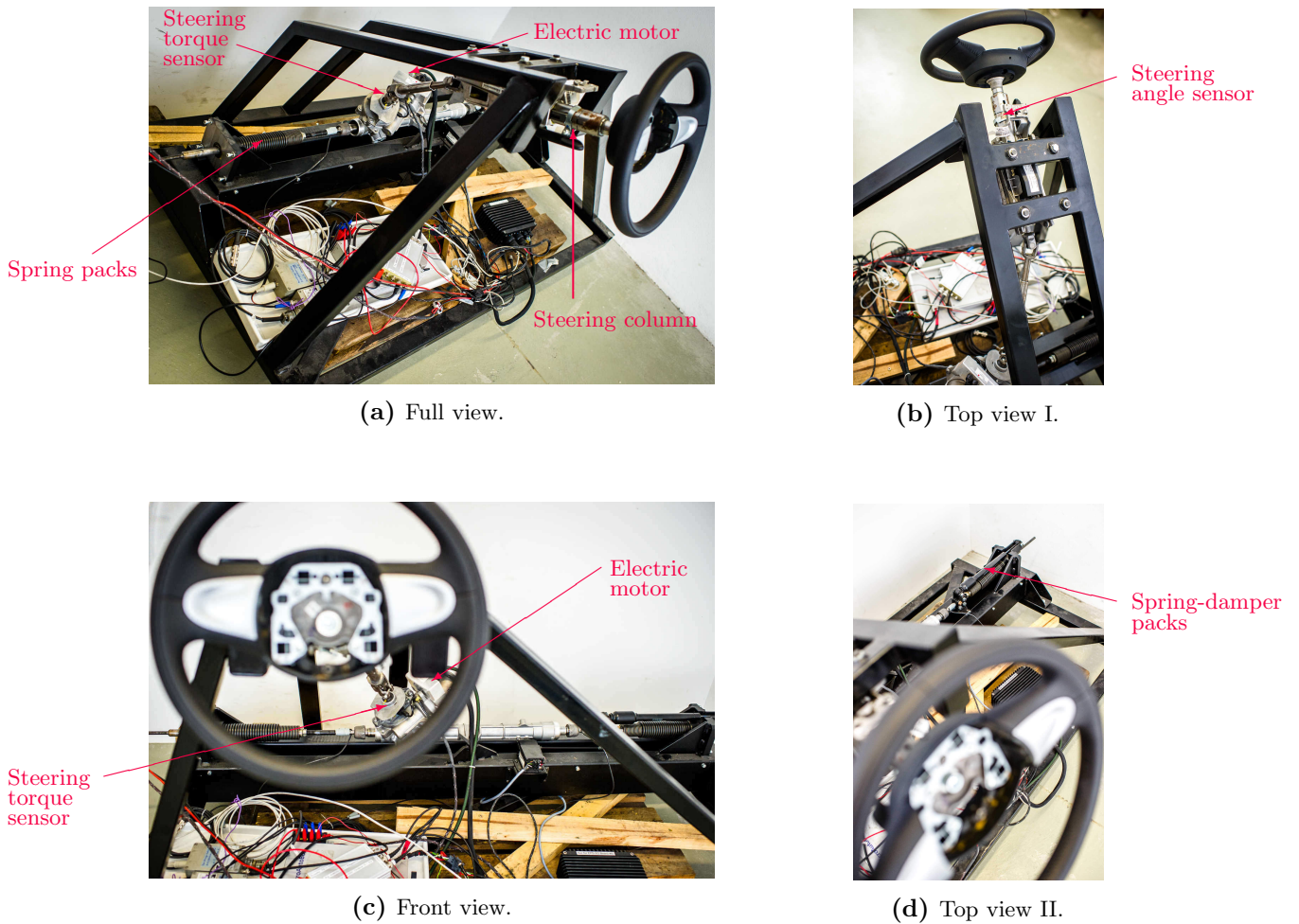


Figure D.2: The EPS test bench for validation of robust state estimation with unknown input recovery.

Bibliography

- [ADM04] M. ARNDT, E.L. DING, and T. MASSEL. Observer based diagnosis of roll rate sensor. In *Proceedings of the American Control Conference (ACC)*, volume 2, pages 1540–1545, 2004.
- [AFK11] S. ANTONOV, A. FEHN, and A. KUGI. Unscented Kalman filter for vehicle state estimation. *Vehicle System Dynamics*, 49(9):1497–1520, 2011.
- [AG15] KISTLER HOLDING AG. Correvit[®] S-350 DataSheet. <http://www.kistler.com/?type=669&fid=20100&model=document>, accessed on 10.09.2015.
- [AH05] H. ABDELLATIF and B. HEIMANN. Accurate modelling and identification of vehicle’s nonlinear lateral dynamics. In *Proceedings of the 16th IFAC World Congress*, 2005.
- [AHH03] H. ABDELLATIF, B. HEIMANN, and J. HOFFMANN. Nonlinear identification of vehicle’s coupled lateral and roll dynamics. In *Proceedings of the 11th IEEE Mediterranean Conference on Control and Automation*, Rhodes, Greece, 2003.
- [AMM97] D. AMMON. *Modellbildung und Systementwicklung in der Fahrzeugdynamik*. B.G. Teubner Stuttgart, 1997.
- [AND01] B.E. ANDERSSON. *Som man frågar får man svar: en introduktion i intervju- och enkätteknik*. Tema nova. Prisma, 2001.
- [ASH02] H. ASH. *Correlation of Subjective and Objective Handling of Vehicle Behaviour*. PhD thesis, University of Leeds, School of Mechanical Engineering, 2002.
- [BAR04] T. BARTHENHEIER. *Potenzial einer fahrertyp- und fahrsituationsabhängigen Lenkradmomentgestaltung*. PhD thesis, Technische Universität Darmstadt, 2004.
- [BB90] H. BUBB and U. BOLTE. Regelungstechnische Simulation der Schnittstelle Mensch-Maschine. *Zeitschrift für Arbeitswissenschaften*, 1990.
- [BBD96] J.-P. BARBOT, T. BOUKHOBZA, and M. DJEMAI. Sliding mode observer for triangular input form. In *Proceedings of the 35th IEEE Conference on Decision and Control*, volume 2, pages 1489–1490, 1996.

- [BCL09] G. BAFFET, A. CHARARA, and D. LECHNER. Estimation of vehicle sideslip, tire force and wheel cornering stiffness. *Control Engineering Practice*, 17(11):1255 – 1264, 2009.
- [BCLT08] G. BAFFET, A. CHARARA, D. LECHNER, and D. THOMAS. Experimental evaluation of observers for tire-road forces, sideslip angle and wheel cornering stiffness. *Vehicle System Dynamics*, 46(6):501–520, 2008.
- [BDK09] B. BANDYOPADHYAY, F. DEEPAK, and K.S. KIM. *Sliding Mode Control Using Novel Sliding Surfaces*, volume 392 of *Lecture Notes in Control and Information Sciences*. Springer Science & Business Media, 2009.
- [BDP11] V.A. BAVDEKAR, A.P. DESHPANDE, and S.C. PATWARDHAN. Identification of process and measurement noise covariance for state and parameter estimation using extended Kalman filter. *Journal of Process Control*, 21(4):585 – 601, 2011.
- [BFU98] G. BARTOLINI, A. FERRARA, and E. USAI. Chattering avoidance by second-order sliding mode control. *IEEE Transactions on Automatic Control*, 43(2):241–246, 1998.
- [BIR92] J. BIRK. Rechnergestützte Analyse und Lösung nichtlinearer Beobachtungsaufgaben. In *Fortschritt-Berichte VDI, Reihe 8, Nr. 294, Düsseldorf: VDI Verlag*, 1992.
- [BJ06] B. BANDYOPADHYAY and S. JANARDHANAN. *Discrete-time Sliding Mode Control*, volume 323 of *Lecture Notes in Control and Information Sciences*. Springer-Verlag, 2006.
- [BÖR04] M. BÖRNER. Adaptive Querdynamikmodelle für Personenkraftfahrzeuge - Fahrzustandserkennung und Sensorfehlertoleranz. In *Fortschritt-Berichte VDI, Reihe 12, Nr. 563, Düsseldorf: VDI Verlag*, 2004.
- [BOT08] S. BOTEV. *Digitale Gesamtfahrzeugabstimmung für Ride und Handling*. VDI-Verlag, Düsseldorf, 2008.
- [BR86] N.F. BENNINGER and J. RIVOIR. Ein neues konsistentes Maß zur Beurteilung der Steuerbarkeit in linearen, zeitinvarianten Systemen. *Regelungstechnik*, 34(12):473 – 479, 1986.
- [CC98] D.C. CHEN and A. CROLLA. Subjective and objective measures of vehicle handling: Drivers & experiments. *Vehicle System Dynamics: International Journal of Vehicle Mechanics and Mobility*, 29:576–597, 1998.
- [CHE95] C. CHEN. *Analog and Digital Control System Design: Transfer-function, State-space, and Algebraic Methods*. Oxford University Press, Inc., 1995.
- [CHE97] D. CHEN. *Subjective and Objective Vehicle Handling Behaviour*. PhD thesis, University of Leeds, School of Mechanical Engineering, 1997.
- [CKA00] D.A. CROLLA, R.P. KING, and H.A.S. ASH. Subjective and objective assessment of vehicle handling performance. In *FISITA World Automotive Congress*, Seoul, Korea, 2000.

- [DCREH10] H. DAHMANI, M. CHADLI, A. RABHI, and A. EL HAJJAJI. Road Bank Angle Considerations for Detection of Impending Vehicle Rollover. In *6th IFAC Symposium Advances in Automotive Control*, pages 31–36, 2010.
- [DEC09] M. DECKER. *Zur Beurteilung der Querdynamik von Personenkraftwagen*. PhD thesis, Fakultät für Maschinenwesen der TU München, 2009.
- [DET05] F. DETTKI. *Methoden zur objektiven Bewertung des Geradeauslaufs von Personenkraftwagen*. PhD thesis, Universität Stuttgart, Fakultät für Maschinenbau, 2005.
- [DFL05] J. DAVILA, L. FRIDMAN, and A. LEVANT. Second-order sliding-mode observer for mechanical systems. *IEEE Transactions on Automatic Control*, 50(11):1785–1789, 2005.
- [DFP06] J. DAVILA, L. FRIDMAN, and A. POZNYAK. Observation and identification of mechanical systems via second order sliding modes. *International Journal of Control*, 79(10):1251–1262, 2006.
- [DM05] E.L. DING and T. MASSEL. Estimation of vehicle roll angle. In *Proceedings of the 16th IFAC World Congress*, 2005.
- [DON77] E. DONGES. Ein Zwei-Ebenen-Modell des menschlichen Lenkverhaltens im Kraftfahrzeug. *Bericht Nr. 27 des Forschungsinstituts für Anthropotechnik*, 1977.
- [DP13] L. DEVRIES and D.A. PALEY. Observability-based optimization for flow sensing and control of an underwater vehicle in a uniform flowfield. In *American Control Conference (ACC)*, pages 1386–1391, 2013.
- [DRA69] B. DRAŽENOVIĆ. The invariance conditions in variable structure systems. *Automatica*, 5(3):287 – 295, 1969.
- [DSH⁺06] L. DIEBOLD, W. SCHINDLER, J. HAUG, C. DÄSCH, and M. LAHTI. Anwendung eines Einspurmodells zur Fahrdynamiksimulation und -analyse. *Automobil-technische Zeitschrift*, 108(11):962 – 967, 2006.
- [DVCL09] M. DOUMIATI, A. VICTORINO, A. CHARARA, and D. LECHNER. Lateral load transfer and normal forces estimation for vehicle safety: experimental test. *Vehicle System Dynamics*, 47(12):1511–1533, 2009.
- [DVL⁺10] M. DOUMIATI, A. VICTORINO, D. LECHNER, G. BAFFET, and A. CHARARA. Observers for vehicle tyre/road forces estimation: experimental validation. *Vehicle System Dynamics*, 48(11):1345–1378, 2010.
- [ENG94] A. ENGELS. *Geradeauslaufkriterien für Pkw und deren Bewertung*. PhD thesis, Technische Universität Carolo-Wilhelmina zu Braunschweig, Fakultät für Maschinenbau und Elektrotechnik, 1994.
- [ES98] C. EDWARDS and S. SPURGEON. *Sliding Mode Control: Theory and Applications*. Taylor & Francis Ltd, 1998.

- [ES15] C. EDWARDS and Y. SHTESSEL. Adaptive dual layer second-order sliding mode control and observation. In *American Control Conference (ACC)*, pages 5853–5858, July 2015.
- [EUR06] EUROPEAN COMMISSION. Impact Assessment for Euro 6 emission limits for light duty vehicles - Commission Staff Working Document, Brussels, Belgium, 2006.
- [EUR10] EUROPEAN COMMISSION. Demography report 2010 - older, more numerous and diverse Europeans - Commission Staff Working Document, 2010.
- [EUR15] EUROPEAN COMMISSION. Road Safety evolution in the EU, http://ec.europa.eu/transport/road_safety/specialist/statistics/index_en.htm, accessed on 10.09.2015.
- [FB06] T. FLOQUET and J.-P. BARBOT. A canonical form for the design of unknown input sliding mode observers. In *Advances in Variable Structure and Sliding Mode Control*, volume 334 of *Lecture Notes in Control and Information Sciences*. Springer Verlag, 2006.
- [FB07] T. FLOQUET and J.-P. BARBOT. Super twisting algorithm-based step-by-step sliding mode observers for nonlinear systems with unknown inputs. *International Journal of Systems Science*, 38(10):803–815, 2007.
- [FES06] T. FLOQUET, C. EDWARDS, and S.K. SPURGEON. On sliding mode observers for systems with unknown inputs. In *9th International Workshop on Variable Structure Systems (VSS)*, pages 214–219, 2006.
- [FIL88] A. F. FILIPPOV. *Differential Equations with Discontinuous Righthand Sides: Control Systems (Mathematics and its Applications)*. Springer, 1st edition, 1988.
- [FRI12] L. FRIDMAN. Sliding Mode Enforcement after 1990: Main Results and Some Open Problems. In *Sliding Modes after the First Decade of the 21st Century*, volume 412 of *Lecture Notes in Control and Information Sciences*, pages 3–57. Springer Berlin Heidelberg, 2012.
- [FRÖ08] M. FRÖHLICH. *Ein robuster Zustandsbeobachter für ein semiaktives Fahrwerkregelsystem*. PhD thesis, Technische Universität München, Fakultät für Maschinenwesen, 2008.
- [FWE02] J. FREDRIKSSON, H. WEIEFORS, and B. EGARDT. Powertrain control for active damping of driveline oscillations. *Vehicle System Dynamics*, 37(5):359–376, 2002.
- [GA01] M.S. GREWAL and A.P. ANDREWS. *Kalman Filtering: Theory and Practice Using MATLAB*. John Wiley & Sons, Inc., 2nd edition, 2001.
- [GB81] J.P. GAUTHIER and G. BORNARD. Observability for any $u(t)$ of a class of nonlinear systems. *IEEE Transactions on Automatic Control*, 26(4):922–926, 1981.
- [GCRP14] M. GADOLA, D. CHINDAMO, M. ROMANO, and F. PADULA. Development and validation of a Kalman filter-based model for vehicle slip angle estimation. *Vehicle System Dynamics*, 52(1):68–84, 2014.

- [GIB11] B.P. GIBBS. *Advanced Kalman Filtering, Least-Squares and Modeling: A Practical Handbook*. John Wiley & Sons, Inc., 2011.
- [GIJ⁺08] H.F. GRIP, L. IMSLAND, T.A. JOHANSEN, T.I. FOSSEN, J.C. KALKKUHL, and A. SUISSA. Nonlinear vehicle side-slip estimation with friction adaptation. *Automatica*, 44(3):611 – 622, 2008.
- [GIJ⁺09] H.F. GRIP, L. IMSLAND, T.A. JOHANSEN, J.C. KALKKUHL, and A. SUISSA. Estimation of road inclination and bank angle in automotive vehicles. In *American Control Conference (ACC)*, pages 426–432, 2009.
- [GIL92] T.D. GILLESPIE. *Fundamentals of Vehicle Dynamics*. Society of Automotive Engineers, Inc., 1st edition, 1992.
- [GMB15a] ROBERT BOSCH GMBH. Angular rate sensor SMG 10x DataSheet. http://www.bosch-semiconductors.de/media/pdf_1/einzeldownloads/airbag_systems/SMG10x_Productinfo.pdf, accessed on 10.09.2015.
- [GMB15b] ROBERT BOSCH GMBH. Yaw sensor DRS-MM 3.7K DataSheet. http://rb-aa.bosch.com/boaasocs/modules-pdf/Bosch_AA_Sensoren_PDFGen.dll?db=BOAAMDB02PRD7&MV_ID=900&CL_ID=20&Prod_ID=716&filename=0265005764.pdf, accessed on 10.09.2015.
- [GMF12] T. GONZALEZ, J.A. MORENO, and L. FRIDMAN. Variable Gain Super-Twisting Sliding Mode Control. *IEEE Transactions on Automatic Control*, 57(8):2100–2105, 2012.
- [GO10] L. GUZZELLA and C.H. ONDER. *Introduction to Modeling and Control of Internal Combustion Engine Systems*. Springer-Verlag Berlin Heidelberg, 2010.
- [GP89] F. GIROSI and T. POGGIO. Representation Properties of Networks: Kolmogorov’s Theorem is Irrelevant. *Neural Computation*, 1(4):465–469, 1989.
- [GUT13] D. GUTJAHR. *Objektive Bewertung querdynamischer Reifeneigenschaften im Gesamtfahrzeugversuch*. PhD thesis, Karlsruher Institut für Technologie, Fakultät für Maschinenbau, 2013.
- [GYNW10] X. GAO, Z. YU, J. NEUBECK, and J. WIEDEMANN. Sideslip angle estimation based on input-output linearisation with tire-road friction adaptation. *Vehicle System Dynamics*, 48(2):217–234, 2010.
- [HAR02] P. HARNETT. *Objective Methods for the Assessment of Passenger Car Steering Quality*. PhD thesis, Cranfield University, School of Engineering, Department of Optical and Automotive Engineering, 2002.
- [HAR07] M. HARRER. *Characterisation of Steering Feel*. PhD thesis, University of Bath, Department of Mechanical Engineering, 2007.
- [HAU83] M.L.J. HAUTUS. Strong detectability and observers. *Linear Algebra and its Applications*, 50(0):353 – 368, 1983.

- [HAY01] S. HAYKIN. *Kalman Filtering and Neural Networks*. John Wiley & Sons, Inc., 2001.
- [HB02] B. HEISSING and H. J. BRANDL. *Subjektive Beurteilung des Fahrverhaltens*. Vogel Industrie Medien GmbH & Co. KG, Würzburg, 2002.
- [HBS⁺05] H. M. HEERSPINK, W. R. BERKOUWER, O. STROOSMA, M. M. VAN PAASSEN, M. MULDER, and J. A. MULDER. Evaluation of Vestibular Thresholds for Motion Detection in the SIMONA Research Simulator. In *Proceedings of the AIAA Modeling and Simulation Technologies Conference and Exhibit*, 2005.
- [HE11] B. HEISSING and M. ERSOY. *Chassis Handbook - Fundamentals, Driving Dynamics, Components, Mechatronics, Perspectives*. Vieweg + Teubner Verlag | Springer Fachmedien Wiesbaden GmbH, 1st edition, 2011.
- [HEN04] R. HENZE. *Beurteilung von Fahrzeugen mit Hilfe eines Fahrermodells*. PhD thesis, Technische Universität Carolo-Wilhelmina zu Braunschweig, Fakultät für Maschinenbau und Elektrotechnik, 2004.
- [HEY88] J.B. HEYWOOD. *Internal Combustion Engine Fundamentals*. McGraw-Hill series in mechanical engineering, 1988.
- [HH03] C. HALFMANN and H. HOLZMANN. *Adaptive Modelle für die Kraftfahrzeugdynamik*. Springer-Verlag Berlin Heidelberg 2003, 1st edition, 2003.
- [HIR09] W. HIRSCHBERG. TM_simple 4.0: A simple to Use Tyre Model. *Graz University of Technology*, 2009.
- [HJ78] R. HOSMAN and VAN DER VAART J. *Vestibular models and thresholds of motion perception - results of tests in a flight simulator*. Delft University of Technology, Department of Aerospace Engineering, 1978.
- [HK77] R. HERMANN and A. J. KRENER. Nonlinear controllability and observability. *IEEE Transactions on Automatic Control*, 22(5):728–740, 1977.
- [HL05] L. HULTMAN and S. LARSSON. Development of a Method for Subjective Expert Evaluation of the Human Driving Geometry. Master's thesis, Luleå University of Technology, Department of Human Work Sciences, 2005.
- [HMCB06] B.C. HAMBLIN, R.D. MARTINI, J.T. CAMERON, and S.N. BRENNAN. Low-order modeling of vehicle roll dynamics. In *Proceedings of American Control Conference*, pages 4008–4015, 2006.
- [HOR85] A. HORN. *Fahrer-Fahrzeug-Kurvenfahrt auf trockener Strasse*. PhD thesis, Technische Universität Braunschweig, Fakultät für Maschinenbau und Elektrotechnik, 1985.
- [HOU08] W. HOULT. *A neuromuscular model for simulating driver steering torque*. PhD thesis, University of Cambridge, Department of Engineering, 2008.

- [HRW07] W. HIRSCHBERG, G. RILL, and H. WEINFURTER. Tire model TMeasy. *Vehicle System Dynamics*, 45:101–119, 2007.
- [HS99] R. HOSMAN and H. STASSEN. Pilot’s perception in the control of aircraft motions. *Control Engineering Practice*, 7(11):1421 – 1428, 1999.
- [HUN11] M. HUNEKE. *Fahrverhaltensbewertung mit anwendungsspezifischen Fahrdynamikmodellen*. PhD thesis, Technische Universität Carolo-Wilhelmina zu Braunschweig, Fakultät für Maschinenbau, 2011.
- [ICDW11] J.T. ILLAN, V. CIARLA, and C.C. DE WIT. Oscillation annealing and driver/tire load torque estimation in Electric Power Steering systems. In *IEEE International Conference on Control Applications (CCA)*, pages 1100–1105, 2011.
- [IFM15] H. IMINE, L. FRIDMAN, and T. MADANI. Identification of vehicle parameters and estimation of vertical forces. *International Journal of Systems Science*, 46(16):2996–3009, 2015.
- [IFSD11] H. IMINE, L. FRIDMAN, H. SHRAIM, and M. DJEMAI. *Sliding Mode Based Analysis and Identification of Vehicle Dynamics*, volume 414 of *Lecture Notes in Control and Information Sciences*. Springer Verlag, 2011.
- [IJF⁺06] L. IMSLAND, T.A. JOHANSEN, T.I. FOSSEN, H.F. GRIP, J.C. KALKKUHL, and A. SUISSA. Vehicle velocity estimation using nonlinear observers. *Automatica*, 42(12):2091 – 2103, 2006.
- [IM11] R. ISERMANN and M. MÜNCHHOF. *Identification of Dynamic Systems*. Springer Verlag Berlin Heidelberg, 2011.
- [ISO88a] ISO7401. Road vehicles - lateral transient response test methods, 1988.
- [ISO88b] ISO8725. Road vehicles - transient open-loop response test method with one period of sinusoidal input, 1988.
- [ISO88c] ISO8726. Road vehicles - transient open-loop response test method with pseudo-random steering input, 1988.
- [ISO91] ISO8855. Road Vehicles - Vehicle dynamics and road-holding ability - Vocabulary, 1991.
- [ISO99] ISO/TR 3888:1975. Road vehicles - test procedure for a severe lane-change manoeuvre, 1999.
- [ISO10] ISO13674. Road vehicles - test method for the quantification of on-centre handling - part 1: Weave test, 2010.
- [ISO12] ISO4138. Passenger cars - steady-state circular driving behaviour - open-loop test methods, 2012.
- [J14] SAE J1441. Standard SAE J1441 - Subjective Rating Scale for Vehicle Handling. 2007-4 (Revised).

- [JAZ14] R.N. JAZAR. *Vehicle Dynamics: Theory and Application*. Springer Science+Business Media New York, 2014.
- [JU97] S. J. JULIER and J. K. UHLMANN. New extension of the Kalman filter to non-linear systems. In *Proc. SPIE 3068, Signal Processing, Sensor Fusion, and Target Recognition VI*, volume 3068, pages 182–193, 1997.
- [JÜR97] T. JÜRGENSOHN. *Hybride Fahrermodelle*. Pro Universitate Verlag Sinzheim, 1997.
- [KAL11] R.E. KALMAN. Lectures on controllability and observability. In E. Evangelisti, editor, *Controllability and Observability*, volume 46 of *C.I.M.E. Summer Schools*, pages 1–149. Springer Berlin Heidelberg, 2011.
- [KD97] U. KIENCKE and A. DAISS. Observation of lateral vehicle dynamics. *Control Engineering Practice*, 5(8):1145 – 1150, 1997.
- [KEC01] V. KECMAN. *Learning and Soft Computing: Support Vector Machines, Neural Networks, and Fuzzy Logic Models*. MIT Press, Cambridge, MA, USA, 2001.
- [KHA02] H.K. KHALIL. *Nonlinear Systems*. Prentice Hall, 3rd edition, 2002.
- [KIM09] J. KIM. Identification of lateral tyre force dynamics using an extended Kalman filter from experimental road test data. *Control Engineering Practice*, 17(3):357 – 367, 2009.
- [KLC12] J. KIM, H. LEE, and S. CHOI. A robust road bank angle estimation based on a proportional-integral H_∞ filter. *Proceedings of the Institution of Mechanical Engineers, Part D: Journal of Automobile Engineering*, 226(6):779–794, 2012.
- [KN01] H.-P. KRÜGER and A. NEUKUM. Bewertung von Handlingeigenschaften - zur methodischen und inhaltlichen Kritik des korrelativen Forschungsansatzes. In *Kraftfahrzeugführung*, pages 245–262. Springer Berlin Heidelberg, 2001.
- [KN05] U. KIENCKE and L. NIELSEN. *Automotive Control Systems: For Engine, Drive-line, and Vehicle*. Springer Berlin Heidelberg New York, 2nd edition, 2005.
- [KNS99] H.-P. KRÜGER, A. NEUKUM, and J. SCHULLER. Bewertung von Fahrzeugeigenschaften - vom Fahrgefühl zum Fahrergefühl. *VDI-Fortschritt-Berichte Reihe 22, Düsseldorf: VDI-Verlag*, 1999.
- [KNW07] L. KÖNIG, J. NEUBECK, and J. WIEDEMANN. Nichtlineare Lenkregler für den querdynamischen Grenzbereich. *at - Automatisierungstechnik*, 55(6):314–321, 2007.
- [KOB03] C. KOBETZ. *Modellbasierte Fahrdynamikanalyse durch ein an Fahrmanövern parameteridentifiziertes querdynamisches Simulationsmodell*. PhD thesis, Fakultät für Maschinenbau, Technische Universität Wien, 2003.
- [KOL09] D. KOLLREIDER. *Identifikation der Reifeneigenschaften als Grundlage zur Fahrdynamikbewertung*. PhD thesis, Technische Universität Graz, Fakultät für Maschinenbau und Wirtschaftsingenieurwesen, 2009.

- [KPM12] C. KUNUSCH, P. PULESTON, and M. MAYOSKY. *Sliding-Mode Control of PEM Fuel Cells*. Advances in Industrial Control. Springer London, 2012.
- [KRA11] C. KRAFT. *Gezielte Variation und Analyse des Fahrverhaltens von Kraftfahrzeugen mittels elektrischer Linearaktuatoren im Fahrwerksbereich*. Karlsruher Schriftenreihe Fahrzeugsystemtechnik. KIT Scientific Publ., 2011.
- [KRE10] E. KREYSZIG. *Advanced Engineering Mathematics*. John Wiley & Sons, 2010.
- [LAH12] M. LAHTI. *Suspension-Tire-Behavior Models*. PhD thesis, Technische Universität Wien, Institut für Mechanik und Mechatronik, 2012.
- [LAN87] S. LANG. *Calculus of Several Variables*. Springer-Verlag New York Inc, 3rd edition, 1987.
- [LEV93] A. LEVANT. Sliding order and sliding accuracy in sliding mode control. *International Journal of Control*, 58(6):1247–1263, 1993.
- [LEV98] A. LEVANT. Robust exact differentiation via sliding mode technique. *Automatica*, 34(3):379–384, 1998.
- [LEV99] A. LEVANT. Controlling output variables via higher order sliding modes. In *European Control Conference (ECC)*, pages 3798–3803, 1999.
- [LEV03] A. LEVANT. Higher-order sliding modes, differentiation and output-feedback control. *International Journal of Control*, 76:924–941, 2003.
- [LEV05] A. LEVANT. Quasi-continuous high-order sliding-mode controllers. *IEEE Transactions on Automatic Control*, 50(11):1812–1816, 2005.
- [LEV07] A. LEVANT. Principles of 2-sliding mode design. *Automatica*, 43(4):576 – 586, 2007.
- [LIM09] J. LIMROTH. *Real-Time Vehicle Parameter Estimation and Adaptive Stability Control*. PhD thesis, Graduate School of Clemson University, 2009.
- [LIT83] L. LITZ. Modale Maße für Steuerbarkeit, Beobachtbarkeit, Regelbarkeit und Dominanz - Zusammenhänge, Schwachstellen, neue Wege. *Regelungstechnik*, 31(5):148 – 158, 1983.
- [LJU79] L. LJUNG. Asymptotic behavior of the extended Kalman filter as a parameter estimator for linear systems. *IEEE Transactions on Automatic Control*, 24(1):36–50, Feb 1979.
- [LJU99] L. LJUNG. *System Identification: Theory for the User*. Prentice Hall Ptr, 2nd edition, 1999.
- [LL14] M. LIVNE and A. LEVANT. Proper discretization of homogeneous differentiators. *Automatica*, 50(8):2007 – 2014, 2014.
- [LNO15] S. LEE, K. NAKANO, and M. OHORI. On-board identification of tyre cornering stiffness using dual Kalman filter and GPS. *Vehicle System Dynamics*, 53(4):437–448, 2015.

- [LS98] H. LIST and P. SCHÖGGL. Objective Evaluation of Vehicle Driveability. *SAE Technical Paper 980204*, 1998.
- [LSBJ95] B. LA SCALA, R. BITMEAD, and M. JAMES. Conditions for stability of the extended Kalman filter and their application to the frequency tracking problem. *Mathematics of Control, Signals and Systems*, 8(1):1–26, 1995.
- [LUE71] D.G. LUENBERGER. An introduction to observers. *IEEE Transactions on Automatic Control*, 16(6):596–602, 1971.
- [MAR03] H.J. MARQUEZ. *Nonlinear Control Systems: Analysis and Design*. John Wiley & Sons, Inc., 1st edition, 2003.
- [MD08] J. A. MORENO and D. DOCHAIN. Global observability and detectability analysis of uncertain reaction systems and observer design. *International Journal of Control*, 81(7):1062–1070, 2008.
- [MEL03] D. MELJNIKOV. *Entwicklung von Modellen zur Bewertung des Fahrverhaltens von Kraftfahrzeugen*. PhD thesis, Fakultät für Maschinenbau, Universität Stuttgart, 2003.
- [MG11] J.A. MORENO and E. GUZMAN. A New Recursive Finite-Time Convergent Parameter Estimation Algorithm. In *Proceedings of the 18th IFAC World Congress*, volume 18, Milano, Italy, 2011.
- [MGV⁺09] M.L. MCINTYRE, T.J. GHOTIKAR, A. VAHIDI, XUBIN SONG, and D.M. DAWSON. A Two-Stage Lyapunov-Based Estimator for Estimation of Vehicle Mass and Road Grade. *IEEE Transactions on Vehicular Technology*, 58(7):3177–3185, 2009.
- [MKDN12] L. MENHOUR, D. KOENIG, and B. D’ANDREA-NOVEL. Road bank and vehicle roll angles estimation based on proportional-integral observer. In *8th IFAC Symposium on Fault Detection, Supervision and Safety of Technical Processes*, volume 8, pages 1185–1190, Mexico City, Mexico, 2012.
- [MLC10] L. MENHOUR, D. LECHNER, and A. CHARARA. Embedded unknown input sliding mode observer to estimate the vehicle roll and road bank angles: Experimental evaluation. In *7th IFAC Symposium on Intelligent Autonomous Vehicles (IAV 2010)*, pages 623–628, Italy, 2010.
- [MO12] J.A. MORENO and M. OSORIO. Strict Lyapunov Functions for the Super-Twisting Algorithm. *IEEE Transactions on Automatic Control*, 57(4):1035–1040, 2012.
- [MON02] G. MONSEES. *Discrete-Time Sliding Mode Control*. PhD thesis, Technische Universität Delft, 2002.
- [MOR09] J.A. MORENO. A linear framework for the robust stability analysis of a Generalized Super-Twisting Algorithm. In *6th International Conference on Electrical Engineering, Computing Science and Automatic Control, CCE*, pages 1–6, 2009.
- [MOS11] S. MOSCHIK. *Steuerbarkeitsmaße für lineare zeitinvariante Systeme*. PhD thesis, Technische Universität Graz, Fakultät für Elektro- und Informationstechnik, 2011.

- [MOYS90] T. MIMURO, M. OHSAKI, H. YASUNAGA, and K. SATOH. Four parameter evaluation method of lateral transient response. *SAE Technical Paper 901734*, 1990.
- [MRF⁺08] N.K. M'SIRDI, A. RABHI, L. FRIDMAN, J. DAVILA, and Y. DELANNE. Second order sliding-mode observer for estimation of vehicle dynamic parameters. *International Journal of Vehicle Design*, 48(3/4):190 – 207, 2008.
- [MT08] H. MEYER-TUVE. *Modellbasiertes Analysetool zur Bewertung der Fahrzeugquerdynamik anhand von objektiven Bewegungsgrößen*. PhD thesis, Technische Universität München, Fakultät für Maschinenwesen, 2008.
- [MT14] G.P. MERKER and R. TEICHMANN, editors. *Grundlagen Verbrennungsmotoren*. Springer Vieweg, 3rd edition, 2014.
- [MTTT80] A. MATSUSHITA, K. TAKANAMI, N. TAKEDA, and M. TAKAHASHI. Subjective evaluation and vehicle behavior in lane-change maneuvers. *SAE Technical Paper 800845*, 1980. Society of Automotive Engineers.
- [MW04] M. MITSCHKE and H. WALLENTOWITZ. *Dynamik der Kraftfahrzeuge*. Springer-Verlag Berlin Heidelberg, 4th edition, 2004.
- [NAL89] A.G. NALECZ. Application of Sensitivity Methods to Analysis and Synthesis of Vehicle Dynamic Systems. *Vehicle System Dynamics*, 18(1-3):1–44, 1989.
- [NKS01] A. NEUKUM, H.-P. KRÜGER, and J. SCHULLER. Der Fahrer als Messinstrument für fahrdynamische Eigenschaften? *Der Fahrer im 21. Jahrhundert*, pages 13–32, (VDI-Berichte, Nr. 1613). Düsseldorf: VDI-Verlag, 2001.
- [NÜS02] M. NÜSSLE. *Ermittlung von Reifeneigenschaften im realen Fahrbetrieb*. PhD thesis, Fakultät für Maschinenbau der Universität Karlsruhe, 2002.
- [NUT09] C. NUTHONG. *Estimation of Tire-Road Friction Forces using Kalman Filtering for Advanced Vehicle Control*. PhD thesis, Universität der Bundeswehr München, Institut für Steuer- und Regelungstechnik, 2009.
- [NVDS90] H. NIJMEIER and A.J. VAN DER SCHAFT. *Nonlinear Dynamical Control Systems*. Springer-Verlag New York Inc., 1990.
- [OCGS06] A. ORTIZ, J. A. CABRERA, A. J. GUERRA, and A. SIMON. An easy procedure to determine magic formula parameters. *Vehicle System Dynamics*, 44(9):689–718, 2006.
- [OGA01] K. OGATA. *Modern Control Engineering*. Prentice Hall PTR, Upper Saddle River, NJ, USA, 4th edition, 2001.
- [ORR06] B.J. ODELSON, M.R. RAJAMANI, and J.B. RAWLINGS. A new autocovariance least-squares method for estimating noise covariances. *Automatica*, 42(2):303 – 308, 2006.
- [OSB99] A. V. OPPENHEIM, R. W. SCHAFER, and J. R. BUCK. *Discrete-time Signal Processing*. Prentice-Hall, Inc., Upper Saddle River, NJ, USA, 2nd edition, 1999.

- [PAC12] H. PACEJKA. *Tire and Vehicle Dynamics*. Butterworth-Heinemann, 3rd edition, 2012.
- [PB97] H. B. PACEJKA and I. J. M. BESSELINK. Magic formula tyre model with transient properties. *Vehicle System Dynamics*, 27:234–249, 1997.
- [PB02] W. PERRUQUETTI and J.P. BARBOT. *Sliding Mode Control in Engineering*. Marcel Dekker, Inc., 2002.
- [PE07] M. PLÖCHL and J. EDELMANN. Driver models in automobile dynamics application. *Vehicle System Dynamics*, 45(7-8):699–741, 2007.
- [PES06] N. PATEL, C. EDWARDS, and S.K. SPURGEON. A sliding mode observer for tyre friction estimation during braking. In *American Control Conference*, pages 5867–5872, 2006.
- [PFE06] P.E. PFEFFER. *Interaction of Vehicle and Steering System Regarding On-Centre Handling*. PhD thesis, University of Bath, Department of Mechanical Engineering, 2006.
- [PH11] P. PFEFFER and M. HARRER. *Lenkungsbandbuch*. Vieweg+Teubner Verlag | Springer Fachmedien Wiesbaden GmbH, 1st edition, 2011.
- [PHL08] P. E. PFEFFER, M. HARRER, and J. LIN. Vehicle dynamics measurements. *Proceedings of the Institution of Mechanical Engineers, Part D: Journal of Automobile Engineering*, 222:801–813, 2008.
- [PIC04] A.J. PICK. *Neuromuscular Dynamics and the Vehicle Steering Task*. PhD thesis, Cambridge University Engineering Department, 2004.
- [PIS00] A. PISANO. *Second Order Sliding Modes: Theory and Applications*. PhD thesis, Dipartimento di Ingegneria Elettrica ed Elettronica, Università degli Studi di Cagliari, 2000.
- [POZ04] A. POZNYAK. Deterministic output noise effects in sliding mode observation. *Variable structure systems: from principles to implementation*, pages 45–79, 2004.
- [POZ10] A. POZNYAK. *Advanced Mathematical Tools for Control Engineers: Volume 1: Deterministic Systems*. Elsevier Science, 2nd edition, 2010.
- [PP02] A. PAPOULIS and S.U. PILLAI. *Probability, Random Variables, and Stochastic Processes*. McGraw-Hill, 4th edition, 2002.
- [PP09] A. POLYAKOV and A. POZNYAK. Reaching Time Estimation for Super-Twisting Second Order Sliding Mode Controller via Lyapunov Function Designing. *IEEE Transactions on Automatic Control*, 54(8):1951–1955, 2009.
- [PRE08] K. PRENNINGER. *Objektive Beurteilung der Fahrdynamik von Kraftfahrzeugen, insbesondere Nutzfahrzeugen, mittels modellbasierter Parameteridentifikation*. PhD thesis, Technische Universität Graz, Fakultät für Maschinenbau und Wirtschaftsingenieurwesen, 2008.

- [RA97] A. RIEDEL and R. ARBINGER. *Subjektive und objektive Beurteilung des Fahrverhaltens von Pkw.* FAT Schriftenreihe, Nr. 139, FAT, Frankfurt, 1997.
- [RA00] A. RIEDEL and R. ARBINGER. *Ergänzende Auswertungen zur subjektiven und objektiven Beurteilung des Fahrverhaltens von Pkw.* FAT Schriftenreihe, Nr. 161, FAT, Frankfurt, 2000.
- [RAJ12] R. RAJAMANI. *Vehicle Dynamics and Control.* Mechanical Engineering Series. Springer New York Dordrecht Heidelberg London, 2nd edition, 2012.
- [RAP04] K. RAPP. *Nonlinear estimation and control in the iron ore pelletizing process: An application and analysis of the Extended Kalman Filter.* PhD thesis, Norwegian University of Science and Technology, 2004.
- [REI90] W. REICHELT. *Ein adaptives Fahrermodell zur Bewertung der Fahrdynamik von Pkw in kritischen Situationen.* PhD thesis, Technische Universität Carolo-Wilhelmina zu Braunschweig, Fakultät für Maschinenbau und Elektrotechnik, 1990.
- [REN07] I. RENNER. *Methodische Unterstützung funktionsorientierter Baukastenentwicklung am Beispiel Automobil.* PhD thesis, Technische Universität München, Lehrstuhl für Produktentwicklung, 2007.
- [RG04] J. RYU and J.C. GERDES. Estimation of vehicle roll and road bank angle. In *Proceedings of the 2004 American Control Conference*, volume 3, pages 2110–2115, 2004.
- [RGYU99] K. REIF, S. GUNTHER, E. YAZ, and R. UNBEHAUEN. Stochastic stability of the discrete-time extended Kalman filter. *IEEE Transactions on Automatic Control*, 44(4):714–728, 1999.
- [RH84] K. ROMPE and B. HEISSING. *Objektive Testverfahren für die Fahreigenschaften von Kraftfahrzeugen.* Verlag TÜV Rheinland GmbH, Köln, 1984.
- [RH11] M. REICHHARTINGER and M. HORN. Finite-time stabilization by robust backstepping for a class of mechanical systems. In *Proceedings of IEEE International Conference on Control Applications (CCA)*, pages 1403–1409, 2011.
- [RH14] M. REICHHARTINGER and M. HORN. Improved Position Control of a Mechanical System Using Terminal Attractors. In *Mechanics and Model-Based Control of Advanced Engineering Systems*, pages 247–254. Springer Vienna, 2014.
- [RIX05] J.J. RIX. *Identification of the closed-loop steering behaviour of a driver.* PhD thesis, Cambridge University Engineering Department, 2005.
- [RMC07] J. RYU, N.K. MOSHCHUK, and SHIH-KEN CHEN. Vehicle state estimation for roll control system. In *American Control Conference (ACC)*, pages 1618–1623, 2007.
- [RPTL11] R. RAJAMANI, D. PIYABONGKARN, V. TSOURAPAS, and J.Y. LEW. Parameter and state estimation in vehicle roll dynamics. *IEEE Transactions on Intelligent Transportation Systems*, 12(4):1558–1567, 2011.

- [RRV00] M. RUSSO, R. RUSSO, and A. VOLPE. Car parameters identification by handling manoeuvres. *Vehicle System Dynamics: International Journal of Vehicle Mechanics and Mobility*, 34(6):423–436, 2000.
- [RS40] P. RIEKERT and T.E. SCHUNCK. Zur Fahrmechanik des gummibereiften Kraftfahrzeuges. *Ingenieur-Archiv XI. Band, Heft 3, S. 210-224*, 1940.
- [RYU04] J. RYU. *State and Parameter Estimation for Vehicle Dynamics Control using GPS*. PhD thesis, Stanford University, Department of Mechanical Engineering, 2004.
- [RZSF⁺12] A. REZAEIAN, R. ZARRINGHALAM, M. SABER FALLAH, W. MELEK, A. KHAJEPOUR, S.K. CHEN, and B. LITKOUHI. Joint Unscented Kalman Filter for Combined Estimation of Vehicle States and Parameters. In *11th International Symposium on Advanced Vehicle Control*, Seoul, South Korea, 2012.
- [SC08] T. SHIM and G. CHINAR. Understanding the limitations of different vehicle models for roll dynamics studies. *Vehicle System Dynamics: International Journal of Vehicle Mechanics and Mobility*, 45(3):191–216, 2008.
- [SCH10] C. SCHIMMEL. *Entwicklung eines fahrerbasierten Werkzeugs zur Objektivierung subjektiver Fahreindrücke*. PhD thesis, Technische Universität München, 2010.
- [SEFL14] Y. SHTESSEL, C. EDWARDS, L. FRIDMAN, and A. LEVANT. *Sliding Mode Control and Observation*. Birkhäuser, 2014.
- [SGG14] M. SAHA, R. GHOSH, and B. GOSWAMI. Robustness and Sensitivity Metrics for Tuning the Extended Kalman Filter. *IEEE Transactions on Instrumentation and Measurement*, 63(4):964–971, 2014.
- [SGMN08] Y. SEBSADJI, S. GLASER, S. MAMMAR, and M. NETTO. Vehicle roll and road bank angles estimation. In *Proceedings of the 17th IFAC World Congress*, pages 7091–7097, Seoul, South Korea, 2008.
- [SH92] R. SCHIESCHKE and R. HIEMENZ. The decisive role the quality of tyre approximation plays in vehicle dynamics simulations. *Vehicle System Dynamics*, 21:156–166, 1992.
- [SHB14] D. SCHRAMM, M. HILLER, and R. BARDINI. *Vehicle Dynamics: Modeling and Simulation*. Springer Berlin Heidelberg, 2014.
- [SHKH09] G. STOCK, J. HOFFMANN, F. KÜÇÜKAY, and R. HENZE. Sensitivität des Durchschnittsfahrers auf Veränderungen in der Fahrdynamik. *Subjektive Fahreindrücke sichtbar machen IV, Korrelation zwischen objektiver Messung und subjektiver Beurteilung in der Fahrzeugentwicklung*, pages 179–198, Haus der Technik Fachbuch Band 108, 2009.
- [SIM06] D. SIMON. *Optimal State Estimation*. John Wiley & Sons, Inc., 2006.
- [SJ08] P. SAHLHOLM and K. H. JOHANSSON. Road Grade Estimation for Look-ahead Vehicle Control. In *Proceedings of the 17th IFAC World Congress*, 2008.

- [SL07] R. F. SCHMIDT and F. LANG, editors. *Physiologie des Menschen*. Springer Medizin Verlag Heidelberg, 30th edition, 2007.
- [SOF08] H. SHRAIM, M. OULADSINE, and L. FRIDMAN. Vehicle parameter and states estimation via sliding mode observers. In *Modern Sliding Mode Control Theory*, volume 375 of *Lecture Notes in Control and Information Sciences*, pages 345–362. Springer Berlin Heidelberg, 2008.
- [SPU08] S. K. SPURGEON. Sliding mode observers: a survey. *Int. J. Systems Science*, 39(8):751–764, 2008.
- [SR08] U. SEIFFERT and G. RAINER. *Virtuelle Produktentstehung für Fahrzeug und Antrieb im Kfz*. Vieweg + Teubner Verlag, 1st edition, 2008.
- [SS89] T. SÖDERSTRÖM and P. STOICA. *System Identification*. Prentice Hall International Ltd, 1989.
- [STE94] R.F. STENGEL. *Optimal Control and Estimation*. Dover Publications, Inc., New York, 1994.
- [STJP06] C. SIERRA, E. TSENG, A. JAIN, and H. PENG. Cornering stiffness estimation based on vehicle lateral dynamics. *Vehicle System Dynamics*, 44:24–38, 2006.
- [STP12] Y.B. SHTESSEL, M. TALEB, and F. PLESTAN. A novel adaptive-gain supertwisting sliding mode controller: Methodology and application. *Automatica*, 48(5):759–769, 2012.
- [SU11] F. SAGLAM and Y.S. UNLUSOY. Identification of low order vehicle handling models from multibody vehicle dynamics models. In *Mechatronics (ICM), IEEE International Conference on*, pages 96–101, 2011.
- [TE09] P. TEMPLIN and B. EGARDT. An LQR torque compensator for driveline oscillation damping. In *IEEE International Symposium on Intelligent Control (ISIC)*, pages 352–356, 2009.
- [TFG12] M. TANELLI, A. FERRARA, and P. GIANI. Combined vehicle velocity and tire-road friction estimation via sliding mode observers. In *IEEE International Conference on Control Applications (CCA)*, pages 130–135, 2012.
- [TØN07] K.K. TØNNE. Stability Analysis of EKF-based Attitude Determination and Control. Master’s thesis, Norwegian University of Science and Technology, Department of Engineering Cybernetics, 2007.
- [TRH12a] R. TAFNER, M. REICHHARTINGER, and M. HORN. Robust online identification of vehicle roll dynamics. In *11th International Symposium on Advanced Vehicle Control*, Seoul, South Korea, 2012.
- [TRH12b] R. TAFNER, M. REICHHARTINGER, and M. HORN. Robust vehicle roll dynamics identification based on roll rate measurements. In *IFAC Workshop on Engine and Powertrain Control, Simulation and Modelling (E-COSM’12)*, pages 72–78, Paris, France, 2012.

- [TRH14a] R. TAFNER, M. REICHHARTINGER, and M. HORN. Estimation of tire parameters via second-order sliding mode observers with unknown inputs. In *13th International Workshop on Variable Structure Systems (VSS)*, pages 1–6, 2014.
- [TRH14b] R. TAFNER, M. REICHHARTINGER, and M. HORN. Robust online roll dynamics identification of a vehicle using sliding mode concepts. *Control Engineering Practice*, 29(0):235 – 246, 2014.
- [TSE01] H.E. TSENG. Dynamic estimation of road bank angle. *Vehicle System Dynamics*, 36(4-5):307–328, 2001.
- [TXH07] H.E. TSENG, L. XU, and D. HROVAT. Estimation of land vehicle roll and pitch angles. *Vehicle System Dynamics*, 45(5):433–443, 2007.
- [UGS09] V. UTKIN, J. GULDNER, and J. SHI. *Sliding Mode Control in Electro-Mechanical Systems*. Taylor & Francis Group, CRC Press, 2nd edition, 2009.
- [UP13] V. I. UTKIN and A. S. POZNYAK. Adaptive sliding mode control with application to super-twist algorithm: Equivalent control method. *Automatica*, 49(1):39 – 47, 2013.
- [UTK92] V. UTKIN. *Sliding Modes in Control and Optimization*. Springer-Verlag Berlin Heidelberg New York, 1992.
- [UTK13] V. UTKIN. On convergence time and disturbance rejection of super-twisting control. *IEEE Transactions on Automatic Control*, 58(8):2013–2017, 2013.
- [VDMW01] R. VAN DER MERWE and E.A. WAN. The square-root unscented Kalman filter for state and parameter-estimation. In *IEEE International Conference on Acoustics, Speech, and Signal Processing*, volume 6, pages 3461–3464, 2001.
- [VDS98] F. M. A VAN DER STEEN. *Self-Motion Perception*. PhD thesis, Technische Universiteit Delft, 1998.
- [VG93] S. T. VENKATARAMAN and S. GULATI. Control of Nonlinear Systems Using Terminal Sliding Modes. *Journal of Dynamic Systems, Measurement, and Control*, 115(3):554–560, 1993.
- [VV08] A. VON VIETINGHOFF. *Nichtlineare Regelung von Kraftfahrzeugen in querdynamisch kritischen Fahrsituationen*. PhD thesis, Universität Karlsruhe, Fakultät für Elektrotechnik und Informationstechnik, 2008.
- [WAG03] A. WAGNER. Ein Verfahren zur Vorhersage und Bewertung der Fahrerreaktion bei Seitenwind. *Schriftreihe des Instituts für Verbrennungsmotoren und Kraftfahrwesen der Universität Stuttgart 23*, 2003.
- [WAN09] J. WANG. A variable forgetting factor RLS adaptive filtering algorithm. In *Proceedings of 3rd IEEE International Symposium on Microwave, Antenna, Propagation and EMC Technologies for Wireless Communications*, pages 1127 –1130, 2009.

- [WBGH06] M. WENTINK, J. BOS, E. GROEN, and R. HOSMAN. Development of the Motion Perception Toolbox. In *AIAA Modeling and Simulation Technologies Conference and Exhibit*. AIAA American Institute of Aeronautics and Astronautics, 2006.
- [WD78] H.D. WEIR and R.J. DIMARCO. Correlation and evaluation of driver/vehicle directional handling data. *SAE Technical Paper 780010*, 1978.
- [WEY15] M. WEYRER. Inbetriebnahme, Modellierung und Regelung eines Prüfstandes für elektrische Lenkunterstützung. Master's thesis, Alpen-Adria-Universität Klagenfurt, Fakultät für technische Wissenschaften, 2015.
- [WI09] D. WESEMEIER and R. ISERMANN. Identification of vehicle parameters using stationary driving maneuvers. *Control Engineering Practice*, 17(12):1426 – 1431, 2009. Special Section: The 2007 {IFAC} Symposium on Advances in Automotive Control.
- [WIL02] A. WILDEN. *Analyse und Modellierung vestibulärer Information in den tiefen Kleinhirnkernen*. PhD thesis, Medizinische Fakultät der Ludwig-Maximilians-Universität zu München, 2002.
- [WMCL06] M. A. WILKIN, W. J. MANNING, D. A. CROLLA, and M. C. LEVESLEY. Use of an extended Kalman filter as a robust tyre force estimator. *Vehicle System Dynamics*, 44:50–59, 2006.
- [WVDM00] E.A. WAN and R. VAN DER MERWE. The unscented Kalman filter for nonlinear estimation. In *The IEEE 2000 Adaptive Systems for Signal Processing, Communications, and Control Symposium*, pages 153–158, 2000.
- [ZAM94] J. ZAMOW. Beitrag zur Identifizierung unbekannter Parameter für fahrdynamische Simulationsmodelle. In *Fortschritt-Bericht VDI, Reihe 12, Nr. 217, Düsseldorf: VDI-Verlag*, 1994.
- [ZBR97] A. ZOMOTOR, H.-H. BRAESS, and R. RÖNITZ. Verfahren und Kriterien zur Bewertung des Fahrverhaltens von Personenkraftwagen - ein Rückblick auf die letzten 20 Jahre (Teil 1). *ATZ Automobiltechnische Zeitschrift*, 99:780–786, 1997.
- [ZBR98] A. ZOMOTOR, H.-H. BRAESS, and R. RÖNITZ. Verfahren und Kriterien zur Bewertung des Fahrverhaltens von Personenkraftwagen - ein Rückblick auf die letzten 20 Jahre (Teil 2). *ATZ Automobiltechnische Zeitschrift*, 100:236–243, 1998.
- [ZOM91] A. ZOMOTOR. *Fahrwerktechnik: Fahrverhalten*. Vogel Buchverlag, 1991.
- [ZOM02] Z. A. ZOMOTOR. *Online-Identifikation der Fahrdynamik zur Bewertung des Fahrverhaltens von Pkw*. PhD thesis, Institut A für Mechanik der Universität Stuttgart, 2002.
- [ZPW94] MAN ZHIHONG, A.P. PAPLINSKI, and H.R. WU. A robust MIMO terminal sliding mode control scheme for rigid robotic manipulators. *IEEE Transactions on Automatic Control*, 39(12):2464–2469, 1994.

-
- [ZSC09] A. K. ZSCHOCKE. *Ein Beitrag zur objektiven und subjektiven Evaluierung des Lenkkomforts von Kraftfahrzeugen*. PhD thesis, Universität Karlsruhe, Fakultät für Maschinenbau, 2009.
- [ZSM09] J. ZEHETNER, P. SCHÖGGL, and K. MEITZ. Simulation of Driveability in Real-time. *SAE Technical Paper 2009-01-1372*, 2009.